Alkaline-Earth Catalysis for Inorganic Polymer Synthesis

Morris, Louis

Award date:
2020

Awarding institution:
University of Bath

Alkaline-Earth Catalysis for Inorganic Polymer Synthesis

Louis Jowan Morris

A thesis submitted for the degree of Doctor of Philosophy

University of Bath

Department of Chemistry

October 2019

Declaration of any previous submission of the work

The material presented here for examination for the award of a higher degree by research has been incorporated into a submission for another degree, specifically:

*The synthesis and characterisation of compound **3** was incorporated into a submission to Cardiff University for the award of Master of Research in Catalysis.*

Declaration of authorship

I am the author of this thesis, and the work described therein was carried out by myself personally, with following exceptions:

*All single-crystal X-ray structures were refined and finalised by Dr Mary F. Mahon, University of Bath. In Chapter 2, powder X-ray diffraction was carried out by Dr George R. Whittell (University of Bristol, Bristol, UK) and electron microscopy studies were carried out by Dr Jean-Charles Eloi (University of Bristol, Bristol, UK). In Chapter 3, samples **P15**-**P18** were synthesised by Fred McMenamy (University of Bath). In Chapter 4, all calculations relating to the computational investigations were carried out by Dr Nasir A. Rajabi and Dr Claire L. McMullin (University of Bath). In Chapter 5, X-ray crystallography of compound **19** was carried out by Dr Brian Patrick (University of British Columbia, Vancouver, British Columbia, Canada).*

Table of contents

I. Acknowledgements

There are many wonderful people with whom I've been lucky enough to share the past three years with and without whom, neither this thesis, nor my life in general would have taken the form that it has.

Firstly, I would like to thank Mike. Your knowledge, insight and creativity never cease to amaze me. Somehow, the gentle encouragements and enthusiasm are contagious. It has been a real joy to work with you and bit by bit, get to know you. If I ever manage to be half the chemist, let alone person that you are, I'll be a very happy man!

Ian. To have had the opportunity to work with you has been an incredible experience, one that took a fair while to dawn on me! To try and put into words what I've learnt from you would be futile. The excitement that you have for good science and the interest and care that you take over your group are inspirational.

Besides being an excellent scientist and great colleague, I wish to thank George Whittell for his contribution to this work and for his easy-going, buoyant personality. I have rarely had a dull moment in his presence. Acknowledgements are also due for Mary Mahon, Jean-Charles Eloi, Nasir Rajabi, Claire McMullin, John Lowe, and Frank Marken for their considerable expertise, helpful discussions, assistance, and hard work in the X-ray crystallography, Electron Microscopy, Computational Chemistry, NMR, and Electrochemistry without which, this thesis would be nothing more than a firelighter printed with a few rambling words (this sentence being a case in point). I would also like to acknowledge the contributions of Fred McMenamy to Chapter 3, and Brian Patrick for taking care of my Canadian crystals.

It has been such fun to work with the Hill group of past and present: Mat, Amanda, Lucia, Bibian, Kieran, Henry, and Ryan. Special thanks go to Andy. A friend from whose unique perspective, scientific rigor, attention to detail and interesting discussions, I've learnt so much. I've also learnt so much from Anne-Fred, with whom I've had the pleasure of passing many hours in the lab and who deserves, not the title of "chemistry mum", but of a true friend and colleague. Without the PhD of David Liptrot, the content of this thesis would be wholly different. To be honest, I tend to take a natural dislike to people with a loud disposition. However, first impressions can be misleading, and I express my thanks to his kindness, helpful conversations, and a genuine willingness to just have a chat! I would also like to thank the Manners group, for providing such a welcoming and friendly environment whenever I would occasionally wonder in. In particular, I wish to thank Diego, Becs, Nikki, Ali, Vince, Sam, Liam, Mitch, and Etienne.

I thank my parents. Obviously, I wouldn't be the person I am (or a life-form at all!) without you, but I really appreciate the opportunities and freedom that you've given myself and my siblings to be creative, individual, and pursue whatever takes our interest. Your encouragement to be the best that I can be and to look at the world with curiosity have certainly left their mark on this thesis.

Laura, you know as well as I do, that the words that follow will barely approach how I really think or feel about you. Needless to say, I cannot begin to imagine what shape the last few years would be like without you, and I always look forward to our future together. Your encouraging, loving, caring, and radiant personality have had an immeasurable impact on me. I'm sorry I was late for dinner again.

II. Publications as a result of this thesis

Chapter 2:

Ferrocene-Containing Polycarbosilazanes via the Alkaline-Earth Catalysed Dehydrocoupling of Silanes and Amines, L. J. Morris, G. R. Whittell, J.-C. Eloi, M. F. Mahon, F. Marken, I. Manners and M. S. Hill, *Organometallics*, 2019, **38**, 3629-3648.

Chapter 4:

Calcium Stannyl Formation by Organostannane Dehydrogenation, L. J. Morris, M. S. Hill, I. Manners, C. L. McMullin, M. F. Mahon and N. A. Rajabi, *Chemical Communications,* 2019, **55**, 12964-12967.

III. Abstract

Synthetic polymers play an increasingly dominant role in almost every aspect of 21st century human life. With notable exceptions, polymers containing significant quantities of elements other than carbon remain a subject of academic curiosity, yet already show potential as useful materials in commodity and speciality applications. Central to this elemental disparity is the requirement for a robust and versatile toolkit of efficient element-element bond forming reactions. Herein, various aspects pertaining to the use of alkaline-earth mediated dehydrocoupling as a tool for inorganic polymer synthesis are investigated in detail.

Initially focussing upon the well-established alkaline-earth mediated dehydrocoupling of silanes and amines, a series of soluble ferrocene-containing metallo-polycarbosilazanes and model molecular compounds were synthesised. Whilst monomer choice was found to be a decisive factor in the ability to yield well-defined polymeric structures, this approach proved to be an effective method to access previously unexplored metallopolymers. Although wider application was limited by the hydrolytic sensitivity of backbone Si-N bonds, the polymers displayed well-behaved reversible electrochemical behaviour and were found to be promising precursors to magnetic ceramic materials, which themselves were subjected to extensive characterisation.

The scope of alkaline-earth mediated cross-metathesis was subsequently expanded to the dehydrocoupling of silanes and alcohols. Besides providing access to hydrolytically robust ferrocene-containing metallo-polysilylethers, extensive investigations into the scope and mechanism of catalysis provided insight into an intricate and complex reaction manifold. Factors such as ionic radius, catalyst and substrate concentration, and active species nuclearity were found to exert a profound influence on mechanism and activity.

The construction of polymer chains composed entirely of other main-group elements provides fascinating materials which often exhibit totally different properties to their carbon-analogues. Since they produce polymer chains formally isoelectronic to polyolefins, organostannanes and phosphine-boranes are monomers of interest, yet their dehydrogenative polymerisation is dominated by transition-metal catalysis. The final portion of this work sought to address this issue by conducting a preliminary investigation into the chemistry of calcium- and magnesium stannyl and phosphidoborane complexes. Structural, spectroscopic, and computational investigations provided valuable insight into virtually unexplored chemistry combining the alkaline-earths and heavier *p*-block elements.

IV. Abbreviations used herein

ADP	Anisotropic Displacement Parameter
Ae	Alkaline-Earth
AIBN	Azo-bis-*iso*butyronitrile
Ar	Aryl
9-BBN	9-borabicyclo[3.3.1]nonane
BDI	β-diketiminate, β-diketiminato
Bn	Benzyl
Bpin, pinB	Pinocolatoboryl
BS	Basis Set
Bu, *n*Bu	*n*-Butyl
18-c-6	18-crown-6
CAAC	Cyclic Alkyl Amino Carbene
Cat.	Catalyst
Cc	Cobaltocene/cobaltocenyl
Cc^+	Cobaltocenium
CDSA	Crystallisation-Driven Self-Assembly
clox	1,1-diphenyl-1-(*para*-chlorophenyl)-methoxy
cod	Cyclooctadiene
COSY	Correlation Nuclear Magnetic Resonance Spectroscopy
Cp	Cyclopentadienyl
Cp*	Pentamethylcyclopentadienyl
CSD	Cambridge Structural Database
CV	Cyclic Coltammetry, Cyclic Voltammogram
X_n	Number Average Degree of Polymerisation
Δ	Heat
$\Delta E_{1/2}$	Difference in midpoint redox potential
ΔE_{peak}	Difference in electrochemical potential at peak current
$\Delta G^‡$	Gibbs Free Energy of Activation
$\Delta S^‡$	Entropy of Activation
DFT	Density Functional Theory
Dipep	2,6-di-*iso*pentylphenyl
Dipp	2,6-di-*iso*propylphenyl
DME	Dimethoxyethane
DNA	Deoxyribonucleic acid

DOSY	Diffusion Ordered Spectroscopy
dpp	2,6-diphenylphenyl
DSC	Differential Scanning Calorimetry
E	Electrochemical potential
$E_{1/2}$	Midpoint electrochemical potential
E_{peak}	Electrochemical potential at peak current
EDX	Energy Dispersive X-ray Spectroscopy
Et	Ethyl
Fc	Ferrocene/ferrocenyl
fc	Ferrocene-diyl
Fc^+	Ferrocenium
FLP	“Frustrated” Lewis-pair
GPC	Gel-Permeation Chromatography
hv	Electromagnetic radiation
Hex, *n*Hex	*n*-Hexyl
HMBC	Heteronuclear multiple bond correlation spectroscopy
HMPA	Hexamethylphosphoramide
HMQC	Heteronuclear Multiple Quantum Coherence Spectroscopy
HOMO	Highest Occupied Molecular Orbital
HRTEM	High-Resolution Transmission Electron Microscopy
HSQC	Heteronuclear Single Quantum Coherence Spectroscopy
*i*Bu	*iso*-Butyl
*i*Pr	*iso*-Propyl
L	Supporting ligand
Ln	Lanthanide
LUMO	Lowest Unoccupied Molecular Orbital
M_n	Number-Average Molecular Weight
M_w	Weight-Average Molecular Weight
Me	Methyl
Mes	Mesityl, 2,4,6-trimethylphenyl
NBO	Natural Bond Orbital
NHC	N-Heterocyclic Carbene
NMR	Nuclear Magnetic Resonance
Oct, *n*Oct	*n-O*ctyl
PEO	Polyethyleneoxide
PDI	Polydispersity Index

PFS	Polyferrocenylsilane
Ph	Phenyl
PXRD	Powder X-ray diffraction
Rc	Ruthenocene/ruthenocenyl
RECP	Relativistic Effective Core Potential
ROMP	Ring-Opening Metathesis Polymerisation
ROP	Ring-Opening Polymerisation
r.t.	Room temperature
SAED	Selected Area Electron Diffraction
SEM	Scanning Electron Microscopy
STEM	Scanning Transmission Electron Microscopy
*t*Bu	*Tertiary*-butyl
TEM	Transmission Electron Microscopy
Tip	2,4,6-tri-*iso*propylphenyl
Tf	Triflate, trifluoromethanesulfonate
TGA	Thermal Gravimetric Analysis
THF	Tetrahydrofuran
TMEDA	*N,N,N',N'*-tetramethylethylenediamine
TOF	Turnover Frequency
WCA	Weakly Coordinating Anion
X	Anionic ligand/leaving group

1 Introduction

1.1 Inorganic polymers

Although humans have made use of, and often modified naturally occurring macromolecules for millennia, it was not until 1907 that Leo Hendrik Baekeland discovered the first fully synthetic polymer, a thermoset resin derived from phenol and formaldehyde known as 'Bakelite'.[1] Around a similar time, and largely due to the efforts of Hermann Staudinger, the consensus that macromolecules were composed of colloidal aggregates of small molecules, "Association Theory",[2] was replaced by a model in which macromolecules are constituted of large numbers of covalently bonded monomer units.[3] It is this theory that forms the foundation of modern polymer science. Synthetic polymers are now found in almost every aspect of the modern world thanks to their wide-ranging properties that are well-suited to a plethora of applications.

Most commercialised polymers are composed entirely of a hydrocarbon-based backbone and, although other heteroatoms such as nitrogen or oxygen are frequently incorporated, their synthesis is most commonly reliant upon the formation of carbon-carbon, or heteroatom-carbon bonds. Despite this relative lack of compositional diversity, organic polymers display an astonishing array of properties and applications through variation of parameters such as molecular structure, chain length and processing methods. The synthesis of polymers based upon other elements in the periodic table i.e. inorganic polymers, however, provides a further variable for chemists to expand and improve the range of properties and applications available to polymeric materials.

1.1.1 Homocatenated inorganic polymers and oligomers

Carbon possesses the remarkable and unusual ability to form highly stable homocatenated chains of essentially unlimited length.[4] Although the constituent E-E σ-bonds are weaker, the heavier members of group 14 are also capable of homocatenation, which results in polymers with highly divergent properties to those of polyolefins (Figure 1.1).[5]

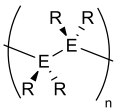

R = H or organic group
E = C, Si, Ge, Sn

Figure 1.1: Polymers with a backbone composed of homocatenated group 14 elements.

For example, σ-conjugation enables polysilanes to demonstrate semi-conductive properties upon oxidation with SbF_5,[6] whilst polystannanes exhibit similar phenomena without the need for modification or doping. Spectroscopic investigations into the electronic structure of oligostannanes $Ph_3Sn(tBu_2Sn)_nSnPh_3$ (n = 1,4), revealed a systematic decrease of the HOMO-LUMO energy gap with increasing chain-length.[7] This feature results from σ-conjugation, which provides a molecular orbital that is delocalised over the length of the oligomeric chain and is manifested in a bathochromic shift of the σ- σ* transition from λ_{max} = 280 nm (n = 1) to 370 nm (n = 4),[7-9] whilst polystannanes typically display λ_{max} values of 375 – 410 nm.[10, 11] These properties have led to the description of polystannanes as "one-dimensional metals" of potential use as "molecular wires" in nanoscale electronic devices.[10-19] Visible-light promoted homolytic Sn-Sn bond cleavage, however, presents a barrier to the practical use of polystannanes[20] and recent efforts to circumvent this drawback include the incorporation of chelating side chains that result in hypervalent tin centres with reduced light-sensitivity.[18, 21, 22] Although reductive Wurtz-type coupling has been employed for each of the heavier group 14 elements, the synthesis of polygermanes has been met with only limited success,[23-27] whilst polysilanes and polystannanes are most reliably prepared *via* a dehydrogenative route from the corresponding hydrosilanes and hydrostannanes.[13, 15, 28-36]

Linear homocatenation of the group 13 elements is challenging due to their reduced number of valence electrons. Although truly polymeric chains of these elements are unknown, well-defined oligomeric compounds of four or more linearly homocatenated boron- (**P-I**)[37] or indium (**P-II**)[38] atoms have been reported (Figure 1.2).

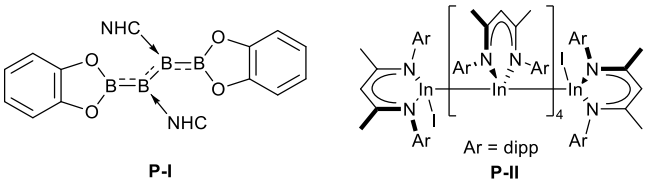

P-I **P-II**

Figure 1.2: Homocatenated group 13 chains.[37, 38]

Cyclic pentamethylarsine undergoes thermal ring-opening-polymerisation (ROP) to provide an insoluble material, polymethylarsine (**P-III**), to which a ladder-like structure has been assigned (Scheme 1.1).[39, 40] Soluble and processable polymers based upon group 15 chains however, remain unrealised. Meanwhile, the naturally occurring allotropes of the heavier group 16 elements, S_8 and Se_8 undergo well-known thermal ROP to provide polymeric sulphur, which depolymerises on cooling (**P-IVa**), and grey selenium respectively (**P-IVb**) (Scheme 1.1).

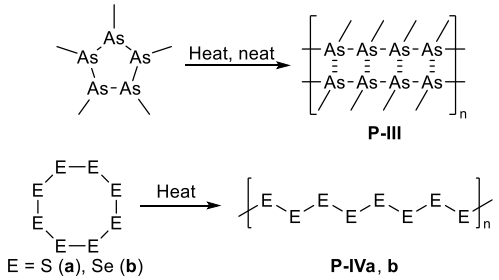

Scheme 1.1: ROP of As_5Me_5 to provide a ladder-type polymethylarsine **PIII**,[39, 40] and the ROP of S_8 and Se_8 to yield polymeric sulphur and selenium (grey selenium).

A more successful and general approach to main-group polymeric chains, is to use a combination of elements, often in alternating sequence. For example, chains of alternating boron and nitrogen atoms can provide polyaminoboranes,[41-48] silicon and oxygen provide widely-used polysiloxanes,[49] and phosphorus and nitrogen make up the backbone of polyphosphazenes.[50-52]

1.1.2 Hybrid-polymers

The incorporation of *p*-block elements into primarily carbon-based frameworks provide "hybrid" polymers. Heteroatomic substitution of just one or two carbon atoms can often result in a substantially different material.[53, 54] Hybrid polymers have received particular attention in the field of π-conjugated materials, where 'doping' the polymer chain or side chain with a heteroatom provides a tool to modulate optoelectronic properties.[53, 55, 56]

1.2 Metallopolymers

The incorporation of metal atoms into macromolecules can result in materials with interesting and exciting properties.[4, 7-18] Although metallopolymers have been the subject of research for over half a century,[57, 58] most early examples suffered from the use of poorly defined and highly reactive organometallic monomers. Furthermore, the products were often inadequately characterised by modern standards. For example, the polycondensation of dilithioferrocene with dichlorosilanes was reported to provide a polyferrocenylsilane,[59-61] whilst polyferrocene was synthesised by a similar route, from dilithioferrocene and diiodoferrocene (**P-V**, Scheme 1.2).[62] Notable exceptions include polyvinylferrocene (**P-VI**), which can be prepared using common styrene-polymerisation routes such as radical polymerisation,[63] and ferrocene-containing polysiloxanes such as **P-VII** (Scheme 1.3).[64]

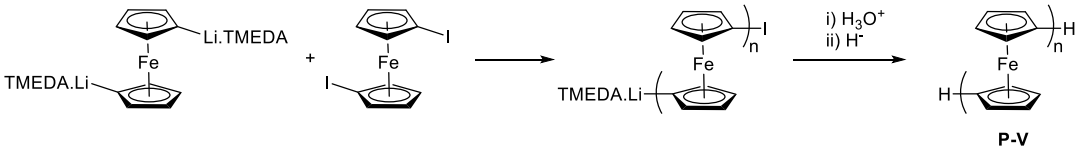

Scheme 1.2: Reaction of dilithioferrocene-TMEDA complex with diiodoferrocene to provide polyferrocene.[62]

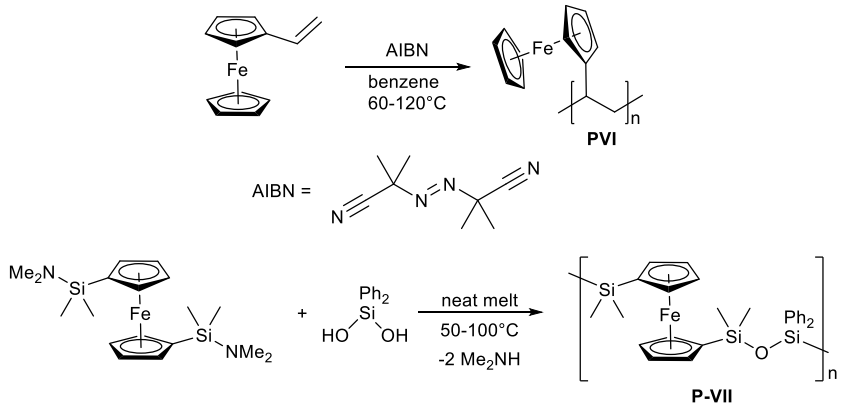

Scheme 1.3: AIBN initiated radical polymerisation of vinylferrocene (top)[63] and the polycondensation of diphenylsilanediol and 1,1'-bis(dimethylaminodimethylsilyl)ferrocene (bottom).[64]

More recently, synthetic approaches and characterisation techniques have improved immeasurably and the field of metallopolymers has witnessed dramatic growth. Well-characterised metallopolymers with a versatile array of properties and structures have been reported.[61, 65] Resulting applications are wide ranging and include; conductive and semiconducting materials,[66] photo- and electroluminescent polymers,[67] photovoltaic devices,[68] liquid crystals,[69] ceramic precursors,[70, 71] ion etching resists,[71, 72] and various biomedical applications.[73-75] The complexation of metal ions can cross-link polymer chains to result in organometallic networks and gels with tuneable electronic properties,[76-78] whilst the incorporation of photo- and electroluminescent complexes enables advantageous tuning and processing compared to small molecules.[61]

1.2.1 Metallocene-containing polymers

Alongside carbonyl complexes such as $[Ni(CO)_4]$,[79, 80] ferrocene, $Fe(C_5H_5)_2$, is the archetypal organometallic compound[81-83] and its incorporation into macromolecular chains has provided a smorgasbord of metallopolymer structures. The strong Fe-Cp bonds of neutral (Fe^{2+}) 18-electron ferrocene, and oxidised (Fe^{3+}) 17-electron ferrocenium moieties make such groups well-suited as constituents of metallopolymers with reversible redox activity at easily accessible potentials.[84] Furthermore, cyclopentadienyl ligands display similar reactivity to other electron-rich aromatic rings, allowing the use of common organic reactions to provide

functionalised monomers. A substantial number of ferrocene-containing polymers had already been reported before 1970,[85] although most suffered from the drawbacks of highly reactive monomers, poor stoichiometric control, and inadequate characterisation.

Polymers containing metallocenes of other transition metals have also received substantial attention, and their incorporation as pendent groups have given rise to a multitude of polymers with useful properties and applications, primarily derived from the reversible electrochemical redox activity of the metallocene moiety.[86] Examples include redox-switchable liquid crystalline polymers,[61, 87] and the application of anion-binding cobaltocenium or ferrocencium-containing polymers as molecular sensors.[88, 89] Metallo-polyelectrolytic multilayers can display reversible assembly and disassembly,[88] and robust redox interfaces may be formed by layer-by-layer assembly of covalently bound metallocene-containing polymers, providing attractive properties for sensing and fuel-cell applications.[90] Reversible redox-behaviour has also been investigated for use in biomedical applications, for example polymers with pendent cobaltocenium groups can form hydrogels which bind to antibiotic compounds (Figure 1.3).[91, 92]

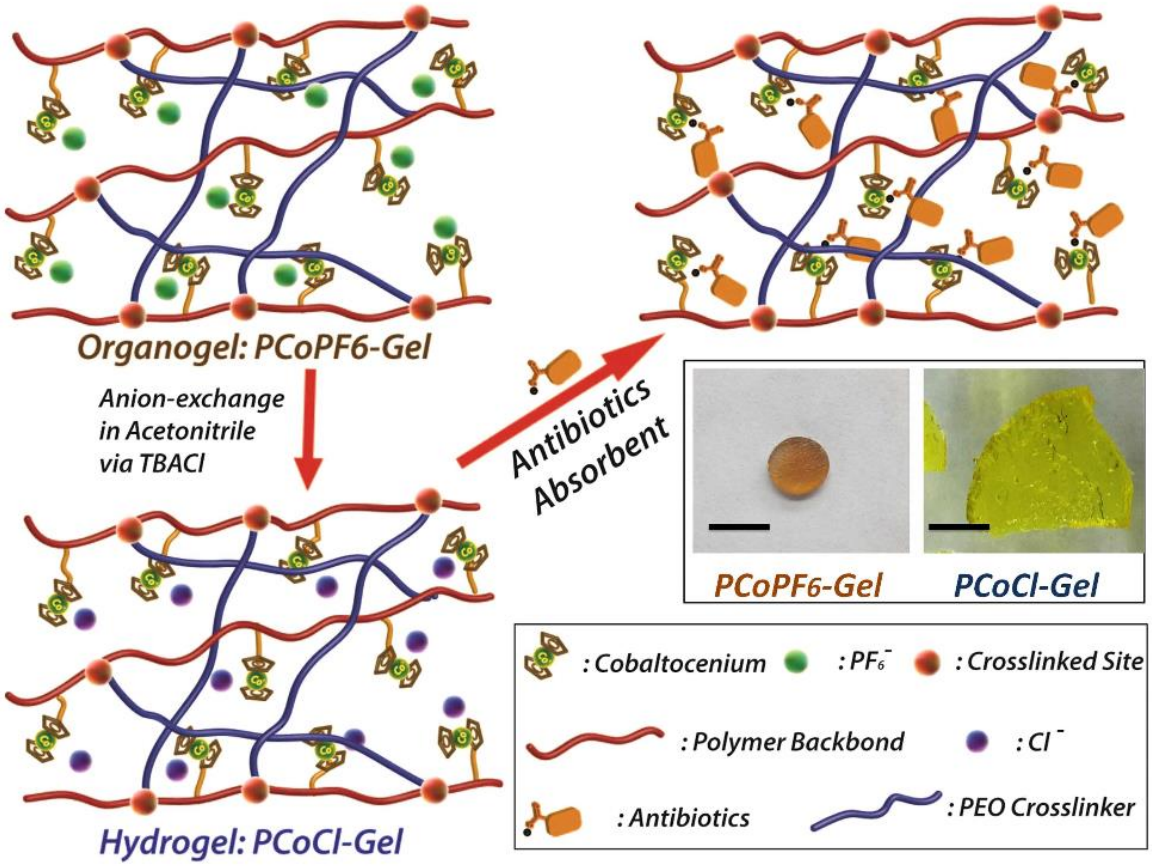

Figure 1.3 A cobaltocenium-containing hydrogel and its adsorption of antibiotics. Reproduced from reference 92 under creative commons license. Copyright 2015 Nature Publishing Group.

Altering the overall charge of a polymer modifies inter-chain interactions and changes macroscopic properties, such as hydrophobicity and polymer-surface interactions.[86] Conjugated polymers such as **P-VIII** incorporate ferrocene into the main-chain and have been used in memory storage, where the redox active ferrocene centres act as a conductivity switch (Figure 1.4),[93] while related donor-acceptor type conjugated polymers including ferrocene could be useful in solar cells.[94]

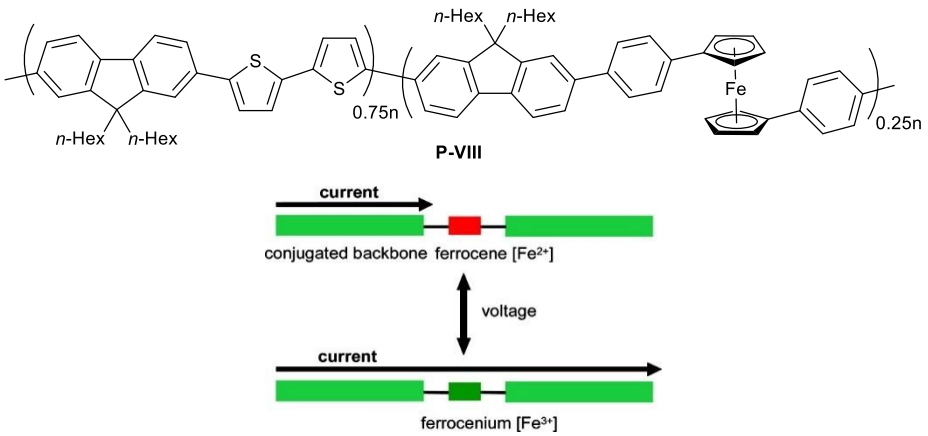

Figure 1.4: Polymer **P-VIII** and postulated mechanism for memory behaviour. Figure reproduced with permission from reference 93, copyright 2019 American Chemical Society.

Metallocene groups may be installed by post polymerisation functionalisation,[86] or through the direct use of a metallocene-functionalised monomer.[60, 86, 88] For example, ring-opening olefin-metathesis polymerisation (ROMP) of ferrocene-containing monomers has been utilised to prepare a conjugated ferrocene-containing poly-ene, **P-IX** (Scheme 1.4).[95]

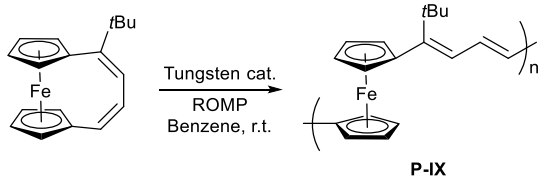

Scheme 1.4: Synthesis of conjugated ferrocene-containing polymer, **P-IX**, *via* tungsten-catalysed ROMP.[95]

ROMP has also been used to prepare polymers with pendent metallocene groups and, being amenable to living chain-growth polymerisation, it has been utilised in the synthesis of well-defined block-copolymers (BCPs). A particularly elegant example was recently reported by Astruc and co-workers, who synthesised a tetrablock co-polymer **P-X**, consisting of four metallocene-containing side chains (Figure 1.5a). Each block displays a reversible redox couple at a slightly different potential, thus allowing the electrochromic polymer to adopt a

range of colours depending on the chemical or electrochemical potential in solution (Figure 1.5b).[96]

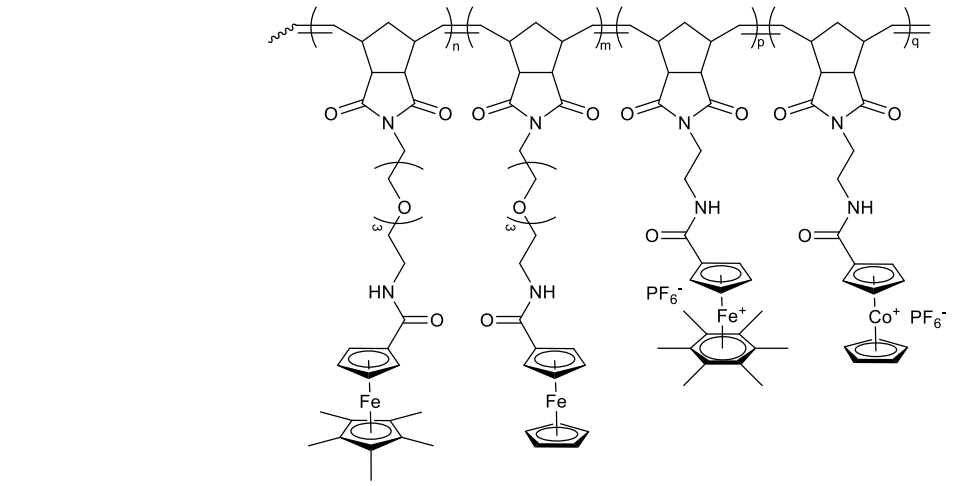

(a) **P-X**

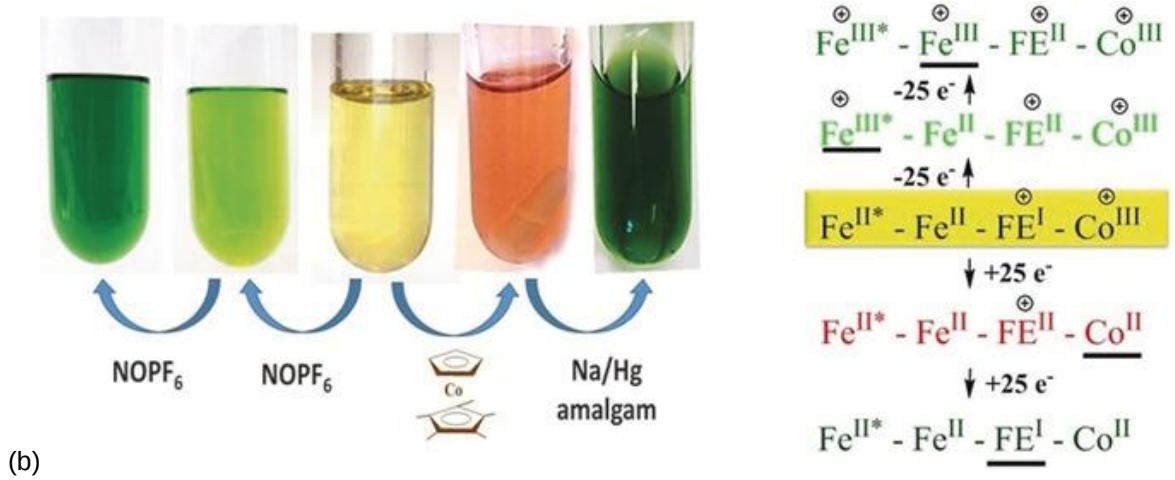

(b)

Figure 1.5: (a) Tetrablock metallopolymer **P-X** prepared by ROMP and (b) its electrochromic behaviour, reported by Astruc and co-workers.[96] (b) Reproduced with permission from reference 96, copyright 2018 John Wiley and Sons.

1.2.2 Main-chain metallocene-containing polymers *via* the ROP of *ansa*-[n]metallocenophanes

Probably the most successful and well-studied route to ferrocene-containing polymers with inorganic linkages is the ROP of *ansa*-bridged ferroceneophanes. Although such compounds have been known for over half a century,[97, 98] it was not until the early 1990s that their potential as monomers for ROP was realised. In a landmark paper, Manners and co-workers showed that the strained *ansa*-bridged dimethylsilyl[1]ferrocenophane underwent thermal ROP to obtain high molecular weight polyferrocenylsilane, **P-XI** (PFS).[99]

A variety of strained *ansa*-bridged metallocenophanes have since been utilised, providing ferrocene-containing polymers with sulphur,[100] tin,[101] germanium,[102] and phosphorus bridges,[103] as well as polymers based on other transition metal sandwich complexes. Polymerisation techniques include cationic,[104] thermal,[99] living anionic (Scheme 1.5),[105] photolytic,[106] solvent-mediated,[107] and transition metal-catalysed routes.[108] Other *ansa*-[n]arenophanes also undergo ROP,[109, 110] albeit PFS remains the most widely explored system. The potential applications of PFS are numerous; for example pyrolysis yields magnetic ceramic materials[70, 111-114] and the presence of iron and silicon results in high resistance to ion beams. As a result, PFS containing BCPs are excellent resists for nanolithography.[112, 115, 116] Furthermore, the ability for such BCPs to undergo crystallisation-driven self-assembly (CDSA) enables exquisite control over the synthesis of self-assembled monodisperse nanostructures. [116-119]

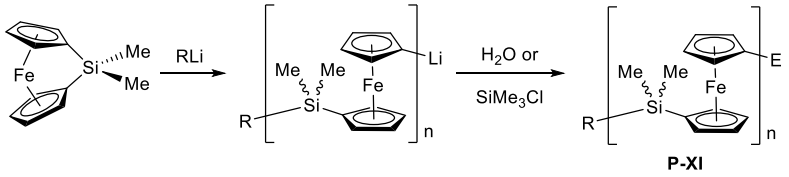

P-XI

Scheme 1.5: Living anionic ring opening polymerisation (ROP) of dimethylsilyl[1]ferrocenophane to yield PFS, **P-XI**. R = Fc, Ph, or *n*-Bu; E = H or $SiMe_3$.

Although ferrocenophanes exist with a plethora of bridging elements including B,[120] Al,[121] As,[122, 123] Ga,[124] Ge,[102] P,[103, 122, 123] S,[100, 125] Se,[100] Sn,[101, 126] and transition metals,[127-129] the ability to undergo ROP is not universal. Ring-strain provides a thermodynamic driving force for polymerisation, the extent and nature of which can be quantified, in part, by analysis of the following geometrical parameters: ring-tilt (α), the angle between the Cp ring-plane and C-E bond (β), the $Cp_{centroid}$-M-$Cp_{centroid}$ angle (δ), the Cp-E-Cp angle (θ), and the torsional angle (τ) for [n]metallocenophanes where n > 1 (Figure 1.6).[130, 131]

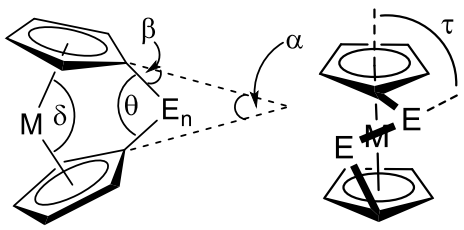

Figure 1.6: depiction of geometrical parameters used to describe *ansa*-bridged metallocenophanes.

The *d*-electron configuration of the sandwiched metal centre and the M-Cp bond strength are also important variables. For example, whereas ring-tilt induces strain for d^6 ferrocene-based metallocenes, d^2 titanocene is 'naturally' bent and hence strain is not manifested by small δ or large θ angles.[130] The relatively weak Ni-Cp bonds at the paramagnetic 20-electron nickel-centre (Figure 1.7) of tricarba[3]nickelocenophane results in dynamic and reversible solvent-mediated ROP to generate polymers **P-XII** and **P-XII'** (Scheme 1.6).[107] Furthermore, nickelocenophanes with even longer carbon-based *ansa* bridges do not display significant ring-tilt, yet still display ROP activity due to significant torsional strain.[132, 133]

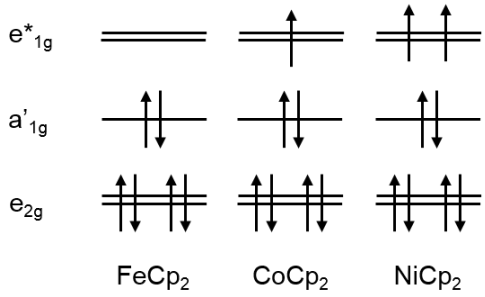

Figure 1.7: Qualitative representation of frontier 3d molecular orbitals for selected first-row metallocene complexes.[84]

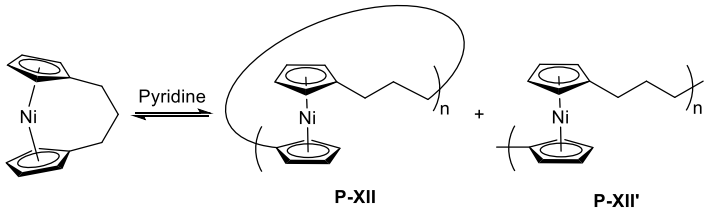

Scheme 1.6: Dynamic reversible polymerisation of tricarba[3]nickelocenophane.[107]

1.2.3 Electrochemistry of PFS

PFS and related tin- or germanium-bridged polymers display two separate redox events of equal intensity in cyclic voltammetry experiments (Figure 1.8).[102, 126, 134] This voltammetric effect is caused by the oxidation of alternate iron centres, whereby through-bond electronic communication perturbs the oxidation potential of remaining Fe^{2+} centres and results in a second peak.[134] The extent of electronic communication can be approximately quantified by the separation of the two redox events, $\Delta E_{1/2}$.[135] Experiments on shorter, monodisperse oligomers show more complex redox behaviour, but increasing chain length into the polymeric regime results in the limiting case of an infinite chain of communicating redox centres.[136] The nature of bridging unit has a profound influence on this phenomenon[137, 138] and the analogous –{CH_2}–bridged polymer displays a peak separation of just $\Delta E_{1/2}$ = 0.1 V, whilst a similar –{CH_2-CH_2}–bridged species displays a single redox event.[134, 139]

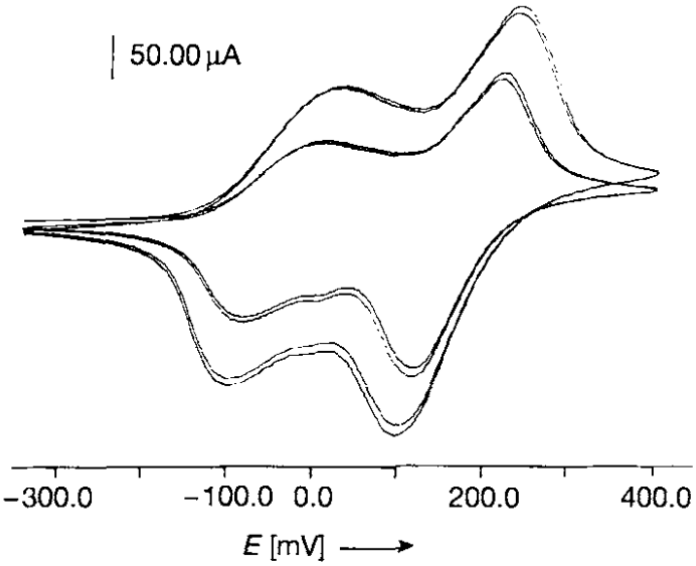

Figure 1.8: Cyclic voltammogram of **P-XI** reproduced with permission from reference 134, copyright 1993 John Wiley and Sons.

The reversible electrochemical behaviour of PFS has provided materials with useful properties. For example, redox responsive inverse opals have been fabricated from cross-linked PFS, to result in colour-changing displays that can cover a wide range of wavelengths (Figure 1.9).[140]

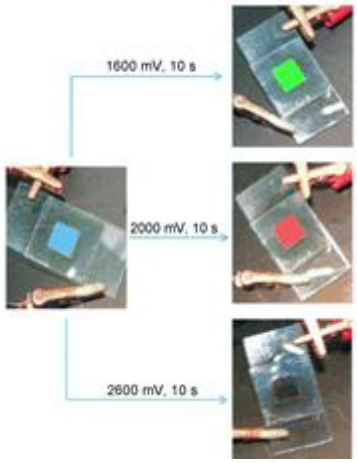

Figure 1.9: Electroactive colour-tuning properties of a polymer-gel inverse opal composed of cross-linked PFS. Figure adapted with permission from reference 140, copyright 2009 John Wiley and Sons.

1.2.4 The limitations of metallocenophane ROP

Photolytically initiated living anionic polymerisation has been utilised for the formation of heterobimetallic block co-polymers such as poly(ferrocenylsilane)-*b*-poly(cobaltoceniumethylene) (**P-XIII**, Scheme 1.7).[141] Although examples of PFS also exist with pendent ferrocene[142] or ruthenocene groups,[143] co-polymers with main chains composed of alternating metallocenes with different metal centres are not currently accessible *via* ROP. Furthermore, the bridging unit must have the correct structural characteristics to promote ROP-inducing strain and be inert whilst the metallocenophane is synthesised from either dilithioferrocene·TMEDA, or a bridged dianionic $(C_5H_4)_2(ER_x)_y$ ligand.[130, 131] The extent of electronic communication between adjacent metal centres is also heavily influenced by the nature of the *ansa*-bridge[138] and, as such, access to a more diverse range of available bridges will be useful for potential application in electronic devices. A possible solution to these drawbacks is adoption of a polycondensation regime, where bifunctional monomers offer a modular platform for the diversification of metallopolymer structure.

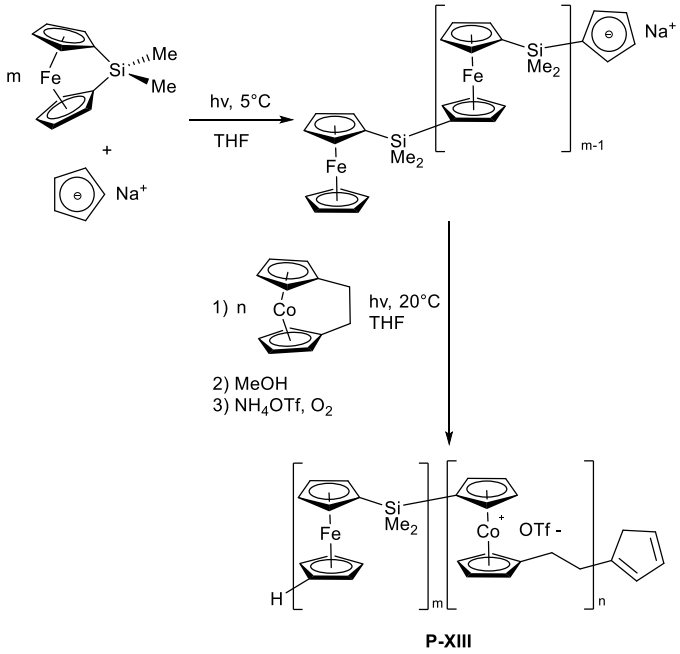

Scheme 1.7: Synthesis of the heterobimetallic block-copolymer, poly(ferrocenylsilane)-*b*-poly(cobaltoceniumethylene) **P-XIII**.[141]

1.3 Polycondensation routes to inorganic polymers

Although polycondensation is one of the most well-established and versatile polymerisation methodologies, it has been met with only limited success in the preparation of inorganic polymers. The predominant reason for this is a lack of efficient element-element (E-E) bond-forming reactions and availability of sufficiently high purity monomers. These requirements

stem from the fundamental theory of step-growth polycondensation that was developed in the early 1930s by Wallace Carothers and Paul Flory,[144, 145] and is described by Equation 1.1.

Equation 1.1:

$$\bar{X}_n = \frac{1 + r}{1 + r - 2rp}$$

In this equation, $\bar{X}_n$ is the number average degree of polymerisation, r is the stoichiometric ratio of monomers, and p is the extent of reaction defined as $p = \frac{N_0 - N}{N_0}$, where N_0 is the initial number of monomer molecules and N is the number of monomer molecules present at time t. Inspection of Equation 1.1 reveals that polymer chains of high molar-mass may only be obtained if perfect stoichiometry and incredibly high conversions are satisfied, in contrast to chain-growth polymerisation where long chains are already formed at low conversions (Figure 1.10). Despite these drawbacks, there are several notable examples of inorganic and metallo-hybrid polymers prepared from step-growth polycondensation.

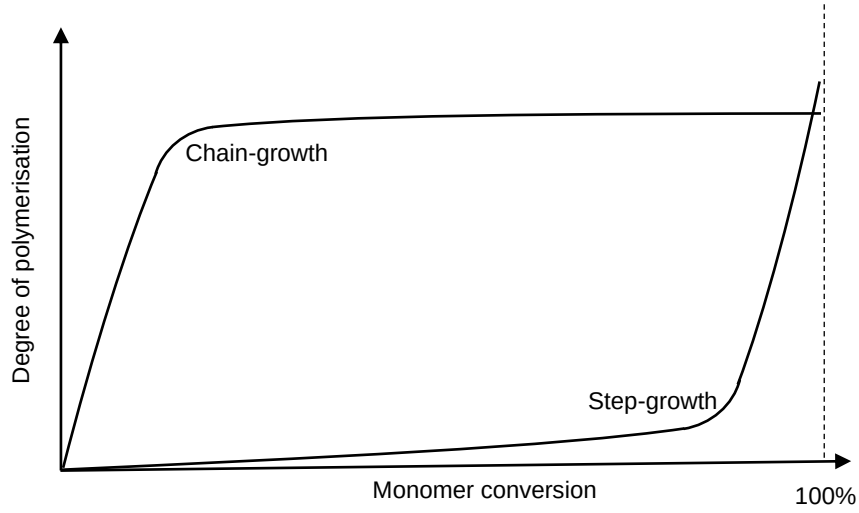

Figure 1.10: Schematic representation of the relationship between degree of polymerisation and monomer conversion for chain-growth and step-growth polymerisation regimes.

1.3.1 Polycondensation routes to metallopolymers

Ferrocene-based polymers with boron-bridges such as **P-XIV** previously eluded ferrocenophane-ROP based routes, yet were successfully accessed (albeit in relatively low molecular weights) by Jäkle and co-workers by *in situ* silane reduction and diborane elimination (Scheme 1.8).[146] Highly metallised ferrocene-containing conjugated polymers such as **P-XV** may also be prepared by a melt-state polycondensation, although this reaction offers poor control and relies upon harsh reaction conditions (Scheme 1.9).[147]

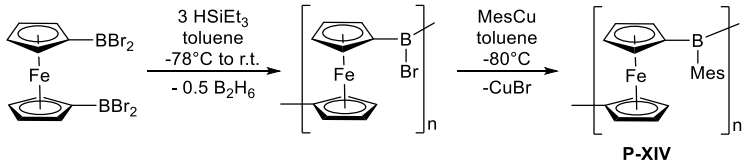

Scheme 1.8: A polycondensation approach to the borylene-bridged polyferrocenylene **P-XIV** reported by Jäkle and co-workers.[146]

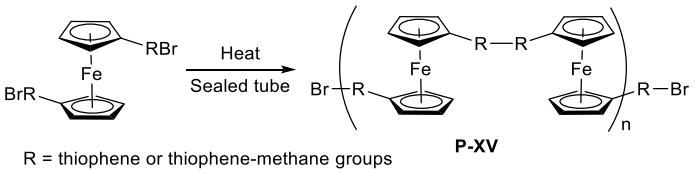

Scheme 1.9: Melt-State polycondensation route to highly metallised ferrocene-containing conjugated polymers.[147]

Conjugated polymetallynes have received significant attention for their potential in electronic applications, and their synthesis has been reliant upon Sonogashira cross-coupling-based polycondensation (Figure 1.11).[148-150] Classical organic polycondensation reactions have also been used to prepare metallopolymers, such as ferrocene-containing polyamides.[151, 152]

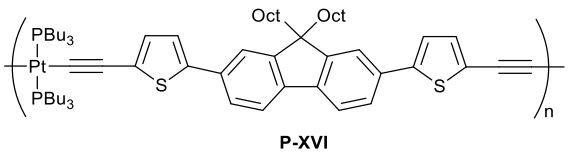

Figure 1.11: A conjugated platinum containing polymetallyne **P-XVI** synthesised *via* Sonogashira cross-coupling.[153]

1.3.2 Polycondensation routes to other inorganic and hybrid polymers

Polyphosphoesters are a class of hybrid polymers which, in addition to their well-established flame-retardant properties,[154-156] have attracted much recent attention for their potential biomedical applications. The latter application arises from excellent biocompatibility due to their similarity to biologically ubiquitous phosphates, for example, the backbone of DNA is formally a polyphosphoester.[157-161] Although they may be prepared by ROP, polyphosphoesters such as **P-XVII** are normally prepared *via* the polycondensation of bisphenols with aryl phosphodichlorides (Scheme 1.10).[157]

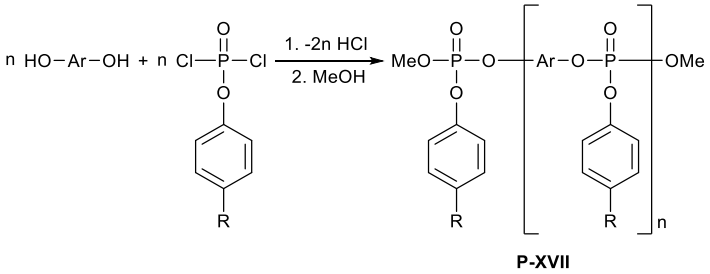

Scheme 1.10: Synthesis of polyphosphoesters *via* the polycondensation of bisphenols with arylphosphodichlorides.[162, 163]

Polyiminoboranes can be thought of as BN analogues of polyacetylene and, hence, are of significant interest due to the potentially useful electronic properties that may arise from a π-conjugated polymer chain consisting of polar B=N bonds. While true high-molecular weight polymers of this type have remained elusive, the Helten group recently adopted an approach where nitrogen atoms are connected by a short, chain-stabilising hydrocarbon bridge.[164, 165] Although the high yielding polycondensation route provided relatively low molecular weight oligomers (**P-XVIII**), higher molar mass hybrid polymers possessing aryl spacer groups (**P-XIX**) were obtained *via* a similar route (Scheme 1.11).[166, 167]

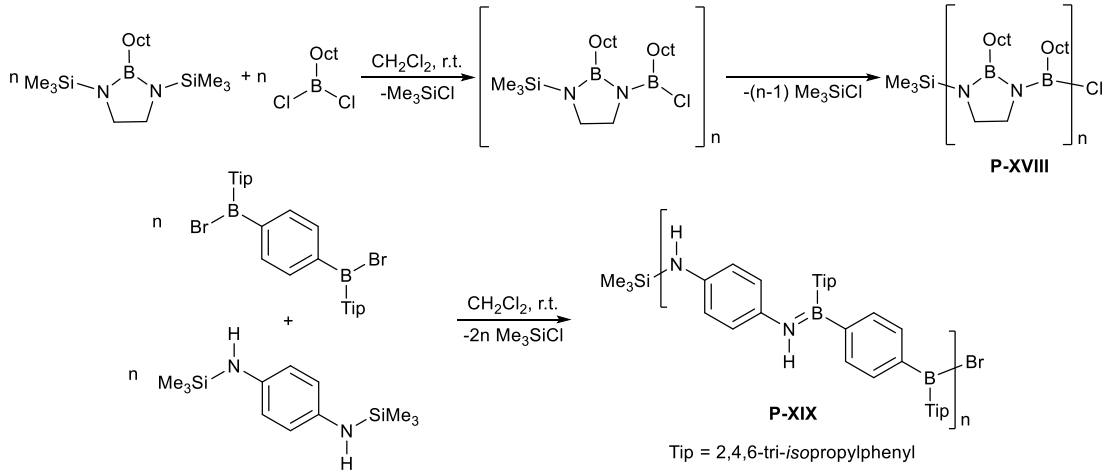

Scheme 1.11: Synthesis of an oligoiminoborane **P-XVIII** (top), and poly(*p*-phenylene-iminoborane) **P-XIX** (bottom) *via* polycondensation of bifunctional halobromides and silazanes.[165, 166]

Polycondensation has also been particularly successful for the synthesis of boron-doped π-conjugated hybrid polymers. The vacant *p*-orbital of trivalent boron, when co-planar, can overlap with carbon-based π-systems to modify the electronic structure and result in properties that are useful for application in optoelectronic devices (Figure 1.12).[55, 56]

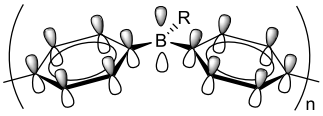

Figure 1.12: Incorporation of trivalent boron into a hypothetical π-conjugated polymer.

Whilst polycondensation reactions that eliminate stoichiometric quantities of halostannanes and silanes or salts can be highly effective (Scheme 1.12),[168, 169] the production of large quantities of waste is a significant drawback towards large-scale production. Furthermore, the preparation of reactive halo- and metallo-monomers suitable for such reactions in sufficient purity, is a general challenge facing polycondensation routes to metallo-, inorganic- and hybrid-polymers. Dehydrocoupling, which uses commonly available element-hydrides to form E-E bonds with H_2 as the only by-product, therefore, is an economically and environmentally attractive alternative.

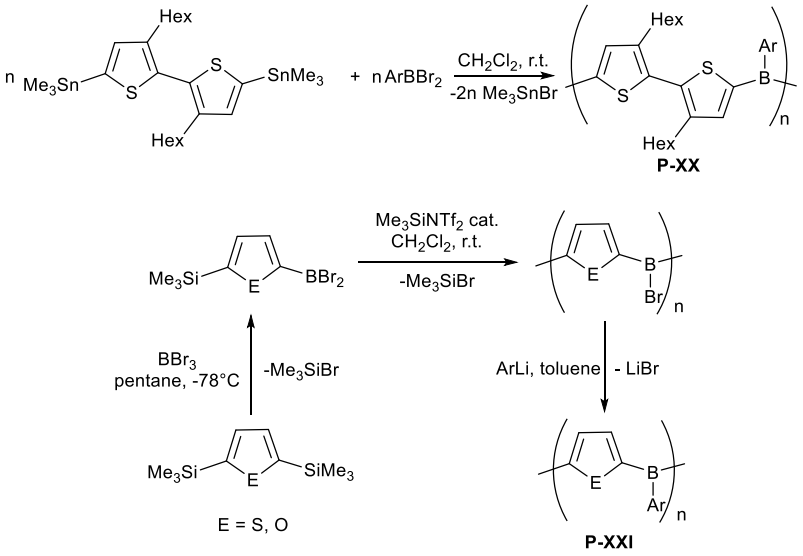

Scheme 1.12: Polycondensation routes to boron-containing π-conjugated polymers.[168, 169]

1.4 Dehydrocoupling

Having been the subject of extensive research with many different catalysts and substrates, a wide variety of E-E bonds may be formed *via* homo- or hetero-dehydrocoupling (Scheme 1.13).[170-173] Since hydrides are ubiquitous and readily available amongst many main group elements, dehydrocoupling has already provided a rich library of *p*-block element-containing polymers.[54, 172, 174-176] Although many interesting and useful examples of dehydrocoupling are known for the late-transition metals, the following sections will predominantly focus upon

redox-neutral dehydrocoupling mechanisms of d^0 early transition metals, lanthanides, *s*-block, and *p*-block elements that are of most relevance to this thesis.

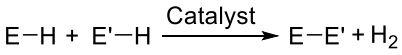

Scheme 1.13: A general dehydrocoupling scheme.

1.4.1 Lewis-acid catalysed dehydrocoupling

Lewis acid reagents can serve as dehydrocoupling catalysts by activating hydridic substrates towards nucleophilic attack from a Lewis-base.[177] The $B(C_6F_5)_3$-catalysed dehydrocoupling of silanes and alcohols reported by Piers and co-workers was proposed to operate by this type of mechanism,[178] as was the phosphonium-mediated catalytic dehydrocoupling of silanes and amines or phenols reported by Stephan's group (Scheme 1.14).[179, 180] Manners and co-workers postulated a similar mechanism for the $B(C_6F_5)_3$-catalysed dehydrocoupling of phosphines and silanes (Scheme 1.14, left),[181] where the involvement of Lewis-acidic $B(C_6F_5)_3$ and Lewis-basic phosphine leads to an "FLP"-like[182-184] silane activation. Elimination of dihydrogen from the resultant charge-separated species provides the dehydrocoupled product. High temperatures could be avoided though addition of PhCN, which allows the reaction to proceed *via* an alternative lower-energy, but also FLP-type mechanism, which provided accelerated reaction rates at room temperature (Scheme 1.14).[181]

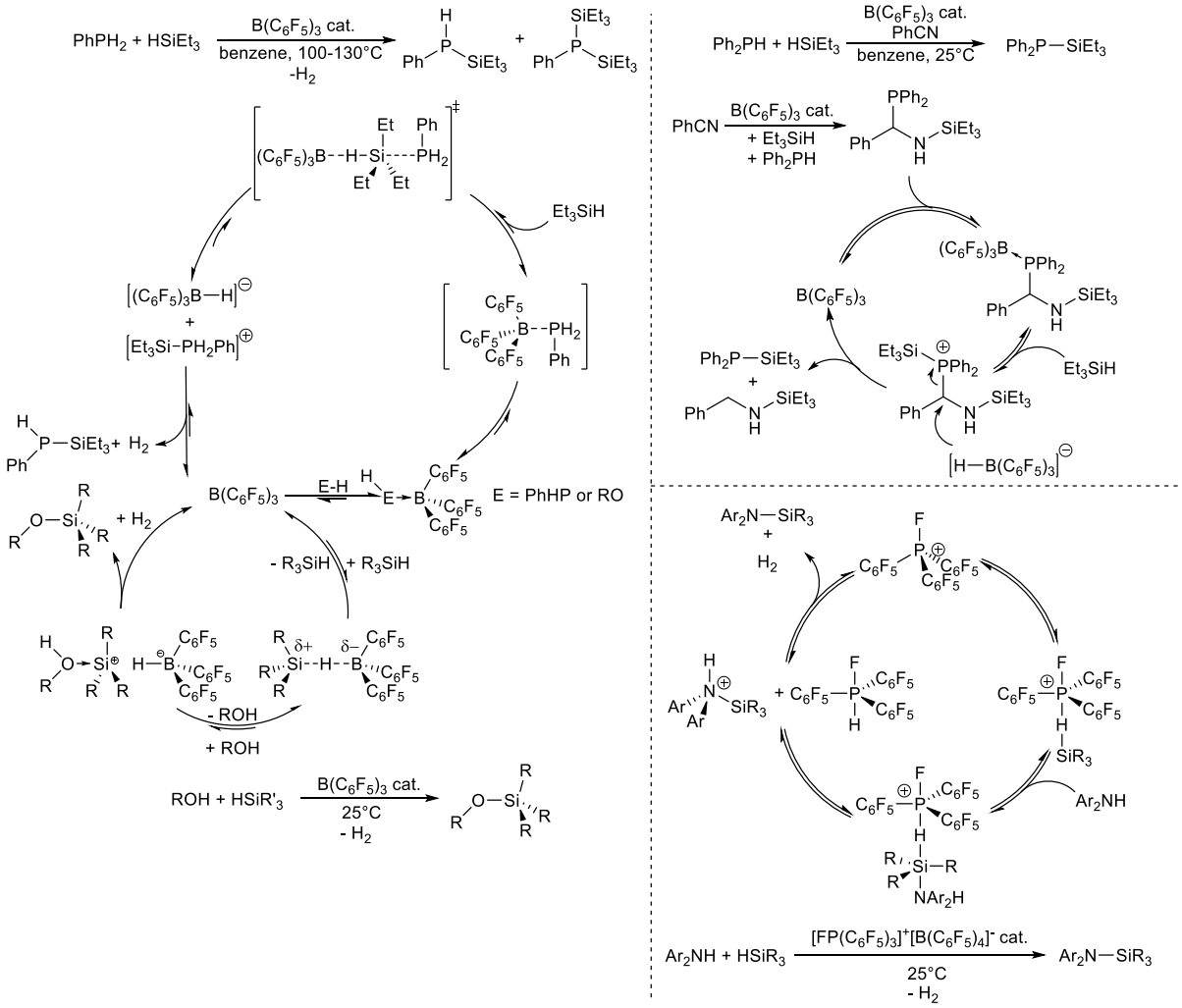

Scheme 1.14: Postulated reaction mechanisms for Lewis acid-catalysed heterodehydrocoupling.[178-181]

1.4.2 Homodehydrocoupling *via* σ-bond metathesis and related mechanisms

The catalytic dehydropolymerisation of phenylsilane was first reported in 1985 by Harrod and co-workers.[28] The reaction was further developed by Tilley and co-workers in the early 1990s, using similar zirconocene and hafnocene pre-catalysts (Scheme 1.15).[31] Detailed mechanistic studies based upon observed stoichiometric metathesis reactions,[32] deuterium labelling and kinetic investigations, established a catalytic cycle involving two four-membered σ-bond metathesis transition states (Scheme 1.15).[30, 31] This type of mechanism has been proposed to operate in a variety of silane dehydropolymerisation systems,[29] as well as other dehydrocoupling reactions such as zirconium-catalysed phosphine or arsine dehydrocoupling.[185, 186]

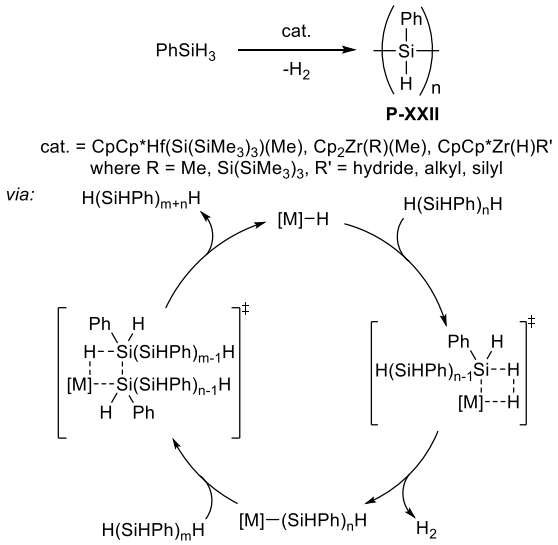

Scheme 1.15: Group 4 catalysed dehydropolymerisation of phenylsilane[28, 31] and proposed mechanism based upon four-membered σ-bond metathesis transition states.[30, 31]

Tilley was also responsible for the first reports of the catalytic dehydropolymerisation of diorganotin dihydrides (Scheme 1.16).[13, 33] Similarity between silanes and stannanes, and the catalysts employed, led to the postulated involvement of a σ-bond metathesis-based mechanism, analogous to that operative for phenylsilane dehydropolymerisation.

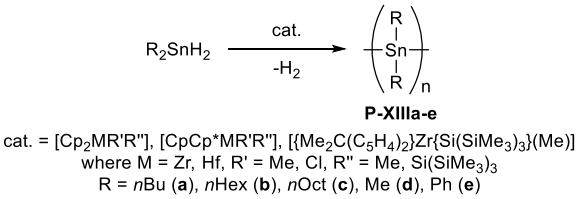

Scheme 1.16: Group 4 catalysed dehydropolymerisation of diorganostannanes.[13, 33]

A subsequent series of investigations, however, favoured an alternative mechanism involving α-hydride elimination of an intermediate stannyl complex to generate transient stannylene species. The latter may insert into Sn-Sn or M-Sn (where M = Zr, Hf) bonds to propagate polystannane chain-growth (Scheme 1.17).[187, 188] Similar α-elimination reactions have since been proposed to operate in Sb-Sb, and As-As dehydrocoupling reactions,[189, 190] and may prove relevant to a number of other dehydrocoupling processes previously thought to proceed by σ-bond metathesis. Distinction between the two mechanisms can be elucidated not only by the experimental trapping of low valent species, but also through measurement of the entropy of activation ($\Delta S^{\ddagger}$), which is significantly more negative for the highly ordered four-membered transition states involved in σ-bond metathesis.[173]

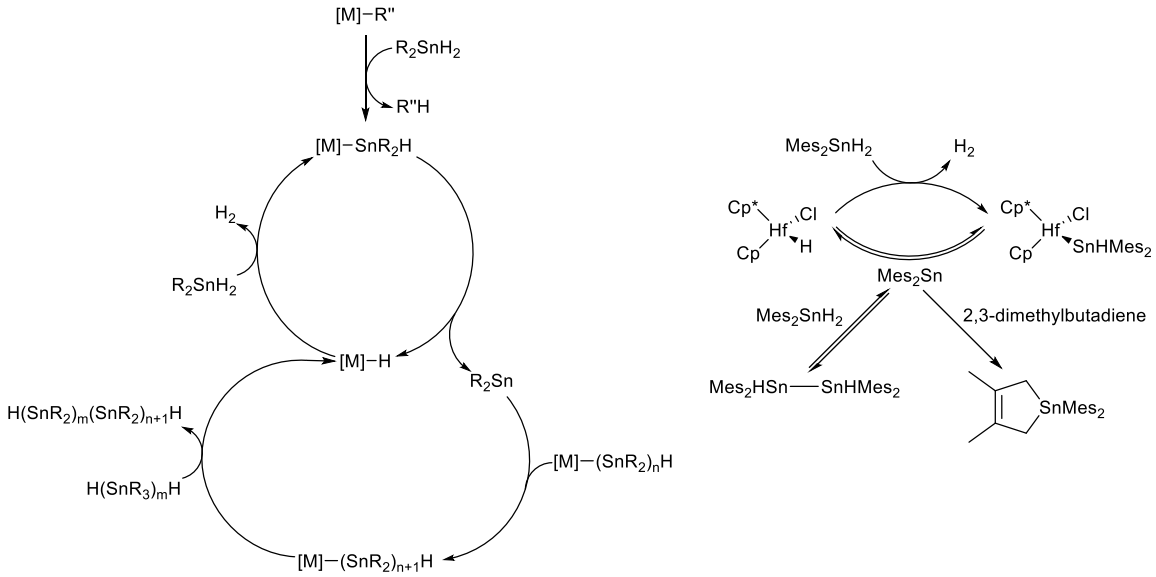

Scheme 1.17: (left) A proposed mechanism for stannane dehydropolymerisation based on α-hydride elimination and stannylene insertion. (right) Supporting stoichiometric reactions.[187, 188, 191]

Caseri and co-workers reported the use of Wilkinson's rhodium catalyst, $[RhCl(PPh_3)_3]$, as a highly effective catalyst for organostannane dehydropolymerisation, capable of selectively favouring high molecular-weight linear polymer over cyclic oligomers.[15, 36] A plausible mechanism involves oxidative addition of the monomer to a Rh(I) centre, reductive elimination of H_2, α-hydride elimination, and stannylene insertion into a Rh-Sn bond (Scheme 1.18). Significantly, experimental results agreed most closely with a metal centred process, where both stannylene and oligostannyl moieties remain within the coordination sphere of rhodium, to result in a chain-growth polymerisation regime.[12, 36]

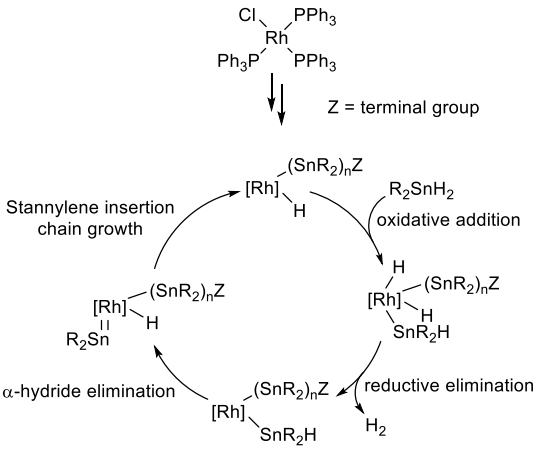

Scheme 1.18: Mechanism proposed for the rhodium-catalysed polymerisation of dialkylstannanes by Caseri and co-workers.[12, 36]

1.4.3 Catalytic amine-borane and phosphine-borane dehydrocoupling

Amines and phosphines form Lewis acid-base adducts with boranes. The resulting amine-boranes and phosphine-boranes are often described as inorganic alkane analogues due to the formally isoelectronic relationship between N-B or P-B and C-C bonds.[192, 193] The dative polar-covalent bonds of Lewis acid-base adducts imparts such compounds with significantly different properties to their hydrocarbon analogues. Whereas alkanes require a catalyst, and often harsh conditions, to undergo dehydrogenation, many amine-boranes and phosphine-boranes undergo thermal dehydrogenation upon relatively mild heating, whilst some examples spontaneously eliminate dihydrogen at room temperature. In part, this feature arises from the combination of protic N-H and hydridic B-H bonds within a single molecule (Scheme 1.19). Catalysts help to perform such dehydrogenation reactions under mild conditions and this type of reactivity led to widespread interest into the potential of ammonia-borane as a hydrogen storage medium suitable for use in a hydrogen-based energy economy.[194]

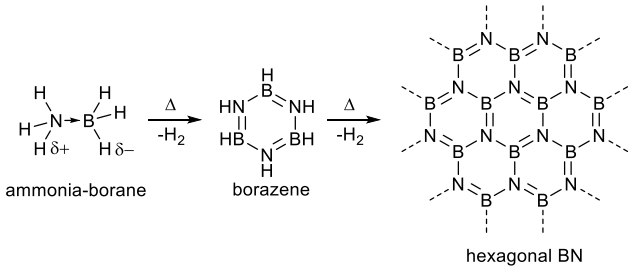

Scheme 1.19: Thermal dehydrogenation of ammonia-borane to afford borazine and/or hexagonal boron-nitride.

Alkenes undergo catalytic addition polymerisation to provide polyolefins. The unsaturated group 13/15 analogues, aminoboranes and phosphinoboranes, may also be utilised as monomers to afford polyaminoboranes and polyphosphinoboranes.[41] In the absence of bulky kinetically stabilising substituents, however, aminoboranes and phosphinoboranes undergo spontaneous and uncontrolled oligomerisation at room temperature. Hence, amine-borane and phosphine-borane dehydropolymerisation catalysts face the two-fold challenge of performing both dehydrogenation, and controlled addition polymerisation.[43]

In 2000, Manners and co-workers reported the rhodium-catalysed dehydrocoupling of phosphine-boranes.[195] Whilst $Ph_2PH{\cdot}BH_3$ yielded the linear dimer **P-XXIVa** and cyclic trimers and tetramers **P-XXIVb** and **c**, primary phosphine-boranes $PhPH_2{\cdot}BH_3$ and *i*-$BuPH_2{\cdot}BH_3$ provided high-molecular weight polymers **P-XXVa** and **b** (Scheme 1.20). Iron, ruthenium, and iridium-based systems have since been reported to yield primary alkyl-[45, 196, 197] and aryl-polyphosphinoboranes,[45, 197-201] but catalytic routes to secondary polyphosphinoboranes remain elusive.

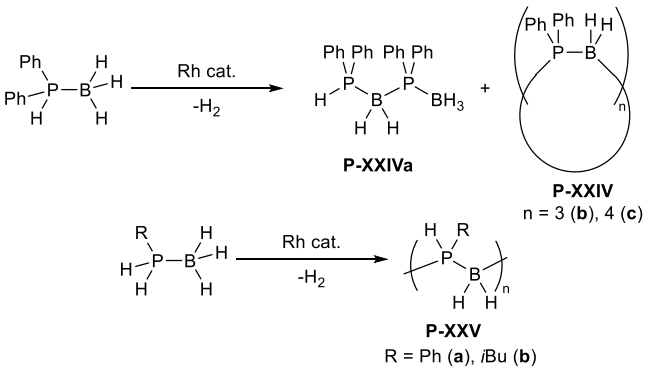

Scheme 1.20: Rhodium-catalysed dehydrogenation/dehydrocoupling of phosphine-boranes reported by Manners and co-workers.

Early investigations into the dehydrocoupling of primary amine-boranes yielded borazines, whilst secondary amine boranes normally provide dimeric species.[202] Challenges in providing controlled reactivity rendered soluble, well-characterised polyaminoboranes inaccessible until 2010.[203] Since then, a variety of catalysts based on iron, iridium, rhodium, ruthenium, and titanium have been reported for amine-borane polymerisation, with most requiring bulky and/or chelating ligands to control reactivity and provide selective access towards linear polymers over oligomeric by-products.[42-48, 204] Until recently, all examples of polyaminoboranes featured *N*-alkyl substituents (**P-XXVI,** Scheme 1.21), since *N*-arylated amine-boranes undergo uncontrolled oligomerisation.[205] Aryl-substituted polyaminoboranes were, however, recently reported by Resendiz-Lara *et al.*, who installed the aryl substituents at boron instead of nitrogen and hence obtained *B*-aryl polyaminoboranes (**P-XVII,** Scheme 1.21), "*inorganic polystyrene*", under iridium catalysis.[206]

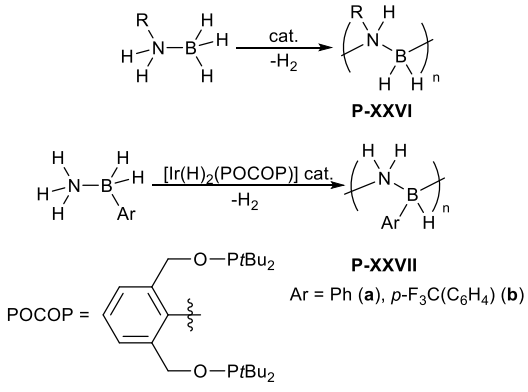

Scheme 1.21: Catalytic dehydropolymerisation of *N*-alkyl and *B*-aryl amine-boranes.

The polymerisation of amine-boranes and phosphine-boranes are mechanistically complex processes, with the exact mechanism being highly dependent upon both monomer and

catalyst.[42, 43] Most investigations have focussed upon model systems such dimethylamine-borane, rather than more challenging polymerisation systems.[45, 207] Detailed mechanistic studies by Weller and co-workers focussed upon the methylamine-borane polymerisation system. It was proposed that whilst amine-borane dehydrogenation and polymer chain-propagation may proceed at a single metal centre, experimental observations were more satisfactorily accounted for by interception of unsaturated aminoborane by a second metal centre, from which polymer chain-growth occurs *via* nucleophilic attack of a rhodium-bound amidoborane on free aminoborane monomers (Scheme 1.22).[204, 208]

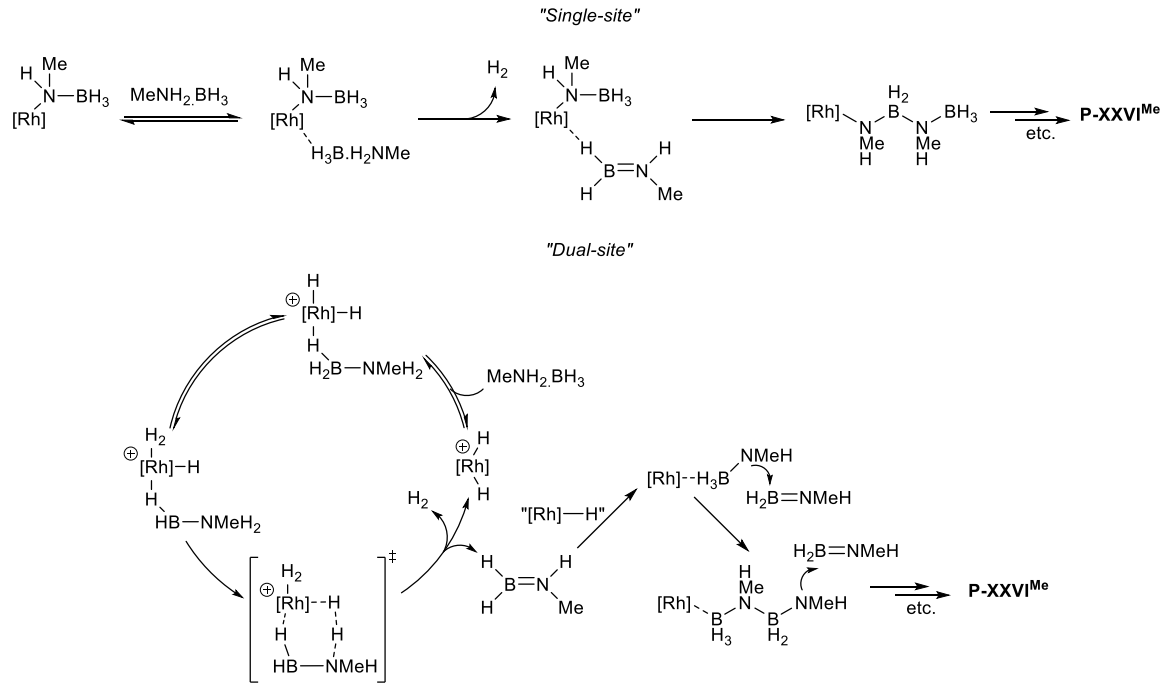

Scheme 1.22: Proposed mechanisms for rhodium-catalysed methylamine-borane dehydropolymerisation involving dehydrogenation and polymerisation either at a single rhodium centre, or separate sites.[204, 208]

This type of on-metal chain growth leads to a highly controlled polymerisation with low polydispersity. Phosphine-borane dehydropolymerisation with similar cationic rhodium-systems was, however, proposed to proceed *via* a reversible chain-transfer step-growth regime.[209] Stoichiometric investigations with model secondary phosphine-boranes suggested that the pre-coordination of phosphine-borane to form σ-complexes plays an important role in on-metal P-B coupling.[210] This type of BH-M interaction appears to be of importance to amine-borane and phosphine-borane dehydrocoupling systems based not only on late transition metals, but also early transition metals and even *s*-block systems, as exemplified by the recent isolation of a calcium-amine-borane σ-complex by Zheng *et al.*.[211]

A step-growth mechanism for amine-borane dehydrogenation/deydrocoupling was proposed by Manners and co-workers for their titanocene catalyst-system, generated *in situ* by addition of *n*BuLi to a [Cp_2TiCl_2] precursor.[212] Mechanistic investigations on this and similar systems have focused upon the dimethylamine-borane system, and proposals involve oxidative addition of an N-H,[213] or B-H[214] bond to the Ti(II) centre to generate a Ti(IV) amidoborane-hydride species. Such a species may undergo subsequent β-hydride elimination to generate the unsaturated aminoborane and a Ti(IV) dihydride, which reductively eliminates dihydrogen to close the cycle (Scheme 1.23). The possible involvement of paramagnetic Ti(III) intermediates has also been discussed.[207]

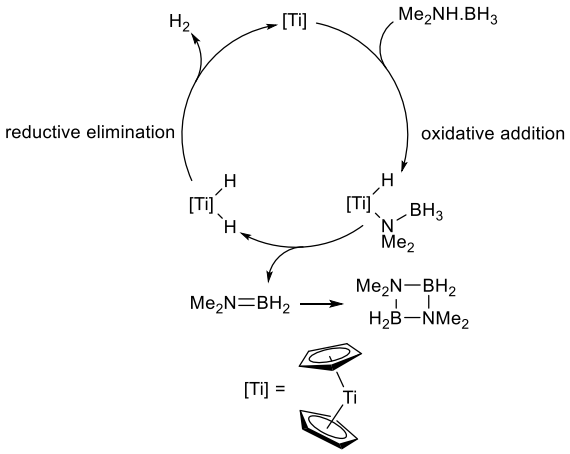

Scheme 1.23: A plausible mechanism for the titanium-catalysed dehydrogenation of dimethylamine-borane involving a Ti(II)/Ti(IV) redox cycle.[212]

Coles *et al.* proposed a redox-neutral mechanism based on σ-bond metathesis and δ-hydride elimination for their Fe(II) system (Scheme 1.24), although mechanistic studies were only performed on the model dimethylamine-borane system.[45] Similar mechanisms have been proposed for alkaline-earth systems by Hill and co-workers (see section 1.5.8).[215, 216] Manners' iron catalyst [$FeCp(CO)_2(OTf)$], which provides low polydispersity polyphosphinoboranes *via* a chain-growth process, was also proposed to operate through redox-neutral σ-bond metathesis steps.[197]

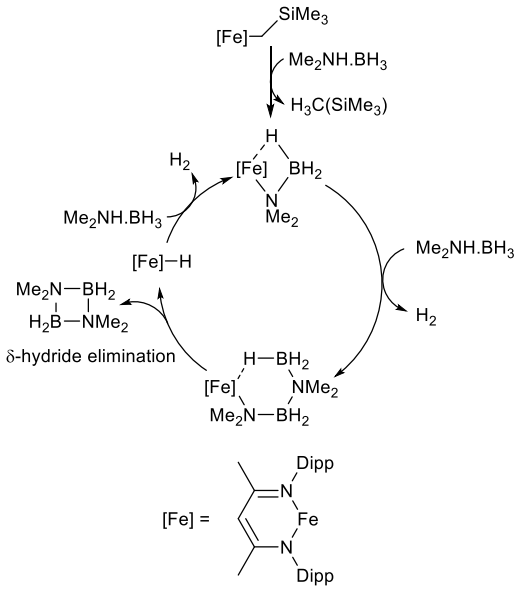

Scheme 1.24: Postulated mechanism for dimethylamine-borane dehydrogenation by a β-diketiminato iron(II) system.[45]

1.4.4 Stoichiometric routes to polyaminoboranes and polyphosphinoboranes

The utilisation of kinetically stabilised monomers enables precious-metal catalysts to be avoided and can sometimes provide access to catalytically inaccessible structures, such as bulky or disubstituted polymers. Alcaraz and co-workers recently reported the low temperature reaction of di-*iso*propylaminoborane with one equivalent of a primary amine, under solvent-less conditions (Scheme 1.25). In this process, amine-exchange generates primary aminoboranes *in situ*, with stoichiometric elimination of di-*iso*propylamine and isolation of high molar mass polyaminoboranes.[217]

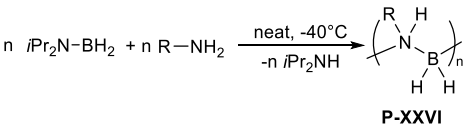

P-XXVI

Scheme 1.25: Synthesis of polyaminoboranes *via* the solvent-less, catalyst-free route reported by Alcaraz and co-workers.[217]

In a related but slightly different approach, the Scheer group have used amines to stabilise phosphinoboranes and arsinoboranes for the preparation of well-defined cationic phosphanyl- and arsanylborane oligomers.[218, 219] In collaboration with Manners and co-workers, this methodology was also used to prepare high molecular weight poly-*tert*-butylphosphinoborane **P-XXVIII** (Scheme 1.26).[220]

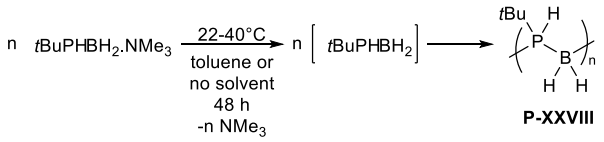

Scheme 1.26: Metal-free head-to-tail polymerisation of *tert*-butylphosphinoborane reported by Manners, Scheer, and co-workers.[220]

Dehydrogenative transition metal-free routes to polyphosphinoboranes are limited to a recent report by Oldroyd *et al.*, who found that cyclic alkyl amino carbenes (CAACs) were able to perform the stoichiometric dehydrogenation of primary and secondary phosphine-boranes (Scheme 1.27). To date, this remains the only direct route from phosphine-borane adduct to secondary polyphosphinoborane.[221]

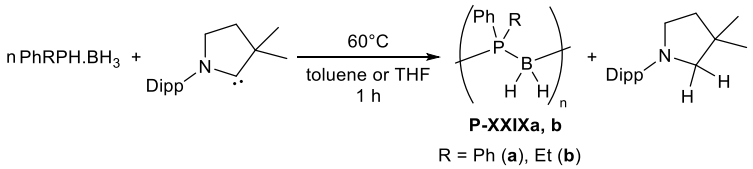

Scheme 1.27: Cyclic alkyl amino carbene (CAAC) mediated polymerisation of phosphineboranes.[221]

1.5 Alkaline-earth catalysed dehydrocoupling

Whilst the majority of dehydrocoupling processes discussed thus far are dependent upon transition metal catalysis or stoichiometric reagents, the abundance of redox-neutral catalytic cycles suggests that the *s*-block metals may able to mediate catalytic dehydrocoupling. This has been particularly well-demonstrated for the alkaline-earth elements, which are discussed henceforth.

1.5.1 Group 2

Although Mg(I) and Ca(I) species have precedent,[222-224] the prohibitively negative Ae^{+}/Ae^{2+} reduction potentials prevent the involvement of redox cycles in catalysis. As such, a defining feature of alkaline-earth mediated catalysis is the persistent and ubiquitous +2 oxidation state. Despite this common characteristic, significant differences in ionic radii from 0.86 Å for Mg^{2+}, to 1.49 Å for Ba^{2+} can result in varied reactivity (Figure 1.13).[225] This characteristic bears comparison to the lanthanides, whose Ln^{3+} cations also display substantial variation in ionic radius due to the lanthanide-contraction effect.

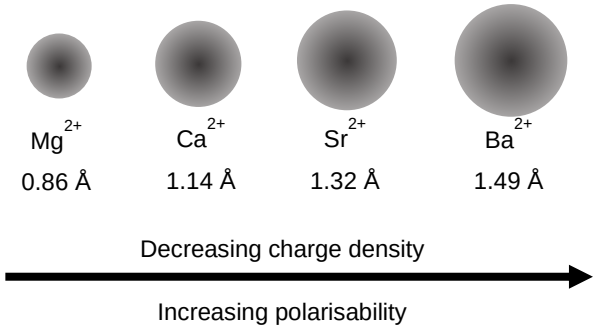

Figure 1.13: Variation in the ionic radius of Ae^{2+} cations.[225]

Another characteristic shared between the alkaline-earths and the rare-earths, is coordination chemistry that is dominated by non-directional ionic bonding. One of the consequences of this characteristic is the propensity for heteroleptic Ae-complexes to participate in Schlenk-type ligand redistribution equilibria, which become more prevalent descending from magnesium to the more diffuse dications of the heavier alkaline-earths (Scheme 1.28).

$$2\ LAeX \rightleftharpoons L_2Ae + AeX_2$$

Scheme 1.28: Schlenk-type ligand redistribution equilibria.

Although simple homoleptic complexes based upon bulky silylated bis-amides (**Ia**-**d**, **IIa**-**d**) and -alkyls (**IIIa**-**d**) have been successfully employed, much of the catalysis and mechanistic understanding of group 2 is founded upon the ability to isolate well-defined heteroleptic complexes. Schlenk-type redistribution equilibria can be suppressed by the utilisation of bulky and/or chelating ligands, which serve to kinetically stabilise heteroleptic complexes with respect to redistribution. Examples include β-diketiminates (**IVa**-**d**, **Va**-**c**, **VIa**-**e**),[226-238] macrocyclic chelating amines,[239-243] bisimidazolinates,[244] aminotropiminates,[245, 246] triazenides,[247] anilido-imines (**VIIa**-**c**),[248] and borates (**VIIIa**).[249-251] Some common alkaline-earth complexes based on these ligands and of relevance to this work are shown in Figure 1.14.

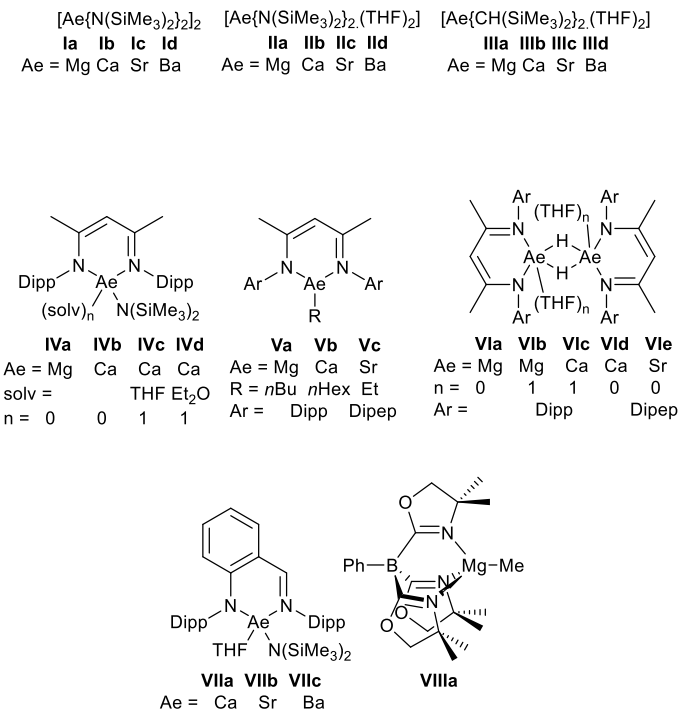

Figure 1.14: Some alkaline-earth complexes relevant to this thesis.

1.5.2 Catalytically relevant reactivity at group 2 centres

Most catalytically relevant alkaline-earth centred reactivity can be summarised by two redox-neutral processes. Firstly, unsaturated double bonds may insert into polar Ae-X bonds *via* a four-membered transition state (Scheme 1.29a). This process has manifested itself in a variety of Ae-mediated catalytic heterofunctionalization reactions, such as the hydroamination,[230, 231, 233, 252-257] hydrophosphination,[248, 254, 258-260] hydroalkoxylation,[261] hydroboration,[262-267] and hydrosilylation[268] of a variety of unsaturated small molecules, including activated alkenes, carbodiimides, ketones, and ketimines. In the absence of multiple-bonds, σ-bond metathesis may occur. Although analogies may be drawn to similar processes already discussed in the context of group 4-mediated dehydrocoupling chemistry (Section 1.4.2), the ionic nature of alkaline-earth coordination complexes, however, results in highly polarised Ae-X bonds. Hence, the outcome of σ-bond metathesis depends on the predisposed polarity of the incoming substrate, where the δ- substituent (e.g. a hydride or amide) is transferred to the Ae-centre and the δ+ substituent (e.g. a proton, borane, or silane) forms a new σ-bond (Scheme 1.29b). In this way, protic substrates may be dehydrocoupled with hydridic partners under alkaline-earth catalysis. Due to the prerequisite polar orthogonality of the substrates, examples of direct homodehydrocoupling by Ae-catalysis are yet to be reported.

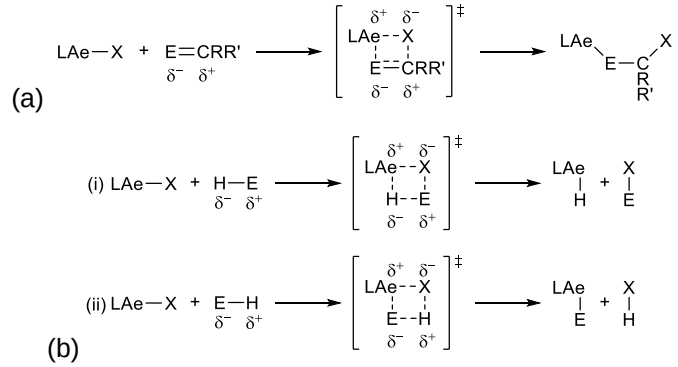

Scheme 1.29: Redox-neutral reactivity modes at alkaline-earth metal centres. (a) Polarised insertion of an unsaturated bond into an Ae-X bond. (b) σ-Bond metathesis with (i) hydridic and (ii) protic substrates.[269]

Interesting recent developments in the chemistry of the heavier alkaline earths have departed from these two well-established modes of reactivity. Of key importance to such reactions is the polarisation of an otherwise non-polar substrate such as alkene, dihydrogen, or benzene, by a highly Lewis-acidic Ae-centre. For example, polarised insertion of unactivated terminal alkenes into the dimeric β-diketiminato calcium hydride **VId** gives alkyl complexes such as the BDI-calcium hexyl, **Vb**.[235, 236, 238] In turn, **Vb** effects the alkylation of benzene *via* pre-coordination and activation of the arene to the Lewis-acidic calcium centre, followed by nucleophilic attack of the alkyl anion to generate a Meisenheimer-type intermediate (Scheme 1.30).[235, 238]

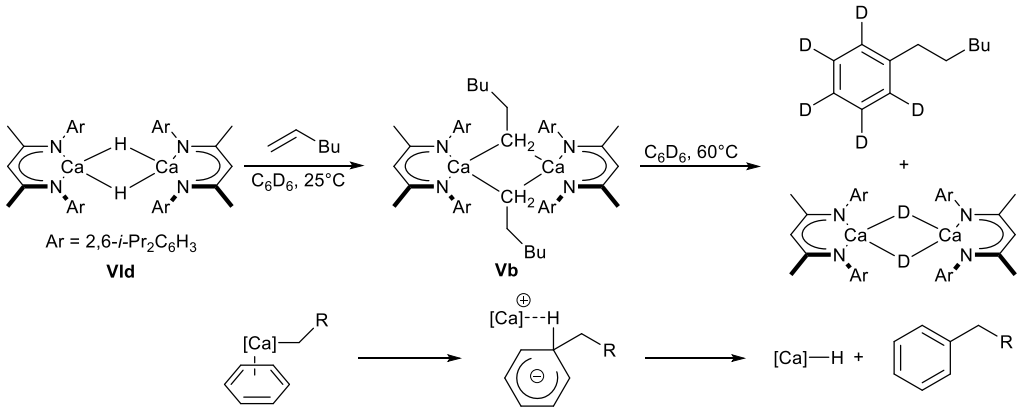

Scheme 1.30: Insertion of un-activated terminal alkenes into a Ca-H bond and subsequent nucleophilic substitution of benzene.[235]

The regeneration of Ae-hydride or deuteride in this process means that, in principle, this reactivity may be realised in a catalytic manner although, thus far, Schlenk-type equilibria are a limitation. The analogous strontium hydride complex **VIe** is even more reactive, and

undergoes multiple ethylene insertions to ultimately yield polyethylene. The resulting ethyl complex **Vc** is such a potent nucleophile, that twofold nucleophilic substitution may take place on a single benzene molecule.[238] Analogous insertion reactions with the BDI-magnesium hydride **VIa** require elevated temperatures, [270] highlighting the importance of ionic-radii effects. Although the resulting BDI-magnesium alkyl complexes are inert towards benzene, they do facilitate the catalytic hydrosilylation of otherwise un-activated *n*-alkenes. Similar calcium-centred benzene coordination-activation is thought to play a role in the very recently reported calcium-catalysed oxidative addition of benzene to the BDI-aluminium(I) complex **IX** (Scheme 1.31).[271] Experimental evidence for the unsupported coordination of neutral arenes to Lewis-acidic Ae-centres has also been provided in a series of recently reported cationic complexes.[272-276]

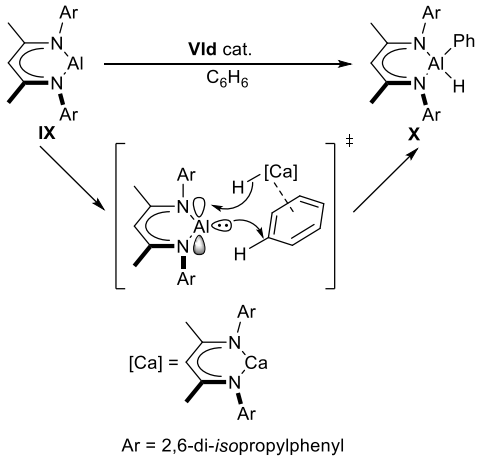

Scheme 1.31: Calcium catalysed oxidative addition of benzene to the BDI-Al(I) compound **IX**.[271]

1.5.3 Silane-amine dehydrocoupling

Catalysts reported for the dehydrocoupling of silanes and amines span the breadth of the periodic table. Examples include lanthanide,[277-280] actinide,[281] transition metal,[282-286] alkali metal,[287] *p*-block elements,[288, 289] metal nanoparticles[290, 291] and the catalytic activation of Si-H bonds by nucleophilic fluoride attack.[292] The first example of Ae-catalysis for this reaction was reported by Buch and Harder in 2007, utilising the calcium azametallocyclopropane pre-catalyst **XI**.[293] Since then, the reaction has been studied using a variety of catalysts by the groups of Sadow,[249] Hill,[294] Sarazin,[295-298] Nembenna,[299] and Parkin.[300]

Sadow's 2011 study with the tris(oxazolinyl)boratomagnesium methyl precatalyst, **VIIIa**, provides evidence for deviation from the concerted four-membered transition states, typically associated with σ-bond metathesis.[249] Although the large negative $\Delta S^{\ddagger}$ value determined was consistent with such a transition state, Hammett studies suggested a reaction pathway that passes through a five-coordinate silicate species. This species is stabilised by electron

withdrawing groups, and generated from nucleophilic attack of a magnesium centred amide on the electrophilic silicon centre. Kinetic isotope effect experiments with $PhMeSiD_2$ suggested that Si-H bond cleavage was not involved in this rate-determining step, which is followed by rapid hydride transfer from silicon to magnesium (Scheme 1.32).

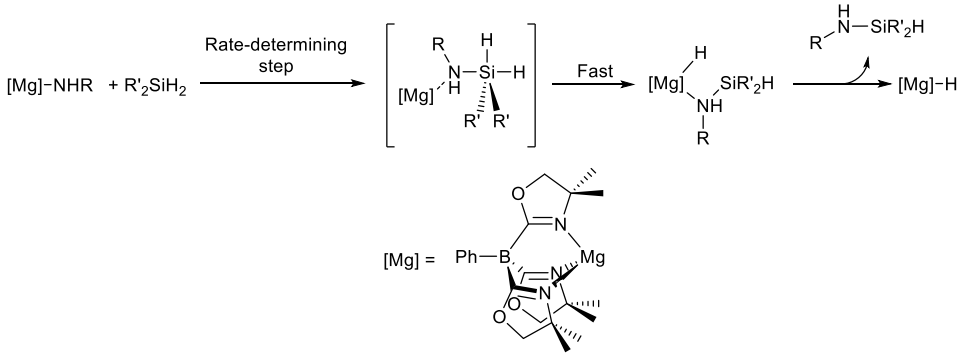

Scheme 1.32: Proposed mechanism for the magnesium-catalysed dehydrocoupling of silanes and amines reported by Sadow and co-workers.[249]

Later experimental and computational investigations by Sarazin, Tobisch, and co-workers on a system involving the anilido-imine barium pre-catalyst **VIIc**, also favoured a mechanism involving stepwise nucleophilic attack, although, in their case, hydride transfer was proposed to be the turnover limiting step and the rate law shown in Equation 1.2 was deduced.[297, 298]

Equation 1.2:

$$\frac{-d[silane]}{dt} = k[Ba]^1[silane]^1[amine]^0$$

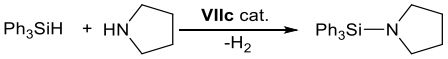

Scheme 1.33: The barium-catalysed dehydrocoupling reaction used to deduce the rate law Equation 1.2.[298]

Whilst both of these studies focussed on mononuclear catalysts with bulky chelating ligands and well-defined reaction centres, the homoleptic bis amides **Ia**-**d**, **IIb**-**d**, and alkyls **IIIb**-**d** were found to offer highly effective alternatives. The absence of bulky chelating ligands, however, results in divergent and complex kinetic profiles consistent with a less-precisely defined active site. Whereas Hill *et.al.* found that the turnover frequency (TOF) of calcium pre-catalyst **Ib** surpassed that of the analogous magnesium or strontium species **Ia** and **Ic**,[294] Sarazin's group found reaction rates to increase from calcium (**IIb**), to strontium (**IIc**), to barium (**IId**).[297] Furthermore, the structurally related alkyl pre-catalysts **IIIb**-**d** provided yet improved rates,

hinting at the involvement of amide-amine equilibria and the persistence of bulky $[N(SiMe_3)_2]^-$ in the coordination sphere of the catalyst.

Kinetic experiments by Hill *et.al.* found further mechanistic variation amongst pre-catalysts **Ia**-**c**. Whilst calcium and magnesium pre-catalysts displayed overall first-order kinetics and a first-order dependence in both catalyst and amine concentration (Equation 1.3), the strontium pre-catalyst was first order in both amine and silane, and second order in catalyst concentration (Equation 1.4). These findings were ascribed to the adoption of a dimeric active species by the larger strontium centre, and involvement of both amine and silane substrates within the rate-determining step.[294]

Equation 1.3:
$$-\frac{d[amine]}{dt}(\mathbf{Ia}, \mathbf{Ib}) = k[cat]^1 amine^1 silane^0$$

Equation 1.4:
$$-\frac{d[amine]}{dt}(\mathbf{Ic}) = k[cat]^2 amine^1 silane^1$$

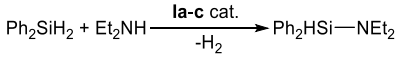

Scheme 1.34: Catalytic dehydrocoupling reaction used to derive rate laws Equation 1.3 and Equation 1.4.

Using the barium-alkyl pre-catalyst **IIId**, Sarazin and co-workers applied this reaction toward the controlled synthesis of oligosilazanes *via* sequential dehydrocoupling (Scheme 1.35, top).[296] This work was ultimately extended to the catalytic dehydropolymerisation of diphenylsilane and *para*-xylylenediamine providing linear (**P-XXX**) and cyclic (**P-XXX'**) polycarbosilazanes (Scheme 1.35, bottom).[295]

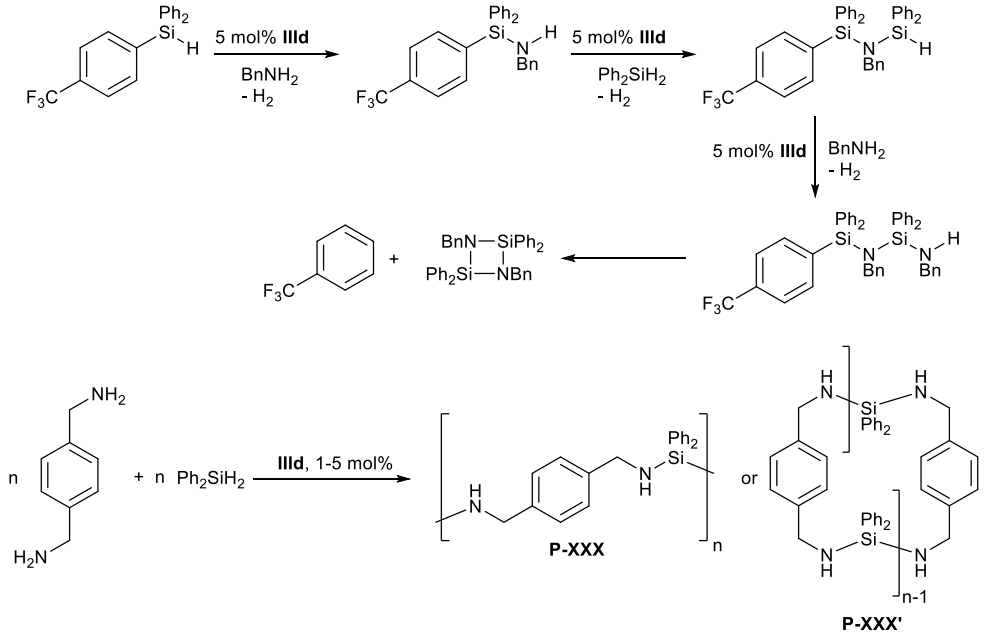

Scheme 1.35: Barium-catalysed stepwise and polycondensation synthesis of oligosilazanes and polycarbosilazanes. Reactions performed at 60°C in benzene.[295, 296]

1.5.4 Silane-silanol and silane-boronic acid dehydrocoupling

Although the formation of Si-O bonds is an important transformation for a wide variety of industrially relevant processes and materials, a dehydrogenative approach using Ae-catalysis has only recently been realised. Sarazin and co-workers utilised bulky alkyl-substituted boronic acids to access barium boroxides **XIIa**-**c** with coordination numbers as low as two.[301] Complex **XIIc** is able to undergo σ-bond metathesis with primary silanes and tertiary alkoxysilanes to afford catalytic formation of B-O-Si linkages (Scheme 1.36).

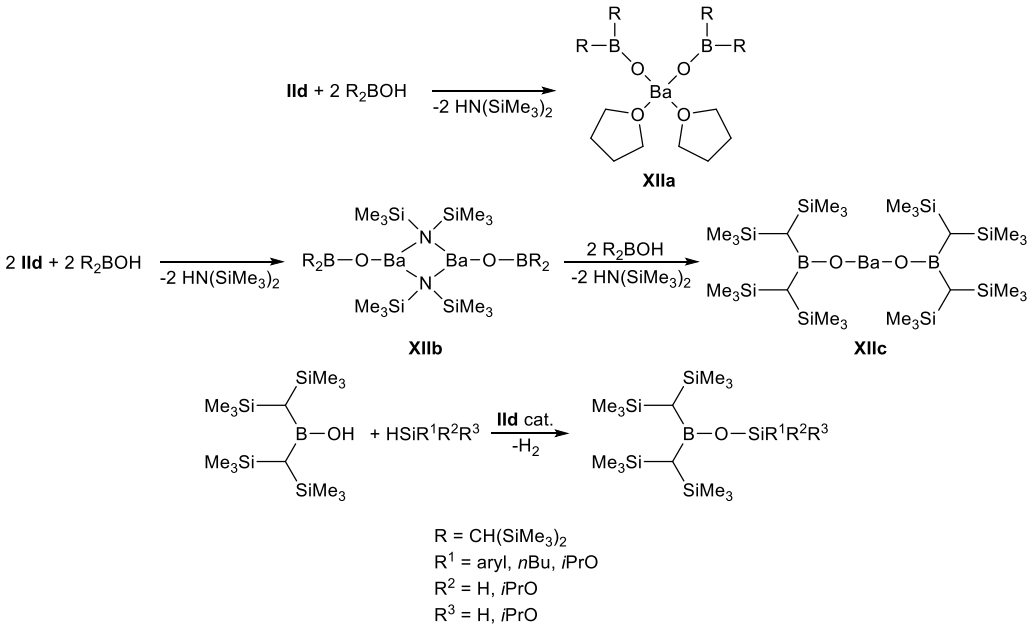

Scheme 1.36: Synthesis of low-coordinate barium-boryloxides from **IId** and resulting catalytic dehydrocoupling of a bulky boronic acid with silanes.[301]

Work by the same group yielded dimeric barium siloxides **XIIIa**, **XIIIb** and **XIV**, by reacting the bulky silanol, $(Me_3Si)_3SiOH$ with the bis-amides **Id** and **IId** (Scheme 1.37). When **Id** was used in catalytic quantities, silanes and silanols could be dehydrocoupled to provide unsymmetrical siloxanes (Scheme 1.37, bottom). Based upon preliminary mechanistic investigations, both the boronic acid and silanol systems were proposed to pass through a rate-limiting step that involves nucleophilic attack of the boroxy or siloxy oxygen on the incoming silane, to produce a five-coordinate intermediate, similar to those previously proposed for silane-amine dehydrocoupling (Scheme 1.38).[298, 302]

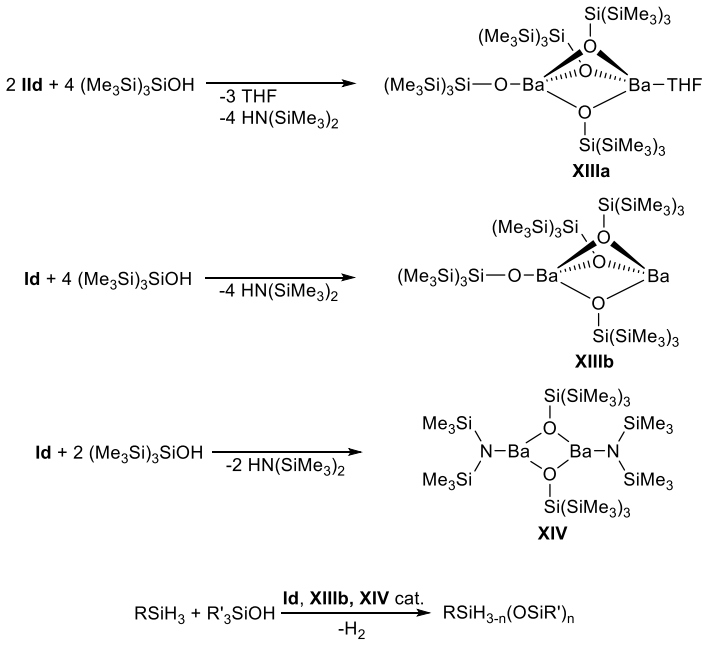

Scheme 1.37: Synthesis of barium siloxides and resulting catalytic dehydrocoupling of silanes and silanols to afford unsymmetrical siloxanes.[303]

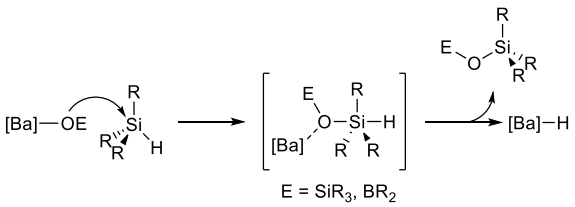

Scheme 1.38: Plausible step-wise rate-limiting step involving nucleophilic attack of boroxy or siloxy oxygen on silicon, consistent with preliminary studies on the barium-catalysed dehydrocoupling of silanes with boronic acids and silanols.[301, 303]

Although related alkali-metal mediated processes are known, alcohol substrates have not been applied towards Ae-mediated catalytic Si-O bond formation, to the best of our knowledge.[304] However, a zinc-catalysed reaction reported by Sadow bears similarity to related alkaline-earth systems due to persistence of the d^{10} Zn^{2+}-centre of pre-catalyst **VIIIb**.[305] Although the related magnesium pre-catalyst **VIIIa** was proposed to facilitate silane-amine dehydrocoupling *via* stepwise nucleophilic attack and hydride transfer steps, Sadow and co-workers proposed the zinc-catalysed silane-alcohol dehydrocoupling to proceed *via* four-membered σ-bond metathesis transition states (Scheme 1.39).

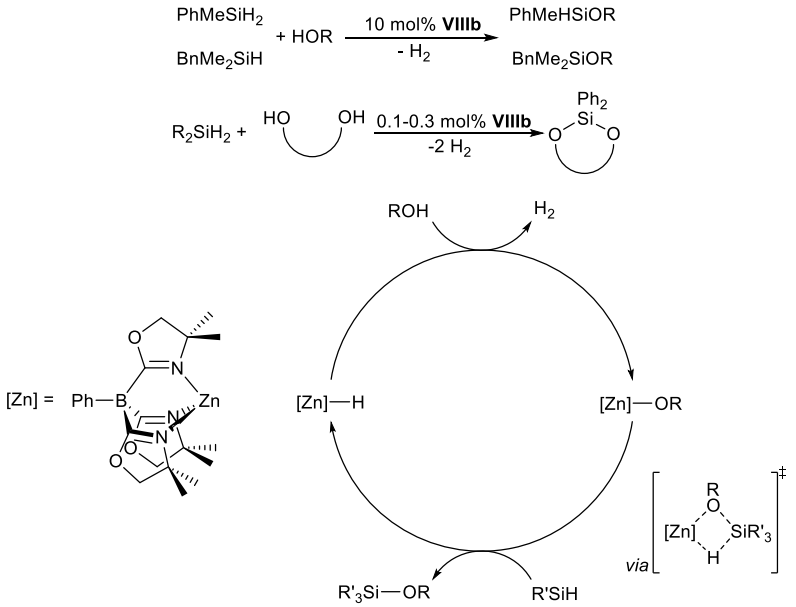

Scheme 1.39: Zinc-catalysed dehydrocoupling of silanes and alcohols and a proposed mechanism.[305]

1.5.5 Dehydrocoupling of silanes and terminal alkynes

Terminal alkynes are relatively acidic and readily undergo deprotonation and metalation with Ae-amides, alkyls, and hydrides to afford the corresponding acetylide complexes.[300, 306] Reacting such acetylide complexes with a silane would be expected to accompany the regeneration of an Ae-hydride with formation of a Si-C bond. Although conceptually simple, the Ae-mediated catalytic dehydrocoupling of silanes and terminal alkynes is limited to two reports, the relative insolubility of Ae-acetylides being a key drawback. Whilst Parkin's group recently reported the use of the tris[(1-isopropylbenzimidazol-2-yl)dimethylsilyl]methyl magnesium methyl and hydride pre-catalysts **XVa** and **XVb**,[300] Buch and Harder utilised the calcium-azacyclometallopropane **XI** (Scheme 1.40).[293]

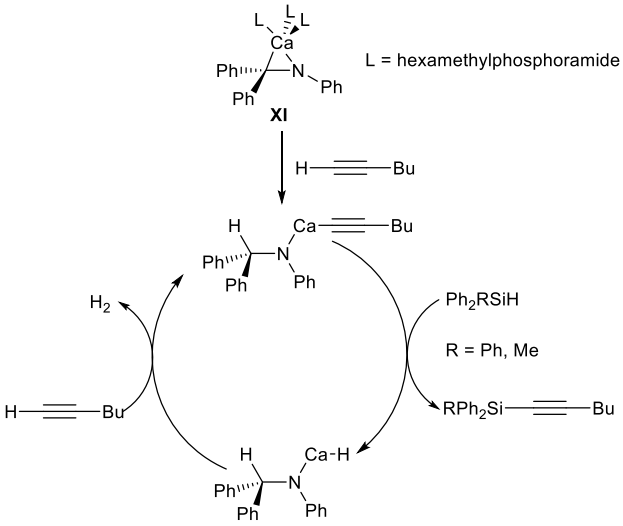

Scheme 1.40: A proposed catalytic cycle for the calcium-catalysed dehydrocoupling of silanes and terminal alkynes.[293]

1.5.6 Dehydrocoupling and desilacoupling of amines with boranes and silaboranes

In contrast to intense study of the dehydrocoupling/dehydrogenation of amine-boranes, the dehydrocoupling of separate amines and boranes has received relatively little attention. A report by Liptrot *et.al.* in 2015 showed that the BDI-magnesium butyl complex, **Va**, was an effective pre-catalyst for the dehydrocoupling of pinacol borane (HBpin) and 9-borabicyclo[3.3.1]nonane (9-BBN), with a variety of aromatic and aliphatic amines (Scheme 1.41).[307] Stoichiometric studies enabled the isolation of intermediates such as the magnesium anilidoborane complex **XVI**, whilst kinetic investigations revealed significant mechanistic variations between the HBpin system (Equation 1.5) and that of 9-BBN (Equation 1.6). Consistent with the observed rate law, the borohydride complex **XVII** was proposed to be an off-cycle resting-state when the latter substrate was used. The proposed catalytic cycle involves an equilibrium between **XVII** and the magnesium hydride **VIa,** and depends on monomerisation and amine pre-coordination to the latter species (Scheme 1.42).

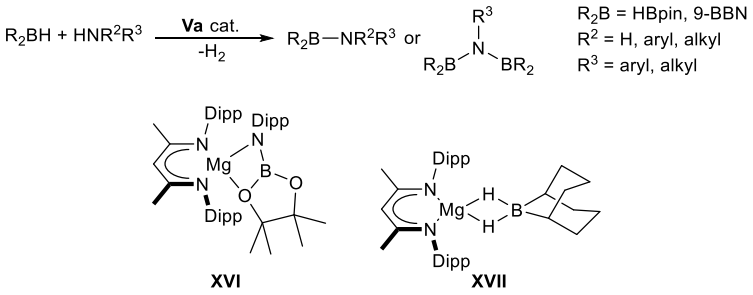

Scheme 1.41: Magnesium-catalysed dehydrocoupling of amines and boranes intermediates proposed to be relevant to catalysis.[307]

Equation 1.5: $$rate = k[\mathbf{Va}]^2[\mathrm{HBpin}]^1[\mathrm{PhNH(Me)}]^0$$

Equation 1.6: $$rate = k[\mathbf{Va}]^{\frac{1}{2}}[\text{9-BBN}]^{-1}[\mathrm{PhNH(Me)}]^2$$

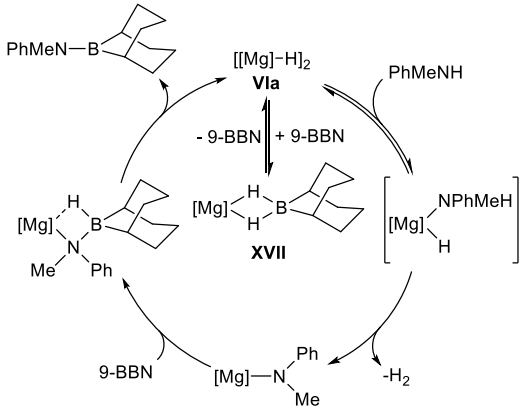

Scheme 1.42: Proposed catalytic cycle for the magnesium-catalysed dehydrocoupling of *N*-methylaniline with 9-BBN.[307]

An extension of this work draws upon the fact that Ae-mediated σ-bond metathesis need not require the involvement of E-H bonds, as shown in Scheme 1.29b. Polar E-E' bonds may also undergo rupture *via* similar four-membered transition states to affect transfer of the E' group to the metal centre. This mode of reaction has resulted in formation of the magnesium silyl complex **XVIII** from pinB-SiMe$_2$Ph (Scheme 1.43a). In the presence of amine, this transformation forms part of a cycle which, using the bis-amides **IIa**-**c**, affords catalytic cross-coupling to generate aminoborane and silane products (Scheme 1.43b).[308]

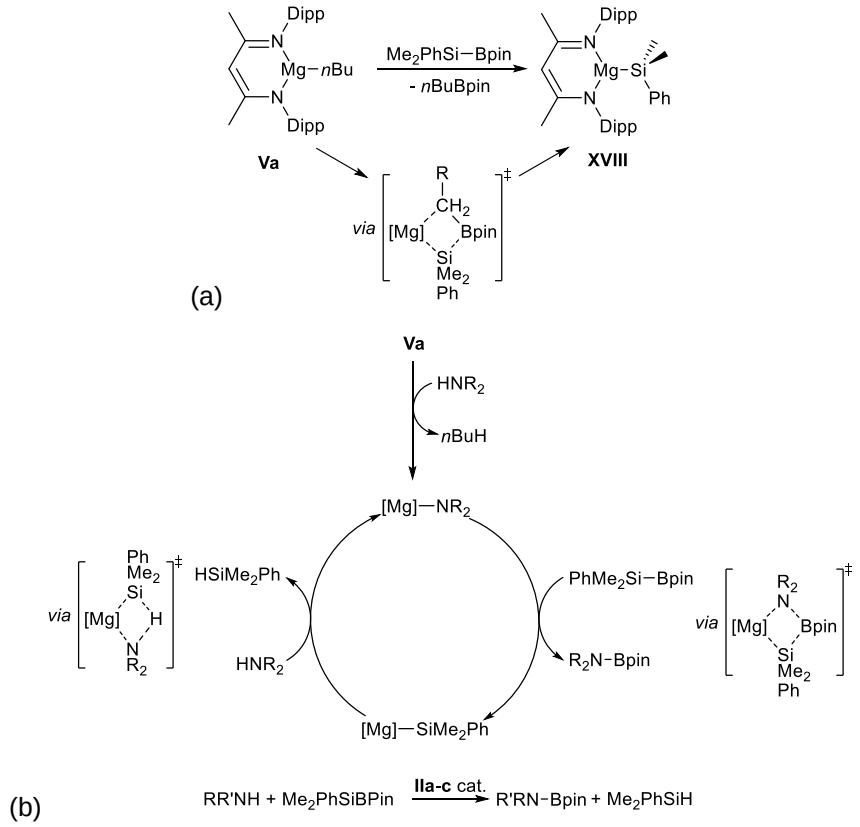

Scheme 1.43: (a) Synthesis of the BDI-magnesium silyl complex **XVIII** *via* σ-bond metathesis of **Va** with $Me_2PhSiBpin$. (b) A hypothetical catalytic cycle based upon similar σ-bond metathesis steps, and the Ae-catalysed desilacoupling of silaboranes and amines.[308]

1.5.7 Alkaline-earth mediated homo-dehydrocoupling

Alkaline-earth mediated homo-dehydrocoupling is virtually unprecedented due to the orthoganal E-H polarity demanded by the polarised transition states involved in catalysis. Recent work with highly charge-separated and coordinatively unsaturated complexes such as hydrides **VId** and **VIe,** and alkyls **Vb** and **Vc**, however, hints at the possibility of inductive activation of relatively non-polar σ-bonds by approach to the highly polarised Ae-complex (Scheme 1.44). Reactions with the unactivated π-bonds of benzene or *n*-alkenes depend on a similar activation mode.[235, 236] Recent reports of Ae-mediated hydrogenation catalysis support this idea,[242, 309-311] and Chapter 4 will explore similar reactivity in the context of organostannane dehydrocoupling.

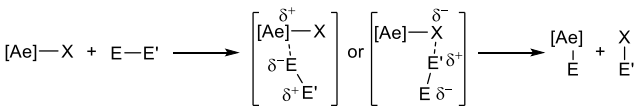

Scheme 1.44: Hypothetical inductive activation and cleavage of a non-polar E-E' bond at an Ae-centre.

Although not a direct dehydrocoupling, the calcium bis-alkyl complex **IIIb** was shown to mediate the reductive coupling of phosphine oxides to the mixed P(V)-P(III) and P(III)-P(III) coupled products $Ph_2P(O)PPh_2$ and $(Ph_2P)_2$ in the presence of phenylsilane. Whilst the mechanism of this unusual reactivity remains unclear, involvement of calcium-hydride intermediates is implicated by the pre-requisite phenylsilane, whilst isolation of the heteroleptic $[Ph_2PO]^-$ derivative **XIX** from **IVc** and $Ph_2P(O)H$ supports the involvement of Ca(II)-P(V) species.[312]

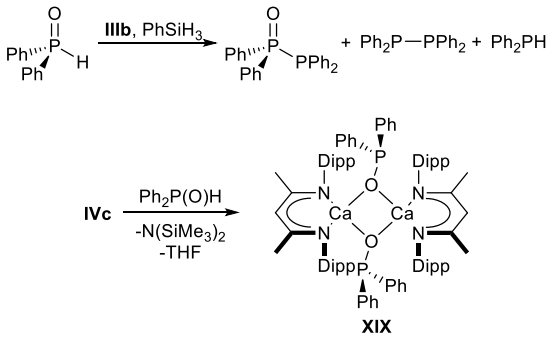

Scheme 1.45: Hydrido-calcium mediated reductive coupling of diphenylphosphine oxide, and the formation of compound **XIX**.[312]

Another rare-example of Ae-mediated homodehydrocoupling relevant to this work, is a preliminary report in the thesis of Dr David Liptrot.[313] In attempting to perform catalytic tin-nitrogen dehydrocoupling, Sn-Sn bonds were instead formed using the magnesium pre-catalyst **Va** and related complexes, in the presence of catalytic quantities of *n*-butylamine (Scheme 1.46). A tentative mechanistic pathway was proposed to involve formation and subsequent dismutation of the initially targeted stannylamine to provide a distannane and regenerate amine. Further investigations into the coupling chemistry of Ph_3SnH mediated by **IVc**, however, revealed a complex manifold of organostannane coupling and redistribution reactions to produce Ph_4Sn and higher oligomers such as octaphenyltristannane, in addition to the anticipated distannane product.

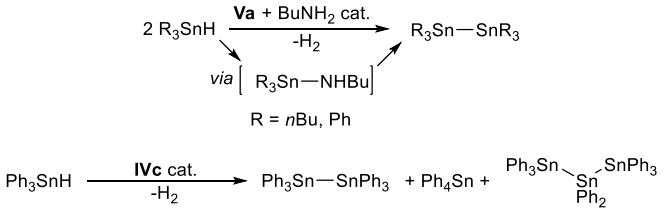

Scheme 1.46: Magnesium- and calcium-mediated dehydrocoupling of organotin(IV) hydrides.[313]

1.5.8 Alkaline-earth mediated amine-borane dehydrocoupling

The N-H bond of amine-boranes are readily deprotonated by Ae-amides, alkyls and hydrides to provide Ae-amidoborane complexes (**XX**-**XXIV**)[216, 314-322] and, in some cases, spontaneous N-B coupling and H_2 elimination can give $[R_2NBH_2NR_2BH_3]^-$ derivatives of the type **XXV** (Scheme 1.47).[216, 318, 320] Although such species are relatively stable, elevated temperatures can promote the formation of dehydrogenated products such as **XXVI** and **XXVII**.[314, 315] Exposing an amidoborane complex to further equivalents of amine-borane can facilitate β-hydride elimination at mild temperatures to produce the unsaturated aminoborane monomer. If kinetically unstable, the aminoborane may undergo dimerisation[216, 320] or be trapped by Ae-amides or -alkyls to generate unsymmetrical diaminoboranes[323] or alkylaminoboranes[319, 322] *via* polarised insertion into Ae-N or Ae-C bonds. Both processes may be extended to the catalytic regime (Scheme 1.47).[215, 323]

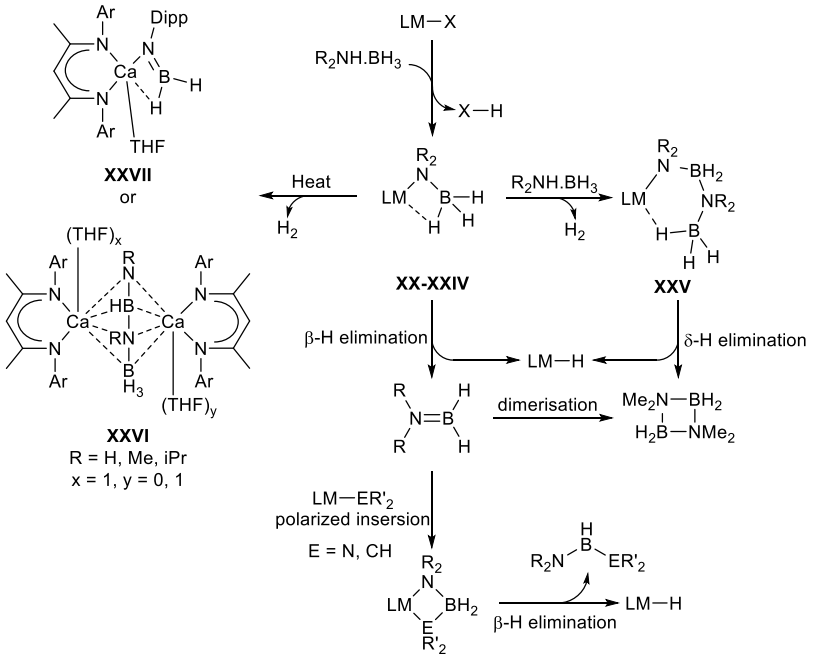

Scheme 1.47: Stoichiometric reactivity of Ae-amidoborane complexes.[216, 314-323]

Magnesium and calcium bis-alkyl complexes **IIIa** and **IIIb** were found to catalyse the dehydrogenation of dimethylamine-borane to afford the corresponding cyclic diborazane. Various stoichiometric experiments were carried out and, taking products and intermediates observed by ^{11}B NMR spectroscopy into account, a catalytic cycle was proposed (Scheme 1.48). The cyclic diborazane can be produced by off-metal dimerization of the unsaturated aminoborane, generated *via* β-hydride elimination of an amidoborane species. Alternatively, δ-hydride elimination of a $[Me_2NBH_2NMe_2BH_3]^-$ derivative provides the same product, whilst β-hydride elimination produces the observed by-products BH_3 and $(Me_2N)_2BH$.[216, 318]

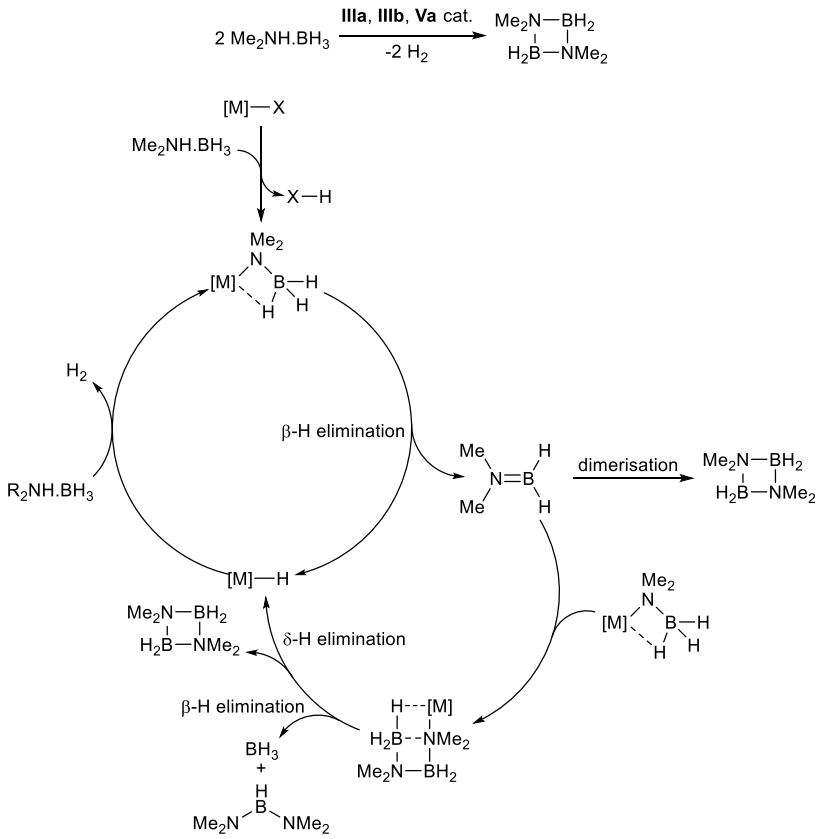

Scheme 1.48: Proposed catalytic cyclic for the Ae-mediated dehydrocoupling of dimethylamine-borane.[216, 318]

The involvement of further equivalents of amine-borane in both β- and δ-hydride elimination processes was suggested to be of great importance (Scheme 1.49), and goes some way to rationalise the high thermal stability of complexes such as **XXVb** and **XXb**. In contrast to most other Ae-mediated dehydrocoupling reactions, the reactivity of magnesium surpasses that of calcium. This attribute may be rationalised by the greater efficacy of the hard, charge-dense magnesium centre to effect hydride-elimination processes.

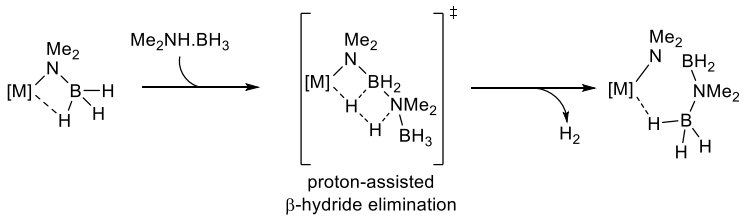

Scheme 1.49: Postulated proton-assisted transition state for β-hydride elimination of an Ae-amidoborane to produce an $[Me_2NBH_2NMe_2BH_3]^-$ derivative.[216]

The *in situ* generation of unsaturated aminoborane was harnessed in the synthesis of unsymmetrical diaminoboranes (Scheme 1.50). This process occurs *via* polarised insertion of aminoborane into the Ae-N bond of an amide intermediate. The ability to trap unsaturated fragments and build well-defined inorganic molecules of higher complexity is an attractive proposition that merits further investigation.

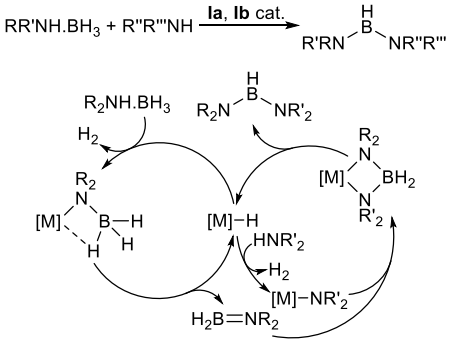

Scheme 1.50: Ae-mediated catalytic dehydrocoupling of amines and amine-boranes to provide unsymmetrical aminoboranes.[323]

A recent publication from the Kays group provides an alternative mechanism for dimethylamine-borane dehydrogenation through the involvement of a non-innocent bidentate ligand (Scheme 1.51).[324] The amidopyridine-derivative **XXVIII** can accept a proton from dimethylamine-borane to become an aminopyridine-coordinated magnesium amidoborane. The latter species undergoes insertion with unsaturated aminoborane and/or deprotonation, avoiding the formation of potentially unstable magnesium hydride species. The high activity of this catalyst system was attributed to reversible protonation of the ligand, which allows **XXVIII** to be regenerated as a stable resting state.

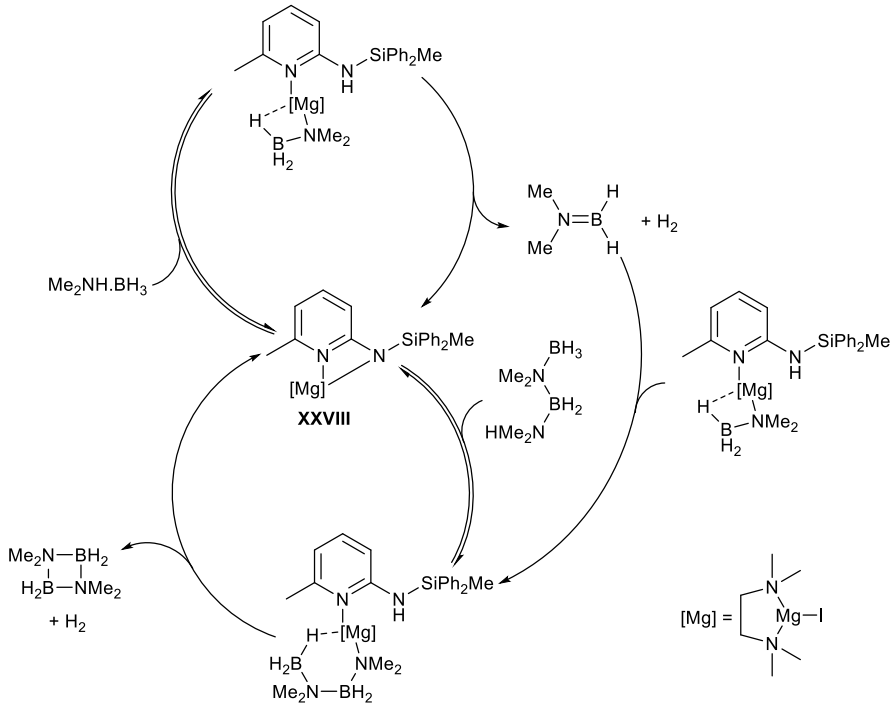

Scheme 1.51: Postulated mechanism for the dehydrogenation of dimethylamine-borane with the magnesium pre-catalyst **XXVIII**.[324]

1.5.9 Alkaline-earth mediated phosphine-borane dehydrocoupling

Although alkali-metal salts of phosphidoboranes are well known and have acted as precursors to the only reported examples of Ae-phosphidoborane complexes,[325] the reactivity of alkaline-earth species toward phosphine-boranes remains unexplored. Conceptually, reaction pathways involving σ-bond metathesis and β-hydride elimination analogous to those of Ae-amidoborane complexes are a realistic possibility. Important differences such as the relatively weak P-B bond and mismatch between soft phosphorus-centred anions, and hard Lewis-acidic Ae-cations must, however, be taken into consideration.

1.6 Aims of this project

The synthesis of polymers containing metal atoms and/or main group E-E bonds has been subject to a relatively recent and intense research effort. Synthetic and characterisation methods have seen dramatic improvements and catalysis has played an important role in this regard. Dehydrocoupling has already proved to be a valuable tool in the synthesis of inorganic polymers, but its application towards the preparation of metallopolymers remains limited. The dehydrocoupling literature remains dominated by transition metal-catalysis, and although redox-neutral Ae-mediated processes, based on σ-bond metathesis and other related mechanisms have made significant advances, they are yet to make a significant impact on polymer chemistry.

This thesis aims to address these shortcomings by applying Ae-catalysed dehydrocoupling towards the synthesis of metallopolymers and main-group inorganic polymers. The polymers thus synthesised will be subject to state-of-the-art solution state and solid-state characterisation techniques. Molecular dehydrocoupling products will provide valuable model-compounds suitable for assessing reactivity as well as providing structural, spectroscopic, and electronic comparison to the polymers through techniques such as single-crystal X-ray diffraction, NMR spectroscopy, and cyclic voltammetry. The products of polymer pyrolysis will also be subjected to materials characterisation techniques such as electron microscopy and spectroscopy, and powder X-ray diffraction. Insight into the fundamental reactivity of Ae-complexes towards relevant main-group substrates will be gained through the use of single-crystal X-ray diffraction, whilst NMR spectroscopy will provide an *in-situ* reaction monitoring tool, as well as providing information on the solution-state behaviour of such coordination complexes.

Chapter 2 takes a well-understood reaction: Ae-catalysed silane-amine dehydrocoupling, and applies it towards the synthesis of ferrocene-containing polycarbosilazanes. The inclusion of ferrocene as a pendent group, or as part of the main polymer chain is facilitated by judicious choice of monomer. The resulting materials were subjected to solution-state characterisation by multinuclear NMR and DOSY, as well as electrochemical analysis. Magnetic ceramics were prepared by polymer pyrolysis and comprehensively investigated by electron microscopy, electron diffraction, and X-ray diffraction.

Chapter 3 seeks to develop a new Ae-mediated catalytic process in the form of silane-alcohol dehydrocoupling, with the aim of preparing ferrocene-containing polysilylethers. Hydrolytically robust Si-O-C linkages address the limited moisture stability of Si-N-C based polymers described in Chapter 2. After thorough optimisation and investigation of the reaction scope, stoichiometric and kinetic experiments uncovered a complex catalytic system beneath a conceptually simple mechanism, and led to the isolation of a series of fully characterised dimeric Ae-alkoxide complexes. Ultimately, the reaction was used to prepare the first examples of ferrocene-containing polysilylethers.

In *Chapter 4*, the thesis pursues an effort to expand Ae-catalysis towards unexplored substrates suitable for the formation of purely inorganic polymer chains *via* dehydrocoupling. The reactivity of organo and hydrido-stannanes towards calcium hydride and alkyl complexes was investigated and, whilst Sn-Sn bond forming catalysis was limited by complex redistribution processes, virtually unprecedented stannyl-calcium complexes were isolated and crystallographically characterised. The nature of hydrido- and organo-calcium mediated Sn-H, Sn-C, and Sn-Sn bond activation was probed experimentally and computationally.

Chapter 5 continues on the theme of expanding the palette of monomers available to the alkaline earths. The reactivity of magnesium and calcium hydride, alkyl, and amide complexes towards diphenylphosphine-borane was explored. Ae-phosphidoborane complexes were hence prepared, and their structural and spectroscopic properties are discussed. Rather than affording dehydrogenated or dehydrocoupled products, attempts to affect phosphine-borane dehydrogenation resulted in diphenylphosphine elimination to provide an unusual phosphinediboronate complex. Phosphine-borane dehydrogenation could, however, be achieved *via* a stepwise stoichiometric deprotonation-hydride abstraction approach using [K{N(SiMe$_3$)$_2$}] and B(C$_6$F$_5$)$_3$. A similar reaction using the previously mentioned β-diketiminato magnesium or calcium phosphidoborane complexes provided a different outcome, resulting in P-B(C$_6$F$_5$)$_3$ adduct formation followed by activation of the BDI-ligand by an unsaturated phosphinoborane.

1.7 References

1. L. H. Baekeland, US Patent, 942600, 1909.
2. G. A. Stahl, *ACS Symposium Series*, 1981, **175**, 25-44.
3. H. Staudinger, *Berichte d. D. Chem. Gesellschaft*, 1920, **53**, 1073.
4. K. Ziegler, E. Holzkamp, H. Breil and H. Martin, *Angewandte Chemie-International Edition*, 1955, **67**, 541-547.
5. E. Rivard, *Chemical Society Reviews*, 2016, **45**, 989-1003.
6. R. West, L. D. David, P. I. Djurovich, K. L. Stearley, K. S. V. Srinivasan and H. Yu, *Journal of the American Chemical Society*, 1981, **103**, 7352-7354.
7. S. Adams and M. Dräger, *Angewandte Chemie-International Edition in English*, 1987, **26**, 1255-1256.
8. S. Harrypersad, L. Liao, A. Khan, R. S. Wylie and D. A. Foucher, *Journal of Inorganic and Organometallic Polymers and Materials*, 2015, **25**, 515-528.
9. S. Adams and M. Dräger, *Journal of Organometallic Chemistry*, 1985, **288**, 295-304.
10. W. Caseri, *Chemical Society Reviews*, 2016, **45**, 5187-5199.
11. M. Trummer, F. Choffat, P. Smith and W. Caseri, *Macromolecular Rapid Communications*, 2012, **33**, 448-460.
12. F. Choffat, P. Smith and W. Caseri, *Advanced Materials*, 2008, **20**, 2225-2229.
13. T. Imori, V. Lu, H. Cai and T. D. Tilley, *Journal of the American Chemical Society*, 1995, **117**, 9931-9940.
14. J. R. Babcock and L. R. Sita, *Journal of the American Chemical Society*, 1996, **118**, 12481-12482.
15. F. Choffat, P. Smith and W. Caseri, *Journal of Materials Chemistry*, 2005, **15**, 1789-1792.
16. F. Choffat, S. Fornera, P. Smith, W. R. Caseri, D. W. Breiby, J. W. Andreasen and M. M. Nielsen, *Advanced Functional Materials*, 2008, **18**, 2301-2308.
17. F. Choffat, Y. Buchmuller, C. Mensing, P. Smith and W. Caseri, *Journal of Inorganic and Organometallic Polymers and Materials*, 2009, **19**, 166-175.
18. J. Pau, A. J. Lough, R. S. Wylie, R. A. Gossage and D. A. Foucher, *Chemistry-a European Journal*, 2017, **23**, 14367-14374.
19. S. Harrypersad and D. Foucher, *Chemical Communications*, 2015, **51**, 7120-7123.
20. F. Choffat, P. Wolfer, P. Smith and W. Caseri, *Macromolecular Materials and Engineering*, 2010, **295**, 210-221.
21. A. Khan, J. Pau, J. Loungxay, T. Magobenny, R. S. Wylie, A. J. Lough and D. Foucher, *Journal of Organometallic Chemistry*, 2019, **900**, 120910.

22. J. Pau, G. M. D'Amaral, A. J. Lough, R. S. Wylie and D. A. Foucher, *Chemistry-a European Journal*, 2018, **24**, 18762-18771.
23. R. G. Jones, R. E. Benfield, R. H. Cragg, A. C. Swain and S. J. Webb, *Macromolecules*, 1993, **26**, 4878-4887.
24. K. Mochida and H. Chiba, *Journal of Organometallic Chemistry*, 1994, **473**, 45-54.
25. T. Hayashi, Y. Uchimaru, N. P. Reddy and M. Tanaka, *Chemistry Letters*, 1992, 647-650.
26. N. Devylder, M. Hill, K. C. Molloy and G. J. Price, *Chemical Communications*, 1996, 711-712.
27. P. R. Deacon, N. Devylder, M. S. Hill, M. F. Mahon, K. C. Molloy and G. J. Price, *Journal of Organometallic Chemistry*, 2003, **687**, 46-56.
28. C. Aitken, J. F. Harrod and E. Samuel, *Journal of Organometallic Chemistry*, 1985, **279**, C11-C13.
29. J. Y. Corey, *Advances in Organometallic Chemistry*, 2004, **51**, 1--52.
30. T. D. Tilley, *Accounts of Chemical Research*, 1993, **26**, 22-29.
31. H. G. Woo, J. F. Walzer and T. D. Tilley, *Journal of the American Chemical Society*, 1992, **114**, 7047-7055.
32. H. G. Woo, R. H. Heyn and T. D. Tilley, *Journal of the American Chemical Society*, 1992, **114**, 5698-5707.
33. T. Imori and T. D. Tilley, *Journal of the Chemical Society-Chemical Communications*, 1993, 1607-1609.
34. H. G. Woo, J. M. Park, S. J. Song, S. Y. Yang, I. S. Kim and W. G. Kim, *Bulletin of the Korean Chemical Society*, 1997, **18**, 1291-1295.
35. H. G. Woo, S. J. Song and B. H. Kim, *Bulletin of the Korean Chemical Society*, 1998, **19**, 1161-1164.
36. F. Choffat, S. Kaeser, P. Wolfer, D. Schmid, R. Mezzenga, P. Smith and W. Caseri, *Macromolecules*, 2007, **40**, 7878-7889.
37. A. Hermann, J. Cid, J. D. Mattock, R. D. Dewhurst, I. Krummenacher, A. Vargas, M. J. Ingleson and H. Braunschweig, *Angewandte Chemie-International Edition*, 2018, **57**, 10091-10095.
38. M. S. Hill, P. B. Hitchcock and R. Pongtavornpinyo, *Science*, 2006, **311**, 1904-1907.
39. J. J. Daly and Sanz, *Helvetica Chimica Acta*, 1970, **53**, 1879-1880.
40. Rheingol.Al, J. E. Lewis and J. M. Bellama, *Inorganic Chemistry*, 1973, **12**, 2845-2850.
41. A. Staubitz, J. Hoffmann and P. Gliese, in *Smart Inorganic Polymers: Synthesis, Properties, and Emerging Applications in Materials and Life Sciences*, eds. E. Hey-Hawkins and M. Hissler, Wiley-VCH, Weinheim, First Edition edn., 2019, ch. 2, pp. 19-39.
42. D. L. Han, F. Anke, M. Trose and T. Beweries, *Coordination Chemistry Reviews*, 2019, **380**, 260-286.
43. A. L. Colebatch and A. S. Weller, *Chemistry-a European Journal*, 2019, **25**, 1379-1390.
44. A. Staubitz, M. E. Sloan, A. P. M. Robertson, A. Friedrich, S. Schneider, P. J. Gates, I. Manners and J. Schmedt auf der Guenne, *Journal of the American Chemical Society*, 2010, **132**, 13332-13345.
45. N. T. Coles, M. F. Mahon and R. L. Webster, *Organometallics*, 2017, **36**, 2262-2268.
46. R. L. Webster, *Dalton Trans.*, 2017, **46**, 4483-4498.
47. A. Staubitz, A. P. Soto and I. Manners, *Angewandte Chemie-International Edition*, 2008, **47**, 6212-6215.
48. J. R. Vance, A. Schafer, A. P. M. Robertson, K. Lee, J. Turner, G. R. Whittell and I. Manners, *Journal of the American Chemical Society*, 2014, **136**, 3048-3064.
49. I. Manners, *Angewandte Chemie - International Edition*, 1996, **35**, 1602-1621.
50. S. Rothemund and I. Teasdale, *Chemical Society Reviews*, 2016, **45**, 5200-5215.
51. H. R. Allcock, *Soft Matter*, 2012, **8**, 7521-7532.
52. M. Deng, S. G. Kumbar, Y. Q. Wan, U. S. Toti, H. R. Allcock and C. T. Laurencin, *Soft Matter*, 2010, **6**, 3119-3132.

53. F. Jäkle and F. Vidal, *Angewandte Chemie – International Edition*, 2019, **58**, 5846-5870.
54. A. M. Priegert, B. W. Rawe, S. C. Serin and D. P. Gates, *Chemical Society Reviews*, 2016, **45**, 922-953.
55. T. M. Swager, *Macromolecules*, 2017, **50**, 4867-4886.
56. H. Helten, *Chemistry-an Asian Journal*, 2019, **14**, 919-935.
57. X. Jiang, R. R. Li, C. Feng, G. L. Lu and X. Y. Huang, *Polymer Chemistry*, 2017, **8**, 2773-2784.
58. P. Yang, P. Pageni, M. P. Kabir, T. Zhu and C. Tang, *ACS Macro Letters*, 2016, **5**, 1293-1300.
59. P. Nguyen, P. Gomez-Elipe and I. Manners, *Chemical Reviews*, 1999, **99**, 1515-1548.
60. A. S. Abd-El-Aziz and I. Manners, *Journal of Inorganic and Organometallic Polymers and Materials*, 2005, **15**, 157-195.
61. G. R. Whittell and I. Manners, *Advanced Materials*, 2007, **19**, 3439-3468.
62. E. W. Neuse and L. Bednarik, *Macromolecules*, 1979, **12**, 187-195.
63. C. U. Pittman, J. C. Lai, D. P. Vanderpool, M. Good and R. Pradole, *Macromolecules*, 1970, **3**, 746--754.
64. W. J. Patterson, S. P. McManus and C. U. Pittman Jr., *Journal of Polymer Science: Polymer Chemistry Edition*, 1974, **12**, 837-850.
65. G. R. Whittell, M. D. Hager, U. S. Schubert and I. Manners, *Nature Materials*, 2011, **10**, 176-188.
66. B. J. Holliday and T. M. Swager, *Chemical Communications*, 2005, 23-36.
67. W. Y. Ng, X. Gong and W. K. Chan, *Chemistry of Materials*, 1999, **11**, 1165-1170.
68. A. Kohler, H. F. Wittmann, R. H. Friend, M. S. Khan and J. Lewis, *Synthetic Metals*, 1994, **67**, 245-249.
69. S. Takahashi, E. Murata, M. Kariya, K. Sonogashira and N. Hagihara, *Macromolecules*, 1979, **12**, 1016-1018.
70. M. J. MacLachlan, M. Ginzburg, N. Coombs, T. W. Coyle, N. P. Raju, J. E. Greedan, G. A. Ozin and I. Manners, *Science*, 2000, **287**, 1460-1463.
71. Q. C. Dong, Z. G. Meng, C. L. Ho, H. G. Guo, W. Y. Yang, I. Manners, L. L. Xu and W. Y. Wong, *Chemical Society Reviews*, 2018, **47**, 4934-4953.
72. J. Y. Cheng, C. A. Ross, V. Z. H. Chan, E. L. Thomas, R. G. H. Lammertink and G. J. Vancso, *Advanced Materials*, 2001, **13**, 1174-1178.
73. Y. Yan, J. Y. Zhang, L. X. Ren and C. B. Tang, *Chemical Society Reviews*, 2016, **45**, 5232-5263.
74. Y. L. Wang, D. Astruc and A. S. Abd-El-Aziz, *Chemical Society Reviews*, 2019, **48**, 558-636.
75. H. B. Gu, S. D. Mu, G. R. Qiu, X. Liu, L. Zhang, Y. F. Yuan and D. Astruc, *Coordination Chemistry Reviews*, 2018, **364**, 51-85.
76. C. Weder, *Journal of Inorganic and Organometallic Polymers and Materials*, 2006, **16**, 101-113.
77. M. A. Hempenius, C. Cirmi, F. Lo Savio, J. Song and G. J. Vancso, *Macromolecular Rapid Communications*, 2010, **31**, 772-783.
78. H. Li, P. Yang, P. Pageni and C. B. Tang, *Macromolecular Rapid Communications*, 2017, **38**, 1700109.
79. L. Mond, C. Langer and F. Quincke, *Journal of the Chemical Society, Transactions*, 1890, **57**, 749-753.
80. W. L. Gilliland and A. A. Blanchard, *Inorganic Syntheses*, 1946, **2**, 234-237.
81. T. J. Kealy and P. L. Pauson, *Nature*, 1951, **168**, 1039-1040.
82. S. A. Miller, J. A. Tebboth and J. F. Tremaine, *Journal of the Chemical Society*, 1952, 632-635.
83. G. Wilkinson, M. Rosenblum, M. C. Whiting and R. B. Woodward, *Journal of the American Chemical Society*, 1952, **74**, 2125-2126.
84. N. J. Long, *Metallocenes: An Introduction to Sandwich Complexes*, Wiley-Blackwell, Oxford, First edition edn., 1998.

85. E. Neuse and H. Rosenberg, *Polymer Reviews*, 1970, **4**, 1-145.
86. R. Pietschnig, *Chemical Society Reviews*, 2016, **45**, 5216-5231.
87. Y. Gao and J. M. Shreeve, *Journal of Inorganic and Organometallic Polymers and Materials*, 2007, **17**, 19-36.
88. L. Zhao, X. Liu, L. Zhang, G. R. Qiu, D. Astruc and H. B. Gu, *Coordination Chemistry Reviews*, 2017, **337**, 34-79.
89. X. Feng, K. Zhang, M. A. Hempenius and G. J. Vancso, *RSC Advances*, 2015, **5**, 106355-106376.
90. X. L. Feng, A. Curnurcu, X. F. Sui, J. Song, M. A. Hernpenius and G. J. Vancso, *Langmuir*, 2013, **29**, 7257-7265.
91. J. Zhang, Y. P. Chen, K. P. Miller, M. S. Ganewatta, M. Bam, Y. Yan, M. Nagarkatti, A. W. Decho and C. Tang, *Journal of the American Chemical Society*, 2014, **136**, 4873-4876.
92. J. Y. Zhang, J. Yan, P. Pageni, Y. Yan, A. Wirth, Y. P. Chen, Y. L. Qiao, Q. Wang, A. W. Decho and C. B. Tang, *Scientific Reports*, 2015, **5**, 11914.
93. T. L. Choi, K. H. Lee, W. J. Joo, S. Lee, T. W. Lee and M. Y. Chae, *Journal of the American Chemical Society*, 2007, **129**, 9842-9843.
94. T. Michinobu, H. Kumazawa, K. Noguchi and K. Shigehara, *Macromolecules*, 2009, **42**, 5903-5905.
95. R. W. Heo, F. B. Somoza and T. Randall, *Journal of the American Chemical Society*, 1998, **120**, 1621-1622.
96. H. B. Gu, R. Ciganda, P. Castel, S. Moya, R. Hernandez, J. Ruiz and D. Astruc, *Angewandte Chemie-International Edition*, 2018, **57**, 2204-2208.
97. K. L. Rinehart, A. K. Frerichs, P. A. Kittle, L. F. Westman, D. H. Gustafson, R. L. Pruett and J. E. McMahon, *Journal of the American Chemical Society*, 1960, **82**, 4111-4112.
98. A. G. Osborne and R. H. Whiteley, *Journal of Organometallic Chemistry*, 1975, **101**, C27-C28.
99. D. A. Foucher, B.-Z. Tang and I. Manners, *Journal of the American Chemical Society*, 1992, **114**, 6246-6248.
100. R. Rulkens, D. P. Gates, D. Balaishis, J. K. Pudelski, D. F. McIntosh, A. J. Lough and I. Manners, *Journal of the American Chemical Society*, 1997, **119**, 10976-10986.
101. R. Rulkens, A. J. Lough and I. Manners, *Angewande Chemie – International Edition in English*, 1996, **35**, 1805-1807.
102. D. A. Foucher, M. Edwards, R. A. Burrow, A. J. Lough and I. Manners, *Organometallics*, 1994, **13**, 4959-4966.
103. C. H. Honeyman, D. A. Foucher, F. Y. Dahmen, R. Rulkens, A. J. Lough and I. Manners, *Organometallics*, 1995, **14**, 5503-5512.
104. R. Resendes, P. Nguyen, A. J. Lough and I. Manners, *Chemical Communications*, 1998, 1001-1002.
105. I. Manners, *Chemical Communications*, 1999, 857-865.
106. M. Tanabe, G. W. M. Vandermeulen, W. Y. Chan, P. W. Cyr, L. Vanderark, D. A. Rider and I. Manners, *Nature Materials*, 2006, **5**, 467-470.
107. R. A. Musgrave, A. D. Russell, D. W. Hayward, G. R. Whittell, P. G. Lawrence, P. J. Gates, J. C. Green and I. Manners, *Nature Chemistry*, 2017.
108. K. Temple, F. Jäkle, J. B. Sheridan and I. Manners, *Journal of the American Chemical Society*, 2001, **123**, 1355-1364.
109. H. Braunschweig, C. J. Adams, T. Kupfer, I. Manners, R. M. Richardson and G. R. Whittell, *Angewandte Chemie-International Edition*, 2008, **47**, 3826-3829.
110. A. Bartole-Scott, H. Braunschweig, T. Kupfer, M. Lutz, I. Manners, T. L. Nguyen, K. Radacki and F. Seeler, *Chemistry-a European Journal*, 2006, **12**, 1266-1273.
111. M. Ginzburg, M. J. MacLachlan, S. M. Yang, N. Coombs, T. W. Coyle, N. P. Raju, J. E. Greedan, R. H. Herber, G. A. Ozin and I. Manners, *Journal of the American Chemical Society*, 2002, **124**, 2625-2639.
112. K. Liu, S. Fournier-Bidoz, G. A. Ozin and I. Manners, *Chemistry of Materials*, 2009, **21**, 1781-1783.

113. R. Petersen, D. A. Foucher, B. Z. Tang, A. Lough, N. P. Raju, J. E. Greedan and I. Manners, *Chemistry of Materials*, 1995, **7**, 2045-2053.
114. B. Z. Tang, R. Petersen, D. A. Foucher, A. Lough, N. Coombs, R. Sodhi and I. Manners, *Journal of the Chemical Society-Chemical Communications*, 1993, 523-525.
115. A. Nunns, J. Gwyther and I. Manners, *Polymer*, 2013, **54**, 1269-1284.
116. R. L. N. Hailes, A. M. Oliver, J. Gwyther, G. R. Whittell and I. Manners, *Chemical Society Reviews*, 2016, **45**, 5358-5407.
117. J. B. Gilroy, T. Gadt, G. R. Whittell, L. Chabanne, J. M. Mitchels, R. M. Richardson, M. A. Winnik and I. Manners, *Nature Chemistry*, 2010, **2**, 566-570.
118. X. S. Wang, G. Guerin, H. Wang, Y. S. Wang, I. Manners and M. A. Winnik, *Science*, 2007, **317**, 644-647.
119. Z. M. Hudson, J. Qian, C. E. Boott, M. A. Winnik and I. Manners, *ACS Macro Letters*, 2015, **4**, 187-191.
120. A. Berenbaum, H. Braunschweig, R. Dirk, U. Englert, J. C. Green, F. Jäkle, A. J. Lough and I. Manners, *Journal of the American Chemical Society*, 2000, **122**, 5765-5774.
121. J. A. Schachner, C. L. Lund, J. W. Quail and J. Muller, *Organometallics*, 2005, **24**, 785-787.
122. D. Seyferth and H. P. Withers, *Organometallics*, 1982, **1**, 1275-1282.
123. D. Seyferth and H. P. Withers, *Journal of Organometallic Chemistry*, 1980, **185**, C1-C5.
124. J. A. Schachner, C. L. Lund, J. W. Quail and J. Muller, *Organometallics*, 2005, **24**, 4483-4488.
125. J. K. Pudelski, D. P. Gates, R. Rulkens, A. J. Lough and I. Manners, *Angewandte Chemie - International Edition*, 1995, **34**, 1506-1508.
126. F. Jäkle, R. Rulkens, G. Zech, D. A. Foucher, A. J. Lough and I. Manners, *Chemistry-a European Journal*, 1998, **4**, 2117-2128.
127. I. Matas, G. R. Whittell, B. M. Partridge, J. P. Holland, M. F. Haddow, J. C. Green and I. Manners, *Journal of the American Chemical Society*, 2010, **132**, 13279-13289.
128. G. R. Whittell, B. M. Partridge, O. C. Presly, C. J. Adams and I. Manners, *Angewandte Chemie-International Edition*, 2008, **47**, 4354-4357.
129. R. Broussier, A. Darold, B. Gautheron, Y. Dromzee and Y. Jeannin, *Inorganic Chemistry*, 1990, **29**, 1817-1822.
130. D. E. Herbert, U. F. J. Mayer and I. Manners, *Angewandte Chemie - International Edition*, 2007, **46**, 5060-5081.
131. A. D. Russell, R. A. Musgrave, L. K. Stoll, P. Choi, H. Qiu and I. Manners, *Journal of Organometallic Chemistry*, 2015, **784**, 24-30.
132. R. Hailes, R. A. Musgrave, A. F. R. Kilpatrick, A. D. Russell, G. R. Whittell, D. O'Hare and I. Manners, *Chemistry – A European Journal*, 2018, **25**, 1044-1054.
133. R. A. Musgrave, R. L. N. Hailes, V. T. Annibale and I. Manners, *Chemical Science*, 2019, Advance article.
134. D. A. Foucher, C. H. Honeyman, J. M. Nelson, B. Z. Tang and I. Manners, *Angewandte Chemie-International Edition in English*, 1993, **32**, 1709-1711.
135. F. Barriere, N. Camire, W. E. Geiger, U. T. Mueller-Westerhoff and R. Sanders, *Journal of the American Chemical Society*, 2002, **124**, 7262-7263.
136. R. Rulkens, A. J. Lough, I. Manners, S. R. Lovelace, C. Grant and W. E. Geiger, *Journal of the American Chemical Society*, 1996, **118**, 12683-12695.
137. P. Aguirre-Etcheverry and D. O'Hare, *Chemical Reviews*, 2010, **110**, 4839-4864.
138. S. Barlow and D. O'Hare, *Chemical Reviews*, 1997, **97**, 637-670.
139. J. M. Nelson, H. Rengel and I. Manners, *Journal of the American Chemical Society*, 1993, **115**, 7035-7036.
140. D. P. Puzzo, A. C. Arsenault, I. Manners and G. A. Ozin, *Angewandte Chemie-International Edition*, 2009, **48**, 943-947.
141. J. B. Gilroy, S. K. Patra, J. M. Mitchels, M. A. Winnik and I. Manners, *Angewandte Chemie - International Edition*, 2011, **50**, 5851-5855.

142. M. J. MacLachlan, J. Zheng, K. Thieme, A. J. Lough, I. Manners, C. Mordas, R. LeSuer, W. E. Geiger, L. M. Liable-Sands and A. L. Rheingold, *Polyhedron*, 2000, **19**, 275-289.
143. M. Erhard, K. Lam, M. Haddow, G. R. Whittell, W. E. Geiger and I. Manners, *Polymer Chemistry*, 2014, **5**, 1264-1274.
144. P. J. Flory, *Journal of the American Chemical Society*, 1936, **58**, 1877-1885.
145. W. H. Carothers, *Transactions of the Faraday Society*, 1936, **32**, 39-49.
146. J. B. Heilmann, M. Scheibitz, Y. Qin, A. Sundararaman, F. Jakle, T. Kretz, M. Bolte, H. W. Lerner, M. C. Holthausen and M. Wagner, *Angewandte Chemie-International Edition*, 2006, **45**, 920-925.
147. Q. Luo, R. Zhang, J. Zhang and J. B. Xia, *Organometallics*, 2019, **38**, 2972-2978.
148. K. Sonogashira, *Journal of Organometallic Chemistry*, 2002, **653**, 46-49.
149. C.-L. Ho, Z.-Q. Yu and W.-Y. Wong, *Chemical Society Reviews*, 2016, **45**, 5264-5295.
150. J. Xiang, C. L. Ho and W. Y. Wong, *Polymer Chemistry*, 2015, **6**, 6905-6930.
151. S. Mehdipour-Ataei and S. Babanzadeh, *Applied Organometallic Chemistry*, 2007, **21**, 360-367.
152. M. S. U. Khan, A. Nigar, M. A. Bashir and Z. Akhter, *Synthetic Communications*, 2007, **37**, 473-482.
153. L. Liu, C. L. Ho, W. Y. Wong, K. Y. Cheung, M. K. Fung, W. T. Lam, A. B. Djurisic and W. K. Chan, *Advanced Functional Materials*, 2008, **18**, 2824-2833.
154. S. Y. Lu and I. Hamerton, *Progress in Polymer Science*, 2002, **27**, 1661-1712.
155. E. D. Weil, S. V. Levchik, M. Ravey and W. M. Zhu, *Phosphorus Sulfur and Silicon and the Related Elements*, 1999, **144**, 17-20.
156. K. S. Annakutty and K. Kishore, *Polymer*, 1988, **29**, 1273-1276.
157. T. Steinbach and F. R. Wurm, *Angewandte Chemie-International Edition*, 2015, **54**, 6098-6108.
158. E. M. Alexandrino, S. Ritz, F. Marsico, G. Baier, V. Mailander, K. Landfester and F. R. Wurm, *Journal of Materials Chemistry B*, 2014, **2**, 1298-1306.
159. S. W. Huang, J. Wang, P. C. Zhang, H. Q. Mao, R. X. Zhuo and K. W. Leong, *Biomacromolecules*, 2004, **5**, 306-311.
160. X. Y. Xu, H. Yu, S. J. Gao, H. Q. Mao, K. W. Leong and S. Wang, *Biomaterials*, 2002, **23**, 3765-3772.
161. J. Wang, H. Q. Mao and K. W. Leong, *Journal of the American Chemical Society*, 2001, **123**, 9480-9481.
162. K. S. Annakutty and K. Kishore, *Polymer*, 1988, **29**, 756-761.
163. K. Kishore, K. S. Annakutty and I. M. Mallick, *Polymer*, 1988, **29**, 762-764.
164. O. Ayhan, N. A. Riensch, C. Glasmacher and H. Helten, *Chemistry-a European Journal*, 2018, **24**, 5883-5894.
165. O. Ayhan, T. Eckert, F. A. Plamper and H. Helten, *Angewandte Chemie – International Edition*, 2016, **55**, 13321-13325.
166. T. Lorenz, M. Crumbach, T. Eckert, A. Lik and H. Helten, *Angewandte Chemie – International Edition*, 2017, **56**, 2780-2784.
167. T. Lorenz, A. Lik, F. A. Plamper and H. Helten, *Angewandte Chemie – International Edition*, 2016, **55**, 7236-7241.
168. A. Lik, L. Fritze, L. Müller and H. Helten, *Journal of the American Chemical Society*, 2017, **139**, 5692-5695.
169. A. Sundararaman, M. Victor, R. Varughese and F. Jäkle, *Journal of the American Chemical Society*, 2005, **127**, 13748-13749.
170. K. Kucinski and G. Hreczycho, *ChemCatChem*, 2017, **9**, 1868-1885.
171. F. Gauvin, J. F. Harrod and H. G. Woo, *Advances in Organometallic Chemistry*, 1998, **42**, 363-405.
172. E. M. Leitao, T. Jurca and I. Manners, *Nature Chemistry*, 2013, **5**, 817-829.
173. R. Waterman, *Chemical Society Reviews*, 2013, **42**, 5629-5641.
174. T. J. Clark, K. Lee and I. Manners, *Chemistry - A European Journal*, 2006, **12**, 8634-8648.
175. B. H. Kim, M. S. Cho and H. G. Woo, *Synlett*, 2004, 761-772.

176. A. R. McWilliams, H. Dorn and I. Manners, *New Aspects in Phosphorus Chemistry*, 2002, **220**, 141-167.
177. R. L. Melen, *Chemical Society Reviews*, 2016, **45**, 775-788.
178. J. M. Blackwell, K. L. Foster, V. H. Beck and W. E. Piers, *Journal of Organic Chemistry*, 1999, **64**, 4887-4892.
179. M. Perez, C. B. Caputo, R. Dobrovetsky and D. W. Stephan, *Proceedings of the National Academy of Sciences of the United States of America*, 2014, **111**, 10917-10921.
180. C. B. Caputo and D. W. Stephan, *Abstracts of Papers of the American Chemical Society*, 2014, **248**.
181. L. P. Wu, S. S. Chitnis, H. J. Jiao, V. T. Annibale and I. Manners, *Journal of the American Chemical Society*, 2017, **139**, 16780-16790.
182. D. W. Stephan, *Organic & Biomolecular Chemistry*, 2008, **6**, 1535-1539.
183. J. S. J. McCahill, G. C. Welch and D. W. Stephan, *Angewandte Chemie-International Edition*, 2007, **46**, 4968-4971.
184. G. C. Welch, R. R. S. Juan, J. D. Masuda and D. W. Stephan, *Science*, 2006, **314**, 1124-1126.
185. R. Waterman, *Current Organic Chemistry*, 2008, **12**, 1322-1339.
186. R. Waterman, *Organometallics*, 2007, **26**, 2492-2494.
187. N. R. Neale and T. D. Tilley, *Journal of the American Chemical Society*, 2002, **124**, 3802-3803.
188. N. R. Neale and T. D. Tilley, *Tetrahedron*, 2004, **60**, 7247-7260.
189. A. J. Roering, J. J. Davidson, S. N. MacMillan, J. M. Tanski and R. Waterman, *Dalton Transactions*, 2008, 4488-4498.
190. R. Waterman and T. D. Tilley, *Angewandte Chemie-International Edition*, 2006, **45**, 2926-2929.
191. J. Guihaume, C. Raynaud, O. Eisenstein, L. Perrin, L. Maron and T. D. Tilley, *Angewandte Chemie-International Edition*, 2010, **49**, 1816-1819.
192. A. Rossin and M. Peruzzini, *Chemical Reviews*, 2016, **116**, 8848-8872.
193. C. W. Hamilton, R. T. Baker, A. Staubitz and I. Manners, *Chemical Society Reviews*, 2009, **38**, 279-293.
194. A. Staubitz, A. P. M. Robertson and I. Manners, *Chemical Reviews*, 2010, **110**, 4079-4124.
195. H. Dorn, R. A. Singh, J. A. Massey, J. M. Nelson, C. A. Jaska, A. J. Lough and I. Manners, *Journal of the American Chemical Society*, 2000, **122**, 6669-6678.
196. C. Marquardt, T. Jurca, K. C. Schwan, A. Stauber, A. V. Virovets, G. R. Whittell, I. Manners and M. Scheer, *Angewandte Chemie-International Edition*, 2015, **54**, 13782-13786.
197. A. Schäfer, T. Jurca, J. Turner, J. R. Vance, K. Lee, V. A. Du, M. F. Haddow, G. R. Whittell and I. Manners, *Angewandte Chemie - International Edition*, 2015, **54**, 4836-4841.
198. U. S. D. Paul, H. Braunschweig and U. Radius, *Chemical Communications*, 2016, **52**, 8573-8576.
199. J. R. Turner, D. A. Resendiz-Lara, T. Jurca, A. Schäfer, J. R. Vance, L. Beckett, G. R. Whittell, R. A. Musgrave, H. A. Sparkes and I. Manners, *Macromolecular Chemistry and Physics*, 2017, **128**, 1700120.
200. H. Dorn, R. A. Singh, J. A. Massey, J. M. Nelson, C. A. Jaska, A. J. Lough and I. Manners, *Journal of the American Chemical Society*, 2000, **122**, 6669-6678.
201. H. Dorn and I. Manners, *Phosphorus Sulfur and Silicon and the Related Elements*, 2001, **168**, 185-190.
202. C. A. Jaska, K. Temple, A. J. Lough and I. Manners, *Journal of the American Chemical Society*, 2003, **125**, 9424-9434.
203. A. Staubitz, M. E. Sloan, A. P. M. Robertson, A. Friedrich, S. Schneider, P. J. Gates, J. Gunne and I. Manners, *Journal of the American Chemical Society*, 2010, **132**, 13332-13345.

204. G. M. Adams, A. L. Colebatch, J. T. Skornia, A. I. McKay, H. C. Johnson, G. C. Lloyd-Jones, S. A. Macgregor, N. A. Beattie and A. S. Weller, *Journal of the American Chemical Society*, 2018, **140**, 1481-1495.
205. H. Helten, A. P. M. Robertson, A. Staubitz, J. R. Vance, M. F. Haddow and I. Manners, *Chemistry-a European Journal*, 2012, **18**, 4665-4680.
206. D. A. Resendiz-Lara, N. E. Stubbs, M. I. Arz, N. E. Pridmore, H. A. Sparkes and I. Manners, *Chemical Communications*, 2017, **53**, 11701-11704.
207. H. Helten, B. Dutta, J. R. Vance, M. E. Sloan, M. F. Haddow, S. Sproules, D. Collison, G. R. Whittell, G. C. Lloyd-Jones and I. Manners, *Angewandte Chemie-International Edition*, 2013, **52**, 437-440.
208. H. C. Johnson, E. M. Leitao, G. R. Whittell, I. Manners, G. C. Lloyd-Jones and A. S. Weller, *Journal of the American Chemical Society*, 2014, **136**, 9078-9093.
209. T. N. Hooper, A. S. Weller, N. A. Beattie and S. A. Macgregor, *Chemical Science*, 2016, **7**, 2414-2426.
210. T. N. Hooper, M. A. Huertos, T. Jurca, S. D. Pike, A. S. Weller and I. Manners, *Inorganic Chemistry*, 2014, **53**, 3716-3729.
211. X. Z. Zheng, J. S. Huang, Y. M. Yao and X. Xu, *Chemical Communications*, 2019, **55**, 9152-9155.
212. T. Jurca, T. Dellermann, N. E. Stubbs, D. A. Resendiz-Lara, G. R. Whittell and I. Manners, *Chemical Science*, 2018, **9**, 3360-3366.
213. Y. Luo and K. Ohno, *Organometallics*, 2007, **26**, 3597-3600.
214. D. Pun, E. Lobkovsky and P. J. Chirik, *Chemical Communications*, 2007, 3297-3299.
215. D. J. Liptrot, M. S. Hill, M. F. Mahon and D. J. MacDougall, *Chemistry - A European Journal*, 2010, **16**, 8508-8515.
216. P. Bellham, M. D. Anker, M. S. Hill, G. Kociok-Köhn and M. F. Mahon, *Dalton Transactions*, 2016, **45**, 13969-13978.
217. C. A. D. Pinheiro, C. Roiland, P. Jehan and G. Alcaraz, *Angewandte Chemie-International Edition*, 2018, **57**, 1519-1522.
218. C. Marquardt, G. Balazs, J. Baumann, A. Virovets and M. Scheer, *Chemistry - A European Journal*, 2017, **23**, 11423-11429.
219. O. Hegen, A. V. Virovets, A. Y. Timoshkin and M. Scheer, *Chemistry-a European Journal*, 2018, **24**, 16521-16525.
220. C. Marquardt, T. Jurca, K. C. Schwan, A. Stauber, A. V. Virovets, G. R. Whittell, I. Manners and M. Scheer, *Angewandte Chemie - International Edition*, 2015, **54**, 13782-13786.
221. N. L. Oldroyd, S. S. Chitnis, V. T. Annibale, M. I. Arz, H. A. Sparkes and I. Manners, *Nature Communications*, 2019, **10**, 1370.
222. M. Westerhausen, *Angewandte Chemie-International Edition*, 2008, **47**, 2185-2187.
223. S. P. Green, C. Jones and A. Stasch, *Science*, 2007, **318**, 1754-1757.
224. S. Krieck, H. Gorls, L. Yu, M. Reiher and M. Westerhausen, *Journal of the American Chemical Society*, 2009, **131**, 2977-2985.
225. R. D. Shannon, *Acta Crystallographica Section A*, 1976, **32**, 751-767.
226. M. H. Chisholm, J. Gallucci and K. Phomphrai, *Chemical Communications*, 2003, 48-49.
227. M. H. Chisholm, J. C. Gallucci and K. Phomphrai, *Inorganic Chemistry*, 2004, **43**, 6717-6725.
228. S. Harder and J. Brettar, *Angewandte Chemie-International Edition*, 2006, **45**, 3474-3478.
229. S. Sarish, S. Nembenna, S. Nagendran, H. W. Roesky, A. Pal, R. Herbst-Irmer, A. Ringe and J. Magull, *Inorganic Chemistry*, 2008, **47**, 5971-5977.
230. M. R. Crimmin, M. Arrowsmith, A. G. M. Barrett, I. J. Casely, M. S. Hill and P. A. Procopiou, *Journal of the American Chemical Society*, 2009, **131**, 9670-9685.
231. A. G. M. Barrett, I. J. Casely, M. R. Crimmin, M. S. Hill, J. R. Lachs, M. F. Mahon and P. A. Procopiou, *Inorganic Chemistry*, 2009, **48**, 4445-4453.

232. M. R. Crimmin, M. S. Hill, P. B. Hitchcock and M. F. Mahon, *New Journal of Chemistry*, 2010, **34**, 1572-1578.
233. M. Arrowsmith, M. R. Crimmin, A. G. M. Barrett, M. S. Hill, G. Kociok-Köhn and P. A. Procopiou, *Organometallics*, 2011, **30**, 1493-1506.
234. C. Jones, S. J. Bonyhady, S. Nembenna and A. Stasch, *European Journal of Inorganic Chemistry*, 2012, 2596-2601.
235. A. S. S. Wilson, M. S. Hill, M. F. Mahon, C. Dinoi and L. Maron, *Science*, 2017, **358**, 1168-1171.
236. A. S. S. Wilson, M. S. Hill and M. F. Mahon, *Organometallics*, 2019, **38**, 351-360.
237. T. X. Gentner, B. Rosch, K. Thum, J. Langer, G. Ballmann, J. Pahl, W. A. Donaubauer, F. Hampel and S. Harder, *Organometallics*, 2019, **38**, 2485-2493.
238. B. Rosch, T. X. Gentner, H. Elsen, C. A. Fischer, J. Langer, M. Wiesinger and S. Harder, *Angewandte Chemie-International Edition*, 2019, **58**, 5396-5401.
239. P. Jochmann, J. P. Davin, T. P. Spaniol, L. Maron and J. Okuda, *Angewandte Chemie-International Edition*, 2012, **51**, 4452-4455.
240. V. Leich, T. P. Spaniol, L. Maron and J. Okuda, *Angewandte Chemie-International Edition*, 2016, **55**, 4794-4797.
241. D. Mukherjee, S. Shirase, K. Beckerle, T. P. Spaniol, K. Mashima and J. Okuda, *Dalton Transactions*, 2017, **46**, 8451-8457.
242. D. Schuhknecht, C. Lhotzky, T. P. Spaniol, L. Maron and J. Okuda, *Angewandte Chemie-International Edition*, 2017, **56**, 12367-12371.
243. S. Banerjee, Ankur, A. Andrews and A. Venugopal, *Chemical Communications*, 2018, **54**, 5788-5791.
244. J. S. Wixey and B. D. Ward, *Dalton Transactions*, 2011, **40**, 7693-7696.
245. S. Datta, M. T. Gamer and P. W. Roesky, *Organometallics*, 2008, **27**, 1207-1213.
246. S. Datta, P. W. Roesky and S. Blechert, *Organometallics*, 2007, **26**, 4392-4394.
247. A. G. M. Barrett, M. R. Crimmin, M. S. Hill, P. B. Hitchcock, G. Kociok-Köhn and P. A. Procopiou, *Inorganic Chemistry*, 2008, **47**, 7366-7376.
248. B. Liu, T. Roisnel, J. F. Carpentier and Y. Sarazin, *Angewandte Chemie-International Edition*, 2012, **51**, 4943-4946.
249. J. F. Dunne, S. R. Neal, J. Engelkemier, A. Ellern and A. D. Sadow, *Journal of the American Chemical Society*, 2011, **133**, 16782-16785.
250. M. Arrowsmith, M. S. Hill and G. Kociok-Köhn, *Organometallics*, 2009, **28**, 1730-1738.
251. M. Arrowsmith, A. Heath, M. S. Hill, P. B. Hitchcock and G. Kociok-Köhn, *Organometallics*, 2009, **28**, 4550-4559.
252. A. G. M. Barrett, C. Brinkmann, M. R. Crimmin, M. S. Hill, P. Hunt and P. A. Procopiou, *Journal of the American Chemical Society*, 2009, **131**, 12906-12907.
253. M. R. Crimmin, I. J. Casely and M. S. Hill, *Journal of the American Chemical Society*, 2005, **127**, 2042-2043.
254. B. Liu, T. Roisnel, J. F. Carpentier and Y. Sarazin, *Chemistry-a European Journal*, 2013, **19**, 13445-13462.
255. B. Liu, T. Roisnel, J. F. Carpentier and Y. Sarazin, *Chemistry-a European Journal*, 2013, **19**, 2784-2802.
256. J. R. Lachs, A. G. M. Barrett, M. R. Crimmin, G. Kociok-Köhn, M. S. Hill, M. F. Mahon and P. A. Procopiou, *European Journal of Inorganic Chemistry*, 2008, 4173-4179.
257. A. Baishya, M. K. Barman, T. Peddarao and S. Nembenna, *Journal of Organometallic Chemistry*, 2014, **769**, 112-118.
258. M. R. Crimmin, A. G. M. Barrett, M. S. Hill, P. B. Hitchcock and P. A. Procopiou, *Organometallics*, 2007, **26**, 2953-2956.
259. T. M. A. Al-Shboul, H. Gorls and M. Westerhausen, *Inorganic Chemistry Communications*, 2008, **11**, 1419-1421.
260. M. R. Crimmin, A. G. M. Barrett, M. S. Hill, P. B. Hitchcock and P. A. Procopiou, *Organometallics*, 2008, **27**, 497-499.
261. C. Brinkmann, A. G. M. Barrett, M. S. Hill, P. A. Procopiou and S. Reidt, *Organometallics*, 2012, **31**, 7287-7297.

262. C. Weetman, M. S. Hill and M. F. Mahon, *Chemistry-a European Journal*, 2016, **22**, 7158-7162.
263. C. Weetman, M. D. Anker, M. Arrowsmith, M. S. Hill, G. Kociok-Köhn, D. J. Liptrot and M. F. Mahon, *Chemical Science*, 2016, **7**, 628-641.
264. C. Weetman, M. S. Hill and M. F. Mahon, *Polyhedron*, 2016, **103**, 115-120.
265. C. Weetman, M. S. Hill and M. F. Mahon, *Chemical Communications*, 2015, **51**, 14477-14480.
266. M. Arrowsmith, M. S. Hill and G. Kociok-Köhn, *Chemistry-a European Journal*, 2013, **19**, 2776-2783.
267. M. Arrowsmith, T. J. Hadlington, M. S. Hill and G. Kociok-Köhn, *Chemical Communications*, 2012, **48**, 4567-4569.
268. F. Buch, H. Brettar and S. Harder, *Angewandte Chemie-International Edition*, 2006, **45**, 2741-2745.
269. M. S. Hill, D. J. Liptrot and C. Weetman, *Chemical Society Reviews*, 2016, **45**, 972-988.
270. L. Garcia, C. Dinoi, M. F. Mahon, L. Maron and M. Hill, *Chemical Science*, 2019, **10**, 8108-8118.
271. S. Brand, H. Elsen, J. Langer, S. Grams and S. Harder, *Angewandte Chemie - International Edition*, 2019, Advance article, doi: 10.1002/anie.201908978.
272. L. Garcia, M. D. Anker, M. F. Mahon, L. Maron and M. S. Hill, *Dalton Transactions*, 2018, **47**, 12684-12693.
273. A. Friedrich, J. Pahl, H. Elsen and S. Harder, *Dalton Transactions*, 2019, **48**, 5560-5568.
274. J. Pahl, A. Friedrich, H. Eisen and S. Harder, *Organometallics*, 2018, **37**, 2901-2909.
275. J. Pahl, S. Brand, H. Elsen and S. Harder, *Chemical Communications*, 2018, **54**, 8685-8688.
276. S. Brand, H. Elsen, J. Langer, W. A. Donaubauer, F. Hampel and S. Harder, *Angewandte Chemie-International Edition*, 2018, **57**, 14169-14173.
277. W. L. Xie, H. F. Hu and C. M. Cui, *Angewandte Chemie-International Edition*, 2012, **51**, 11141-11144.
278. A. E. Nako, W. Y. Chen, A. J. P. White and M. R. Crimmin, *Organometallics*, 2015, **34**, 4369-4375.
279. N. Li and B. T. Guan, *Advanced Synthesis & Catalysis*, 2017, **359**, 3526-3531.
280. A. Pindwal, A. Ellern and A. D. Sadow, *Organometallics*, 2016, **35**, 1674-1683.
281. J. X. Wang, A. K. Dash, J. C. Berthet, M. Ephritikhine and M. S. Eisen, *Journal of Organometallic Chemistry*, 2000, **610**, 49-57.
282. P. Rios, M. Rosello-Merino, O. Rivada-Wheelagham, J. Borge, J. Lopez-Serrano and S. Conejero, *Chemical Communications*, 2018. **54**, 619-622.
283. C. D. F. Konigs, M. F. Muller, N. Aiguabella, H. F. T. Klare and M. Oestreich, *Chemical Communications*, 2013, **49**, 1506-1508.
284. W. D. Wang and R. Eisenberg, *Organometallics*, 1991, **10**, 2222-2227.
285. H. Q. Liu and J. F. Harrod, *Canadian Journal of Chemistry-Revue Canadienne De Chimie*, 1992, **70**, 107-110.
286. H. Q. Liu and J. F. Harrod, *Organometallics*, 1992, **11**, 822-827.
287. S. Anga, Y. Sarazin, J. F. Carpentier and T. K. Panda, *ChemCatChem*, 2016, **8**, 1373-1378.
288. L. Greb, S. Tamke and J. Paradies, *Chemical Communications*, 2014, **50**, 2318-2320.
289. L. K. Allen, R. Garcia-Rodriguez and D. S. Wright, *Dalton Transactions*, 2015, **44**, 12112-12118.
290. J. F. Blandez, I. Esteve-Adell, M. Alvaro and H. Garcia, *Catalysis Science & Technology*, 2015, **5**, 2167-2173.
291. T. Mitsudome, T. Urayama, Z. Maeno, T. Mizugaki, K. Jitsukawa and K. Kaneda, *Chemistry-a European Journal*, 2015, **21**, 3202-3205.

292. R. J. P. Corriu, D. Leclercq, P. H. Mutin, J. M. Planeix and A. Vioux, *Journal of Organometallic Chemistry*, 1991, **406**, C1-C4.
293. F. Buch and S. Harder, *Organometallics*, 2007, **26**, 5132-5135.
294. M. S. Hill, D. J. Liptrot, D. J. MacDougall, M. F. Mahon and T. P. Robinson, *Chemical Science*, 2013, **4**, 4212-4222.
295. C. Bellini, C. Orione, J. F. Carpentier and Y. Sarazin, *Angewandte Chemie - International Edition*, 2016, **55**, 3744-3748.
296. C. Bellini, T. Roisnel, J. F. Carpentier, S. Tobisch and Y. Sarazin, *Chemistry - A European Journal*, 2016, **22**, 15733-15743.
297. C. Bellini, V. Dorcet, J. F. Carpentier, S. Tobisch and Y. Sarazin, *Chemistry - A European Journal*, 2016, **22**, 4564-4583.
298. C. Bellini, J.-F. Carpentier, S. Tobisch and Y. Sarazin, *Angewandte Chemie – International Edition*, 2015, **54**, 7679-7683.
299. A. Baishya, T. Peddarao and S. Nembenna, *Dalton Transactions*, 2017, **46**, 5880-5887.
300. M. Rauch, R. C. Roberts and G. Parkin, *Inorganica Chimica Acta*, 2019, **494**, 271-279.
301. E. Le Coz, V. Dorcet, T. Roisnel, S. Tobisch, J. F. Carpentier and Y. Sarazin, *Angewandte Chemie-International Edition*, 2018, **57**, 11747-11751.
302. J. F. Dunne, S. R. Neal, J. Engelkemier, A. Ellern and A. D. Sadow, *Journal of the American Chemical Society*, 2011, **133**, 16782-16785.
303. E. Le Coz, S. Kahlal, J.-Y. Saillard, T. Roisnel, V. Dorcet, J.-F. Carpentier and Y. Sarazin, *Chemistry - A European Journal*, 2019, Advance article, doi: 10.1002/chem.201903676.
304. A. Harinath, J. Bhattacharjee, S. Anga and T. K. Panda, *Australian Journal of Chemistry*, 2017, **70**, 724-730.
305. D. Mukherjee, R. R. Thompson, A. Ellern and A. D. Sadow, *ACS Catalysis*, 2011, **1**, 698-702.
306. A. G. M. Barrett, M. R. Crimmin, M. S. Hill, P. B. Hitchcock, S. L. Lomas, M. F. Mahon, P. A. Procopiou and K. Suntharalingam, *Organometallics*, 2008, **27**, 6300-6306.
307. D. J. Liptrot, M. S. Hill, M. F. Mahon and A. S. S. Wilson, *Angewandte Chemie - International Edition*, 2015, **54**, 13362-13365.
308. D. J. Liptrot, M. Arrowsmith, A. L. Colebatch, T. J. Hadlington, M. S. Hill, G. Kociok-Kohn and M. F. Mahon, *Angewandte Chemie*, 2015, **54**, 15280-15283.
309. A. S. S. Wilson, C. Dinoi, M. S. Hill, M. F. Mahon and L. Maron, *Angewandte Chemie-International Edition*, 2018, **57**, 15500-15504.
310. H. Bauer, K. Thum, M. Alonso, C. Fischer and S. Harder, *Angewandte Chemie-International Edition*, 2019, **58**, 4248-4253.
311. H. Bauer, M. Alonso, C. Fischer, B. Rosch, H. Elsen and S. Harder, *Angewandte Chemie-International Edition*, 2018, **57**, 15177-15182.
312. M. S. Hill, M. F. Mahon and T. P. Robinson, *Chemical Communications*, 2010, **46**, 2498-2500.
313. D. J. Liptrot, PhD Thesis, University of Bath, 2014.
314. J. Spielmann, G. Jansen, H. Bandmann and S. Harder, *Angewandte Chemie - International Edition*, 2008, **47**, 6290-6295.
315. J. Spielmann and S. Harder, *Journal of the American Chemical Society*, 2009, **131**, 5064-5065.
316. J. Spielmann, M. Bolte and S. Harder, *Chemical Communications*, 2009, 6934.
317. J. Spielmann, D. F. J. Piesik and S. Harder, *Chemistry-a European Journal*, 2010, **16**, 8307-8318.
318. D. J. Liptrot, M. S. Hill, M. F. Mahon and D. J. MacDougall, *Chemistry-a European Journal*, 2010, **16**, 8508-8515.
319. P. Bellham, M. S. Hill, D. J. Liptrot, D. J. MacDougall and M. F. Mahon, *Chemical Communications*, 2011, **47**, 9060.
320. M. S. Hill, M. Hodgson, D. J. Liptrot and M. F. Mahon, *Dalton Transactions*, 2011, **40**, 7783-7790.

321. S. Harder, J. Spielmann and B. Tobey, *Chemistry-a European Journal*, 2012, **18**, 1984-1991.
322. P. Bellham, M. S. Hill, G. Kociok-Köhn and D. J. Liptrot, *Dalton Transactions*, 2013, 737-745.
323. P. Bellham, M. S. Hill, G. Kociok-Köhn and D. J. Liptrot, *Chemical Communications*, 2013, **49**, 1960-1962.
324. A. C. A. Ried, L. J. Taylor, A. M. Geer, H. E. L. Williams, W. Lewis, A. J. Blake and D. L. Kays, *Chemistry-a European Journal*, 2019, **25**, 6840-6846.
325. K. Izod, J. M. Watson, S. M. El-Hamruni, R. W. Harrington and P. G. Waddell, *Organometallics*, 2017, **36**, 2218-2227.

2 Ferrocene-Containing Polycarbosilazanes *via* the Alkaline-Earth Catalysed Dehydrocoupling of Silanes and Amines

2.1 Introduction

The ring opening polymerisation (ROP) of strained ferrocenophanes can be a highly effective method for metallopolymer synthesis (see Chapter 1, Section 1.2.2). Structural variation can be achieved by varying the spacer and sidechains,[1-3] but the prerequisite strained ferrocenophane monomer precludes access towards polymer architectures such as alternating sequences or longer inter-ferrocene bridges. A polycondensation approach would circumvent these limitations, but requires precise stoichiometry and a highly efficient element-element (E–E) bond forming reaction to reach high monomer conversions and high polymer molecular weights.[4, 5]

Although dehydrocoupling is a promising approach for metallopolymer synthesis, examples of its use in the preparation of ferrocene-containing polymers are limited to two examples, both dependant on rhodium catalysis. A low molecular weight polyferrocenylthioether (**P-XXXI**) reported by Yamamoto and co-workers,[6] and pendent-ferrocene containing polyphosphinoboranes (**P-XXXIIa, b**), reported by the Hey-Hawkins group (Scheme 2.1).[7]

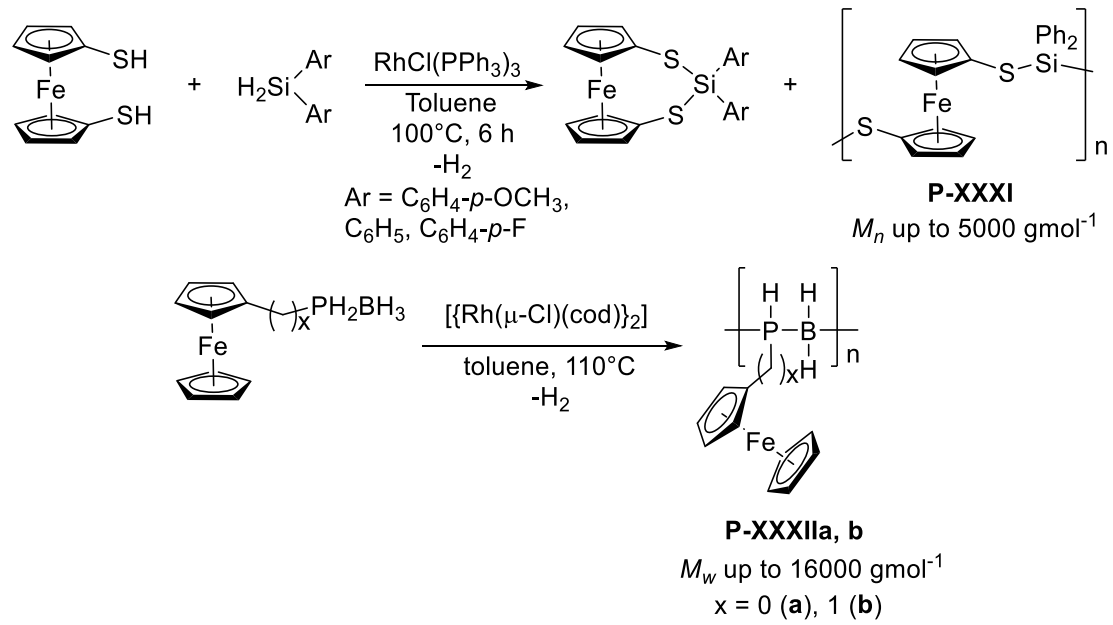

Scheme 2.1 Ferrocene-containing polymers synthesised *via* catalytic dehydrocoupling.[6, 7]

The alkaline-earth (Ae) catalysed dehydrocoupling of silanes and amines has been thoroughly studied with a wide array of pre-catalysts.[8-16] In particular, the groups of Hill,[12] and Sarazin[14-16] have demonstrated that homoleptic bis-amides $[M\{N(SiMe_3)_2\}_2]_2$ (**Ia**-**d**), $[M\{N(SiMe_3)_2\}_2.(THF)_2]$ (**IIb**-**d**) and bis-alkyls $[M\{CH(SiMe_3)_2\}_2.(THF)_2]$ (**IIIb**-**d**) (M = Mg (**a**), Ca (**b**), Sr (**c**), Ba (**d**)) are particularly effective pre-catalysts and have the advantage of avoiding complex ligands and lengthy syntheses. Since this catalysis is well understood, and has the proven capability of specifically forming Si-N bonds in high yields, it is an ideal candidate for the preparation of polysilazanes or polycarbosilazanes *via* a dehydrocoupling, polycondensation route. This potential was recently realised by Sarazin and co-workers, who utilised pre-catalyst **IIId** to yield soluble linear (**P-XXX**) or cyclic polycarbosilazanes (**P-XXX'**) from diphenylsilane and *p*-xylylenediamine monomers (Scheme 2.2).[13] Building on this work, the use of ferrocene-containing silanes and/or amines could in principle, lead to previously unexplored metallo-polycarbosilazanes. Our efforts to pursue this concept are described henceforth.

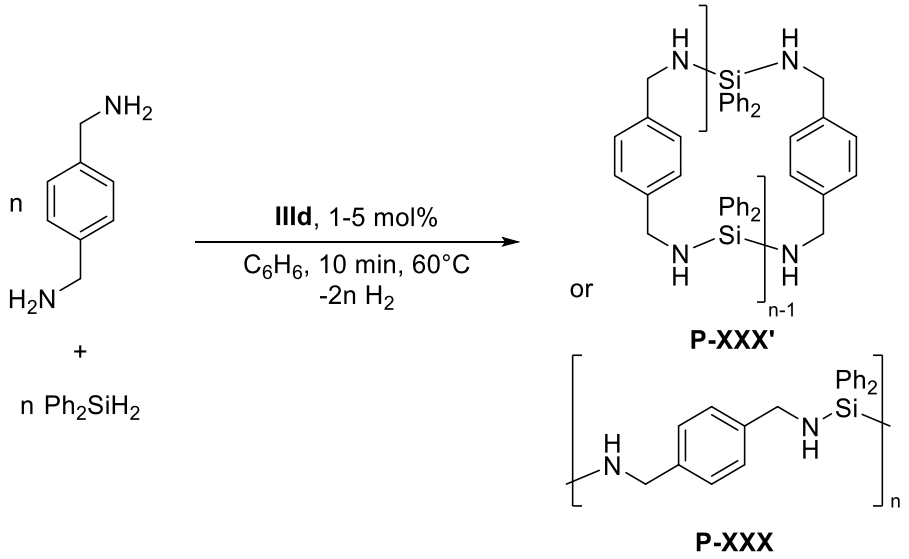

Scheme 2.2 The barium catalysed dehydrocoupling of *p*-xylylenediamine and diphenylsilane to yield cyclic or linear polycarbosilazanes, as reported by Sarazin and co-workers.[13]

2.2 Results and discussion

2.2.1 Catalytic dehydrocoupling of compound 1 with benzyl amine.

In the knowledge that diphenylsilane was a suitable monomer for polycarbosilazane formation *via* dehydrocoupling, an organometallic analogue, $Fc(SiPhH_2)$ (**1**) was prepared from lithioferrocene and phenylchlorosilane. The product was purified by sublimation, yielding single crystals, from which the compound's structure was confirmed by X-ray diffraction (Figure 2.1).

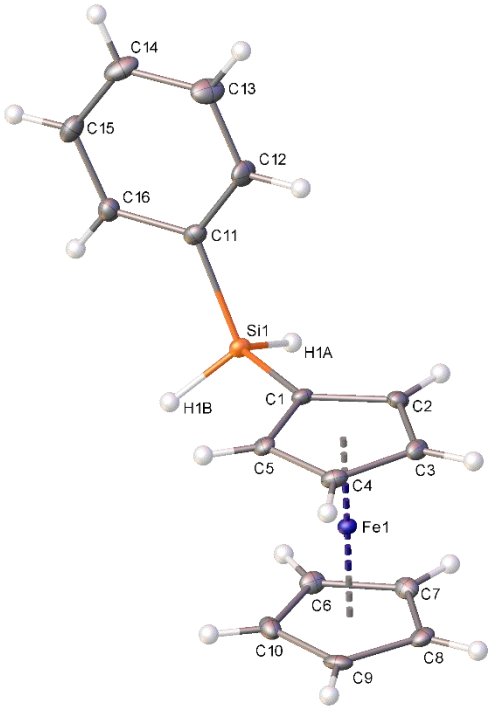

Figure 2.1 X-ray crystal structure of compound **1**. Thermal ellipsoids are shown at the 30% probability level.

As a model reaction, compound **1** was subjected to dehydrocoupling with two equivalents of benzylamine and 5 mol% **IIb** (Scheme 2.3). After 30 minutes at room temperature, 50% conversion of the starting materials was accomplished. On heating at 60°C for a further 16 hours, the bis-coupled product **2** was obtained in quantitative spectroscopic yield (Scheme 2.3).

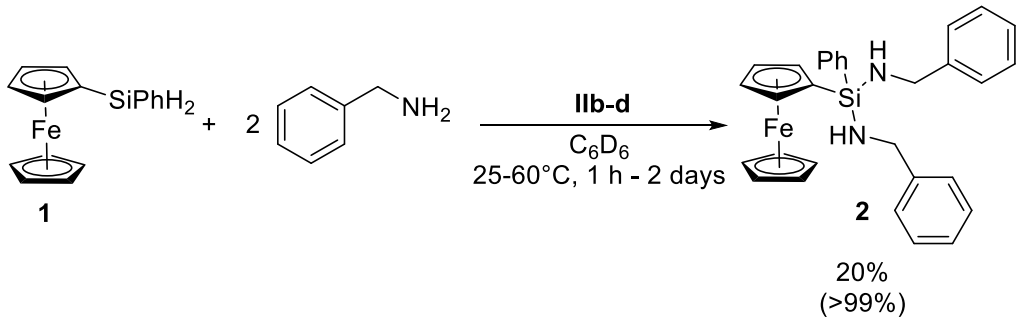

Scheme 2.3 The Ae-catalysed dehydrocoupling reaction of compound **1** and benzylamine to give compound **2**. The spectroscopic yield is shown in parentheses and was determined by ^{1}H NMR spectroscopy of the crude reaction mixture.

Compound **2** crystallised as pale-orange needles in the orthorhombic space group, *Pbcn*, by slow evaporation of a toluene solution (Figure 2.2). The reaction time could be reduced to 20 minutes under strontium or barium catalysis (5 mol% of **IIc** or **IId**), achieving quantitative spectroscopic yield of **2** at room temperature. The increase in reaction rate on descending group two of the periodic table is a common feature in Ae-catalysis and is attributed to an increase in ionic radius, polarizability, and electropositivity.[12, 15, 16] Although the homoleptic Ae-alkyl complexes (**IIIb**-**d**) have been demonstrated to provide increased rates relative to their amide congeners,[16] the amides **IIb**-**d** meet the requirements for quantitative Si-N bond formation and are less synthetically demanding. For this reason, further catalysis described within this chapter makes use of the barium amide pre-catalyst, **IId**, unless otherwise specified**.**

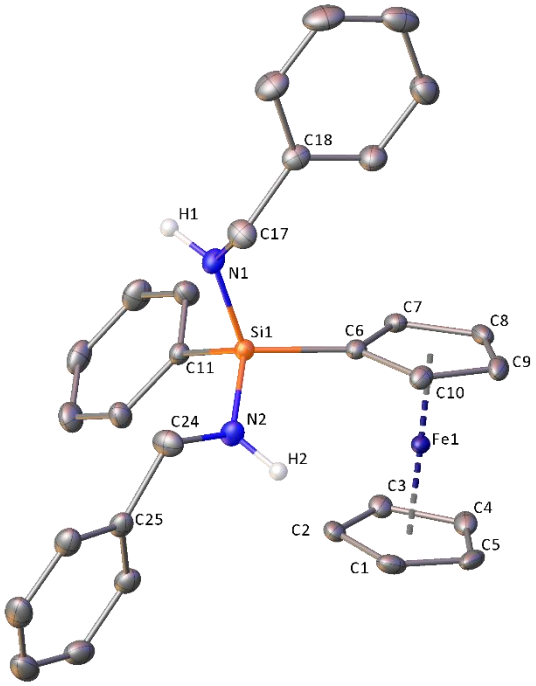

Figure 2.2 X-ray crystal structure of compound **2**. Thermal ellipsoids are shown at the 30% probability level. Hydrogen atoms are omitted for clarity except for those bound to nitrogen.

2.2.2 Synthesis and characterisation of polycarbosilazanes with ferrocene pendent to the main-chain.

Having established that **IId** catalyses the quantitative dehydrocoupling of monomer **1** with two equivalents of benzyl amine, the bifunctional amine 1,4-$(H_2NCH_2)_2C_6H_4$ was investigated as a comonomer. Equimolar quantities of **1** and 1,4-$(H_2NCH_2)_2C_6H_4$ were dehydrocoupled in toluene using 5 mol% **IId** with immediate and vigorous release of hydrogen gas. After stirring at 60°C for two hours to ensure full conversion, the reaction mixture was precipitated into

pentane at -78°C. The solution was decanted, and after prolonged vacuum drying a pale-orange solid (**P1**) was obtained (Scheme 2.4). Analysis by ^{1}H NMR spectroscopy was consistent with the formation of two new Si-N bonds per molecule of **1** to provide a polymer with a polycarbosilazane backbone and pendent ferrocene groups. Although cyclic products cannot be ruled out, a lack of Si-H resonances discounts the possibility of silane-terminated linear polymers. Two well-defined resonances at δ 3.61 and 0.77 ppm, however, were assigned to chain-end CH_2 and NH_2 groups, respectively, allowing the average degree of polymerisation ($X_{n,\ end\ group}$) to be estimated by integration relative to the respective mid-chain resonances at δ 4.37-4.07 (CH_2) and 1.49 ppm (NH_2) (Figure 2.3). Hence with $X_{n,\ end\ group}$ = 22, an estimated molecular weight ($M_{n,\ end\ group}$) of ~10000 Da was determined (Table 2.1, **P1**).

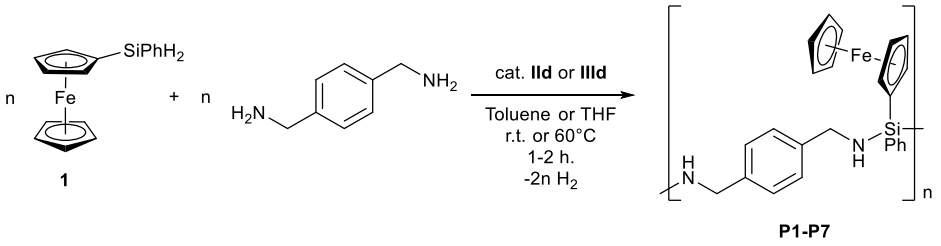

Scheme 2.4 Synthesis of polymers **P1-P7**.

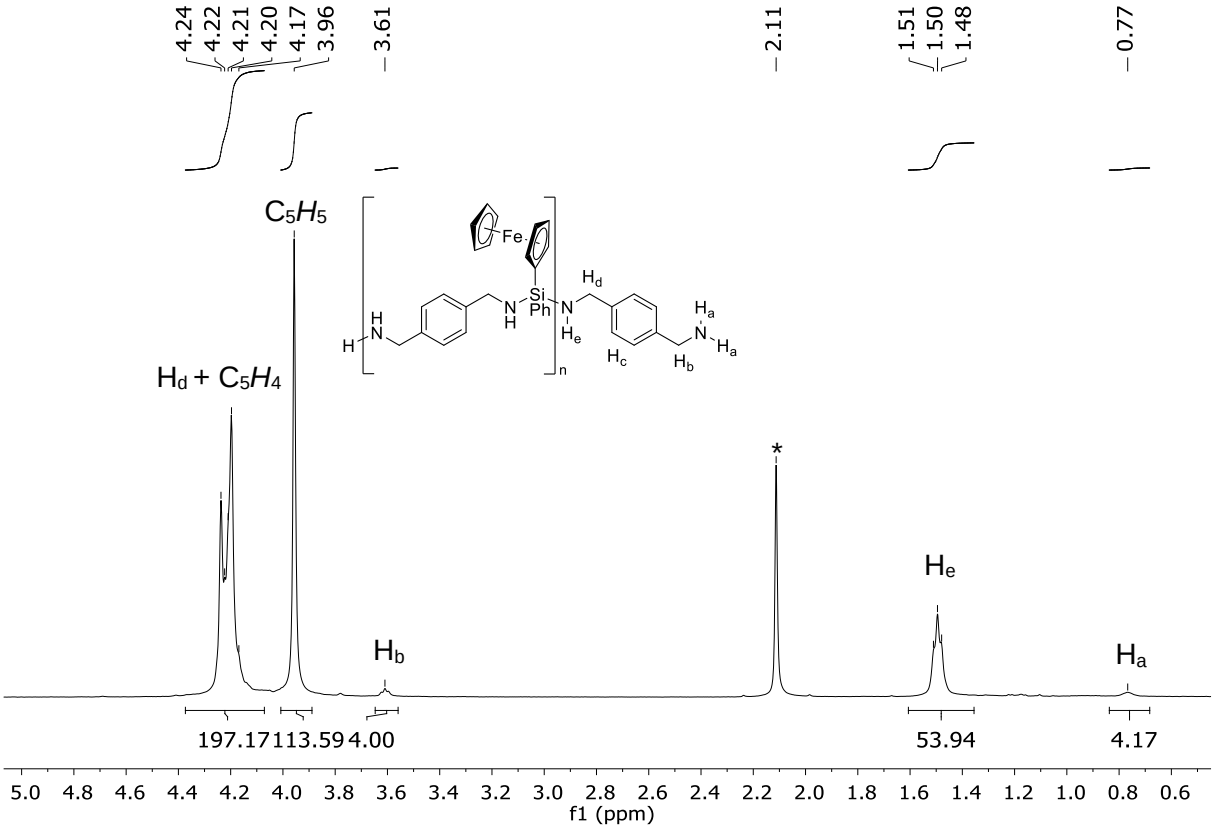

Figure 2.3: Expanded ^{1}H NMR spectrum (500 MHz, C_6D_6) of **P1**. * = entrapped toluene solvent.

The presence of hydrolytically sensitive backbone Si-N bonds precluded molecular weight determination by Gel-Permeation Chromatography (GPC). M_n values within broad agreement to those obtained by end-group analysis were, however, provided by diffusion ordered NMR spectroscopy (DOSY), which was calibrated to monodisperse polystyrene standards using a protocol described by Grubbs *et.al.*.[17] A decrease in catalyst loading to 3.3 mol% had no significant impact on $M_{n,\ DOSY}$ (Table 2.1, **P2**), whereas 1 mol% was insufficient for polymer formation, returning only oligomeric species (Table 2.1, **P3**). The molecular weight was not significantly influenced by changing to the alkyl pre-catalyst **IIId**, and although switching the solvent to THF allowed the use of higher concentrations, the molecular weight remained unchanged (Table 2.1, **P4**, **P5**). A slightly elevated temperature of 60°C helped to ensure high conversions at shorter reaction times relative to room-temperature (Table 2.1, **P6**). The possibility of catalyst deactivation-limited molecular weight was ruled out by comparing an aliquot obtained after two hours at 60°C with the product obtained after adding an additional 5 mol% **IIb** and stirring at 60°C for a further two hours (Table 2.1, **P7a**, **P7b**). Deviation from a 1:1 stoichiometry resulted in substantial molecular weight loss, as expected for a step-growth polycondensation.[4, 5] Polymers **P1**-**P7** all display end-group resonances in their ^{1}H NMR spectra, in contrast to the analogous cyclic ferrocene-free polycarbosilazanes reported by Sarazin and co-workers at a 1:1 reaction stoichiometry.[13]

Table 2.1 Ba-catalysed dehydropolymerisation of **1** and *p*-xylylenediamine. [a] Number average molecular weight calculated from ^{1}H NMR end-group analysis. [b] Degree of polymerisation calculated from ^{1}H NMR end-group analysis. [c] Number average molecular weight estimated by ^{1}H DOSY NMR spectroscopy. * Product obtained following addition of a further 5 mol% **IId** to the reaction mixture after two hours.

Polymer	Catalyst	Ratio Si:N:Ba	Solvent (concentration/M)	Temperature/°C (time/hours)	$M_{n,\ end\ group}$ / (g mol^{-1})[a]	$X_{n,\ end\ group}$[b]	$M_{n,\ DOSY}$ / (g mol^{-1})[c]
P1	**IId**	20:40:1	Toluene (0.48)	60 (2)	9800	22.7	12600
P2	**IId**	30:60:1	Toluene (0.48)	60 (2)	9000	20.9	11600
P3	**IId**	100:200:1	Toluene (0.48)	60 (2)	1800	4.0	1700
P4	**IIId**	30:60:1	Toluene (0.48)	60 (2)	11000	25.6	11900
P5	**IId**	30:60:1	THF (1.33)	25 (1)	9300	21.7	12200
P6	**IId**	30:60:1	Toluene (0.46)	25 (3)	17400	41.0	21700
P7a	**IId**	30:60:1	Toluene (0.46)	25 (3)	12400	29.2	12200
P7b	**IId**	25:50:2*	Toluene (0.46)	25 (5)	10500	24.7	14300

2.2.3 Dehydrocoupling of compound 3 with benzyl amine

With the objective of synthesising an organometallic polymer with ferrocene as part of the main polymer chain, the bifunctional ferrocenylsilane **3** was identified as a viable monomer.

Compound **3** was prepared from dilithioferrocene·TMEDA and phenylchlorosilane. Sublimation provided the pure product as single crystals, from which the molecular structure was confirmed by X-ray diffraction analysis (Figure 2.4).

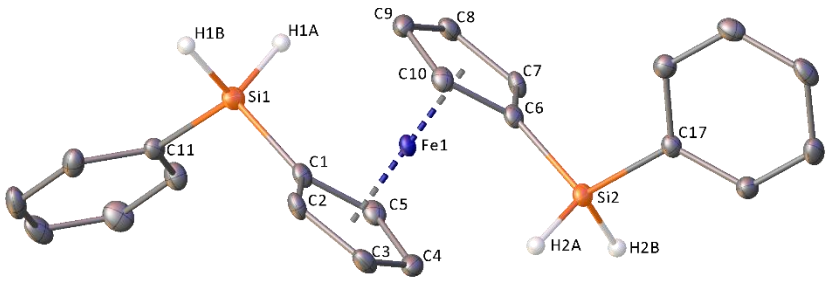

Figure 2.4: X-ray crystal structure of compound **3**. Thermal ellipsoids are shown at the 30% probability level and hydrogen atoms are omitted for clarity, except for those bound to silicon.

In the presence of 10 mol% **IId**, **3** was reacted with two equivalents of benzyl amine (Scheme 2.5). However, the ^{1}H NMR spectrum of the reaction mixture after 16 hours at 60°C revealed an intractable mixture of compounds.

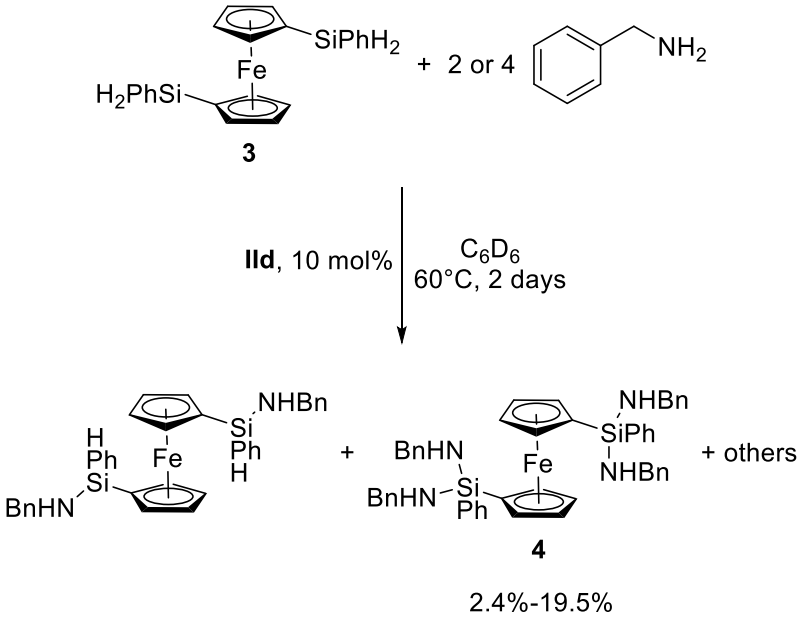

Scheme 2.5 The Ba-catalysed dehydrocoupling of compound **3** with benzyl amine to yield compound **4**. Isolated yields of crystalline product shown.

After removing solvent under vacuum, the crude product was re-dissolved in hexane/toluene and cooled to -30°C, depositing orange crystalline blocks of the tetra-substituted product, **4**, the molecular structure of which was confirmed by X-ray diffraction (Figure 2.5). Compound **4** displays similar structural parameters to compound **2**, and could be rationally synthesised in higher yield by following the same protocol at a 1:4 molar ratio. It crystallises in the triclinic space group, *P-1* with half a molecule per unit cell, and the iron centre coincident with a crystallographic inversion centre.

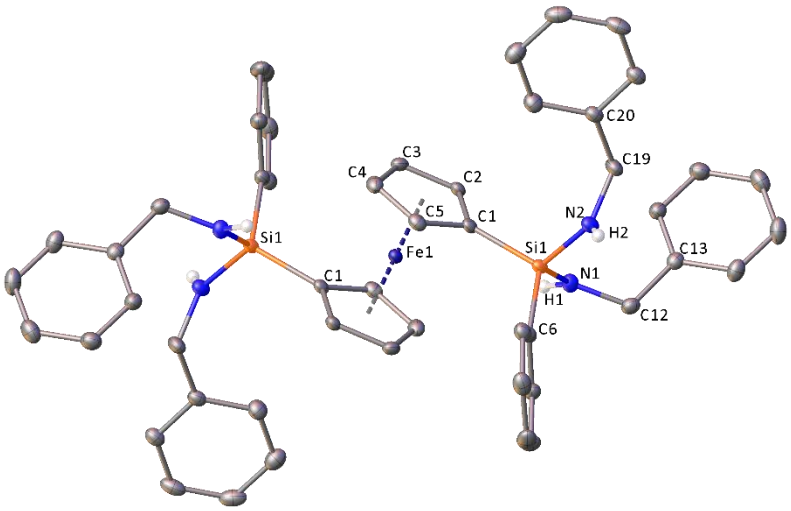

Figure 2.5 X-ray crystal structure of **4**. Thermal ellipsoids are shown at the 30% probability level. Hydrogen atoms are omitted for clarity, except for those bound to nitrogen.

2.2.4 Synthesis of polycarbosilazanes with ferrocene in the main polymer chain

The bifunctional amine, 1,4-$(H_2NCH_2)_2C_6H_4$ was reacted with **3** at 60°C and 5 mol% **IId**, yielding polymer **P8** after solvent evaporation. As expected from the model reaction with benzyl amine (Section 2.2.3), poor chemoselectivity was observed, and multiple overlapping signals precluded detailed assignment of the ^{1}H NMR spectrum. Multiple Si-H environments suggested several different repeat units. This is likely to be due to extensive branching and cross-linking to form a network-type structure (Scheme 2.6). The reaction was repeated at higher concentration and after precipitation into pentane, a material (**P9**) with a similarly complex ^{1}H NMR spectrum was obtained. **P9** displayed a significantly higher diffusion coefficient compared to **P8** (from DOSY, Table 2.2). However, molecular weights estimated from DOSY were uninformative in this case, since a branched or network-type structures are likely to have a significantly different hydrodynamic radius compared to the polystyrene calibration standards. Lower catalyst loadings resulted in a decrease in the estimated degree of polymerisation (Table 2.2, **P10**).

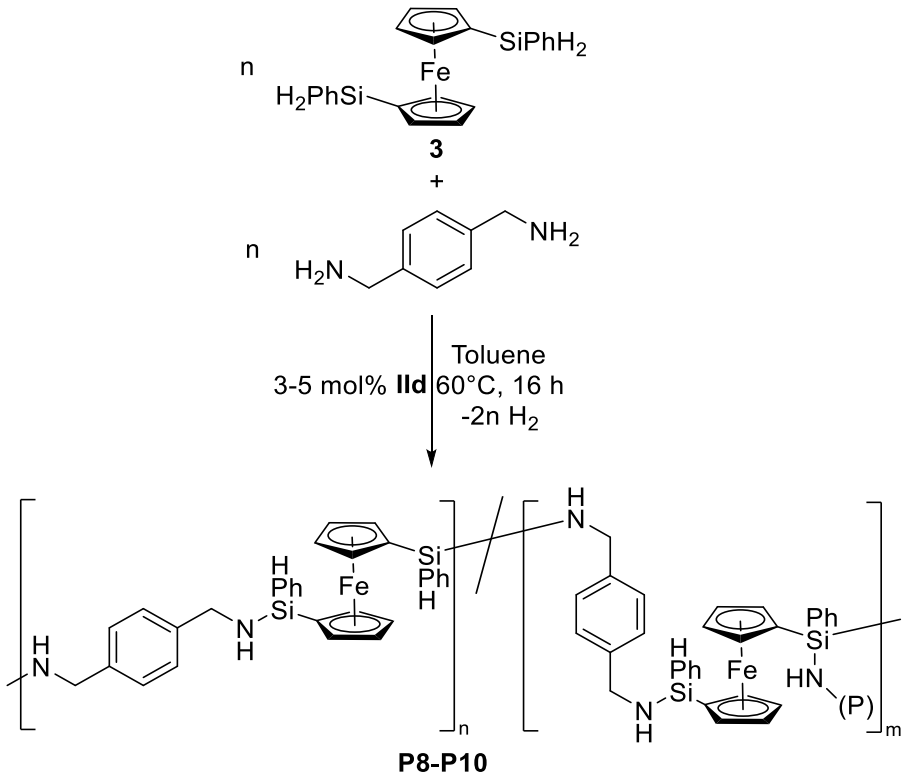

Scheme 2.6 Synthesis of polymers **P8-P10**. Note that the structure shown is simplified. Numerous repeat units are possible depending on the extent of substitution at silicon, some may give rise to oligomeric or polymeric side chains, which are shown is this scheme as '(P)'.

Table 2.2 Dehydropolymerisation of **3** and *p*-xylylenediamine catalysed by compound **IIb**. Reactions were performed in toluene at 60°C for 2 hours, except for **P8**, where polymerisation was carried out at 60°C for 16 hours. [a] Number average molecular weight estimated by ^{1}H DOSY NMR spectroscopy. *DOSY of **P9** displayed two different diffusion coefficients.

Polymer	Ratio Si:N:Ba	Concentration / M	$M_{n,\,DOSY}$ / (g mol^{-1}) [a]
P8	40:40:1	0.10	3600
P9	40:40:1	0.39	19200, 27800*
P10	60:60:1	0.39	5200

2.2.5 Dehydrocoupling of fc(NH$_2$)$_2$ with secondary silanes

Detailed characterisation and rational synthesis of **P8**-**P10** was challenged by their poorly defined nature, and this prompted an alternative approach. One option was to attempt polymerisation with an amine-functionalised ferrocene. Hence, fc(NH$_2$)$_2$ was dehydrocoupled with an equimolar equivalent of diphenylsilane and 5 mol% **IId** in d$_8$-THF. Although clean and quantitative conversion was observed, rather than providing the expected polymer, a cyclic silazane[3]ferrocenophane, **5**, was obtained (Scheme 2.7).

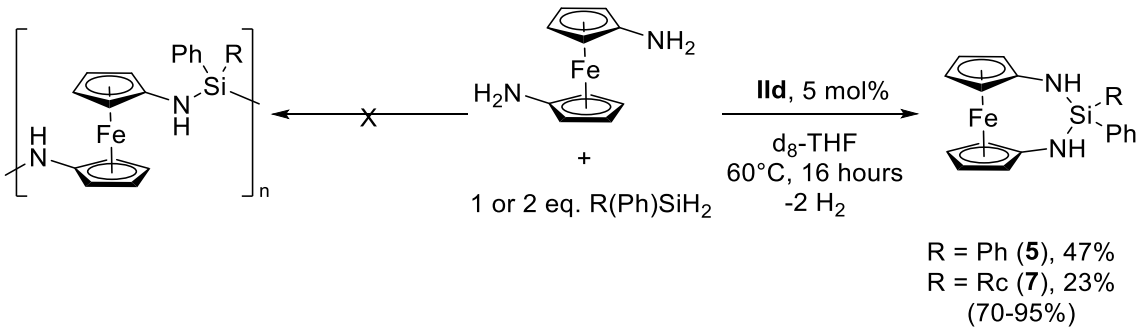

Scheme 2.7 Barium-catalysed dehydrocoupling of $fc(NH_2)_2$ and dihydrosilanes to yield compounds **5** and **7**. Values in parentheses refer to the spectroscopic yield determined by integration of ^1H NMR of the crude product.

Compound **5** persisted as the major product in 70% spectroscopic yield, even when two molar equivalents of diphenylsilane were used. Single crystals were grown from a THF solution by hexane vapour diffusion and the molecular structure was confirmed by X-ray diffraction (Figure 2.6). In addition to a multitude of ferrocene-based N-heterocyclic carbenes and 1,1'-bisamino, amido, and imido-ferrocene based chelating ligands, several examples of nitrogen-containing *ansa*-bridged metallocenophanes can be found in the literature.[18-32] However, compound **5** is notable as the first example of a metallocenophane with an –{N-Si-N}– *ansa* bridge, to the best of our knowledge.

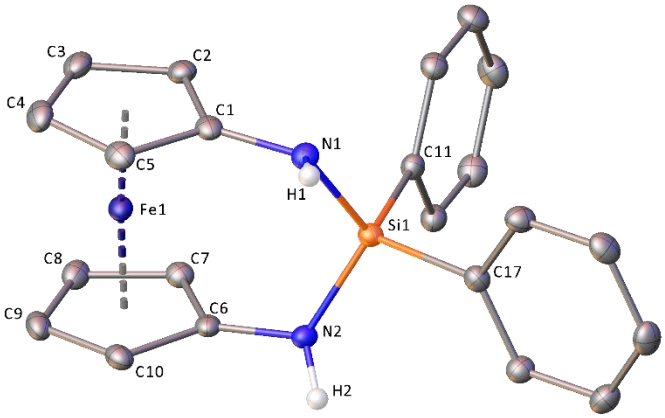

Figure 2.6 X-ray crystal structure of **5**. Thermal ellipsoids are shown at the 30% probability level and, except for those bound to nitrogen, H-atoms are omitted for clarity.

Replacing diphenylsilane with the hydrosilane-functionalised ruthenocene **6** (Figure 2.7), presented the possibility of accessing an unusual bimetallic metallocenophane. Compound **6** was synthesised *via* an method analogous to that for compound **1**, and was purified by sublimation to yield single crystals, from which the molecular structure was confirmed by X-ray diffraction (Figure 2.7). Coupling equimolar quantities of $fc(NH_2)_2$ and **6** with 5 mol% **IId** in d_8-THF at 60°C provided the bimetallic silazane[3]ferrocenophane **7**, which prevails regardless of reaction stoichiometry. The molecular structure of **7** was confirmed by X-ray diffraction after layering hexane above the crude reaction mixture to obtain single crystals (Figure 2.8).

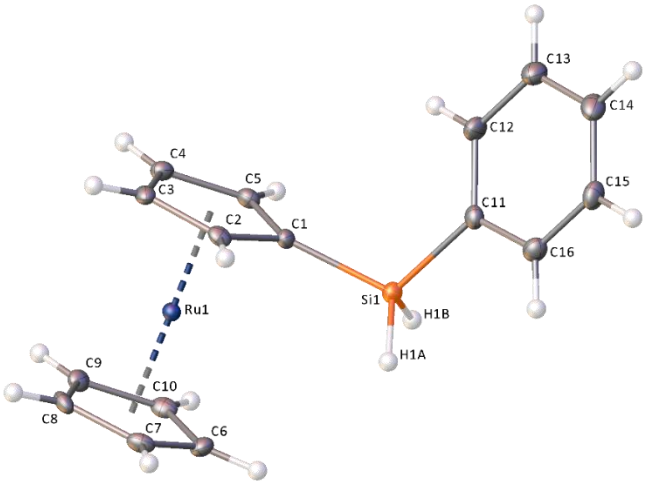

Figure 2.7 X-ray crystal structure of compound **6**. Thermal ellipsoids are shown at the 30% probability level.

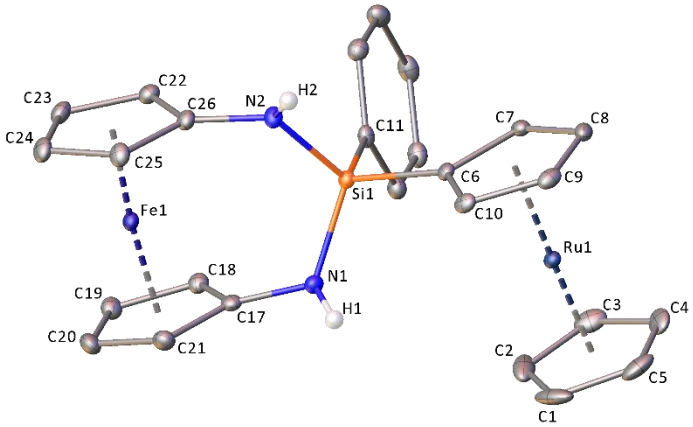

Figure 2.8 X-ray crystal structure of **7**. Thermal ellipsoids are shown at 30% probability level. Hydrogen atoms are omitted for clarity, except for those bound to nitrogen.

Compounds **5** and **7** are structurally similar with very little ring-tilt, a relatively linear Cp-Fe-Cp angle (δ) (Figure 2.9), and insignificant geometrical distortion of the *ansa*-bridge (Table 2.3).The release of ring strain typically provides a thermodynamic driving force for the ring opening polymerisation (ROP) of metallocenophanes and although ring-tilt is not necessarily indicative of strain,[33-36] differential scanning calorimetry (DSC) of **5** and **7** provided no evidence of a thermal ROP process (see Appendix i.6).

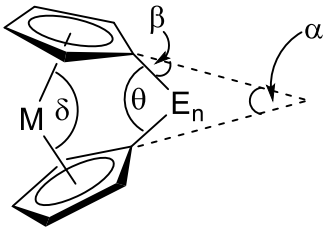

Figure 2.9 Depiction of geometric parameters α, β, δ, and θ in [n]metallocenophanes.

Table 2.3 Geometric analysis for compounds **5** and **7**.

Compound	α/°	β/°	δ/°	θ/°
5	4.61	3.37	175.51	11.14
7	6.30	3.62	174.41	12.09

2.2.6 Synthesis of well-defined main-chain ferrocene-containing polycarbosilazanes *via* steric control

Whilst primary amines have a tendency to afford disubstituted products when coupled with secondary hydrosilanes, the steric demands of secondary amines can provide kinetic control and good selectivity towards singly coupled silazanes.[12, 14, 15] Hence, attention was turned to the bifunctional secondary amine, *N*,*N*'-dimethyl-*p*-xylylenediamine, 1,4-(H(Me)NCH$_2$)$_2$C$_6$H$_4$. This monomer has already been the subject of investigation by Sarazin's group, who found that dehydrocoupling with one equivalent of diphenylsilane yielded an amino-silazane (1-(Me(H)NCH$_2$)-(C$_6$H$_4$)-4-(CH$_2$N(SiPh$_2$H)Me), Scheme 2.8) rather than the desired polymer.[14] Repeating Sarazin's reaction with two molar equivalents of diphenylsilane returns quantitative spectroscopic yields of the *N*,*N*'-silylated product, 1,4-(Me(SiPh$_2$H)CH$_2$)$_2$C$_6$H$_4$ (**8**), of which the molecular structure was confirmed by X-ray diffraction after crystallisation from toluene at -30°C (Figure 2.10).

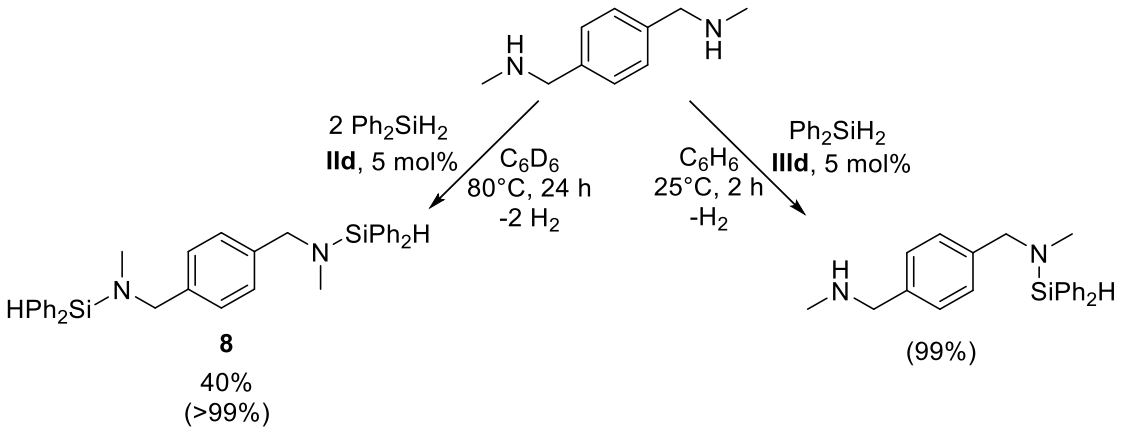

Scheme 2.8 The barium catalysed dehydrocoupling of diphenylsilane and *N,N'*-dimethyl-*p*-xylylenediamine to provide 1-(Me(H)NCH$_2$)-(C$_6$H$_4$)-4-(CH$_2$N(SiPh$_2$H)Me),[14] or compound **8**.

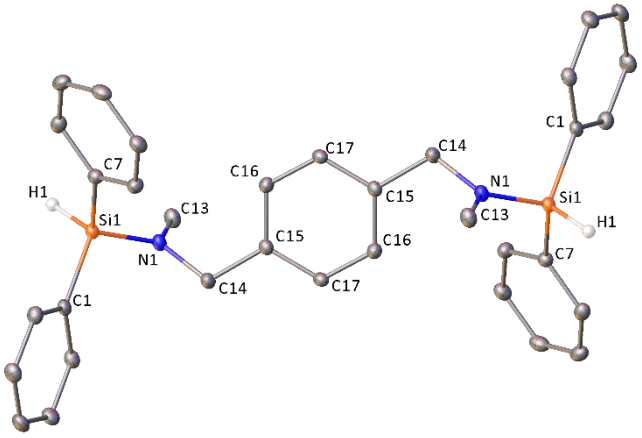

Figure 2.10 X-ray crystal structure of compound **8**. Thermal ellipsoids are shown at the 30% probability level and hydrogen atoms are omitted for clarity except those bound to silicon.

The controlled formation of one Si-N bond per silicon atom suggested that well-defined linear polymer with ferrocene as part of the main-chain would be accessible from *N,N'*-dimethyl-*p*-xylylenediamine in combination with **3**. This proved to be the case, and an orange solid (**P11**) was obtained by precipitating the reaction mixture into pentane at -78°C after 16 hours at 60°C in toluene, with 5 mol% **IId** (Scheme 2.9).

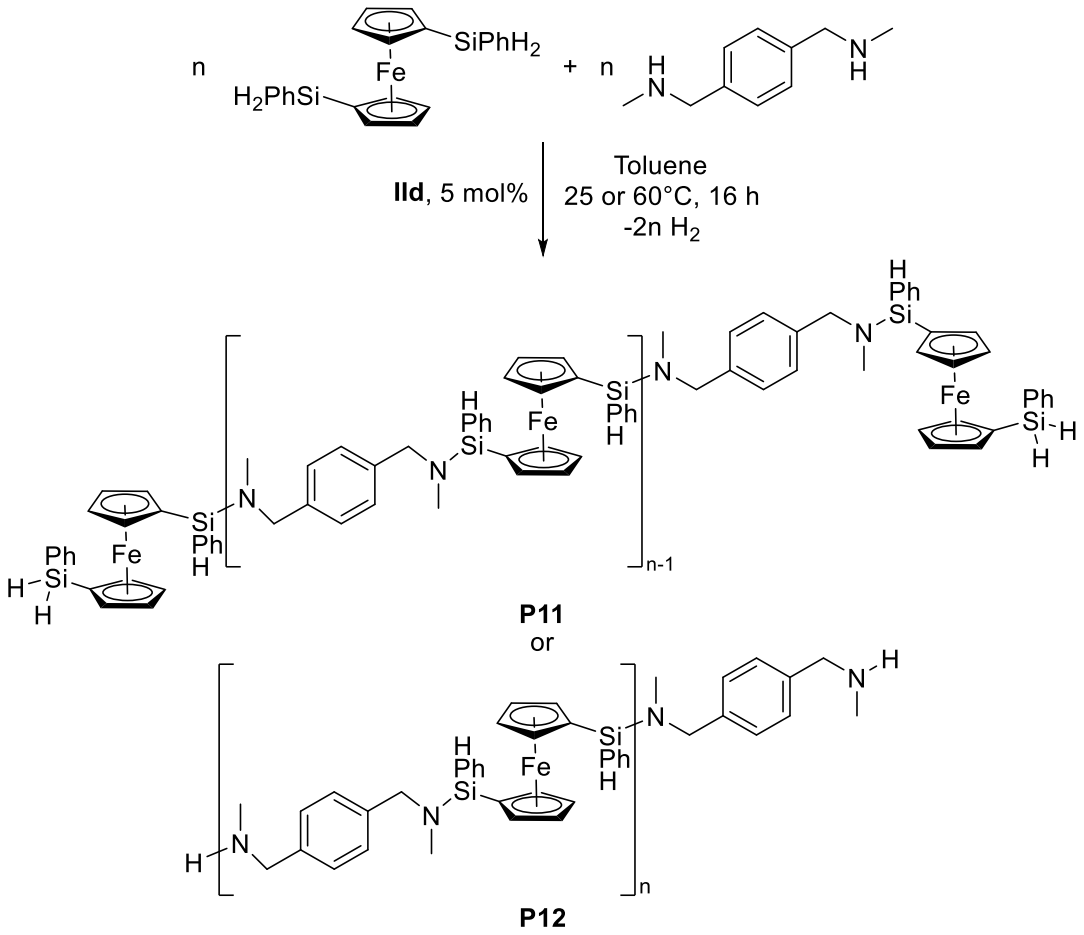

Scheme 2.9 Synthesis of polymers **P11** and **P12** *via* the barium catalysed dehydrocoupling of **3** and *N*,*N*'-dimethyl-*p*-xylylenediamine.

The ^{1}H NMR spectrum (Figure 2.11) of **P11** clearly displays separate peaks corresponding to mid-chain SiH groups (δ 5.64 ppm) and terminal SiH_2 moieties (doublets at δ 5.10, 5.04 ppm), without clear evidence for amine termini. Although the ^{29}Si{^{1}H} NMR spectrum displayed two resonances at δ -10.23, -10.32 ppm, they could not be unambiguously assigned. End-group integral analysis provided an estimated molecular weight of $M_{n,\ end\ group}$ = 5300 Da, which, in this case, disagrees with that obtained by DOSY measurement ($M_{n,\ DOSY}$ = 10000 Da, Table 2.4). This discrepancy can be tentatively ascribed to a relatively rigid polymer chain and hence substantial deviation from the ideal spherical case, or alternatively, a combination of low molecular weight linear species and higher molecular weight cyclics which would evade detection by end-group analysis. At room temperature and a higher concentration, **P12** was isolated (Scheme 2.9). In contrast to **P11**, **P12** displays terminal $CH_2N(H)Me$ groups, but lacks Si-H resonances in the ^{1}H NMR spectrum (Figure 2.12). Furthermore, a number average molecular weight of ~17000 Da was estimated by both end-group integration and DOSY (Table 2.4).

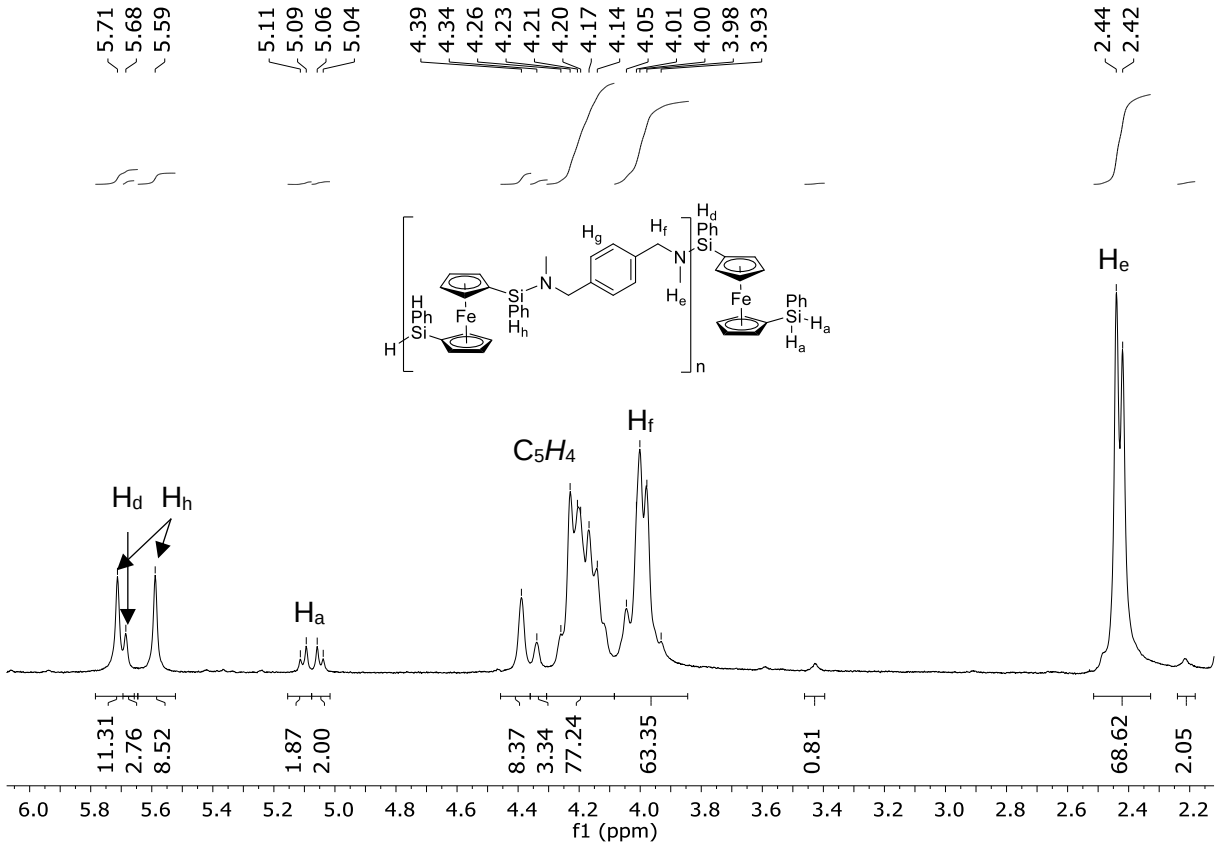

Figure 2.11: Expanded ^{1}H NMR spectrum (500 MHz, C_6D_6) of polymer **P11**.

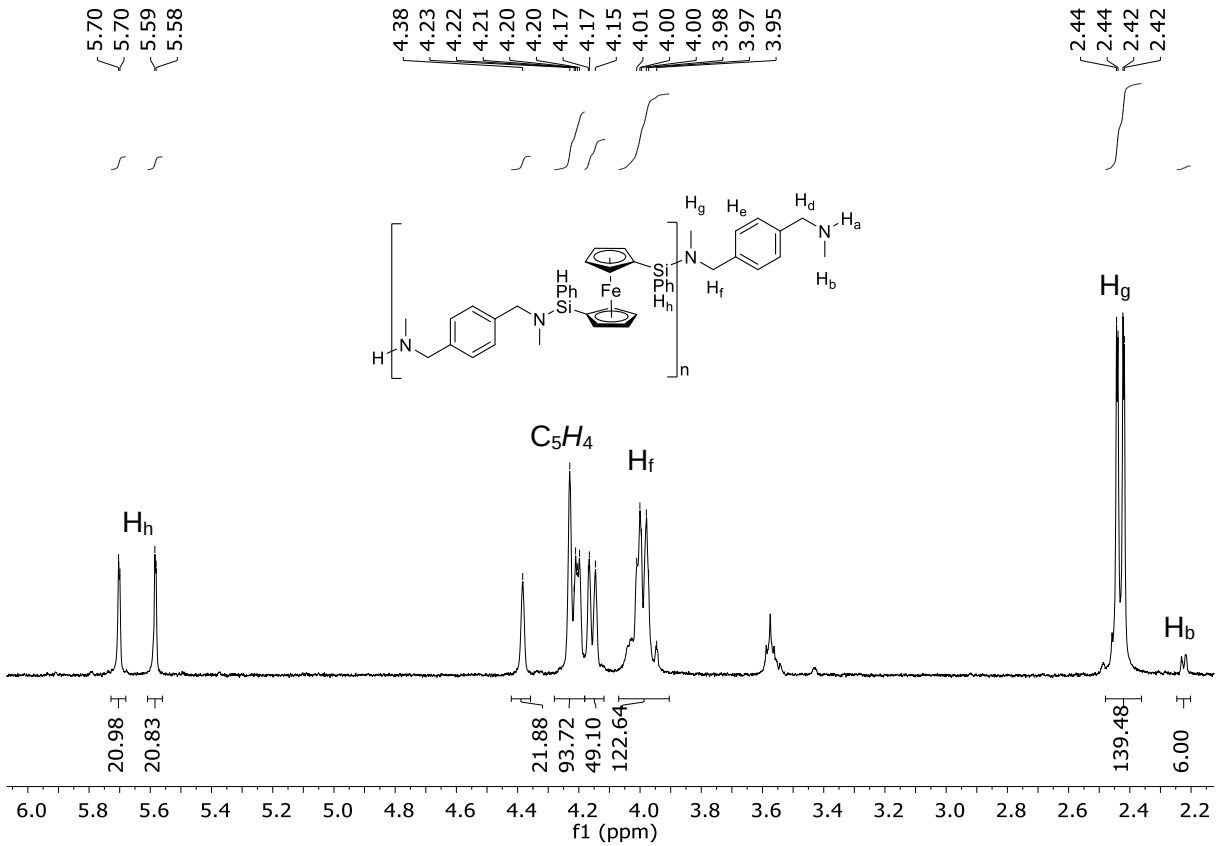

Figure 2.12: Expanded ^{1}H NMR spectrum (500 MHz, C_6D_6) of polymer **P12**.

A well-defined linear polymer is also the predicted outcome of a dehydrocoupling reaction between a bis-tertiary silane and bis-primary amine, since only one Si-H bond is available per silicon centre, and primary amines do not typically couple with two equivalents of tertiary silane under Ae-catalysis.[12, 15] This hypothesis was proven correct on coupling 1,1'-bis(dimethylsilyl)ferrocene with 1,4-$(H_2NCH_2)_2C_6H_4$ under barium catalysis (3.3 mol% **IId**), to yield a gummy solid, **P13**, which was purified by precipitation into hexane at -78°C (Scheme 2.10).

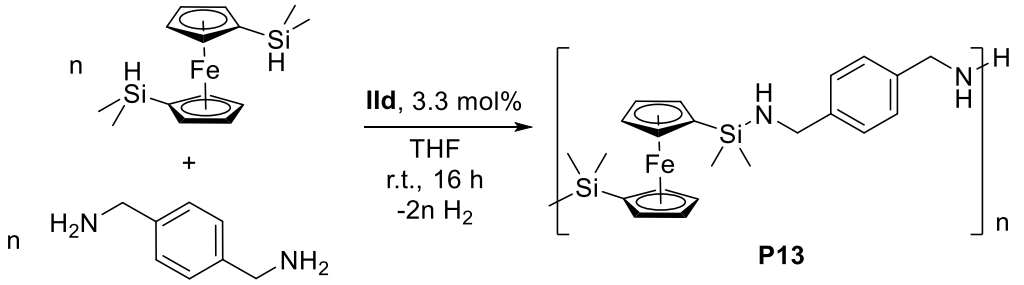

Scheme 2.10 Synthesis of polymer **P13**.

The ^{1}H NMR spectrum of **P13** is simple to interpret, with an absence of Si-H resonances and a well-defined triplet at δ 3.62 ppm, corresponding to terminal C*H*$_2$NH$_2$ groups. Estimated number average molecular weights of $M_{n,\ end\ group}$ = 6500 Da and $M_{n,\ DOSY}$ = 5500 Da were obtained by end-group integration and DOSY respectively (Table 2.4).

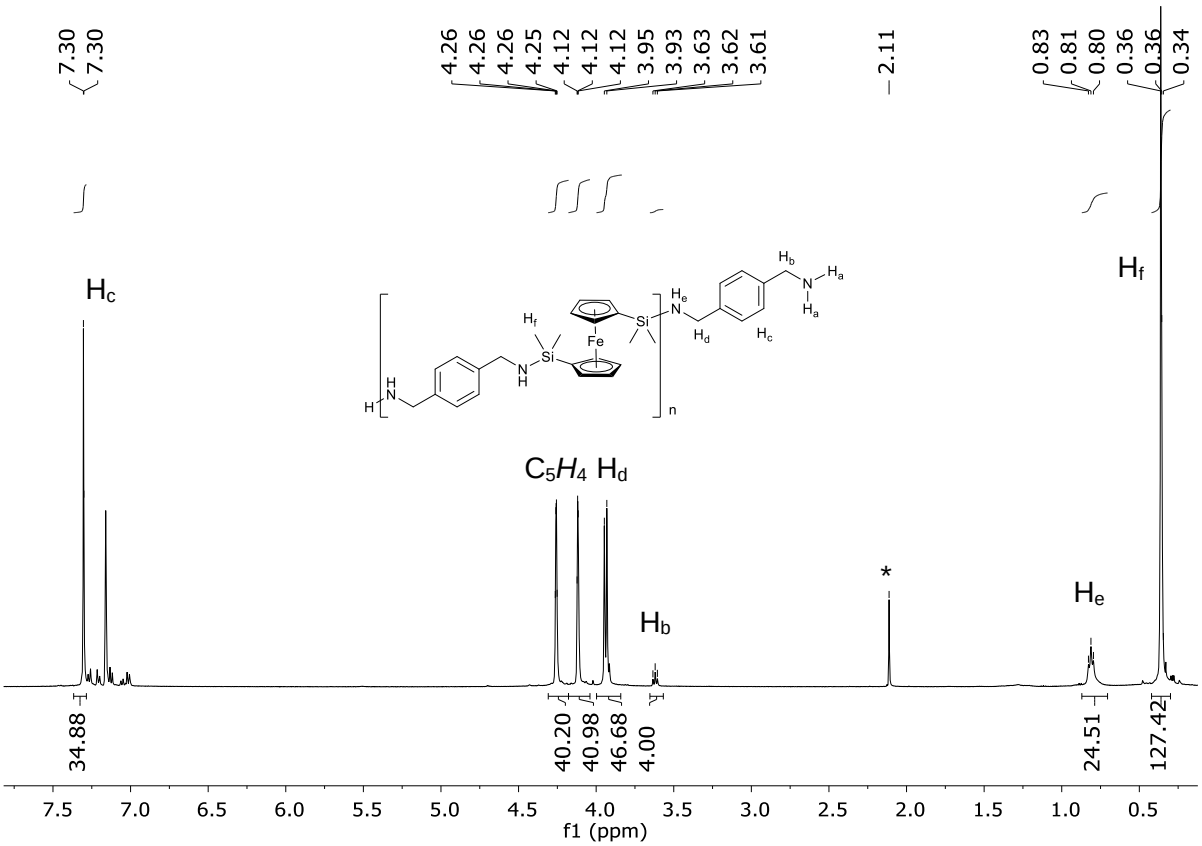

Figure 2.13: ^{1}H NMR spectrum (500 MHz, C_6D_6) of **P13**.* = entrapped toluene.

Table 2.4 Catalytic dehydrocoupling of compound **3** with *N*,*N*'-dimethyl-*p*-xylylenediamine and of 1,1'-bis(dimethylsilyl)ferrocene with *p*-xylylenediamine. Each reaction was carried out with the pre-catalyst **IId** and was stirred for 16 hours to ensure complete conversion. [a] Number average molecular weight calculated from ^{1}H NMR end-group analysis. [b] Degree of polymerisation calculated from ^{1}H NMR end-group analysis. [c] Number average molecular weight estimated by ^{1}H DOSY NMR spectroscopy.

Polymer	Silane	Amine	Ratio Si:N:Ba	Solvent (concentration / M)	Temperature / °C	$M_{n,\,end\,group}$ / (gmol^{-1})[a]	$X_{n,\,end\,group}$[b]	$M_{n,\,DOSY}$ / (gmol^{-1})[c]
P11	**3**	1,4-(H(Me)NCH$_2$)$_2$C$_6$H$_4$	40:40:1	Toluene (0.06)	60	5300	8	10300
P12	**3**	1,4-(H(Me)NCH$_2$)$_2$C$_6$H$_4$	40:40:1	Toluene (0.46)	25	16900	30	17600
P13	fc(SiMe$_2$H)$_2$	1,4-(H$_2$NCH$_2$)$_2$C$_6$H$_4$	60:60:1	THF (0.74)	25	6500	10	5500

2.2.7 Electrochemical studies

The presence of multiple redox-active sites within a single macromolecule often furnish ferrocene-containing polymers with interesting electrochemical properties.[1, 37, 38] The cyclic voltammogram of **P1** consists of a single electron Fe^{3+}/Fe^{2+} redox event that is fully reversible. $E_{1/2}$ lies very close to that of the reference ferrocene system, but at slightly lower potential than

monomer **1**, possibly due to increased electron density at iron on replacing Si–H with Si–N bonds (Figure 2.14, Table 2.5). The model system of compound **2** offers a direct comparison with **P1**, since both are the product of a double dehydrocoupling of **1** with two amine molecules and hence display almost identical $E_{1/2}$ values. Normally, larger molecules with lower diffusion coefficients (D) display lower peak currents (I_{peak}): $I_{peak} \propto D^{\frac{1}{2}}$ as described by the Randles-Sevcik equation (Equation 2.1).[39] However, I_{peak} depends on the number of electrons per molecule diffusing to the electrode (n): $I_{peak} \propto n^{\frac{3}{2}}$. For a polymer, n can be approximated to the degree of polymerisation (X) (i.e. the number of ferrocene moieties per macromolecule), D decreases by a factor $(molecular\ volume)^{-0.6}$,[40] and the concentration c, decreases by a factor $1/X$. If the molecular volume is assumed proportional to X, these factors compensate, and a similar peak current is predicted for both systems.

Equation 2.1: The Randles-Sevcik equation. F Faraday constant, A is the electrode area, c is the concentration, R is the gas constant, D is the diffusion coefficient, n is the number of electrons transferred, and T is the absolute temperature.

$$I_{peak} = 0.446\, n^{3/2} D^{1/2} F^{3/2} \mathrm{Ac} \sqrt{\frac{v}{RT}}$$

Although peak currents are similar for **P1** and **2**, the former displays a smaller peak separation (ΔE_{peak}), typical of a multiple-electron transfer process (Table 2.5).[41] Although the peak-to-peak separation can be described by the equation: $\Delta E_{peak} = 2.218\ \frac{RT}{nF}$,[39] this relates to the ideal system, which is unlikely to be satisfied in the polymer systems described here. Furthermore, **P1** displays a sharper reduction peak, a feature which may be due to partial adsorption of the multiply oxidised polymer to the electrode surface (Figure 2.14).

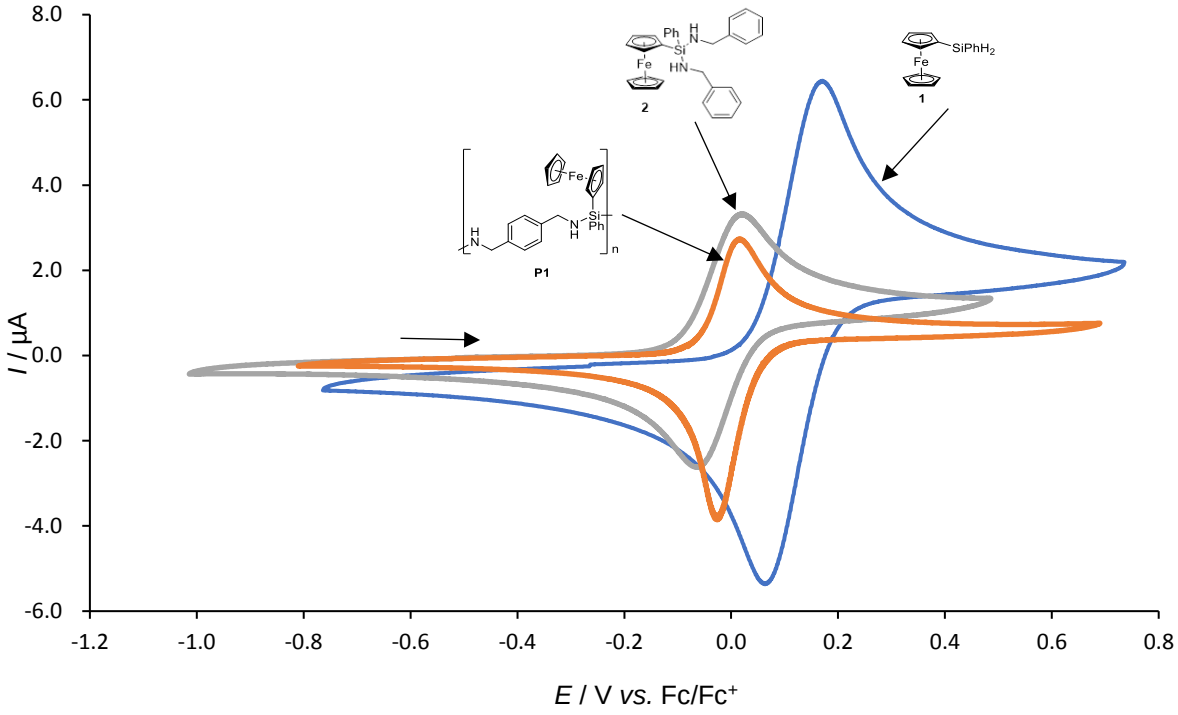

Figure 2.14: Cyclic voltammogram of polymer **P1**, compared to compounds **1**, and **2**, each ca. 1 mM in molecular or monomer concentration obtained with a 1 mm diameter platinum disc electrode immersed in dichloroethane containing 0.1 M NBu_4PF_6 with at a scan rate of 100 mVs^{-1}.

The main-chain ferrocene containing polymers, **P9** and **P11** (Figure 2.15), display positively shifted $E_{1/2}$ values compared to **P1** (Table 2.5), probably due to decreased electron density at iron resulting from the presence of silicon substituents on both cyclopentadienyl rings. The hydrosilane monomer **3** displays a higher $E_{1/2}$ value, similar to that of compound **4** (Figure 2.16, Table 2.5).

The somewhat broadened peaks of **P9** compared to **P11** are consistent with a highly polydisperse polymer with a poorly defined structure. The substantial difference in peak current between **P9**, **P11**, and **P13** can be rationalised on account of the number average molar mass (M_n), with high M_n values (**P11** ~ 10000 Da) resulting in lower peak currents than polymers of low M_n (**P13** ~ 5500 Da) due to slower diffusion (Figure 2.15, Table 2.5). **P1**, also of relatively high molar mass (~ 12600 Da) however, presented a much higher peak current than **P11**. This can be tentatively explained by relatively fast charge transfer from the pendent ferrocene, compared to redox centres within the polymer chain itself. The symmetrical redox waves of polymers **P11** and **P13** contrast with that of **P1**, indicating that polymer adsorption to the electrode surface is less significant in these cases.

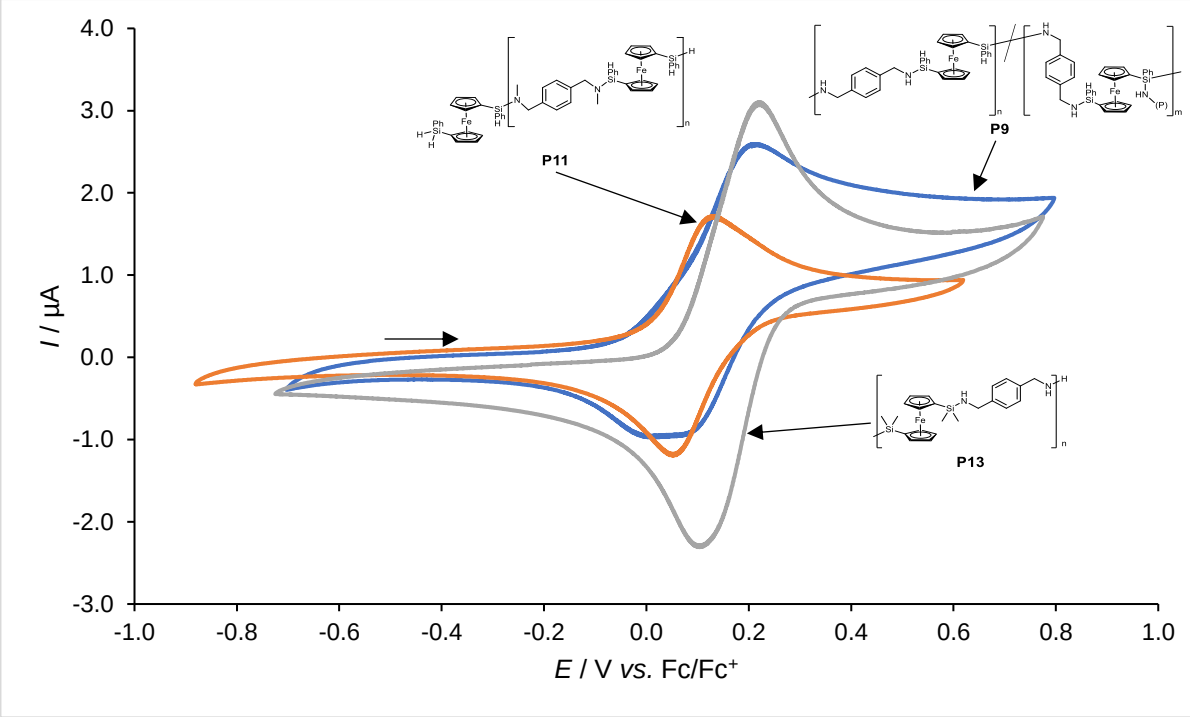

Figure 2.15: Cyclic voltammogram of polymers **P9**, **P11**, and **P13**, each ca. 1 mM in monomer concentration obtained with a 1 mm diameter platinum disc electrode immersed in dichloroethane containing 0.1 M NBu_4PF_6 with at a scan rate of 100 mVs^{-1}.

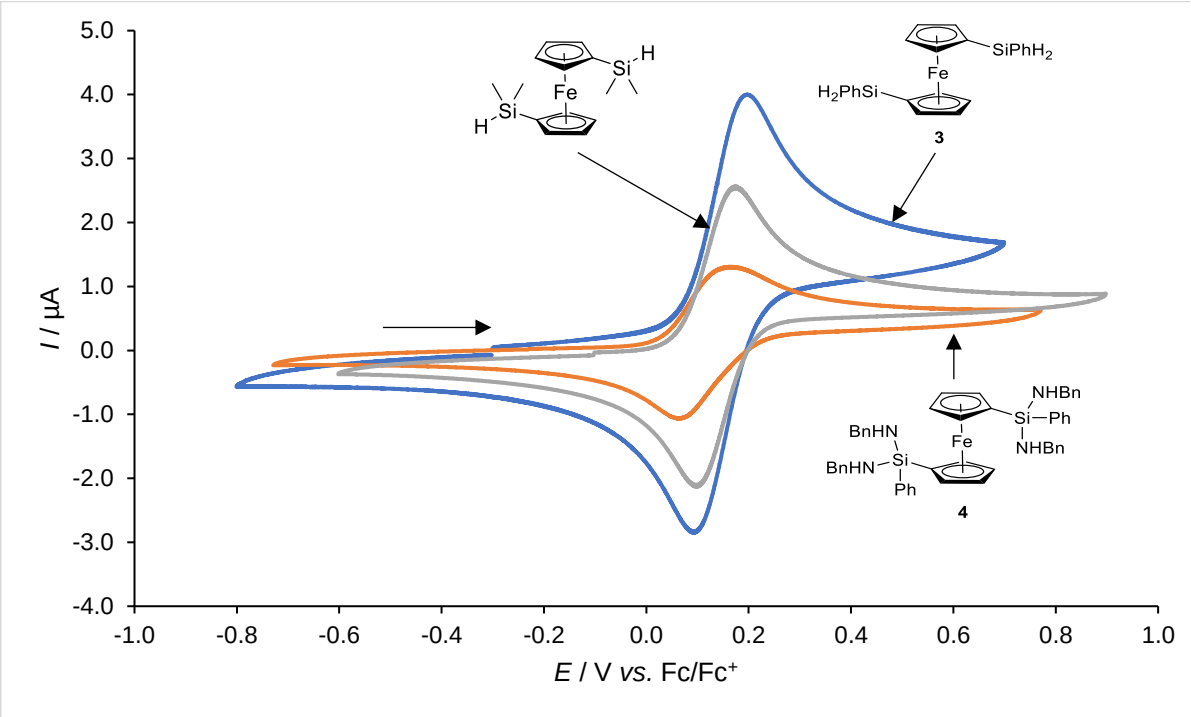

Figure 2.16: Cyclic voltammograms of compounds **3** (1 mM), **4** (0.4 mM), and $fc(SiMe_2H)_2$ (1 mM) obtained with a 1 mm diameter platinum disc electrode immersed in dichloroethane containing 0.1 M NBu_4PF_6 with at a scan rate of 100 mVs^{-1}.

Compound **5** displays a reversible redox event centred close to the reference ferrocene system at $E_{1/2}$ = 0.031 V. Compound **7** exhibits a negatively shifted peak at -0.019 V for the Fe^{2+}/Fe^{3+} oxidation event, and an irreversible peak at 0.90 V corresponding to oxidation of the Ru^{2+} centre to Ru^{3+}. The two reduction peaks at -0.187 and -0.405 V cannot be meaningfully interpreted due to instability of Cp-Ru^{III} bonds towards the PF_6^- anion (Figure 2.17).

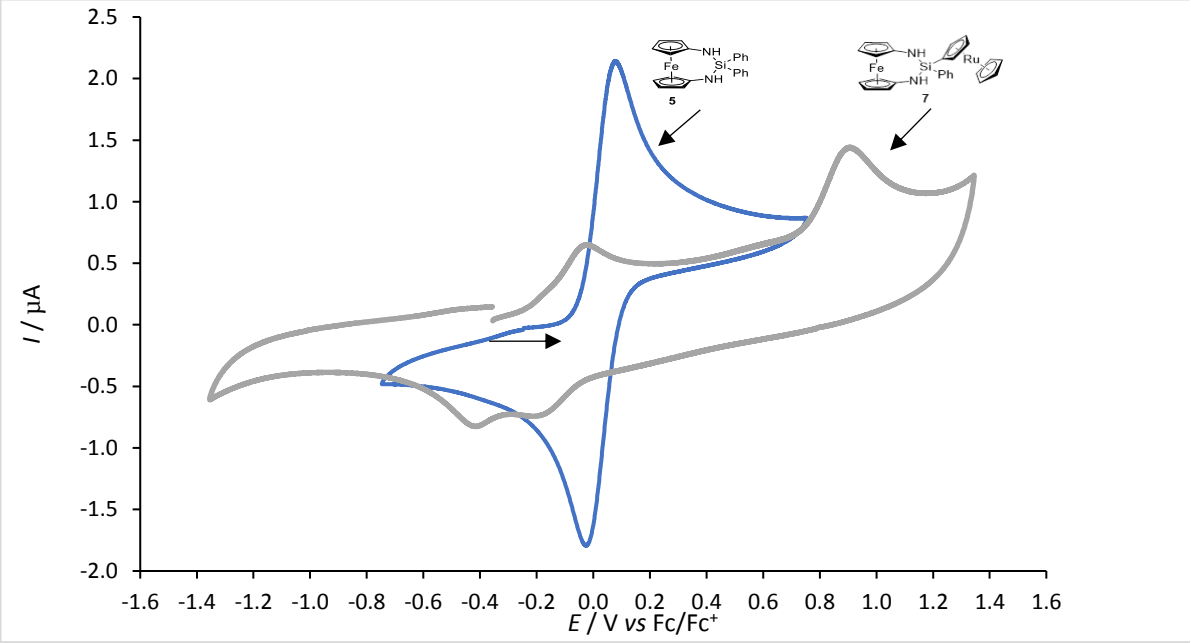

Figure 2.17: Cyclic voltammogram of compounds **5** (0.5 mM) and **7** (0.4 mM), obtained with a 1 mm diameter platinum disc electrode immersed in dichloroethane containing 0.1 M NBu_4PF_6 with at a scan rate of 100 mVs^{-1}.

Table 2.5 Cyclic voltammetry data for samples dissolved in ca. 1 mM molecular/monomer concentration obtained at a 1 mm diameter platinum disc electrode immersed in dichloroethane containing 0.1 M NBu_4PF_6 at 100 mV/s. Potentials are referenced to ferrocene/ferrocenium. Compound **7** is omitted from the table, since the presence of more than one irreversible events makes comparison to the other systems inappropriate. [a] Approximate concentration of molecular systems or of monomer in polymer systems.[b] The midpoint potential is defined here as $E_{1/2}$ = ½($E_{peak,ox}$ + $E_{peak,red}$). [c] A shoulder peak occurs at $E_{1/2}$ = -0.02 V vs. Fc/Fc^+ possibly due to oligomer impurities or adsorption.

Compound	Concentration [a]	$E_{1/2}$ / V [b]	ΔE_{peak} / mV	$I_{peak, ox}$ / µA	$I_{peak, red}$ / µA
P1	1 mM	0.001	41	2.45	-3.87
1	1 mM	0.115	100	5.44	-5.78
2	1 mM	-0.016	90	3.40	-3.49
P9	1 mM	0.078	108	2.34	-2.54
P11	1 mM	0.065	87	1.52	-1.64
3	1 mM	0.115	95	3.73	-3.99
4	0.4 mM	0.128	100	1.26	-1.39
P13	1 mM	0.171	85	2.33	-3.29
$fc(SiMe_2H)_2$	1 mM	0.119	74	2.53	-2.65
5	0.6 mM	0.031	109	2.20	-2.31

2.2.8 Thermogravimetric analysis

In addition to the proven utility of ferrocene-containing polymers as precursors to magnetic ceramic materials,[42-49] the use of silicon-containing polymers such as polysilanes, polysilazanes, and polycarbosilazanes as precursors for SiC, Si_3N_4, and Si/C/N ceramics is well established.[50-54] Hence the ferrocene-containing polycarbosilazanes described within this chapter are promising candidates as ceramic precursors.

The polymers thermal properties were first investigated by thermal gravimetric analysis (TGA). When heated to 800°C at 10°C/min under a flow of N_2, all polymers displayed a major weight loss event between ca. 300-550°C (Figure 2.18). Those polymers which were synthesised in toluene also presented a minor weight-loss below 200°C, assigned to the loss of entrapped solvent which was unavoidable even after prolonged vacuum treatment prior to TGA. As a result, ceramic yields discussed henceforth take the relative mass at 200°C to equal 100%. Uncorrected TGA traces can be found in Appendix i.6.

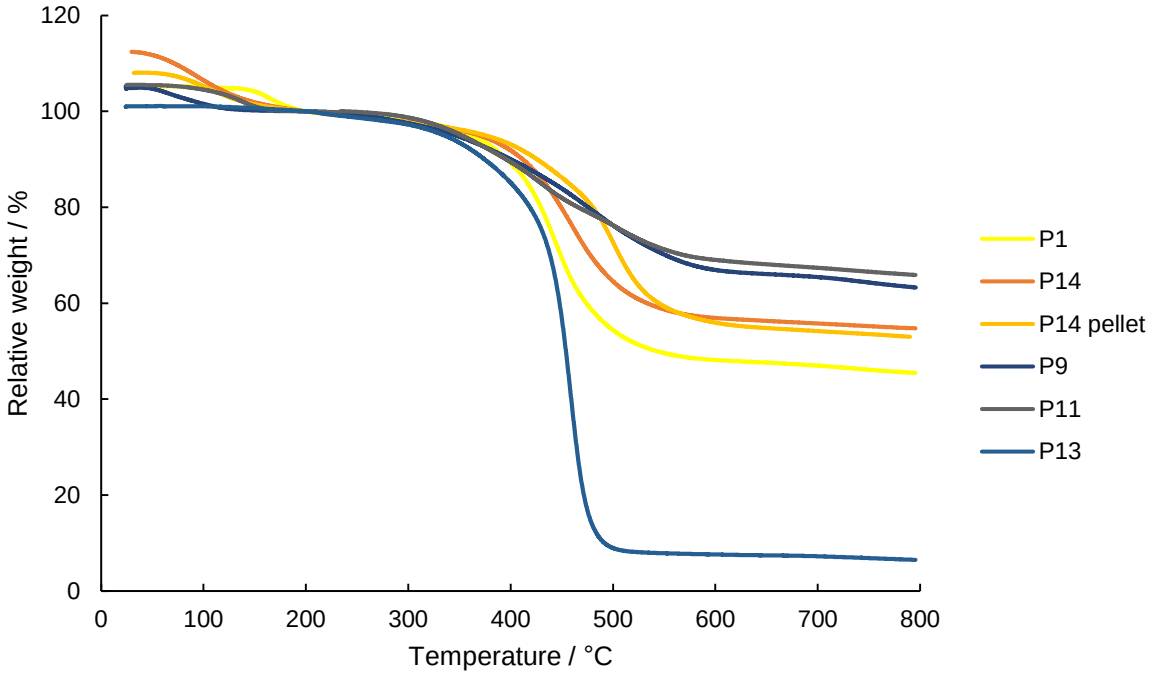

Figure 2.18 TGA traces of ferrocene-containing polycarbosilazanes, heated to 800°C at 10°C/min under a flow of N_2. To account for loss of entrapped solvent, the mass at 200°C is taken to equal 100%. Uncorrected thermograms can be found in Appendix i.6.

For a linear polymer, **P1** has a respectable ceramic yield of 43% (Table 2.6). For comparison, the ceramic yields of linear polyferrocenylsilane (PFS) vary depending on the substituents at silicon, but lie in the range of 17-58% at 600°C.[42, 49] The presence of appreciable quantities of pyrolysised material following TGA implies that **P1** is able to undergo crosslinking reactions at a rate competitive with depolymerisation and loss of volatile fragments. Pre-crosslinked precursors sometimes help improve ceramic yields.[45] With this in mind, a polymerisation of **1** and 1,4-$(H_2NCH_2)_2C_6H_4$ was carried out and, once the polymerisation appeared complete, 0.2 equivalents of phenylsilane were added to the unquenched reaction mixture. Immediate bubbling ensued, followed by a rapid increase in viscosity, eventually becoming an immobile mass. Although insolubility prevented precipitation or solution processing, quenching with non-dried THF and vacuum drying resulted in a spongy material (**P14**), which presented a slightly improved ceramic yield (55%) by TGA compared to **P1**. Processing **P14** into a compressed pellet slightly delayed the onset temperature (Figure 2.18), but neither improved the ceramic yield (Table 2.6), nor gave rise to shape retention (Figure 2.19).

a) 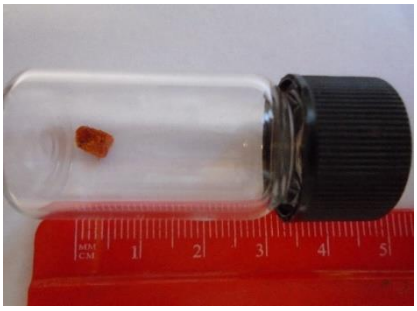 b) 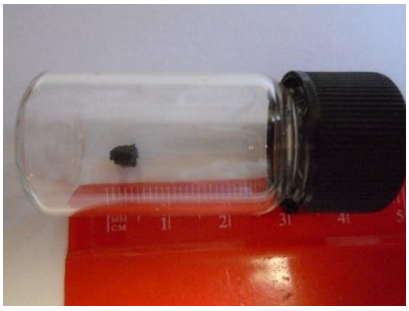

Figure 2.19: A pellet of polymer **P14** a) before TGA and b) following TGA.

TGA of **P9** gave a higher ceramic yield of 61% which was initially attributed to a branched and partially cross-linked polymer structure. However, the well-defined linear polymer **P11** had the highest ceramic yield of all (64%), emphasising that cross-linking during pyrolysis is more important than pre-crosslinking in this class of polymers. By contrast, **P13** was almost entirely lost during pyrolysis, with a ceramic yield of <6%, suggesting a phenyl substituent and/or hydride at silicon are critical during formation of non-volatile ceramic material.

Table 2.6 Ceramic yields obtained after analysis of polymers by TGA at 10°C/min up to 800°C under a flow of N_2. Yields given are corrected for loss of entrapped solvent, with the mass at 200°C taken to equal 100%.

Sample	Ceramic yield / %
P1	43
P14	55
P9	61
P11	64
P13	6

2.2.9 Pyrolysis and ceramic characterisation

Encouraged by promising TGA results, polymers **P5** and **P8** were pyrolysed on a preparative scale using the same heating protocol under a flow of N_2 in a tube furnace. The resulting charcoal coloured powders, **P5py** and **P8py**, were attracted to a bar magnet, suggesting that they contained metallic iron or magnetite (Figure 2.20).

Figure 2.20: Photograph of **P5py** responding to a bar magnet.

The pyrolysed materials were characterised by powder X-ray diffraction (PXRD), and gave broad, low intensity diffraction patterns. The maxima at 2θ = 44° (*d* = 2.05 Å) and 2θ = 63° (d = 1.43 Å) were assigned to α-Fe, as was a sharper peak at 2θ = 82° (*d* = 1.17 Å).[55] Hematite (α-Fe_2O_3), probably the result of brief exposure to air when removed from the furnace, was identified by peaks at 2θ = 35° (*d* = 2.52 Å), 2θ = 72° (*d* = 1.31 Å), and 2θ = 83° (*d* = 1.16 Å).[56] A broad maximum at 2θ = 69° was also observed in both samples, but its assignment was precluded by the lack of other diagnostic peaks. Ceramics obtained from the pyrolysis of PFS at relatively low temperatures also give low intensity diffraction patterns indicative of relatively non-crystalline and/or very small iron nanoparticles.[42, 43, 45, 46] Although the low intensity diffraction maxima of **P5py** and **P8py** at low angle were not amenable to meaningful Scherrer analysis, an estimated crystallite size of 13 nm could be elucidated from the relatively intense peaks at 2θ = 82° and 2θ = 83°.

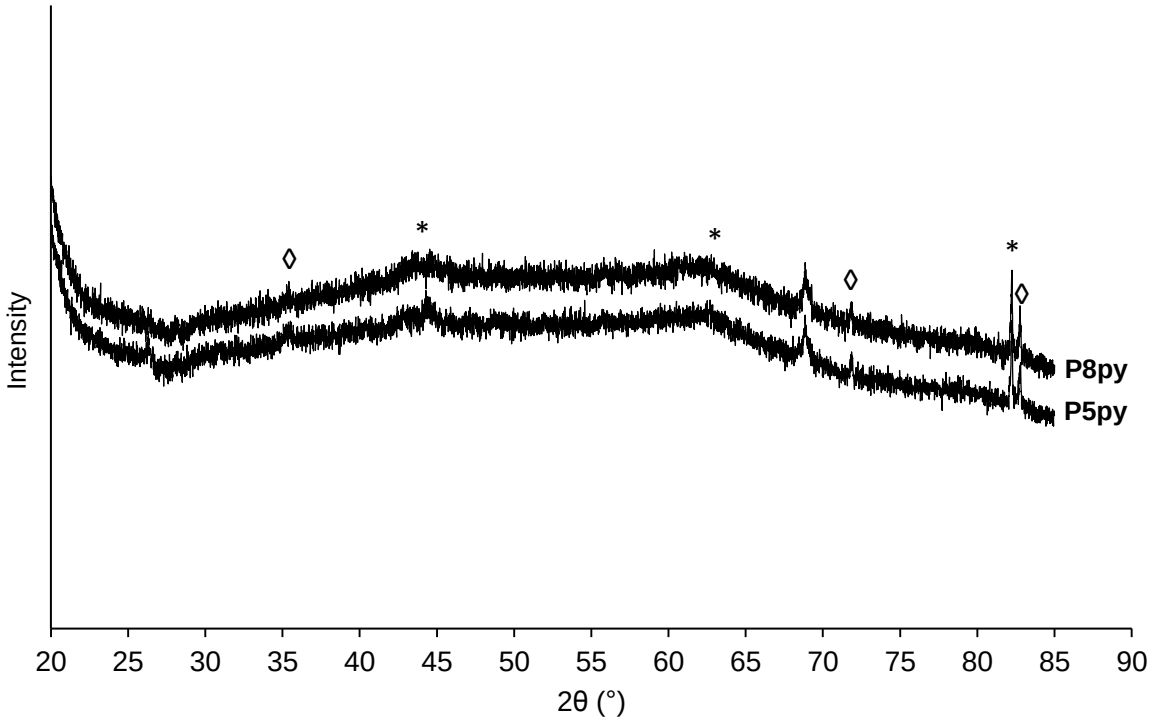

Figure 2.21 Powder X-ray diffraction patterns for ceramics **P5py** (bottom) and **P8py** (top), produced from polymers **P5** and **P8** respectively, after being heated to 800°C at 10°C/min, then immediately allowed to cool to ambient temperature under an atmosphere of N_2. * = αFe, ◊ = Fe_2O_3.

A relatively non-porous morphology was observed by scanning electron microscopy (SEM) (Figure 2.22, Figure 2.24), and the map sum EDX spectrum shows a composition of predominantly silicon, oxygen, and iron for both samples (Figure 2.23, Figure 2.25). **P8py** (which was obtained from a non-precipitated polymer) also contained significant quantities of barium (from residual catalyst), as well as sodium, sulfur, aluminium, and chlorine contamination.

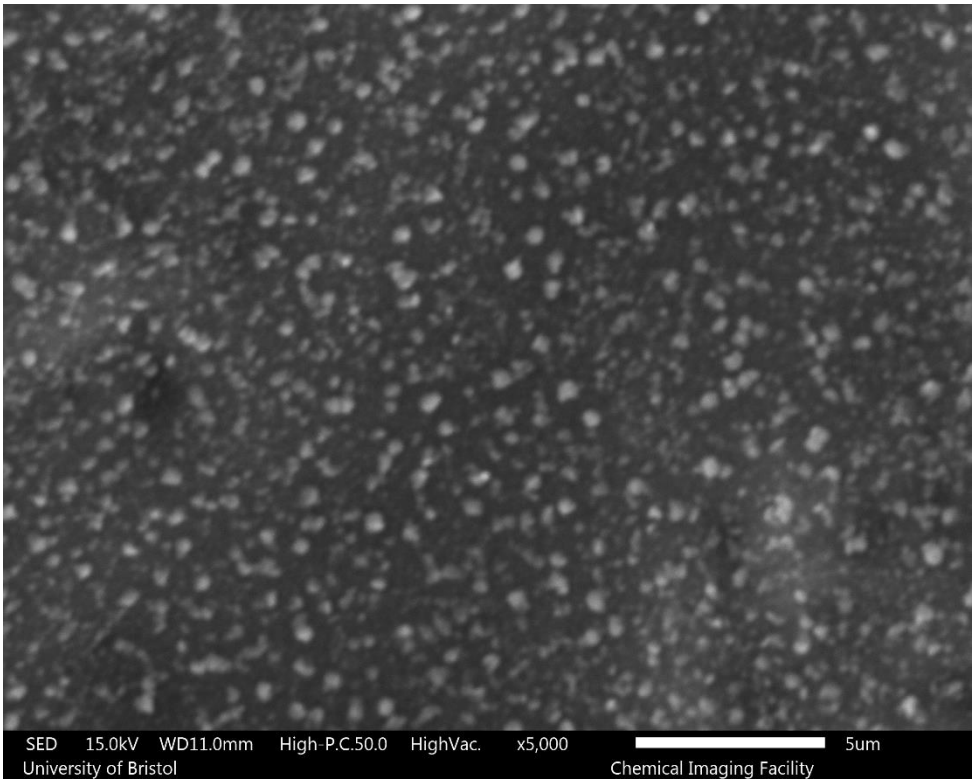

Figure 2.22 SEM micrograph of **P5py**, using secondary electron detector, at 15.0 kV accelerating voltage and a working distance of 11.0 mm.

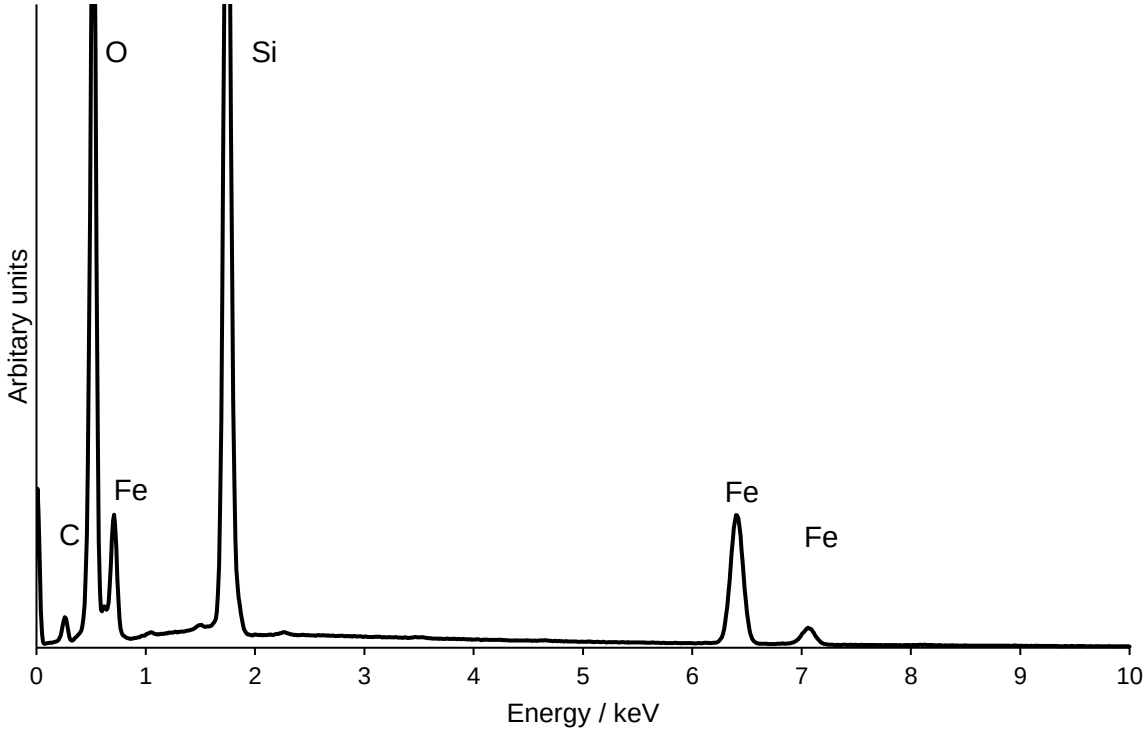

Figure 2.23 Map sum EDX spectrum of **P5py**, taken over the 25x20 µm area shown in Figure 2.22.

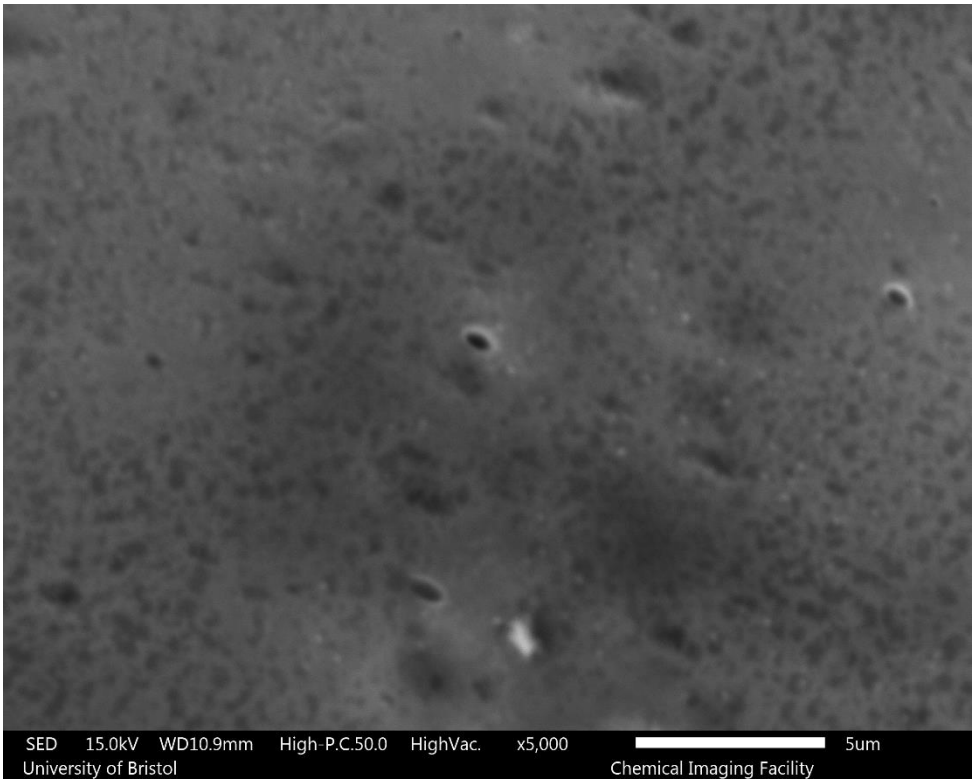

Figure 2.24 SEM micrograph of **P8py**, using secondary electron detector, at 15.0 kV accelerating voltage and a working distance of 10.9 mm.

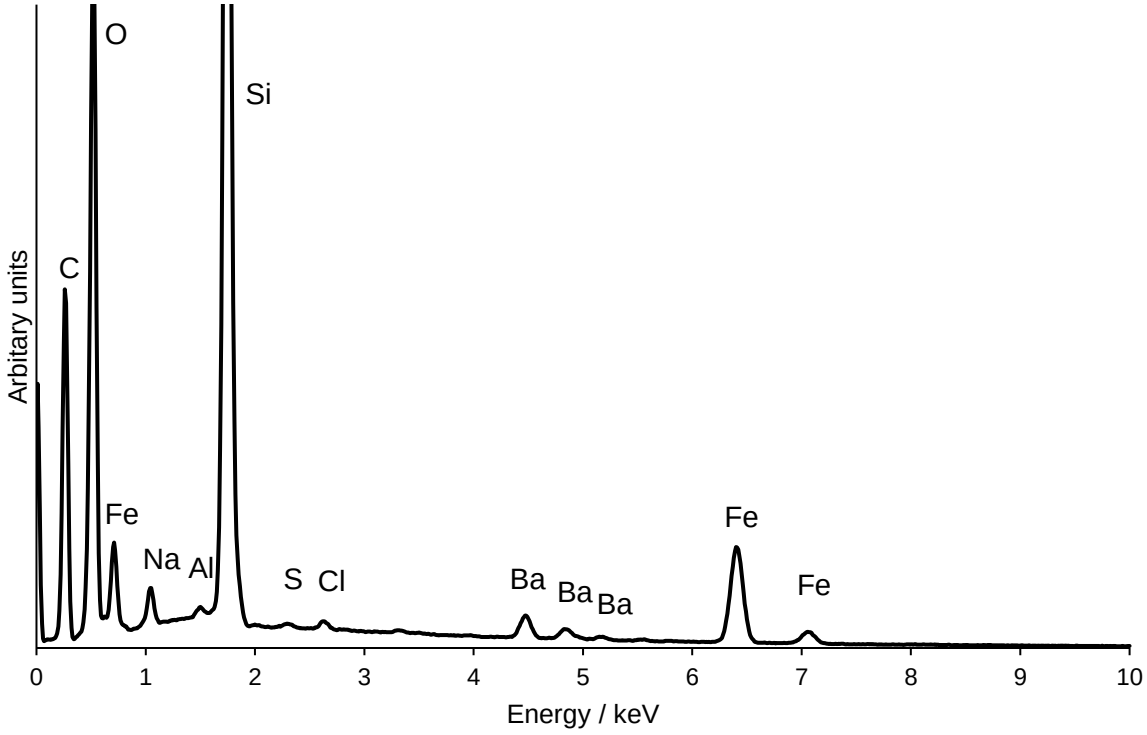

Figure 2.25 Map sum EDX spectrum of **P8py**, taken over the 25x20 µm area shown in Figure 2.24.

Transmission Electron Microscopy (TEM) and dark-field Scanning Transmission Electron Microscopy (STEM) was carried out after embedding finely ground samples in resin and microtoming. **P5py** and **P8py** appeared similar, with nanoparticles homogeneously dispersed throughout a matrix of lower contrast (Figure 2.26, Figure 2.27). Depending on the sample and region studied, the average nanoparticle size varied between 9 nm and 16 nm (Figure 2.26).

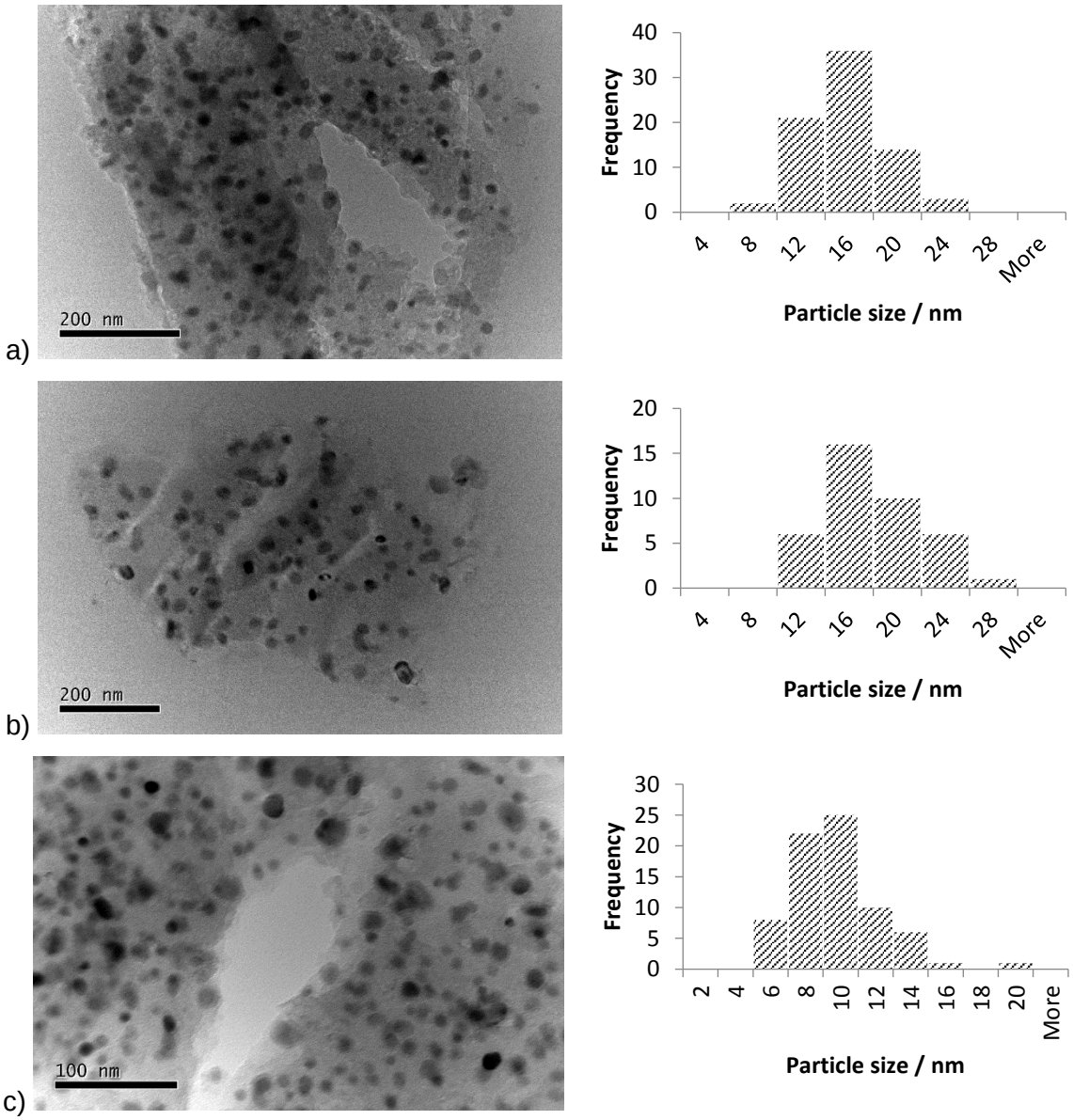

Figure 2.26: TEM micrograph and histogram showing the size distribution of iron nanoparticles for a) **P8py**, b) **P5py** site A, c) **P5py** site B.

a) 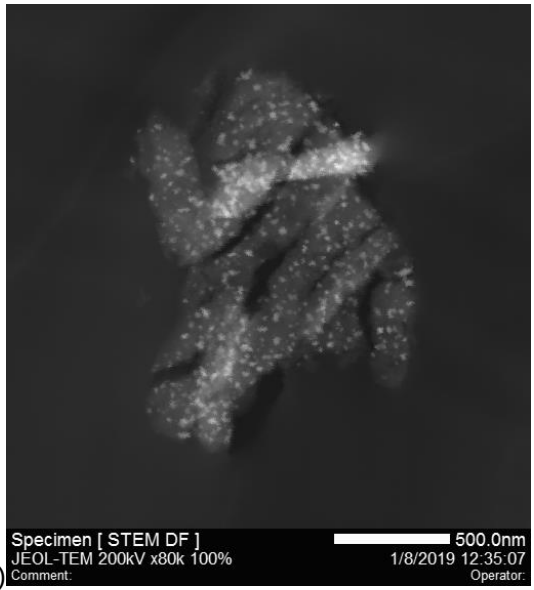

b) 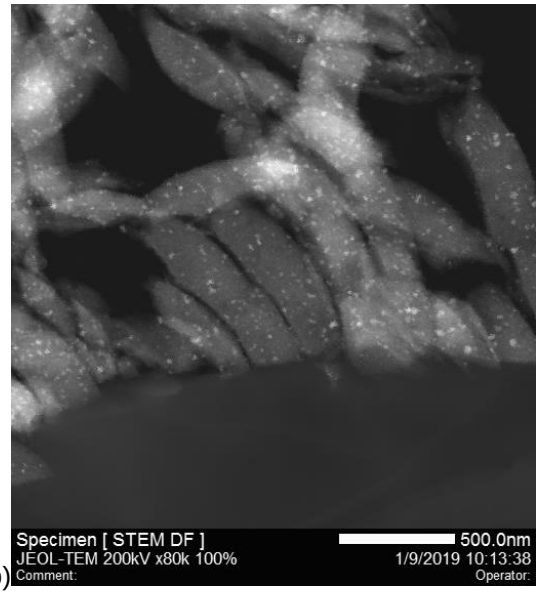

Figure 2.27: STEM dark-field micrographs of a) **P5py** and b) **P8py**.

EDX clarified the elemental composition of the nanoparticles and surrounding matrix, with the iron localised in the nanoparticles, and the matrix predominantly composed of silicon and carbon. Other elements present in significant quantities were barium (from the polymerisation catalyst), oxygen (likely introduced during sample preparation), and nitrogen (Figure 2.28 and Figures i.6, i.7 in Appendix i).

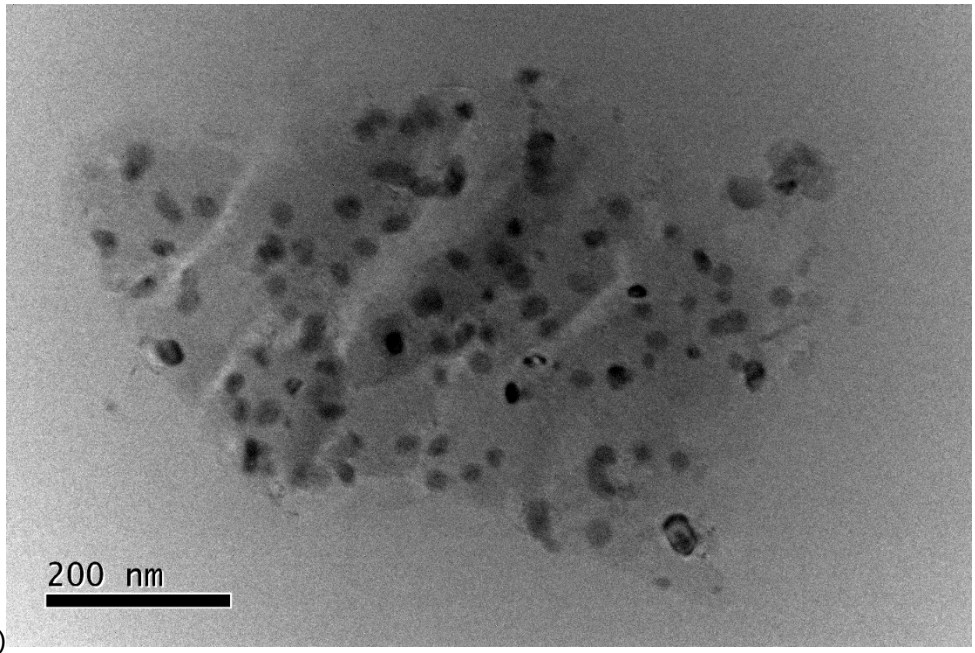

a)

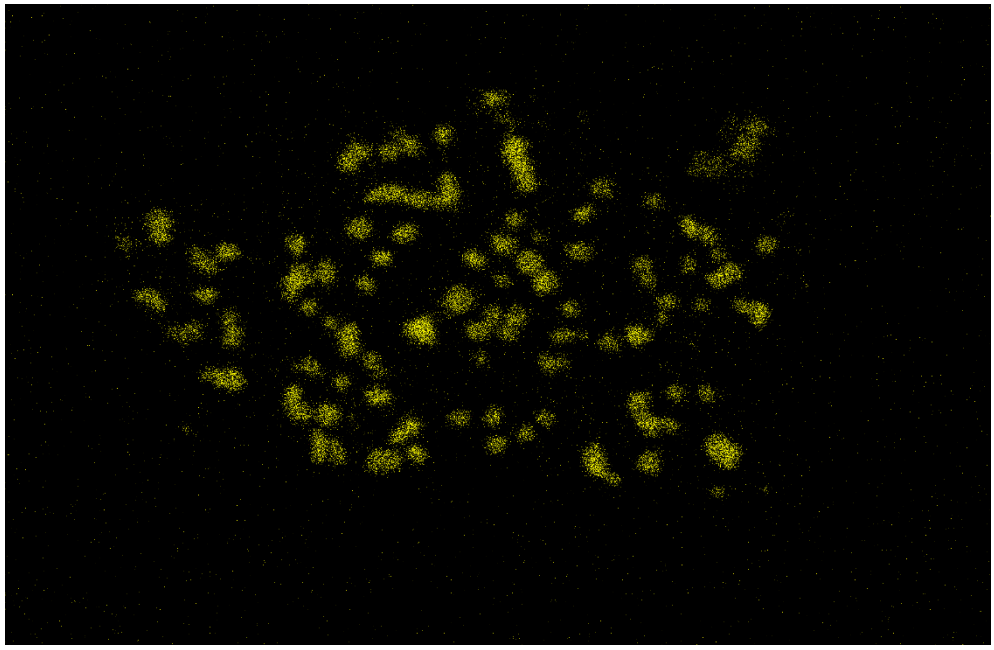

b)

Figure 2.28 a) TEM micrograph and b) FeKα1 EDX map of **P5py**.

The nanoscopic structure was further investigated by High Resolution Transmission Electron Microscopy (HRTEM). The nanoparticles showed lattice fringes of *d*-spacing 0.217 nm, which corresponds to the (110) plane of α-Fe (Figure 2.29a, d). A polycrystalline diffraction pattern was obtained by Selected Area Electron Diffraction (SAED), with clear diffraction rings corresponding to the (110) and (211) lattice planes of α-Fe (Figure 2.29c, f). In agreement with PXRD, the surrounding matrix was predominantly devoid of lattice fringes, albeit some regions of graphitised carbon could be resolved (d = 0.365 nm (002)) (Figure 2.29b, e).

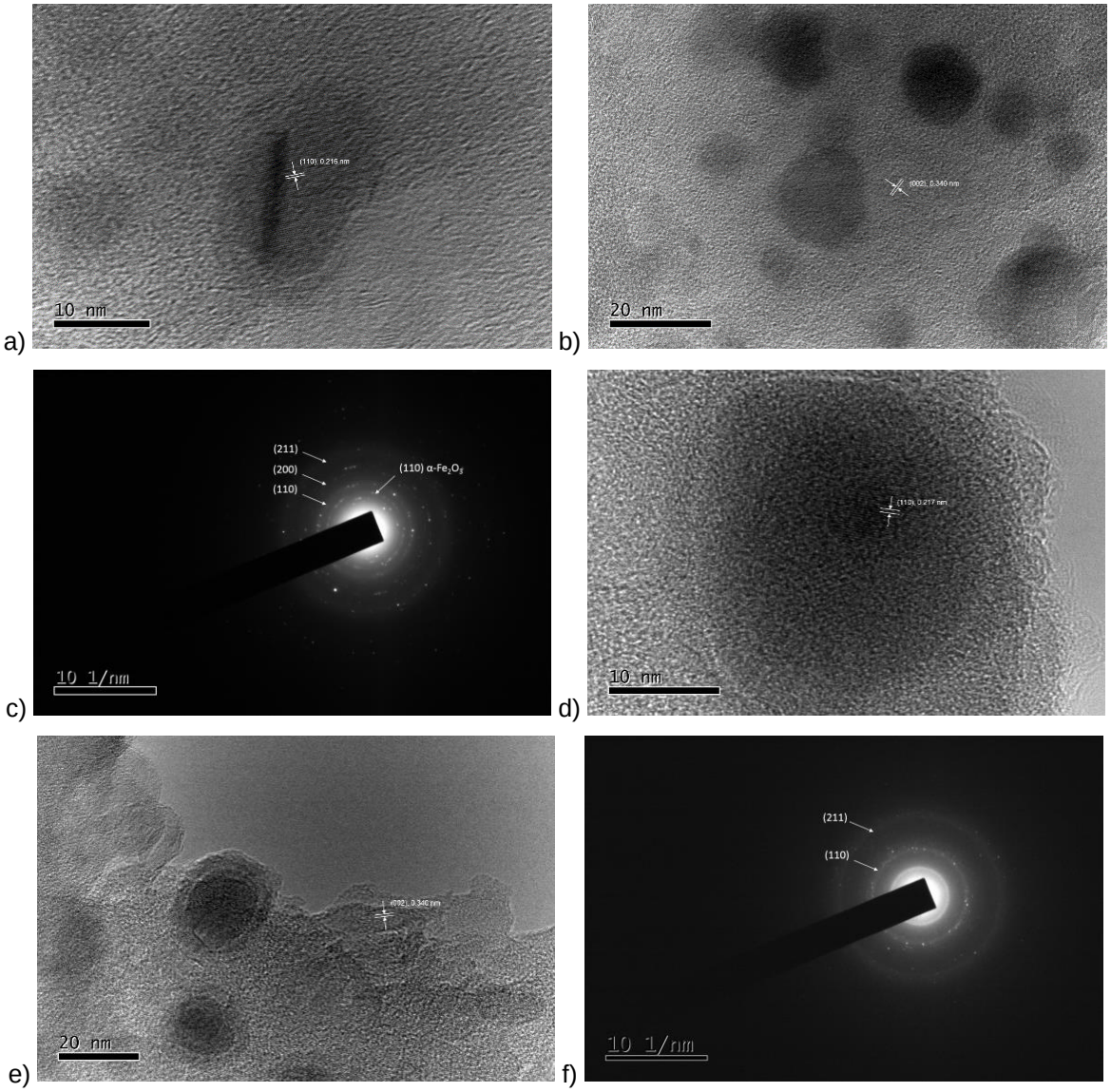

Figure 2.29: a) and b) HRTEM micrographs, and c) Selected Area Electron Diffraction for **P5py**, d) and e) HRTEM micrographs, and f) SAED diffraction pattern of **P8py**. Indexed reflections refer to the α-Fe phase unless stated otherwise.

The magnetic properties of **P5py** and **P8py** are likely to lie on the borderline between superparamagnetism and ferromagnetism. The former phenomenon is the product of single-domain particles below a size of approximately 14 nm, whilst ferromagnetism is typically observed for larger, multi-domain particles which are able to retain magnetic hysteresis in the absence of external magnetic field.[57] The resulting pyrolysed material appears to be unaffected by structural variation of the polymeric precursor (main chain *vs.* pendent ferrocene), but future studies focussing on pyrolysis conditions would merit attention in order to fine-tune the ceramic's magnetic properties.[43]

2.3 Conclusions

In conclusion, ferrocene-containing polycarbosilazanes can be conveniently accessed *via* the Ae-catalysed dehydrocoupling of silanes and amines. Synthetically accessible bis(amide) pre-catalysts may be used, with readily prepared or commercially available monomers. Soluble, well characterised linear polymers with ferrocene pendent to, or part of, the polymer chain can be yielded selectively through careful choice of monomer and, in some cases, estimated M_n values in excess of 20000 Da were achieved. The catalytic dehydrocoupling reaction was also used to isolate unusual silazane[3]ferrocenophanes. Iron centres in the polymers display reversible redox activity, but act as isolated redox centres without electronic communication, as determined by cyclic voltammetry. Pyrolysis of the polymers under N_2 provides magnetic ceramic materials with good yields in most cases. The resulting materials responded to an external magnetic field, and extensive characterisation described a structure of α-Fe nanoparticles embedded within an amorphous silicon carbide/nitride matrix. Although deliberate pre-crosslinking of the polymers gave slight improvements in ceramic yield, it was not essential, and high ceramic yields are likely to be the result of cross-linking reactions *in situ*, enabled by residual functionality of the polymer backbone.

In summary, dehydrocoupling reactions such as those described in the chapter are promising routes towards novel materials with interesting and useful properties. However, moisture sensitivity of Si–N bonds in the polymer backbone limits characterisation, processing and ultimately, application of these materials. In the following chapter, the principles of Ae-catalysed dehydrocoupling will be extended towards alcohol substrates in an effort to form hydrolytically robust polymers *via* Ae-catalysed Si–O bond formation.

2.4 Experimental details

2.4.1 Synthesis of $Fc(SiPhH_2)$ 1

In the glove box, a Schlenk flask was charged with 4.0 g ferrocene (21.5 mmol) and 0.30 g KOtBu (2.7 mmol), then dissolved in approx. 50 ml THF. Another Schlenk flask was charged with 25.3 ml *t*BuLi (1.7 M in pentane, 43 mmol). The flasks were transferred to a Schlenk line, cooled to -78°C, and the *t*BuLi added dropwise to the ferrocene solution. The yellow suspension was stirred at -78°C for a further hour and 5.8 ml $SiPhH_2Cl$ (40 mmol) was added dropwise over 5 minutes. The reaction mixture was slowly warmed to ambient temperature, and stirred for a further 90 minutes. Volatiles were removed under reduced pressure, yielding a viscous orange slurry. The product was extracted with two portions of hexane followed by cannula filtration. Removal of the solvent yielded the crude product as a viscous orange oil. Prolonged sublimation at 70°C onto a cold finger and the walls of a Schlenk flask yielded the pure product as orange crystals suitable for single-crystal X-ray diffraction analysis. Yield 3.4

g, 54%. ^{1}H NMR (300 MHz, C_6D_6) δ 7.69 – 7.58 (m, 2H, *o*-C_6H_5), 7.27 – 7.06 (m, 3H, *m,p*-C_6H_5), 5.14 (s, 2H, SiH_2), 4.17 (t, *J* = 1.6 Hz, 2H, 2,5-Si(C_5H_4), 4.13 (t, *J* = 1.8 Hz, 2H, 3,4-Si C_5H_4), 3.98 (s, 5H, C_5H_5). ^{13}C{^{1}H} NMR (126 MHz, C_6D_6) δ 135.58 (*o-Ph*), 133.47 (*i-Ph*), 129.92 (*m-Ph*), 128.37 (*p-Ph*), 75.08 (3,4-C_5H_4), 72.16 (2,5- C_5H_4), 69.04 (C_5H_5), 61.15 (1- C_5H_4Si). ^{29}Si{^{1}H} NMR (99 MHz, C_6D_6) δ -35.81. Analysis calculated for $C_{16}H_{16}FeSi$: C 65.76, H 5.52, N 0%. Found: C 65.66, H 5.39, N 0%.

2.4.2 Reaction of benzyl amine with 1 to give FcSi(Ph)(HNBn)$_2$ 2

To a J. Youngs NMR tube was added 10 mg **1** ($3.42x10^{-5}$ mol), 7.48 µl benzyl amine ($6.84x10^{-5}$ mol), and 0.5 ml C_6D_6. 1 mg **IIb** ($2x10^{-6}$ mol) was dissolved in 0.1 ml C_6D_6 in a vial, and added *via* pipette to the NMR tube resulting in immediate effervescence. On heating at 60°C for 16 hours, quantitative conversion to FcSi(Ph)(NHBn)$_2$ **2** was observed. Slow evaporation of a toluene solution yielded long, yellow crystalline needles, suitable for single crystal X-ray diffraction analysis. Yield 3.5 mg, 20.4%. Alternatively, compounds **IIc** or **IId** could be used in the place of compound **IIb** at the same molar loading, reaching quantitative conversion to **2** after 20 minutes at room temperature followed by 1 hour at 60°C, or after 20 minutes at room temperature respectively. ^{1}H NMR (500 MHz, C_6D_6) δ 7.88 – 7.81 (m, 2H, *o*-Si*Ph*), 7.35 – 7.24 (m, 7H *o*-CH_2*Ph* + *m,p*-Si*Ph*), 7.23 – 7.18 (m, 4H, *m*-CH_2*Ph*), 7.14 – 7.07 (m, 2H, *p*-CH_2*Ph*), 4.20 (dd, *J* = 2.0, 1.4 Hz, 2H, 2,5-C_5H_4), 4.19 (dd, *J* = 2.0, 1.4 Hz, 2H, 3,4-C_5H_4), 4.13 (d, *J* = 2.5 Hz, 2H, NHCH_2), 4.12 (d, *J* = 2.1 Hz, 2H, NHCH_2), 3.93 (s, 5H, C_5H_5), 1.43 (t, *J* = 8.0 Hz, 2H, N*H*). ^{13}C{^{1}H} NMR (126 MHz, C_6D_6) δ 144.52 (*i*-Si*Ph*), 137.98 (*i*-CH_2*Ph*), 135.02 (*o*-Si*Ph*), 129.75 (*o*-CH_2*Ph*), 128.65 (*m*-CH_2*Ph*), 128.11 (*p*-Si*Ph*), 127.36 (*m*-Si*Ph*), 126.79 (*p*-CH_2*Ph*), 74.30 (2,5-C_5H_4), 71.36 (3,4-C_5H_4), 68.86 (C_5H_5), 46.07 (CH_2). ^{29}Si{^{1}H} NMR (99 MHz, C_6D_6) δ -21.34. Analysis calculated for $C_{30}H_{30}FeN_2Si$: C 71.71, H 6.02, N 5.57%. Found: C 71.71, H 5.86, N 5.43%.

2.4.3 Synthesis of P1-P7

In the glove box, a 5 ml solution of 1.05 g **1** (3.6 mmol) and 0.49 g *p*-xylylenediamine (3.6 mmol) was made up in toluene (0.72 M) and stirred overnight before use to ensure complete dissolution. A Schlenk flask was charged with 1 ml of the stock solution (0.72 mmol) and heated to 60°C. The catalyst was added to another Schenk flask, dissolved in 0.5 ml toluene, and added *via* cannula to the monomer solution. Immediate and vigorous effervescence was accompanied by the appearance of an intense purple colour, and the reaction was stirred at 60°C for a further 2 hours to ensure complete conversion. Polymers were isolated by precipitation into pentane at -78°C, cannula filtration, and removal of solvent under vacuum.

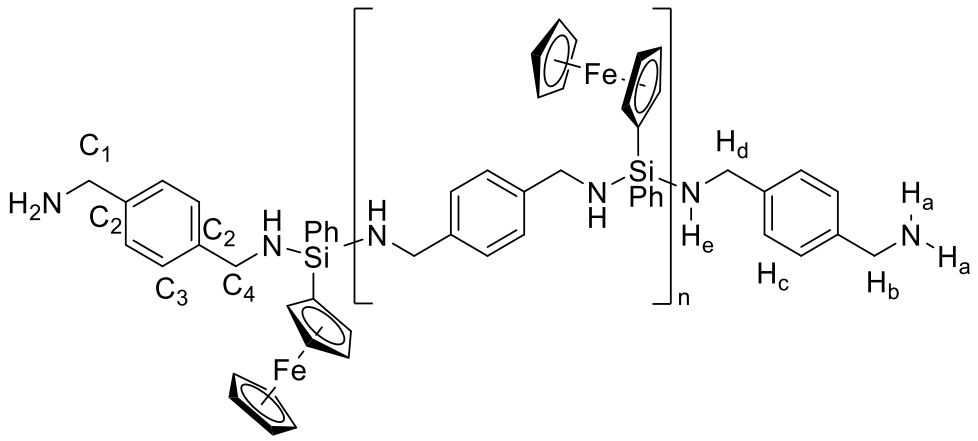

Figure 2.30 Labelling scheme used in ^{1}H and ^{13}C NMR assignment for polymers **P1**-**P7**.

Polymer **P1** was synthesised according to the general procedure, using 21.6 mg **IId** (0.035 mmol, 5 mol%). Isolated yield following precipitation: 0.105 g, 33%. ^{1}H NMR (500 MHz, C_6D_6) δ 7.88 (d, *J* = 6.6 Hz, 49H, *o-Ph*Si), 7.38 (s, 91H, H_c), 7.29 (q, *J* = 7.7, 7.0 Hz, 88H, *m,p-Ph*Si), 4.37 – 4.07 (m, 197H, H_d + C_5H_4), 3.96 (s, 114H, C_5H_5), 3.61 (t, *J* = 7.2 Hz, 4H, H_b), 1.49 (t, *J* = 7.8 Hz, 54H, H_e), 0.77 (s, 4H, H_a). ^{13}C{^{1}H} NMR (126 MHz, C_6D_6) δ 142.83 (C_2), 138.12 (*i-Ph*Si), 135.07 (*o-Ph*Si), 129.75 (*m-Ph*Si), 128.35 (*p-Ph*Si), 127.52 (C_3), 74.37 (2,5-C_5H_4), 71.39 (3,4-C_5H_4), 68.92 (C_5H_5), 68.64 (1- C_5H_4), 45.95 (C_1, C_4). ^{29}Si{^{1}H} NMR (99 MHz, C_6D_6) δ -21.46.

Polymer **P2** was synthesised according to the general procedure, using 14.3 mg **IId** (0.024 mmol, 3.3 mol%). Isolated yield following precipitation: 0.172 g, 57%. ^{1}H NMR (500 MHz, C_6D_6) δ 7.88 (dq, *J* = 5.7, 2.1 Hz, 50H, *o-Ph*Si), 7.38 (s, 81H, H_c), 7.35 – 7.23 (m, 81H, *m,p-Ph*Si), 4.30 – 4.14 (m, 183H, H_d + C_5H_4), 3.96 (s, 104H, C_5H_5), 3.61 (t, *J* = 7.0 Hz, 4H, H_b), 1.49 (t, *J* = 7.9 Hz, 54H, H_e), 0.77 (s, 4H, H_a). ^{13}C{^{1}H} NMR (126 MHz, C_6D_6) δ 142.83 (C_2), 138.12 (*i-Ph*Si), 135.08 (*o-Ph*Si), 129.75 (*m-Ph*Si), 128.35 (*p-Ph*Si), 127.52 (C_3), 74.37 (2,5-C_5H_4), 71.39 (3,4-C_5H_4), 68.92 (C_5H_5), 68.64 (1- C_5H_4), 45.95 (C_1, C_4). ^{29}Si{^{1}H} NMR (99 MHz, C_6D_6) δ -21.46.

Polymer **P3** was synthesised according to the general procedure, using 4.3 mg **IId** (0.007 mmol, 1 mol%). Isolated yield following precipitation: 0.200 g, 62%. ^{1}H NMR (500 MHz, C_6D_6) δ 7.87 – 7.80 (m, 5H, *o*-Si*Ph*), 7.80 – 7.75 (m, 2H, *o*-Si*Ph*), 7.33 (dd, *J* = 5.5, 1.8 Hz, 5H, H_c), 7.31 – 7.19 (m, 12H, *m,p-Ph*Si), 5.91 (d, *J* = 5.7 Hz, 0H, Si*H*), 5.63 (t, *J* = 2.3 Hz, 1H, Si*H*), 5.10 (s, 0H, Si*H*), 4.25 – 4.09 (m, 23H, C_5H_4 + H_d), 3.99 – 3.94 (m, 2H, H_d), 3.94 – 3.92 (m, 2H, C_5H_5), 3.92 – 3.90 (m, 8H, C_5H_5), 3.56 (q, *J* = 6.8 Hz, 4H, H_b), 1.53 – 1.39 (m, 5H, H_e), 1.08 (t, *J* = 8.2 Hz, 0H, H_e), 0.72 (s, 4H, H_a). ^{13}C{^{1}H} NMR (126 MHz, C_6D_6) δ 142.83 (C_2),

142.29 (C_2), 138.12 (*i-Ph*Si), 135.06 (*o-Ph*Si), 130.09 (*m-Ph*Si), 129.74 (*m-Ph*Si), 128.35 (*p-Ph*Si), 127.51 (C_3), 127.49 (C_3), 127.40 (C_3), 74.58 (2,5-C_5H_4), 74.35 (2,5-C_5H_4), 71.87 (3,4-C_5H_4), 71.73 (3,4-C_5H_4), 71.37 (3,4-C_5H_4), 68.90 (C_5H_5), 68.63 (1- C_5H_4), 46.58 (C_1), 45.93 (C_4). $^{29}Si\{^1H\}$ NMR (99 MHz, C_6D_6) δ -21.45.

Polymer **P6** was synthesised according to the general procedure, using 14.3 mg **IIId** (0.024 mmol, 3.3 mol%). Isolated yield following precipitation: 0.192 g, 63%.^{1}H NMR (500 MHz, C_6D_6) δ 7.92 – 7.83 (m, 64H, *o-Ph*Si), 7.38 (s, 104H, H_c), 7.34 – 7.24 (m, 99H, *m,p-Ph*Si), 4.30 – 4.12 (m, 223H, H_d + C_5H_4), 3.96 (s, 128H, C_5H_5), 3.61 (t, J = 7.1 Hz, 4H, H_b), 1.49 (t, J = 7.8 Hz, 70H, H_e), 0.77 (s, 3H, H_a). $^{13}C\{^1H\}$ NMR (126 MHz, C_6D_6) δ 142.83 (C_2), 138.12 (*i-Ph*Si), 135.07 (*o-Ph*Si), 129.75 (*p-Ph*Si), 128.35 (*m-Ph*Si), 127.52 (C_3), 74.37 (2,5-C_5H_4), 71.39 (3,4-C_5H_4), 68.92 (C_5H_5), 68.64 (1-C_5H_4), 45.95 (C_1, C_4). $^{29}Si\{^1H\}$ NMR (99 MHz, C_6D_6) δ -21.45.

P5. A Schenk flask was charged with 0.105 g **1** (0.36 mmol), 0.049 g *p*-xylylenediamine (0.36 mmol), and 0.25 ml THF. The monomer solution was stirred for 1 hour until completely dissolved before a THF solution of **IId** was added (7.1 mg, 0.012 mmol, 3.3 mol%, in 0.02 ml THF). Immediate and vigorous effervescence was accompanied by the appearance of an intense purple colour. The reaction was stirred for a further hour, before the viscous solution was diluted with a further 0.5 ml THF and precipitated into non-dried hexane. The polymer was isolated as a pale orange solid following filtration and removal of solvent under vacuum. Yield 60.5 mg, 39.6%. ^{1}H NMR (500 MHz, C_6D_6) δ 7.92 – 7.84 (m, 55H, *o-Ph*Si), 7.38 (s, 90H, H_c), 7.33 – 7.24 (m, 86H, *m,p-Ph*Si), 4.29 – 4.12 (m, 223H, H_d + C_5H_4), 3.96 (s, 108H, C_5H_5), 3.61 (t, J = 7.1 Hz, 4H, H_b), 1.49 (t, J = 7.8 Hz, 63H, H_e), 0.77 (s, 4H, H_a). $^{13}C\{^1H\}$ NMR (126 MHz, C_6D_6) δ 142.83 (C_2), 138.12 (*i-Ph*Si), 135.07 (*o-Ph*Si), 129.75 (*p-Ph*Si), 128.35 (*m-Ph*Si) 127.52 (C_3), 74.37 (2,5-C_5H_4), 71.39 (3,4-C_5H_4), 68.93 (C_5H_5), 68.64 (1-C_5H_4), 45.95 (C_1, C_4). $^{29}Si\{^1H\}$ NMR (99 MHz, C_6D_6) δ -21.45.

P6. A Schenk flask was charged with 0.126 g **1** (0.43 mmol), 0.059 g *p*-xylylenediamine (0.43 mmol), and 0.6 ml toluene. The monomer solution was stirred for 1 hour until completely dissolved before a toluene solution of **IId** was added (8.7 mg, 0.014 mmol, 3.3 mol%, in 0.33 ml toluene). Immediate and vigorous effervescence was accompanied by the appearance of an intense purple colour. The reaction was stirred for two hours at room temperature before precipitating twice into non-dried hexane. The polymer was isolated as a pale orange solid following filtration and removal of solvent under vacuum. Yield 90.6 mg, 49.6%. ^{1}H NMR (500 MHz, C_6D_6) δ 7.88 (dt, J = 5.9, 2.3 Hz, 92H, *o-Ph*Si), 7.38 (s, 180H, H_c), 7.33 – 7.23 (m, 171H, *m* + *p-Ph*Si), 4.29 – 4.14 (m, 369H, H_d + C_5H_4), 3.96 (s, 206H, C_5H_4),

3.61 (t, *J* = 6.9 Hz, 4H, H_b), 1.49 (t, *J* = 7.8 Hz, 92H, H_e), 0.77 (s, 4H, H_a). $^{13}C\{^1H\}$ NMR (126 MHz, C_6D_6) δ 142.83 (C_2), 138.12 (*i*-Si*Ph*), 135.07 (*o*-Si*Ph*), 129.75 (*p*-Si*Ph*), 128.14 (*m*-Si*Ph*), 127.52 (C_3), 74.37 (2,5-C_5H_4), 71.39 (3,4-C_5H_4), 68.93 (C_5H_5), 68.64 (1-C_5H_4), 45.95 (C_4). $^{29}Si\{^1H\}$ NMR (99 MHz, C_6D_6) δ -21.45.

P7a and **P7b**. A Schenk flask was charged with 0.126 g **1** (0.43 mmol), 0.059 g *p*-xylylenediamine (0.43 mmol), and 0.6 ml toluene. The monomer solution was stirred for 1 hour until completely dissolved before a toluene solution of **IId** was added (8.7 mg, 0.014 mmol, 3.3 mol%, in 0.33 ml toluene). Immediate and vigorous effervescence was accompanied by the appearance of an intense purple colour. After stirring for two hours at room temperature, half of the reaction mixture was removed and precipitated twice into non-dried hexane, yielding **P7a**. Yield 13.9 mg (7.6%). ^1H NMR (500 MHz, C_6D_6) δ 7.91 – 7.83 (m, 75H, *o-Ph*Si), 7.38 (d, *J* = 2.0 Hz, 126H, H_c), 7.29 (d, *J* = 7.3 Hz, 104H, *m* + *p-Ph*Si), 4.28 – 4.13 (m, 293H, H_d + C_5H_4), 3.96 (d, *J* = 2.2 Hz, 139H, C_5H_5), 3.61 (t, *J* = 7.1 Hz, 4H, H_b), 1.50 (t, *J* = 7.7 Hz, 78H, H_e), 0.77 (s, 4H, H_a). $^{13}C\{^1H\}$ NMR (126 MHz, C_6D_6) δ 142.84 (C_2), 138.12 (*i*-Si*Ph*), 135.08 (*o*-Si*Ph*), 129.75 (*p*-Si*Ph*), 128.15 (*m*-Si*Ph*), 127.52 (C_3), 74.37 (2,5-C_5H_4), 71.39 (3,4-C_5H_4), 68.93 (C_5H_5), 68.64 (1-C_5H_4), 45.95 (C_4). $^{29}Si\{^1H\}$ NMR (99 MHz, C_6D_6) δ -21.45.

A further 4.4 mg **IId** (0.007 mmol) in 0.150 ml toluene was added without visual change. The reaction was stirred for a further two hours before precipitating twice into non-dried hexane to yield **P7b**. Yield 30.3 mg (16.6%). NMR spectra were very similar to that of **P7a**. ^1H NMR (500 MHz, C_6D_6) δ 7.93 – 7.82 (m, 60H), 7.38 (s, 89H), 7.34 – 7.24 (m, 89H), 4.30 – 4.11 (m, 226H), 3.96 (s, 126H), 3.61 (t, *J* = 6.8 Hz, 4H), 1.49 (t, *J* = 7.8 Hz, 63H), 0.77 (s, 4H). $^{13}C\{^1H\}$ NMR (126 MHz, C_6D_6) δ 142.83, 138.12, 135.08, 129.75, 128.14, 127.52, 74.37, 71.39, 68.92, 68.64, 45.95. $^{29}Si\{^1H\}$ NMR (99 MHz, C_6D_6) δ -21.46.

2.4.4 Synthesis of fc(SiPhH$_2$)$_2$ 3

In the glove box, a Schlenk flask was charged with 3.26 g ferrocene (18 mmol) and 6.45 ml *N*,*N*,*N*',*N*'-tetramethylethylenediamine (TMEDA) (43 mmol). Another Schlenk flask was charged with 17.0 ml 2.5 M *n*BuLi in hexanes (43 mmol). The ferrocene and TMEDA were dissolved/suspended in ~80 ml hexane, and on the Schlenk line, the *n*BuLi solution was added dropwise with stirring. The reaction mixture was stirred at room temperature for 16 hours and the resultant pale orange suspension allowed to settle before cannula filtration. The pale orange solid (dilithioferrocene) was washed with two portions of hexane, then re-suspended in ~50 ml fresh hexane. The suspension was cooled to 0 °C, and 4.7 ml $SiPhH_2Cl$ (35 mmol) was added dropwise. The reaction was allowed to reach room temperature, and stirred for a further 16 hours. The product was extracted from the LiCl by-product with hexane, cannula filtered, and solvent removed under reduced pressure to obtain a sticky orange residue.

Prolonged sublimation onto a dry-ice cold finger and the walls of a Schlenk flask at 140 °C yielded the pure product as orange crystals suitable for single-crystal X-ray diffraction analysis. Yield 1.98 g, 28.4%. ^{1}H NMR (300 MHz, C_6D_6) δ 7.65 – 7.56 (m, 4H, *o*-C_6H_5), 7.20 – 7.09 (m, 6H, *m,p*-C_6H_5), 5.10 (s, 4H, SiH_2), 4.20 (t, *J* = 1.7 Hz, 4H, 2,5-C_5H_4), 4.13 (t, *J* = 1.9 Hz, 4H, 3,4-C_5H_4). ^{13}C{^{1}H} NMR (126 MHz, C_6D_6) δ 135.56 (*o*-Ph), 133.24 (*i*-Ph), 129.97 (*m*-Ph), 128.39 (*p*-Ph), 75.83 (3,4-C_5H_4), 72.92 (2,5-C_5H_4), 61.91 (1-C_5H_4). ^{29}Si{^{1}H} NMR (99 MHz, C_6D_6) δ -35.83. Analysis calculated for $C_{22}H_{22}Si_2Fe$: C 66.32 H 5.57 N 0.00%. Found: C 66.27, H 5.48, N 0.00%.

2.4.5 Reaction of benzyl amine with 3 to yield 4

To a J. Youngs NMR tube was added 10 mg **3** ($2.5x10^{-5}$ mol), 5.48 µl benzyl amine ($5x10^{-5}$ mol), and 0.5 ml C_6D_6. 1.5 mg **IId** ($2.5x10^{-6}$ mol) was dissolved in 0.1 ml C_6D_6 and added to the NMR tube. The reaction mixture was heated to 60°C for 16 hours, after which no further reaction was observed. Multinuclear NMR of the crude reaction mixture revealed a mixture of reaction products, precluding detailed characterisation. Solvent was removed under vacuum, and the crude product was re-dissolved in a hexane/toluene mixture. Cooling to -30°C resulted in the isolation of orange crystalline blocks, identified by single crystal X-ray diffraction analysis as compound **4**. Yield 0.5 mg, 2.4%. The reaction was also carried out following the same procedure, but with a 1:2 Si:N ratio; **3** (10 mg, $2.5x10^{-5}$ mol) and benzyl amine ($1.0x10^{-4}$ mol). In this case, a higher yield of crystals were obtained, enabling full characterisation by NMR spectroscopy and elemental microanalysis. Yield 4.0 mg, 19.5% ^{1}H NMR (500 MHz, C_6D_6) δ 7.83 – 7.75 (m, 4H, o-SiPh), 7.30 – 7.22 (m, 14H, *m*+*p*-Si*Ph*, *o*-NHCH2*Ph*), 7.19 (dd, *J* = 8.4, 6.8 Hz, 8H, *m*-NHCH2*Ph*), 7.13 – 7.07 (m, 4H, *p*-NHCH2*Ph*), 4.13 (t, J = 1.7 Hz, 4H, *2,5*-C_5H_4), 4.12 (t, J = 1.6 Hz, 4H, *3,*4-C_5H_4), 4.06 (d, J=1.7 Hz, 4H, NHCH_2), 4.04 (s, br, 4H, NHCH_2), 1.41 (t, *J* = 8.0 Hz, 4H, N*H*). ^{13}C{^{1}H} NMR (126 MHz, C_6D_6) δ 144.46 (*i*-NHCH2*Ph*), 137.84 (*i*-Si*Ph*), 135.03 (*o*-Si*Ph*), 129.81 (*m*-Si*Ph*), 128.62 (*m*-$NHCH_2Ph$), 127.39 (*m*-$NHCH_2Ph$), 126.76 (*p*-$NHCH_2Ph$), 74.65 (*3,4*-C_5H_4), 72.22 (*2,5*-C_5H_4), 68.86 (*1*-C_5H_4), 46.02 (CH_2). ^{29}Si{^{1}H} NMR (99 MHz, C_6D_6) δ -21.32. Analysis calculated for $C_{50}H_{50}FeN_4Si_2$: C 73.33, H 6.15, N 6.84%. Found: C 73.28, H 6.35, N 6.66%.

2.4.6 Synthesis of P8

To a Schlenk flask was added 120 mg **3** (0.3 mmol), 41 mg *p*-xylylenediamine (0.3 mmol), and 2 ml toluene. 9 mg **IId** (0.015 mmol) was dissolved in 1 ml toluene and added to the monomer solution resulting in immediate effervescence and a colour change to purple. After heating to 60°C for 16 hours to ensure complete conversion, the reaction was quenched by addition of 1 ml non-dried hexane. After prolonged drying under vacuum, the product was recovered as a pale orange powder, 105 mg, 60%. ^{1}H NMR (500 MHz, C_6D_6) δ 8.12 – 7.63 (m, 390H *o*-Si*Ph*), 7.52 – 7.19 (m, 1015H, *m,p*-Si*Ph* + C_6H_4), 5.88 – 5.75 (m, 63H, Si*H*), 5.73 (s, 22H,

Si*H*), 5.64 (d, *J* = 6.1 Hz, 19H, Si*H*), 5.56 (d, *J* = 9.7 Hz, 8H, Si*H*), 4.61 – 3.80 (m, 1230H, C_5H_4 + CH_2), 3.58 (br, s, 1H, CH_2NH_2), 3.51 (t, 2H, CH_2NH_2), 1.75 – 1.03 (m, 131H, N*H*). $^{13}C\{^1H\}$ NMR (126 MHz, C_6D_6) δ 139.84 (*i*-Si*Ph*), 135.19 (*o*-Si*Ph*), 135.17 (*o*-Si*Ph*), 135.13 (*o*-Si*Ph*), 135.10 (*o*-Si*Ph*), 135.08 (*o*-Si*Ph*), 130.08 (Si*Ph*), 129.96 (*p*-Si*Ph*), 129.10 (*Ar*), 128.92 (*m*-Si*Ph*), 127.54 (C_6H_4), 127.07 (C_6H_4), 76.73 (2,4-C_5H_4), 76.60 (2,4- C_5H_4), 76.52 (2,4- C_5H_4), 75.36 (C_5H_4), 74.50 (C_5H_4), 74.35 (C_5H_4), 73.67 (C_5H_4), 73.57 (C_5H_4), 73.45 (C_5H_4), 73.23 (C_5H_4), 72.89 (C_5H_4), 63.42 (1- C_5H_4), 63.29 (1- C_5H_4), 51.27 (CH_2). $^{29}Si\{^1H\}$ NMR (99 MHz, C_6D_6) δ -14.20.

2.4.7 Synthesis of polymers P9-P10

In the glovebox, a 3.33 ml solution of **3** (0.96 g, 2.4 mmol) and *p*-xylylenediamine (0.33 g, 2.4 mmol) was made up in toluene (0.72 M) and stirred overnight to aid dissolution. A Schlenk flask was charged with 0.6 ml of the stock solution (0.43 mmol) and heated to 60°C. The catalyst was added to another Schenk flask, dissolved in 0.5 ml toluene, and added *via* cannula to the monomer solution. Immediate and vigorous effervescence was accompanied by the appearance of an intense purple colour, and the reaction was stirred at 60°C for a further 2 hours to ensure complete conversion. Polymers were isolated by precipitation into pentane at -78°C, cannula filtration, and removal of solvent under vacuum.

Polymer **P9** was synthesised according to the general procedure, using 13.1 mg **IId** (0.022 mmol, 5 mol%). Isolated yield following precipitation: 0.110 g, 48%. ^1H NMR (500 MHz, C_6D_6) δ 7.97 – 7.63 (m, 44H, *o*-Si*Ph*), 7.47 – 7.19 (m, 143H, *m,p*-Si*Ph* + C_6H_4), 5.79 (s, br 6H, Si*H*), 5.74 (s, 0H, Si*H*), 5.72 (s, 0H, Si*H*), 5.62 (d, *J* = 11.3 Hz, 7H, Si*H*), 4.60 – 4.38 (m, 10H, C_5H_4), 4.38-4.31 (m, 9H, CH_2), 4.31 – 3.89 (m, 137H, C_5H_4 + CH_2), 3.85 (s, 4H, CH_2), 3.60 (s, 4H, CH_2NH_2), 3.51 (s, 1H, CH_2NH_2), 1.45 (d, *J* = 32.6 Hz, 9H, N*H*), 1.10 (s, 3H, N*H*), 0.76 (s, 3H, NH_2). $^{13}C\{^1H\}$ NMR (126 MHz, C_6D_6) δ 135.17 (*o*-Si*Ph*), 135.08 (*o*-Si*Ph*), 135.06 (*o*-Si*Ph*), 76.71 (C_5H_4), 74.35 (C_5H_4), 73.66 (C_5H_4), 72.88 (C_5H_4), 63.28 (1- C_5H_4), 51.22 (CH_2), 47.00 (CH_2), 45.89 (CH_2). ^{29}Si NMR (99 MHz, C_6D_6, determined from ^1H-^{29}Si HMQC) δ -14.15

Polymer **P10** was synthesised according to the general procedure, using 8.7 mg **IId** (0.014 mmol, 3.3 mol%). Isolated yield following precipitation: 0.120 g, 52%. ^1H NMR (500 MHz, C_6D_6) δ 7.92 – 7.68 (m, 28H, *o*-Si*Ph*), 7.43 – 7.19 (m, 58H, *m,p*-Si*Ph* + C_6H_4), 5.79 (s, 3H, Si*H*), 5.74 (s, 0H, Si*H*), 5.73 (s, 0H, Si*H*), 5.66 – 5.55 (m, 8H, Si*H*), 4.44 (s, 1H), 4.41 (s, 4H), 4.33 (m, CH_2), 4.31 – 3.89 (m, 79H, C_5H_4 + CH_2), 3.86 (d, *J* = 7.8 Hz, 2H, CH_2), 3.59 (s, 4H, CH_2NH_2), 3.51 (s, 1H, CH_2NH_2), 1.91 – 1.26 (m, 87H, N*H*), 1.06 (d, *J* = 47.1 Hz, 8H, N*H*), 0.76 (s, 3H, N*H*), 0.44 (s, 22H, N*H*). $^{13}C\{^1H\}$ NMR (126 MHz, C_6D_6) δ 142.29 (1-C_6H_4), 142.20 (1-C_6H_4), 135.16 (*o*-Si*Ph*), 135.07 (*o*-Si*Ph*), 135.05 (*o*-Si*Ph*), 130.14 (*m*-Si*Ph*), 129.02 (Si*Ph*), 127.47 (2,5-C_6H_4), 127.05 (2,5-C_6H_4), 76.70 (C_5H_4), 75.84 (C_5H_4), 75.35 (C_5H_4), 75.31 (C_5H_4), 75.17 (C_5H_4), 75.11 (C_5H_4), 74.80 (C_5H_4), 74.35 (C_5H_4), 74.22 (C_5H_4), 74.10 (C_5H_4), 73.66

(C_5H_4), 73.46 (C_5H_4), 72.88 (C_5H_4), 72.54 (C_5H_4), 72.51 (C_5H_4), 72.42 (C_5H_4), 47.01 (CH_2). ^{29}Si NMR (99 MHz, C_6D_6, determined from ^{1}H-^{29}Si HMQC) δ -14.13, -16.24.

An attempted polymerisation using 2.6 mg **IId** (0.0043 mmol, 1 mol%) was carried out using the general procedure for **P9-P10**. The ^{1}H NMR spectrum of the product showed predominantly starting material, and no polymeric products by DOSY.

2.4.8 Reaction of 1,1'-bis(amino)ferrocene with Ph_2SiH_2 to yield 5

To a J. Youngs NMR tube was added 10 mg fc(NH_2)$_2$ (0.0463 mmol), 17.2 µl diphenylsilane (0.0926 mmol), and 0.5 ml d_8-THF. 1.4 mg **IId** (0.0023 mmol) was dissolved in 0.1 ml d_8-THF in a vial, and transferred to the NMR tube. On heating to 60°C for 16 hours, complete consumption of fc(NH_2)$_2$ was obtained. Compound **5** was isolated in the form of large orange blocks suitable for single crystal X-ray diffraction by diffusion of hexane into a THF solution at room temperature. Isolated yield 8.6 mg, 47.5%. ^{1}H NMR (500 MHz, C_6D_6) δ 7.80 – 7.73 (m, 4H, *o-Ph*), 7.25 – 7.16 (m, 6H, *m,p-Ph*), 3.82 (t, *J* = 1.9 Hz, 4H, 2,4-C_5H_4), 3.80 (t, *J* = 1.8 Hz, 4H, 3,5-C_5H_4), 2.09 (s, 2H, N*H*). ^{13}C{^{1}H} NMR (126 MHz, C_6D_6) δ 135.83 (*i-Ph*), 135.57 (*o-Ph*), 130.47 (*m-Ph*), 128.35 (*p-Ph*), 97.95 (1-C_5H_4), 66.16 (3,5- C_5H_4), 65.93 (2,4- C_5H_4). ^{29}Si{^{1}H} NMR (99 MHz, C_6D_6) δ -16.08. Analysis calculated for $C_{22}H_{20}FeN_2Si$: C 66.67, H. 5.09, N 7.07%. Found: C 66.48, H 5.16, N 6.91%. Melting point 200°C (Determined by DSC).

This reaction was also carried out using the same method, but with 4.6 mg fc(NH_2)$_2$ (2.10×10^{-5} mol), 2.89 µl diphenylsilane (0.0210 mmol), and 0.7 mg **IId** (0.0012 mmol), yielding the same product in 95% spectroscopic yield. The product was not isolated in this case.

2.4.9 Synthesis of Rc(($SiPhH_2$)) 6

A Schlenk flask was charged with 0.98 g ruthenocene (4.23 mmol) and 59 mg KOtBu (0.53 mmol), dissolved in THF, and cooled to -78°C. Another Schlenk was charged with 5 ml *t*BuLi (1.7 M solution in pentane), which was added dropwise to the ruthenocene solution *via* cannula. The reaction mixture was stirred at -78°C for a further 30 minutes before 1.3 ml $PhSiH_2Cl$ (9.75 mmol) was slowly added. After removing from the cold bath, the reaction was stirred for 90 minutes. The solvent was removed under reduced pressure, and the product was extracted twice with hexane. The crude product was obtained as a yellow residue following removal of solvent under vacuum. The pure product was collected as an off-white crystalline solid by sublimation at 65°C. A colourless plate obtained from the sublimation was selected for single crystal X-ray diffraction analysis. ^{1}H NMR (300 MHz, C_6D_6) δ 7.69 – 7.59 (m, 3H, *m,p*-C_6H_5), 7.24 – 7.17 (m, 2H, *o*-C_6H_5), 5.11 (s, *J* = 1.5 Hz, 2H, SiH_2), 4.60 (t, *J* = 1.5 Hz, 2H, 2,5-C_5H_4), 4.55 (t, *J* = 1.7 Hz, 2H, 3,4-C_5H_4), 4.40 (s, 5H, C_5H_5). ^{13}C{^{1}H} NMR (126 MHz, C_6D_6) δ 135.11 (*o*-C_6H_5), 133.45 (*i*-C_6H_5) 129.49 (*m*-C_6H_5), 127.92 (*p*-C_6H_5), 76.26 (3,4-

C_5H_4), 73.34 (2,5-C_5H_4), 70.93 (C_5H_5). $^{29}Si\{^1H\}$ NMR (99 MHz, C_6D_6) δ -36.82. Analysis calculated for $C_{16}H_{16}RuSi$: C 56.95, H 4.78, N 0.00%. Found: C 57.07, H 4.90, N 0.00%.

2.4.10 Reaction of 1,1'-bis(amino)ferrocene with 6 to yield 7

To a J. Youngs NMR tube was added 4.9 mg $fc(NH_2)_2$ ($2.2x10^{-5}$ mol), 7.0 mg **6** ($2.1x10^{-5}$ mol), and 0.5 ml d_8-THF. 0.6 mg **IId** ($1x10^{-6}$ mol) was dissolved in 0.1 ml d_8-THF in a vial, and transferred to the NMR tube. After heating to 60°C for 16 hours, complete conversion was obtained, with 80% spectroscopic yield of the ferrocenophane product **7**. Addition of a hexane layer to the NMR tube yielded crystals suitable for single crystal X-ray diffraction analysis on standing at room temperature for several days. Yield 3 mg, 23%. ^1H NMR (500 MHz, d_8-THF) δ 7.96 – 7.88 (m, 2H, *o-Ph*), 7.46 – 7.39 (m, 3H, *m,p-Ph*), 4.64 (t, *J* = 1.6 Hz, 2H, 2,5-RuC_5H_4), 4.50 (t, *J* = 1.6 Hz, 2H, 3,4-RuC_5H_4), 4.49 (s, 5H, RuC_5H_5), 3.99 (dt, *J* = 2.5, 1.4 Hz, 2H, 2-FeC_5H_4), 3.72 (tt, *J* = 2.2, 1.1 Hz, 2H, 3-FeC_5H_4), 3.65 (dt, *J* = 2.5, 1.4 Hz, 2H, 5-FeC_5H_4), 3.35 (dt, *J* = 2.6, 1.4 Hz, 2H, 4-FeC_5H_4), 2.88 (s, 2H, N*H*). $^{13}C\{^1H\}$ NMR (126 MHz, d_8-THF) δ 138.70 (*i-Ph*), 136.62 (*o-Ph*), 130.44 (*m-Ph*), 128.23 (*p-Ph*), 99.86 (1-FeC_5H_4), 75.95 (3,4-RuC_5H_4), 73.32 (2,5-RuC_5H_4), 71.71 (RuC_5H_5), 70.99 (1-RuC_5H_4) 69.13 (2-FeC_5H_4), 65.99 (5-FeC_5H_4), 64.84 (3-FeC_5H_4), 62.72 (4-FeC_5H_4). $^{29}Si\{^1H\}$ NMR (99 MHz, d_8-THF) δ -7.41. Analysis calculated for $C_{26}H_{24}FeN_2RuSi$: C 56.84, H 4.40, N 5.10%. Found: C 56.61, H 4.27, N 5.13%. Melting point (determined by DSC): 261°C.

2.4.11 Reaction of *N,N'*-dimethyl-*p*-xylylenediamine with two equivalents of diphenylsilane in the presence of IId to yield 8

To a J. Youngs NMR tube was added 10 µl *N,N'*-dimethyl-*p*-xylyenediamine ($6.21x10^{-5}$ mol), 24.6 µl Ph_2SiH_2 ($1.24x10^{-4}$ mol), and 0.5 ml C_6D_6. 1.9 mg **IId** ($3.15x10^{-6}$ mol) was dissolved in 0.1 ml C_6D_6 and added to the NMR tube. After heating to 60°C overnight, 90% of Ph_2SiH_2 was obtained, and after a further 24 hours at 80°C, complete conversion resulted in near quantitative spectroscopic yield of **8**. Colourless blocks suitable for single crystal X-ray diffraction could be obtained by slow cooling of a hot toluene solution to room temperature, or room temperature toluene solution to -30°C. Yield 13.4 mg, 40%. ^1H NMR (500 MHz, C_6D_6) δ 7.73 – 7.66 (m, 8H, *o*-Si*Ph*), 7.25 (s, 4H, $CH_2C_6H_4CH_2$), 7.23 – 7.18 (m, 12H, *m,p*-Si*Ph*), 5.69 (s, 2H, Si*H*), 4.00 (s, 4H, CH_2), 2.45 (s, 6H, NCH_3). $^{13}C\{^1H\}$ NMR (126 MHz, C_6D_6) δ 139.34 (1-$CH_2C_6H_4CH_2$), 135.60 (*i*-S*Ph*), 135.48 (*o*-Si*Ph*), 129.91 (*m*-Si*Ph*), 128.42 (*p*-Si*Ph*), 128.31 (2,3-$CH_2C_6H_4CH_2$), 55.57 (NCH_2), 35.34 (NCH_3). $^{29}Si\{^1H\}$ NMR (99 MHz, C_6D_6) δ -10.99. Analysis calculated for $C_{34}H_{36}N_2Si_2$: C 77.22, H 6.86, N 5.30%. Found: C 77.29, H 6.94, N 5.23%.

2.4.12 Synthesis of polymer P11

A Schlenk flask was charged with 48.3 µl *N,N'*-dimethyl-*p*-xylylenediamine (0.30 mmol), 120 mg **3** (0.30 mmol), and 4 ml toluene. 9 mg **IId** (0.015 mmol) was dissolved in 1 ml toluene

and added to the monomer solution. The reaction was heated to 60°C for 16 hours to ensure complete conversion. The reaction mixture was cooled to -78°C and precipitated by addition of a large excess of pentane. Following filtration and solvent removal under vacuum, **P11** was obtained as a pale orange solid. Yield 0.084 g, 50%. ^{1}H NMR (500 MHz, C_6D_6) δ 7.80 (t, *J* = 7.4 Hz, 40H, *o-Ph*SiH), 7.68 – 7.52 (m, 5H, *o-Ph*SiH$_2$), 7.28 (dd, *J* = 9.7, 5.7 Hz, 94H, *m,p-Ph*Si, H_g), 5.68 (s, 2H, H_d), 5.64 (d, *J* = 59.3 Hz, 17H, H_h), 5.10 (d, *J* = 5.9 Hz, 2H, H_a), 5.04 (d, *J* = 6.0 Hz, 2H, H_a), 4.38 (s, 8H, C_5H_4), 4.34 (s, 3H C_5H_4), 4.31 – 4.08 (m, 70H, C_5H_4), 4.01 (dd, *J* = 19.7, 13.0 Hz, 53H, H_f), 2.44 (s, 41H, H_e), 2.42 (s, 43H, H_e). ^{13}C{^{1}H} NMR (126 MHz, C_6D_6) δ 139.54 (C_6), 136.99 (*i-Ph*Si), 136.95 (*i-Ph*Si), 135.59 (*p-Ph*Si), 135.17 (*o-Ph*Si), 135.12 (*o-Ph*Si), 135.10 (*o-Ph*Si), 130.11 (*m-Ph*Si), 130.06 (*m-Ph*Si), 128.35 (C_7), 75.83 (C_5H_4), 75.74 (C_5H_4), 75.67 (C_5H_4), 75.62 (C_5H_4), 75.31 (C_5H_4), 75.26 (C_5H_4), 75.23 (C_5H_4), 72.99 (C_5H_4), 72.86 (C_5H_4), 72.75 (C_5H_4), 72.69 (C_5H_4), 66.22 (1- C_5H_4), 55.20 (C_5), 35.24 (C_4), 35.22 (C_4). ^{29}Si{^{1}H} NMR (99 MHz, C_6D_6) δ -10.23, -10.32.

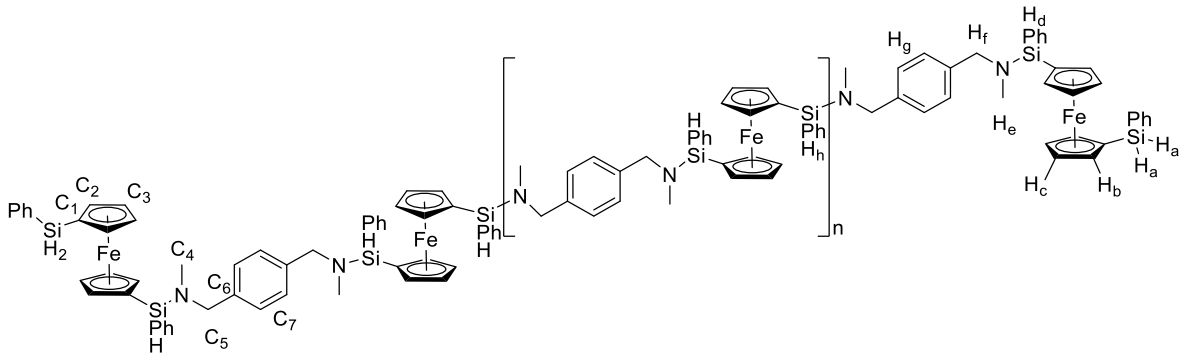

Figure 2.31 Labelling scheme used for the assignment of ^{1}H and ^{13}C NMR for polymer **P11**.

2.4.13 Synthesis of polymer P12

A Schlenk flask was charged with 0.6 ml of a 0.72 M solution (0.43 mmol) of *N*,*N*'-dimethyl-*p*-xylylenediamine and compound **3** in toluene. 12.9 mg **IId** (0.022 mmol, 5 mol%) was dissolved in 0.33 ml toluene and added to the monomer solution, resulting in immediate effervescence. After stirring at room temperature for 16 hours, the product was precipitated twice into non-dried hexane and obtained as a slightly sticky orange residue. 31.5 mg, 13% yield. ^{1}H NMR (500 MHz, C_6D_6) δ 7.85 – 7.73 (m, 126H, *o-Ph*SiH), 7.35 – 7.22 (m, 317H, *m,p-Ph*Si, H_e), 5.70 (d, *J* = 2.2 Hz, 29H, H_h), 5.58 (d, *J* = 2.1 Hz, 29H, H_h), 4.38 (s, 45H), 4.23 (s, 60H, C_5H_4), 4.22 – 4.18 (m, 62H, C_5H_4), 4.17 (s, 33H, C_5H_4), 4.15 (s, 31H, C_5H_4, 4.07 – 3.91 (m, 168H, H_f), 3.54 (m, 4H, H_d) 2.43 (dd, *J* = 10.4, 2.4 Hz, 192H, H_g), 2.22 (d, J = 6.2 Hz, 6H, H_b) 0.62 (s, br, 2H, H_a). ^{13}C{^{1}H} NMR (126 MHz, C_6D_6) δ 139.54 (C_3), 136.99 (*i-Ph*Si), 136.95 (*i-Ph*Si), 135.17 (*o-Ph*Si), 135.10 (*o-Ph*Si), 130.11 (*m-Ph*Si), 130.07 (*m-Ph*Si), 128.36 (*p*-Si*Ph*), 128.33 (C_4), 75.67 (C_5H_4), 75.62 (C_5H_4), 75.26 (C_5H_4), 75.23 (C_5H_4), 72.87 (C_5H_4), 72.85 (C_5H_4), 72.76

(C_5H_4), 66.22 (1- C_5H_4), 55.19 (C_2), 35.24 (C_1), 35.22 (C_1). $^{29}Si\{^1H\}$ NMR (99 MHz, C_6D_6) δ -10.22, -10.32.

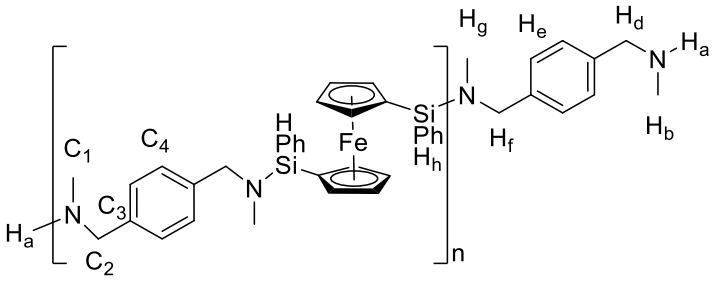

Figure 2.32 Labelling scheme used for the assignment of ^1H and ^{13}C NMR for polymer **P12**.

2.4.14 Synthesis of 1,1'-bis(dimethylsilyl)ferrocene

1,1'-bis(dimethylsilyl)ferrocene was synthesised according to a modified literature procedure.[58, 59] A Schlenk flask was charged with 1.0 g ferrocene (5.5 mmol), 0.8 ml TMEDA (5.3 mmol), and hexane. The mixture was stirred at room temperature, and 4.3 ml *n*BuLi (2.5 M in hexanes, 11 mmol) was added. After stirring at room temperature overnight, the yellow suspension was filtered and the 1,1'-dilithioferrocene·TMEDA product washed with toluene. The yellow solid was re-suspended in fresh toluene, cooled to 0°C, and 1.21 ml dimethylchlorosilane was added dropwise. The reaction mixture was allowed to warm to room temperature and stirred for 16 hours. After filtering and washing the LiCl byproduct with toluene, the solvent was removed under vacuum to yield the crude product as an orange oil. The product was purified by flash column chromatography using a hexane eluent and silica stationary phase. The products eluted as a broad orange band and collected as nine fractions, of which the first five contained the desired product in >98% purity. Isolated yield: 0.617 g, 37%. ^1H NMR (500 MHz, C_6D_6) δ 4.68 (hept, J = 3.7 Hz, 2H, Si*H*), 4.24 – 4.18 (m, 4H, 2,5- C_5H_4), 4.05 (t, J = 1.7 Hz, 4H, 3,4- C_5H_4), 0.27 (d, J = 3.7 Hz, 12H, CH_3). $^{13}C\{^1H\}$ NMR (126 MHz, C_6D6) δ 74.03 (3,4-C_5H_4), 71.93 (2,5- C_5H_4), 68.32 (1- C_5H_4), -2.87 (CH_3). $^{29}Si\{^1H\}$ NMR (99 MHz, C_6D6) δ -18.68.

2.4.15 Synthesis of polymer P13

A Schlenk flask was charged with 25.2 mg *p*-xylylenediamine (0.185 mmol), 50µl 1,1'-bis(dimethylsilyl)ferrocene (0.185 mmol), and 0.2 ml THF. 3.7 mg **IId** (0.006 mmol) was dissolved in 0.05 ml THF and added to the monomer solution. The reaction mixture immediately became a deep purple colour and bubbled enthusiastically. After stirring at room temperature for 16 hours, the solution was diluted with 1.5 ml THF and precipitated into non-dried hexane at -78°C. Following filtration and removal of solvent under vacuum, the product was obtained as a sticky orange residue. Isolated yield 56.5 mg, 70 %. ^1H NMR (500 MHz,

C_6D_6) δ 7.30 (s, br, 35H, Ar*H*), 4.26 (q, *J* = 1.9 Hz, 35H, 2,5-C_5H_4), 4.16 – 4.06 (m, 35H, 3,4-C_5H_4), 3.94 (d, *J* = 8.0 Hz, 44H, H_c), 3.62 (t, *J* = 7.2 Hz, 4H, H_b), 0.81 (t, *J* = 8.0 Hz, 25H, H_d + H_a), 0.36 (s, br, 127H, C*H3*). $^{13}C\{^1H\}$ NMR (126 MHz, C_6D_6) δ 142.92 (*1*-C_6H_4), 127.38 (2,6-C_6H_4), 73.59 (3,4-C_5H_4), 71.79 (2,5- C_5H_4), 46.61 (C_1), 46.33 (C_2), -0.15 (CH_3). $^{29}Si\{^1H\}$ NMR (99 MHz, C_6D_6) δ -1.71.

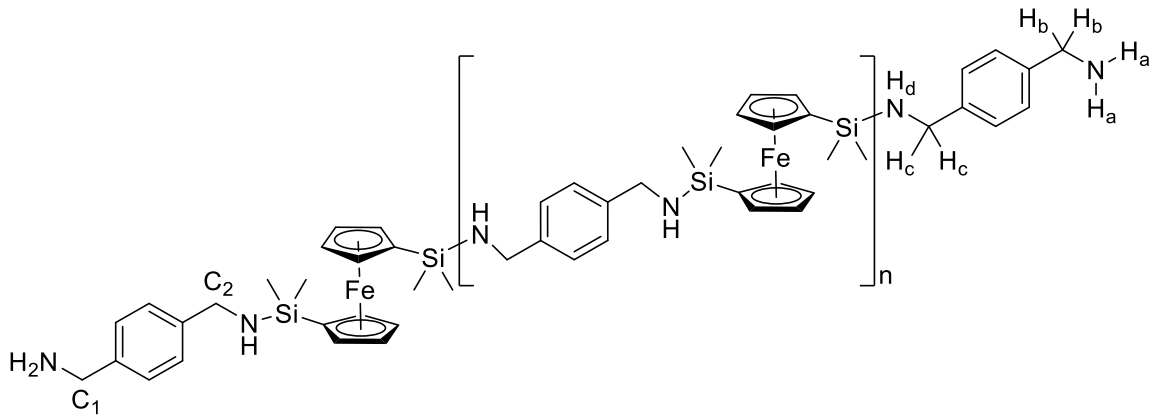

Figure 2.33 Labelling scheme used in the assignment of the ^1H and ^{13}C NMR for polymer **P13**.

2.4.16 Synthesis of polymer P14

In the glove box, 0.210 g compound **1** (0.72 mmol) and 0.098 g *p*-xylylenediamine (0.72 mmol) were dissolved in 1 ml THF in a Schlenk flask. 14.3 mg compound **IId** (0.024 mmol) was dissolved in 0.1 ml THF, and added to the stirred monomer solution, resulting in an immediate colour change to purple, and vigorous bubbling. The reaction was stirred for 45 minutes, then 17.8 µl $PhSiH_3$ (0.144 mmol) was added. The reaction mixture resumed bubbling and rapidly increased in viscosity, becoming an immobile mass after a few seconds. The bubbling subsided, and the Schlenk flask was removed from the glove box. Most of the solvent was removed under vacuum, before backfilling with air in order to quench the catalyst and purple colouration. The product was isolated as an insoluble spongy orange solid following prolonged vacuum drying. Addition of solvent (benzene, toluene, or THF) resulted in swelling to an orange gel, precluding characterisation by NMR spectroscopy. A small amount of soluble material could be extracted from the gel with C_6D_6. The ^1H NMR spectrum of this extract resembled that of polymers **P1-P7**, and was assumed to be a fraction of polymer which was not cross-linked by addition of phenylsilane. A pellet of **P14** could be obtained by compressing a 30 mg sample of the polymer in a KBr press in the glove box.

2.4.17 X-ray crystallography

Compound	**1**	**2**	**3**	**4**	**5**	**6**	**7**	**8**
Empirical formula	$C_{16}H_{16}FeSi$	$C_{30}H_{30}FeN_2Si$	$C_{22}H_{22}FeSi_2$	$C_{50}H_{50}FeN_4Si_2$	$C_{22}H_{20}FeN_2Si$	$C_{16}H_{16}RuSi$	$C_{26}H_{24}FeN_2RuSi$	$C_{34}H_{36}N_2Si_2$
Formula weight	292.23	502.50	398.42	818.97	396.34	337.45	549.48	528.83
Temperature/K	150.01(10)	150.00(10)	150.00(10)	150.00(10)	150.00(10)	150.00(10)	150.00(10)	150.00(10)
Crystal system	monoclinic	orthorhombic	monoclinic	triclinic	triclinic	monoclinic	monoclinic	monoclinic
Space group	*Cc*	*Pbcn*	*P2₁/n*	*P-1*	*P-1*	*Cc*	*C2/c*	*P2₁/c*
a/Å	5.8712(3)	34.1850(3)	6.18596(9)	9.2527(7)	8.9354(5)	5.78450(10)	28.2223(3)	10.0737(6)
b/Å	26.4890(14)	7.52336(7)	26.0832(4)	9.8933(6)	9.0139(4)	27.1843(5)	7.60411(6)	9.8529(4)
c/Å	8.8144(4)	19.60595(15)	12.14067(17)	13.0738(5)	12.4980(5)	8.86997(16)	19.59268(18)	14.9732(9)
α/°	90	90	90	104.141(4)	80.283(4)	90	90	90
β/°	95.427(5)	90	102.4996(15)	94.661(5)	79.612(4)	95.3880(17)	91.3615(9)	106.882(6)
γ/°	90	90	90	114.135(7)	64.527(5)	90	90	90
Volume/Å^3	1364.69(12)	5042.38(8)	1912.46(5)	1036.63(12)	889.14(8)	1388.62(4)	4203.51(7)	1422.12(14)
Z	4	8	4	1	2	4	8	2
ρ_{calc}g/cm^3	1.422	1.324	1.384	1.312	1.480	1.614	1.737	1.235
μ/mm^{-1}	1.171	5.399	7.515	3.778	7.492	9.771	12.022	1.317
F(000)	608.0	2112.0	832.0	432.0	412.0	680.0	2224.0	564.0
Crystal size/mm^3	0.534 × 0.373 × 0.233	0.261 × 0.163 × 0.083	0.143 × 0.049 × 0.046	0.135 × 0.123 × 0.083	0.249 × 0.178 × 0.117	0.407 × 0.162 × 0.078	0.175 × 0.175 × 0.073	0.122 × 0.102 × 0.058
Radiation	MoKα (λ = 0.71073)	CuKα (λ = 1.54184)	CuKα (λ = 1.54184)	CuKα (λ = 1.54184)	CuKα (λ = 1.54184)	CuKα (λ = 1.54184)	CuKα (λ = 1.54184)	CuKα (λ = 1.54184)
2Θ range for data collection/°	7.14 to 54.952	9.02 to 146.298	6.778 to 139.072	7.124 to 146.064	7.23 to 145.924	6.502 to 146.032	6.266 to 146.212	9.174 to 146.61
Index ranges	-7 ≤ h ≤ 7, -34 ≤ k ≤ 33, -11 ≤ l ≤ 11	-42 ≤ h ≤ 41, -9 ≤ k ≤ 8, -24 ≤ l ≤ 24	-4 ≤ h ≤ 7, -31 ≤ k ≤ 30, -14 ≤ l ≤ 14	-11 ≤ h ≤ 11, -9 ≤ k ≤ 12, -16 ≤ l ≤ 15	-11 ≤ h ≤ 10, -7 ≤ k ≤ 11, -15 ≤ l ≤ 15	-6 ≤ h ≤ 7, -32 ≤ k ≤ 33, -10 ≤ l ≤ 10	-34 ≤ h ≤ 34, -6 ≤ k ≤ 9, -24 ≤ l ≤ 24	-12 ≤ h ≤ 12, -12 ≤ k ≤ 12, -18 ≤ l ≤ 18
Reflections collected	5535	74183	11042	9888	7992	5769	22525	3344
Independent reflections	2444 [R_{int} = 0.0233, R_{sigma} = 0.0306]	5063 [R_{int} = 0.0426, R_{sigma} = 0.0149]	3569 [R_{int} = 0.0202, R_{sigma} = 0.0215]	4121 [R_{int} = 0.0328, R_{sigma} = 0.0416]	3530 [R_{int} = 0.0252, R_{sigma} = 0.0299]	2149 [R_{int} = 0.0227, R_{sigma} = 0.0222]	4208 [R_{int} = 0.0352, R_{sigma} = 0.0205]	3344 [R_{int} = 0.0559, R_{sigma} = 0.0311]
Data/restraints/parameters	2444/2/171	5063/2/315	3569/0/242	4121/2/267	3530/2/243	2149/2/171	4208/2/288	3344/0/178
Goodness-of-fit on F^2	1.054	1.042	1.023	1.024	1.058	1.061	1.060	1.129
Final *R* indexes [I>=2σ (I)]	R_1 = 0.0229, wR_2 = 0.0567	R_1 = 0.0260, wR_2 = 0.0679	R_1 = 0.0262, wR_2 = 0.0679	R_1 = 0.0361, wR_2 = 0.0862	R_1 = 0.0372, wR_2 = 0.0946	R_1 = 0.0228, wR_2 = 0.0589	R_1 = 0.0241, wR_2 = 0.0647	R_1 = 0.0357, wR_2 = 0.0960
Final *R* indexes [all data]	R_1 = 0.0237, wR_2 = 0.0572	R_1 = 0.0282, wR_2 = 0.0695	R_1 = 0.0292, wR_2 = 0.0697	R_1 = 0.0407, wR_2 = 0.0892	R_1 = 0.0395, wR_2 = 0.0964	R_1 = 0.0228, wR_2 = 0.0589	R_1 = 0.0250, wR_2 = 0.0653	R_1 = 0.0426, wR_2 = 0.0977
Largest diff. peak/hole / e Å^{-3}	0.24/-0.25	0.36/-0.23	0.33/-0.29	0.30/-0.28	0.77/-0.39	0.46/-0.44	0.77/-0.60	0.26/-0.21
Flack parameter	-0.011(12)					-0.011(12)		

Notes on crystallographic refinement

For compounds **1** and **6**, H1A and H1B, attached to Si1, were located and refined without restraints. For compounds **2**, **4**, **5** and **7**, nitrogen bound hydrogen atoms were located and refined at a distance of 0.98 Å from the relevant parent atom. The asymmetric unit of **4** comprises half of a molecule in which the iron center is coincident with a crystallographic inversion center. The structure of **5** is a textbook presentation of 'almost but not quite' in terms of symmetry, being metrically close to a monoclinic *C* unit cell. However, the latter was not supported, even by invoking a twin law. Ultimately, the crystal was single, and the solution was broker, as presented here, in space group *P*-1. Integration of the raw data for **8** took account of the fact that the sample was a two-component twin (53:47 ratio), by virtue of a 180° rotation about the *c* axis. Half of one molecule was seen to comprise the asymmetric unit, the remainder being generated *via* an inversion center intrinsic to the space group. H1 was located and refined without restraints.

2.5 References

1. R. L. N. Hailes, A. M. Oliver, J. Gwyther, G. R. Whittell and I. Manners, *Chemical Society Reviews*, 2016, **45**, 5358-5407.
2. T. J. Peckham, J. A. Massey, C. H. Honeyman and I. Manners, *Macromolecules*, 1999, **32**, 2830-2837.
3. E. K. Sarbisheh, J. E. Flores, J. F. Zhu and J. Muller, *Chemistry-a European Journal*, 2016, **22**, 16836-16847.
4. P. J. Flory, *Journal of the American Chemical Society*, 1936, **58**, 1877-1885.
5. W. H. Carothers, *Transactions of the Faraday Society*, 1936, **32**, 39-49.
6. I. Yamaguchi, H. Ishii, T. Sakano, K. Osakada and T. Yamamoto, *Applied Organometallic Chemistry*, 2001, **15**, 197-203.
7. S. Pandey, P. Lonnecke and E. Hey-Hawkins, *European Journal of Inorganic Chemistry*, 2014, **2014**, 2456-2465.
8. F. Buch and S. Harder, *Organometallics*, 2007, **26**, 5132-5135.
9. J. F. Dunne, S. R. Neal, J. Engelkemier, A. Ellern and A. D. Sadow, *Journal of the American Chemical Society*, 2011, **133**, 16782-16785.
10. M. Rauch, R. C. Roberts and G. Parkin, *Inorganica Chimica Acta*, 2019, **494**, 271-279.
11. A. Baishya, T. Peddarao and S. Nembenna, *Dalton Transactions*, 2017, **46**, 5880-5887.
12. M. S. Hill, D. J. Liptrot, D. J. MacDougall, M. F. Mahon and T. P. Robinson, *Chemical Science*, 2013, **4**, 4212.
13. C. Bellini, C. Orione, J. F. Carpentier and Y. Sarazin, *Angewandte Chemie - International Edition*, 2016, **55**, 3744-3748.
14. C. Bellini, T. Roisnel, J. F. Carpentier, S. Tobisch and Y. Sarazin, *Chemistry - A European Journal*, 2016, **22**, 15733-15743.
15. C. Bellini, V. Dorcet, J. F. Carpentier, S. Tobisch and Y. Sarazin, *Chemistry - A European Journal*, 2016, **22**, 4564-4583.
16. C. Bellini, J.-F. Carpentier, S. Tobisch and Y. Sarazin, *Angewandte Chemie International Edition*, 2015, **54**, 7679-7683.
17. W. Li, H. Chung, C. Daeffler, J. A. Johnson and R. H. Grubbs, *Macromolecules*, 2012, **45**, 9595-9603.
18. B. Wrackmeyer, E. V. Klimkina and W. Milius, *Zeitschrift Fur Anorganische Und Allgemeine Chemie*, 2010, **636**, 784-794.

19. H. Bhattacharjee, S. Dey, J. F. Zhu, W. Sun and J. Muller, *Chemical Communications*, 2018, **54**, 5562-5565.
20. T. C. Auch, H. Braunschweig, K. Radacki, R. Sigritz, U. Siemeling and S. Stellwag, *Zeitschrift Fur Naturforschung Section B-a Journal of Chemical Sciences*, 2008, **63**, 920-922.
21. F. Walz, E. Moos, D. Garnier, R. Koppe, C. E. Anson and F. Breher, *Chemistry-a European Journal*, 2017, **23**, 1173-1186.
22. J. Oetzel, N. Weyer, C. Bruhn, M. Leibold, B. Gerke, R. Pottgen, M. Maier, R. F. Winter, M. C. Holthausen and U. Siemeling, *Chemistry-a European Journal*, 2017, **23**, 1187-1199.
23. C. Moser, F. Belaj and R. Pietschnig, *Phosphorus Sulfur and Silicon and the Related Elements*, 2015, **190**, 837-844.
24. B. Wrackmeyer, E. V. Klimkina and W. Milius, *Zeitschrift Fur Naturforschung Section B-a Journal of Chemical Sciences*, 2009, **64**, 1401-1412.
25. B. Wrackmeyer, E. V. Klimkina and W. Milius, *Zeitschrift Fur Naturforschung Section B-a Journal of Chemical Sciences*, 2007, **62**, 1259-1266.
26. B. Wrackmeyer, E. V. Klimkina and W. Milius, *Zeitschrift Fur Anorganische Und Allgemeine Chemie*, 2007, **633**, 1964-1972.
27. B. Wrackmeyer, E. V. Klimkina and W. Milius, *Polyhedron*, 2007, **26**, 3496-3504.
28. B. Wrackmeyer, E. V. Klimkina and W. Milius, *Zeitschrift Fur Anorganische Und Allgemeine Chemie*, 2006, **632**, 2331-2340.
29. B. Wrackmeyer, E. V. Klunkina, W. Millus, O. L. Tok and M. Herberhold, *Inorganica Chimica Acta*, 2005, **358**, 1420-1428.
30. B. Wrackmeyer, E. V. Klimkina and W. Milius, *Inorganic Chemistry Communications*, 2004, **7**, 884-888.
31. B. Wrackmeyer, E. V. Klimkina and W. Milius, *Inorganic Chemistry Communications*, 2004, **7**, 412-416.
32. B. Wrackmeyer, E. V. Klimkina, H. E. Maisel, W. Milius and M. Herberhold, *Inorganica Chimica Acta*, 2004, **357**, 1703-1710.
33. R. A. Musgrave, A. D. Russell and I. Manners, *Organometallics*, 2013, **32**, 5654--5667.
34. R. Hailes, R. A. Musgrave, A. F. R. Kilpatrick, A. D. Russell, G. R. Whittell, D. O'Hare and I. Manners, *Chemistry – A European Journal*, 2018, **25**, 1044-1054.
35. A. D. Russell, R. A. Musgrave, L. K. Stoll, P. Choi, H. Qiu and I. Manners, *Journal of Organometallic Chemistry*, 2015, **784**, 24-30.
36. R. A. Musgrave, A. D. Russell, D. W. Hayward, G. R. Whittell, P. G. Lawrence, P. J. Gates, J. C. Green and I. Manners, *Nature Chemistry*, 2017, **9**, 743-750.
37. S. Schottner, R. Hossain, C. Ruttiger and M. Gallei, *Polymers*, 2017, **9**, 491.
38. K. H. Zhang, M. M. Zhang, X. L. Feng, M. A. Hempenius and G. J. Vancso, *Advanced Functional Materials*, 2017, **27**, 1702784.
39. A. C. Fisher, *Electrode Dynamics*, Oxford University Press, Oxford, 1996.
40. C. R. Wilke and P. Chang, *AIChE Journal*, 1955, **1**, 264-270.
41. J. B. Flanagan, S. Margel, A. J. Bard and F. C. Anson, *Journal of the American Chemical Society*, 1978, **100**, 4248-4253.
42. R. Petersen, D. A. Foucher, B. Z. Tang, A. Lough, N. P. Raju, J. E. Greedan and I. Manners, *Chemistry of Materials*, 1995, **7**, 2045-2053.
43. M. Ginzburg, M. J. MacLachlan, S. M. Yang, N. Coombs, T. W. Coyle, N. P. Raju, J. E. Greedan, R. H. Herber, G. A. Ozin and I. Manners, *Journal of the American Chemical Society*, 2002, **124**, 2625-2639.
44. K. Liu, S. B. Clendenning, L. Friebe, W. Y. Chan, X. B. Zhu, M. R. Freeman, G. C. Yang, C. M. Yip, D. Grozea, Z. H. Lu and I. Manners, *Chemistry of Materials*, 2006, **18**, 2591-2601.
45. M. J. MacLachlan, M. Ginzburg, N. Coombs, T. W. Coyle, N. P. Raju, J. E. Greedan, G. A. Ozin and I. Manners, *Science*, 2000, **287**, 1460-1463.

46. K. Kulbaba, A. Cheng, A. Bartole, S. Greenberg, R. Resendes, N. Coombs, A. Safa-Sefat, J. E. Greedan, H. D. H. Stover, G. A. Ozin and I. Manners, *Journal of the American Chemical Society*, 2002, **124**, 12522-12534.
47. J. Galloro, M. Ginzburg, H. Miguez, S. M. Yang, N. Coombs, A. Safa-Sefat, J. E. Greedan, I. Manners and G. A. Ozin, *Advanced Functional Materials*, 2002, **12**, 382-388.
48. K. Liu, S. Fournier-Bidoz, G. A. Ozin and I. Manners, *Chemistry of Materials*, 2009, **21**, 1781-1783.
49. B. Z. Tang, R. Petersen, D. A. Foucher, A. Lough, N. Coombs, R. Sodhi and I. Manners, *Journal of the Chemical Society-Chemical Communications*, 1993, 523-525.
50. S. J. Lenhart, Y. D. Blum and R. M. Laine, *Corrosion*, 1989, **45**, 503-506.
51. M. Birot, J. P. Pillot and J. Dunogues, *Chemical reviews*, 1995, **95**, 1443-1477.
52. E. Kroke, Y. L. Li, C. Konetschny, E. Lecomte, C. Fasel and R. Riedel, *Materials Science & Engineering R-Reports*, 2000, **26**, 97-199.
53. Y. D. Blum, K. B. Schwartz and R. M. Laine, *Journal of Materials Science*, 1989, **24**, 1707-1718.
54. A. S. Bernard, A. Viard, D. Fonblanc, A. Lale, C. Salameh, M. Wynn, P. Champagne, F. Babonneau, G. Chollon, C. Gervais, A. Viard, D. Fonblanc, M. Schmidt, A. Lale and C. Salameh, *Chemistry A European Journal*, 2017, **23**, 9076-9090.
55. J. D. Hanawalt, H. W. Rinn and L. K. Frevel, *Industrial and Engineering Chemistry Analytical Edition*, 1938, **10**, 457-512.
56. M. C. Morris, H. F. McMurdie, E. H. Evans, B. Paretzkin, H. S. Parker, N. C. Panagiotopoulos and C. R. Hubbard, in *National Bureau of Standards (U.S.) Monograph 25*, 1981, vol. 18, p. 37.
57. D. L. Leslie-Pelecky and R. D. Rieke, *Chemistry of Materials*, 1996, **8**, 1770-1783.
58. R. J. P. Corriu, N. Devylder, C. Guerin, B. Henner and A. Jean, *Organometallics*, 1994, **13**, 3194-3202.
59. R. Jain, H. Choi, R. A. Lalancette and J. B. Sheridan, *Organometallics*, 2005, **24**, 1468-1476.

3 Alkaline-Earth Mediated Catalytic Dehydrocoupling of Silanes and Alcohols for the Preparation of Metallo-polysilylethers

3.1 Introduction

The formation of silicon-oxygen bonds is a transformation of considerable importance. Polysiloxanes are widely used, with the highly robust and flexible Si-O-Si unit resulting in excellent thermoxidative stability and low temperature elasticity, which is suitable for a variety of applications. The Si-O-C linkage that makes up silyl ethers has been less explored at the macromolecular level, but also presents opportunities for the synthesis of hybrid organic/inorganic materials suitable for speciality applications.[1-7] Silyl ethers are also widely used in synthetic organic chemistry; for example as protecting and directing groups,[8-11] or in kinetic resolution.[12, 13] Historically, Si-O-C linkages have been accessed *via* reaction of an alcohol with chlorosilane,[14] yet this strategy is limited by high reactivity and moisture sensitivity of the chlorosilane substrate as well as the stoichiometric generation of HCl, which further limits functional group tolerance. The catalytic dehydrocoupling of hydrosilanes with alcohols (also known as hydrosilane alcoholysis) is a promising alterative. Reported catalysts for this reaction are almost exclusively transition metal-based,[1, 9, 12, 13, 15-43] but there are also examples of Lewis- and Brønstead base catalysis,[8, 10, 11, 44-46] as well as boron-[44, 47-49] and phosphorus-based[49, 50] Lewis acid catalysis. The use of main-group compounds in the place of transition metal catalysts is an interesting and attractive proposition, allowing the use of expensive and toxic precious metals to be avoided. Lewis acidic main-group catalysts, however, often suffer from low activity due to competitive Lewis acid-base adduct formation with the alcohol substrate.[49] Catalytic hydrosilylation is also a viable route towards the formation of Si-O-C linkages,[51] finding application in the synthesis of polysilylethers[1, 52-54] and modification of polysilanes.[55] Addition polymerisation, however, has an entropic disadvantage compared condensation polymerisation, especially dehydropolymerisation, where loss of dihydrogen provides a thermodynamic driving-force.

To the best of our knowledge, there are no reports of catalytic silane-alcohol dehydrocoupling mediated by alkaline-earth (Ae) metals. Conceptually, it is easy to extend the suite of Ae-catalysed heterodehydrocoupling towards alcohols. The formation of B-N,[56] Si-O-B,[57] Si-O-Si,[58] Si-N[59-67], and Si-C≡C[59, 67] bonds *via* Ae-catalysed dehydrocoupling of protic (amine, boronic acid, silanol, or terminal alkyne) and hydridic substrates (borane or silane) are known. These reactions can be rationalised to share a simplified mechanism of the type shown in Scheme 3.1, which proceeds *via* a series of steps involving σ-bond metathesis at the redox-

inactive Ae^{2+} centre. This mechanism depends on the orthogonally predisposed E-H and E'-H bond polarity, and invokes the generation of Ae-amide, -boroxy, -siloxy, or -acetylide species and Ae-hydride intermediates. In theory, an alcohol is a suitable substrate since it features a protic O-H bond. This would allow an Ae-alkoxide to form, yielding an Si-O bond following σ-bond metathesis with a silane. The resulting Ae-hydride is open to protonolysis by a further equivalent of alcohol, thus eliminating H_2 and closing the catalytic cycle.

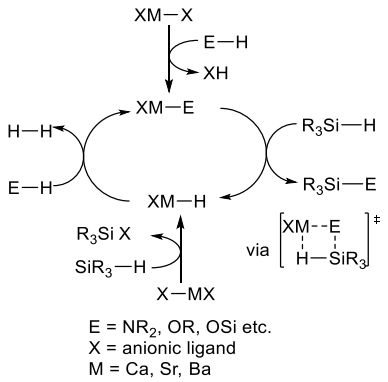

Scheme 3.1: A simplified hypothetical mechanism for the Ae-mediated catalytic dehydrocoupling of silanes with amines or alcohols.

This chapter will present efforts to develop and understand catalytic silane-alcohol dehydrocoupling, mediated by the heavier alkaline earths. Subsequently, the reaction will be applied to the synthesis of hitherto unknown metallo-polysilylethers, to access materials with improved moisture tolerance compared to the ferrocene-containing polycarbosilazanes described in Chapter 2.

3.2 Results and discussion

3.2.1 Dehydrocoupling of alcohols with phenylsilane

First, the dehydrocoupling reactivity of phenylsilane towards primary- secondary- and tertiary-alcohols was investigated using catalytic quantities of compounds **IIb-d** and **IIIb-d** (Scheme 3.2).

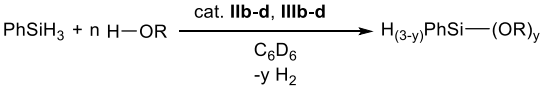

Scheme 3.2: The Ae-catalysed dehydrocoupling of alcohols with phenylsilane.

Catalysis proceeded with good to excellent rates at room temperature (Table 3.1). Quantitative conversion of 1-hexanol and benzyl alcohol was achieved in under 60 minutes at a 2.5 mol%

catalyst loading in most cases. Catalyst loading could be decreased to 1 mol% or even 0.5 mol% with strontium and barium. In contrast, calcium required higher catalyst loadings to achieve appreciable results. By altering the Si:O stoichiometry, good selectivity towards either the doubly coupled ($(RO)_2SiPhH$) or triply coupled ($(RO)_3SiPh$) silyl ethers was achieved, although longer reaction times were necessary to obtain good spectroscopic yields of the latter. Whilst the singly coupled silyl ethers ($(RO)SiPhH_2$) could sometimes be observed *in situ* after short reaction times (<10 minutes), they were never observed at higher conversions. Even when the reaction was carried out at a 1:1 Si:O ratio, the doubly coupled product was obtained, returning 0.5 eq. unreacted $PhSiH_3$. Furthermore, after complete alcohol conversion was obtained, the product distribution slowly shifted towards the triply coupled thermodynamic product, returning phenyl silane (see Table 3.1 entries 15 and 16).

The reaction also proceeded efficiently with more sterically encumbered secondary- and tertiary-alcohols (*iso*-propanol and *tert*-butanol). The greater steric demands clarify a trend in reaction rate on moving down group two, where Ca << Sr <Ba. Doubly coupled products were favoured whilst singly coupled products were only observed at low conversion under calcium catalysis for *i*PrOH, and with improved selectivity at short reaction times for *t*BuOH. In both cases, however, the singly coupled product rapidly redistributes to the doubly coupled product and $PhSiH_3$. Whilst $(i\text{PrO})_3SiPh$ was accessible in 95% selectivity under strontium or barium catalysis, the fully substituted product $(t\text{BuO})_3SiPh$ remained inaccessible even with extended reaction times and elevated temperatures. By contrast, only 10% spectroscopic yield of this product could be obtained under calcium catalysis after one day at an Si:O:Ca ratio of 40:120:1.

Qualitatively, the bis-alkyl complexes **IIIb**-**d** did not give improved results compared to their amide congeners **IIb**-**d**. Moving to even bulkier substrates such as DippOH (Dipp = 2,6-diisopropylphenyl) or Ph_3COH required higher temperatures, longer reaction times and higher catalyst loading to reach good conversion. These reactions further illuminate the qualitative reactivity trend on descending group two.

Table 3.1: Ae-catalysed dehydrocoupling of phenylsilane with various alcohols.

All reactions performed at room temperature in C_6D_6 unless otherwise specified. [a] Reaction performed at 85°C. [b] m: minutes, h: hours, d: days. [c] Conversion of alcohol determined by the relative integral of starting material and products in the *in situ* ^{1}H NMR spectrum.

Entry	Pre-catalyst	Alcohol	Si:O:Ae	Time[b]	Products	Conversion[c] / %
1[a]	No catalyst	HexOH	1:3:0	7 d.	$HexOSiPhH_2$	2
2	**IIb**		40:40:1	10 m.	$(HexO)_2SiPhH$ + $(HexO)_3SiPh$	99 (93:7)
3	**IIb**		40:80:1	5 m.	$(HexO)_2SiPhH$ + $(HexO)_3SiPh$	99 (86:14)
4	**IIb**		40:120:1	16 h.	$(HexO)_2SiPhH$ + $(HexO)_3SiPh$	99 (3:97)
5	**IIb**		100:300:1	16 h.	$(HexO)_3SiPh$	98
6	**IIc**		40:120:1	240 m.	$(HexO)_3SiPh$	99
7	**IIc**		200:600:1	2 d.	$(HexO)_2SiPhH$ + $(HexO)_3SiPh$	94 (32:68)
8	**IId**		40:120:1	60 m.	$(HexO)_3SiPh$	97
9	**IId**		200:600:1	240 m.	$(HexO)_3SiPh$	97
10[a]	No catalyst	BnOH	1:3:0	7 d.	$BnOSiPhH_2$	3
11	**IIb**		40:120:1	2 d.	$(BnO)_2SiPhH$ + $(BnO)_3SiPh$	97 (3:97)
12	**IIc**		40:120:1	240 m.	$(BnO)_2SiPhH$ + $(BnO)_3SiPh$	99 (2:98)
13	**IIc**		100:200:1	16 h.	$(BnO)_2SiPhH$ + $(BnO)_3SiPh$	95 (19:81)
14	**IId**		40:40:1	30 m.	$(BnO)_2SiPhH$ + $(BnO)_3SiPh$	99 (94:6)
15	**IId**		40:80:1	10 m.	$(BnO)_2SiPhH$ + $(BnO)_3SiPh$	99 (87:13)
16	**IId**		40:80:1	16 h.	$(BnO)_2SiPhH$ + $(BnO)_3SiPh$	99 (15:85)
17	**IId**		40:120:1	16 h.	$(BnO)_2SiPhH$ + $(BnO)_3SiPh$	99 (3:97)
18	**IId**		200:600:1	60 m.	$(BnO)_2SiPhH$ + $(BnO)_3SiPh$	96 (17:83)
19	**IIIb**		40:120:1	16 h.	$(BnO)_2SiPhH$ + $(BnO)_3SiPh$	99 (6:94)
20	**IIIc**		40:120:1	15 m.	$(BnO)_3SiPh$	99
21	**IIId**		40:120:1	60 m.	$(BnO)_3SiPh$	99
22[a]	No catalyst	*i*PrOH	1:2:0	7 d.	$iPrOSiPhH_2$	<1
23	**IIb**		40:40:1	240 m.	$iPrOSiPhH_2$ + $(iPrO)_2SiPhH$	99 (7:93)
24	**IIb**		40:80:1	16 h.	$(iPrO)_2SiPhH$ + $(iPrO)_3SiPh$	99 (99:1)
25	**IIb**		40:120:1	16 h.	$(iPrO)_2SiPhH$ + $(iPrO)_3SiPh$	76 (90:10)
26	**IIc**		40:80:1	5 m.	$(iPrO)_2SiPhH$ + $(iPrO)_3SiPh$	99 (99:1)
27	**IIc**		40:120:1	180 m.	$(iPrO)_2SiPhH$ + $(iPrO)_3SiPh$	94 (5:95)
28	**IIc**		200:400:1	16 h.	$iPrOSiPhH_2$ + $(iPrO)_2SiPhH$	99 (3:97)
29	**IId**		40:80:1	45 m.	$(iPrO)_2SiPhH$ + $(iPrO)_3SiPh$	99 (98:2)
30	**IId**		200:400:1	16 h.	$iPrOSiPhH_2$ + $(iPrO)_2SiPhH$ + $(iPrO)_3SiPh$	99 (2:95:3)
31	**IIIb**		40:80:1	15 m.	$(iPrO)_2SiPhH$ + $(iPrO)_3SiPh$	99 (98:2)
32	**IIIc**		40:80:1	10 m.	$(iPrO)_2SiPhH$ + $(iPrO)_3SiPh$	99 (98:2)
33	**IIId**		40:80:1	15 m.	$(iPrO)_2SiPhH$ + $(iPrO)_3SiPh$	99 (98:2)
34[a]	No catalyst	*t*BuOH	1:3:0	7 d.	N/A	0
35	**IIb**		40:40:1	16 h.	$tBuOSiPhH_2$ + $(tBuO)_2SiPhH$	99 (9:91)
36	**IIc**		40:80:1	16 h.	$tBuOSiPhH_2$ + $(tBuO)_2SiPhH$	99 (4:96)
37	**IId**		40:40:1	10 m.	$tBuOSiPhH_2$ + $(tBuO)_2SiPhH$	99 (93:7)
38	**IId**		40:40:1	16 h.	$tBuOSiPhH_2$ + $(tBuO)_2SiPhH$	99 (50:50)
39	**IId**		40:80:1	16 h.	$tBuOSiPhH_2$ + $(tBuO)_2SiPhH$	96 (7:93)
40	**IId**		40:120:1	16 h.	$(tBuO)_2SiPhH$	67
41	**IId**		100:200:1	16 h.	$tBuOSiPhH_2$ + $(tBuO)_2SiPhH$	94 (5:95)
42	**IIIb**		40:80:1	240 m.	$tBuOSiPhH_2$ + $(tBuO)_2SiPhH$	94 (28:72)
43	**IIIc**		40:80:1	15 m.	$(tBuO)_2SiPhH$	99
44	**IIId**		40:80:1	16 h.	$tBuOSiPhH_2$ + $(tBuO)_2SiPhH$	99 (1:99)
45[a]	**IId**	DippOH	20:20:1	4 d.	$DippOSiPhH_2$	35
46[a]	**IIb**	Ph_3COH	20:20:1	3 d.	$Ph_3COSiPhH_2$	2
47[a]	**IIc**		20:20:1	3 d.	$Ph_3COSiPhH_2$	17
48[b]	**IId**		20:20:1	3 d.	$Ph_3COSiPhH_2$	96

3.2.2 Dehydrocoupling of alcohols with diphenylsilane

Diphenylsilane was also investigated as a substrate (Scheme 3.3). Although rates were somewhat reduced compared to phenylsilane, quantitative alcohol conversion under strontium or barium catalysis could be obtained in under 24 hours for 1-hexanol and benzyl alcohol at room temperature (Table 3.2). A mixture of singly- and doubly coupled products were obtained in all cases, with selectivity generally skewed towards the singly coupled product $(RO)Si(H)Ph_2$. Whilst increasing temperature to 60°C resulted in an improved rate, it did not

have a significant impact on the product distribution. Prolonged reaction times resulted in slow redistribution towards the doubly coupled product $(RO)_2SiPh_2$, which could be obtained with good selectivity when the reaction was performed at a 1:2 Si:O ratio.

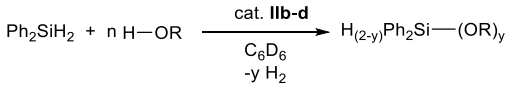

Scheme 3.3: The Ae-catalysed dehydrocoupling of alcohols with diphenylsilane.

The secondary alcohol, *iso*-propanol, provided better selectivity, forming $(RO)Si(H)Ph_2$ at a 1:1 Si:O ratio, and $(RO)_2SiPh_2$ at 1:2 Si:O (Sr or Ba catalysis). Calcium generally struggled to reach high conversions, even at elevated temperature and prolonged reaction times. Quantitative conversion of *tert*-butanol to (tBuO)$Si(H)Ph_2$ was possible, but the highly encumbered doubly coupled product was inaccessible. Under barium catalysis, catalyst loadings could be reduced to 1 mol% with a moderate decrease in reaction rate, which further decreased on reducing catalyst to 0.5 mol%. Coupling of pinacol $((H_3C)_2COH)_2$ with diphenylsilane provided quantitative consumption of both Si-H bonds to yield the cyclic silyl ether regardless of the Si:O ratio.

Table 3.2: Ae-catalysed dehydrocoupling of diphenylsilane with various alcohols. Reactions carried out in C_6D_6, [a] m: minutes, h: hours, d: days. [b] Conversion of alcohol determined by the relative integral of starting material and products in the *in situ* ^{1}H NMR spectrum.

Entry	Pre-catalyst	Alcohol	Si:O:Ae	Time[a]	Temp / °C	Product	Conversion[b] / %
1	**IIb**	HexOH	40:40:1	1 d.	25	$HexOSi(H)Ph_2$ + $(HexO)_2SiPh_2$	99 (75:25)
2	**IIc**	HexOH	40:40:1	1 d.	25	$HexOSi(H)Ph_2$ + $(HexO)_2SiPh_2$	99 (88:12)
3	**IId**	HexOH	40:40:1	120 m.	25	$HexOSi(H)Ph_2$ + $(HexO)_2SiPh_2$	99 (88:12)
4	**IId**	HexOH	40:40:1	180 m.	60	$HexOSi(H)Ph_2$ + $(HexO)_2SiPh_2$	99 (88:12)
5	**IIb**	HexOH	40:80:1	1 d.	60	$HexOSi(H)Ph_2$ + $(HexO)_2SiPh_2$	79 (47:53)
6	**IIc**	HexOH	40:80:1	1 d.	60	$HexOSi(H)Ph_2$ + $(HexO)_2SiPh_2$	97 (12:88)
7	**IId**	HexOH	40:80:1	2 d.	25	$HexOSi(H)Ph_2$ + $(HexO)_2SiPh_2$	92 (27:73)
8	**IId**	HexOH	40:80:1	1 d.	60	$HexOSi(H)Ph_2$ + $(HexO)_2SiPh_2$	97 (12:88)
9	**IId**	HexOH	100:200:1	1 d.	60	$HexOSi(H)Ph_2$ + $(HexO)_2SiPh_2$	96 (11:89)
10	**IId**	HexOH	200:400:1	1 d.	60	$HexOSi(H)Ph_2$ + $(HexO)_2SiPh_2$	87 (26:74)
11	**IIb**	BnOH	40:40:1	4 d.	25	$BnOSi(H)Ph_2$ + $(BnO)_2SiPh_2$	59 (90:10)
12	**IIc**	BnOH	40:40:1	1 d.	25	$BnOSi(H)Ph_2$ + $(BnO)_2SiPh_2$	99 (78:22)
13	**IId**	BnOH	40:40:1	45 m.	25	$BnOSi(H)Ph_2$ + $(BnO)_2SiPh_2$	99 (73:27)
14	**IId**	BnOH	40:40:1	4 d.	25	$BnOSi(H)Ph_2$ + $(BnO)_2SiPh_2$	99 (26:74)
15	**IId**	BnOH	40:80:1	1 d.	60	$BnOSi(H)Ph_2$ + $(BnO)_2SiPh_2$	99 (6:94)
16	**IId**	BnOH	200:400:1	1 d.	60	$BnOSi(H)Ph_2$ + $(BnO)_2SiPh_2$	95 (4:96)
17	**IIb**	*i*PrOH	40:40:1	5 d.	25	$iPrOSi(H)Ph_2$	33
18	**IIb**	*i*PrOH	40:40:1	2 d.	60	$iPrOSi(H)Ph_2$ + $(iPrO)_2SiPh_2$	99 (98:2)
19	**IIc**	*i*PrOH	40:40:1	1 d.	25	$iPrOSi(H)Ph_2$ + $(iPrO)_2SiPh_2$	99 (97:3)
20	**IId**	*i*PrOH	40:40:1	15 m.	25	$iPrOSi(H)Ph_2$ + $(iPrO)_2SiPh_2$	99 (97:3)
21	**IId**	*i*PrOH	100:100:1	120 m.	60	$iPrOSi(H)Ph_2$ + $(iPrO)_2SiPh_2$	99 (93:7)
22	**IId**	*i*PrOH	200:200:1	1 d.	60	$iPrOSi(H)Ph_2$ + $(iPrO)_2SiPh_2$	97 (94:6)
23	**IId**	*i*PrOH	40:80:1	1 d.	25	$iPrOSi(H)Ph_2$ + $(iPrO)_2SiPh_2$	95 (6:94)
24	**IIb**	*t*BuOH	40:40:1	1 d.	60	$tBuOSi(H)Ph_2$	99
25	**IIc**	*t*BuOH	40:40:1	1 d.	60	$tBuOSi(H)Ph_2$	99
26	**IId**	*t*BuOH	40:40:1	60 m.	60	$tBuOSi(H)Ph_2$	99
27	**IId**	*t*BuOH	100:100:1	1 d.	60	$tBuOSi(H)Ph_2$	99
28	**IId**	*t*BuOH	200:200:1	1 d.	60	$tBuOSi(H)Ph_2$	30
29	**IId**	*t*BuOH	40:80:1	7 d.	60	$tBuOSi(H)Ph_2$	55
30	**IId**	$((H_3C)_2COH)_2$	20:40:1	1 d.	25	$Ph_2Si(OC(CH_3)_2C(CH_3)_2O)$	99

3.2.3 Dehydrocoupling of benzyl alcohol with ferrocenylsilane 1

Compound **1** can be thought of as an organometallic analogue of diphenylsilane and hence was coupled with two equivalents of benzyl alcohol under barium catalysis (5 mol% **IId**) (Scheme 3.4). The resulting ferrocene-containing silyl ether **9** was formed in quantitative spectroscopic yields in under three days at room temperature.

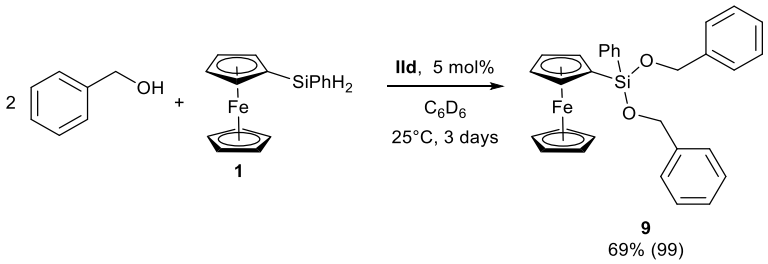

Scheme 3.4: Dehydrocoupling of compound **1** with two equivalents of benzyl alcohol, catalysed by 5 mol% compound **IIId**. Yield reported for isolated crystalline compound with spectroscopic yield shown in parentheses.

Single crystals of compound **9** were grown from a hexane/toluene solution at -30°C. The molecular structure was determined by X-ray diffraction and displays features typical for ferrocene-containing compounds and silyl ethers (Figure 3.1). Although analogous to compound **2**, replacement of NH linkages with oxygen results in a conformational change of the benzyl substituents, which are arranged with a mutually orthogonal disposition in compound **9** (*cf.* compound **2**, where benzyl substituents are orientated away from one another). The ferrocenyl moieties pack in a staggered fashion (Figure 3.2).

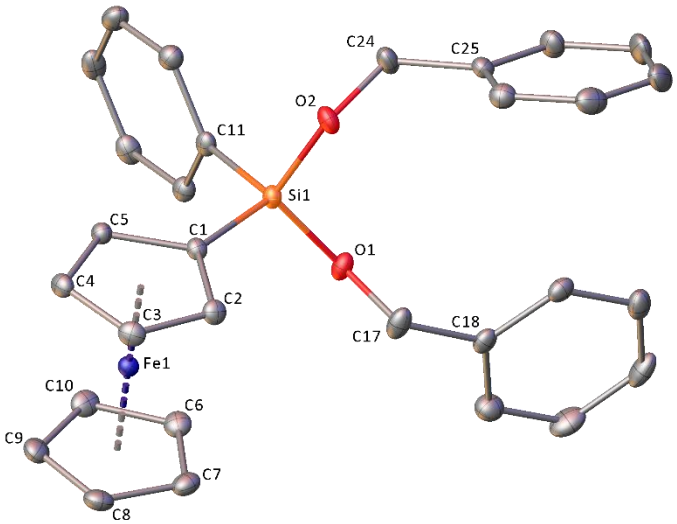

Figure 3.1: X-ray crystal structure of compound **9**. Thermal ellipsoids are shown at the 30% probability level.

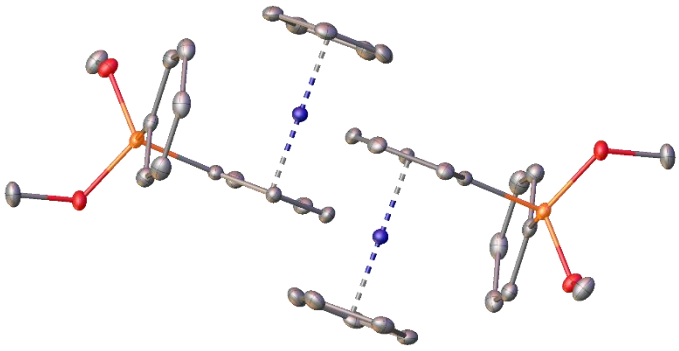

Figure 3.2: Image showing packing of the ferrocenyl substituents in X-ray crystal structure of compound **9**. Thermal ellipsoids are shown at the 30% probability level, with hydrogen atoms and phenyl substituents of the benzyl groups omitted for clarity.

3.2.4 Dehydrocoupling alcohols with tertiary silanes

Unsurprisingly, given their greater steric demands, tertiary silanes (Scheme 3.5) presented a challenge and required barium catalysis, long reaction times, and elevated temperatures (Table 3.3). Nevertheless, good to moderate spectroscopic yields could still be obtained for benzyl alcohol and *iso*-propanol with triphenylsilane whilst 1-hexanol returned very low conversions. Replacement of the aryl-substituents at silicon with alkyls resulted in significantly reduced activity; low conversions were possible for dimethyl(phenyl)silane, but triethylsilane was essentially inactive towards Si-O bond formation. Similar trends were identified by Sarazin and co-workers in barium-catalysed dehydrocoupling of silanes and amines,[65] and of silanes and silanols.[58]

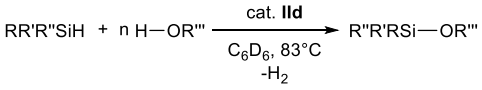

Scheme 3.5: The Ba-catalysed dehydrocoupling of alcohols with tertiary silanes.

Table 3.3: Dehydrocoupling of tertiary silanes with various alcohols.

Reactions were carried out in C_6D_6 at 83°C with 5 mol% compound **IId** as a pre-catalyst. [a] Conversion of alcohol determined by the relative integral of starting material and products in the *in situ* ^{1}H NMR spectrum.

Entry	Silane	Alcohol	Time/days	Product	Conversion[a] / %
1	Et_3SiH	BnOH	4	N/A	0
2	$Me_2(Ph)SiH$	BnOH	4	$BnOSi(Ph)Me_2$	50
3	Ph_3SiH	BnOH	4	$BnOSiPh_3$	83
4	Et_3SiH	HexOH	7	N/A	0
5	$Me_2(Ph)SiH$	HexOH	7	$HexOSi(Ph)Me_2$	4
6	Ph_3SiH	HexOH	7	$HexOSiPh_3$	8
7	Et_3SiH	*i*PrOH	5	N/A	0
8	$Me_2(Ph)SiH$	*i*PrOH	5	$iPrOSi(Ph)Me_2$	24
9	Ph_3SiH	*i*PrOH	5	$iPrOSiPh_3$	41
10	Et_3SiH	*t*BuOH	7	N/A	0
11	$Me_2(Ph)SiH$	*t*BuOH	7	N/A	0
12	Ph_3SiH	*t*BuOH	7	N/A	0

3.2.5 Stoichiometric NMR experiments

In order to gain mechanistic insight, stoichiometric reactions were carried out. A reaction between the calcium bis-amide **IIb** and three equivalents of *iso*-propanol in C_6D_6 resulted in a new trimethylsilyl resonance at δ 0.10 ppm in the ^{1}H NMR spectrum, corresponding to $HN(SiMe_3)_2$. Pronounced broadening of the *iso*-propyl resonances and a shift in the THF peaks to chemical shifts characteristic of free THF in C_6D_6 (Scheme 3.6, Figure 3.3)[68] imply displacement of coordinated THF by *iso*-propanol, which coordinates to unreacted $\{Ca(N(SiMe_3)_2)_2\}$ (δ 0.29 ppm) and a calcium *iso*-propoxide species. Subsequent addition of phenylsilane (three equivalents) resulted in immediate H_2 evolution and appearance of the dehydrocoupled product $PhSi(H)(OiPr)_2$ in the ^{1}H NMR spectrum (Scheme 3.6, Figure 3.3).

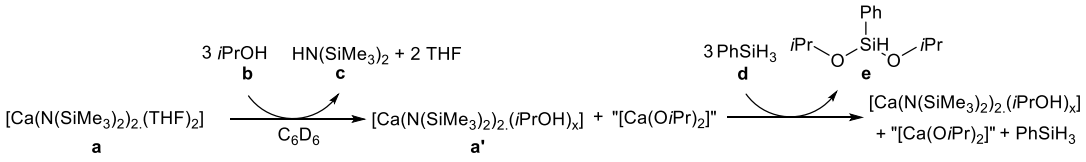

Scheme 3.6: Sequential addition of *iso*-propanol, then phenylsilane to a C_6D_6 solution of **IIb**.

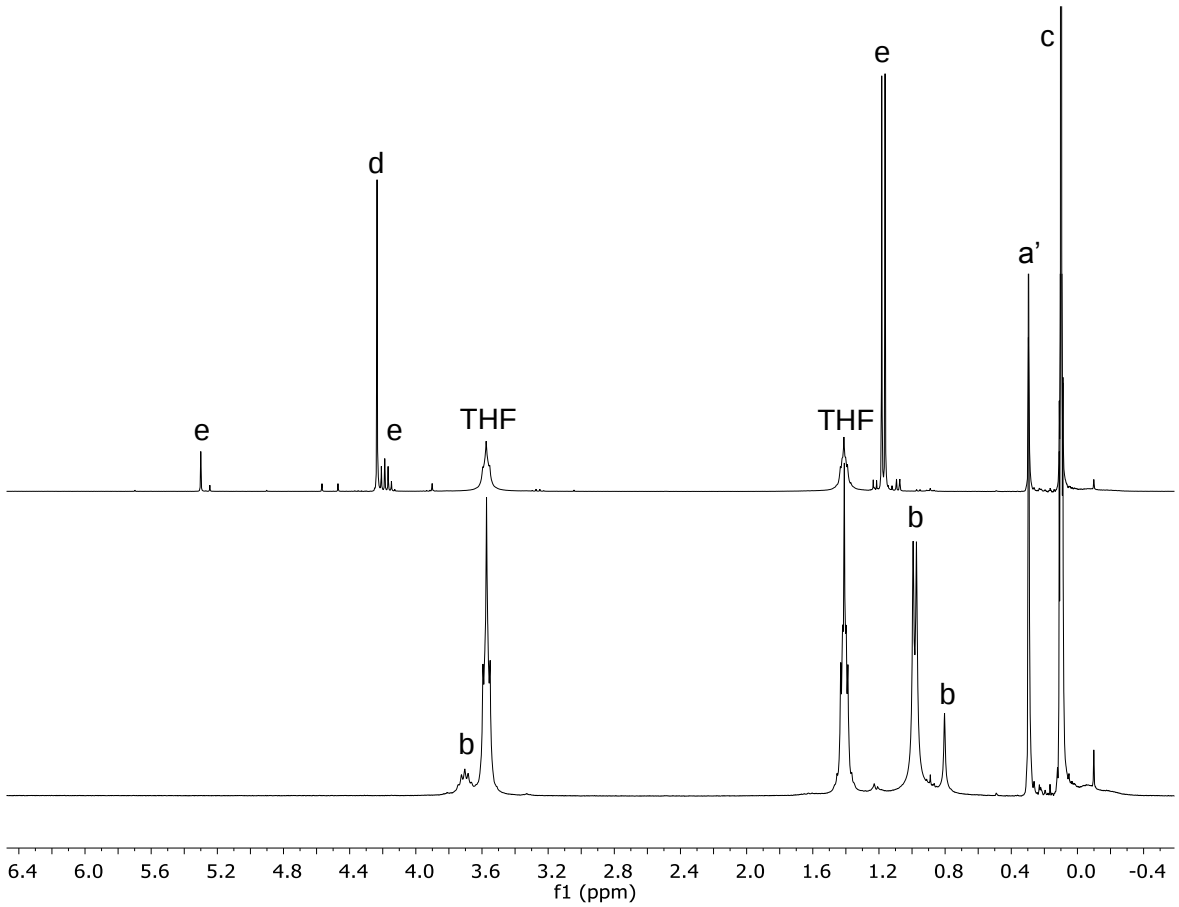

Figure 3.3: Expanded ^{1}H NMR spectra (300 MHz, 298 K, C_6D_6) of **IIb** with sequential addition of *iso*-propanol (bottom), then phenylsilane (top).

Adding three equivalents of $PhSiH_3$ to a C_6D_6 solution of **IIb** resulted in generation of a new trimethylsilyl-containing species at δ 0.22 ppm, corresponding to the silazane $PhSi(H)_2N(SiMe_3)_2$, which results from σ-bond metathesis between **IIb** and phenylsilane to form a Si-N bond and generate a calcium-hydride species (Scheme 3.7, Figure 3.4). In the absence of bulky and/or chelating ligands, such hydride species are likely to be unstable with respect to redistribution and, on standing, a light insoluble precipitate (presumably CaH_2) was observed to form. Subsequent addition of *iso*-propanol protonates the remaining amide ligand, eliminating the expected dehydrocoupling product $PhSi(H)(O\textit{i}Pr)_2$ (Scheme 3.7, Figure 3.4). These observations are similar to pre-catalyst activation proposed to occur in analogous silane-amine dehydrocoupling.[61, 65, 69, 70]

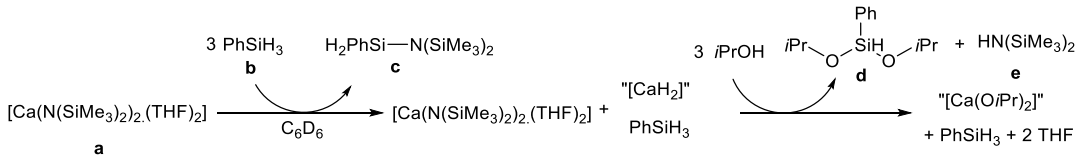

Scheme 3.7: The sequential addition of phenylsilane then *iso*-propanol to a C_6D_6 solution of **IIb**.

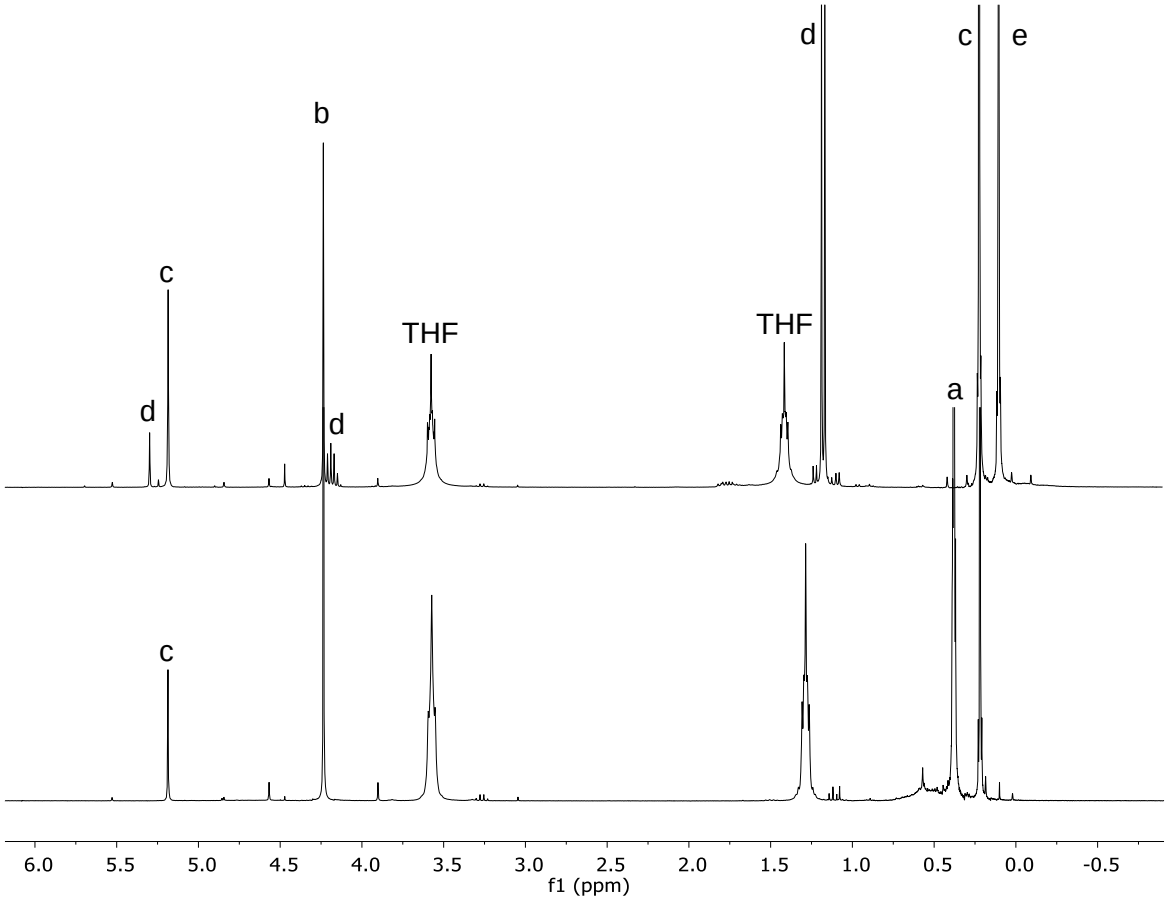

Figure 3.4: Expanded ^{1}H NMR spectra (300 MHz, 298 K, C_6D_6) of **IIb** with sequential addition of phenylsilane (bottom) then *iso*-propanol (top).

A similar study was carried out with diphenylsilane (Scheme 3.8, Figure 3.5). In this case, the expected product of σ-bond metathesis, $Ph_2Si(H)N(SiMe_3)_2$ was not observed, suggesting that under catalytically relevant conditions, direct reaction of diphenylsilane to produce a calcium-hydride species does not occur. Rather, **IIb** evidently persists until exposure to alcohol. Crystallographic verification of proposed calcium *iso*-propoxide species could not be achieved, however. Consequently, it was decided to undertake similar experiments with a bulkier alcohol, to facilitate crystallisation of a well-defined, low nuclearity alkoxide.

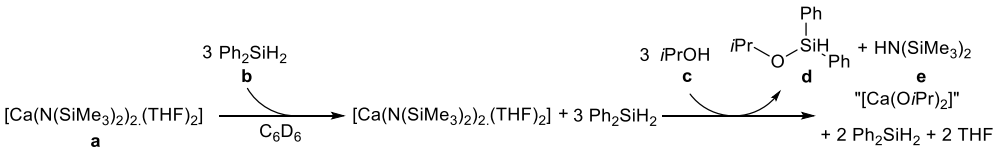

Scheme 3.8: The sequential addition of diphenylsilane then *iso*-propanol to a C_6D_6 solution of **IIb**.

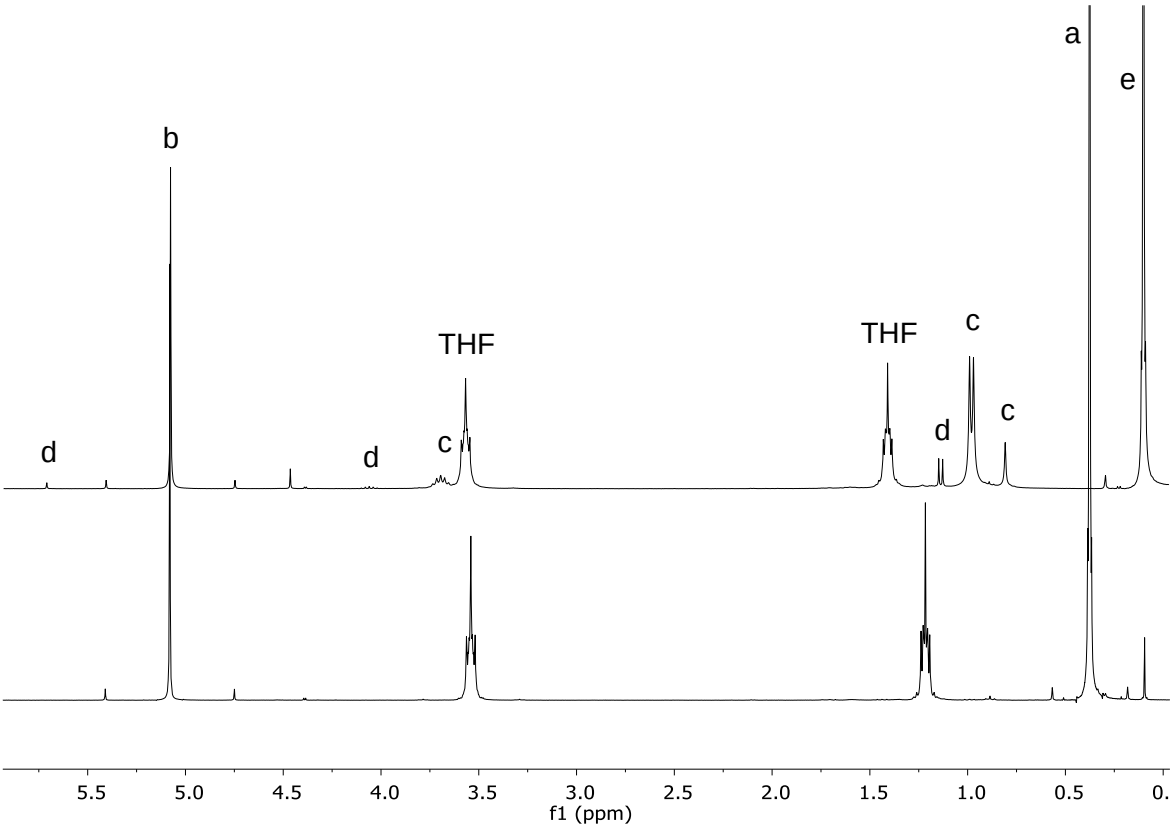

Figure 3.5: Expanded ^{1}H NMR spectra (300 MHz, 298 K, C_6D_6) of **IIb** with sequential addition of diphenylsilane (bottom) then *iso*-propanol (top).

3.2.6 Isolation and crystallographic characterisation of calcium, strontium, and barium alkoxides

Compound **IIb** was reacted with two equivalents of triphenylmethanol in C_6D_6, resulting in the formation of $HN(SiMe_3)_2$ and deposition of X-ray quality crystals of compound **10a** from the hot solution. The reaction was also carried out on a preparative scale in toluene with similar results, while analogous strontium- and barium-alkoxides (**10b**, and **10c**) could also be obtained in a similar fashion and crystallised by slow evaporation of a THF/toluene solution (Scheme 3.9).

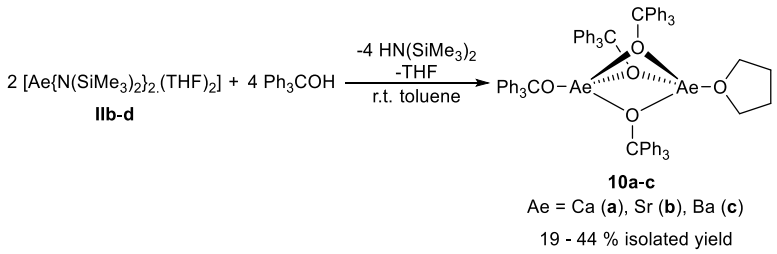

Scheme 3.9: Synthesis of compounds **10a**-**c**.

Compounds **10a**-**c** were subjected to single-crystal X-ray diffraction and crystallise as colourless blocks in the monoclinic $P2_1/n$ space group. They structurally similar, consisting of an asymmetric dimer with three μ_2-bridged alkoxide ligands, a terminal κ^1-alkoxide at Ae1, and a THF molecule coordinating to Ae2 (Figure 3.6). In each case, one of the bridging alkoxide ligands is tilted towards Ae1, with an Ae1-phenyl interaction maintaining similar Ae1-C33 (3.33-3.37 Å) and Ae1-C38 (3.17-3.29 Å) distances in all three compounds (Table 3.4). The Ae1-O2 bond increases in length on descending the group, resulting in increased tilting. This is reflected in the Ae1-O2-C20 angle, which decreases from 120.85(9)° (**10a**) to 115.66(11)° (**10b**), to 111.00(16)° (**10c**). The second bridging alkoxide ligand is tilted towards Ae2 with a significant Ae2-phenyl interaction. This is most pronounced in the case of strontium (Ca2-(C46-51) = 2.85-3.39 Å, Sr2-(C46-51) = 2.97-3.36 Å, Ca2-(C46-51) = 3.14-3.50 Å), and results in substantial deviation of the C39-C46-controid angle from linearity (Figure 3.7) (167.371° (**10a**, Ae = Ca), 166.166° (**10b**, Ae = Sr), 167.16(19)° (**10c**, Ae = Ba)). The Ae2-C46 distances increase down the group, resulting in a slight decrease in the tilt of this alkoxide ligand towards Ae2 (Ae2-O3-C39 increasing from 114.93(9)° (**10a**) to 115.08(11)° (**10b**) to 116.27(17)° (**10c**)). The third bridging alkoxide ligand maintains a relatively symmetrical bridging mode, without significant Ae-aryl interactions. The bridging alkoxide ligands in compounds **10a**-**c** all feature elongated Ae-O bonds (2.20-2.38 Å (**10a**), 2.33-2.57 Å (**10b**), 2.46-2.75 Å (**10c**)), with the asymmetric nature of the dimer giving rise to significant variation amongst the three ligands. The Ae1-O1 distance (2.0945(12) Å for **10a**) from the terminal alkoxide is significantly shorter than Ae-O distances for bridging alkoxide ligands. The bridging oxygen atoms are located asymmetrically, with O2 and O4 located closer to Ae2, and O3 located closer to Ae1. This can be rationalised by the Ae-phenyl interaction, which pushes the phenyl ring closer to one Ae centre, and the oxygen atom closer to the other Ae centre. O4 of the non-tilted bridging alkoxide is drawn closer to Ae2 on electrostatic grounds, due to the absence of a terminal alkoxide ligand on that side of the dimer. Additionally, the π-Ae induced tilting of the O3-alkoxide forces the THF ligand towards one side, resulting in an O3-Ae2-O5 angle of 168-172°.

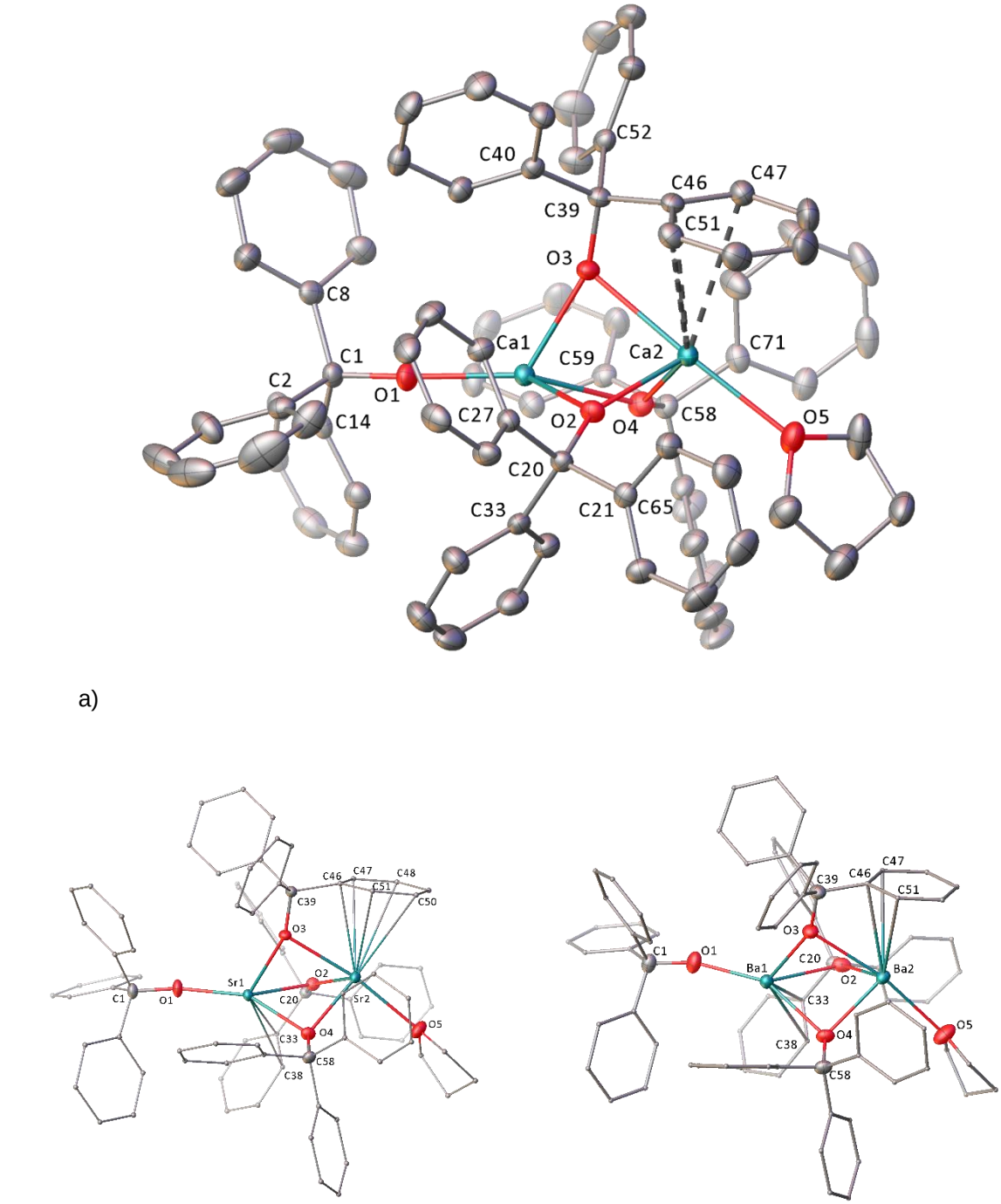

Figure 3.6: X-ray crystal structures of compounds a) **10a**, b) **10b** and c) **10c**. Thermal ellipsoids are shown at the 50% probability level**,** and hydrogen atoms are omitted for clarity. For a) and c), only the major component of the disordered THF ligand is shown. For b) and c) ligand substituents are shown as wireframes for clarity.

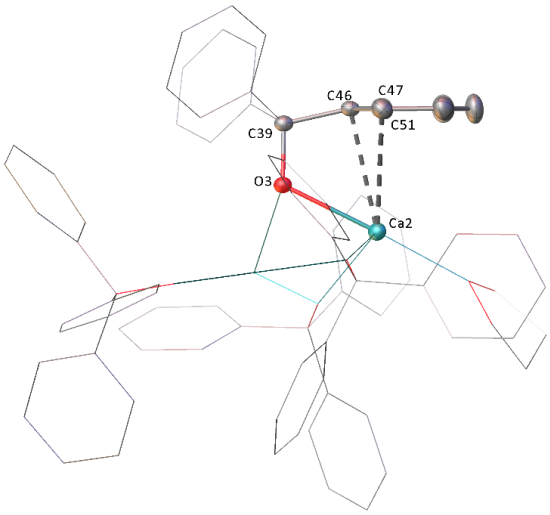

Figure 3.7: Image highlighting the intramolecular Ca-aryl interaction in the X-ray crystal structure of compound **10a**. Thermal ellipsoids are shown at the 50% probability level, hydrogen atoms are omitted, and the remainder of the molecule is shown in wireframe model for clarity.

Table 3.4: Selected distances (Å) and angles (°) from the X-ray crystal structures of compounds **10a**-**c.**

Compound	**10a**	**10b**	**10c**
Ae1-O1	2.0945(12)	2.2464(14)	2.376(2)
Ae1-O2	2.3554(11)	2.5141(14)	2.703(2)
Ae1-O3	2.2376(11)	2.3713(13)	2.524(2)
Ae1-O4	2.3435(11)	2.4984(14)	2.660(2)
Ae2-O2	2.2025(11)	2.3339(13)	2.4583(19)
Ae2-O3	2.3831(11)	2.5697(14)	2.733(2)
Ae2-O4	2.2420(11)	2.3861(14)	2.537(2)
Ae2-O5	2.3815(13)	2.5623(15)	2.753(2)
Ae1-C33	3.36835(3)	3.332(2)	3.336(3)
Ae1-C38	3.1735(17)	3.179(2)	3.294(3)
Ae1-C60	3.1422(16)	3.19515(8)	3.292(3)
Ae2-C46	2.8469(15)	2.970(2)	3.143(3)
Ae2-C47	3.0580(17)	3.090(2)	3.246(3)
Ae2-C48	3.39258(4)	3.352(2)	3.48756(3)
Ae2-C50	3.36489(3)	3.357(2)	3.49719(4)
Ae2-C51	3.0030(17)	3.113(2)	3.268(3)
Ae2-C76	3.28372(3)	3.29443(7)	3.331(3)
Ae1-O1-C1	168.04(10)	161.57(13)	158.2(2)
Ae1-O2-C20	120.85(9)	115.66(11)	111.00(16)
C20-O2-Ae2	152.58(10)	154.91(12)	157.15(18)
Ae1-O3-C39	157.06(9)	155.54(12)	152.86(18)
C39-O3-Ae2	114.93(9)	115.08(11)	116.27(17)
Ae1-O4-C58	132.66(10)	132.75(12)	132.98(18)
C58-O4-Ae2	133.48(10)	130.30(12)	127.11(17)

Whilst numerous crystallographically characterised Ae-aryloxides exist in the literature, there are surprisingly few examples of simple, non-chelating Ae-alkoxides. Ruhlandt-Senge and co-workers reported a series of ether-coordinated Ae-fluoroalkoxides ($[(R_2O)_nM(OC(CF_3)_3)_2]$, R_2O = THF (**XXIXa**, **d**), DME (**XXIXb**, **e**, **g**), diglyme (**XXIXc**, **f**, **h**), n = 4 (**XXIXa**, **d**), 2 (**XXIXb**, **c**, **e**-**g**), 3 (**XXIXh**), M = Ca (**XXIXa**-**c**), Sr (**XXIXd**-**f**), Ba (**XXIXg**, **h**)). Compounds **XXIXa**-**h** were prepared by reaction of the perfluorinated alcohol with either ammonia-activated Ae-metal or alcoholysis of compounds **IIb**-**d**.[71] These compounds are all monomeric, with coordinative saturation achieved by ether coordination. Control over *cis*/*trans* geometry was achieved through ether choice and the O-Ae bond provided the only significant interaction between the fluoroalkoxide ligand and metal centre. A later publication by the same group reports the bimetallic Ae-K-fluoroalkoxides of strontium and barium ($[(THF)_3M\text{-}\mu\text{-}(OC(CF_3)_3)_3K(THF)]$, M = Sr (**XXXa**), Ba (**XXXb**)), in which three fluoroalkoxide ligands bridge the M- and K-centres in a μ_2 fashion, with coordinative saturation achieved *via* a combination of THF coordination, and K-F interactions.[72]

Analogy can be drawn between compounds **XXXa**, **b** and **10a**-**c** by the importance of electrostatic interactions between the δ+ Ae centre and δ- fluorine or phenyl π-system to achieve greater coordinative saturation in the dimeric structure. The structures of **10a**-**c** also bear some similarity to homo and heterometallic alkali/alkaline-earth 2,6-diphenylphenolate (Odpp) complexes, which are stabilised by multiple secondary Ae-π-arene interactions.[73-76] Although the flanking nature of the 2,6-diphenylphenolate ligand might be expected to result in closer Ae-arene interactions compared to the cone-like triphenylmethoxide ligand, the Ae2-C_{Ar} distances in compounds **10a**-**c** are comparable with (even shorter for **10b**) those of the related homobimetallic dimers, $[(Odpp)Ca\text{-}\mu\text{-}(Odpp)_2]_2$ (**XXXI**), $[(Odpp)Sr\text{-}\mu\text{-}(Odpp)_3Sr]$ (**XXXIIa**), and $[(Odpp)Sr\text{-}\mu\text{-}(Odpp)_3Sr]$ (**XXXIIb**).[73]

Tacke and co-workers reported the crystal structure of a monomeric analogue of **10a**, $[Ca(OCPh_3)_2(THF)_4]$ (**XXXIII**), which displays a *cis*-octahedral geometry.[77] Hanusa and co-workers also described the calcium alkoxides, $[Ca(clox)_2(THF)_3]$ (**XXXIV**) and $[Ca(\mu\text{-clox})(clox)(THF)]_2$ (clox = $OC(Ph)_2(CH_2C_6H_4Cl)$) (**XXXV**), the latter of which features a dimeric structure with two bridging- and two terminal clox ligands.[78] The terminal Ca-O bond of **10a** is of a similar length to that in **XXXV** but is significantly shorter than literature examples of monomeric calcium alkoxides (**XXIX**,[71] **XXXIII**[77]). This is principally due to the less sterically demanding four-coordinate geometry at calcium in compounds **10a**-**c** and **XXXV**, compared to the octahedral calcium centres in compounds **XXIX**-**XXX** and **XXXIII**. The bridging Ae-μ-O bond lengths of **10a**-**c** are similar to those in the literature dimeric alkoxides (**XXX**, **XXXV**).[72, 78] Interestingly, **XXXV** lacks close Ca-aryl interactions, possibly due to the presence of a second coordinating THF molecule.

Compounds **10a**-**c** also merit comparison to the dimeric barium siloxides [{$(Me_3Si)_3SiO$}Ba{μ-$OSi(SiMe_3)_3$}$_3$Ba$(THF)_n$] (**XIIIa**, **b**, n = 0 or 1) very recently reported by Sarazin and co-workers.[58] **XIIIa** and **b** display a similar structure to **10a**-**c**, with a terminal siloxide and three μ_2-siloxides bridging the two barium centres. Notably, the absence of barium-arene interactions results in a more symmetrical ligand arrangement, with the THF ligand of **XIIIb** aligned with the *pseudo* C_3 rotational axis of the dimeric core.

Gratifyingly, compounds **10a-c** proved to be competent dehydrocoupling catalysts when added to a d_8-THF solution of triphenylmethanol and phenylsilane, returning >90% spectroscopic yield of the singly coupled product $Ph_3COSiPhH_2$ after two days at 60°C (Table 3.5).

Table 3.5: Dehydrocoupling of Ph_3COH and $PhSiH_3$ catalysed by compounds **10a**-**c**. Reactions performed at 60°C in d_8-THF, at a Si:O:Ae ratio of 20:20:1. [a] Conversion of alcohol determined by the relative integral of starting material and products in the *in situ* ^{1}H NMR spectrum.

Entry	Pre-catalyst	Time/hours	Product	Conversion[a] / %
1	**10a**	48	$Ph_3COSiPhH_2$	95
2	**10b**	48	$Ph_3COSiPhH_2$	93
3	**10c**	48	$Ph_3COSiPhH_2$	95

3.2.7 Kinetic investigation of Ic, IIb-d and IIId: overall reaction order and TOF

After exploring reaction scope and the nature of catalyst activation, a brief kinetic investigation was undertaken. The dehydrocoupling of *tert*-butanol with diphenylsilane was chosen for this purpose, since it generally proceeds at a rate amenable to kinetic analysis and with complete selectivity towards the 1:1 coupled product (Scheme 3.10).

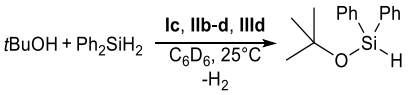

Scheme 3.10: The reaction used for a kinetic analysis of the catalytic dehydrocoupling of silanes and alcohols.

The identity of metal centre, and the presence or absence of coordinated THF molecules in the pre-catalyst was found to have a substantial effect on the overall reaction order. The strontium pre-catalyst **IIc** displayed complex sigmoidal kinetics which suggest changing mechanisms and/or active species during catalysis. By contrast, both the calcium analogue, **IIb** and THF-free dimeric strontium precatalyst, **Ic** follow partial zero-order kinetics (Figure 3.8).

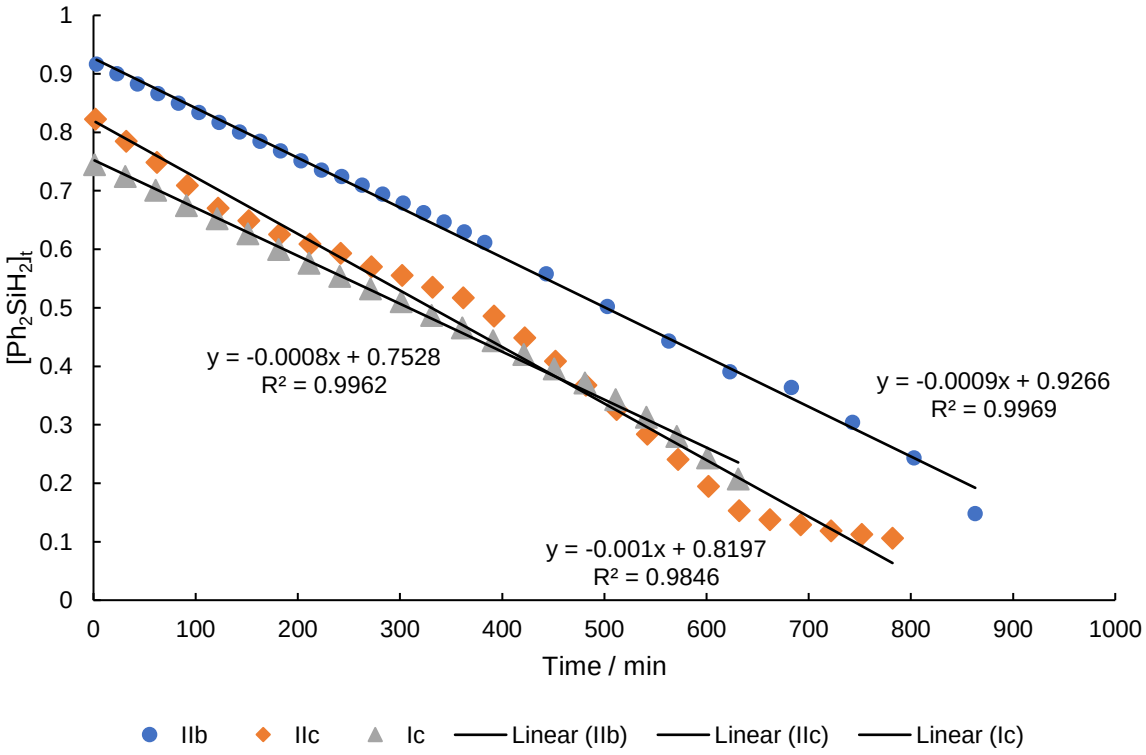

Figure 3.8: Overall zero order plots of $[Ph_2SiH_2]_t/[Ph_2SiH_2]_0$ against time for pre-catalysts **IIb**, **IIc**, and **Ic**.

Data for the barium pre-catalysts (**IId** and **IIId**) was consistent with overall second-order reaction kinetics (Figure 3.9). The change in reaction mechanism on descending group two from strontium to barium is probably the result of a less constrained catalytic platform in the coordination sphere of the larger, softer Ba^{2+} cation.

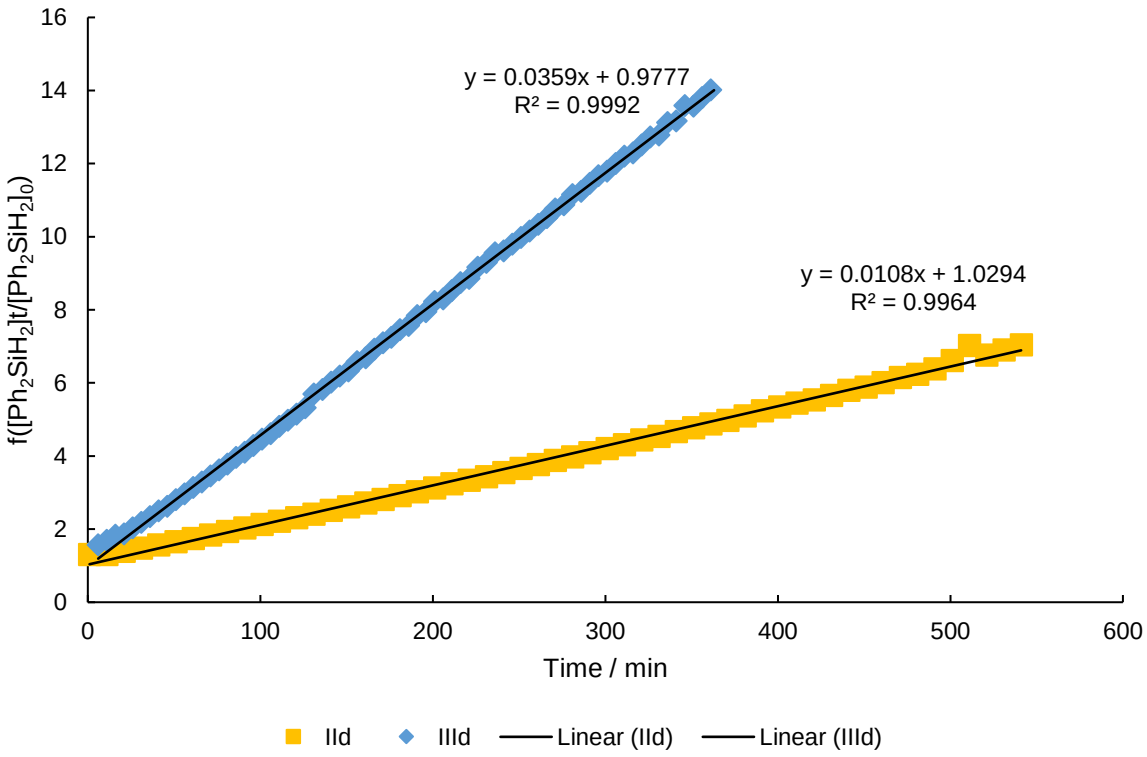

Figure 3.9: Overall second order plot of $1/([Ph_2SiH_2]_t/[Ph_2SiH_2]_0)$ against time for pre-catalysts **IId** and **IIId**.

Turnover frequency (TOF) was influenced by the identity of Ae, following the trend Ba>Sr>Ca, with a larger ionic radius and less crowded Ae coordination sphere resulting in higher TOF (Table 3.6, Figure 3.10). Whilst this trend has been previously noted for other Ae-catalysed processes,[58, 61, 64, 79] it is less pronounced here, and all three Ae metals return TOFs of a similar magnitude. A plausible explanation is that the coordination sphere of the Ae-centre is saturated by alcohol molecules, reducing the influence of ionic radius.

Switching from amide pre-catalyst **IId**, to alkyl **IIId** was accompanied by a significant increase in TOF (Table 3.6, Figure 3.10). Similar effects have been observed in silane-amine dehydrocoupling,[64] where amide/amine equilibria of the type shown in Scheme 3.11 can reduce the number of metal centres present as active, on-cycle intermediates.[61, 80, 81] By contrast, protonation of the $\{HC(SiMe_3)_2\}$ alkyl ligand is both irreversible, and heavily favoured by the relative pKa of substrate and pre-catalyst.[64, 65] Alcohols, however, are more acidic than amines such that, under a large excess of alcohol, acid-base equilibria are unlikely to be influential during silane-alcohol dehydrocoupling. As such, the greater TOF of **IIId** is tentatively attributed to coordination of bis(trimethylsilyl)amine to the metal centre. The TOF of **IIc** was also assessed in d_8-THF, but kinetic analysis was unfeasible due to the extremely deleterious effect of this coordinating solvent on activity.

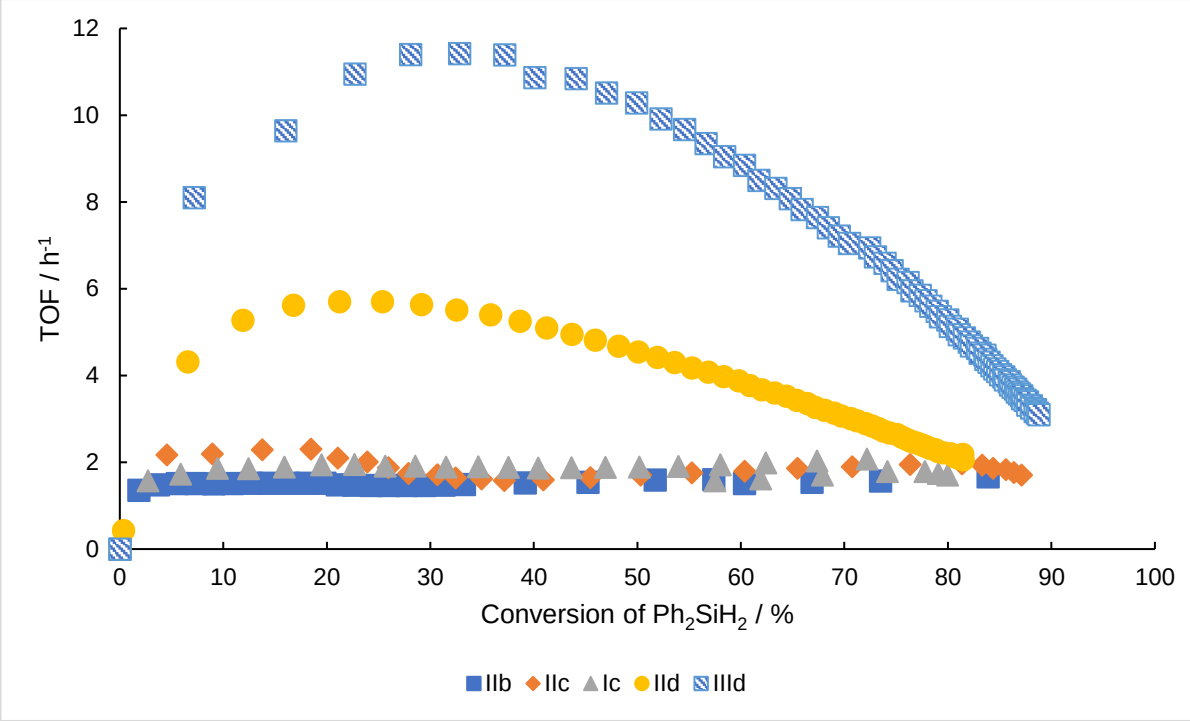

Figure 3.10: Plot of TOF *vs.* Ph_2SiH_2 conversion for a variety of Ae pre-catalysts.

Table 3.6: Turn over frequencies (TOF) at 298 K and 0.087 mol dm^{-3} substrate concentration for the catalytic dehydrocoupling of *tert*-butanol and diphenylsilane (1:1 Si/O stoichiometry). * Average TOF between 10% and 80% conversion.

Pre-catalyst	Turnover frequency (TOF) / h^{-1} *	Overall reaction order
IIb	1.52	0
IIc	1.84	variable
Ic	1.92	0
IId	3.56	2
IIId	7.1	2

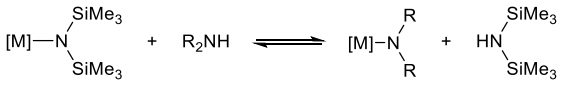

Scheme 3.11: Amine-mediated equilibrium between Ae-bis(trimethylsilyl)amide and bis(trimethylsilyl)amine.[61, 80, 81]

3.2.8 Kinetic investigation of IId: order in catalyst

Owing to its unambiguous reaction order and favourable rate, **IId** was taken forward for a more in-depth kinetic investigation. In order to determine order in catalyst, the observed second-order rate constant, k_{obs}, was measured for a range of initial **IId** loadings from 1-9 mol% (Figure 3.11, Figure 3.13). When plotted against $[Ba]^2$, a linear relationship was found for catalyst loadings between 1.4 mol% and 3.3 mol%, consistent with a second-order dependence on [Ba] and the likely action of a dinuclear active species during the rate determining process (Figure 3.12). Such behaviour is common for the heavier alkaline-earths, especially in the absence of bulky chelating ligands.[61, 79, 82]

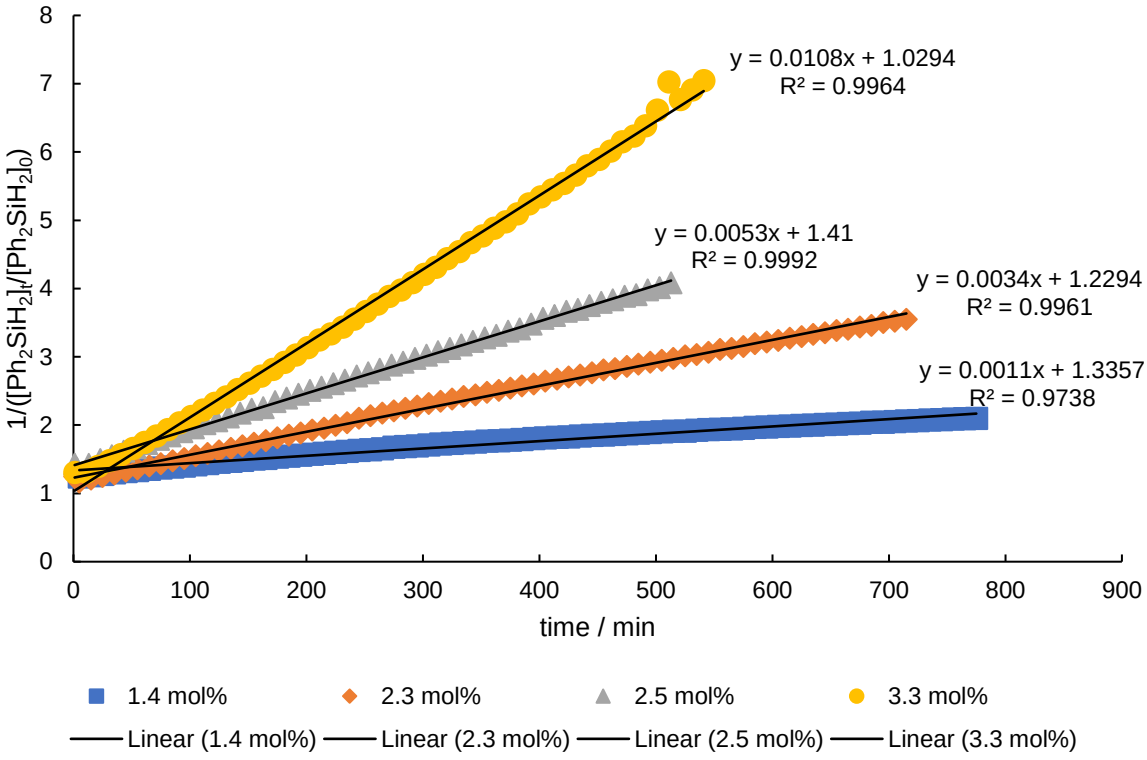

Figure 3.11: Overall second order plot of $1/([Ph_2SiH_2]_t/[Ph_2SiH_2]_0)$ against time for a variety of initial **IId** concentrations up to 3.3 mol%.

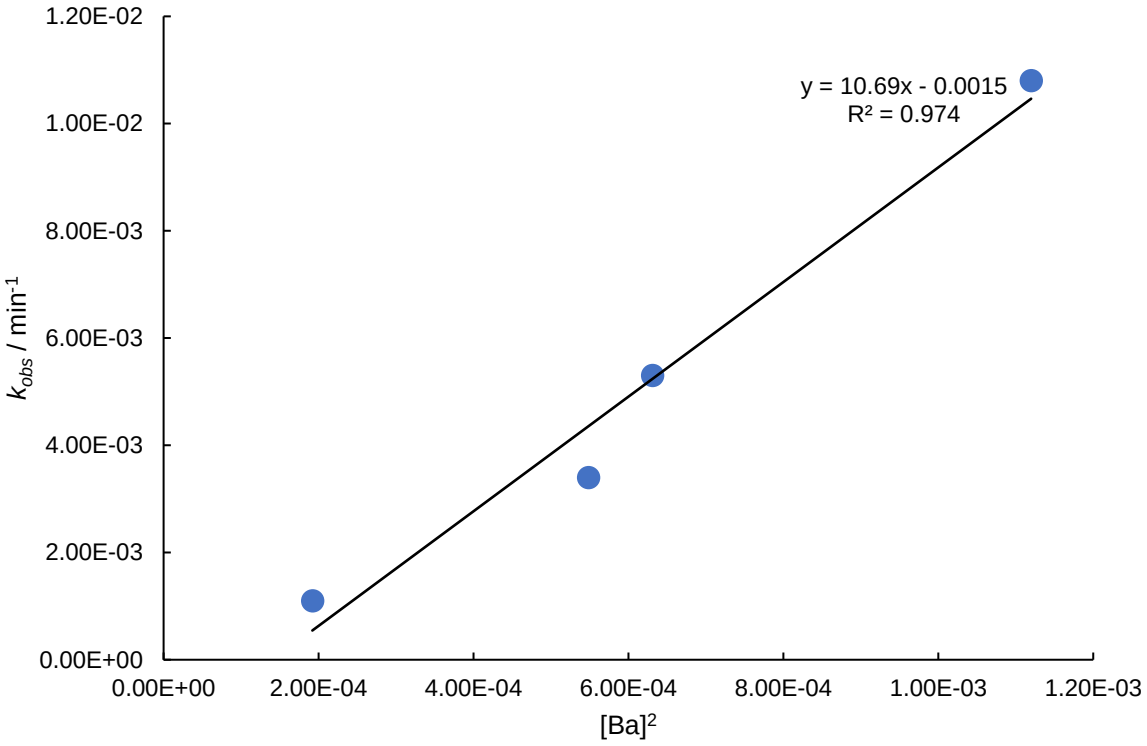

Figure 3.12: Plot of rate constant, k_{obs} against $[Ba]^2$, demonstrating a second order dependence of rate on the initial concentration of **IId** up to a 3.3 mol% loading.

Where catalyst loadings exceed 3.3 mol%, an inverse correlation between [Ba] and k_{obs} was observed, although the reaction maintained overall second order kinetics (Figure 3.14). This counter-intuitive effect has previously been observed in Ae-catalysed aminoalkene hydroamination and can be rationalised by invoking the formation of high molecularity barium alkoxide aggregates at increased barium concentration.[79] Higher aggregates of this type reduce the effective number of active sites available and are not surprising given that crystallographically characterised barium-containing complexes tend to exhibit large cluster-like structures in the absence of bulky ligands.[83-85]

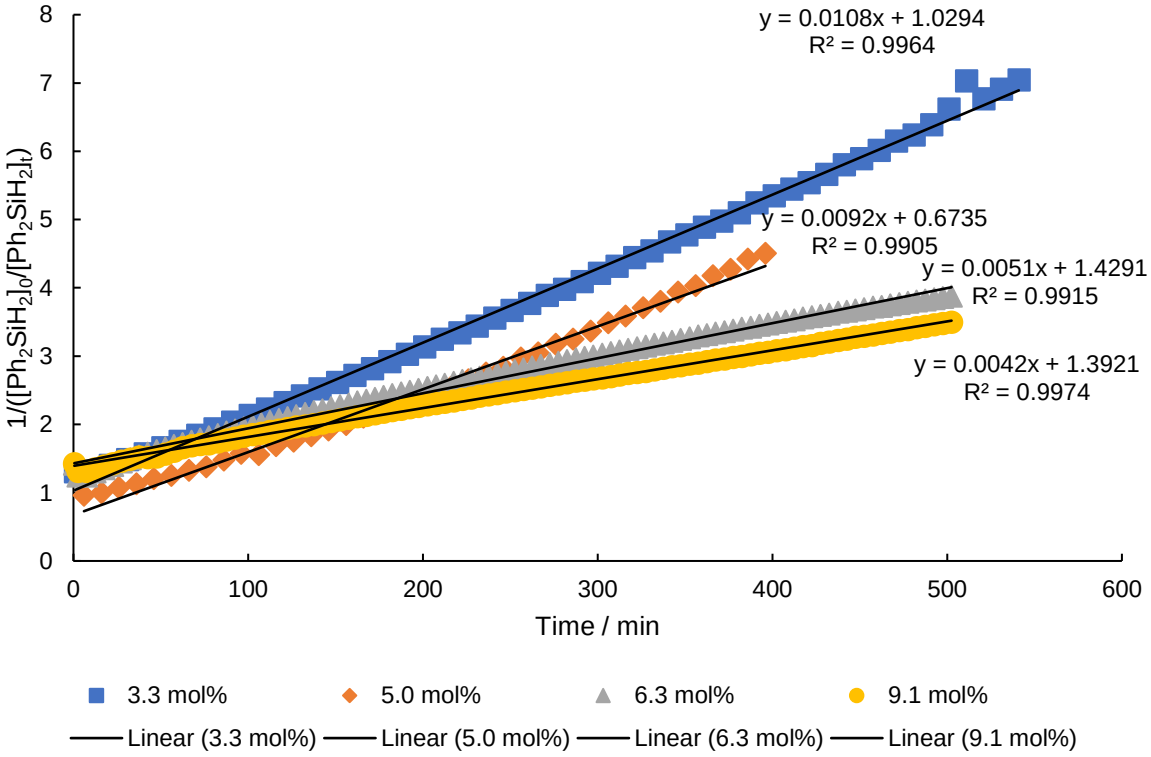

Figure 3.13: Overall second order plot of $1/([Ph_2SiH_2]_t/[Ph_2SiH_2]_0)$ against time for a variety of initial **IId** concentrations above 3.3 mol%.

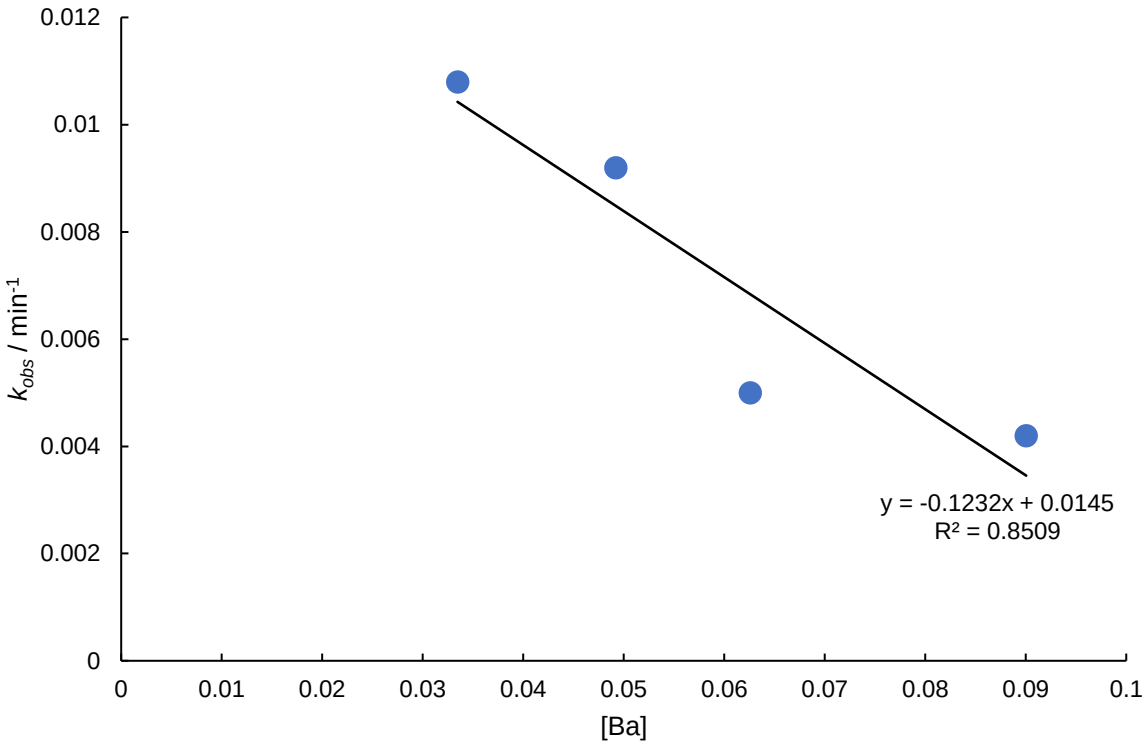

Figure 3.14: Plot of rate constant, k_{obs} against [Ba], for initial **IId** concentrations above 3.3 mol%.

3.2.9 Kinetic investigation of IId: order in substrates

Pseudo first-order experiments (Figure 3.15, Figure 3.16) provided an apparent first order dependence in both [Ph_2SiH_2] and [*tert*-butanol]. Furthermore, the rate increased by an order of magnitude under a ten-fold excess of silane and decreased by a similar magnitude when a ten-fold excess of alcohol was used. Substrate inhibition is not uncommon in Ae-catalysis[58, 61, 79, 82, 86] and, whilst product inhibition can also be a significant consideration,[86] it is unlikely to be important in this case due to the poor donor properties of silyl ethers.[87, 88]

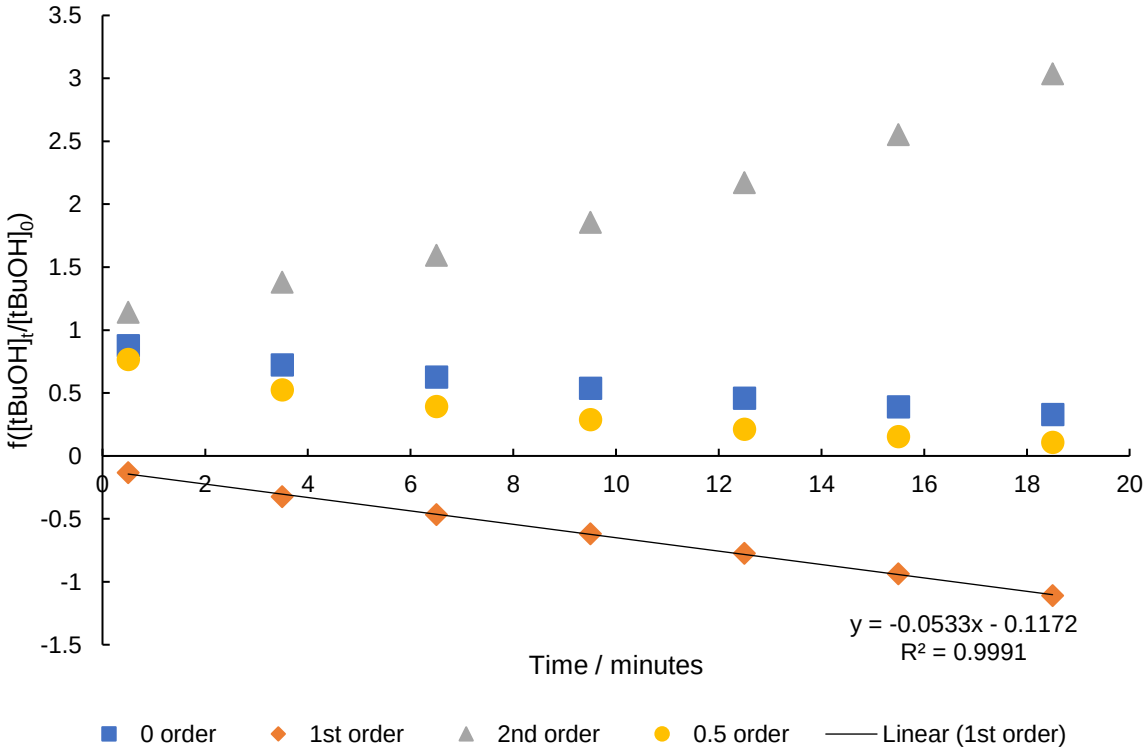

Figure 3.15: Plot of $f([tBuOH]_t/[tBuOH]_0)$ under pseudo-first order conditions with a ten-fold excess of Ph_2SiH_2 and 3 mol% **IIb**.

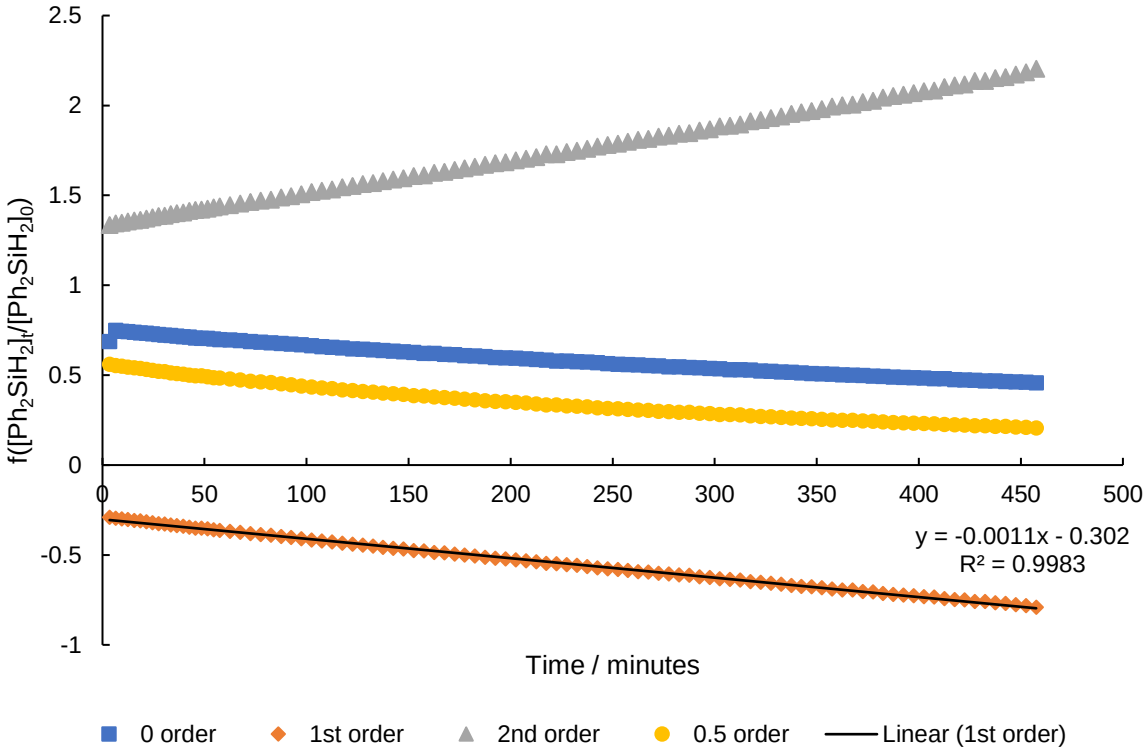

Figure 3.16: Plot of $f([Ph_2SiH_2]_t/[Ph_2SiH_2]_0)$ under pseudo-first order conditions with a ten-fold excess of *tert*-BuOH and 4 mol% **IIb**.

3.2.10 Discussion of kinetic results for pre-catalyst IId

With results in hand, an overall rate equation, Equation 3.1, can be proposed for [Ba] < 3.5 mol%.

Equation 3.1:

$$\frac{-d[silane]}{dt} = k[Ba]^2[silane]^1[alcohol]^1$$

By contrast, an overall first-order rate, Equation 3.2, was proposed by Sadow for the analogous zinc-catalysed process[89] and by both Sadow[69] and Sarazin[65, 70] for Ae-catalysed silane-amine dehydrocoupling.

Equation 3.2:

$$\frac{-d[silane]}{dt} = k[cat.]^1[silane]^1[\text{E-H}]^0$$

Where E-H = 3,5-dimethylphenol, pyrrolidine, or *tert*-butylamine, cat. = **VIIIa**, **VIIIb**, **VIIc**.

The mononuclear complexes (**VIIc**, **VIIIa** and **b**) with bulky chelating ligands employed in these studies, however, result in a well-defined active site and a turnover limiting step involving silane activation at the metal centre. Poly-nuclearity and the lack of bulky chelating ligands in the active species studied in this thesis are likely to provide a less-constrained environment and the operation of a more complex mechanism involving more than one metal centre. A similar effect was observed by Hill *et.al.* in strontium-catalysed silane-amine dehydrocoupling.[61]

A rate equation with an overall first order dependence in both alcohol and silane was also derived by Piers and co-workers in their $B(C_6F_5)_3$ catalysed reaction.[44] Here, the Lewis acid activates silane towards nucleophilic attack by an alcohol molecule, resulting in a turnover-limiting step involving both substrates. Whilst it is plausible for a barium-centre to act as a Lewis acid and activate the Si-H bond in a similar way, nucleophilic attack by neutral alcohol implies the formation of an anionic bariate species, which seems unlikely in a coordination environment containing several alkoxide ligands. A more likely explanation for the involvement of alcohol in the rate equation is that the presence of one or more alcohol molecules in the coordination sphere facilitate Si-H/Ba-O metathesis. Similar explanations have been previously been put forward for other Ae-mediated processes.[61, 90]

With these considerations in hand, a mechanism can be proposed where an equilibrium exists between coordinatively saturated, and unsaturated species. The former may be on- or off-cycle, and the latter may activate diphenylsilane towards alcohol-assisted attack from an alkoxide moiety (Scheme 3.12). Whether this process proceeds in a stepwise fashion *via* a silicate intermediate, or in a concerted manner remains unclear, but both have been put forward for other Ae-mediated dehydrocoupling processes.[61, 65, 69, 89] The reluctance of alkyl-substituted tertiary silanes to undergo dehydrocoupling (Table 3.3) also indicates that

accumulation of negative charge at the silicon centre (and hence stepwise character) could be an important factor.[58] The resulting silicate and/or barium hydride species undergo rapid protonolysis to close the cycle and regenerate a barium alkoxide (Scheme 3.13).

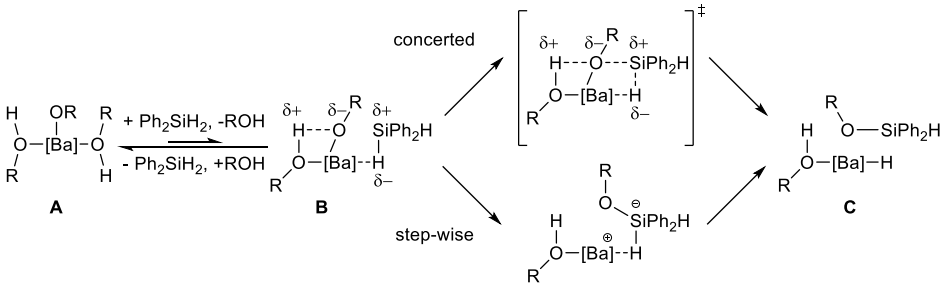

Scheme 3.12: Proposed mechanisms for the rate limiting Si-O bond-forming step. The catalyst is depicted as a monomeric species for simplicity.

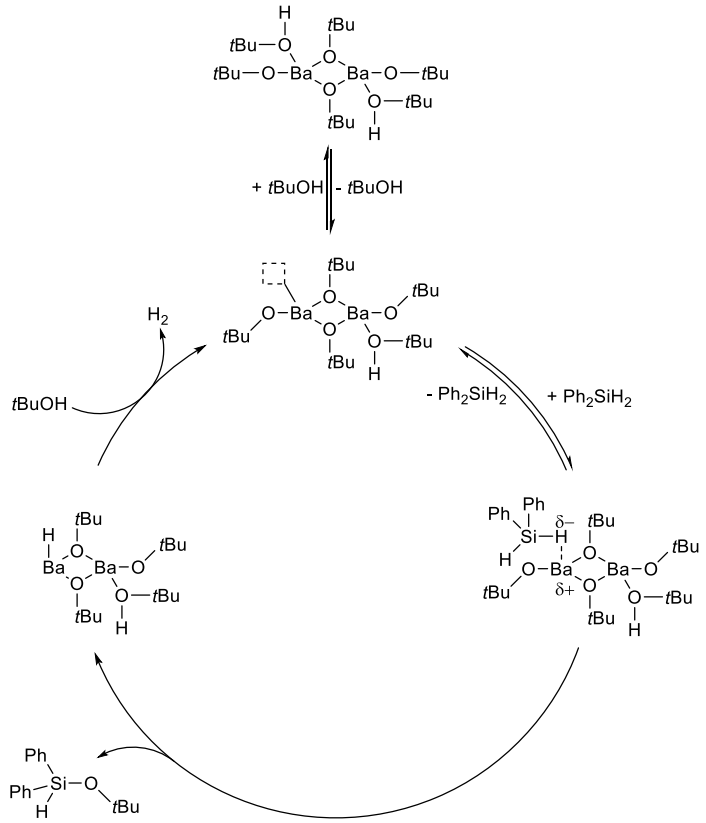

Scheme 3.13: Proposed and simplified catalytic cycle based on a dimeric active species.

Whilst it is tempting to draw conclusions based on the rate equation, poorly-defined speciation involving dimers and higher aggregates as well as significant substrate inhibition effects are likely to result in a complex reaction manifold consisting of several inter-related side reactions and off-cycle species, whose relative importance in the overall rate equation is highly dependent on variables such as substrate and catalyst concentration. The contrasting effects

that different pre-catalysts have on the overall reaction order further emphasises the complex interplay between reaction variables and mechanism.

3.2.11 Synthesis of ferrocene-containing polysilylethers

Having established the viability of Ae-catalysed Si-O dehydrocoupling in molecular systems, the reaction was taken forward as a tool to prepare ferrocene-containing polysilylethers. In section 3.2.3, it was shown that ferrocene-containing silyl ether **9** is formed selectively and quantitatively from **1** and two equivalents of benzyl alcohol, under barium catalysis in C_6D_6. Replacing benzyl alcohol with the bifunctional analogue, 1,4-$(HOCH_2)_2C_6H_4$ (1,4-benzenedimethanol), necessitated a change in solvent to THF on account of the diol's poor solubility in hydrocarbon solvents. Nevertheless, dehydrocoupling proceeded smoothly with 1.25 - 5.0 mol% **IId** and, after 2 h, polymers **P15**-**P18** were isolated as pale-orange solids by precipitation into non-dried hexane (Scheme 3.14).

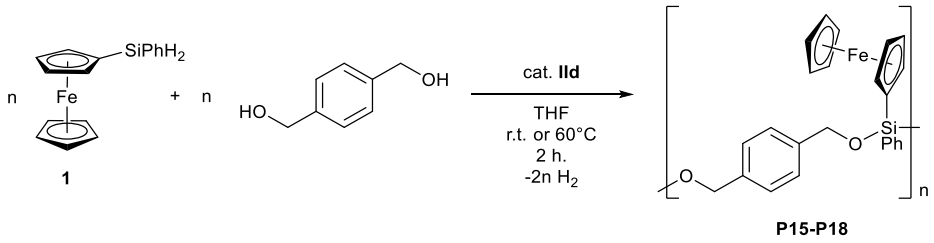

Scheme 3.14: Synthesis of polymers **P15**-**P18**.

Polysilylethers with ferrocene in the main polymer chain were also targeted. Based on the reaction scope study in section 3.2.2, however, dehydrocoupling between the bifunctional ferrocenylsilane **3** and 1,4-benzenedimethanol would be unlikely to provide a well-defined linear polymer, since diphenylsilane and **1** both give complete selectivity towards bis-coupled products when coupled with primary alcohols. Secondary alcohols, however, provided better selectivity towards mono-coupled products, hence, the bifunctional alcohol, 1,4-$(CH(CH_3)OH)_2(C_6H_4)$ was taken forward as a co-monomer.

Equimolar quantities of **3** and 1,4-$(CH(CH_3)OH)_2(C_6H_4)$ were coupled in THF at 0.6 M concentration and with 5 mol% **IIb** at 60°C. Rapid bubbling ensued, and the orange reaction mixture rapidly became viscous, which eventually prevented stirring. After heating to 60°C for 16 hours, the gum-like mixture was redissolved in non-dried THF and precipitated into hexane at -78°C to provide **P19** as a soft, glassy, orange solid. Concerned that the highly viscous reaction mixture may lead to poor mass-transport and low molecular weight, the reaction was repeated at half the original concentration. This time, stirring was possible for a full 16 hours, and the product, **P20**, had a similar appearance.

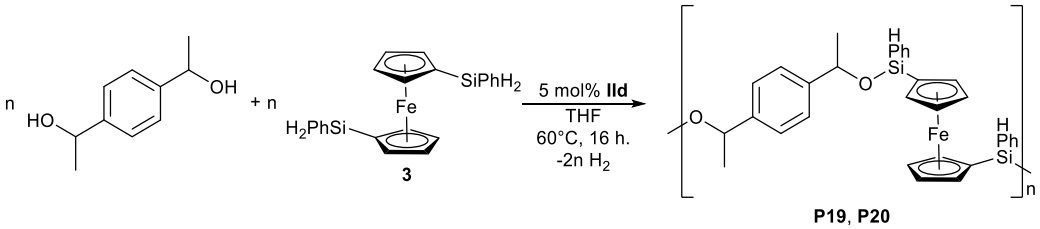

Scheme 3.15: Synthesis of oligomers **P19** and **P20**.

3.2.12 Spectroscopic and chromatographic characterisation of ferrocene-containing polysilylethers

Polymers **P15**-**P18** display almost identical ^{1}H, $^{13}C\{^{1}H\}$, and $^{29}Si\{^{1}H\}$ NMR spectra. The $^{29}Si\{^{1}H\}$ spectrum displays a single resonance at -24.28 ppm, whilst the ^{1}H NMR spectrum (Figure 3.17) shows well-defined peaks for the cyclopentadienyl and aromatic protons. The methylene protons are split into two doublets at δ 4.99, and 4.94 ppm in a similar manner to the ^{1}H NMR spectrum of the molecular analogue, compound **9**. Whilst weak apparent singlets at δ 4.88 and 4.82 ppm are candidates for chain-end methylene groups, their identity could not be unambiguously assigned. The lack of silicon-hydride resonances in the ^{1}H NMR spectra, suggest that polymers **P15**-**P18** contain a high molar mass or cyclic/linear ratio.

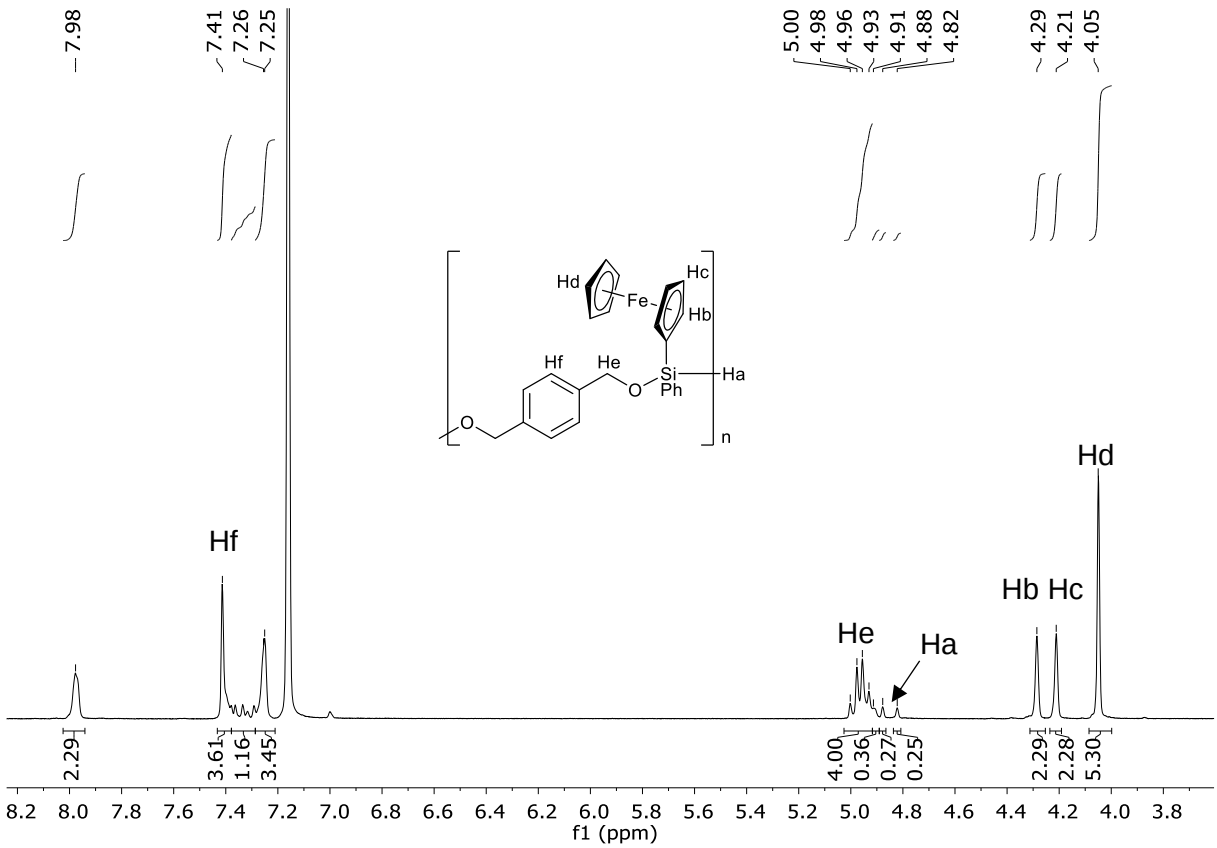

Figure 3.17: Expanded ^{1}H NMR spectrum (500 MHz, C_6D_6) of **P15**.

Polymers **P15**-**P18** have structures analogous to the polycarbosilazanes **P1**-**P7** but may be handled in non-dried solvents and stored in the ambient atmosphere. Although silyl ethers are not as hydrolytically robust as siloxanes, they offer a significant improvement over carbosilazanes and, in the case of **P15**-**P18**, moisture tolerance is enhanced by non-polar aromatic side chains, which protect the backbone from nucleophilic attack by water.

This improved stability allowed the molecular weight of **P15**-**P18** to be determined by gel permeation chromatography (GPC) (Table 3.7). All polymers displayed a bimodal distribution with a polymeric fraction eluting before an oligomeric (*ca.* ~1000-2000 Da) fraction (Appendix i.5, Figure i.2). Polymers prepared with a 2.5 mol% pre-catalyst loading (**P15**, **P18**) presented the highest M_n values, in excess of 20000 Da for the polymeric fraction. Increasing the reaction temperature to 60°C did not affect M_n significantly, but slightly increased the polydispersity (**P18**). Increasing the pre-catalyst loading to 5 mol% decreased M_n in the final product (**P17**), possibly a consequence of some of the diol being sequestered by the barium centre as an alkoxide ligand during catalysis and a resultant deviation of the reaction stoichiometry away from the ideal 1:1 ratio. Decreasing **IId** to 1.25 mol% resulted only in oligomeric products of high polydispersity (**P16**). Diffusion ordered NMR spectroscopy (DOSY) was also employed to provide estimated M_n values, using the method described by Grubbs *et.al.* and utilised in

Chapter 2.[91] Whilst DOSY returned values of a similar magnitude to GPC (Table 3.7), a minor discrepancy was apparent between the two techniques, particularly for the higher molar mass samples (**P15** and **P18**). A possible explanation for this may be attributed to the bimodal distribution; whereas GPC can discriminate polymeric and oligomeric fractions, DOSY measures an overall mean diffusion coefficient, such that the final M_n will be substantially influenced by the relative population of polymer and oligomer in the final product.

P19 displays a broad and complex ^{1}H NMR spectrum, from which the various proton environments could nevertheless be assigned. A broad singlet at δ 0.45 ppm was identified as O*H* termini, whilst multiplets at δ 1.29 and 4.54 ppm were assigned to chain-end C*H* and CH_3 environments, respectively, and were clearly separated from the corresponding mid-chain resonances at δ 1.53 – 1.36 and 5.09 – 4.92 ppm. A doublet resonance at δ 5.73 ppm suggested that some SiH_2 termini were also present. The significant relative intensity of chain-end resonances suggested that **P19** consists of low-molecular weight oligomeric material. This was supported by both DOSY and GPC, with estimated M_n values of <10000 Da and a PDI of 2.2. The ^{1}H NMR spectrum of **P20** was even broader than that of **P19** and, although this precluded detailed assignment, the spectra were otherwise similar. Unfortunately, DOSY was uninformative for **P20** due to the broad ^{1}H NMR spectrum, albeit GPC provided evidence for a high polydispersity material with M_n = 7000 Da, PDI = 3.0, and a distribution of chain lengths ranging from low-molecular weight oligomers to polymeric material in excess of 15000 Da.

Table 3.7: Synthesis of polymers and oligomers **P14-P19** using pre-catalyst **IId**. [a] Number average molecular weight estimated by ^{1}H DOSY NMR spectroscopy relative to monodisperse polystyrene standards. [b] Number average molecular weight estimated by Gel Permeation Chromatography (GPC), determined from polymeric fraction of bimodal distribution relative to monodisperse polystyrene standards. *Meaningful M_n not possible due to very broad ^{1}H NMR spectrum. **Overall M_n and PDI: bimodal distribution could not be deconvoluted.

Sample	Diol	Silane	Si:O:Ba	$C_{monomer}$[a] (mol dm^{-3})	Temperature/°C (time/hours)	$M_{n,\,DOSY}$ / (g mol^{-1})[b]	$M_{n,\,GPC}$ / (g mol^{-1})[c]	PDI_{GPC}[d]
P14		**1**	40:80:1	0.36	25 (2)	17000	23200	1.6
P15	1,4-$(HOCH_2)_2$-(C_6H_4)	**1**	80:160:1	0.41	25 (2)	7000	2000*	3.9**
P16		**1**	20:40:1	0.29	25 (2)	15000	12300	1.8
P17		**1**	40:80:1	0.36	60 (2)	35000	21500	2.1
P18	1,4-$(CH(CH_3)OH)$-(C_6H_4)	**3**	40:40:1	0.6	60 (16)	7000	2900	2.2
P19		**3**	40:40:1	0.3	60 (16)	-*	5000	3.0

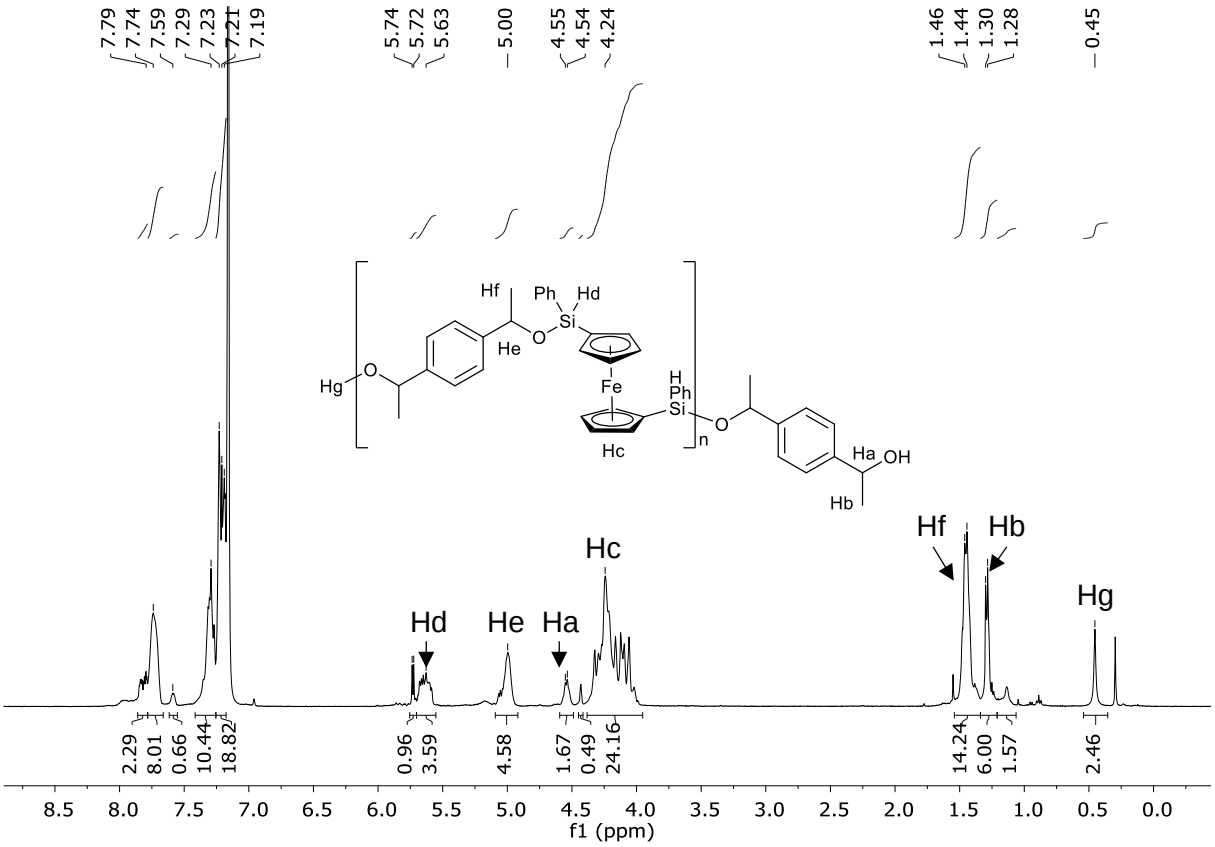

Figure 3.18: ^{1}H NMR spectrum (500 MHz, C_6D_6) of **P19**.

3.2.13 Electrochemical analysis of P15, P19 and compound 9

The electrochemical behaviour of **P15** and **P19** was investigated by cyclic voltammetry (CV) and compared to the model compound **9** and parent monomers **1** and **3**, whose electrochemical behaviour was discussed in Chapter 2, Section 2.2.7. All samples displayed a single, fully reversible redox wave corresponding to the Fe^{2+}/Fe^{3+} redox couple (Figure 3.19). The midpoint potential, $E_{1/2}$, of the coupled silyl ethers was shifted towards lower potentials compared to hydrosilane monomers **1** and **3**, reflecting the electron withdrawing effect of the oxygen substituents (Table 2.5). **P15** displays a very similar $E_{1/2}$ value to compound **9**, indicating essentially identical electronic environments at iron, whilst the monocoupled silylether-hydride motif of **P19** gives rise to a redox potential that resides between those of the bis-coupled materials and the hydrosilane monomers. As a result of slower diffusion, peak currents of the oligomeric materials are substantially lower than the small molecule **9**. In contrast to **P1** and compound **2**, the effect of slow diffusion is not offset by the presence of multiple redox centres in this case, indicating that a relatively small number of ferrocene moieties per oligomer undergo redox activity at the electrode. The redox wave of **P19** is slightly broadened, complicating accurate measurement of the peak separation (ΔE_{peak}). A relatively

large ΔE_{peak} value was observed for **P15** compared to the analogous polycarbosilazane, **P1**, which may also be a result of a relatively few-electron redox process.

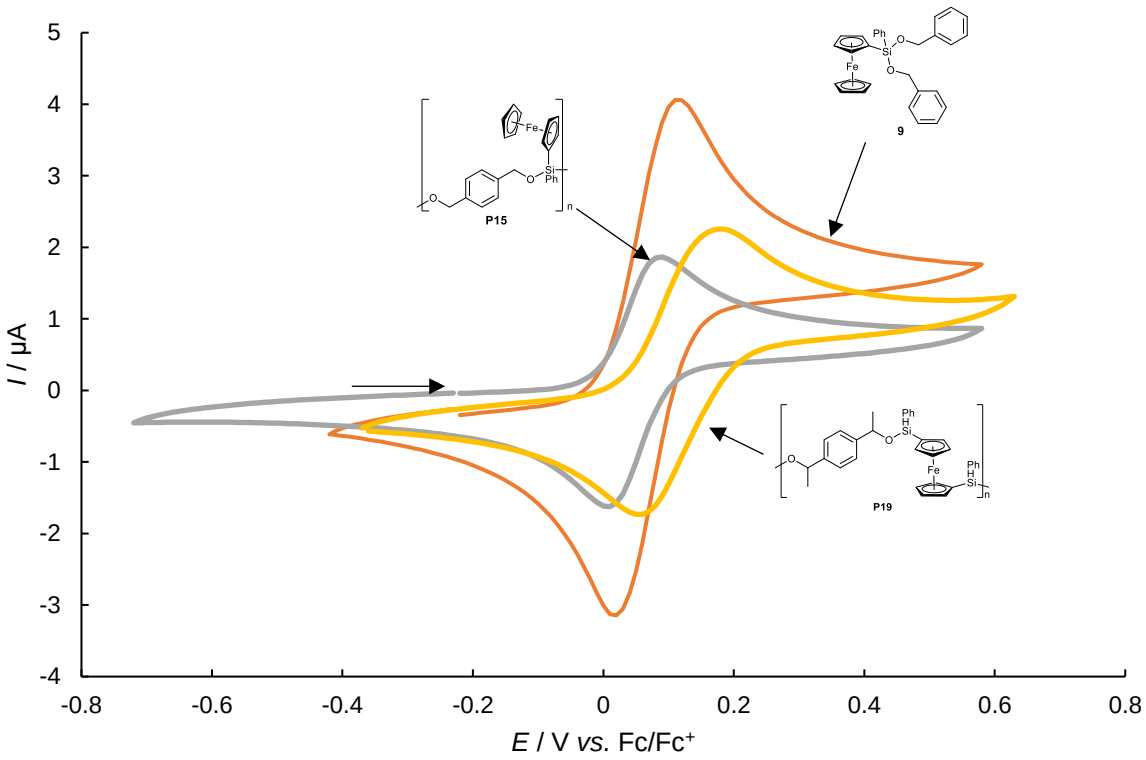

Figure 3.19: Cyclic voltammogram of compound **9**, polymer **P15**, and oligomer **P19**. Voltammetry carried out in 1 mM molecular or monomer concentration with a 1 mm diameter platinum disc electrode immersed in dichloroethane containing 0.1 M NBu_4PF_6 and a scan rate of 100 mVs^{-1}.

Table 3.8: Cyclic voltammetry data for samples dissolved in ca. 1 mM molecular/monomer concentration obtained at a 1 mm diameter platinum disc electrode immersed in dichloroethane containing 0.1 M NBu_4PF_6 at 100 mV/s. Potentials are referenced to ferrocene/ferrocenium. [a] Approximate concentration of molecular systems or of monomer in polymer systems.[b] The midpoint potential is defined here as $E_{1/2} = ½(E_{p,ox} + E_{p,red})$. Cyclic voltammograms of compounds **1** and **3** can be found in Chapter 2, Section 2.2.7.

Compound	Concentration [a]	$E_{1/2}$ / V [b]	ΔE_{peak} / mV	$I_{peak, ox}$ / µA	$I_{peak, red}$ / µA
1	1 mM	0.115	100	5.44	-5.78
9	1 mM	0.045	90	3.78	-4.13
P15	1 mM	0.040	80	1.81	-1.90
3	1 mM	0.115	95	3.73	-3.99
P19	1 mM	0.060	120	2.16	-2.17

3.2.14 Thermal analysis of ferrocene-containing polysilylethers

Although polysiloxanes have been extensively utilised as precursors to silicon oxycarbide glasses,[92-94] the pyrolysis of polysilylethers remains virtually unexplored.[95] To this end, **P16**

and **P19** were subjected to thermogravimetric analysis (TGA) (Figure 3.20, Table 3.9). **P16** displays a well-defined onset temperature at 360°C, with most mass-loss occurring below 600°C to provide a final ceramic yield of 36% at 800°C. The onset temperature of **P19** occurs at approximately 300°C, and weight loss proceeds in a gradual and stepwise manner, eventually providing a 49% ceramic yield. The ceramic yields are respectable for linear ferrocene-containing polymers. For comparison, linear polyferrocenylsilane (PFS) provides ceramic yields of 17-58%,[96, 97] whilst ferrocene-containing polycarbosilazanes **P1** and **P11** give values of 43% and 64% respectively (Chapter 2: Section 2.2.8, Table 2.6). It is also worth noting that, despite the low molecular weight of **P19**, the ceramic yield is good, reflecting the importance of *in situ* cross-linking reactions during pyrolysis. With enhanced crosslinking processes it may be possible to achieve very high ceramic yields.[98]

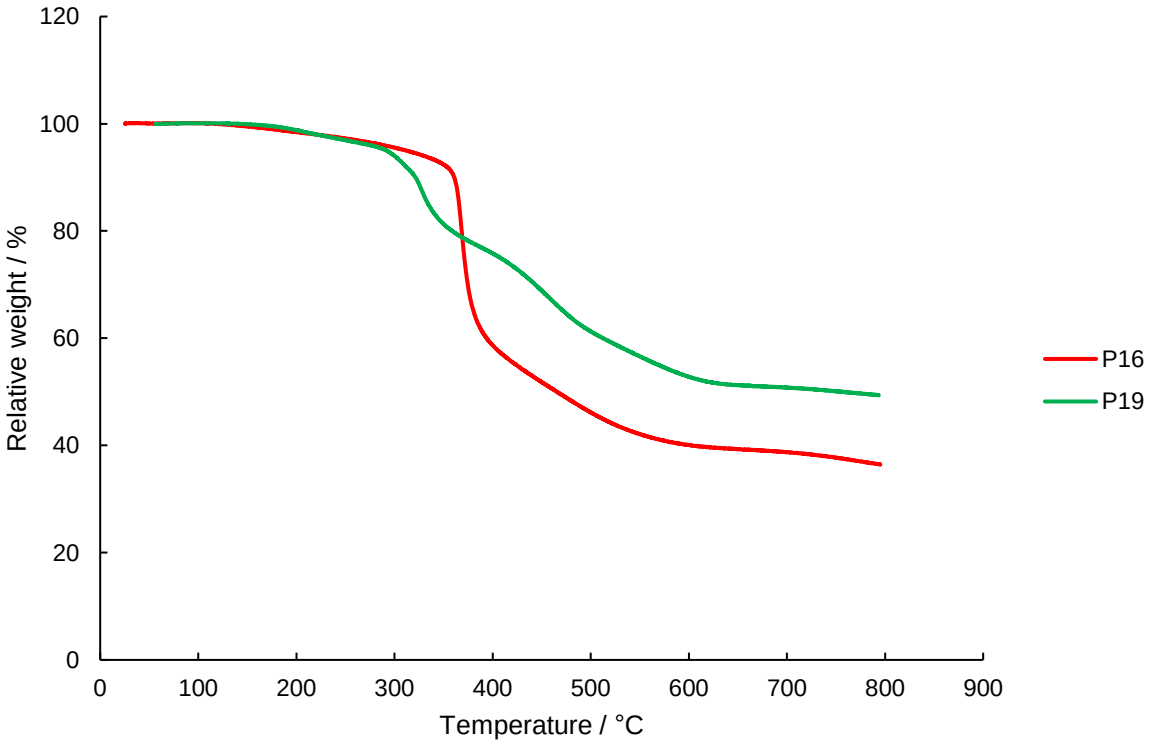

Figure 3.20: TGA traces **P16** and **P19**, heated to 800°C at 10°C/min under a flow of N_2.

Table 3.9: Ceramic yields of ferrocene-containing polysilylethers at 800°C, determined by TGA (10°C/min, under flow of N_2).

Sample	**Ceramic yield** / %
P16	36
P19	49

The pyrolysed material obtained from TGA was attracted to a bar magnet, suggesting a similar structure to those of **P5py** and **P8py** described in Chapter 2 (Section 2.2.9), with iron, or

magnetite nanoparticles embedded within a matrix, which, in this case, is likely to be a silica-like material.[99] Whilst a thorough compositional analysis of the pyrolysed material is beyond the scope of this study, future comparison to the nitrogen-containing ceramics **P5py** and **P8py** would merit further attention.

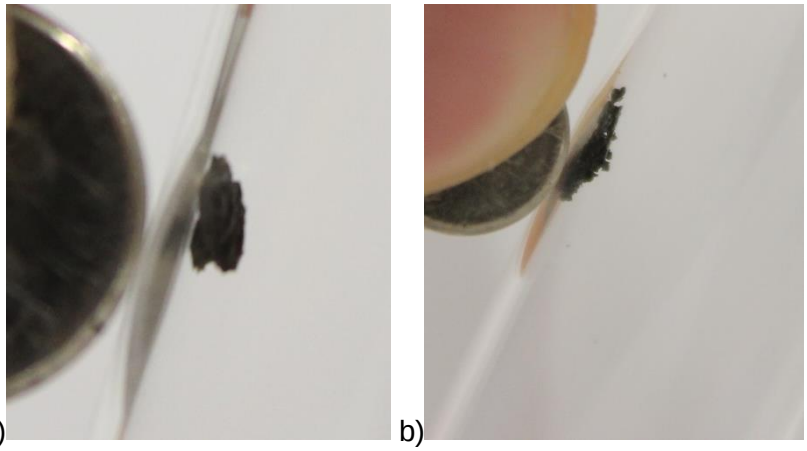

Figure 3.21: Photographs demonstrating magnetisation of the pyrolysed material obtained from TGA of a) **P16** and b) **P18**.

3.3 Conclusions

Homoleptic bis-amide and bis-alkyl complexes of the heavier alkaline-earths act as efficient and general catalysts for the dehydrocoupling of silanes with alcohols. Although good discrimination of phenylsilane towards silyl ethers with two- or three- Si-O bonds could be obtained for primary and secondary alcohols, such selectivity is dependent upon parameters such as catalyst choice, reaction duration, and temperature. Mono-substitution was only accessible for very bulky alcohols, and redistribution towards the more highly substituted thermodynamic products was generally observed where the steric demands of the substrate allowed. Using triphenylmethanol, a series of dimeric Ae-alkoxides **10a**-**c** were isolated and crystallographically characterised. Kinetic and stoichiometric investigations suggest that, whilst pre-catalyst activation to an alkoxide species appears essentially irreversible, higher reaction rates were observed for the alkyl pre-catalyst **IIId** compared to the amide **IId**. A possible explanation for this is that $HN(SiMe_3)_2$ produced from the latter precatalyst has an inhibitory effect on catalysis. Turnover frequency (TOF) increases down group two, with the larger, less charge-dense cations providing a less constrained catalytic platform. Kinetic investigations on the barium pre-catalyst **IId** suggest that the active species in catalysis are dimeric, with the formation of less catalytically efficient higher aggregates at higher catalyst concentration. A turnover limiting step implicating both silane and alcohol is invoked by the kinetic data, and is tentatively rationalised by an alcohol-promoted Si-O bond-forming step.

Increasing alcohol concentration, however, has a strong inhibitory effect, suggesting that de-coordination to deliver a coordinatively unsaturated species is important.

Barium-catalysed Si-O dehydrocoupling was applied to the synthesis of previously unknown ferrocene-containing polysilylethers, with ferrocene pendent to- or part of the main polymer chain, depending on monomer choice. These materials are hydrolytically robust and display fully reversible electrochemical behaviour, with ferrocene moieties behaving as isolated redox centres. GPC found that, whilst main-chain ferrocene-containing oligosilylethers were of low molar mass, estimated M_n values in excess of 20000 Da were achieved for pendent ferrocene-containing polysilylethers. Furthermore, TGA under a nitrogen atmosphere provides magnetic ceramic materials in a respectable yield and future improvements through the introduction of additional crosslinking during pyrolysis may lead to very high values.[98]

Having explored the utility of Ae-catalysis for the synthesis of organic/inorganic hybrid metallopolymers and investigated properties of the resulting materials, the remainder of this thesis will be concerned with the goal of forming “truly inorganic” group 14 and group 13/15 chains. Since alkaline-earth mediated reactivity for this purpose is essentially absent from the literature, we must first probe the fundamental reactivity of some alkaline-earth complexes towards model *p*-block substrates.

3.4 Experimental details

3.4.1 Catalytic dehydrocoupling reactions

Liquid alcohols: In the glove box, a quantity of silane (0.04-0.05 mmol) was added to a J. Youngs NMR tube containing a C_6D_6 solution of the desired quantity of Ae catalyst (0.5 ml). The open NMR tube was transferred to a sealed Schlenk flask, removed from the glove box and, using standard Schlenk techniques, the alcohol was added *via* syringe. The NMR tube was sealed against a flow of argon, removed from the Schlenk flask and immediately subjected to vigorous shaking. Release of hydrogen gas was often observed and the reaction was monitored by ^{1}H NMR spectroscopy.

Solid alcohols (Ph_3COH, pinacol): In the glove box, a C_6D_6 solution containing the desired quantity of Ae catalyst (0.2 ml) was added to a J. Young’s NMR tube containing a C_6D_6 solution (0.4 ml) of the silane and alcohol (0.04-0.05 mmol). The NMR tube was sealed, shaken, removed from the glove box, and the reaction was monitored by ^{1}H NMR spectroscopy.

3.4.2 Synthesis of compound 9

A J. Young’s NMR tube was charged with 50 mg **1** (0.171 mmol) and a C_6D_6 solution of **IId** (5.1 mg, 0.0086 mmol, 0.6 ml) was added. The NMR tube was transferred to a Schlenk flask and, using standard Schlenk techniques, 35.5 µl benzyl alcohol (0.342 mmol) was added *via*

syringe. The NMR tube was sealed against a flow of argon. After three days at room temperature, solvent was removed under vacuum, and the crude product extracted into hexane, from which single crystals were obtained at -30°C. Yield 59.2 mg, 69%. ^{1}H NMR (300 MHz, C_6D_6) δ 8.03 – 7.92 (m, 2H, *o*-Si*Ph*), 7.37 (ddq, *J* = 6.9, 1.5, 0.7 Hz, 4H, *o*-CH_2*Ph*), 7.29 – 7.17 (m, 6H, *m,*p-Si*Ph*, *m*-CH_2*Ph*), 7.13 – 7.02 (m, 2H, *p*-CH_2*Ph*), 4.95 (d, *J* = 12.7 Hz, 2H, C*H*$_2$), 4.90 (d, *J* = 12.9 Hz, 3H, C*H*$_2$), 4.28 (t, *J* = 1.6 Hz, 2H, 2,5-C_5H_4), 4.20 (t, *J* = 1.7 Hz, 2H, 3,4-C_5H_4), 4.04 (s, 5H, C_5H_5). ^{13}C{^{1}H} NMR (126 MHz, C_6D_6) δ 141.15 (*i*-CH_2*Ph*), 135.08 (*o*-SiPh), 134.44 (*i*-Si*Ph*), 130.54 (*m*-Si*Ph*), 128.62 (*m*-CH_2*Ph*), 128.34 (*p*-Si*Ph*), 127.46 (*p*-CH_2*Ph*), 126.84 (*o*-CH_2*Ph*), 74.35 (3,4-C_5H_4), 71.73 (2,5- C_5H_4), 69.21 (C_5H_5), 65.44 (OCH_2), 64.59 (*1*-C_5H_4Si). ^{29}Si NMR (99 MHz, C_6D_6) δ -24.27. Analysis calculated for $C_{30}H_{28}FeO_2Si$: C 71.43, H 5.59%. Found: C 71.54, H 5.52%.

3.4.3 Stoichiometric reactions of compound IIb with *i*-PrOH and $PhSiH_3$ or Ph_2SiH_2

In the glove box, 7.3 mg **IIb** (0.0145 mmol) was dissolved in 0.5 ml C_6D_6 and transferred to a J. Young's NMR tube, which was placed in a sealed Schlenk flask. Using standard Schlenk techniques, 3.3 µl *i*PrOH (0.0435 mmol) was added *via* syringe, and the NMR tube sealed against a flow of argon. Following analysis by ^{1}H NMR spectroscopy, the NMR tube was returned to the glove box and 5.4 µl $PhSiH_3$ (0.0435 mmol) or 8.1 µl Ph_2SiH_2 (0.0435 mmol) was added. The reaction mixture was again analysed by ^{1}H NMR spectroscopy.

The reaction was repeated with the order of addition reverse: silane first (in the glove box), followed by alcohol (on the Schlenk line *via* syringe).

3.4.4 Synthesis of compound 10a

In a J. Young's NMR tube, 11.1 mg **IIb** (0.022 mmol) and 11.4 mg Ph_3COH (0.044 mmol) were dissolved in 0.5 ml C_6D_6. 5.4µl $PhSiH_3$ (0.044 mmol) was subsequently added, and the reaction mixture heated to 60°C for 3 days. There was no evidence of the anticipated dehydrocoupling product ($Ph_3COSiPhH_2$) by NMR spectroscopy. Compound **10a** crystallised directly from the reaction mixture and was isolated as large colourless blocks suitable for single crystal X-ray diffraction. Some degree of THF ligand exchange takes place in THF solution, hence the reported NMR spectrum in THF-d_8 refers to the partially deuterated compound. Yield 4.1 mg, 31%. Reversing the order of addition for $PhSiH_3$ and Ph_3COH followed by heating to 80°C for 7 days also resulted in the crystallisation of compound **10a** (yield 4.2 mg, 32%), as did undertaking the reaction at 60°C for 3 days in the absence of $PhSiH_3$ (yield 5.7 mg, 44%). ^{1}H NMR (500 MHz, C_6D_6) δ 7.52 – 7.40 (m, 24H, *o*-C_6H_5), 7.03 – 6.89 (m, 36H, *m*+*p*-C_6H_5), 2.35 (s, 4H, 2,5-THF), 0.77 (s, 4H, 3,4-THF). ^{13}C{^{1}H} NMR (126 MHz, C_6D_6) δ 153.57 (*i*-C_6H_5), 128.55 (*o*-C_6H_5), 128.35 (*m*-C_6H_5),126.10 (*p*-C_6H_5), 68.20 (2,5-THF), 24.82 (3,4-THF). ^{1}H NMR (500 MHz, THF-d_8) δ 9.27 (d, *J* = 7.6 Hz, 24H, *o*-C_6H_5), 8.94

(t, *J* = 7.5 Hz, 24H, *m*-C_6H_5), 8.86 (t, *J* = 7.1, 6.4 Hz, 12H, *p*-C_6H_5), 5.48 (m, 3H, 2,5-THF), 3.66 – 3.62 (m, 3H, 3,4-THF). $^{13}C\{^1H\}$ NMR (126 MHz, THF-d_8) δ 129.40 (*o*-C_6H_5), 127.37 (*m*-C_6H_5), 125.46 (*p*-C_6H_5), 67.97 (2,5-THF), 25.86 (3,4-THF). Analysis calculated for $C_{80}H_{68}Ca_2O_5$: C 80.78, H 5.76 %. Found: C 80.64, H 5.72 %.

3.4.5 Synthesis of compound 10b

A Schlenk flask was charged with 94 mg Ph_3COH (0.36 mmol), 100 mg **IIc** (0.18 mmol), and dry toluene (~3 ml). The reaction mixture was stirred and, following dissolution, a colourless precipitate formed. After 30 minutes, the reaction mixture was filtered. The resulting colourless solid was washed with toluene and dried under vacuum. X-ray quality crystals of compound **10b** were obtained by slow evaporation of a THF solution in the glove box. Compound **10b** is soluble in ethereal solvents, but only sparingly soluble in aromatic solvents such as benzene and toluene. Some degree of THF ligand exchange takes place in THF solution, hence the NMR spectrum in THF-d_8 refers to the partially deuterated compound. Yield 22 mg, 19%. ^1H NMR (500 MHz, THF-d_8) δ 7.43 (d, *J* = 7.7 Hz, 24H, *o*-C_6H_5), 7.02 (t, *J* = 7.5 Hz, 24H, *m*-C_6H_5), 6.95 (t, *J* = 7.1 Hz, 12H, *p*-C_6H_5), 3.65 – 3.60 (m, 2H, 2,5-THF), 1.80 – 1.75 (m, 2H, 3,4-THF). $^{13}C\{^1H\}$ NMR (126 MHz, THF-d_8) δ 155.42 (*i*-C_6H_5), 129.55 (*o*-C_6H_5), 127.13 (*m*-C_6H_5), 125.05 (*p*-C_6H_5), 84.43 (O*C*(C_6H_5)$_3$), 68.27 (2,5-THF), 26.43 (3,4-THF). Analysis calculated for $C_{80}H_{68}O_5Sr_2$: C 74.80, H 5.34 %. Found: C 74.63, H 5.16 %.

Performing the reaction in C_6D_6 on 0.022 mmol scale in a sealed J. Young's NMR tube also resulted in the formation of a colourless precipitate, but heating to 84°C allowed a few X-ray quality crystals to be collected from the walls of the NMR tube.

3.4.6 Synthesis of compound 10c

Compound **10c** was synthesised and crystallised following the same procedure as **10b**, using 170 mg Ph_3COH (0.66 mmol) and 200 mg **IId** (0.33 mmol). Compound **10c** is soluble in ethereal solvents, but only sparingly soluble in aromatic solvents such as benzene and toluene. Yield 22 mg, 19%. ^1H NMR (500 MHz, THF-d_8) δ 7.38 (d, *J* = 7.6 Hz, 12H, *o*-C_6H_5), 7.25 (d, *J* = 7.5 Hz, 12H, *o*-C_6H_5), 7.17 – 6.82 (m, 36H, *m*+*p*-C_6H_5), 3.65 – 3.59 (m, 4H), 1.80 – 1.75 (m, 4H). $^{13}C\{^1H\}$ NMR (126 MHz, THF-d_8) δ 155.48 (*i*-C_6H_5), 129.47 (*o*-C_6H_5), 129.38 (*o*-C_6H_5), 128.27 (*m*-C_6H_5), 127.29 (*m*-C_6H_5), 125.94 (*p*-C_6H_5), 111.07 (O*C*(C_6H_5)$_3$), 68.26 (2,5-THF), 26.43 (3,4-THF). Analysis calculated for $C_{80}H_{68}O_5Ba_2$: C 69.42, H 4.95%. Found: C 68.96, H 4.92%.

3.4.7 General procedure for catalytic dehydrocoupling reactions for kinetic analysis

In the glove box, a quantity of Ph_2SiH_2 was added to a J. Youngs NMR tube containing a C_6D_6 solution of the known quantities of Ae catalyst and internal standard (hexamethylbenzene). A quantity of C_6D_6 was added to satisfy the final total volume of 600 µl. The open NMR tube was transferred to a sealed Schlenk flask, removed from the glove box and, using standard

Schlenk techniques, *tert*-butanol was added *via* syringe so that it remained on the upper walls of the NMR tube. The NMR tube was sealed against a flow of argon, removed from the Schlenk flask without shaking and taken immediately to the NMR spectrometer. After locking and shimming, the sample was removed from the spectrometer and subjected to vigorous shaking before re-inserting and commencing analysis. The reaction was followed by recording ^{1}H NMR spectra at regular intervals. *In situ* concentrations were determined by integration of the NMR spectrum and normalised with respect to the internal standard, hence they are reported unit-less.

Turnover frequencies (TOF) were calculated using the following equation:

$TOF\ (min^{-1}) = \frac{([silane]_0 - [silane]_t)}{[Ae].t}$, and were plotted against conversion of silane, where conversion is defined as:

$$\mathrm{X}_{silane} = 100 \times \frac{([silane]_0 - [silane]_t)}{[silane]_0}$$

'Standard conditions' for kinetic runs: 9.7 µl Ph_2SiH_2 (0.052 mmol), 5.0 µl *t*BuOH (0.052 mmol), substrate concentration 0.087 mol dm^{-3} in C_6D_6 (total volume 600µl), and a 3.3 mol% catalyst loading.

For pre-catalyst **IIc** a kinetic run was also carried out following the above procedure, but in d_8-THF solvent.

Overall reaction order was determined by plotting the appropriate zero-, first-, second-, and half-order plots against time, based on [silane] at different [Ba]. [silane] was determined by integration of the Si*H* resonance and normalisation with respect to the integral of the resonance corresponding to the hexamethylbenzene internal standard. Order in [silane] and [alcohol] were determined by conducting kinetic runs under pseudo first-order conditions with a ten-fold excess of the other substrate. Order in [Ba] was determined by plotting the observed rate constant, k_{obs}, obtained from the appropriate overall second-order plot against [Ba] or [Ba]^2, at concentrations from 1-10 mol%. The inhibitory effect of *tert*-butanol was investigated by conducting a series of experiments at different initial alcohol concentrations, using a ten-fold excess of diphenylsilane and 3 mol% [Ba] (both with respect to standard conditions).

3.4.8 Synthesis of polymers P15-P18

In the glove box, an equimolar THF solution of **1** and 1,4-benzenedimethanol (0.48 M) was transferred to a Schlenk flask. A quantity of **IId** was added as a 0.03 M solution in THF, and the reaction mixture was stirred at the desired temperature for two hours and precipitated into

non-dried hexane. The colourless supernatant was decanted and the resulting material was vacuum dried to yield polymers **P15**-**P18** as pale orange solids.

P15: Polymerisation was carried out at 25°C, 0.72 mmol scale (1.5 ml stock 0.48 M solution), with 2.5 mol% **IId** (0.5 ml stock 0.03 M THF solution). After 5 minutes, the reaction mixture became viscous and immobile and an additional 3.5 ml THF was added to aid stirring. Yield: 79 mg, 26%. ^{1}H NMR (500 MHz, C_6D_6) δ ^{1}H NMR (500 MHz, C_6D_6) δ 7.98 (br, 2H, *o*-Si(C_6H_5)), 7.41 (s, 4H, C_6H_4), 7.26 (br, 3H, *m*+*p*-Si(C_6H_5)), 4.99 (d, *J* = 12.8 Hz, 2H), 4.94 (d, *J* = 12.7 Hz, 2H), 4.91, 4.88, 4.82, 4.29 (br, 2H, 2,5-C_5H_4Si), 4.21 (br, 2H, 3,4-C_5H_4Si), 4.05 (s, 5H, C_5H_5). ^{13}C{^{1}H} NMR (126 MHz, C_6D_6) δ 140.16 (1,4-C_6H_4), 135.11 (*o*-Si(C_6H_5), 134.46 (*i*-Si(C_6H_5), 130.55 (*m*-Si(C_6H_5), 128.35 (*p*-Si(C_6H_5), 126.98 (2,3-C_6H_4), 74.40 (2,5-C_5H_4Si), 71.77 (2,5-C_5H_4Si), 69.26 (C_5H_5), 65.35 (OCH_2), 64.62 (1-C_5H_4Si). ^{29}Si NMR (79 MHz) δ -24.34 (from ^{29}Si-^{1}H HMQC).

P16: Polymerisation was carried out at 25°C, 0.36 mmol scale (0.75 ml stock 0.48 M solution), with 1.25 mol% **IId** (0.125 ml stock 0.03 M solution). Yield: 22 mg, 14%. ^{1}H NMR (500 MHz, C_6D_6) δ 7.98 (br, 2H, *o*-Si(C_6H_5)), 7.41 (s, 4H, C_6H_4), 7.25 (br, 3H, *m*+*p*-Si(C_6H_5)), 4.99 (d, *J* = 12.8 Hz, 2H), 4.94 (d, *J* = 12.3 Hz, 2H). 4.88, 4.82, 4.28 (br, 2H, 2,5-C_5H_4Si), 4.21 (br, 2H, 3,4-C_5H_4Si), 4.05 (s, 5H, C_5H_5). ^{13}C{^{1}H} NMR (126 MHz, C_6D_6) δ 140.16 (1,4-C_6H_4), 135.11 (*o*-Si(C_6H_5), 134.46 (*i*-Si(C_6H_5), 130.55 (*m*-Si(C_6H_5), 128.35 (*p*-Si(C_6H_5), 126.98 (2,3-C_6H_4), 74.40 (2,5-C_5H_4Si), 71.77 (2,5-C_5H_4Si), 69.26 (C_5H_5), 65.36 (OCH_2), 64.62 (1-C_5H_4Si). ^{29}Si NMR (79 MHz) δ -24.35 (from ^{29}Si-^{1}H HMQC).

P17: Polymerisation was carried out at 25°C, 0.72 mmol scale (1.5 ml stock 0.48 M solution), with 5.0 mol% **IId** (1.0 ml stock 0.03 M THF solution). After 5 minutes, the reaction mixture became viscous and immobile and an additional 3.0 ml THF was added to aid stirring. Yield: 130 mg, 42%. ^{1}H NMR (500 MHz, C_6D_6) δ 7.97 (br, 2H, *o*-Si(C_6H_5)), 7.41 (s, 4H, C_6H_4), 7.25 (br, 3H, *m*+*p*-Si(C_6H_5)), 4.99 (d, *J* = 12.8 Hz, 2H), 4.94 (d, *J* = 12.3 Hz, 2H), 4.91, 4.88, 4.82, 4.32, 4.29 (br, 2H, 2,5-C_5H_4Si), 4.21 (br, 2H, 3,4-C_5H_4Si), 4.05 (s, 5H, C_5H_5). ^{13}C{^{1}H} NMR (126 MHz, C_6D_6) δ 140.16 (1,4-C_6H_4), 135.11 (*o*-Si(C_6H_5), 134.46 (*i*-Si(C_6H_5), 130.55 (*m*-Si(C_6H_5), 128.35 (*p*-Si(C_6H_5), 126.98 (2,3-C_6H_4), 74.40 (2,5-C_5H_4Si), 71.77 (2,5-C_5H_4Si), 69.26 (C_5H_5), 65.35 (OCH_2), 64.62 (1-C_5H_4Si). ^{29}Si NMR (79 MHz) δ -24.05 (from ^{29}Si-^{1}H HMQC).

P18: Polymerisation was carried out at 60°C, 0.72 mmol scale (1.5 ml stock 0.48 M solution), with 2.5 mol% **IId** (0.5 ml stock 0.03 M solution). Yield: 127 mg, 41%. ^{1}H NMR (500 MHz, C_6D_6) δ 7.97 (br, 2H, *o*-Si(C_6H_5)), 7.41 (s, 4H, C_6H_4), 7.25 (br, 3H, *m*+*p*-Si(C_6H_5)), 4.99 (d, *J* = 12.9 Hz, 2H, OCH_2), 4.94 (d, *J* = 12.7 Hz, 2H, OCH_2), 4.88, 4.82, 4.34 – 4.26 (br, 2H, 2,5-C_5H_4Si), 4.21 (br, 2H, 3,4-C_5H_4Si), 4.05 (s, 5H, C_5H_5). ^{13}C{^{1}H} NMR (126 MHz, C_6D_6) δ 140.16 (1,4-C_6H_4), 135.11 (*o*-Si(C_6H_5), 134.46 (*i*-Si(C_6H_5), 130.55 (*m*-Si(C_6H_5), 128.30 (*p*-Si(C_6H_5),

126.98 (2,3-*C*$_6$H$_4$), 74.40 (2,5-*C*$_5$H$_4$Si), 71.77 (2,5-*C*$_5$H$_4$Si), 69.26 (*C*$_5$H$_5$), 65.35 (O*C*H$_2$), 64.62 (1-*C*$_5$H$_4$Si). ^{29}Si NMR (99 MHz, C$_6$D$_6$) δ -24.28.

3.4.9 Synthesis of oligomer P19

In the glove box, a Schlenk flask was charged with 150 mg compound **3** (0.38 mmol), and 62.6 mg 1,4-(CH(CH$_3$)OH)$_2$(C$_6$H$_4$) (α,α'-dimethyl-1,4-benzenediethanol) (0.38 mmol), dissolved in 0.4 ml THF. The flask was transferred to the Schlenk line, heated to 60°C, and a 0.2 ml THF solution of **IId** (11 mg, 0.019 mmol, 5 mol%) was added *via* cannula with stirring. Immediate and vigorous bubbling occurred and, after 10 minutes, the reaction mixture became too viscous for stirring to take place. After heating overnight at 60°C, the immobile orange mixture was dissolved in approx. 3 ml non-dried THF, then precipitated into non-dried hexane at -78°C. The colourless supernatant was decanted from the pale-orange precipitate, which was dried under vacuum to yield **P19** as a soft, glassy orange solid. Yield 65 mg, 31%. ^{1}H NMR (400 MHz, C$_6$D$_6$) δ 7.86 – 7.78 (m, 2H, *o*-(C$_6$*H*$_5$)Si termini), 7.78 – 7.66 (m, 8H, *o*-(C$_6$*H*$_5$)Si), 7.59 (m, 1H), 7.38 – 7.26 (m, 10H, C$_6$*H*$_4$), 7.26 – 7.18 (m, 19H, *m*+*p*-(C$_6$*H*$_5$)Si), 5.73 (d, J = 4.9 Hz, 1H, Si*H*$_2$ termini), 5.70 – 5.55 (m, 4H, *H3*), 5.09 – 4.92 (m, 5H, *H4*), 4.54 (t, J = 6.4 Hz, 2H, *H1*), 4.47 – 3.95 (m, 24H, (C$_5$*H*$_4$)Si), 1.53 – 1.36 (m, 14H, *H5*), 1.29 (m, 6H, *H2*), 1.19 – 1.07 (m, 2H), 0.45 (s, 2H, O*H*). ^{13}C{^{1}H} NMR (126 MHz, C$_6$D$_6$) δ 145.71 (*C3*), 144.84 (*C7*), 135.86-125.21 (*i*-(*C*$_6$H$_5$)Si), 134.77 (*o*-(*C*$_6$H$_5$)Si), 134.60, 134.52, 130.47 (*m*-(*C*$_6$H$_4$)Si), 125.91 (*C4*), 125.69 (*p*-(*C*$_6$H$_4$)Si), 125.63 (*p*-(*C*$_6$H$_5$)Si), 75.73-74.05 (3,4-(*C*$_5$H$_4$)Si), 73.00-72.50 (*C3* + 2,5-(*C*$_5$H$_4$)Si), 70.06 (*C1*), 65.85 (1-(*C*$_5$H$_4$)Si), 26.80 (*C4*), 26.69 (*C4*), 25.68 (*C2*). Unfortunately, ^{29}Si chemical shifts could not be determined by 1D ^{29}Si{^{1}H} or ^{29}Si-^{1}H HMQC NMR spectroscopy, even at higher sample concentrations and a large number of scans due to very poor signal/noise ratio.

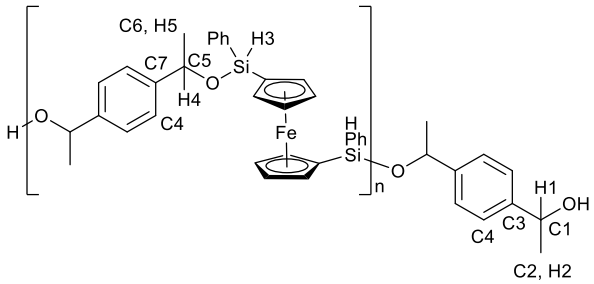

Figure 3.22: Numbering scheme used for the assignment of **P19**.

3.4.10 Synthesis of oligomer P20

A THF solution (2.00 ml, 0.88 mol dm^{-3}) containing 700 mg **3** (1.76 mmol) and 293 mg 1,4-(CH(CH$_3$)OH)$_2$(C$_6$H$_4$) (1.76 mmol) was prepared in the glove box and 340 µl (0.30 mmol) was added to a Schlenk flask containing an additional 390 µl THF. A THF solution (500 µl, 0.30 mol dm^{-3}) of **IId** (90 mg, 0.149 mmol) was prepared and 50 µl (0.015 mmol, 5 mol%) was

added to the Schlenk flask. The bubbling reaction mixture was stirred, removed from the glove box, and heated to 60°C (with stirring) for 16 hours. Approximately 2 ml non-dried THF was added to the orange solution, which was then precipitated into hexane at -78°C. **P20** was isolated as a sticky orange solid following filtration and drying under vacuum. Yield: 49 mg, 30%. The broad, complex NMR spectra precluded detailed and unambiguous peak assignment. ^{1}H NMR (500 MHz, C_6D_6) δ 8.1-7.65 (br, m, 53H, *o*-(C_6H_5)Si), 7.60 (br, 12H), 7.40-7.10 (br, m, 145H, *m*+*p*-(C_6H_5)Si, C_6H_4), 5.86 (s, 1H, Si*H*), 5.80 (s, 1H, Si*H*), 5.73 (d, *J* = 6.1 Hz, 1H, SiH_2 termini), 5.70-5.48 (br, 7H, Si*H*), 5.20 (br, 18H, (C_6H_4)C*H*CH_3), 5.10-4.92 (m, br, 18H, (C_6H_4)C*H*CH_3), 4.65-4.48 (m, br, 10H, (C_6H_4)C*H*CH_3OH), 4.45-3.80 (m, br, 121H, Si(C_5H_4)), 2.25, 1.58-1.33 (br, m, 94H, (C_6H_4)CHC*H*$_3$), 1.33-1.24 (m, 19H, (C_6H_4)CHC*H*$_3$OH), 0.44 (s, br, 19H, O*H*), 0.23-0.07 (m, br, 21H). ^{13}C{^{1}H} NMR (126 MHz, C_6D_6) δ 145.44 (1,4-(*C*$_6$H$_4$)CHCH$_3$), 135.58 (2,3-(*C*$_6$H$_4$)CHCH$_3$), 135.21 (Si(*C*$_6$H$_5$)), 134.77 (2,3-(*C*$_6$H$_4$)CHCH$_3$), 130.48 (Si(*C*$_6$H$_5$)), 129.90 (Si(*C*$_6$H$_5$)), 125.81, 75.81 (Si(*C*$_5$H$_4$)), 75.29 (Si(*C*$_5$H$_4$)), 74.87 (Si(*C*$_5$H$_4$)), 73.44 (Si(*C*$_5$H$_4$)), 72.62 (Si(*C*$_5$H$_4$)), 71.72 (*C*HCH$_3$), 70.04 (*C*HCH$_3$OH), 27.36 (CH*C*H$_3$), 26.81 (CH*C*H$_3$), 25.73 (CH*C*H$_3$OH). Unfortunately, ^{29}Si chemical shifts could not be determined by 1D ^{29}Si{^{1}H} or ^{29}Si-^{1}H HMQC NMR spectroscopy, even at higher sample concentrations and a large number of scans due to very poor signal/noise ratio.

3.4.11 X-ray crystallography

Identification code	**9**	**10a**	**10b**	**10c**
Empirical formula	$C_{30}H_{28}O_2SiFe$	$C_{80}H_{68}Ca_2O_5$	$C_{80}H_{68}O_5Sr_2$	$C_{80}H_{68}Ba_2O_5$
Formula weight	504.46	1189.50	1284.58	1384.02
Temperature/K	150.00(10)	150.0(2)	150.0(2)	150.00(10)
Crystal system	monoclinic	monoclinic	monoclinic	monoclinic
Space group	$P2_1/c$	$P2_1/n$	$P2_1/n$	$P2_1/n$
a/Å	9.66699(11)	14.1741(2)	14.2357(3)	14.4666(2)
b/Å	13.88167(14)	20.1986(2)	20.1492(5)	20.0425(2)
c/Å	18.19176(19)	21.7177(3)	21.9137(5)	22.1077(2)
α/°	90	90	90	90
β/°	93.2768(10)	91.166(1)	90	89.3850(10)
γ/°	90	90	90	90
Volume/Å^3	2437.23(4)	6216.42(14)	6285.7(2)	6409.69(12)
Z	4	4	4	4
ρ_{calc}g/cm^3	1.375	1.271	1.357	1.434
μ/mm^{-1}	5.628	0.238	1.752	9.907
F(000)	1056.0	2512.0	2656.0	2800.0
Crystal size/mm^3	0.288 × 0.191 × 0.091	0.399 × 0.259 × 0.239	0.153 x 0.205 x 0.233	0.213 × 0.197 × 0.101
Radiation	CuKα (λ = 1.54184)	MoKα (λ = 0.71073)	MoKα (λ = 0.71073)	CuKα (λ = 1.54184)
2Θ range for data collection/°	8.016 to 146.246	6.7 to 60.228	6.588 to 60.148	7.268 to 147.21
Index ranges	-11 ≤ h ≤ 11, -13 ≤ k ≤ 17, -22 ≤ l ≤ 22	-19 ≤ h ≤ 16, -28 ≤ k ≤ 28, -29 ≤ l ≤ 29	-19 ≤ h ≤ 18, -28 ≤ k ≤ 28, -30 ≤ l ≤ 30	-17 ≤ h ≤ 17, -24 ≤ k ≤ 20, -27 ≤ l ≤ 27
Reflections collected	29803	56141	70840	86586
Independent reflections	4866 [R_{int} = 0.0450, R_{sigma} = 0.0271]	16569 [R_{int} = 0.0371, R_{sigma} = 0.0464]	16838 [R_{int} = 0.0574, R_{sigma} = 0.0651]	12847 [R_{int} = 0.0555, R_{sigma} = 0.0295]
Data/restraints/parameters	4866/0/307	16569/8/805	16838/2/792	12847/2/793
Goodness-of-fit on F^2	1.014	1.014	1.011	1.016
Final R indexes [I>=2σ (I)]	R_1 = 0.0298, wR_2 = 0.0749	R_1 = 0.0445, wR_2 = 0.0925	R_1 = 0.0422, wR_2 = 0.0718	R_1 = 0.0328, wR_2 = 0.0774
Final R indexes [all data]	R_1 = 0.0326, wR_2 = 0.0766	R_1 = 0.0745, wR_2 = 0.1065	R_1 = 0.0781, wR_2 = 0.0827	R_1 = 0.0384, wR_2 = 0.0812
Largest diff. peak/hole / e Å^{-3}	0.36/-0.35	0.53/-0.41	0.65/-0.54	0.73/-1.52

In compound **10a**, C77 (THF ligand) was modelled to take account of 75:25 disorder, and the hydrogen atoms attached to C22, C26 and C71 were located and refined without restraints. For compound **10b**, H26 and H51 were both located, and each refined subject to being a distance of 0.93 Å from the relevant parent atom. For compound **10c**, C79 was modelled to take account of 65:35 disorder. C-C distance restraints were added for bonds pertaining to the arising, partial-occupancy carbon atoms.

3.5 References

1. S. Vijjamarri, V. K. Chidara and G. D. Du, *ACS Omega*, 2017, **2**, 582-591.
2. S. Vijjamarri, S. Streed, E. M. Serum, M. P. Sibi and G. D. Du, *ACS Sustainable Chemistry & Engineering*, 2018, **6**, 2491-2497.
3. Y. F. Zhang, Z. W. Zhu, Z. G. Bai, W. Jiang, F. Q. Liu and J. Tang, *RSC Advances*, 2017, **7**, 16616-16622.
4. C. Cheng, A. Watts, M. A. Hillmyer and J. F. Hartwig, *Angewandte Chemie-International Edition*, 2016, **55**, 11872-11876.
5. A. M. Issam and M. Haris, *Journal of Inorganic and Organometallic Polymers and Materials*, 2009, **19**, 454-458.
6. S. Minegishi, M. Ito, A. Kameyama and T. Nishikubo, *Journal of Polymer Science A-Polymer Chemistry*, 2000, **38**, 2254-2259.
7. T. Nishikubo, A. Kameyama, Y. Kimura and T. Nakamura, *Macromolecules*, 1996, **29**, 5529-5534.
8. A. A. Toutov, K. N. Betz, M. C. Haibach, A. M. Romine and R. H. Grubbs, *Organic Letters*, 2016, **18**, 5776-5779.
9. M. Mirza-Aghayan, R. Boukherroub and M. Bolourtchian, *Journal of Organometallic Chemistry*, 2005, **690**, 2372-2375.
10. A. Weickgenannt and M. Oestreich, *Chemistry-an Asian Journal*, 2009, **4**, 406-410.
11. A. Grajewska and M. Oestreich, *Synlett*, 2010, 2482-2484.
12. S. Rendler, G. Auer and M. Oestreich, *Angewandte Chemie-International Edition*, 2005, **44**, 7620-7624.
13. X. Dong, A. Weickgenannt and M. Oestreich, *Nature Communications*, 2017, **8**, 15547.
14. C. Eaborn, *Journal of Organometallic Chemistry*, 1975, **100**, 43-57.
15. Y. Li and Y. Kawakami, *Macromolecules*, 1999, **32**, 6871-6873.
16. S. Pramanik, A. Fernandes, V. Liautard, M. Pucheault, F. Robert and Y. Landais, *Chemistry-a European Journal*, 2019, **25**, 728-732.
17. J. Schobel, M. Burgard, C. Hils, R. Dersch, M. Dulle, K. Volk, M. Karg, A. Greiner and H. Schmalz, *Angewandte Chemie-International Edition*, 2017, **56**, 405-408.
18. H. B. Li, H. F. Guo, Z. W. Li, C. Wu, J. Li, C. L. Zhao, S. X. Guo, Y. Ding, W. He and Y. D. Li, *Chemical Science*, 2018, **9**, 4808-4813.
19. U. Schubert and C. Lorenz, *Inorganic Chemistry*, 1997, **36**, 1258-1259.
20. D. R. Schmidt, S. J. O'Malley and J. L. Leighton, *Journal of the American Chemical Society*, 2003, **125**, 1190-1191.
21. E. Peterson, A. Y. Khalimon, R. Sirnionescu, L. G. Kuzmina, J. A. K. Howard and G. I. Nikonov, *Journal of the American Chemical Society*, 2009, **131**, 908-909.
22. R. A. Corbin, E. A. Ison and M. M. Abu-Omar, *Dalton Transactions*, 2009, 2850-2855.
23. T. C. Bedard and J. Y. Corey, *Journal of Organometallic Chemistry*, 1992, **428**, 315-333.
24. S. X. Xin and J. F. Harrod, *Journal of Organometallic Chemistry*, 1995, **499**, 181-191.
25. B. T. Gregg and A. R. Cutler, *Organometallics*, 1994, **13**, 1039-1043.
26. D. Mukherjee, R. R. Thompson, A. Ellern and A. D. Sadow, *ACS Catalysis*, 2011, **1**, 698-702.
27. Y. Satoh, M. Igarashi, K. Sato and S. Shimada, *ACS Catalysis*, 2017, **7**, 1836-1840.
28. I. Yamaguchi, H. Ishii, T. Sakano, K. Osakada and T. Yamamoto, *Applied Organometallic Chemistry*, 2001, **15**, 197-203.
29. X. L. Luo and R. H. Crabtree, *Journal of the American Chemical Society*, 1989, **111**, 2527-2535.
30. R. J. P. Corriu and J. J. E. Moreau, *Journal of Organometallic Chemistry*, 1976, **120**, 337-346.
31. J. Ohshita, R. Taketsugu, Y. Nakahara and A. Kunai, *Journal of Organometallic Chemistry*, 2004, **689**, 3258-3264.

32. D. E. Barber, Z. Lu, T. Richardson and R. H. Crabtree, *Inorganic Chemistry*, 1992, **31**, 4709-4711.
33. S. Chang, E. Scharrer and M. Brookhart, *Journal of Molecular Catalysis A*, 1998, **130**, 107-119.
34. M. K. Chung, G. Ferguson, V. Robertson and M. Schlaf, *Canadian Journal of Chemistry-Revue Canadienne De Chimie*, 2001, **79**, 949-957.
35. X. G. Fang, J. Huhmann-Vincent, B. L. Scott and G. J. Kubas, *Journal of Organometallic Chemistry*, 2000, **609**, 95-103.
36. K. Kucinski and G. Hreczycho, *ChemCatChem*, 2017, **9**, 1868-1885.
37. R. L. Miller, S. V. Maifeld and D. Lee, *Organic Letters*, 2004, **6**, 2773-2776.
38. Y. N. Li and Y. Kawakami, *Macromolecules*, 1999, **32**, 8768-8773.
39. Y. N. Li and Y. Kawakami, *Macromolecules*, 1999, **32**, 3540-3542.
40. S. V. Maifeld, R. L. Miller and D. Lee, *Tetrahedron Letters*, 2002, **43**, 6363-6366.
41. H. Ito, A. Watanabe and M. Sawamura, *Organic Letters*, 2005, **7**, 1869-1871.
42. H. Ito, K. Takagi, T. Miyahara and M. Sawamura, *Organic Letters*, 2005, **7**, 3001-3004.
43. W. Caseri and P. S. Pregosin, *Organometallics*, 1988, **7**, 1373-1380.
44. J. M. Blackwell, K. L. Foster, V. H. Beck and W. E. Piers, *Journal of Organic Chemistry*, 1999, **64**, 4887-4892.
45. Y. Tanabe, H. Okumura, A. Maeda and M. Murakami, *Tetrahedron Letters*, 1994, **35**, 8413-8414.
46. F. Le Bideau, T. Coradin, J. Henique and E. Samuel, *Chemical Communications*, 2001, 1408-1409.
47. J. Cella and S. Rubinsztajn, *Macromolecules*, 2008, **41**, 6965-6971.
48. D. Q. Zhou and Y. Kawakami, *Macromolecules*, 2005, **38**, 6902-6908.
49. R. L. Melen, *Chemical Society Reviews*, 2016, **45**, 775-788.
50. M. Perez, C. B. Caputo, R. Dobrovetsky and D. W. Stephan, *Proceedings of the National Academy of Sciences of the United States of America*, 2014, **111**, 10917-10921.
51. W. Sattler, S. Ruccolo, M. R. Chaijan, T. N. Allah and G. Parkin, *Organometallics*, 2015, **34**, 4717-4731.
52. C. Y. Li, X. F. Hua, Z. H. Mou, X. L. Liu and D. M. Cui, *Macromolecular Rapid Communications*, 2017, **38**, 1700590.
53. M. C. Lipke, A. L. Liberman-Martin and T. D. Tilley, *Angewandte Chemie International Edition*, 2016, **56**, 2260-2294.
54. X.-Y. Zhai, S.-B. Hu, L. Shi and Y.-G. Zhou, *Organometallics*, 2018, **37**, 2342-2347.
55. P. T. K. Lee and L. Rosenberg, *Dalton Transactions*, 2017, **46**, 8818-8826.
56. D. J. Liptrot, M. S. Hill, M. F. Mahon and A. S. S. Wilson, *Angewandte Chemie - International Edition*, 2015, **54**, 13362-13365.
57. E. Le Coz, V. Dorcet, T. Roisnel, S. Tobisch, J. F. Carpentier and Y. Sarazin, *Angewandte Chemie-International Edition*, 2018, **57**, 11747-11751.
58. E. Le Coz, S. Kahlal, J.-Y. Saillard, T. Roisnel, V. Dorcet, J.-F. Carpentier and Y. Sarazin, *Chemistry - A European Journal*, 2019, *Advance Article,* doi: 10.1002/chem.201903676.
59. F. Buch and S. Harder, *Organometallics*, 2007, **26**, 5132-5135.
60. J. F. Dunne, S. R. Neal, J. Engelkemier, A. Ellern and A. D. Sadow, *Journal of the American Chemical Society*, 2011, **133**, 16782-16785.
61. M. S. Hill, D. J. Liptrot, D. J. MacDougall, M. F. Mahon and T. P. Robinson, *Chemical Science*, 2013, **4**, 4212.
62. C. Bellini, C. Orione, J. F. Carpentier and Y. Sarazin, *Angewandte Chemie - International Edition*, 2016, **55**, 3744-3748.
63. C. Bellini, T. Roisnel, J. F. Carpentier, S. Tobisch and Y. Sarazin, *Chemistry - A European Journal*, 2016, **22**, 15733-15743.
64. C. Bellini, V. Dorcet, J. F. Carpentier, S. Tobisch and Y. Sarazin, *Chemistry - A European Journal*, 2016, **22**, 4564-4583.

65. C. Bellini, J.-F. Carpentier, S. Tobisch and Y. Sarazin, *Angewandte Chemie – International Edition*, 2015, **54**, 7679-7683.
66. A. Baishya, T. Peddarao and S. Nembenna, *Dalton Transactions*, 2017, **46**, 5880-5887.
67. M. Rauch, R. C. Roberts and G. Parkin, *Inorganica Chimica Acta*, 2019, **494**, 271-279.
68. G. R. Fulmer, A. J. M. Miller, N. H. Sherden, H. E. Gottlieb, A. Nudelman, B. M. Stoltz, J. E. Bercaw and K. I. Goldberg, *Organometallics*, 2010, **29**, 2176-2179.
69. J. F. Dunne, S. R. Neal, J. Engelkemier, A. Ellern and A. D. Sadow, *Journal of the American Chemical Society*, 2011, **133**, 16782-16785.
70. C. Bellini, V. Dorcet, J. F. Carpentier, S. Tobisch and Y. Sarazin, *Chemistry - A European Journal*, 2016, **22**, 4564-4583.
71. W. D. Buchanan, M. A. Guino-O and K. Ruhlandt-Senge, *Inorganic Chemistry*, 2010, **49**, 7144-7155.
72. W. D. Buchanan and K. Ruhlandt-Senge, *Chemistry-a European Journal*, 2013, **19**, 10708-10715.
73. G. B. Deacon, C. M. Forsyth and P. C. Junk, *Journal of Organometallic Chemistry*, 2000, **607**, 112-119.
74. M. F. Zuniga, G. B. Deacon and K. Ruhlandt-Senge, *Inorganic Chemistry*, 2008, **47**, 4669-4681.
75. M. F. Zuniga, G. B. Deacon and K. Ruhlandt-Senge, *Chemistry-a European Journal*, 2007, **13**, 1921-1928.
76. W. D. Buchanan, D. G. Allis and K. Ruhlandt-Senge, *Chemical Communications*, 2010, **46**, 4449-4465.
77. J. P. Dunne, M. Tacke, C. Selinka and D. Stalke, *European Journal of Inorganic Chemistry*, 2003, 1416-1425.
78. K. F. Tesh, T. P. Hanusa, J. C. Huffman and C. J. Huffman, *Inorganic Chemistry*, 1992, **31**, 5572-5579.
79. M. Arrowsmith, M. R. Crimmin, A. G. M. Barrett, M. S. Hill, G. Kociok-Köhn and P. A. Procopiou, *Organometallics*, 2011, **30**, 1493-1506.
80. A. G. M. Barrett, M. R. Crimmin, M. S. Hill, G. Kociok-Köhn, J. R. Lachs and P. A. Procopiou, *Dalton Transactions*, 2008, 1292-1294.
81. A. G. M. Barrett, I. J. Casely, M. R. Crimmin, M. S. Hill, J. R. Lachs, M. F. Mahon and P. A. Procopiou, *Inorganic Chemistry*, 2009, **48**, 4445-4453.
82. C. Brinkmann, A. G. M. Barrett, M. S. Hill, P. A. Procopiou and S. Reidt, *Organometallics*, 2012, **31**, 7287-7297.
83. B. Borup, J. A. Samuels, W. E. Streib and K. G. Caulton, *Inorganic Chemistry*, 1994, **33**, 994-996.
84. M. Veith, S. Mathur, V. Huch and T. Decker, *European Journal of Inorganic Chemistry*, 1998, 1327-1332.
85. W. J. Evans, D. G. Giarikos, M. A. Greci and J. W. Ziller, *European Journal of Inorganic Chemistry*, 2002, 453-456.
86. M. R. Crimmin, M. Arrowsmith, A. G. M. Barrett, I. J. Casely, M. S. Hill and P. A. Procopiou, *Journal of the American Chemical Society*, 2009, **131**, 9670-9685.
87. J. Pahl, H. Elsen, A. Friedrich and S. Harder, *Chemical Communications*, 2018, **54**, 7846-7849.
88. R. West and T. J. Barton, *Journal of Chemical Education*, 1980, **57**, 165-169.
89. D. Mukherjee, R. R. Thompson, A. Ellern and A. D. Sadow, *ACS Catalysis*, 2011, **1**, 698-702.
90. C. Brinkmann, A. G. M. Barrett, M. S. Hill and P. A. Procopiou, *Journal of the American Chemical Society*, 2012, **134**, 2193-2207.
91. W. Li, H. Chung, C. Daeffler, J. A. Johnson and R. H. Grubbs, *Macromolecules*, 2012, **45**, 9595-9603.
92. A. M. Wilson, G. Zank, K. Eguchi, W. Xing, B. Yates and J. R. Dahn, *Chemistry of Materials*, 1997, **9**, 1601-1606.

93. M. Adam, C. Vakifahmetoglu, P. Colombo, M. Wilhelm and G. Grathwohl, *Journal of the American Ceramic Society*, 2014, **97**, 959-966.
94. J. K. Li, K. Lu, T. S. Lin and F. Y. Shen, *Journal of the American Ceramic Society*, 2015, **98**, 1753-1761.
95. V. Belot, R. J. P. Corriu, D. Leclercq, P. H. Mutin and A. Vioux, *Journal of Non-Crystalline Solids*, 1994, **176**, 33-44.
96. B. Z. Tang, R. Petersen, D. A. Foucher, A. Lough, N. Coombs, R. Sodhi and I. Manners, *Journal of the Chemical Society-Chemical Communications*, 1993, 523-525.
97. R. Petersen, D. A. Foucher, B. Z. Tang, A. Lough, N. P. Raju, J. E. Greedan and I. Manners, *Chemistry of Materials*, 1995, **7**, 2045-2053.
98. M. Ginzburg, M. J. MacLachlan, S. M. Yang, N. Coombs, T. W. Coyle, N. P. Raju, J. E. Greedan, R. H. Herber, G. A. Ozin and I. Manners, *Journal of the American Chemical Society*, 2002, **124**, 2625-2639.
99. M. J. MacLachlan, M. Ginzburg, N. Coombs, N. P. Raju, J. E. Greedan, G. A. Ozin and I. Manners, *Journal of the American Chemical Society*, 2000, **122**, 3878-3891.

4 Activation of Organo- and Hydrido Stannanes and Distannanes by Calcium Hydride and Alkyl Complexes

4.1 Introduction

Although formally isoelectronic to polyolefins, the physical and chemical properties of polystannanes are vastly different. Notably, the low energy σ-σ* transition results in a pale-orange colour, σ-conjugation and semi-conducting properties. This character makes them promising candidates as one-dimensional “molecular wires” in future nanoscale electronic applications.[1-6] Reductive Wurtz type coupling and synthetic electrochemistry have been used to prepare linear and branched polystannanes[7-10] and well-defined oligostannanes have provided valuable model compounds through stepwise routes.[1, 5, 11] Although polystannanes can be similarly prepared *via* stoichiometric polycondensation,[6, 12-14] perhaps the most reliable, versatile and widely used route to polystannanes is transition metal-catalysed dihydrostannane dehydropolymerisation (Scheme 4.1).[15-20]

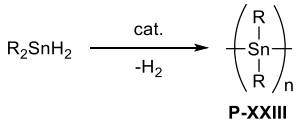

P-XXIII

Scheme 4.1: Catalytic dehydropolymerisation of dihydrostannanes.

First reported by Imori and Tilley in 1993,[15] the group four-catalysed dehydropolymerisation of tin dihydrides is of particular relevance to Ae-catalysis since, by analogy to silane dehydropolymerisation, the reaction was initially proposed to proceed *via* redox-neutral σ-bond metathesis at the d^0 metal centre.[16, 21-23] Subsequent mechanistic investigations favoured a pathway involving α-hydride elimination and the generation of a stannylene, capable of propagating chain-growth by insertion into M-Sn or Sn-H bonds (Scheme 1.17, Scheme 4.2).[24-26] Since both mechanisms involve redox-neutral metal centres, we surmised that tin dihydrides may be activated at an Ae^{2+} centre *via* similar mechanisms, leading to transition metal-free catalytic dehydropolymerisation.

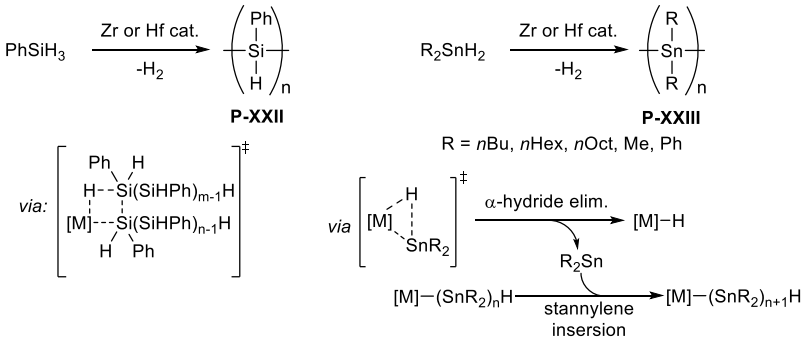

Scheme 4.2: Group 4 catalysed dehydropolymerisation of phenylsilane *via* proposed σ-bond metathesis pathway[22] and of diorganostannanes *via* proposed α-hydride elimination and stannylene insertion.[24-26]

Literature examples of alkaline-earth mediated tin chemistry are predominantly focussed on Mg-promoted Wurtz-type coupling, forming Sn-Sn and Sn-Si bonded compounds *via* the implied formation of magnesium stannides.[27-30] Stannyl magnesium halides,[31, 32] magnesium stannides,[27] and calcium stannides[33] have been reported to result from Grignard stannolysis or oxidative addition of a distannane to the parent Ae-metal. Examples of well characterised Ae-stannides, however, are limited to Westerhausen's calcium stannide, **XXXVI**[34] and the charge-separated species **XXXVII**, **XXXVIIIa** and **XXXVIIIb** reported by Uhlig and co-workers (Scheme 4.3).[35] To date, therefore, compound **XXXVI** is the only crystallographically characterised example of a molecular Ca-Sn bond.

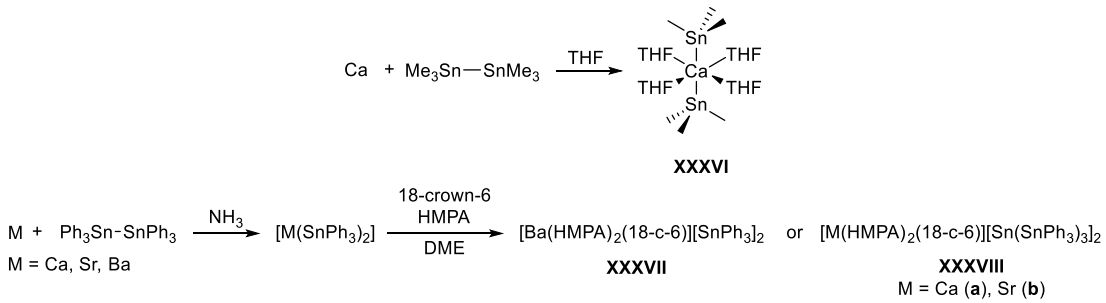

Scheme 4.3: Stannyl derivatives of the heavier alkaline earths.[34, 35]

The reactivity of calcium-hydride and -alkyl complexes towards tin-containing substrates is, to the best of our knowledge, unknown. This is primarily due to the dearth of conveniently accessible calcium hydride[36-48] and -alkyl[49-61] complexes until relatively recently. Ligand redistribution at calcium and tin also present significant challenges.[14, 35, 43, 62-64] The Hill group recently reported a highly reactive and coordinatively unsaturated β-diketiminato (BDI) calcium hydride, **VId**.[44] Amongst other reactions,[47, 65] this compound enabled previously

unprecedented access to BDI-calcium *n*-alkyl complexes, such as [(BDI)CaHex]$_2$, **Vb**, through insertion of an unactivated terminal alkene into the Ca-H bond.[44, 46, 65] The extremely nucleophilic nature of the resulting alkyl complexes was exemplified by heterolysis of dihydrogen[65] and alkylation of benzene.[44] Motivated by the prospect of calcium-catalysed dihydrostannane polymerisation and an interest in isolating calcium derivatives of the heavier tetrels, this chapter reports our preliminary investigations into the reactivity of compounds **VId** and **Vb** towards a variety of organotin compounds.

4.2 Results and discussion

4.2.1 Reaction of compound VId with Ph_3SnH

Addition of Ph_3SnH (2-3 eq.) to a C_6D_6 solution of **VId** resulted in immediate bubbling and the gradual formation of a pale orange colouration (Scheme 4.4). Analysis of the reaction mixture by $^{119}Sn\{^1H\}$ NMR spectroscopy after 60 minutes revealed quantitative conversion of Ph_3SnH and appearance of a new resonance at δ -138.9 ppm. A second, less intense resonance at δ -126.0 ppm was identified as Ph_4Sn.[66] The formation of a new BDI-containing compound, **11**, was made apparent by a new resonance at δ 4.75 ppm, corresponding to the γ-C*H* of the BDI ligand, and a second singlet of half the relative intensity at δ 3.84 ppm. The latter signal displayed satellite peaks separated by 94 Hz, within the typical range for $^2J(^{117/119}Sn\text{-}^1H)$ coupling constants (Figure 4.1).[66] The NMR spectra remained unchanged after standing overnight and the crude product was recrystallised from a hexane/toluene solution at -30°C, yielding colourless blocks of compound **11** suitable for single-crystal X-ray diffraction analysis.

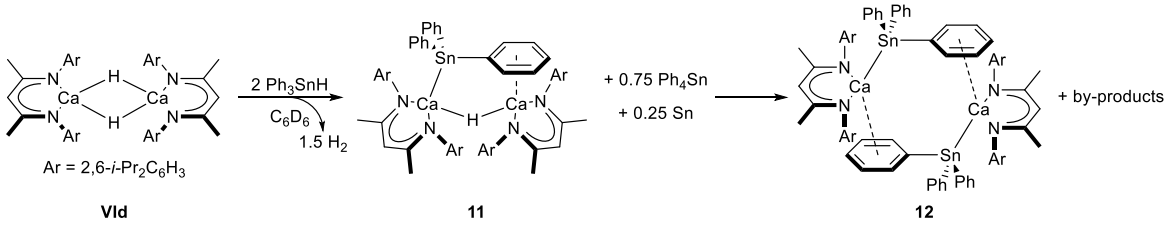

Scheme 4.4: Reaction of **VId** with Ph_3SnH to give compounds **11** and **12**.

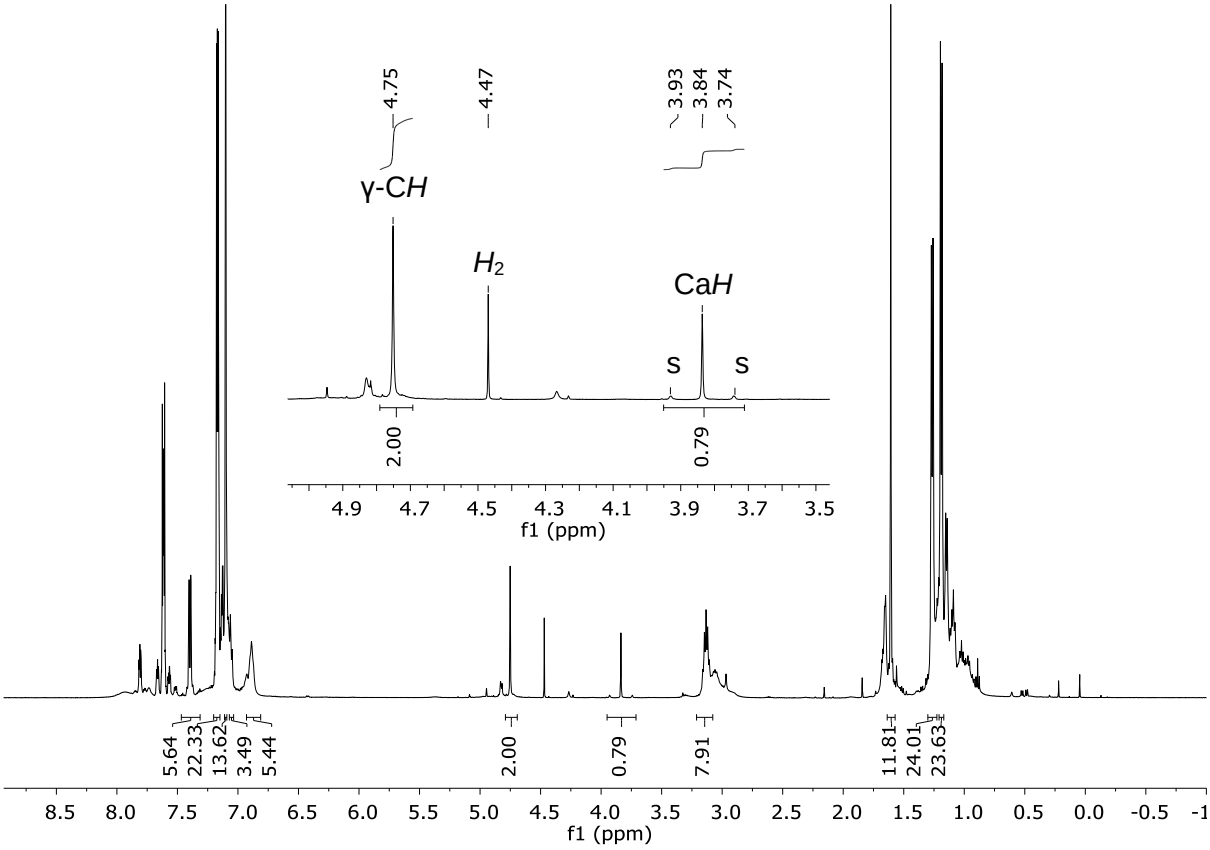

Figure 4.1: ^{1}H NMR spectrum (500 MHz, C_6D_6) of the reaction between **VId** and Ph_3SnH after 16 hours at room temperature. Inset: expansion of the methine/Ca hydride region expanded, s = $^{117/119}$Sn satellite peaks.

The X-ray crystal structure of compound **11** (Figure 4.2) consists of an unsymmetrical dinuclear calcium species, which crystallises in the monoclinic *P2₁/n* space group. Two {(BDI)Ca} units are connected by a μ^2-bridging hydride ligand and a triphenylstannide ligand, which coordinates to Ca1 *via* Sn1, and to Ca2 *via* an unusual η^6 interaction through the (C30-C35) phenyl substituent. The importance of secondary interactions in the stabilisation of alkaline-earth complexes is well established, yet Ca-π interactions are still a relatively rare phenominum.[67-73] Although unsupported η^6 calcium-arene interactions were recently reported for otherwise 'naked' [(BDI)Ca]$^+$ cations by the groups of Harder[74, 75] and Hill,[76] the Ca-arene centroid distances in these compounds (*ca*. 2.9 Å) are significantly longer than for compound **11** (2.5999(9) Å). The latter value is more akin to those reported by Westerhausen[77, 78] and Niemeyer[79] (2.60-2.74 Å) for *N*-mesityl and *N*-di-*iso*propylphenyl substituents that are part of a coordinated anion. The π-interaction is strong enough to slightly elongate the Sn1-C30 bond length (2.2258(19) Å) relative to Sn1-C36 and Sn1-C42 (2.190(2), 2.174(2) Å), and distort the coordination environment of tin towards a trigonal pyramidal geometry; the bond angle defined by C30-Sn1-Ca1 is just 96.16(5)° compared to 127.45(6)° for C36-Sn1-Ca1, and 129.08(6)°

for C42-Sn1-Ca1. The sum of angles provided by the equatorial substituents about the tin centre amounts to 354.53°, with Sn1 lying only 0.3307(13) Å out of the plane defined by Ca1, C36, and C42. Despite such perturbations, the Ca-Sn bond is of a similar length (3.2137(4) Å), to that of Westerhausen's calcium stannide **XXXVI**.[34]

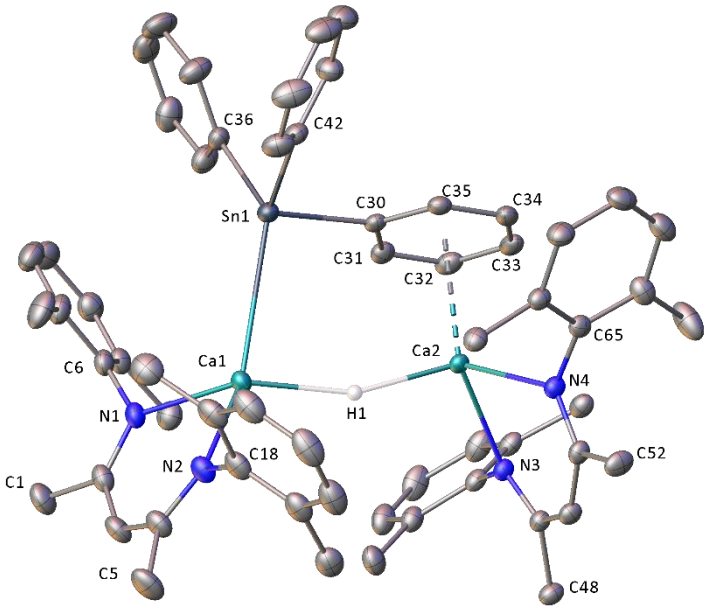

Figure 4.2: X-ray crystal structure of compound **11**. Solvent molecules, *iso*-propyl methyl groups, and hydrogen atoms are omitted for clarity except for the calcium-bound hydride. Thermal ellipsoids are shown at the 30% probability level. Selected bond lengths (Å) and angles (°). Sn1-Ca1 3.2137(4), Sn1-C30 2.2258(19), Sn1-C36 2.190(2), Sn1-C42 2.174(2), Ca2-C30 3.0649(18), Ca2-C31 2.9837(19), Ca2-C32 2.904(2), Ca2-C33 2.864(2), Ca2-C35 2.9815(19), Ca1-N1 2.3306(17), Ca1-N2 2.3275(18) Ca2-N3 2.3443(16), Ca2-N4 2.3318(15), C30-Sn1-Ca1 96.16(5), C36-Sn1-Ca1 127.45(6), C36-Sn1-C30 98.48(8), C42-Sn1-Ca1 129.08(6), C42-Sn1-C30 98.61(7), C42-Sn1-C36 98.00(8).

On standing for several days, the deposition of crystalline Ph_4Sn (confirmed by identification of the unit cell by single crystal X-ray diffraction) from the reaction mixture was accompanied by development of an opaque, dark brown colouration which was tentatively attributed to colloidal $Sn^{(0)}$, resulting from ligand redistribution at the tin centre. New minor resonances at δ 5.02 ppm and -158.0 ppm in the respective ^{1}H and $^{119}Sn\{^{1}H\}$ NMR spectra suggested the presence of new BDI- and tin-containing compounds. Removal of solvent from the reaction mixture, extraction into hexane/toluene, and slow crystallisation at -30°C eventually yielded single crystals of the hydride-free dimeric calcium stannide **12** (Scheme 4.4).

Compound **12** crystallises as colourless blocks in the triclinic space group, *P-1*, with the unit cell containing half a molecule of the centrosymmetric dimer (Figure 4.3). Each *pseudo*-four-coordinate calcium centre is σ-coordinated to the nitrogen atoms of the BDI ligand and to the triphenylstannide anion *via* a direct Ca-Sn bond. Dimer propagation occurs in a similar manner to **11**, through two η^6 Ca-phenyl π interactions. At 2.5376(19) Å, the Ca1-centroid of **12** is slightly shorter than that of **11**, whilst the Ca-Sn distance of 3.3221(6) Å is similar in both cases. Whilst tetrahedral geometry at tin is somewhat distorted, the three C-Sn-C and Ca-Sn-C angles fall within a much closer range (92.91-97.30° and 111.37-130.80° respectively) than the corresponding angles in **11**. Furthermore, the Ca-arene interaction results in the Sn1-C30-centroid angle deviating from linearity (169.9(2)° for **12** compared to 176.57(13)° for **11**). The two triphenylstannide anions are accommodated by projection of the calcium centre some 1.339(3) Å out of the mean plane defined by the BDI ligand.

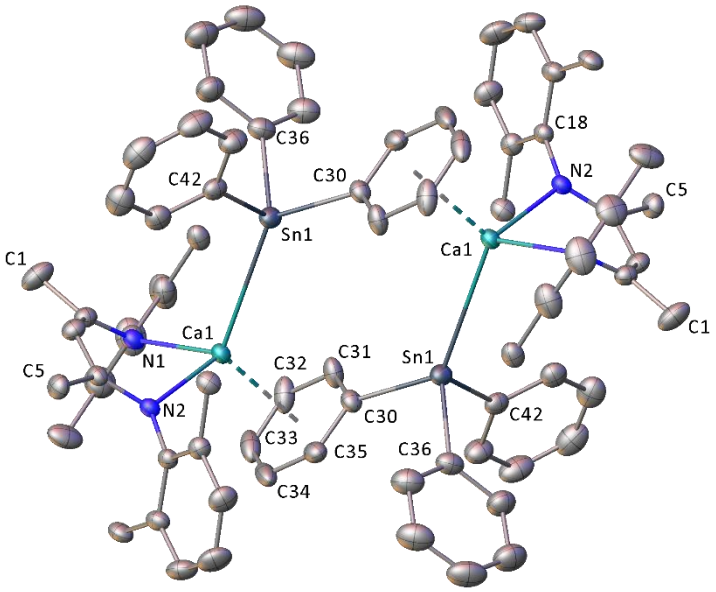

Figure 4.3 X-ray crystal structure of compound **12**. Solvent molecules, *iso*-propyl methyl groups, and hydrogen atoms are omitted for clarity. Thermal ellipsoids are shown at the 30% probability level. Selected bond lengths (Å) and angles (°): Sn1-Ca1' 3.221(5), Sn1-C30 2.222(3), Sn1-C36 2.218(3), Sn1-C42 2.196(3), Ca1'-C30 2.857(3), Ca1'-C31 2.836(3), Ca1'-C32 2.851(3), Ca1'-C33 2.901(3), Ca1'-C34 2.987(3), Ca1'-C35 2.917(3), Ca1-N1 2.319(2), Ca1-N2 2.330(2), C30-Sn1-Ca1 130.80(8), C36-Sn1-Ca 122.05(9), C36-Sn1-C30 94.66(12), C42-Sn1-Ca1 111.37(9), C42-Sn1-C30 92.91(11), C42-Sn1-C36 97.30(12). Primed atoms generated by the symmetry operation 1-x, 1-y, 1-z.

4.2.2 Calculated electronic structure of compounds 11 and 12

Figure 4.4 shows selected molecular orbitals of compounds **11** and **12**, as calculated by Density Functional Theory (DFT). The HOMOs of both compounds are of a similar energy (*ca*. -4.45 eV) and comprise primarily of the filled 5p orbitals of the anionic tin-centres towards the cationic calcium centre(s). The LUMO is predominantly located on the π*-system of the coordinated arene, and is much lower in energy for **11**, where it extends over the π*-system of the BDI ligand (LUMO -4.29eV (**11**) *cf.* -1.95eV (**12**)). The Ca-arene interactions (**11**: HOMO-27, HOMO-28; **12**: HOMO-21, HOMO-22) are also largely electrostatic in nature and originate from interactions between the Lewis acidic calcium centres and the almost degenerate pair of highest energy filled π-orbitals associated with the coordinated C_6H_5 rings.

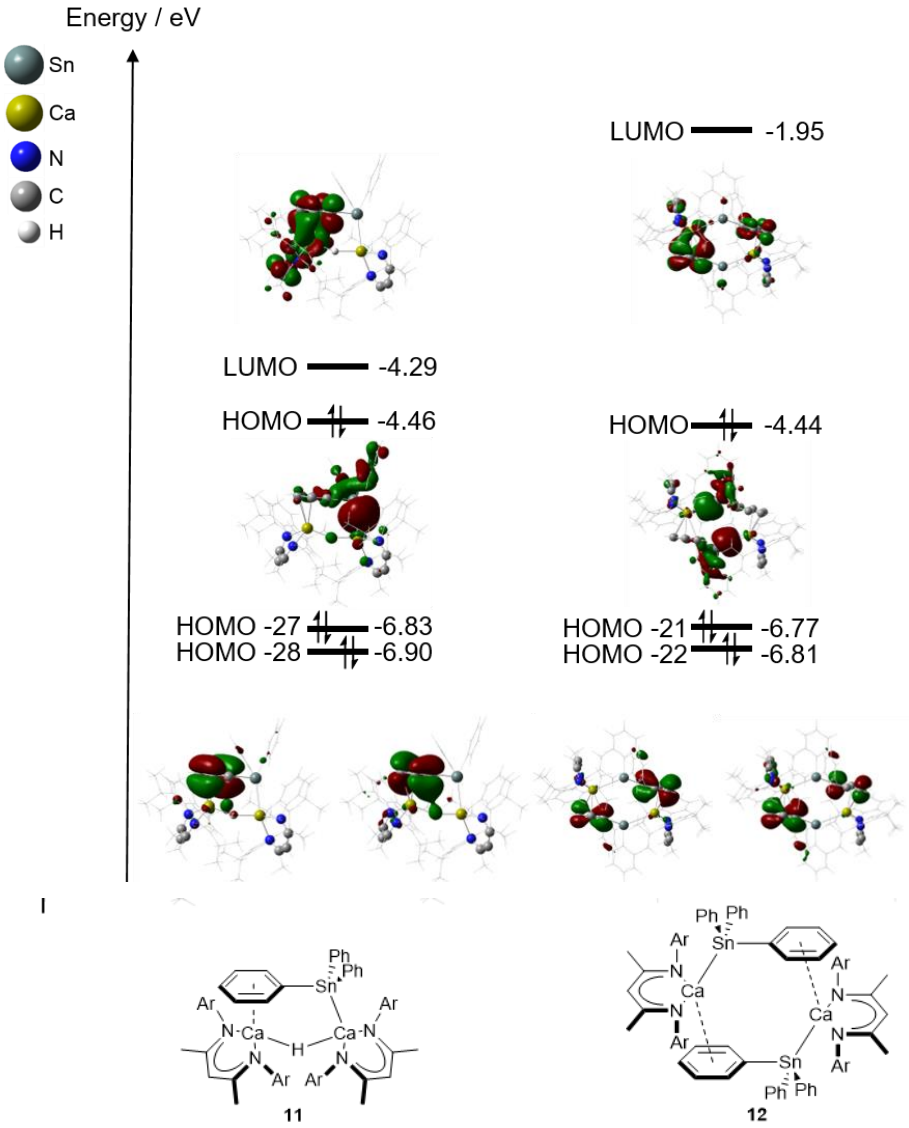

Figure 4.4: Selected molecular orbitals and energies (eV) of compounds **11** (left) and **12** (right) computed with BP86/BS1 (see Section 4.5 for further details).

4.2.3 Variable temperature NMR study of compound 11

Whilst compound **11** displays an unsymmetrical structure in the solid state (Figure 4.2), the *in situ* ^{1}H NMR spectrum in C_6D_6 (Figure 4.1) provides a single set of equivalent BDI and Sn*Ph*$_3$ environments at 298 K, indicating dynamic behaviour. Although a reaction repeated in d_8-toluene provided similar observations at 298 K, cooling the reaction mixture to 246 K in the NMR spectrometer resulted in significant broadening of the γ-C*H* resonance at δ 4.71 ppm, which eventually splits into two well resolved signals at δ 4.60 and 4.83 ppm below 211 K (Figure 4.5). The calcium hydride resonance at δ 3.83 ppm remained unchanged and retains $^{117/119}$Sn satellite peaks. Similarly, a single set of resonances are observed for the tin-bound phenyl substituents at 298 K, whereas below 220 K they are replaced by a set of multiplets which integrate with a relative intensity of 2:1:2, relative to the two γ-C*H* protons of the BDI ligand, at δ 6.05, 6.72, and 8.10 ppm, respectively. Although the triphenylstannide anion apparently undergoes free rotation at room temperature ($\Delta G^{\ddagger}$ = 48 kJ mol^{-1}),[80] persistence of the Ca-arene interaction observed in the solid state is apparent at temperatures < ca. 220 K.

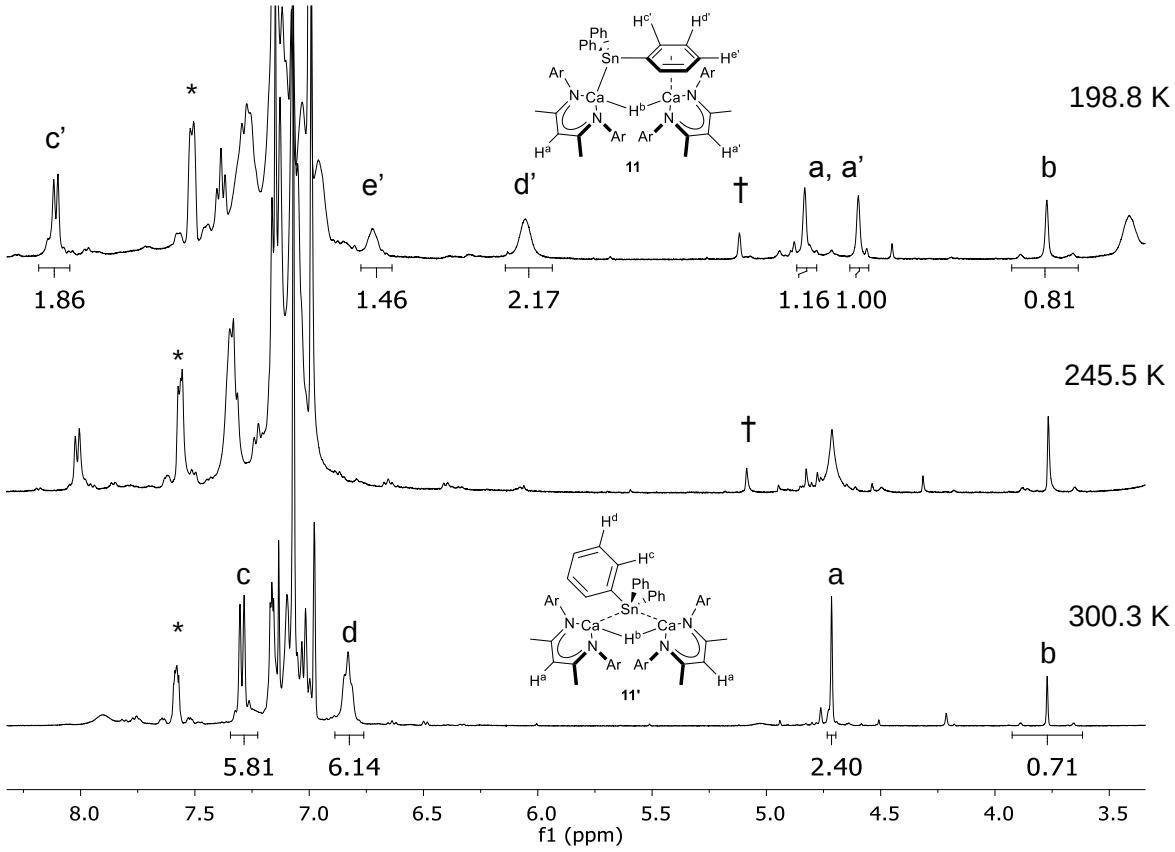

Figure 4.5: Expanded variable temperature *in situ* ^{1}H NMR spectrum (d_8-toluene, 400 MHz) of reaction between **VId** and Ph_3SnH (1:2) to give **11** after 24 hours at room temperature. * = Ph_4Sn, † = compound **12,** Ar = 2,6-di-*iso*propylphenyl.

4.2.4 Computational investigations into the reaction between VId and Ph_3SnH

The reaction between compound **VId** and Ph_3SnH was computationally investigated using DFT by Dr Nasir Rajabi and Dr Claire McMullin (University of Bath). Occurrence of a bridging hydride ligand in compound **11** suggests that a dimeric structure is retained throughout, and calculated mechanisms of other reactions involving **VId** provide similar results.[44, 46, 47, 81] The thermal monomerisation of BDI-calcium,[44] and magnesium[82] complexes to highly reactive monomeric species, however, is also an important consideration, and both scenarios were calculated in this study. Pathway **I** (Figure 4.6) proceeds *via* monomerisation of **VId** to provide intermediate **A**, a process that is endergonic by some +33.7 kcal mol^{-1}. The monomeric calcium hydride **A** reacts with Ph_3SnH to form the bimetallic bridging-hydride species **B.** Formation of new H─H and Ca─Sn bonds are formed *via* transition state $\mathbf{TS_{BC}}$ at +37.9 kcal mol^{-1}, in which the tin centre is deprotonated form a dihydrogen complex, **C.** Release of dihydrogen is exergonic, and the resulting monomeric calcium stannide species **D**, may dimerise to provide **12**, or recombine with the monomeric hydride **A** to yield compound **11**.

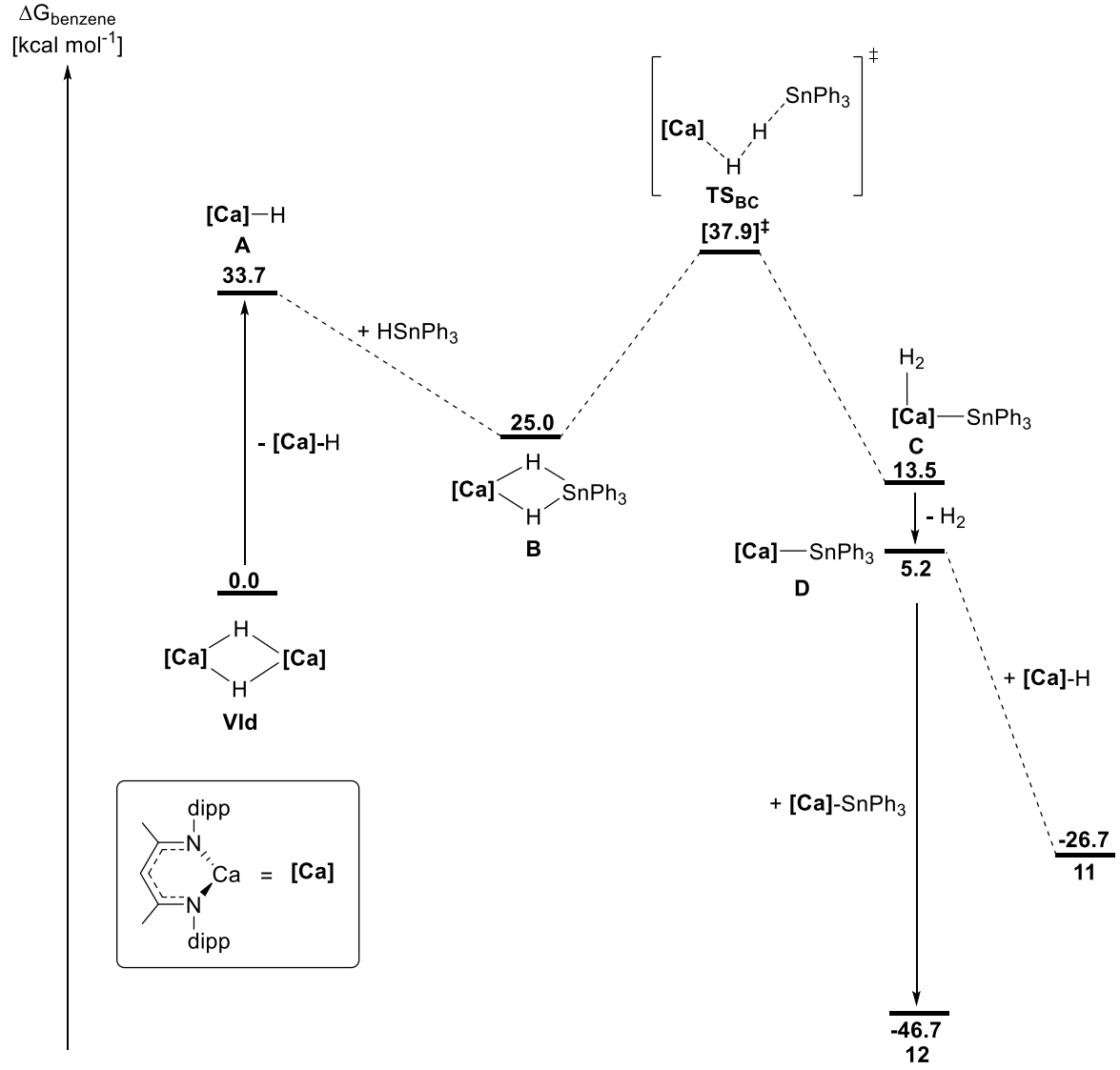

Figure 4.6: DFT calculated (BP87-D3(BJ)-benzene/BS2//BP86/BS1) energy profile (kcal mol^{-1}) for reaction pathway **I** of the formation of **11** and **12** from **VId** and Ph_3SnH.

Pathway **II** (Figure 4.7) proceeds without monomerisation. Formation of encounter complex **E** is endergonic by +7.6 kcal mol^{-1}, whilst the Sn─H^a bond and Ca─H^b bonds are broken *via* the dimeric transition state $\mathbf{TS_{EF}}$ at +8.3 kcal mol^{-1}. Intermediate **F** consists of a hydride-bridged dimeric dihydrogen complex and a $[SnPh_3]^-$ anion. Formation of the Ca^b─Sn bond proceeds *via* isomerisation to provide the unsymmetrical dimer **G** at -3.0 kcal mol^{-1}. Dihydrogen loss provides species **H** at -11.9 kcal mol^{-1}, from which **11** is formed at -26.7 kcal mol^{-1} through realisation of the Ca-π arene interaction. Natural Bond Orbital (NBO) analysis of $\mathbf{TS_{EF}}$ showed partial charges of -0.03 and -0.25 on H^a and H^b respectively (Figure 4.8), emphasising that the reaction is essentially an acid-base reaction where Ph_3SnH is deprotonated by a calcium

hydride. The newly formed H–H bond in the subsequent intermediate **F** remains substantially polarised, with partial charges of +0.01 (H^a) and -0.27 (H^b).

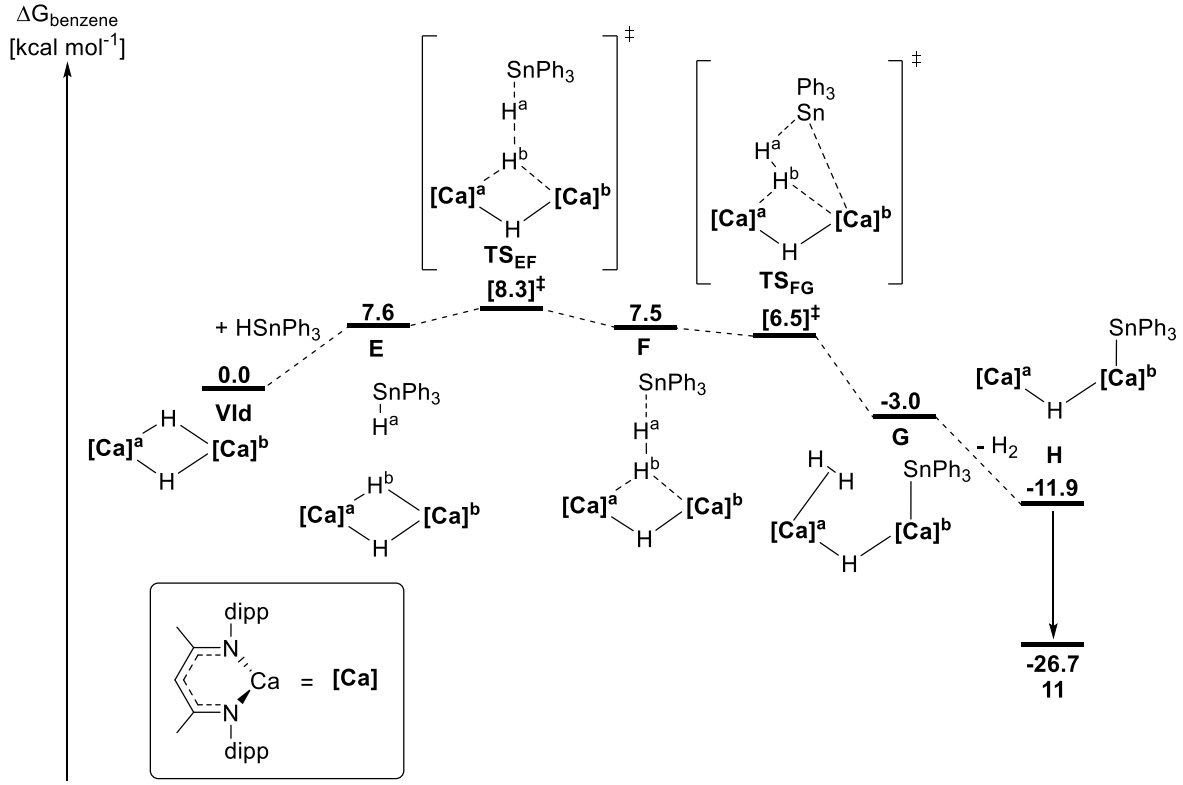

Figure 4.7: DFT calculated (BP87-D3(BJ)-benzene/BS2//BP86/BS1) energy profile (kcal mol^{-1}) for pathway **II** of the formation of **11** from **VId** and Ph_3SnH.

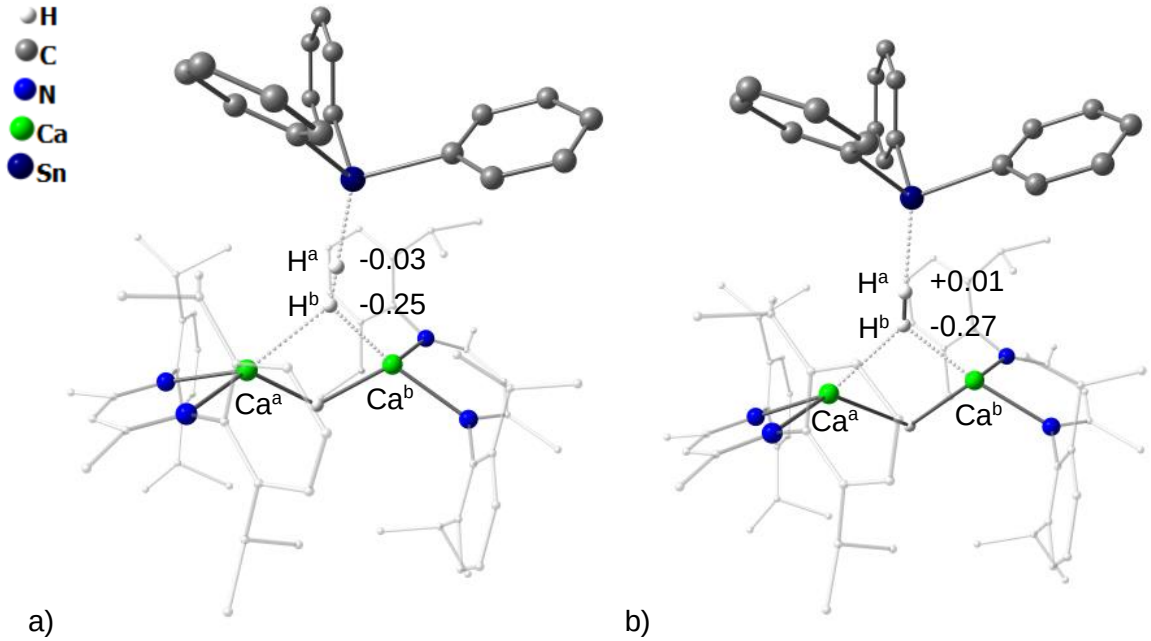

Figure 4.8: Transition state $\mathbf{TS_{EF}}$ and intermediate **F**, showing calculated NBO charges of H^a and H^b. BDI ligand frameworks shown as wireframe for clarity.

DFT was also used to probe the reaction of **11** with a second molecule of Ph_3SnH (Figure 4.9). Encounter complex **I**, at -22.3 kcal mol^{-1} (relative to **VId**) must undergo only slight rearrangement of the BDI-ligands to accommodate the incoming Ph_3SnH molecule. The following transition state, $\mathbf{TS_{IJ}}$ (Figure 4.10) at -12.1 kcal mol^{-1} is kinetically accessible under experimental conditions, allowing cleavage of the Sn^b—H^b bond, and formation of the H^a—H^b bond. Intermediate **J** contains two $[Ph_3Sn]^-$ anions, each coordinated to Ca^a *via* a Ca-Sn bond, while decoordination of H_2 from Ca^b provides intermediate **K** at -38.9 kcal mol^{-1}. Formation of **12** involves transfer of $[Sn^bPh_3]^-$ from Ca^a to Ca^b *via* a low isomerisation barrier which is consistent with the fluxionality of **11** observed by variable temperature NMR (Section 4.2.3), and the overall transformation from **VId** to **12** is -46.7 kcal mol^{-1} downhill.

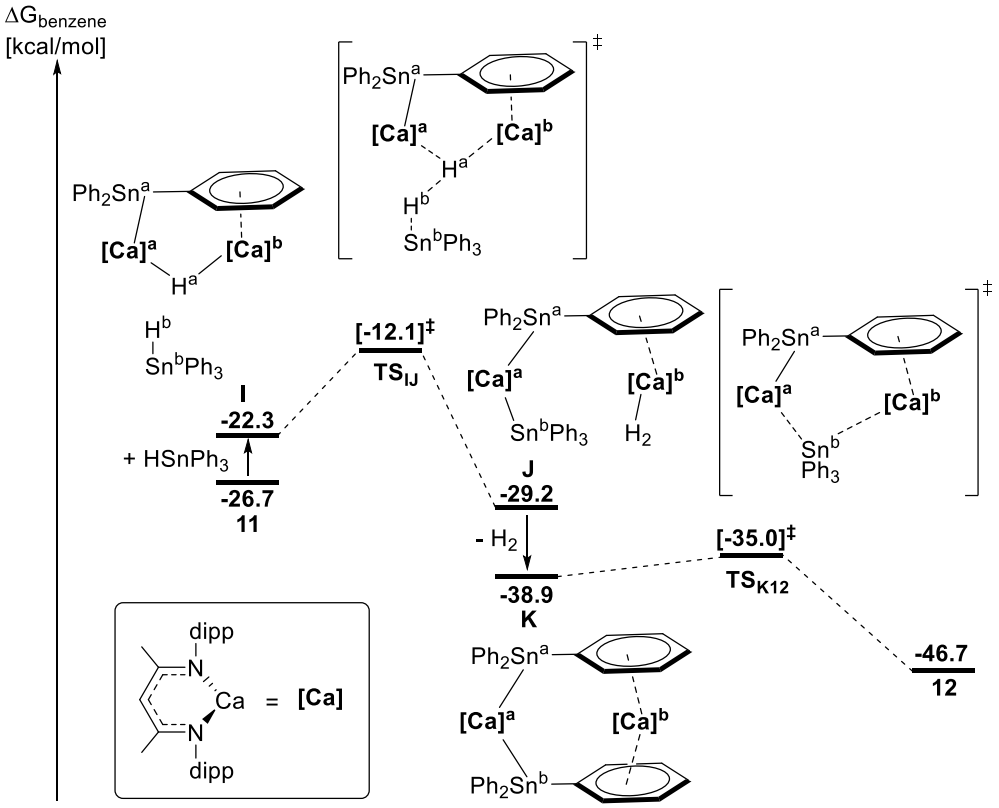

Figure 4.9: DFT calculated (BP87-D3(BJ)-benzene/BS2//BP86/BS1) energy profile (kcal mol^{-1}) for the reaction of **11** with Ph_3SnH.

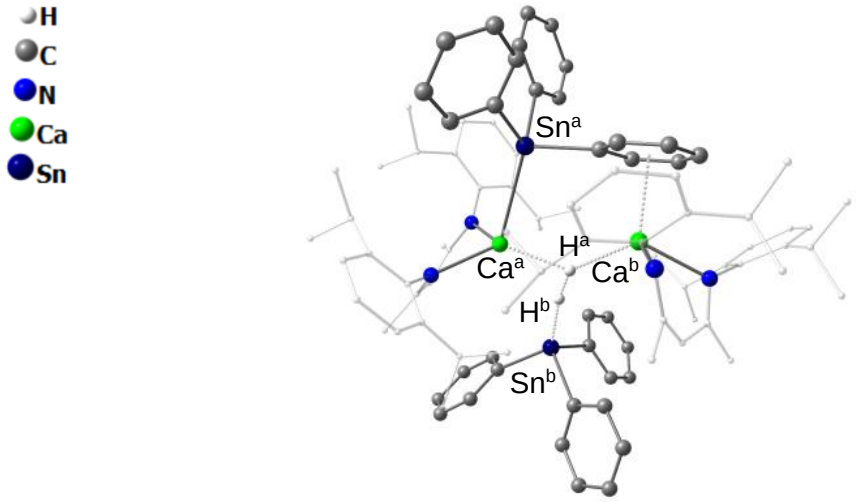

Figure 4.10: Transition state TS_{IJ}. BDI ligand frameworks shown as wireframe for clarity.

In summary, DFT analysis suggests that monomerisation and pathway **I** are kinetically inaccessible under the room-temperature reaction conditions, and that retention of a dimeric structure allows **11** to be formed *via* a low barrier exergonic pathway **II**. Whilst reaction of **11** with Ph_3SnH to provide **12** is both thermodynamically favourable and kinetically accessible, experimental observations suggest that this process is in competition with redistribution of

Ph_3SnH to provide Ph_4Sn, $Sn^{(0)}$, and H_2. Since Ph_3SnH cannot be detected in the reaction mixture by *in situ* NMR spectroscopy, subsequent formation of **12** could originate either from reaction of **11** with Ph_4Sn, or by redistribution *via* monomeric intermediate **D** (Figure 4.6). Unfortunately, Ph_3SnH redistribution was not amenable to computational analysis due to the generation of metallic tin. In pursuit of a greater understanding of this complex reactivity, further experiments involving other aryltin(IV) hydrides were carried out.

4.2.5 Hydrido-calcium mediated activation and redistribution of aryltin(IV) hydrides

As already eluded to, exposing **VId** to an excess of Ph_3SnH produces Ph_4Sn in the place of Sn-Sn coupled products or compound **12.**. Reaction of **VId** with four equivalents of Ph_3SnH provides quantitative conversion of both starting materials after three hours at 40°C, with deposition of colloidal $Sn^{(0)}$ and crystalline Ph_4Sn (Scheme 4.6). Heating to 40°C for a further three days resulted in partial redistribution of **11** to compound **12** and the homoleptic BDI-calcium complex, **XXXIX**.[83] A plausible mechanism for this process involves phenyl-transfer to generate Ph_4Sn and a species of the type [(BDI)Ca(H)(Ph_2HSn)Ca(BDI)], which is susceptible to further attack by Ph_3SnH (Scheme 4.5). The cascade ultimately culminates in a highly reactive stannane derivative [(BDI)Ca(H)(H_3Sn)Ca(BDI)], which may decompose to regenerate **VId** and SnH_2 or SnH_4.

This hypothesis was supported by a reaction performed between *in situ* generated **11** and an equimolar quantity of Bu_3SnH. After one hour at room temperature, analysis by ^1H and $^{119}Sn\{^1H\}$ NMR spectroscopy revealed a mixture of Bu_3SnPh, Bu_3SnH, Ph_4Sn, and compound **11**. After standing for a further 40 hours, the reaction mixture became black and opaque. ^1H and $^{119}Sn\{^1H\}$ NMR spectroscopy confirmed that quantitative conversion of Bu_3SnH to Bu_3SnPh had occurred. Minor quantities of **VId**, unreacted **11**, and the redistribution products Ph_4Sn and **XXXIX** were also present. A plausible mechanism for this process, therefore, occurs *via* Sn-Ph/Sn-H metathesis with dimeric retention (Scheme 4.5). Thermal redistribution of tin-bound aryl groups is well known,[14] and similar redistribution has been observed under reductive conditions such as those reported for the synthesis of **XXXVIIIa** by Uhlig and co-workers.[35] Phenylsilane undergoes similar redistribution to diphenylsilane and SiH_4 in the presence of **VId**,[84] reactivity which has also been mediated by lanthanide hydride complexes.[85-88]

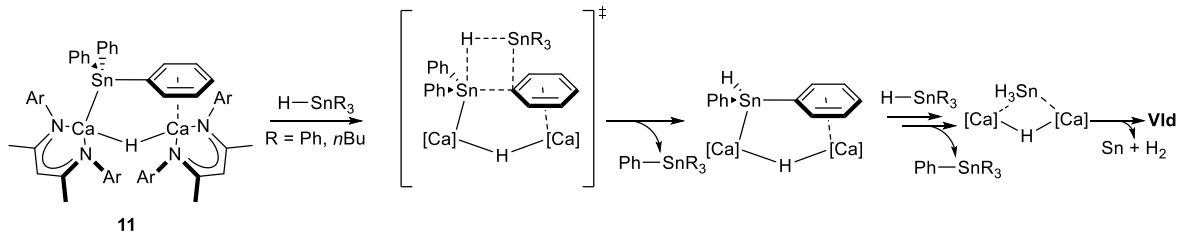

Scheme 4.5: Plausible mechanism for the formation of Ph_4Sn or $n Bu_3SnPh$ from compound **11** and Ph_3SnH or $n Bu_3SnH$.

Reaction of Ph_2SnH_2 and **VId** (2:1) in C_6D_6 also resulted in quantitative conversion of the starting materials to **11**, H_2, Ph_4Sn, and $Sn^{(0)}$ in less than 30 minutes at room temperature. The reaction was repeated with a 20-fold excess of Ph_2SnH_2 (Sn/Ca = 10:1). In this case, the reaction took five days to reach completion. Following the reaction progress by *in situ* $^{119}Sn\{^1H\}$ NMR spectroscopy (Figure 4.11) revealed the sequential redistribution of Ph_2SnH_2 (δ -234.1 ppm) to Ph_3SnH (δ -162.8 ppm) and finally, Ph_4Sn (δ -126.4 ppm).[89]

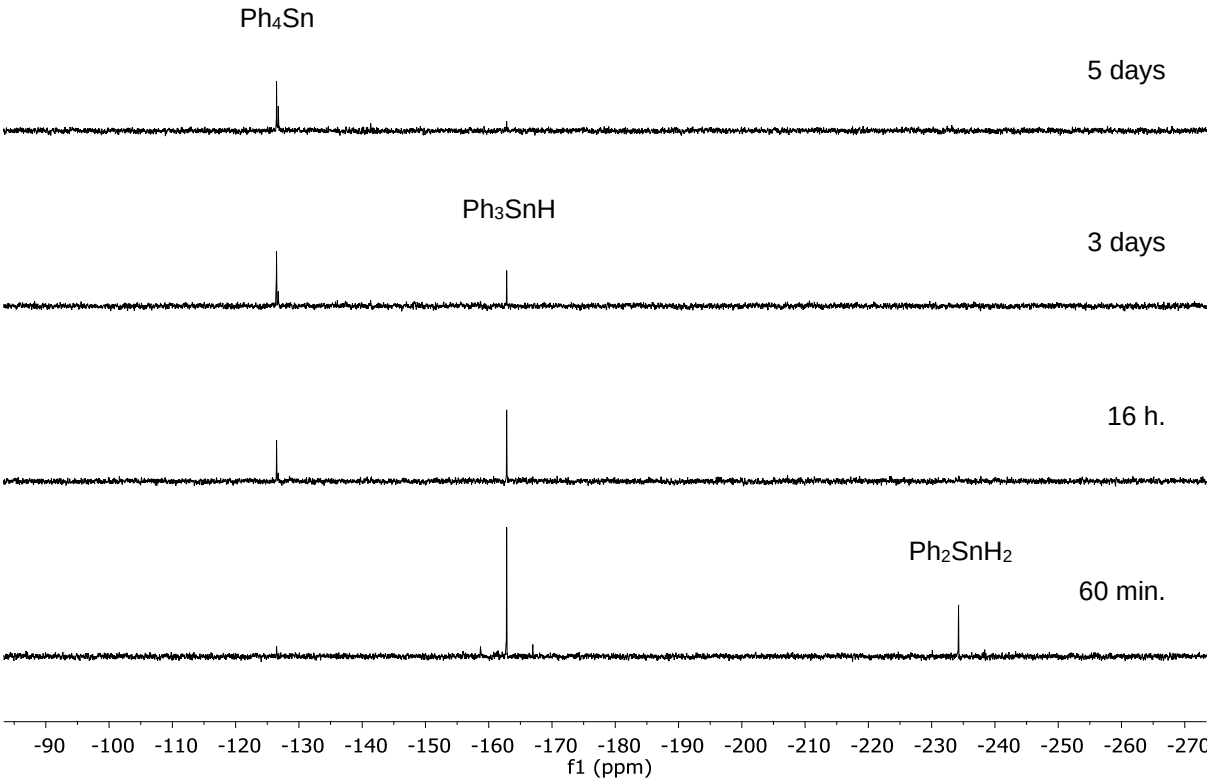

Figure 4.11: *in situ* $^{119}Sn\{^1H\}$ NMR spectra (C_6D_6, 186 MHz, 298 K) following the course of the catalytic redistribution of Ph_2SnH_2 to Ph_4Sn, $Sn^{(0)}$ and H_2 over five days. Reaction carried out with 5 mol% **VId** at room temperature.

The stoichiometric reaction of $MesSnH_3$ with **VId** (2:1) led to vigourous bubbling and a black colouration in a matter of minutes, with a complex mixture of unidentifiable products evidenced by ^1H NMR spectroscopy. Interestingly, the $^{119}Sn\{^1H\}$ NMR spectrum was absent of resonances and provided no evidence for the expected redistribution products, Mes_2SnH_2 and Mes_3SnH. This may be due to decomposition of the proposed intermediate [(BDI)Ca(H)($MesH_2Sn$)Ca(BDI)] *via* transfer of the mesityl group to calcium, rather than by Sn–Mes/Sn–H metathesis and generation of [(BDI)Ca(H)(H_3Sn)Ca(BDI)]. It is suggested that the resultant organocalcium species [(BDI)Ca(H)(Mes)Ca(BDI)] is likely to be unstable with respect to both Schlenk-type redistribution, and reaction with the C_6D_6 solvent,[44, 90] hence the only identifiable compound in the ^1H NMR spectrum is **XXXIX**.

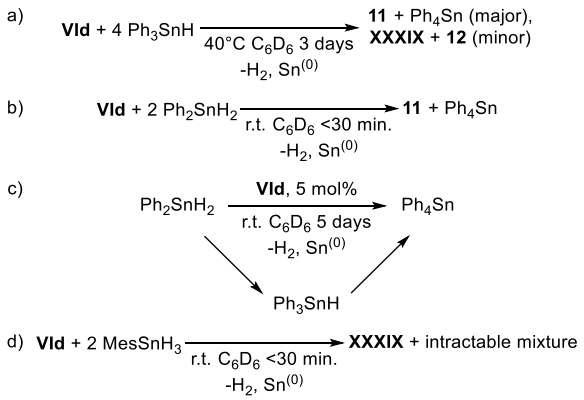

Scheme 4.6: Reactions of **VId** with: a) 4 eq. Ph_3SnH, b) 2 eq. Ph_2SnH_2, c) 20 eq. Ph_2SnH_2, d) 2 eq. $MesSnH_3$.

4.2.6 Reactivity of VId and Vb towards Ph_4Sn

The postulated mechanism discussed in section 4.2.4 for the formation of **12** from **11** involves monomerisation of the latter species into two fragments: [(BDI)Ca($SnPh_3$)] and [(BDI)CaH], which each dimerise to give **12** and **VId** (Figure 4.6, Figure 4.7). Regeneration of **VId**, however, could not be detected by *in situ* ^1H NMR spectroscopy. Hence, it was postulated that any **VId** regenerated may react with Ph_4Sn to produce a further molecule of **11**.

To test this hypothesis, two equivalents of Ph_4Sn were added to a C_6D_6 solution of **VId**. After 24 hours at room temperature, half of the initial **VId** could be detected by *in situ* ^1H NMR spectroscopy, along with the characteristic BDI γ-C*H* and Ca-*H* singlets for compound **11** at δ 4.75 and 3.83 ppm. Two new singlets at δ 4.80 and 4.78 ppm resonated with a relative intensity of 1:2 (Figure 4.12). Elevating the temperature to 40°C and/or allowing the reaction to proceed for up to five days did not significantly increase spectroscopic yield of either product and instead resulted in the formation of small quantities of **12**, and large quantities of **XXXIX**. Selectivity towards the unidentified product could be maximised by adjustment of the reaction

stoichiometry, reaching a maximum of 1:1 relative to **11** at an overall 2:1 Ca/Sn ratio. Furthermore, a doublet at δ 6.78 ppm and triplet at 7.09 ppm were observed upfield of the aromatic region and each integrated 1:1 relative to the singlet at δ 4.78 ppm (Figure 4.12). These signals were tentatively identified as a dimeric BDI calcium phenyl-hydride species, **13** ([(BDI)Ca(μ^2-Ph)(μ^2-H)Ca(BDI)], Scheme 4.7). The resonance at δ 4.80 ppm is assigned to the bridging hydride, the shielded aromatic resonances at δ 6.5-6.7 ppm to the *meta* and *para* protons of the phenyl anion, and the singlet at δ 4.78 ppm to the γ-C*H* of the BDI ligands. Repeated attempts to isolate and crystallise this species, however, were thwarted by low spectroscopic yield, poor selectivity, and thermal instability.

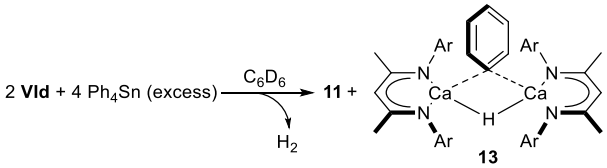

Scheme 4.7: The reaction of **VId** with Ph_4Sn to produce **11** and proposed calcium phenyl species **13**. Through redistribution, the byproducts $Sn^{(0)}$, **XXXIX**, and **12** were also present in the reaction mixture, but are omitted from the scheme for clarity.

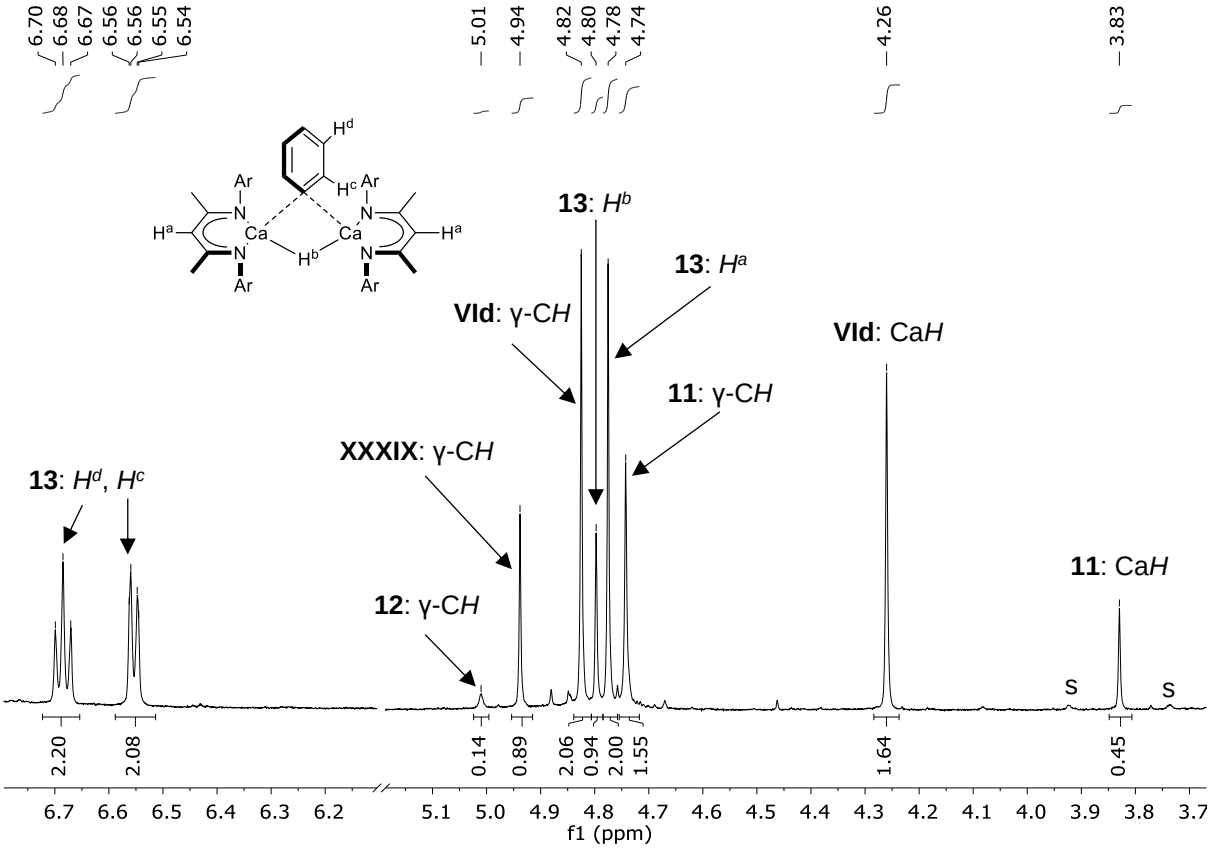

Figure 4.12: Expanded *in situ* ^{1}H NMR spectrum (500 MHz, C_6D_6, 298 K) of the reaction between **VId** and Ph_4Sn (3:1 Ca:Sn ratio) after 24 h at room temperature, s = $^{117/119}$Sn satellites.

An analogous reaction between Ph_4Sn and the potent nucleophile $[(BDI)CaHex]_2$ (**Vb**), was carried out. After 48 hours at 40°C, the $^{119}Sn\{^1H\}$ NMR spectrum displayed a new resonance at δ -98.3 ppm, which was identified to be $HexSnPh_3$.[91] Unfortunately, poor solubility of both substrates in C_6D_6 and the greater steric demands of the hexyl substituent resulted in low reaction rates. Whilst a slightly elevated temperature (40°C) facilitated partial conversion of the tin substrate, Schlenk-type ligand redistribution and thermal decomposition precluded the identification of any resultant calcium-containing species. As such, the homoleptic complex **XXXIX** was the only major product present in the ^1H NMR spectrum. The positive identification of $HexSnPh_3$, however, supports a mechanism in which the calcium-bound hexyl or hydride anion acts as a nucleophile toward the tin centre, resulting in transfer of an anionic phenyl 'leaving group' to the calcium and release of a molecule of either $HexSnPh_3$ or Ph_3SnH. The former is inert towards onward reactivity, whereas the latter tin hydride can react with a second equivalent of **VId** to produce compound **11** (Scheme 4.8).

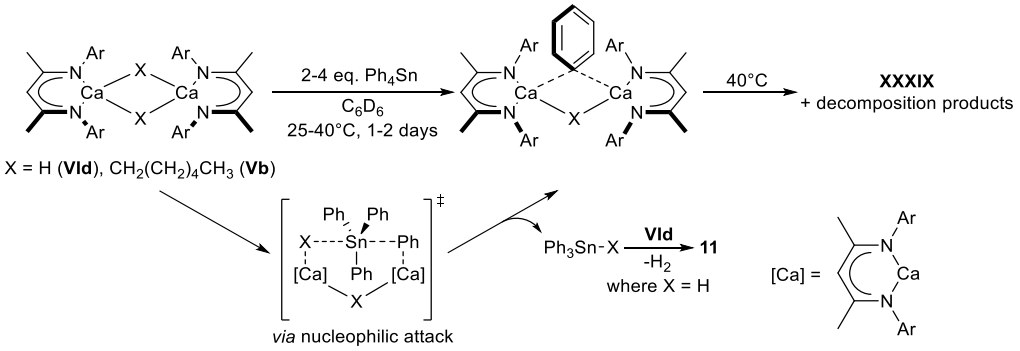

Scheme 4.8: Plausible mechanism for the reaction between Ph_4Sn and **VId** or **Vb**. Ar = 2,6-di-*iso*propylphenyl.

4.2.7 Reactivity of VId and Vb towards $Ph_3Sn{-}SnPh_3$

Whilst attempts to form tin-tin bonds were unsuccessful, **VId** was found to mediate the facile rupture of tin-tin bonds (Scheme 4.9). An equimolar reaction between **VId** and $(Ph_3Sn)_2$ provides Ph_4Sn and compound **11** as the major identifiable products in the *in situ* ^1H and $^{119}Sn\{^1H\}$ NMR spectra.

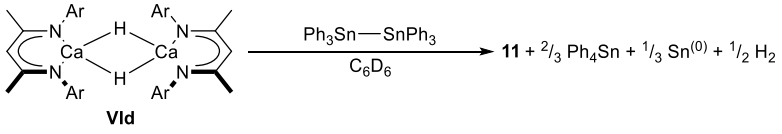

Scheme 4.9: The calcium hydride mediated cleavage of hexaphenyldistannane. Ar = 2,6-di-*iso*propylphenyl.

A similar mechanism to that presented in Scheme 4.8 can be postulated, with nucleophilic attack of a calcium hydride at tin, causing the displacement of a $[Ph_3Sn]^-$ anion to calcium, and elimination of Ph_3SnH (Scheme 4.10).

The reaction of $(Ph_3Sn)_2$ with **Vb** was also carried out, with the presence of $HexSnPh_3$ in the $^{119}Sn\{^1H\}$ NMR spectrum suggesting nucleophilic attack of the hexyl anion towards $(Ph_3Sn)_2$ to be a viable pathway. Low reaction rates arising from the poor solubility of both substrates demanded an elevated temperature, resulting in widespread redistribution that prevented the identification of any other products by ^1H NMR spectroscopy (Scheme 4.10).

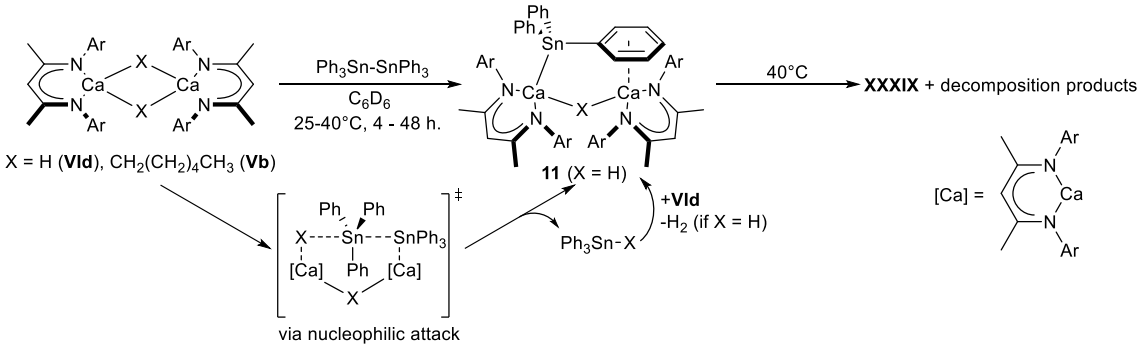

Scheme 4.10: Plausible mechanism for the reaction between $(Ph_3Sn)_2$ and compounds **VId** or **Vb**. Ar = 2,6-di-*iso*propylphenyl.

4.2.8 Computational investigation into the reaction between VId and Ph_4Sn.

Figure 4.13 displays the DFT-calculated reaction mechanism for the reaction between **VId** and Ph_4Sn. The first transition state could not be located due to an extremely flat potential energy surface, but formation of the resulting intermediate **L** is endergonic by only +9.5 kcal mol^{-1}. The five-coordinate tin centre of **L** adopts a trigonal bipyramidal geometry, with the stannate moiety interacting with Ca^b *via* a bridging hydride (H^a—Sn = 1.900 Å, Ca^b—H^a = 2.382 Å), and with Ca^a through an η^6-π interaction (Figure 4.14a). The Sn—C^a bond length is elongated to 2.381 Å (*vs.* 2.284 Å for Sn—C^b), thus activating it towards Sn—C^a cleavage *via* transition state $\mathbf{TS_{L13}}$ at +12.5 kcal mol^{-1}, where the Sn—C^a, and Ca^b—H^a distances are further increased to 3.151 Å and 2.758 Å, respectively (Figure 4.14b). Finally, elimination of Ph_3SnH provides species **13**.

The involvement of an arene-calcium interaction is reminiscent of the calculated mechanism for the nucleophilic alkylation of benzene, in which the arene is activated towards nucleophilic attack by an *n*-alkyl anion through pre-coordination to the calcium centre.[44] Furthermore, weakening and lengthening of the Sn-C^a bond is substantiated by slightly elongated Sn1-C30 bond lengths in the X-ray crystal structures of compounds **11** (Figure 4.2, Sn1-C30 =

2.2258(19) Å *cf.* Sn1-C36 = 2.190(2) Å) and **12** (Figure 4.3, Sn1-C30 = 2.222(3) Å *cf.* Sn1-C36 = 2.218(3) Å). The computed reaction mechanism is in agreement with the *in situ* NMR studies of Section 4.2.6 and, whilst the overall transformation from **VId** to **13** involves a low barrier, it lacks a significant thermodynamic driving force. As a result, the equilibrium is shifted towards the formation of **11** by rapid consumption of *in situ* generated Ph_3SnH by a further equivalent of **VId**.

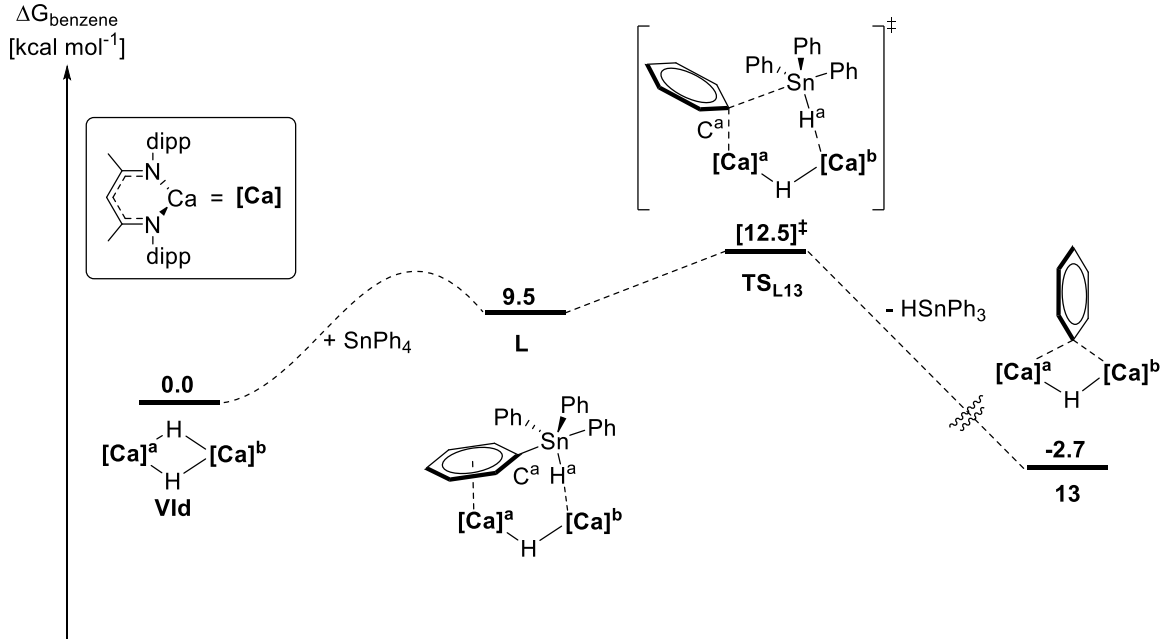

Figure 4.13: DFT calculated (BP87-D3(BJ)-benzene/BS2//BP86/BS1) energy profile (kcal mol^{-1}) for the reaction of **VId** with Ph_4Sn to give Ph_3SnH and **13**.

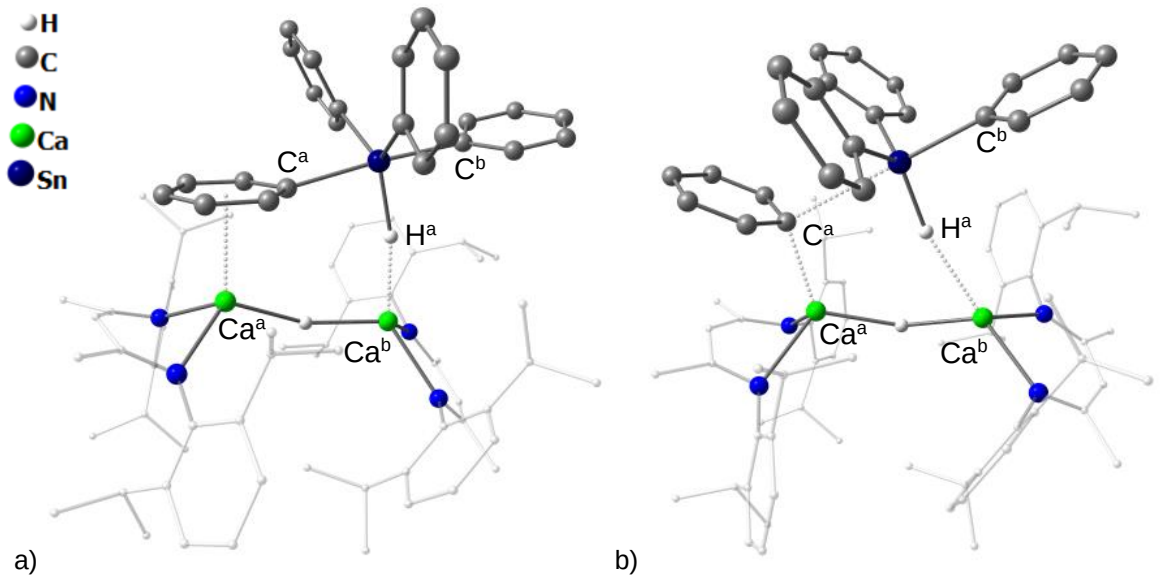

a) b)

Figure 4.14: a) intermediate **L**, and b) transition state $\mathbf{TS_{L13}}$. BDI ligand frameworks shown as wireframe for clarity.

4.2.9 Computation investigations into the reaction between VId and $(Ph_3Sn)_2$.

The calculated pathway for the reaction between **VId** and $(Ph_3Sn)_2$ shown in Figure 4.15 displays some similarities to that in Figure 4.13. Addition of $(Ph_3Sn)_2$ to **VId** gives the van-der-Waals encounter complex, **M** at +8.7 kcal mol^{-1}. The hydride H^a then acts as a nucleophile and attacks Sn^a *via* $\mathbf{TS_{MN}}$, at +12.7 kcal mol^{-1} and in which the Sn^a–Sn^b bond is lengthened from 2.850 Å (calculated for Ph_3Sn–$SnPh_3$) to 2.869 Å in $\mathbf{TS_{MN}}$ (Figure 4.16a). The Sn^a–Sn^b bond is further elongated to 2.949 Å on the formation of intermediate **N** (Figure 4.16a), which resides at +5.2 kcal mol^{-1} and contains a formal stannate anion. The trigonal bipyramidal Sn^a centre bonds to tetrahedral Sn^b and to Ca^a *via* a bridging hydride, with Ca^a–H^a and H^a–Sn^a distances of 2.296 Å and 2.144 Å, respectively. Although the Sn-Sn bond breaking/Sn-Ca bond forming transition state separating **N** from the Ca-Sn bonded intermediate **O** at +11.9 kcal mol^{-1} could not be located due to a very flat potential energy surface, dissociation of Ph_3SnH from **O** was computed to be -14.9 kcal mol^{-1} downhill. The overall process is exergonic by only -3.1 kcal mol^{-1}, therefore, consumption of Ph_3SnH by **VId** and elimination of H_2 provides a thermodynamic driving force. The low kinetic barriers are consistent with the experimental reaction conditions.

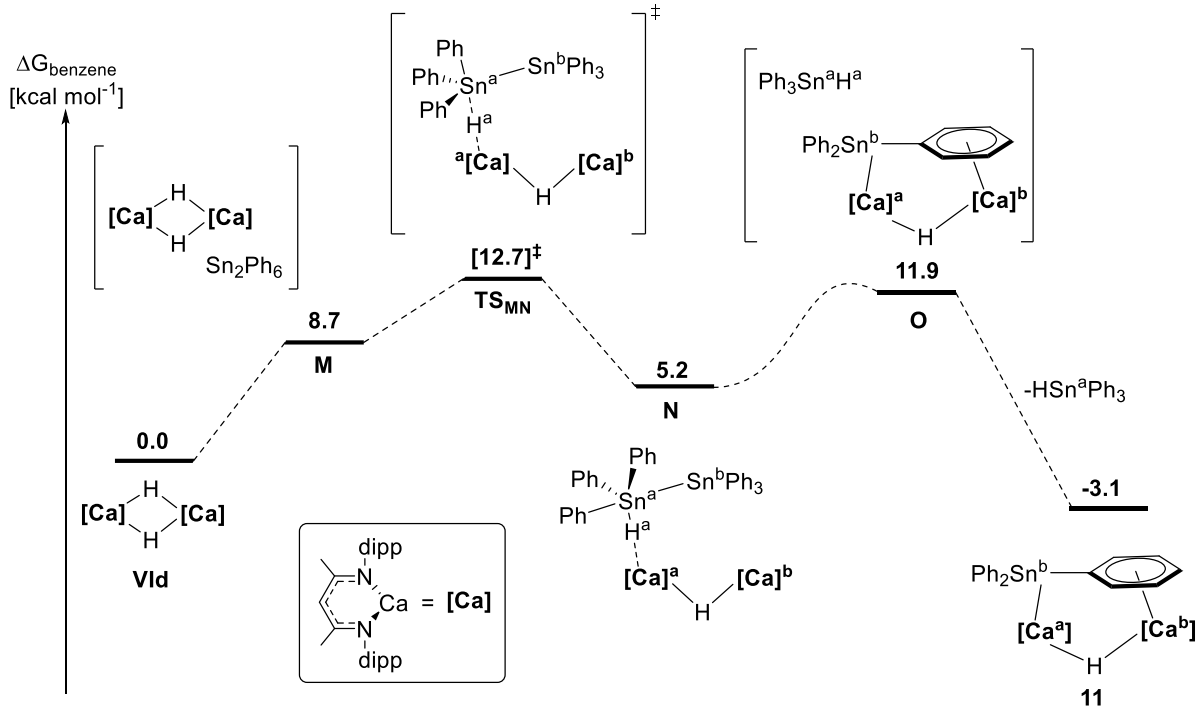

Figure 4.15: DFT calculated (BP87-D3(BJ)-benzene/BS2//BP86/BS1) energy (kcal mol^{-1}) profile for the reaction of **VId** with $(Ph_3Sn)_2$ to give Ph_3SnH and **11**.

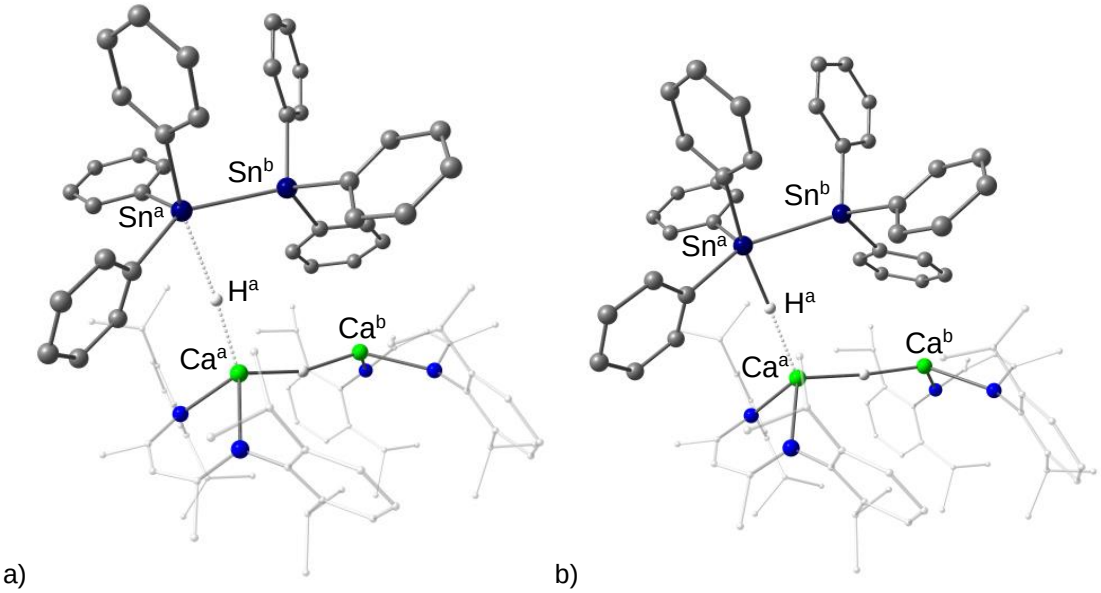

a) b)

Figure 4.16: a) transition state **TS$_{MN}$**, and b) intermediate **N**. BDI ligand frameworks shown as wireframe for clarity.

4.2.10 Triphenylphosphine oxide promoted formation of a monomeric terminal calcium stannide complex

Although compound **11** could be selectively generated *in situ*, redistribution to **12** in solution limits its wider synthetic utility and repeated attempts to scale up and isolate larger quantities

of either compound were unsuccessful. Furthermore, both compounds co-crystallise from the same solvent system, and careful extraction of the crude product into hexane and/or successive fractional crystallisation was necessary to avoid contamination by the Ph_4Sn by-product. Furthermore, the presence of both hydride and stannide ligands potentially complicates the interpretation of any onward reactivity.

Inspired by examples of Lewis base-activated Ae-complexes,[92-94] an equimolar amount of triphenylphosphine oxide was added to an *in situ* generated C_6D_6 solution of compound **11** and Ph_4Sn (from **VId** and $(Ph_3Sn)_2$). After 24 hours, the reaction mixture took on a turbid brown appearance, with the ^1H NMR spectrum showing the generation of a new BDI-containing compound with a single, sharp γ-C*H* resonance at δ 5.23 ppm, in addition to several minor products. The $^{119}Sn\{^1H\}$ NMR spectrum revealed the presence of Ph_4Sn, **11**, and **12** as well as a new major product, resonating as a doublet at δ -146 ppm with a coupling constant of $^3J(^{31}P\text{-}^{117/119}Sn)$ = 10 Hz. This coupling constant is consistent with the few $^3J(^{31}P\text{-}^{117/119}Sn)$ coupling constants that have been reported to date.[95, 96] The $^{31}P\{^1H\}$ NMR spectrum showed complete consumption of the phosphine oxide, with a major resonance at δ 36.4 ppm, which displayed $^{117/119}Sn$ satellites ($^3J(^{31}P\text{-}^{117/119}Sn)$ = 10 Hz), in addition to some minor peaks at δ 88-89 ppm and 71 ppm. Recrystallisation of the crude products from a hexane/toluene mixture at room temperature eventually confirmed the major product as the triphenylphosphine oxide adduct **14** (Scheme 4.11).

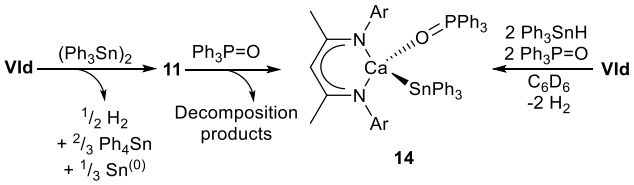

Scheme 4.11: Formation of compound **14** from **VId** or **11**.

A few crystals of the known compound $[(BDI)Ca(OPPh_2)]_2$ (**XIX**) were also identified by comparison to the published unit cell parameters.[97] A plausible mechanism for the formation of **14** involves coordination of phosphine oxide to calcium, favouring monomerisation of **11** to generate monomeric BDI-calcium hydride and stannide species and their respective Ph_3PO adducts. Subsequent dimerization and decomposition processes ensue, and crystals of compound **14** are eventually isolated. Consistent with the observation of **XIX** and the various unidentified by-products in the reaction mixture, triphenylphosphine oxide is known to undergo complex calcium-hydride mediated reduction chemistry.[97] Compound **14** can also be accessed in higher yields and with greater selectivity in a single-step process, reacting **VId** with two equivalents of Ph_3SnH and Ph_3PO. This reaction mixture immediately developed a

red colouration, which gradually faded to yellow over the course of a few hours to provide clean conversion to compound **14**, which was crystallised from a saturated toluene solution at -30°C (Scheme 4.11).

Compound **14** crystallises in the monoclinic space group, $P2_1/c$. Its monomeric structure consists of a distorted tetrahedral calcium centre chelated by the BDI ligand and coordinated to $[Ph_3Sn]^-$ *via* a Ca-Sn bond, and $OPPh_3$ through oxygen (Figure 4.17). The bulky stannide and phosphine oxide ligands are forced apart, with an O1-Ca1-Sn1 angle of 122.09(4)°, whilst the N1-Ca1-N2 angle (81.07(6)°) and N-Ca bond lengths (2.30-2.32 Å) are similar to those in **11** and **12**. The calcium centre is projected 1.449(2) Å out of the plane defined by the BDI ligand: significantly more than the analogous distortions observed in **11** and **12** (0.668(3)/0.744(3) Å and 1.339(3) Å respectively). The calcium-tin bond length (3.2304(4) Å) is similar to those in compounds **11**, **12**, and **XXXVI**. Although the terminal stannide ligand is slightly tilted away from the phosphine oxide (see Ca-Sn-C angles), the phenyl substituents are arranged in symmetrically, such that the *pseudo*-tetrahedral geometry of the tin centre is otherwise unperturbed. The Ca-O and O-P bond lengths are similar to those of the alkyl-calcium Ph_3PO adduct $[(Ph_3PO)_2Ca(CH(SiMe_3)_2)_2]$ (**XL**) previously reported by Hill *et.al.*,[97] and the Ca1-O1-P1 angle lies close to linearity (173.47(10)°).

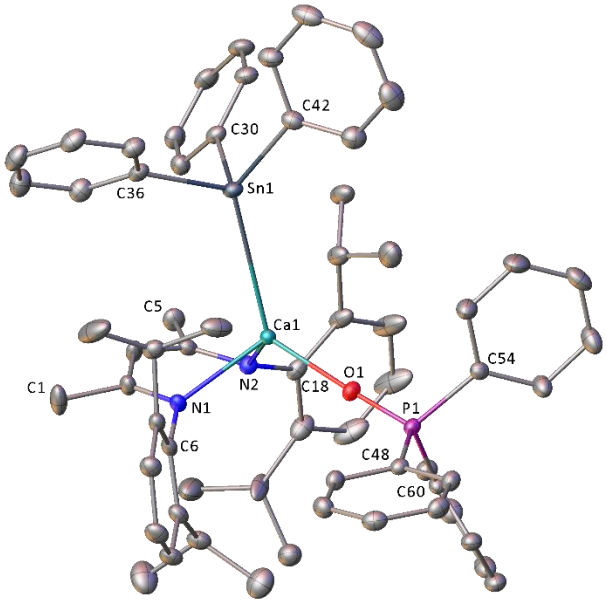

Figure 4.17: X-ray crystal structure of compound **14**. Thermal ellipsoids are shown at the 30% probability level and hydrogen atoms are omitted for clarity. Where disorder is present, only the major component is shown. Selected bond lengths (Å) and angles (°): Sn1-Ca1 3.2304(4), Sn1-C30 2.195(2), Sn1-C36 2.199(2), Sn1-C42 2.192(2), Ca1-N1 2.3014(17), Ca1-N2 2.3189(16), Ca1-O1 2.2020(15), P1-O1 1.5044(15), P1-C48 1.797(2), P1-C54 1.800(2), P1-C60 1.799(2), O1-Ca1-Sn1 122.09(4), O1-Ca1-N1 105.76(6), O1-Ca1-N2 112.13(6), N1-Ca1-Sn1 109.38(4), N2-Ca1-Sn1 117.58(4), Ca1-O1-P1 173.47(10), N2-Ca1-N1 81.07(6), C30-Sn1-Ca1 105.87(5), C36-Sn1-Ca1 118.23(6), C42-Sn1-Ca1 128.90(6).

4.2.11 Stoichiometric reactivity of VId towards alkyltin(IV) hydrides

Having found aryl-stannane redistribution to be an obstacle towards the calcium mediated formation of tin-tin bonds, the reactivity of less labile alkyl stannanes[62] towards **VId** was investigated. The $^{119}Sn\{^{1}H\}$ NMR spectrum (Figure 4.18) of a reaction between compound **VId** and two equivalents of nBu$_3$SnH (Scheme 4.12) showed almost complete conversion of the tin-hydride to a new species resonating at δ -162.5 ppm after five days at room temperature. The signal was tentatively assigned to a calcium stannide, [(BDI)Ca(Sn(nBu)$_3$)], which was formed in conjunction with minor quantities of the distannane, (nBu$_3$)Sn-Sn(nBu$_3$) identified by a peak at δ -83.7 ppm.[14] Although inspection of the corresponding ^{1}H NMR spectrum (Figure 4.19) also confirmed the presence of new BDI-containing species (characterised by a γ-C*H* resonance at δ 4.80 ppm), repeated efforts to crystallographically characterise this compound were unsuccessful and hampered by a low conversion of the starting calcium hydride **VId,** and redistribution to the homoleptic complex **XXXIX**. The reduced rate and low conversion of this

transformation in comparison to the analogous reactions with the aryltin hydrides described above is rationalised to be a likely consequence of the relatively destabilising effect of the *n*-butyl substituents on the resulting stannide anion.

The secondary stannane, (tBu)$_2$SnH$_2$ reacted at an enhanced rate. Although only the starting calcium hydride **VId** was observable by ^{1}H NMR spectroscopy**,** the ^{119}Sn{^{1}H} NMR spectrum revealed near quantitative consumption of the tin dihydride (δ -118.33 ppm) to (tBu)$_2$(H)Sn-Sn(H)(tBu)$_2$ (δ -83.08 ppm)[98] in under 24 hours *via* what is effectively a catalytic dehydrocoupling reaction (Scheme 4.12). Despite failing to detect any reaction intermediates, the formation of tin-tin bonds and lack of organostannane redistribution under stoichiometric reaction conditions provided the opportunity to extend this reactivity into the catalytic domain.

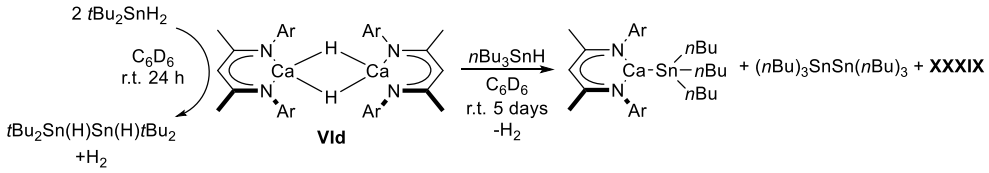

Scheme 4.12: Stoichiometric reactivity of **VId** towards alkyl stannanes.

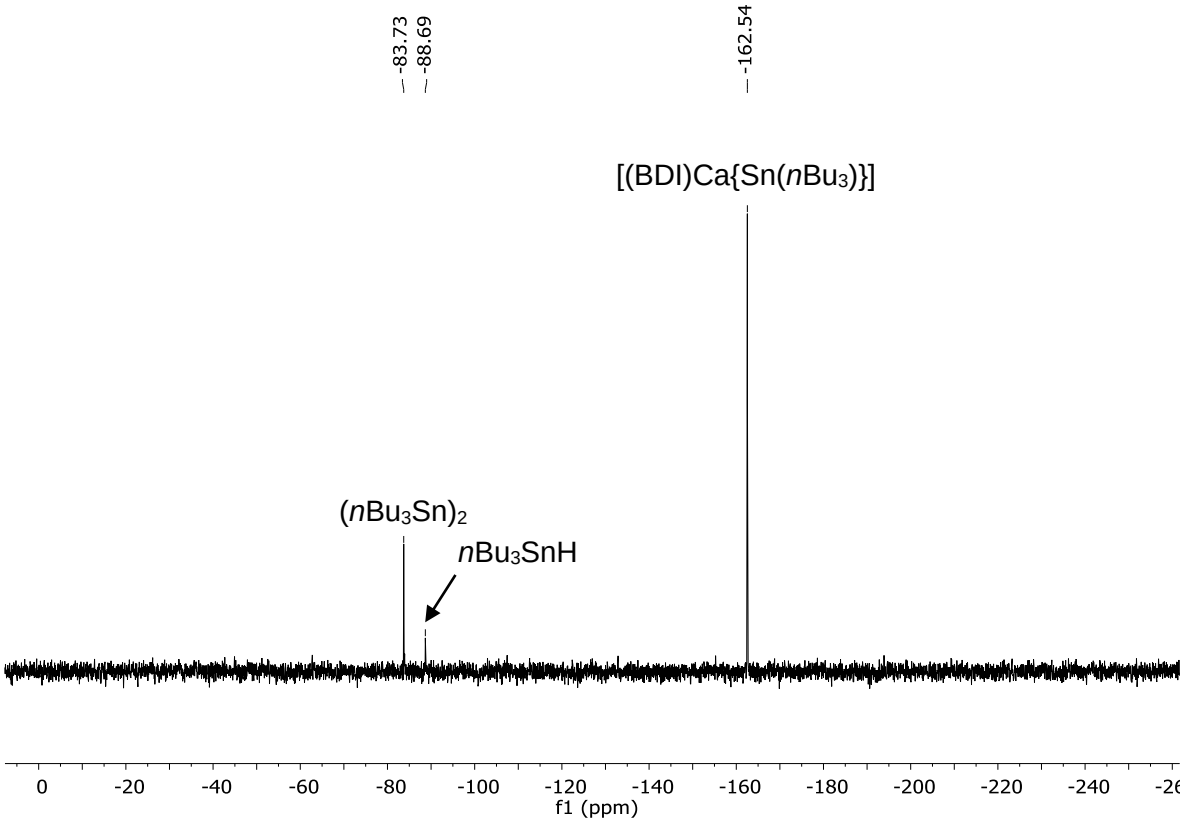

Figure 4.18: Expanded ^{119}Sn{^{1}H} (186 MHz) NMR spectrum (C_6D_6, 298 K) of the reaction between **VId** and Bu_3SnH (2 eq.) after five days at room temperature.

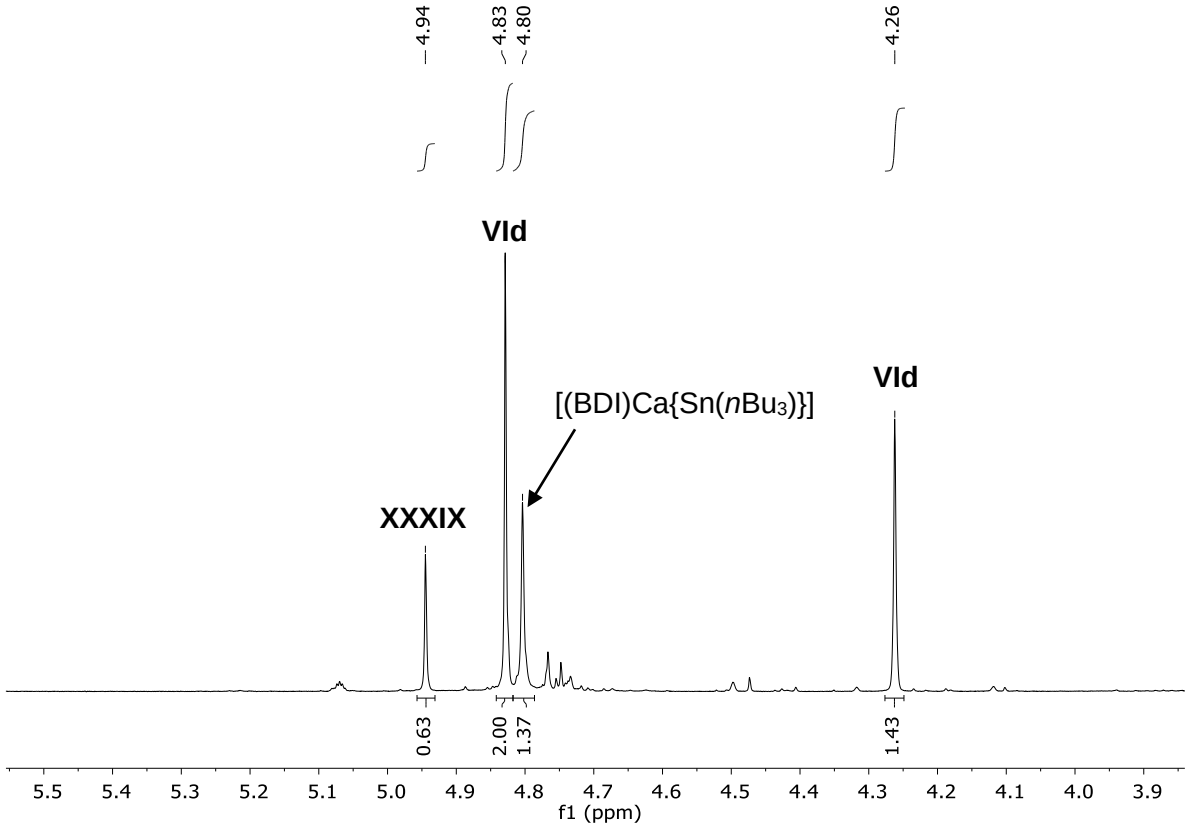

Figure 4.19: Expanded ^{1}H (500 MHz) NMR spectrum (C_6D_6, 298 K) of the reaction between **VId** and Bu_3SnH (2 eq.) after five days at room temperature.

4.2.12 Calcium-mediated catalytic dehydrocoupling of dialkyltin dihydrides

Whilst catalytic dehydrocoupling of nBu$_3$SnH provided only 12% spectroscopic yield of (nBu$_3$Sn)$_2$ (5 mol% **VId**, C_6D_6, three days, 25-60°C), tBu$_2$SnH$_2$ was converted to (tBu)$_2$Sn(H)Sn(H)(tBu)$_2$ in 57% spectroscopic yield after 48 hours at room temperature (2.5 mol% **VId**). Given the susceptibility of heteroleptic calcium complexes with the ^{dipp}BDI ligand to redistribute to **XXXIX** at elevated temperatures, room temperature was maintained, and conversion plateaued to a maximum of 60% after one week.

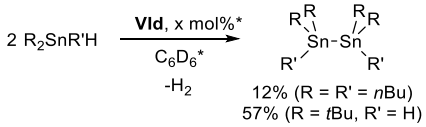

Scheme 4.13: Catalytic dehydrocoupling of nBu$_3$SnH and tBu$_2$SnH$_2$. *For nBu$_3$SnH: 5 mol% **VId**, 16 h r.t., then 24 h 40°, then 24 h 60°C, for tBu$_2$SnH$_2$: 2.5 mol% **VId**, 50 h r.t..

Catalytic dehydrocoupling of nBu$_2$SnH$_2$ reached conversions in excess of 90% after 16 hours (C_6D_6, 2.5 mol% **VId**, Scheme 4.14). The *in situ* $^{119}Sn\{^{1}H\}$ NMR spectrum (Figure 4.20) displayed a major resonance at δ -190 ppm which can be assigned to linear poly-di-*n*-

butylstannane (**P-XXIIIa**).[4, 15, 16, 19, 20, 99] Several minor peaks in the range of δ -200 to -220 ppm are assigned to the 5 and 6 membered cyclic oligomers (nBu$_2$Sn)$_{5/6}$ and Sn-H terminated linear oligomers.[14] The high linear/cyclic selectivity was confirmed by ^{1}H NMR spectroscopy (Figure 4.21), in which a triplet corresponding to the δ-CH_3 of cyclic oligostannanes at δ 1.04 ppm integrates with approximately 10% relative intensity of the corresponding signal for linear **P-XXIIIa** (δ 1.12 ppm).[4, 15, 16, 19, 20, 99]

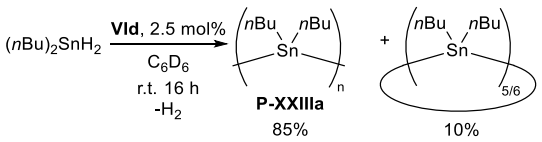

Scheme 4.14: The catalytic dehydrocoupling of di-*n*-butylstannane.

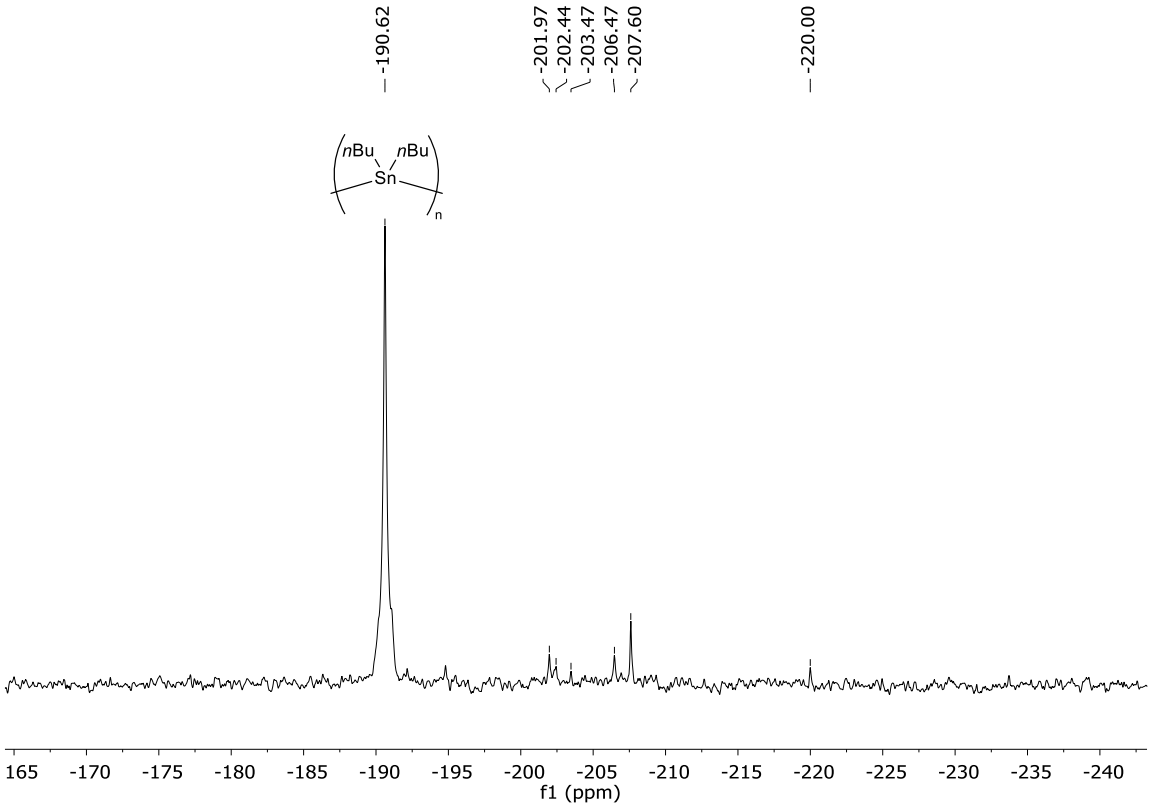

Figure 4.20: ^{119}Sn{^{1}H} NMR spectrum (186 MHz, C_6D_6) of the dehydrocoupling of (nBu)$_2$SnH$_2$ with 2.5 mol% **VId** after 16 hours at room temperature.

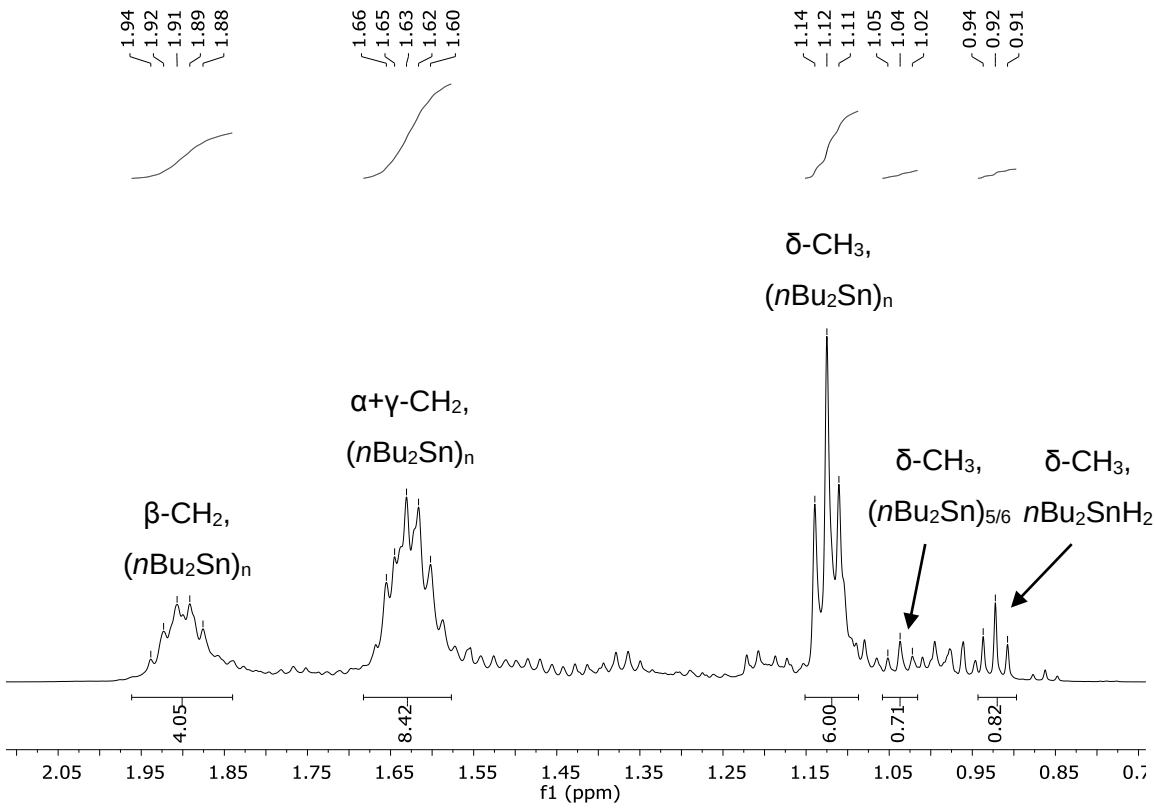

Figure 4.21: ^{1}H NMR spectrum (500 MHz, C_6D_6) of the dehydrocoupling of (nBu)$_2$SnH$_2$ with 2.5 mol% **VId** after 16 hours at room temperature.

The stability of alkyl-substituted Sn-Sn bonds towards compound **VId** was investigated by exposing (nBu)$_3$Sn-Sn(nBu)$_3$ to an equimolar C_6D_6 solution of the calcium hydride. After 16 hours at room temperature, partial conversion of the distannane to nBu$_3$SnH was revealed by appearance of a resonance at δ -88.7 ppm. Although tin-tin bonds of alkyl oligostannanes are clearly less labile than their aryl congeners, Sn-Sn bond cleavage may be substantial enough to ultimately complicate future attempts to prepare high molecular weight polystannanes under calcium catalysis.

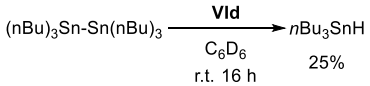

Scheme 4.15: Cleavage of hexa-*n*-butyldistannane by **VId**. Approximate spectroscopic yield determined by integration of the ^{119}Sn{^{1}H} spectrum.

4.3 Conclusions

In summary, we have shown that reactivity of the coordinatively unsaturated β-diketiminato calcium hydride **VId** can be extended beyond organic substrates. Sn-H, Sn-C, and Sn-Sn

bonds can be activated to form BDI-supported calcium stannide complexes (**11** and **12**) possessing rare Ca-Sn bonds. Although these reactions appear to proceed through dimeric intermediates, addition of a mild Lewis base promotes formation of a monomeric, terminal stannide in the form of triphenylphosphine oxide adduct, **14**. Activation of Sn-aryl bonds is facile and leads to rapid redistribution at the tin centre, ultimately yielding Ph_4Sn, $Sn^{(0)}$, and H_2. Replacing aryl for alkyl substituents suppresses redistribution and allows tin-tin bond formation to proceed. *In situ* NMR reactions provided evidence for the formation of the distannanes, $(n\text{Bu})_3\text{Sn-Sn}(n\text{Bu})_3$ and $(t\text{Bu})_2\text{(H)Sn-Sn(H)}(t\text{Bu})_2$, and the linear polystannane $((n\text{Bu})_2\text{Sn})_n$ (**P-XXIIIa**). Although calcium-mediated catalytic dehydropolymerisation has not yet been scaled up successfully, a certain degree of Sn-Sn bond lability in the presence of compound **VId** remains a concern and was demonstrated by the formation of small quantities of $(n\text{Bu})_3\text{SnH}$ from $((n\text{Bu})_3\text{Sn})_2$ and **VId**. A thorough mechanistic investigation into calcium catalysed Sn-Sn dehydrocoupling would be of interest in the future. More generally, an exploration of the reactivity of compounds **11,12** and **14** towards the full palette of inorganic and organic substrates available to the organometallic chemist may be fruitful. Facile tin-to-calcium aryl transfer provides a tantalising glimpse of the possibility of accessing unusual aryl calcium complexes, the realisation of which may provide a route towards organocalcium-mediated arene C-H activation and biaryl coupling. Finally, extending the reactivity of the heavier alkaline-earths towards the other *p*-block elements is an exciting subject for future exploration.

4.4 Experimental section

4.4.1 Reaction of VId with 3 equivalents Ph_3SnH and crystallisation of compound 11.

A C_6D_6 solution (0.6 ml) containing 23 mg Ph_3SnH (0.0654 mmol) was added to a J. Young's NMR tube containing 20 mg **VId** (0.0218 mmol). The reaction mixture bubbled and was left at room temperature overnight. Analysis by ^1H and ^{119}Sn NMR spectroscopy showed complete conversion of both starting materials, and formation of one new BDI-containing product and Ph_4Sn. Solvent was removed under vacuum; the dark brown residue was extracted with hexane/toluene (~1:2 ratio) and filtered into a vial. Cooling the solution to -30°C resulted in crystallisation of the Ph_4Sn by-product. Following filtration, the solution was again cooled to -30°C, resulting in the formation of a second crop of crystals. ^1H NMR spectroscopy revealed the crystals to be a co-crystallised mixture of compounds **11** and **12**. A suitable single crystal of the former compound was selected under the microscope, confirming the structure of the asymmetrical dimeric stannyl-calcium hydride **11**. ^1H NMR (500 MHz, C_6D_6) δ 7.39 (dd, J = 7.7 Hz, 1.2 Hz, $^3J_{1H\text{-}117/119Sn}$ = 24.4 Hz, 6H, *o*-$(C_6H_5)_3$Sn), 7.1 (m, 12H, NAr-C*H*), 7.05 (m, 3H, *p*-$(C_6H_5)_3$Sn) 6.88 (m, 6H *m*-$(C_6H_5)_3$Sn), 4.75 (s, 2H, NC(CH_3)C*H*), 3.83 (s, $^2J_{1H\text{-}117/119Sn}$ = 93.7 Hz, 1H, Ca-*H*), 3.13 (hept, J = 6.8 Hz, 8H, $(H_3C)_2$C*H*), 1.60 (s, 12H, NC(C*H*$_3$)CH), 1.26

(d, J = 6.8 Hz, 24H, (H_3C)$_2$CH), 1.18 (d, J = 6.8 Hz, 24H, (H_3C)$_2$CH). ^{13}C NMR (126 MHz, C_6D_6) δ 166.14 (N*C*(CH$_3$)CH), 145.61 (NAr-C$_{ipso}$), 142.09 (NAr-C$_{ortho}$), 139.20 (*o*-Sn(*C*$_6$H$_5$)$_3$), 127.97 (*m*-Sn(*C*$_6$H$_5$)), 125.75 (*p*-Sn(*C*$_6$H$_5$)), 125.43 (NAr-C$_{para}$), 124.25 (NAr-C$_{meta}$), 95.21 (NC(CH$_3$)*C*H), 28.66 ((H$_3$C)$_2$*C*H), 25.61 ((H$_3$*C*)$_2$CH), 24.53 (NCC*H$_3$*), 24.47 ((H$_3$*C*)$_2$CH). ^{119}Sn NMR (186 MHz, C_6D_6) δ -139.82. Meaningful elemental analysis could not be obtained due to co-crystallisation with compound **12**, preventing isolation of the pure compound.

4.4.2 Reaction of VId with 2 equivalents Ph_3SnH and crystallisation of compound 12.

A solution of 12 mg Ph_3SnH (0.034 mmol) in 0.3 ml C_6D_6 was added to a J. Young's NMR tube containing 11 mg **VId** (0.016 mmol) in 0.3 ml C_6D_6. The reaction mixture immediately became a pale-yellow colour, which darkened to orange over the course of two hours at room temperature. The solvent was removed under vacuum, the resulting residue was extracted with a hexane/toluene mixture and filtered. Cooling the solution to -30°C resulted in the formation of air-sensitive colourless block-like crystals of compound **12** suitable for single-crystal X-ray diffraction analysis. Yield 5.1 mg, 20%. ^{1}H NMR (300 MHz, C_6D_6) δ 8.01 (d, *J* = 7.4 Hz, 12H, *o*-(C$_6$*H*$_5$)$_3$Sn), 7.34 (t, *J* = 7.2 Hz, 12H, *m*-(C$_6$*H*$_5$)$_3$Sn), 7.23 – 7.12 (6H, *p*-(C$_6$*H*$_5$)$_3$Sn), 7.08 (m, 12H, NAr-C*H*), 5.02 (s, 2H, NC(CH$_3$)C*H*), 2.97 (m, 8H, (H$_3$C)$_2$C*H*), 1.71 (s, 12H, NC(C*H$_3$*)CH), 1.17 (d, *J* = 6.9 Hz, 24H, (*H$_3$*C)$_2$CH), 0.90 (d, *J* = 6.6 Hz, 24H, (*H$_3$*C)$_2$CH). ^{13}C{^{1}H} NMR (126 MHz, d$_8$-toluene) δ 165.92 (N*C*(CH$_3$)CH), 155.50 (*i*-(*C*$_6$H$_5$)$_3$Sn), 146.66 (NAr-C$_{ipso}$), 142.46 (NAr-C$_{ortho}$), 138.42 (*o*-(*C*$_6$H$_5$)$_3$Sn), 127.52 (*m*-(*C*$_6$H$_5$)$_3$Sn), 126.03 (*p*-(*C*$_6$H$_5$)$_3$Sn), 124.19 (NAr-C$_{para}$), 123.95 (NAr-C$_{meta}$), 91.23 (NC(CH$_3$)*C*H), 28.51 ((H$_3$C)$_2$*C*H), 24.77 (NC(*C*H$_3$)CH), 24.45 ((H$_3$*C*)$_2$CH), 24.41 ((H$_3$*C*)$_2$CH). ^{119}Sn{^{1}H} (186 MHz, d$_8$-toluene) δ -160.56 ppm. Meaningful elemental analysis could not be obtained due to co-crystallisation with compound **11**, preventing isolation of the pure compound.

4.4.3 Attempted preparative (Schlenk) scale synthesis of compound 11

From $(Ph_3Sn)_2$: In the glove box, a Schlenk flask was charged with 100 mg **VId** (0.109 mmol) and 76 mg $(Ph_3Sn)_2$. Toluene (3 ml) was added with stirring, resulting in a slightly cloudy pale-yellow solution, which was stirred for 16 h at room temperature, during which time it developed a brown colouration. Volatiles were removed under vacuum, and the product was extracted into hexane in order to separate it from the Ph_4Sn by-product. The resulting orange solution was evaporated to dryness under vacuum, yielding compound **11** in approx. 75% purity, contaminated with **VId**, **12**, and [(BDI)$_2$Ca]. Although recrystallisation of the crude product from a hexane/toluene mixture was undertaken, the resulting product was a mixture of compounds **11** and **12**. When a C_6D_6 solution of the crude product was left to stand at room temperature for five days, further redistribution occurred, with the solution containing a mixture of **11**, **12**, and **XXXIX** in an approximate 3:2:2 ratio.

From Ph_3SnH: In a Schlenk flask in the glove box, 100 mg **VId** (0.109 mmol) was dissolved in 2 ml toluene with stirring. Ph_3SnH (76 mg, 0.218 mmol) was dissolved in 2 ml toluene in a vial, then added *via* pipette. The resulting yellow solution was stirred for 3 h, after which the procedure was followed as described above for the reaction with $(Ph_3Sn)_2$. Yield 83 mg, orange powder.

4.4.4 Reaction of VId with four equivalents of Ph_3SnH.

To a J. Young's NMR tube containing 10 mg **VId** (0.0109 mmol) was added a 0.5 ml C_6D_6 solution of Ph_3SnH (15.4 mg, 0.0436 mmol). The reaction bubbled immediately and became pale yellow. The reaction mixture was heated to 40°C for 3 hours. Subsequent analysis by ^1H and $^{119}Sn\{^1H\}$ NMR spectroscopy revealed almost quantitative conversion to compound **11** and Ph_4Sn. Further heating at 40°C for a further 3 days result in partial conversion to compounds **12** and **XXXIX**.

4.4.5 Reaction of compound 11 with *n*Bu_3SnH.

A 0.5 ml C_6D_6 solution containing 11.5 mg Ph_3SnH (0.032 mmol) was added to a J. Young's NMR tube containing 15 mg **VId** (0.016 mmol), resulting in immediate and vigorous release of H_2 gas. After 5 hours at room temperature, 4.2 µl *n*Bu_3SnH (0.032 mmol) was added. After a further hour at room temperature, analysis by ^1H and $^{119}Sn\{^1H\}$ NMR spectroscopy revealed a mixture of *n*Bu_3SnPh, *n*Bu_3SnH, Ph_4Sn, and compound **11**. After standing for 40 hours, the reaction mixture became black and opaque, with complete conversion of *n*Bu_3SnH to Bu_3SnPh, along with the formation of **XXXIX** and small quantities of **VId** in addition to unreacted **11** and Ph_4Sn.

4.4.6 Reaction of VId with Ph_2SnH_2

A solution of Ph_2SnH_2 (10 µl, 0.052 mmol) in 0.6 ml C_6D_6 was added to a J. Young's NMR tube containing 24 mg **VId** (0.026 mmol). The reaction mixture bubbled and immediately became orange in colour. Analysis of the reaction mixture after approx. 30 minutes by $^{119}Sn\{^1H\}$ NMR spectroscopy showed complete consumption of Ph_2SnH_2 to Ph_4Sn and **11**. After 16 hours at room temperature, the reaction became a dark brown turbid mixture. ^1H NMR spectroscopy showed the presence of **VId**, $[(BDI)_2Ca]$, **12**, and **11** in a 10:1:6:2 ratio, whilst the $^{119}Sn\{^1H\}$ showed a slight increase in concentration of **12**.

4.4.7 Catalytic reaction of Ph_2SnH_2 with VId

Ph_2SnH_2 (19 µl, 0.10 mmol) was added to a J. Young's NMR tube containing a C_6D_6 solution (0.6 ml) of **VId** (4.6 mg, 0.005 mmol). The reaction mixture bubbled vigorously and rapidly became first orange in colour, then black after 10 minutes. Analysis of the reaction mixture after approx. 60 minutes by $^{119}Sn\{^1H\}$ NMR spectroscopy showed partial conversion of Ph_2SnH_2 to Ph_3SnH. After 16 hours at room temperature, most of the Ph_2SnH_2 was consumed,

with Ph_3SnH as the major product and Ph_4Sn as a minor product. After a further 4 days at room temperature, almost complete conversion to Ph_4Sn as the only soluble tin-containing product was observed.

4.4.8 Reaction of VId with $MesSnH_3$

To a J. Young's NMR tube containing 0.5 ml of a C_6D_6 solution of $MesSnH_3$ (12.5 mg, 0.052 mmol) was added 24 mg **VId** (0.026 mmol). The reaction mixture immediately became orange and bubbled vigorously. After a few minutes, the reaction mixture became opaque and dark brown then black. Subsequent analysis by ^1H NMR showed predominantly **XXXIX** and other poorly defined products. The $^{119}Sn\{^1H\}$ NMR spectrum did not contain any observable resonances.

4.4.9 Reaction of VId with Ph_4Sn

A J. Young's NMR tube was charged with 10 mg **VId** (0.0109 mmol) and 3, 5, or 19 mg Ph_4Sn (0.073, 0.011, 0.044 mmol respectively). C_6D_6 (0.6 ml) was added, and the reaction monitored by ^1H and $^{119}Sn\{^1H\}$ NMR spectroscopy. Approximately 50% conversion of **VId** could be achieved after 24 hours at 25-35°C, with **13** and **11** as the major products. Elevated temperatures (40°C) and extended reaction times (up to five days) did not significantly increase the spectroscopic yield either product but led to the formation of small quantities of **12** and large quantities of **XXXIX**.

4.4.10 Reaction of Vb with Ph_4Sn

15.7 mg Ph_4Sn (0.0368 mmol) was added to a J. Youngs' NMR tube containing 20 mg **Vb** (0.0184 mmol) and 0.6 ml C_6D_6. The reaction mixture was heated to 40°C for 48 hours, after which ^1H NMR spectroscopy revealed almost complete conversion to **XXXIX**. $^{119}Sn\{^1H\}$ NMR spectroscopy showed the partial consumption of Ph_4Sn, and formation of $(Hex)SnPh_3$, which was identified by comparison to literature NMR spectra.[91]

4.4.11 Reaction of VId with $(Ph_3Sn)_2$

A J. Young's NMR tube was charged with 20.0 mg **VId** (0.0218 mmol) and 15.3 mg $(Ph_3Sn)_2$ (0.0218 mmol). C_6D_6 (0.6 ml) was added and the tube shaken, the reaction mixture bubbled, and full conversion of both starting materials was observed by ^1H and ^{119}Sn NMR spectroscopy after approximately four hours. **11** was the only BDI-containing product, with Ph_4Sn also observed as a by-product. Initially pale yellow, the reaction mixture darkened over time, eventually becoming turbid and dark brown in colour. ^1H and $^{119}Sn\{^1H\}$ NMR spectroscopy showed that on standing for extended periods of time (>24 h.), **12** was gradually formed. Although crystallisation of the reaction products from toluene or a toluene/hexane mixture generally resulted in the co-crystallisation of both **11** and **12** contaminated with Ph_4Sn, this

could be partially avoided through filtering and discarding the first crop of crystals (predominantly Ph_4Sn) from the reaction mixture.

4.4.12 Reaction of Vb with $(Ph_3Sn)_2$

C_6D_6 (0.6 ml) was added to a J. Young's NMR tube containing 10.3 mg $(Ph_3Sn)_2$ (0.0147 mmol) and 8.0 mg **Vb** (0.0073 mmol). The reaction mixture was heated to 40°C for 48 hours, after which ^{1}H and $^{119}Sn\{^{1}H\}$ NMR spectroscopy revealed that most of the starting material had been converted to **XXXIX** and (Hex)$SnPh_3$, along with minor quantities **12** and Ph_4Sn.

4.4.13 Synthesis of compound 14

To a J. Young's NMR tube containing 20 mg **VId** (0.0218 mmol) and 15.3 mg $(Ph_3Sn)_2$ (0.0218 mmol) was added 0.6 ml C_6D_6. After 6 hours, analysis by ^{1}H and $^{119}Sn\{^{1}H\}$ NMR spectroscopy revealed complete conversion to **11** and Ph_4Sn. Ph_3PO, 6.1 mg (0.0218 mmol) was added and the reaction mixture was left for 24 hours, during which time it took on a turbid dark brown appearance. The solvent was removed under vacuum and the residue taken up in toluene/hexane (1:1, 0.5 ml), from which crystals of **14** suitable for single-crystal X-ray diffraction analysis were obtained colourless blocks at room temperature. Crystals of the known compound **XIX** were also obtained from the same sample, and identified by comparison of the unit cell with that reported in the literature.[97] Yield 8 mg, 17%. Analysis calculated for $C_{65}H_{71}CaN_2OPSn$: C 71.89, H 6.59, N 2.58. Found: C 69.82, H 6.61, N 2.78. ^{1}H NMR (500 MHz, C_6D_6) δ 8.11 (d, J = 7.3 Hz, 6H, *o*-$(C_6H_5)_3Sn$), 7.30 (t, J = 7.2 Hz, 6H, *m*-$(C_6H_5)_3Sn$), 7.22 (t, J = 7.1 Hz, 3H, *p*-$(C_6H_5)_3Sn$), 7.12 (d, J = 7.5 Hz, 4H, NAr_{meta}), 7.06 (t, J = 7.7 Hz, 2H, NAr_{para}), 7.04-6.94 (m, 9H, *m*+*p*-$(C_6H_5)_3PO$), 6.84 (m, 6H, *o*-$(C_6H_5)_3PO$), 5.23 (s, 1H, $NC(CH_3)CH$), 3.29 (hept, J = 6.4 Hz, 4H, $(H_3C)_2CH$), 1.84 (s, 6H, $NC(CH_3)CH$), 1.19 (d, J = 6.8 Hz, 6H, $(H_3C)_2CH$), 1.04 (d, J = 7.0 Hz, 6H, $(H_3C)_2CH$), 0.94 (d, J = 6.8 Hz, 6H, $(H_3C)_2CH$), 0.87 (d, J = 6.6 Hz, 6H, $(H_3C)_2CH$). $^{13}C\{^{1}H\}$ NMR (126 MHz, C_6D_6) δ 165.81 ($NC(CH_3)CH$), 156.49 (*i*-$Sn(C_6H_5)_3$), 146.91 (NAr-C_{ipso}), 141.88 (NAr-C_{ortho}), 141.30 (NAr-C_{ortho}), 138.85 (*o*-$Sn(C_6H_5)_3$), 133.02 (d, J_{31P} = 2.9 Hz, *p*-$(C_6H_5)_3PO$), 131.89 (d, J_{31P} = 11.0 Hz, *m*-$(C_6H_5)_3PO$), 129.35 (d, J_{31P} = 12.8 Hz, *o*-$(C_6H_5)_3PO$), 129.02 (d, J_{31P} = 107.3 Hz, *i*-$(C_6H_5)_3PO$), 127.80 (*m*-$Sn(C_6H_5)_3$), 125.88 (*p*-$Sn(C_6H_5)_3$), 124.15 (NAr-C_{meta}), 123.96 (NAr-C_{para}), 123.64 (NAr-C_{meta}), 90.49 ($NC(CH_3)CH$), 28.90 ($(H_3C)_2CH$), 28.12 ($(H_3C)_2CH$), 26.41 ($(H_3C)_2CH$), 24.71 ($NCCH_3$), 24.63 ($(H_3C)_2CH$), 24.38 ($(H_3C)_2CH$), 22.96 ($(H_3C)_2CH$). $^{119}Sn\{^{1}H\}$ NMR (186 MHz, C_6D_6) δ -146 (d, $^{3}J_{31P}$ = 10 Hz). $^{31}P\{^{1}H\}$ NMR (202 MHz, C_6D_6) δ 36.4 (s, satellite peaks: d, $^{3}J_{117/119Sn}$ = 10 Hz).

Single-step procedure: A J. Young's NMR tube was charged with 20 mg **VId** (0.0218 mmol) and 13.5 mg Ph_3PO (0.0437 mmol) and a C_6D_6 solution (0.6 ml) containing Ph_3SnH (15.3 mg,

0.0438 mmol) was added. The reaction mixture bubbled and immediately became a deep red colour. The reaction mixture was left to stand at room temperature for 16 h, after which it had turned yellow. Analysis by ^{1}H, $^{119}Sn\{^{1}H\}$, and $^{31}P\{^{1}H\}$ NMR spectroscopy showed formation of **14** in almost quantitative spectroscopic yield. After removing volatiles under vacuum, the crude product was recrystallised from a concentrated toluene solution at -30°C and washed with minimal toluene. Yield 10 mg, 21%.

4.4.14 Reaction of VId with Bu_3SnH

5.86 µl *n*Bu_3SnH (0.0436 mmol) was added to a J. Young's NMR tube containing a 0.6 ml C_6D_6 solution of 20 mg **VId** (0.0218 mmol). The reaction was left at room temperature and monitored by ^{1}H and $^{119}Sn\{^{1}H\}$ NMR spectroscopy over a period of 5 days.[14]

4.4.15 Reaction of VId with *t*Bu_2SnH_2

10.6 µl *t*Bu_2SnH_2 (0.0436 mmol) was added to an NMR tube containing either 10 mg (0.0109 mmol) or 20 mg (0.0218 mmol) **VId** dissolved in 0.6 ml C_6D_6. The reaction was monitored by ^{1}H and $^{119}Sn\{^{1}H\}$ NMR spectroscopy and the products identified by comparison to the literature.[98]

4.4.16 General procedure for NMR-scale catalytic dehydrocoupling of alkyl stannanes.

20 µl of the alkyl stannane was added to a J. Young's NMR tube containing a 0.5 ml C_6D_6 solution of **VId** (2.5-5 mol%). The NMR tube was protected from light with aluminium foil and the reaction was monitored by ^{1}H and $^{119}Sn\{^{1}H\}$ NMR spectroscopy. The products were identified by comparison of the *in situ* NMR spectra with literature values.[14, 98]

4.4.17 Reaction of VId with $(Bu_3Sn)_2$

11.2 µl $(Bu_3Sn)_2$ (0.0218 mmol) was added to a J. Young's NMR tube containing 10 mg **VId** (0.0109 mmol) in 0.5 ml C_6D_6. The reaction was left at room temperature for 16 h then analysed by ^{1}H and $^{119}Sn\{^{1}H\}$ NMR spectroscopy.

4.4.18 X-ray crystallography

Identification code	**11**	**12**	**14**
Empirical formula	$C_{86}H_{113}Ca_2N_4Sn$	$C_{61}H_{72}CaN_2Sn$	$C_{65}H_{71}CaN_2OPSn$
Formula weight	1401.65	991.97	1085.97
Temperature/K	150.00(10)	150.00(10)	150.00(10)
Crystal system	monoclinic	triclinic	monoclinic
Space group	$P2_1/n$	P-1	$P2_1/c$
a/Å	23.4972(2)	11.7067(3)	13.8086(1)
b/Å	15.1546(1)	13.9755(4)	16.6672(1)
c/Å	24.4653(2)	17.1606(5)	25.6761(2)
α/°	90	76.575(3)	90
β/°	114.523(1)	86.913(2)	103.509(1)
γ/°	90	76.718(2)	90
Volume/Å^3	7926.00(12)	2657.83(13)	5745.88(7)
Z	4	2	4
ρ_{calc}g/cm^3	1.175	1.240	1.255
μ/mm^{-1}	4.022	4.950	4.895
F(000)	2988.0	1044.0	2272.0
Crystal size/mm^3	0.219 × 0.069 × 0.064	0.33 × 0.174 × 0.127	0.113 × 0.064 × 0.021
Radiation	CuKα (λ = 1.54184)	CuKα (λ = 1.54184)	CuKα (λ = 1.54184)
2Θ range for data collection/°	6.818 to 146.172	6.672 to 146.364	6.376 to 146.87
Index ranges	-28 ≤ h ≤ 29, -18 ≤ k ≤ 18, -27 ≤ l ≤ 30	-14 ≤ h ≤ 14, -17 ≤ k ≤ 15, -21 ≤ l ≤ 21	-17 ≤ h ≤ 16, -20 ≤ k ≤ 20, -28 ≤ l ≤ 31
Reflections collected	110586	32255	76338
Independent reflections	15819 [R_{int} = 0.0427, R_{sigma} = 0.0224]	10578 [R_{int} = 0.0378, R_{sigma} = 0.0350]	11514 [R_{int} = 0.0532, R_{sigma} = 0.0315]
Data/restraints/parameters	15819/120/892	10578/410/742	11514/11/692
Goodness-of-fit on F^2	1.029	1.056	1.017
Final R indexes [I>=2σ (I)]	R_1 = 0.0324, wR_2 = 0.0834	R_1 = 0.0415, wR_2 = 0.1080	R_1 = 0.0304, wR_2 = 0.0682
Final R indexes [all data]	R_1 = 0.0374, wR_2 = 0.0870	R_1 = 0.0454, wR_2 = 0.1117	R_1 = 0.0381, wR_2 = 0.0711
Largest diff. peak/hole / e Å^{-3}	0.69/-0.41	2.06/-1.22	0.50/-0.48

Notes on crystallographic refinement:

The asymmetric unit in **11** contains one molecule of the organometallic complex, one molecule of toluene and one molecule of hexane with half site-occupancy. The latter is disordered with itself about a crystallographic inversion centre – and was ultimately modelled using Kratzert's FragmentDB plugin for Olex2.[100] The hydride (H1) in the main feature was located and refined without restraints.

The asymmetric unit in **12** comprises half of one dimer molecule and 3 solvent regions that are additively equivalent to two toluene molecules. Carbon atoms C13, C14, C16 and C17 in the main feature were modelled to take account of 50:50 disorder. The toluene based on C48/C48A was also modelled to take account of 50:50 disorder, while the entities based on C2_1 and C2_2 (both crystallographically disordered) were treated using Kratzert's Fragment-DB algorithm.[100] ADP and distance restraints were employed in disordered areas, to assist in achieving a chemically sensible convergence. The highest residual electron density peak is a ripple associated with the tin centre.

The hydrogen atoms attached to C27 and C28 in the structure of **14** were located and refined at a distance of 0.98 Å from their respective parent atoms, and the *iso*-propyl group based on

C24 was disordered in its entirety in a 70:30 ratio. Distance and ADP restraints were included in the disordered region, to assist convergence.

4.5 Computational details

DFT calculations were performed by Dr Nasir Rajabi and Dr Claire McMullin at the University of Bath and were run with Gaussian 09 (Revision D.01).[101] The Ca and Sn centres were described with the Stuttgart RECPs and associated basis sets,[102] and 6-31G** basis sets were used for all other atoms (BS1).[103, 104] A polarization function was also added to Sn (ζd = 0.180). Initial BP86[105, 106] optimizations were performed using the 'grid = ultrafine' option, with all stationary points being fully characterized via analytical frequency calculations as either minima (all positive eigenvalues) or transition states (one negative eigenvalue). IRC calculations and subsequent geometry optimizations were used to confirm the minima linked by each transition state. All energies were recomputed with a larger basis set (BS2) featuring cc-pVTZ for Ca, cc-pVTZ-PP for Sn and 6-311++G** on the other atoms. Corrections for the effect of benzene (ε = 2.2706) solvent were run using the polarizable continuum model and BS2.[107] Single-point dispersion corrections to the BP86 results employed Grimme's D3 parameter set with Becke-Johnson damping as implemented in Gaussian.[108] The BP86-optimised geometries of **11**, **12**, $\mathbf{TS_{EF}}$, and **F** were used for the NBO (Natural Bonding Orbital) studies to generate molecular orbital diagrams.

4.6 References

1. S. Adams and M. Dräger, *Angewandte Chemie-International Edition in English*, 1987, **26**, 1255-1256.
2. K. Takeda and K. Shiraishi, *Chemical Physics Letters*, 1992, **195**, 121-126.
3. V. Y. Lu and T. D. Tilley, *Macromolecules*, 2000, **33**, 2403-2412.
4. M. Trummer, F. Choffat, P. Smith and W. Caseri, *Macromolecular Rapid Communications*, 2012, **33**, 448-460.
5. S. Harrypersad, L. Liao, A. Khan, R. S. Wylie and D. A. Foucher, *Journal of Inorganic and Organometallic Polymers and Materials*, 2015, **25**, 515-528.
6. J. Pau, A. J. Lough, R. S. Wylie, R. A. Gossage and D. A. Foucher, *Chemistry-a European Journal*, 2017, **23**, 14367-14374.
7. N. Devylder, M. Hill, K. C. Molloy and G. J. Price, *Chemical Communications*, 1996, 711-712.
8. P. R. Deacon, N. Devylder, M. S. Hill, M. F. Mahon, K. C. Molloy and G. J. Price, *Journal of Organometallic Chemistry*, 2003, **687**, 46-56.
9. M. Okano and K. Watanabe, *Electrochemistry Communications*, 2000, **2**, 471-474.
10. M. Okano, K. Watanabe and S. Totsuka, *Electrochemistry*, 2003, **71**, 257-259.
11. L. R. Sita, *Organometallics*, 1992, **11**, 1442-1444.
12. J. S. Dhindsa, B. F. Jacobs, A. J. Lough and D. A. Foucher, *Dalton Transactions*, 2018, **47**, 14094-14100.
13. S. Harrypersad and D. Foucher, *Chemical Communications*, 2015, **51**, 7120-7123.
14. A. Khan, R. A. Gossage and D. A. Foucher, *Canadian Journal of Chemistry-Revue Canadienne De Chimie*, 2010, **88**, 1046-1052.

15. T. Imori and T. D. Tilley, *Journal of the Chemical Society-Chemical Communications*, 1993, 1607-1609.
16. T. Imori, V. Lu, H. Cai and T. D. Tilley, *Journal of the American Chemical Society*, 1995, **117**, 9931-9940.
17. H. G. Woo, J. M. Park, S. J. Song, S. Y. Yang, I. S. Kim and W. G. Kim, *Bulletin of the Korean Chemical Society*, 1997, **18**, 1291-1295.
18. H. G. Woo, S. J. Song and B. H. Kim, *Bulletin of the Korean Chemical Society*, 1998, **19**, 1161-1164.
19. F. Choffat, P. Smith and W. Caseri, *Journal of Materials Chemistry*, 2005, **15**, 1789-1792.
20. F. Choffat, S. Kaeser, P. Wolfer, D. Schmid, R. Mezzenga, P. Smith and W. Caseri, *Macromolecules*, 2007, **40**, 7878-7889.
21. T. Imori and T. D. Tilley, *Polyhedron*, 1994, **13**, 2231-2243.
22. H. G. Woo, J. F. Walzer and T. D. Tilley, *Journal of the American Chemical Society*, 1992, **114**, 7047-7055.
23. H. G. Woo, R. H. Heyn and T. D. Tilley, *Journal of the American Chemical Society*, 1992, **114**, 5698-5707.
24. J. Guihaume, C. Raynaud, O. Eisenstein, L. Perrin, L. Maron and T. D. Tilley, *Angewandte Chemie-International Edition*, 2010, **49**, 1816-1819.
25. N. R. Neale and T. D. Tilley, *Tetrahedron*, 2004, **60**, 7247-7260.
26. N. R. Neale and T. D. Tilley, *Journal of the American Chemical Society*, 2002, **124**, 3802-3803.
27. C. Tamborski and E. J. Soloski, *Journal of the American Chemical Society*, 1961, **83**, 3734.
28. R. Hummeltenberg, K. Jurkschat and F. Uhlig, *Phosphorus Sulfur and Silicon and the Related Elements*, 1997, **123**, 255-261.
29. C. Kayser, R. Klassen, M. Schurmann and F. Uhlig, *Journal of Organometallic Chemistry*, 1998, **556**, 165-167.
30. U. Hermann, M. Schurmann and F. Uhlig, *Journal of Organometallic Chemistry*, 1999, **585**, 211-214.
31. H. M. J. C. Creemers, J. G. Noltes and G. J. M. van der Kerk, *Journal of Organometallic Chemistry*, 1968, **14**, 217-221.
32. J. C. Lahournere and J. Valade, *Journal of Organometallic Chemistry*, 1970, **22**, C3-C4.
33. M. Westerhausen and T. Hildenbrand, *Journal of Organometallic Chemistry*, 1991, **411**, 1-17.
34. M. Westerhausen, *Angewandte Chemie-International Edition in English.*, 1994, **33**, 1493-1495.
35. U. Englich, K. Ruhlandt-Senge and F. Uhlig, *Journal of Organometallic Chemistry*, 2000, **613**, 139-147.
36. S. Harder and J. Brettar, *Angewandte Chemie-International Edition*, 2006, **45**, 3474-3478.
37. P. Jochmann, J. P. Davin, T. P. Spaniol, L. Maron and J. Okuda, *Angewandte Chemie-International Edition*, 2012, **51**, 4452-4455.
38. V. Leich, T. P. Spaniol and J. Okuda, *Inorganic Chemistry*, 2015, **54**, 4927-4933.
39. V. Leich, T. P. Spaniol, L. Maron and J. Okuda, *Angewandte Chemie-International Edition*, 2016, **55**, 4794-4797.
40. A. Causero, G. Ballmann, J. Pahl, H. Zijlstra, C. Farber and S. Harder, *Organometallics*, 2016, **35**, 3350-3360.
41. B. Maitland, M. Wiesinger, J. Langer, G. Ballmann, J. Pahl, H. Elsen, C. Farber and S. Harder, *Angewandte Chemie-International Edition*, 2017, **56**, 11880-11884.
42. D. Schuhknecht, C. Lhotzky, T. P. Spaniol, L. Maron and J. Okuda, *Angewandte Chemie-International Edition*, 2017, **56**, 12367-12371.
43. A. Causero, G. Ballmann, J. Pahl, C. Färber, J. Intemann and S. Harder, *Dalton Transactions*, 2017, **46**, 1822-1831.

44. A. S. S. Wilson, M. S. Hill, M. F. Mahon, C. Dinoi and L. Maron, *Science*, 2017, **358**, 1168-1171.
45. H. Bauer, M. Alonso, C. Farber, H. Elsen, J. Pahl, A. Causero, G. Ballmann, F. De Proft and S. Harder, *Nature Catalysis*, 2018, **1**, 40-47.
46. A. S. S. Wilson, M. S. Hill and M. F. Mahon, *Organometallics*, 2019, **38**, 351-360.
47. J. Dyall, M. S. Hill, M. F. Mahon, L. Teh and A. S. S. Wilson, *Dalton Transactions*, 2019, **48**, 4248-4254.
48. X. H. Shi, G. R. Qin, Y. Wang, L. X. Zhao, Z. Z. Liu and J. Cheng, *Angewandte Chemie-International Edition*, 2019, **58**, 4356-4360.
49. F. G. N. Cloke, P. B. Hitchcock, M. F. Lappert, G. A. Lawless and B. Royo, *Journal of the Chemical Society-Chemical Communications*, 1991, 724-726.
50. C. Eaborn, S. A. Hawkes, P. B. Hitchcock and J. D. Smith, *Chemical Communications*, 1997, 1961-1962.
51. F. Feil and S. Harder, *Organometallics*, 2000, **19**, 5010-5015.
52. S. Harder, F. Feil and K. Knoll, *Angewandte Chemie-International Edition*, 2001, **40**, 4261-4264.
53. S. Harder, F. Feil and A. Weeber, *Organometallics*, 2001, **20**, 1044-1046.
54. M. R. Crimmin, A. G. M. Barrett, M. S. Hill, D. J. MacDougall, M. F. Mahon and P. A. Procopiou, *Chemistry - A European Journal*, 2008, **14**, 11292-11295.
55. M. P. Coles, S. E. Sozeril, J. D. Smith, P. B. Hitchcock and I. J. Day, *Organometallics*, 2009, **28**, 1579-1581.
56. M. R. Crimmin, A. G. M. Barrett, M. S. Hill, D. J. MacDougall, M. F. Mahon and P. A. Procopiou, *Dalton Transactions*, 2009, 9715-9717.
57. K. Yan, G. Schoendorff, B. M. Upton, A. Ellern, T. L. Windus and A. D. Sadow, *Organometallics*, 2013, **32**, 1300-1316.
58. M. Kohler, A. Koch, H. Gorls and M. Westerhausen, *Organometallics*, 2016, **35**, 242-248.
59. I. V. Basalov, B. Liu, T. Roisnel, A. V. Cherkasov, G. K. Fukin, J. F. Carpentier, Y. Sarazin and A. A. Trifonov, *Organometallics*, 2016, **35**, 3261-3271.
60. A. Koch, M. Wirgenings, S. Krieck, H. Gorls, G. Pohnert and M. Westerhausen, *Organometallics*, 2017, **36**, 3981-3986.
61. B. M. Wolf, C. Stuhl, C. Maichle-Mossmer and R. Anwander, *Journal of the American Chemical Society*, 2018, **140**, 2373-2383.
62. J. L. Wardell, in *Chemistry of Tin*, ed. P. J. Smith, Springer Science, Dordrecht, 2 edn., 1998, ch. 4, pp. 95-137.
63. K. C. Molloy, in *Chemistry of Tin*, ed. P. J. Smith, Springer Science, Dordrecht, 2 edn., 1998, ch. 5, pp. 138-175.
64. M. S. Hill, D. J. Liptrot and C. Weetman, *Chemical Society Reviews*, 2016, **45**, 972-988.
65. A. S. S. Wilson, C. Dinoi, M. S. Hill, M. F. Mahon and L. Maron, *Angewandte Chemie-International Edition*, 2018, **57**, 15500-15504.
66. B. Wrackmeyer, *Annual Reports on NMR Spectroscopy,* 1999, **38**, 203-264.
67. S. C. Rosca, C. Dinoi, E. Caytan, V. Dorcet, M. Etienne, J. F. Carpentier and Y. Sarazin, *Chemistry-a European Journal*, 2016, **22**, 6505-6509.
68. S. C. Rosca, E. Caytan, V. Dorcet, T. Roisnel, J. F. Carpentier and Y. Sarazin, *Organometallics*, 2017, **36**, 1269-1277.
69. S. C. Rosca, V. Dorcet, T. Roisnel, J. F. Carpentier and Y. Sarazin, *Dalton Transactions*, 2017, **46**, 14785-14794.
70. S. C. Rosca, V. Dorcet, J. F. Carpentier and Y. Sarazin, *Inorganica Chimica Acta*, 2018, **475**, 59-64.
71. M. F. Zuniga, G. B. Deacon and K. Ruhlandt-Senge, *Inorganic Chemistry*, 2008, **47**, 4669-4681.
72. W. D. Buchanan and K. Ruhlandt-Senge, *Chemistry-a European Journal*, 2013, **19**, 10708-10715.

73. W. D. Buchanan, D. G. Allis and K. Ruhlandt-Senge, *Chemical Communications*, 2010, **46**, 4449-4465.
74. J. Pahl, S. Brand, H. Elsen and S. Harder, *Chemical Communications*, 2018, **54**, 8685-8688.
75. J. Pahl, A. Friedrich, H. Eisen and S. Harder, *Organometallics*, 2018, **37**, 2901-2909.
76. L. Garcia, M. D. Anker, M. F. Mahon, L. Maron and M. S. Hill, *Dalton Transactions*, 2018, **47**, 12684-12693.
77. C. Loh, S. Seupel, H. Gorls, S. Krieck and M. Westerhausen, *Organometallics*, 2014, **33**, 1480-1491.
78. C. Loh, S. Seupel, A. Koch, H. Gorls, S. Krieck and M. Westerhausen, *Dalton Transactions*, 2014, **43**, 14440-14449.
79. S. O. Hauber, F. Lissner, G. B. Deacon and M. Niemeyer, *Angewandte Chemie-International Edition*, 2005, **44**, 5871-5875.
80. D. J. Duncalf, P. B. Hitchcock and G. A. Lawless, *Journal of Organometallic Chemistry*, 1996, **506**, 347-349.
81. M. S. Hill, M. F. Mahon, A. S. S. Wilson, C. Dinoi, L. Maron and E. Richards, *Chemical Communications*, 2019, **55**, 5732-5735.
82. L. Garcia, C. Dinoi, M. F. Mahon, L. Maron and M. Hill, *Chemical Science*, 2019, **10**, 8108-8118.
83. S. Harder, *Organometallics*, 2002, **21**, 3782-3787.
84. A. S. S. Wilson, PhD thesis, University of Bath, 2018.
85. I. Castillo and T. D. Tilley, *Journal of the American Chemical Society*, 2001, **123**, 10526-10534.
86. I. Castillo and T. D. Tilley, *Organometallics*, 2000, **19**, 4733-4739.
87. I. Castillo and T. D. Tilley, *Organometallics*, 2001, **20**, 5598-5605.
88. A. D. Sadow and T. D. Tilley, *Organometallics*, 2001, **20**, 4457-4459.
89. C. Zeppek, J. Pichler, A. Torvisco, M. Flock and F. Uhlig, *Journal of Organometallic Chemistry*, 2013, **740**, 41-49.
90. B. Rosch, T. X. Gentner, H. Elsen, C. A. Fischer, J. Langer, M. Wiesinger and S. Harder, *Angewandte Chemie-International Edition*, 2019, **58**, 5396-5401.
91. G. M. Allan, R. A. Howie, J. N. Low, J. M. S. Skakle, J. L. Wardell and S. Wardell, *Polyhedron*, 2006, **25**, 695-701.
92. A.-F. Pecharman, A. L. Colebatch, M. S. Hill, C. L. Mcmullin, M. F. Mahon and C. Weetman, *Nature Communications*, 2017, **8**, 15022.
93. K. Yuvaraj, I. Douair, A. Paparo, L. Maron and C. Jones, *Journal of the American Chemical Society*, 2019, **141**, 8764-8768.
94. A.-F. Pecharman, N. A. Rajabi, M. S. Hill, C. L. McMullin and M. F. Mahon, *Chemical Communications*, 2019, **55**, 9035-9038.
95. A. C. T. Kuate, R. A. Lalancette, T. Bannenberg and F. Jäkle, *Angewandte Chemie-International Edition*, 2018, **57**, 6552-6557.
96. J. W. Chen, D. A. M. Parra, R. A. Lalancette and F. Jäkle, *Angewandte Chemie-International Edition*, 2015, **54**, 10202-10205.
97. M. S. Hill, M. F. Mahon and T. P. Robinson, *Chemical Communications*, 2010, **46**, 2498-2500.
98. U. Englich, U. Hermann, I. Prass, T. Schollmeier, K. Ruhlandt-Senge and F. Uhlig, *Journal of Organometallic Chemistry*, 2002, **646**, 271-276.
99. W. Caseri, *Chemical Society reviews*, 2016, **45**, 5187-5199.
100. D. Kratzert, J. J. Holstein and I. Krossing, *Journal of Applied Crystallography*, 2015, **48**, 933-938.
101. M. J. Frisch, G. W. Trucks, H. B. Schlegel, G. E. Scuseria, M. A. Robb, J. R. Cheeseman, G. Scalmani, V. Barone, B. Mennucci, G. A. Petersson, H. Nakatsuji, M. Caricato, X. Li, H. P. Hratchian, A. F. Izmaylov, J. Bloino, G. Zheng, J. L. Sonnenberg, M. Hada, M. Ehara, K. Toyota, R. Fukuda, J. Hasegawa, M. Ishida, T. Nakajima, Y. Honda, O. Kitao, H. Nakai, T. Vreven, J. A. J. Montgomery, J. E. Peralta, F. Ogliaro, M. Bearpark, J. J. Heyd, E. Brothers, K. N. Kudin, V. N. Staroverov, R. Kobayashi, J.

Normand, K. Raghavachari, A. Rendell, J. C. Burant, S. S. Iyengar, J. Tomasi, M. Cossi, N. Rega, J. M. Millam, M. Klene, J. E. Knox, J. B. Cross, V. Bakken, C. Adamo, J. Jaramillo, R. Gomperts, R. E. Stratmann, O. Yazyev, A. J. Austin, R. Cammi, C. Pomelli, J. W. Ochterski, R. L. Martin, K. Morokuma, V. G. Zakrzewski, G. A. Voth, P. Salvador, J. J. Dannenberg, S. Dapprich, A. D. Daniels, O. Farkas, J. B. Foresman, J. V. Ortiz, J. Cioslowski and D. J. Fox, GAUSSIAN 09, Gaussian Ic., Pittsburgh, PA, 2009.

102. D. Andrae, U. Haussermann, M. Dolg, H. Stoll and H. Preuss, *Theoretica Chimica Acta*, 1990, **77**, 123-141.
103. P. C. Harihara and J. A. Pople, *Theoretica Chimica Acta*, 1973, **28**, 213-222.
104. W. J. Hehre, R. Ditchfield and J. A. Pople, *Journal of Chemical Physics*, 1972, **56**, 2257-2261.
105. A. D. Becke, *Physical Review A*, 1988, **38**, 3098-3100.
106. J. P. Perdew, *Physical Review B*, 1986, **33**, 8822-8824.
107. J. Tomasi, B. Mennucci and R. Cammi, *Chemical Reviews*, 2005, **105**, 2999-3093.
108. S. Grimme, S. Ehrlich and L. Goerigk, *Journal of Computational Chemistry*, 2011, **32**, 1456-1465.

5 Alkaline-Earth Mediated Reactivity of Phosphine-Boranes

5.1 Introduction

Chains of alternating group 13/15 elements can be thought of as "*inorganic polyolefins"* on the basis that polar covalent N-B or P-B bonds are formally isoelectronic to C-C bonds.[1-3] Polyaminoboranes have been used as precursors to hexagonal boron nitride (hBN),[1, 4] whilst polyphosphinoboranes show potential as flame-retardant materials, boron-phosphide ceramic precursors,[5] and as electron-beam resists for soft lithography.[6-8]

Like polyolefins, polyaminoboranes and polyphosphinoboranes are synthesised *via* the formal addition polymerisation of an unsaturated monomer. Unlike most olefins however, monomeric aminoboranes and phosphinoboranes are prone to spontaneous and uncontrolled oligomerisation unless stabilised by bulky substituents. Hence, they must be generated *in situ* from a kinetically stabilised precursor,[9, 10] or by dehydrogenation of the parent amine-borane or phosphine-borane in a catalytic[6, 7, 11-27] or stoichiometric manner (Scheme 5.1).[28]

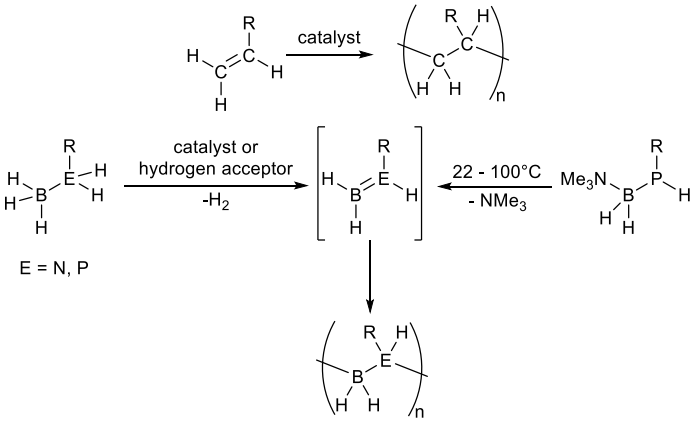

Scheme 5.1: Addition polymerisation of olefins and amino- or phosphinoboranes.

Ae-mediated amine-borane dehydrogenation has been thoroughly studied over the course of the last 15 years (see Chapter 1, Section 1.5.8, for a more detailed discussion of this chemistry). Ae-amidoborane complexes are readily formed from synthetically accessible precursors and display high thermal stability,[29-38] only undergoing dehydrogenation at high temperatures.[29, 30] When exposed to an excess of amine-borane, however, catalytic dehydrogenation is facile and the resulting aminoborane may dimerise to the cyclic diborazane, or be trapped by Ae-amides or -alkyls to generate unsymmetrical diaminoboranes[39] or alkylaminoboranes.[34, 37]

By contrast, the reactivity of Ae-complexes towards phosphine-boranes remains unexplored. Furthermore, phosphine-borane dehydrogenation and polymerisation catalysts are far less widespread than those for amine-boranes.[40] Literature examples of Ae-phosphidoboranes are confined to a series of compounds (**XLIa** and **b**, **XLII**) prepared *via* salt metathesis of AeI_2 (Ae = Mg, Ca, Sr) with anisole-substituted lithium or potassium phosphidoborane derivatives (Figure 5.1).[41]

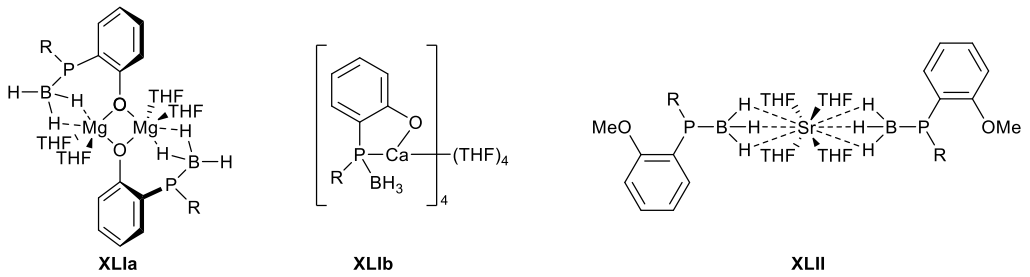

Figure 5.1: Mg, Ca, and Sr phosphidoboranes reported by Izod and co-workers.[41] R = $CH(SiMe_3)_2$.

In this chapter, the reactivity of BDI-magnesium and calcium complexes towards the secondary phosphine-borane, $Ph_2PH{\cdot}BH_3$ will be explored in an effort to expand the catalogue of known Ae-phosphidoborane complexes. The reactivity of these complexes towards phosphine-borane dehydrogenation/dehydrocoupling will be investigated as part of a wider effort to develop transition metal-free routes to polyphosphinoboranes.

5.2 Results and discussion

5.2.1 Reaction of Va with $Ph_2PH{\cdot}BH_3$

An equimolar reaction of **Va** with $Ph_2PH{\cdot}BH_3$ in d_8-toluene resulted in formation of a cloudy colourless suspension at room temperature. *In situ* ^{1}H NMR spectroscopy revealed complete consumption of the characteristic upfield α-C*H*$_2$ butyl resonance of **Va** within minutes, resulting in a broad and uninformative spectrum. The well-defined quartet of doublets at δ -39.43, and the quartet at δ 1.65 ppm in the respective ^{11}B and ^{31}P NMR spectra of $Ph_2PH{\cdot}BH_3$ were replaced by broad resonances centred at approx. δ -34, and -60 ppm, respectively. Single crystals were deposited on slowly cooling the reaction mixture from 80°C to -30°C, providing structural confirmation of the BDI-magnesium phosphidoborane complex **15** by X-ray diffraction (Figure 5.2).

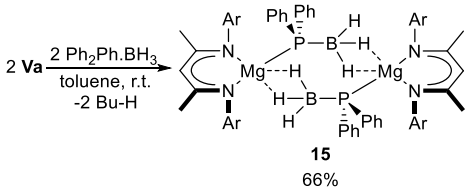

Scheme 5.2: Synthesis of compound **15**. Yield shown refers to isolated product of analytical purity, Ar = 2,6-di-*iso*propylphenyl.

The solid-state structure of compound **15** consists of a non-centrosymmetric dimer containing two magnesium centres, each coordinated by a BDI ligand and linked through a bridging diphenylphosphidoborate ligand. The core of the dimer is maintained through two Mg-P bonds and bridging B-H-Mg contacts. The five-coordinate magnesium centres display distorted square-based pyramidal geometries, with hydrogen, phosphorus and nitrogen atoms at the vertices. The magnesium centres project from the mean planes defined by the N-C-C-C-N atoms of the BDI ligands by 0.910(3) and 0.905(3) Å for Mg1 and Mg2, respectively, whilst the phosphorus-bound phenyl substituents are pushed slightly away from the flanking dipp groups, distorting the tetrahedral geometry of phosphorus (C30-P1-Mg1 = 125.55(9)° *cf.* C30-P1-B1 = 103.88(14)°). The P-B bonds are of a length (*ca.* 1.94 Å) consistent with other diphenylphosphidoborate complexes (1.89-1.98 Å).

With the exception of the potassium salt [(18-crown-6)K][Ph_2PBH_3][42] and the tin-complex [$Me_3Sn(Ph_3PBH_3)$],[43] all examples of crystallographically characterised diphenylphosphidoborate complexes in the Cambridge Structural Database (CSD) are transition-metal centred. Although B-H-M agostic-type interactions are common,[7, 12, 26, 44] they are absent from many complexes (particularly late transition metals)[42, 45-50] and all are monomeric. Furthermore, crystallographically characterised examples of BDI-Ca and Mg amidoboranes are almost exclusively monomeric, with the exception of [(BDI)M(*i*PrNHBH$_3$)]$_2$ (**XXIa**[51] and **b**[36], M = Mg, Ca) and [(BDI)Mg(H_2NBH_2)]$_2$ (**XLIII**),[52] which are structurally reminiscent of compound **15**.

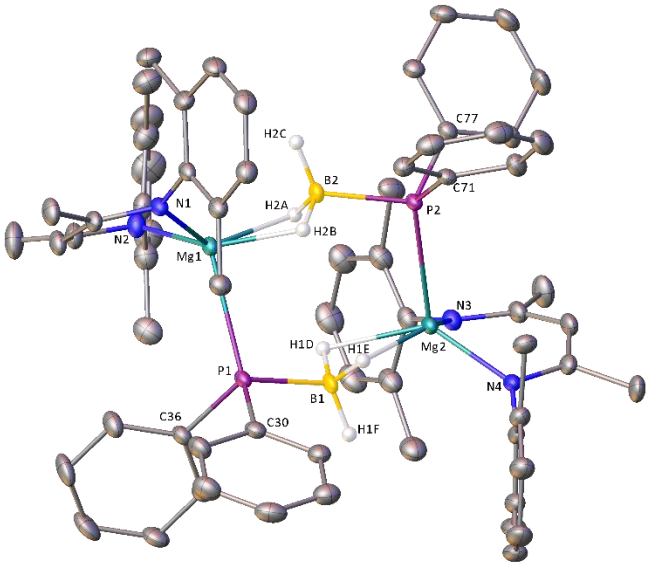

Figure 5.2: X-ray crystal structure of compound **15**. Disordered solvent molecules are omitted for clarity, as are *iso*-propyl methyl groups and hydrogen atoms, except for those bound to boron. Thermal ellipsoids are shown at the 30% probability level. Selected bond lengths (Å) and angles (°): P1-Mg1 2.7001(10), P1-C30 1.841(3), P1-C36 1.833(3), P1-B1 1.944(3), P2-Mg2 2.6931(10), P2-C71 1.848(3), P2-C77 1.836(3), P2-B2 1.939(3), Mg1-N1 2.046(2), Mg1-N2 2.056(3), Mg2-N3 2.057(2), Mg2-N4 2.047(2), C30-P1-Mg1 125.55(9), C30-P1-B1 103.88(14), C36-P1-Mg1 114.78(10), C36-P1-C30 97.62(12), C36-P1-B1 110.15(13), B1-P1-Mg1 104.10(10), C71-P2-Mg2 124.79(9), C71-P2-B2 103.86(13), C77-P2-Mg2 115.57(9), C77-P2-C71 98.33(12), C77-P2-B2 109.74(13), B2-P2-Mg2 103.70(9), N1-Mg1-P1 117.89(7), N1-Mg1-N2 96.38(10), N2-Mg1-P1 112.39(8), N3-Mg2-P2 112.10(7), N4-Mg2-P2 119.06(7), N4-Mg2-N3 96.12(10).

The broad resonances in the ^{1}H NMR spectrum of compound **15** at 298 K may originate from a monomer-dimer equilibrium in the solution state. Although detailed investigation of this phenomenon by variable temperature NMR spectroscopy was thwarted by poor solubility at low temperature, sharp and well-defined NMR spectra were obtained on warming the sample to 349 K, consistent with a fluxional process occurring on an NMR time-scale (Figure 5.3). The ^{1}H NMR spectrum displays a single BDI environment, with a γ-C*H* BDI methine resonance located at δ 4.95 ppm. A single resonance was observed in the ^{11}B NMR spectrum, consisting of a quartet of doublets ($^{1}J_{1H}$ = 91.1 Hz, $^{2}J_{31P}$ = 44.3 Hz) at δ -34.0 ppm, and the ^{31}P{^{1}H} NMR spectrum contained one broad resonance centred at δ -57.1 ppm (Figure 5.4).

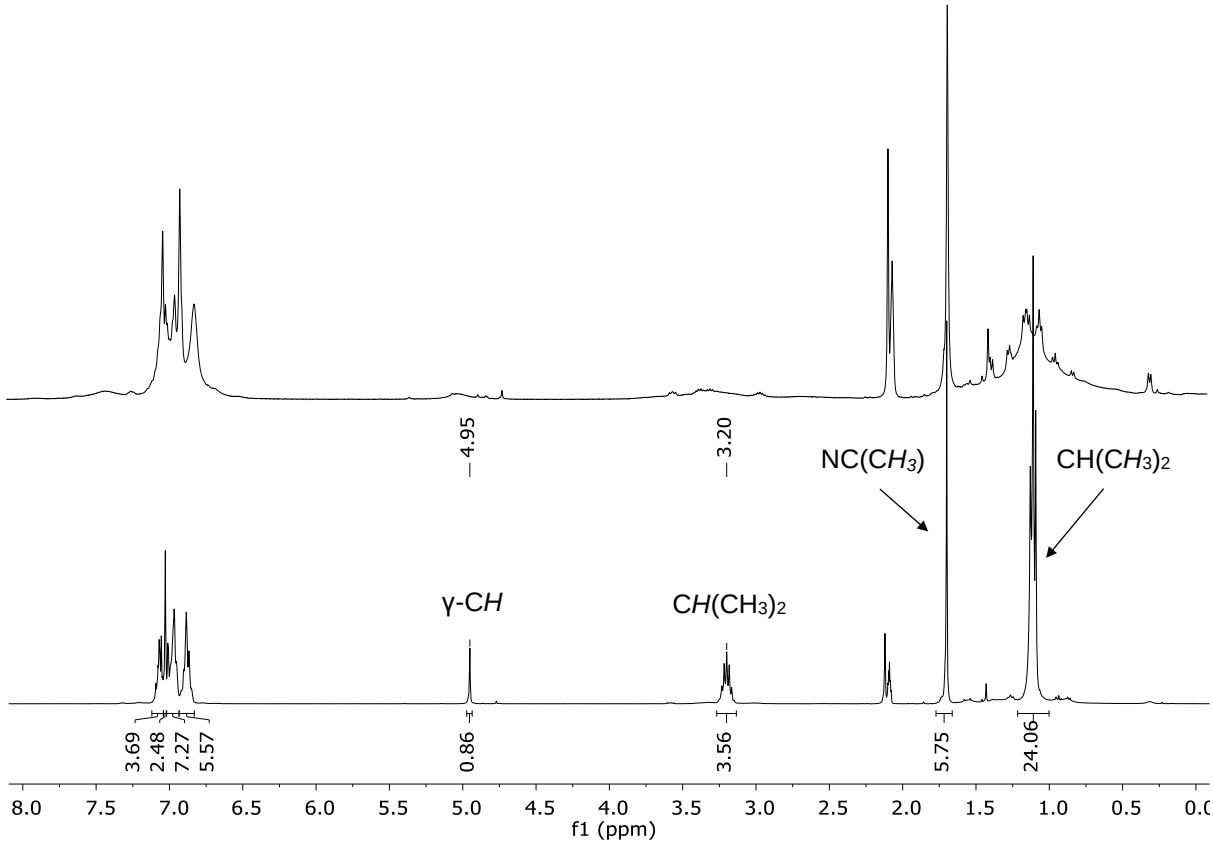

Figure 5.3: ^{1}H NMR spectra of compound **15** (400 MHz, d_8-toluene) top: 298 K, bottom: 349 K.

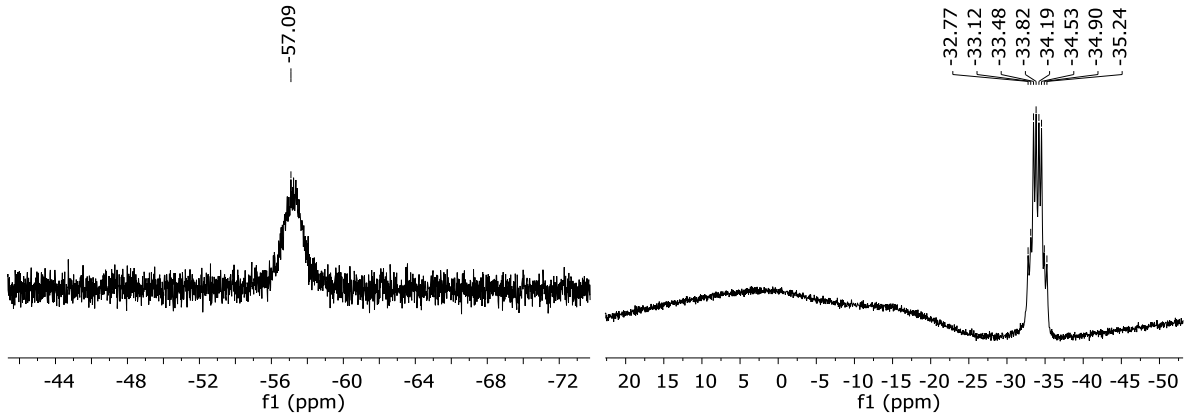

Figure 5.4: left: ^{31}P{^{1}H} (162 MHz) and right: ^{11}B (128 MHz) NMR spectra of compound **15** (349 K, d_8-toluene).

5.2.2 Reaction of compounds IVb and IVc with $Ph_2PH{\cdot}BH_3$

The BDI-calcium amide **IVb** was reacted with $Ph_2PH{\cdot}BH_3$ in toluene for 16 hours at room temperature and, after evaporating the reaction mixture to dryness, the resulting pale-yellow solid was washed with hexane. Analagous to compound **15**, the room-temperature ^{1}H NMR spectrum of the product contains broadened resonances, which resolve into well-defined

peaks at 320 K in d_8-toluene. The close similarity of the resulting spectrum to that of compound **15** provides strong evidence for formation of the BDI-calcium diphenylphosphinoborate complex, **16a**. A single BDI environment is observed in the ^{1}H NMR spectrum, with the γ-C*H* proton resonating at δ 5.03 ppm. The ^{11}B and ^{31}P{^{1}H} spectra are both broad, with resonances that appear downfield relative to compound **15**, at δ -30.2, and -45.0 ppm, respectively.

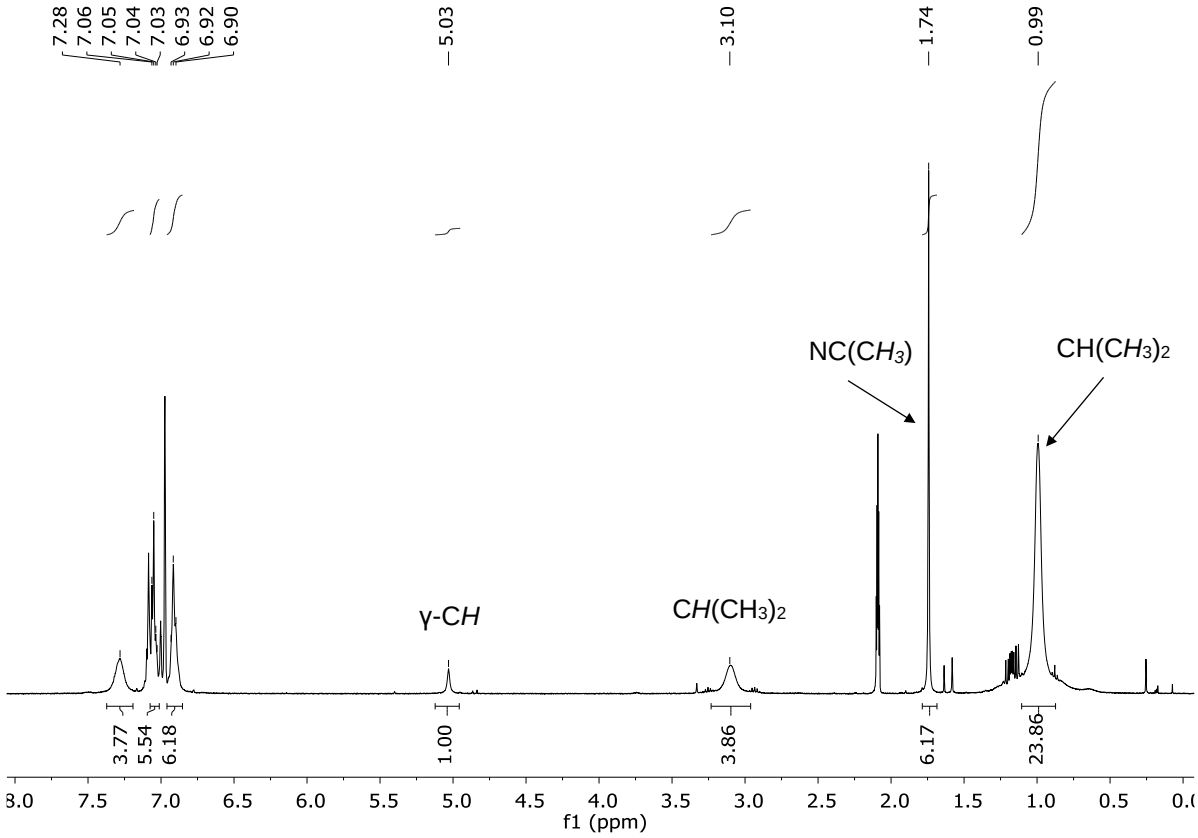

Figure 5.5: ^{1}H NMR spectrum of compound **16a** (400 MHz, 320.6 K, d_8-toluene).

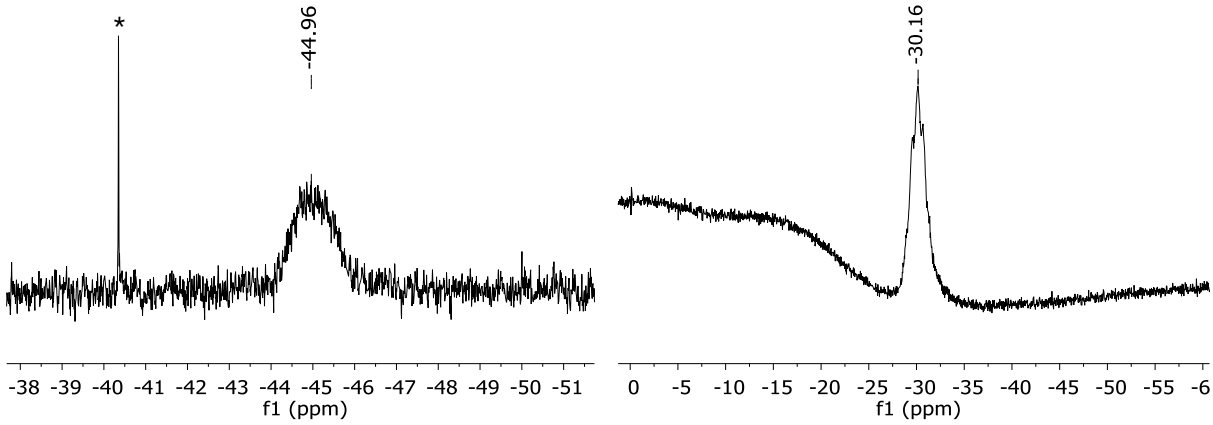

Figure 5.6: left: ^{31}P{^{1}H} (162 MHz) and right: ^{11}B (128 MHz) NMR spectra of compound **16a** (320.6 K, d_8-toluene). * = trace Ph_2PH impurity.

Whilst repeated attempts to obtain single-crystals of compound **16a** were unsuccessful, addition two equivalents of THF to a C_6D_6 solution yielded the monomeric THF adduct **16b**. Compound **16b** could also be obtained directly from reaction of THF-solvated BDI-calcium amide **IVc** with one equivalent of $Ph_2PH{\cdot}BH_3$ or the dimeric THF-solvated BDI-calcium hydride **VIc** with two equivalents of $Ph_2PH{\cdot}BH_3$ in toluene. Compound **16b** can be isolated in an analytically pure form by cooling a saturated toluene solution to -30°C to yield colourless single crystals suitable for X-ray diffraction analysis.

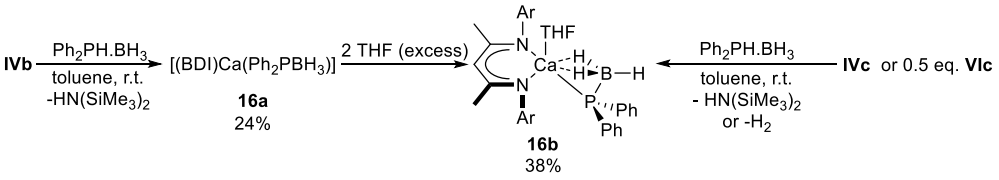

Scheme 5.3: Synthesis of compounds **16a** and **16b**. Yields shown refer to isolated products of analytical purity, Ar = 2,6-di-*iso*propylphenyl.

Compound **16b** crystallises in the triclinic space group *P-1*, with the calcium centre adopting a heavily distorted *pseudo*-trigonal bipyramidal geometry, where Ca1, N1, N2, and B1 sit close to the equatorial plane (O1-Ca1-X = 91.70(4)° – 100.03(3)° where X = N or B). A THF molecule resides in an axial position, with P1 located below the equatorial plane (Figure 5.7). The Ca1-P1 bond length (2.8962(4) Å) is close to that of Izod's calcium phosphidoborane **XLIb** (2.878 Å) and is similar to the Ca-P bond lengths of borane-free calcium diphenylphosphinate complexes (2.872-3.038 Å).[53-57] The P1-B1 bond length (1.9689(15) Å) is essentially identical to **XLIb** and slightly longer than that of compound **15**. The C-P-B and C-P-C angles stay close to the ideal tetrahedral angle of 109°, suggesting that the negative charge resides in a phosphorus-centred sp^3-like lone-pair, which interacts in a side-on fashion with the calcium centre. The phosphidoborate anion displays two B-H agostic-type interactions with calcium, contributing to the unusual geometry at phosphorus (Ca1-P1-B1 = 65.54(4) Å), a feature that has also been observed in related transition-metal phosphidoborate complexes.[7, 12, 26, 44]

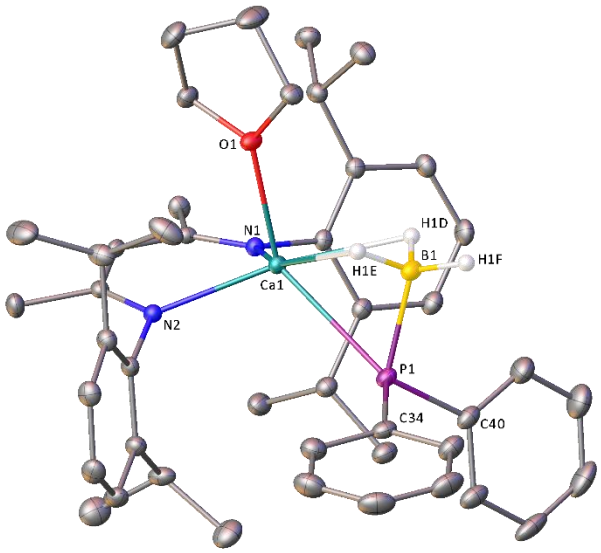

Figure 5.7: X-ray crystal structure of compound **16b**. Thermal ellipsoids are shown at the 30% probability level and hydrogen atoms are omitted for clarity, except for those bound to boron. Only the major component of the disordered THF ligand is shown. Selected bond lengths (Å) and angles (°): Ca1-P1 2.8962(4), Ca1-O1 2.3238(9), Ca1-N1 2.3432(10), Ca1-N2 2.3361(10), Ca1-B1 2.7463(15), P1-C34 1.8269(14), P1-C40 1.8235(14), P1-B1 1.9689(15), O1-Ca1-P1 130.28(2), O1-Ca1-N1 99.30(3), O1-Ca1-N2 100.03(3), O1-Ca1-B1 91.70(4), N1-Ca1-P1 121.86(3), N1-Ca1-B1 131.63(4), N2-Ca1-P1 112.58(3), N2-Ca1-N1 80.10(3), N2-Ca1-B1 143.99(4), B1-Ca1-P1 40.74(3), C34-P1-Ca1 127.88(4), C34-P1-B1 105.31(6), C40-P1-Ca1 127.29(5), C40-P1-C34 104.66(6), C40-P1-B1 108.07(7), B1-P1-Ca1 65.54(4), P1-B1-Ca1 73.72(5).

5.2.3 Reactions of $Ph_2PH{\cdot}BH_3$ with Ae-hydrides VIa, c, d

Compounds **15**, **16a,** and **16b** could also be prepared from a 2:1 reaction of $Ph_2PH{\cdot}BH_3$ with the dimeric BDI-Ae hydride complexes **VIa**, **VId,** and **VIc**, respectively (Scheme 5.4, top). The reaction reaches completion within minutes (as observed by ^{1}H, ^{11}B, and ^{31}P NMR spectroscopy) and is accompanied by vigorous release of H_2 gas. In contrast, when a d_8-toluene or C_6D_6 solution of $Ph_2PH{\cdot}BH_3$ was reacted with an equimolar quantity of either compound **VIa** or **VId**, a complex but sharp ^{1}H NMR spectrum was obtained. A toluene solution of the crude product was cooled to -30°C or evaporated at room temperature to yield single crystals of the respective BDI-magnesium, and calcium-hydrido-phosphidoborate complexes, **17** and **18** (Scheme 5.4, bottom).

Compound **17** crystallises as a dimer, with two {(BDI)Mg} units linked by a μ_2-bridging hydride ligand and a diphenylphosphidoborate anion. The latter coordinates to Mg1 through P1, and to Mg2 *via* two agostic-type B-H-Mg interactions. The Mg1-P1 (2.7241(6) Å) and P1-B1

(1.9610(19) Å) bonds are slightly longer than those of compound **15** (Mg-P = 2.7001(10), 2.6931(10) Å, P-B = 1.944(3), 1.939(3) Å), whilst the Mg-N bond lengths are similar in both compounds.

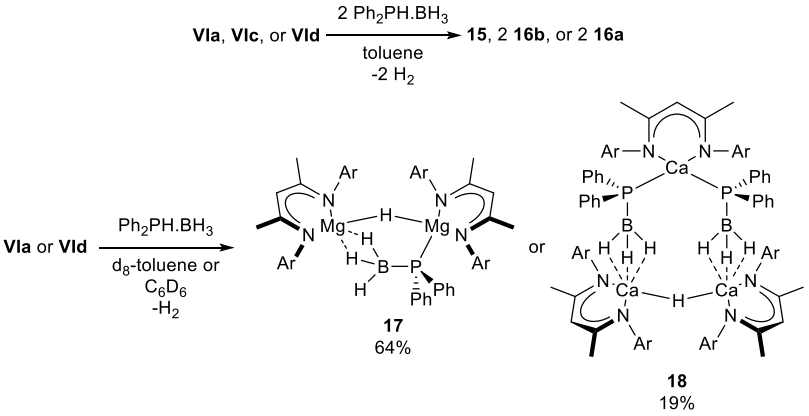

Scheme 5.4: Reactions of BDI-Ae hydride complexes with $Ph_2PH{\cdot}BH_3$. Isolated yields shown, Ar = 2,6-di-*iso*propylphenyl.

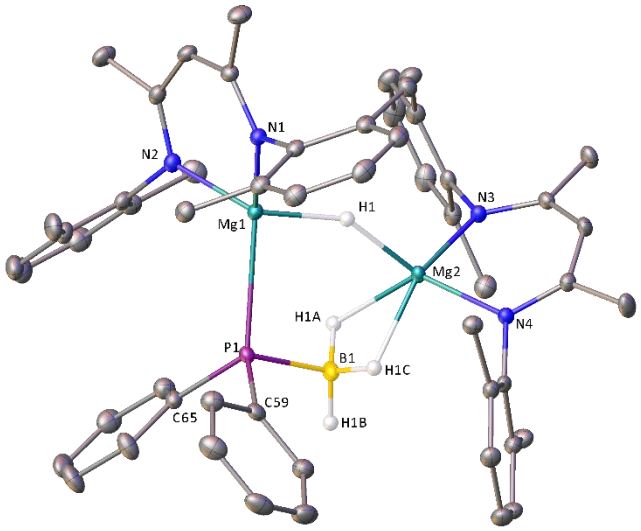

Figure 5.8: X-ray crystal structure of compound **17**. Thermal ellipsoids are shown at the 30% probability level. *Iso*-propyl methyl groups and hydrogen atoms are omitted for clarity, except for those bound to boron and magnesium. Disordered toluene molecules are not shown. Selected bond lengths (Å) and angles (°): P1-Mg1 2.7241(6), P1-C59 1.8337(17), P1-C65 1.8406(16), P1-B1 1.9610(19), Mg1-N1 2.0814(14), Mg1-N2 2.0614(14), Mg2-N3 2.0543(13), Mg2-N4 2.0572(14), C59-P1-Mg1 118.37(5), C59-P1-C65 100.23(7), C59-P1-B1 106.22(8),C65-P1-Mg1 124.34(6), C65-P1-B1 105.29(8), B1-P1-Mg1 100.71(6), N1-Mg1-P1 140.40(4), N2-Mg1-P1 109.74(4), N2-Mg1-N1 93.48(6), N3-Mg2-N4 92.64(5).

Re-dissolving crystals of compound **17** in d_8-toluene produced a complex ^{1}H NMR spectrum which contained an unidentified minor species with resonances assigned to BDI and Ph_2P environments (Figure 5.9). The $^{31}P\{^1H\}$ NMR spectrum contained a major resonance at δ -46.5 ppm and a minor species at δ -42.8 ppm which, by ^{31}P-^1H HMBC NMR spectroscopy, was found to correspond to the minor species in the ^{1}H NMR spectrum (Figure 5.10). These observations may indicate that compound **17** exists in equilibrium with other species in solution, possibly *via* monomerization. Addition of a few drops of d_8-THF to the same d_8-toluene solution, however, resulted in a clean and well-defined ^{1}H NMR spectrum comprising of two BDI-containing species, which, consistent with the composition of **17**, were assigned to the THF-adduct derivatives, $[LMgH{\cdot}THF]_2$ (**VIb**)[32] and $[LMg\{Ph_2PBH_3\}{\cdot}THF]$, (Figure 5.9).

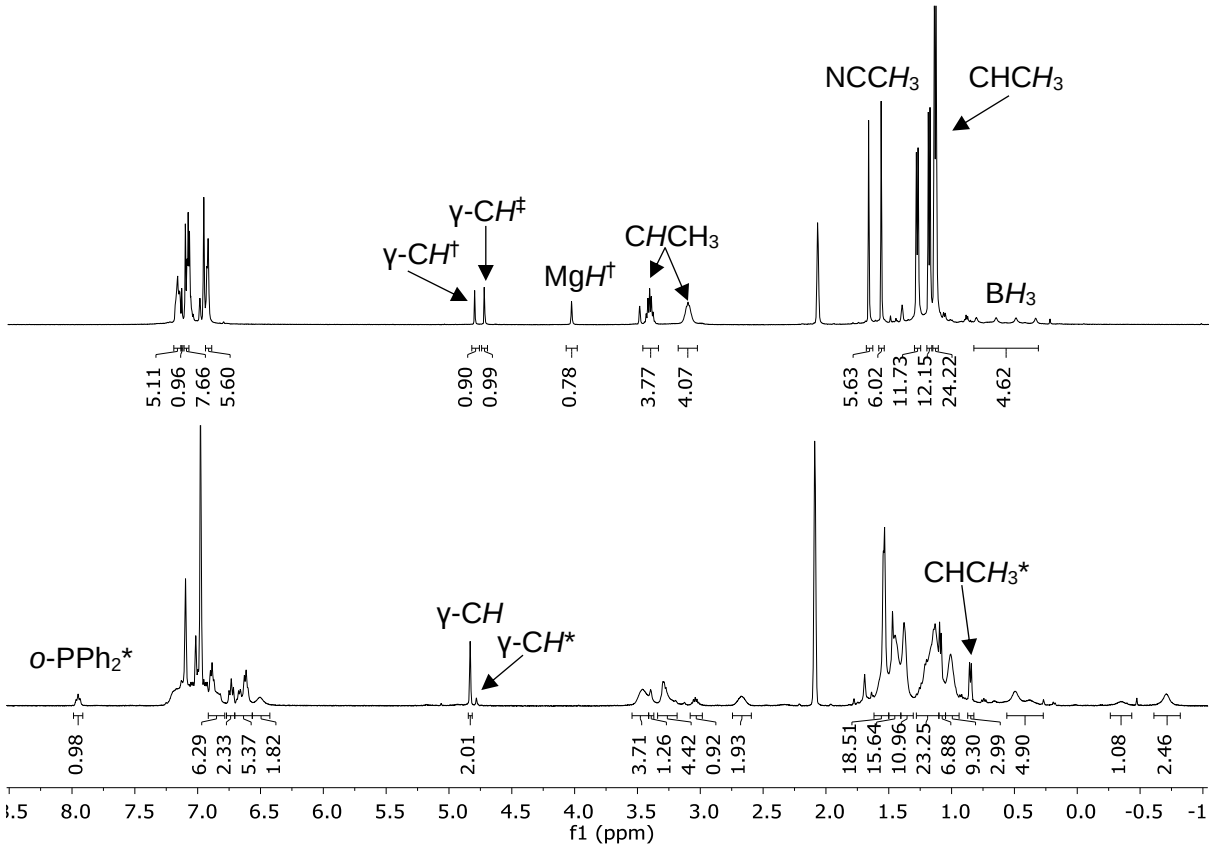

Figure 5.9: ^{1}H NMR spectra (500 MHz, 298 K) of compound **17** dissolved in d_8-toluene (bottom) and d_8-toluene + d_8-THF (top). * = unidentified species formed in solution, † = **VIb**, ‡ = $[LMg\{Ph_2PBH_3\}{\cdot}THF]$.

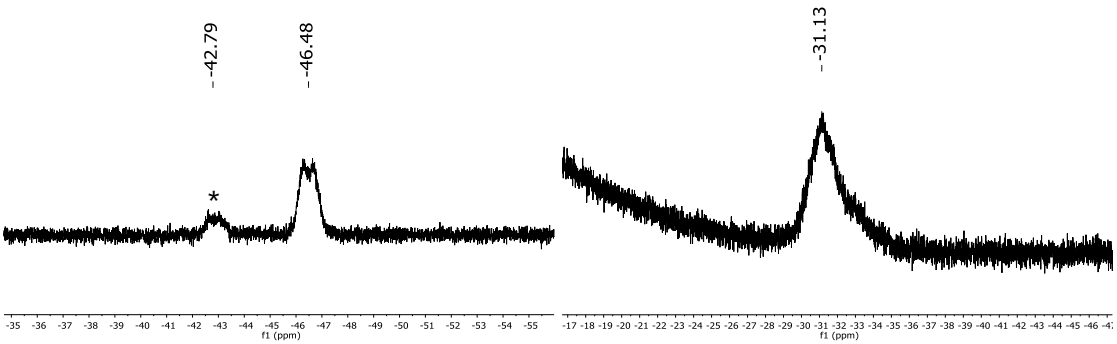

Figure 5.10: left: $^{31}P\{^{1}H\}$ (162 MHz) and right: ^{11}B (128 MHz) NMR spectra of compound **17** (320.6 K, d_8-toluene). * = unidentified species formed in solution.

Compound **18** contains three {(BDI)Ca} units, two diphenylphosphidoborate anions and one μ_2-bridging hydride, which connects {(BDI)Ca2} with {(BDI)Ca1}. Both diphenylphosphidoborate ligands coordinate to Ca1 *via* phosphorus and to each of the Ca2 and Ca3 atoms through three agostic-type B-H-Ca interactions. The P1-B1-Ca2 and P2-B2-Ca3 angles are close to linearity (174.51(51)/176.32(14)°) and the –{Ca-P-BH_3-Ca-H-Ca-H_3B-P}- macrocycle displays a twisted geometry with a *pseudo*-C_2 rotational axis about Ca1/H1 (ignoring asymmetry arising from the BDI ligand orientation). The Ca2-N and Ca3-N bonds (2.333(2)-2.3690(19) Å) are longer than for Ca1-N (2.3069(18), 2.3124(18) Å). Although the N-Ca-N bond angles (*ca.* 80°) are narrower than those of the magnesium compounds **15** and **17** (N-Mg-N = 92-96°), they are similar to that of compound **16b**, reflecting the larger ionic radius of Ca^{2+} *vs.* Mg^{2+}. Due to the nearby phosphorus-bound phenyl groups, Ca1 projects some 1.476(2) Å out of the mean plane defined by the N1/N2-containing BDI ligand, in contrast to Ca2 and Ca3, which are almost co-planar to their ligands. The geometry at both phosphorus atoms is almost perfectly tetrahedral, whilst the P-B bond lengths are slightly shorter, and Ae-P bonds significantly longer than those of **15**, **16b**, and **17**. Although isolated crystals of compound **18** displayed one major BDI-environment in the ^{1}H NMR spectrum, the presence of several other peaks suggests a dynamic system involving dissociation of the trimer in solution albeit the exact nature of this phenomenon remains unclear at this stage. Broad resonances were observed at δ -45.5 and -30.4 ppm in the respective $^{31}P\{^{1}H\}$ and ^{11}B NMR spectra.

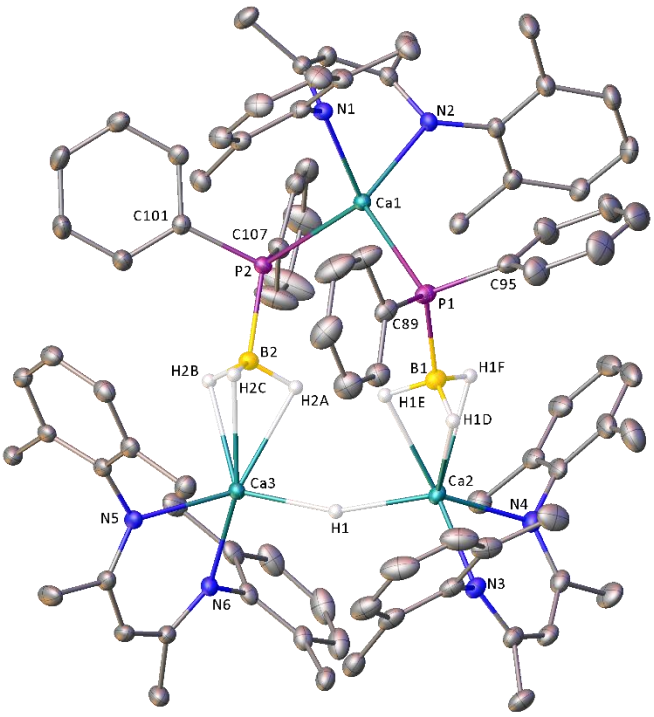

Figure 5.11: X-ray crystal structure of compound **18**. Thermal ellipsoids are shown at the 30% probability level. *Iso*-propyl methyl groups and hydrogen atoms are omitted for clarity, except for those bound to boron and calcium. Disordered toluene molecules are not shown. Selected bond lengths (Å) and angles (°): Ca1-P1 2.9811(7), Ca1-P2 3.0307(7), Ca1-N1 2.3069(18), Ca1-N2 2.3124(18), Ca2-N3 2.333(2), Ca2-N4 2.3498(19), Ca2-B1 2.602(3), Ca3-N5 2.3550(18), Ca3-N6 2.3690(19), Ca3-B2 2.634(3), P1-C89 1.835(3), P1-C95 1.840(3), P1-B1 1.946(3), P2-C101 1.839(2), P2-C107 1.842(3), P2-B2 1.945(3), P1-Ca1-P2 115.80(2), N1-Ca1-P1 107.16(5), N1-Ca1-P2 115.23(5), N1-Ca1-N2 82.40(6), N2-Ca1-P1 117.83(5), N2-Ca1-P2 113.70(5), N3-Ca2-N4 79.52(7), N3-Ca2-B1 118.83(8), N4-Ca2-B1 117.63(8), N5-Ca3-N6 79.67(6), N5-Ca3-B2 111.59(7), N6-Ca3-B2 139.47(8), C89-P1-Ca1 120.90(8), C89-P1-C95 103.03(12), C89-P1-B1 107.01(12), C95-P1-Ca1 110.49(8), C95-P1-B1 108.29(11), B1-P1-Ca1 106.59(9), C101-P2-Ca1 109.04(8), C101-P2-C107 100.63(11), C101-P2-B2 107.33(11), C107-P2-Ca1 114.51(8), C107-P2-B2 106.48(12), B2-P2-Ca1 117.35(9), P1-B1-Ca2 174.51(15), P2-B2-Ca3 176.32(14).

5.2.4 Reaction of compound 15 with $Ph_2PH{\cdot}BH_3$

Having established the ease by which $Ph_2PH{\cdot}BH_3$ deprotonation yields well-defined complexes containing Ae-phosphorus bonds, we endeavoured to induce P-B dehydrocoupling *via* the mechanisms outlined in Scheme 1.47 and Scheme 1.48 through the addition of a further phosphine-borane equivalent. Addition of $Me_2NH{\cdot}BH_3$ to calcium amidoborane complex **XXb** results in the formation of the cyclic dimer $(Me_2NBH_2)_2$ (presumably *via* formal elimination and dimerisation of the unsaturated aminoborane, $Me_2N{=}BH_2$), and compounds **XXVa**-**e** are formed by spontaneous H_2 elimination and N-B bond formation at room

temperature. The analogous reaction of **15** with $Ph_2PH{\cdot}BH_3$ in C_6D_6, however, provided NMR spectra devoid of the anticipated phosphinoborane oligomers or P-B coupled products analogous to **XXVa**-**e**. Rather, generation of stoichiometric quantities of Ph_2PH was revealed by the presence of a sharp doublet of quintets centred at δ -40.70 ppm in the ^{31}P NMR spectrum (Figure 5.12), which collapsed to a singlet in the $^{31}P\{^1H\}$ spectrum, and a characteristic doublet in the ^1H NMR spectrum (δ 5.20 ppm, $^1J_{31P}$ = 216 Hz, Figure 5.13). A second, broad resonance at δ -24.83 ppm in the ^{31}P NMR spectrum was accompanied by a single, well defined BDI-environment in the ^1H NMR spectrum (γ-C*H* = δ 4.96 ppm), corresponding to the resultant magnesium complex, **19** (Scheme 5.5).

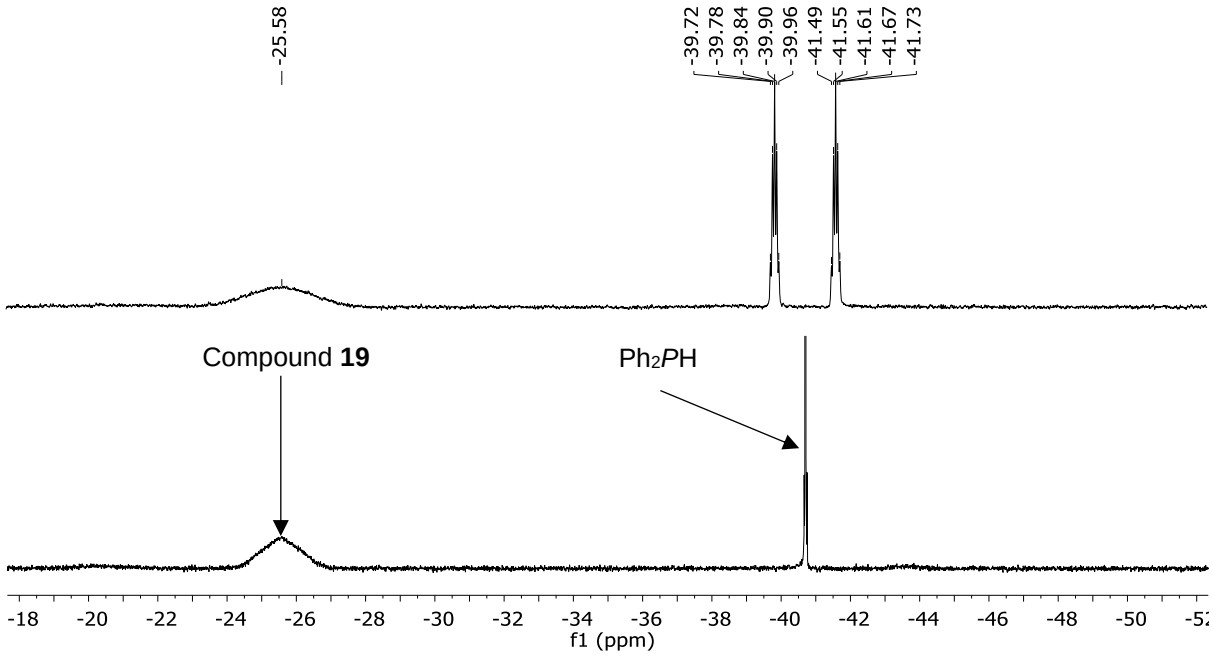

Figure 5.12: Expanded *in situ* ^{31}P (top) and $^{31}P\{^1H\}$ (bottom) NMR spectra (122 MHz, 298 K, d_8-toluene) of the reaction between compound **15** and two equivalents of $Ph_2PH{\cdot}BH_3$.

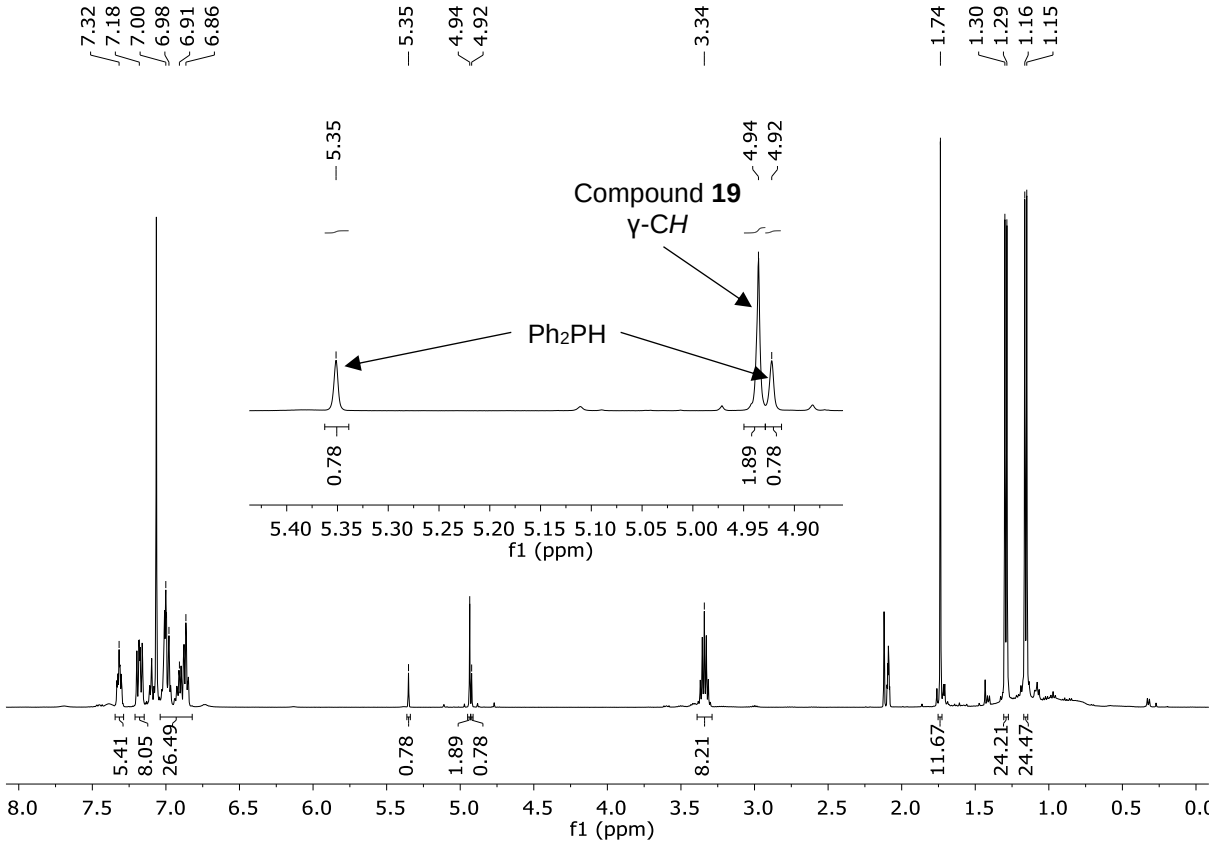

Figure 5.13: *in situ* ^{1}H NMR spectrum (500 MHz, 298 K, d_8-toluene) of the reaction between compound **15** with two equivalents of $Ph_2PH{\cdot}BH_3$. Inset: expanded spectrum to show resonances of γ-C*H* and Ph_2PH protons.

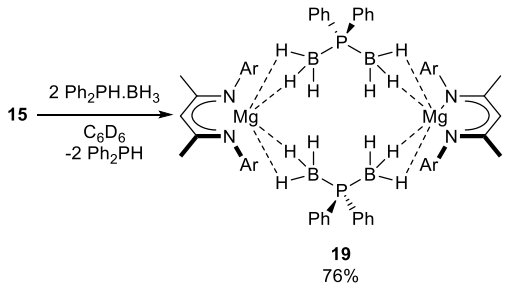

Scheme 5.5: Synthesis of compound **19**. Ar = 2,6-di-*iso*propylphenyl.

Compound **19** was deposited as a colourless crystalline solid on concentration of the C_6D_6 reaction mixture and was isolated in analytical purity after washing thoroughly with hexane. Crystals suitable for single-crystal X-ray diffraction analysis were obtained by slow cooling of a saturated toluene solution from 80°C to room temperature. The molecular structure of compound **19** was confirmed as a dimeric BDI-magnesium phosphinodiboronate complex (Figure 5.14). Although several examples of alkali-phosphinodiboronate salts and related *f*-block complexes have been reported,[58-64] the majority contain alkyl-substituted phosphorus centres and compound **19** is, to the best of our knowledge, the second crystallographically

characterised example of the $[(H_3B)_2PPh_2]^-$ anion; the other being the 18-crown-6 potassium salt, $[(18\text{-crown-6})K\{(H_3B)_2PPh_2\}]$ (**XLIV**) reported by Wagner and co-workers.[65] Compound **19** crystallises in the triclinic space group *P-1*, with a unit cell containing two crystallographically independent dimer halves (molecules *A* and *B*), and two regions of disordered toluene. The $[(H_3B)_2PPh_2]^-$ anion bridges the magnesium centres *via* B-H-Mg agostic-type interactions. In molecule *B*, the anion bridges asymmetrically, with a near linear Mg1-B1-P1 angle (171.76(12)°) resulting in three Mg-H-B interactions, and a bent Mg1'-B2-P1 geometry (136.69(9)°) provided by two Mg-H-B interactions. Molecule *A* contains a more symmetrically disposed anion, which engages with both magnesium centres *via* two Mg-H-B interactions per boron centre. The anion is structurally similar in both molecules, with very slight increases in the B-P-B and C-P-C angles compared to those of **XLIV**. The P-B bond lengths are slightly shorter than in **XLIV**, with molecule *A* featuring one long and one short P-B distance per $[(H_3B)_2PPh_2]^-$ anion, as a result of the asymmetrical binding mode. A similar effect is observed in **XLIV**, where one of the BH_3 moieties interacts with the potassium centre, lengthening the corresponding B-P bond. The phosphorus and magnesium centres display distorted tetrahedral and *pseudo*-tetrahedral geometries, respectively, with typical Mg-N bond lengths and N-Mg-N angles.

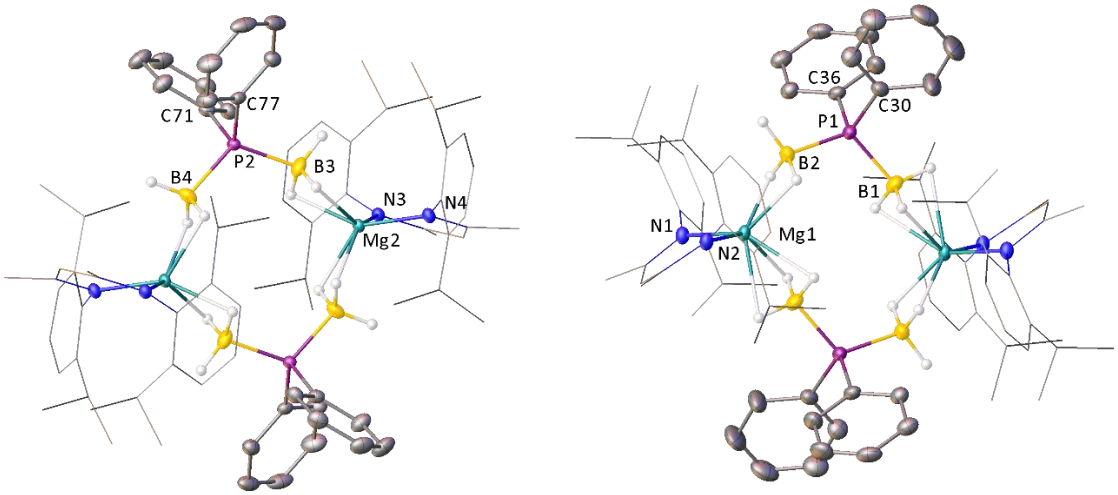

Figure 5.14: X-ray crystal structure of compound **19**, showing both crystallographically independent centrosymmetric dimers (left: molecule *A*, right: molecule *B*). Thermal ellipsoids are shown at the 30% probability level. For clarity, the BDI-ligands are shown in wireframe view and hydrogen atoms are omitted except for those bound to boron. Solvent molecules (toluene) present within in the crystal lattice are not shown. Selected bond lengths (Å) and angles (°) for molecule *A*: P2-C71 1.8142(14), P2-C77 1.8191(13), P2-B3 1.9152(17), P2-B4 1.9197(16), Mg2-N3 2.0493(11), Mg2-N4 2.0401(12), B4-Mg2[2] 2.3973(16), C71-P2-C77 103.68(6), C71-P2-B3 108.24(7), C71-P2-B4 108.46(7), C77-P2-B3 110.83(7), C77-P2-B4 109.70(7), B3-P2-B4 115.25(8), N4-Mg2-N3 95.12(5), P2-B4-Mg2[2] 153.63(10). Selected bond lengths (Å) and angles (°) for molecule *B*: P1-C30 1.8197(16), P1-C36 1.8195(16), P1-B1 1.9121(17), P1-B2 1.9221(17), Mg1-N1 2.0435(12), Mg1-N2 2.0402(12), Mg1-B2[1] 2.4204(18), C30-P1-B1 110.63(8), C30-P1-B2 110.24(8), C36-P1-C30 102.31(7), C36-P1-B1 108.61(8), C36-P1-B2 108.70(8), B1-P1-B2 115.50(8), N1-Mg1-B2[1] 110.15(6), N2-Mg1-N1 95.12(5), N2-Mg1-B2[1] 116.03(6), P1-B2-Mg1[1] 136.69(9). Symmetry operations used: [1]1-X,-1-Y,-Z; [2]2-X,1-Y,1-Z.

5.2.5 Reaction of [K(Ph_2PBH_3)] with $B(C_6F_5)_3$

The lability of P-B bonds is an apparent limitation that prevents β-hydride elimination and/or P-B coupling to affect magnesium-mediated catalytic dehydrocoupling of phosphine-boranes. This deduction demanded an alternative approach to promote hydride loss from **15** and generate an unsaturated phosphinoborane and subsequent oligomers. Previous research by Anker *et.al.* had demonstrated that the strongly Lewis acidic borane, $B(C_6F_5)_3$, may abstract a hydride from [K{Me_2NBH_3}] to provide the cyclic diborazane,$(Me_2NBH_2)_2$, and the potassium borohydride complex, [K{$HB(C_6F_5)_3$}] (**XLVa**) (Scheme 5.6, top).[66] Similarly, BDI-Ca and Mg complexes **XXa, b** and **XXVb** also undergo hydride abstraction to generate the corresponding BDI-Ae-$[HB(C_6F_5)_3]^-$ complexes (**XLVIa-c**) and $(Me_2NBH_2)_2$, when treated with $B(C_6F_5)_3$

(Scheme 5.6, bottom).[66, 67] We, therefore, surmised that similar reactivity may be accessible to phosphine-boranes, enabling oligomerisation to proceed *via* stepwise deprotonation and hydride abstraction.

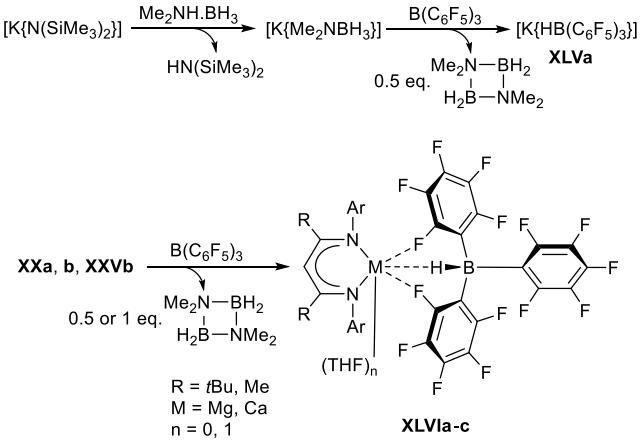

Scheme 5.6: Reactivity of potassium, magnesium, and calcium amidoborane complexes with $B(C_6F_5)_3$ to provide the cyclic dimer, $(Me_2NBH_2)_2$, and derivatives of the $[HB(C_6F_5)_3]^-$ anion.[66, 67] Ar = 2,6-di-*iso*propylphenyl.

Treatment of $Ph_2PH{\cdot}BH_3$ with an equimolar C_6D_6 solution of $[K\{N(SiMe_3)_2\}]$ provided $[K\{Ph_2PBH_3\}]$ (Figure 5.15).[42] Subsequent addition of $B(C_6F_5)_3$ and heating to 60°C for approximately 16 hours resulted in the deposition of colourless plate-like crystals of **XLVa**.[66, 68] Although **XLVa** is barely soluble in C_6D_6, the $[HB(C_6F_5)_3]^-$ anion could be clearly identified as the only species present in the ^{19}F NMR spectrum, and was also visible as a weak signal at δ -22 ppm in the ^{11}B NMR spectrum (Figure 5.16) by comparison to the published spectroscopic data.[66, 68] Although **XLVa** is a known compound, only its bis-TMEDA complex **XLVb** has been crystallographically characterised.[55] Hence, for completeness, the TMEDA-free X-ray crystal structure is shown in Figure 5.17a. **XLVa** forms a three-dimensional lattice in the solid state, with close contacts between the potassium cations and *ortho*-, *meta*-, and *para*-fluorine atoms as well as the boron-bound hydride (Figure 5.17b). Analysis of the *in situ* $^{31}P\{^1H\}$ NMR spectrum (Figure 5.15) after $B(C_6F_5)_3$ addition revealed a major peak at δ -17.5 ppm in addition to minor resonances at δ -3.7 and +3.3 ppm, as well as Ph_2PH at δ -39.7 ppm. The resonance at δ -17.5 ppm is consistent with the formation of cyclic trimeric and/or tetrameric phosphinoboranes **P-XXIVb** and **c**, an assignment which is further supported by the appearance of a signal at δ -30.0 ppm in the ^{11}B NMR (Figure 5.16).[16]

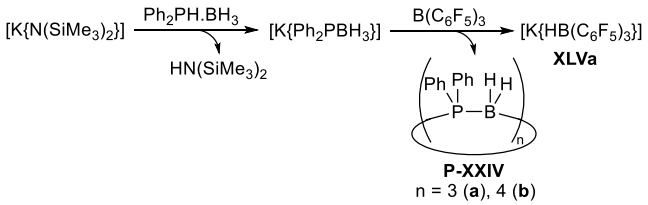

Scheme 5.7: Sequential deprotonation and hydride abstraction of $Ph_2PH{\cdot}BH_3$ by [K{$N(SiMe_3)_2$}].

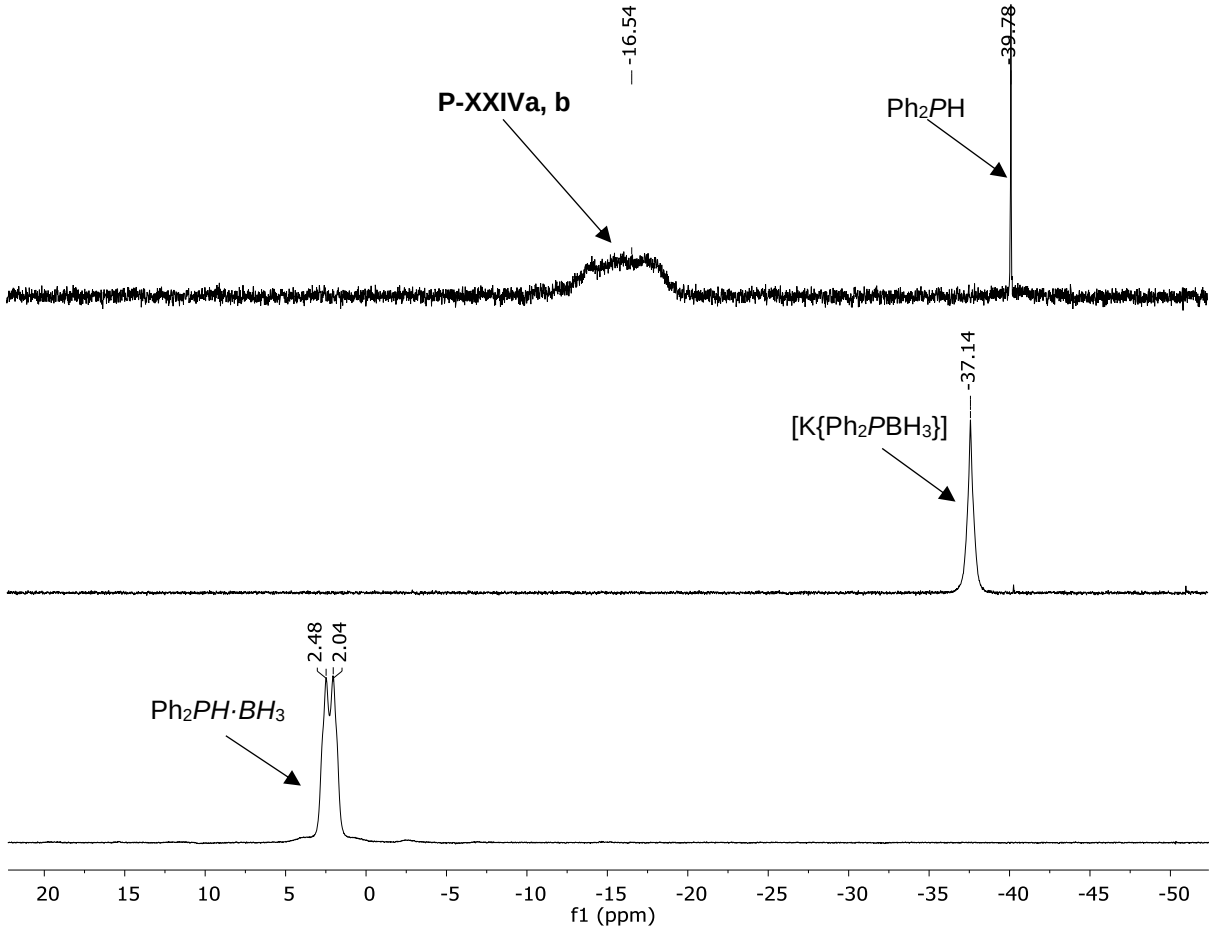

Figure 5.15: Expanded *in situ* $^{31}P\{^1H\}$ NMR spectra (122 MHz, 298 K, C_6D_6) of the reaction sequence shown in Scheme 5.7. Bottom: $Ph_2PH{\cdot}BH_3$, middle: 60 minutes after the addition of [K{$N(SiMe_3)_2$}], top: after addition of $B(C_6F_5)_3$ and heating for approx. 16 hours.

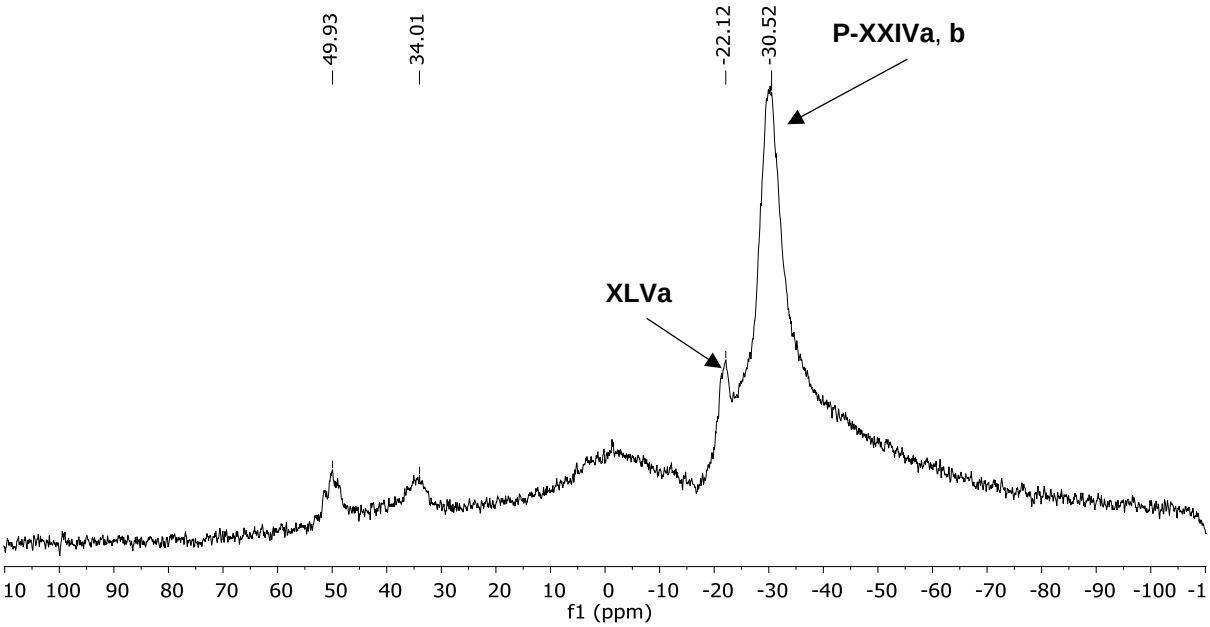

Figure 5.16: *in situ* ^{11}B NMR spectrum (96 MHz, 298 K, C_6D_6) of the reaction shown in Scheme 5.7 after addition of $B(C_6F_5)_3$ and heating to 60°C for approx. 16 hours.

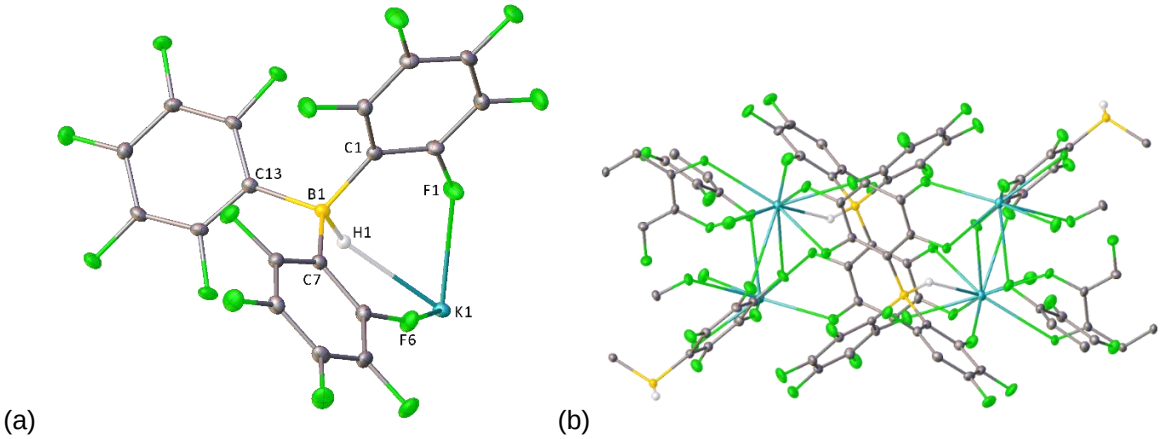

Figure 5.17: X-ray crystal structure of **XLVa.** (a) asymmetric fragment, (b) unit cell packing. Thermal ellipsoids shown at 30% probability level.

5.2.6 Reaction of compound 16a with $B(C_6F_5)_3$

Encouraged by the ability of $B(C_6F_5)_3$ to effect hydride-abstraction promoted phosphine-borane oligomerisation from [K{Ph_2PBH_3}], compound **16a** was exposed to an equimolar solution of $B(C_6F_5)_3$ in d_8-toluene. Although the ^1H NMR spectrum demonstrated clean and quantitative conversion to a new BDI-containing species (**20a**) after a few minutes, the anticipated doublet of the $[HB(C_6F_5)_3]^-$ anion was absent from the ^{11}B NMR spectrum. Instead, two broad resonances were observed at δ -11.0 and -32.3 ppm. A downfield shift in the $^{31}P\{^1H\}$ NMR spectrum resulted in a broad resonance at δ -2.05 ppm. After vacuum drying, the pale-

yellow residue was re-dissolved in toluene and colourless block-like single crystals of compound **20a.toluene** were obtained by slow evaporation at room temperature.

Single-crystal X-ray diffraction revealed the molecular structure of **20a** to be an ion-pair resulting from $[(C_6F_5)_3B\text{-}P(Ph_2)BH_3]^-$ adduct formation. The Lewis acidic $[(BDI)Ca]^+$ cation achieves coordinative saturation through an unusual η^6 interaction with the solvent, resulting in crystallisation of the toluene adduct, **20a.toluene** (Scheme 5.8). The toluene ligand is labile in solution, and dissolving crystals of **20a.toluene** in C_6D_6 results in the release of one equivalent of free toluene (Figure 5.18).[69]

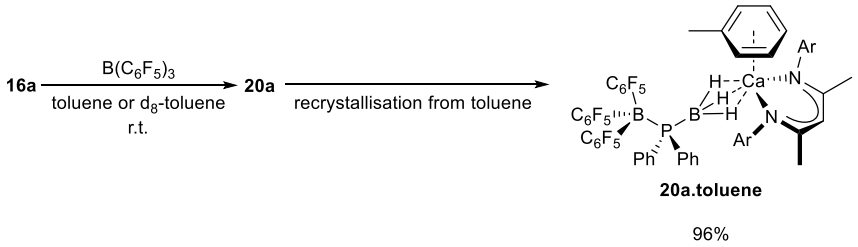

Scheme 5.8: Synthesis of compound **20a.toluene**. Ar = 2,6-di-*iso*propylphenyl.

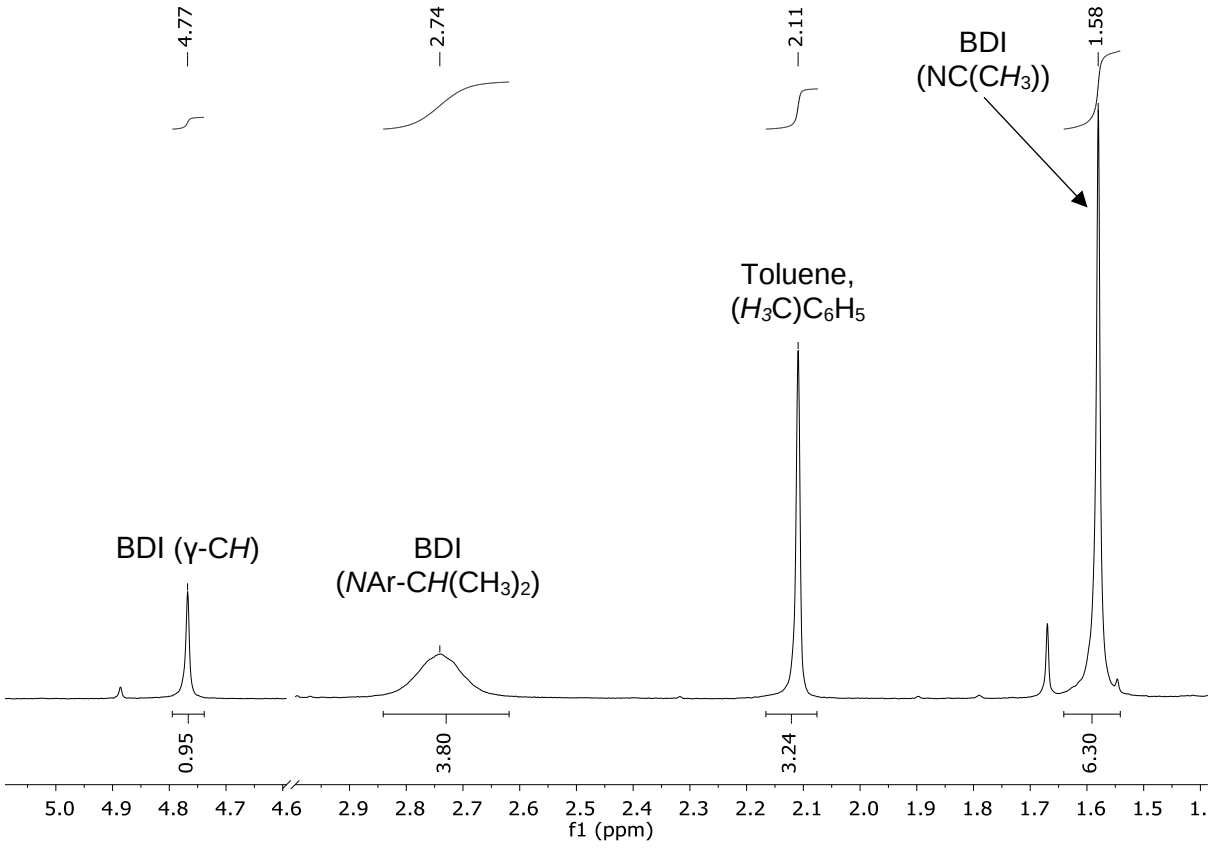

Figure 5.18: Expanded ^{1}H NMR spectrum (300 MHz, C_6D_6, 298 K) obtained from crystals of **20a.toluene** re-dissolved in C_6D_6, showing selected peaks of the BDI-ligand and the C*H*$_3$ resonance corresponding to free-toluene displaced from the calcium centre.

Compound **20a.toluene** crystallises in the triclinic space group, *P-1* (Figure 5.19). The *pseudo*-four-coordinate calcium centre is coordinated to the BDI ligand *via* N1 and N2, to the $[(C_6F_5)_3B\text{-}PPh_2\text{-}BH_3]^-$ anion *via* three B-H-Ca interactions, and to the π-system of a neutral toluene molecule *via* an asymmetric η^6 interaction. Until very recently, the coordination of neutral arenes to alkaline-earth centres was unknown. Charge-separated $[(BDI)Ae]^+[WCA]^-$ species (WCA = weakly coordinating anion: $[B(C_6F_5)_4]^-$ or $[Al\{OC(CF_3)_3\}_4]^-$) are known to coordinate neutral arenes *via* $\eta^{2,3,or\ 6}$ interactions to give complexes **XLVIIa**-**i**.[70-72] Whilst this class of complexes include magnesium-toluene adducts **XLVIIb**, **c**, and **h**,[71, 72] **20a.toluene** is the first crystallographically characterised interaction between a calcium cation and neutral toluene molecule. Previously reported magnesium toluene adducts were sensitive to ligand bulk and WCA choice, with the bulkier ^{tBu}BDI ligand, and/or $[B(C_6F_5)_4]^-$ anion (prone to η^1-F-Mg contacts) resulting in ring slippage, to produce η^3- or η^2-arene binding modes (**XLVIIc**, **e**, **g**-**i**).[70-72] **20a.toluene**, however, retains an unperturbed η^6-coordination mode despite the presence of Ca-H_3B interactions. This can be rationalised by the 'elongated' $[(C_6F_5)_3B\text{-}PPh_2\text{-}BH_3]^-$ anion, whose $\{H_3B\text{-}PPh_2\}$ unit effectively provides a spacer between the $[(BDI)Ca]^+$ cation and bulky C_6F_5 groups, allowing toluene coordination to take place. With calcium sitting 1.3821(18) Å out of the BDI mean plane, a coordination site is provided for the toluene ligand at the *pseudo*-tetrahedral metal-centre (Figure 5.19b). Ca1 is located 2.6391(10) Å from the centroid of the toluene ring and is coordinated in an asymmetric fashion with Ca-C distances ranging from 2.843(2) Å (Ca1-C33) to 3.1365(19) Å (Ca1-C30). The average Ca-C distance of 2.979 Å is slightly longer than those of the calcium-benzene adducts **XLVIId** and **f** (average distance *ca.* 2.93 Å).[70, 71] All bonds in the aromatic ring of toluene are essentially identical in length, demonstrating unperturbed aromaticity.

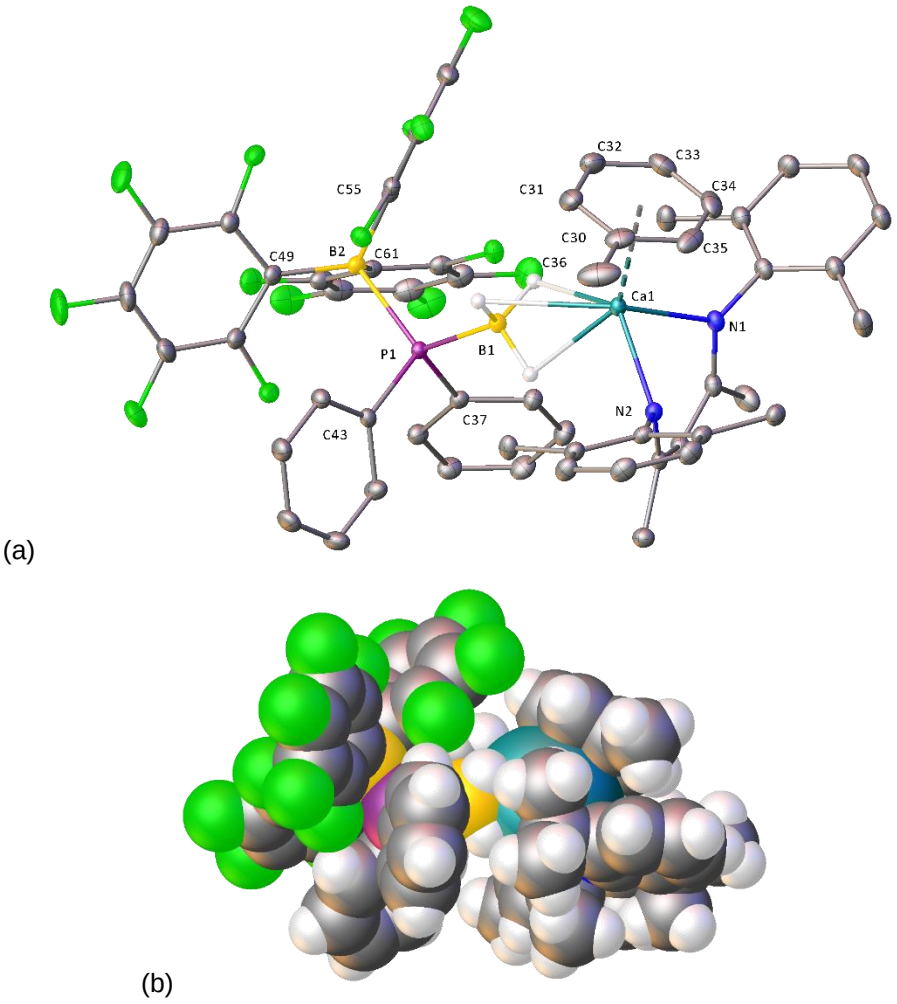

Figure 5.19: X-ray crystal structure of compound **20a.toluene.** (a) Thermal ellipsoids displayed at the 30% probability level with *iso*-propyl methyl groups and hydrogen atoms omitted except those bound to boron. (b) Space filling model demonstrating the coordination site occupied by toluene. Selected bond lengths (Å) and angles (°): Ca1-N1 2.3147(14), Ca1-N2 2.2904(14), Ca1-C30 3.1365(19), Ca1-C31 3.044(2), Ca1-C32 2.905(2), Ca1-C33 2.843(2), Ca1-C34 2.9055(19), Ca1-C35 3.0416(19), Ca1-(C30-C35 centroid) 2.6391(10), Ca1-(C30-C35 centroid plane) 2.6215(11), P1-C37 1.8343(17), P1-C43 1.8382(16), P1-B1 1.9469(18), P1-B2 2.1368(18), C49-B2 1.640(2), C55-B2 1.640(2), C61-B2 1.639(2), C30-C31 1.388(3), C30-C35 1.396(3), C30-C36 1.502(3), C31-C32 1.389(3), C32-C33 1.381(3), C33-C34 1.379(3), C34-C35 1.383(3), N1-Ca1-(C30-C35 centroid) 110.05(5), N1-Ca1-(C30-C35 normal) 105.58(7), N2-Ca1-(C30-C35 centroid) 109.50(4), N2-Ca1-(C30-C35 centroid) 114.48(7), N2-Ca1-N1 84.76(5), C30-C31-C32 120.7(2), C33-C32-C31 120.3(2), C34-C33-C32 119.8(2), C33-C34-C35 119.9(2), C34-C35-C30 121.2(2), C37-P1-C43 103.82(7), C37-P1-B1 105.99(8), C37-P1-B2 109.52(7), C43-P1-B1 106.29(8), C43-P1-B2 114.17(7), B1-P1-B2 116.06(7), C49-B2-P1 110.52(11), C49-B2-C55 111.11(13), C55-B2-P1 104.30(10), C61-B2-P1 102.97(11), C61-B2-C49 114.13(13), C61-B2-C55 113.02(13).

The phosphidodiborate anions, $[(C_6F_5)_3M\text{-}PPh_2\text{-}BH_3]^-$ (M = B, Al), have previously been reported by Lancaster and co-workers in the form of the Et_2O solvated lithium salts **XLVIIIa** and **b**, and were prepared by the addition of $M(C_6F_5)_3$ to the lithium phosphidoborate, $[Li\{PPh_2BH_3\}]$ (Scheme 5.9).[73] By contrast, addition of $B(C_6F_5)_3$ to the lithium amidoborate, $[Li\{Me_2NBH_3\}]$ leads to $[Li\{HB(C_6F_5)_3\}]$ and aminoborane oligomers.[73] The phosphidodiborate anion of **20a.toluene** displays essentially identical geometrical parameters to that of **XLVIIIa**, with near-perfect tetrahedral geometry at P1, and a slightly flattened tetrahedron at B2. The difference in length between the P1-B1 (1.9469(18) Å) and P1-B2 (2.1368(18) Å) bonds can be rationalised on simple steric grounds. Whilst the anion of **XLVIIIa** coordinates to Li through two BH_3 interactions, the metal centre of **20a.toluene** coordinates *via* three BH_3 interactions, leading to a near-linear Ca-B-P geometry.

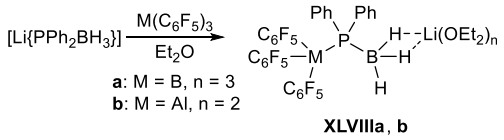

Scheme 5.9: Synthesis of compounds **XLVIIIa** and **b**.[73]

5.2.7 Reaction of compound 15 with $B(C_6F_5)_3$

Compound **15** was reacted with $B(C_6F_5)_3$ in C_6D_6 to provide quantitative and almost instantaneous conversion to the $B(C_6F_5)_3$ adduct, **20b** (Scheme 5.10), which was identified by the similarity of its ^1H, $^{31}P\{^1H\}$, and ^{11}B NMR spectra to those of compound **20a** (Figure 5.21, Figure 5.22).

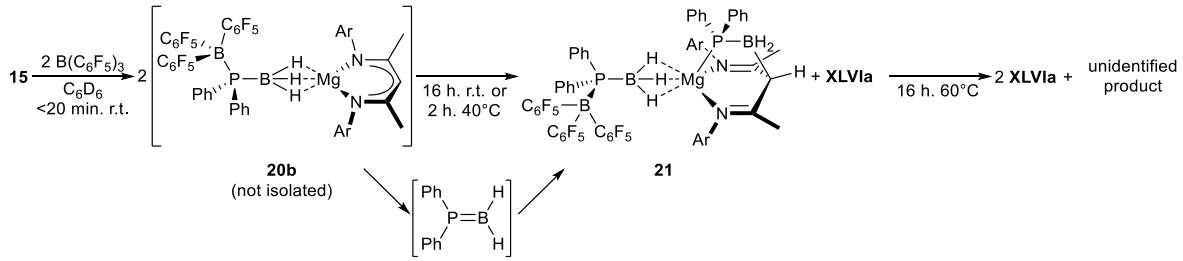

Scheme 5.10: Reaction of compound **15** with $B(C_6F_5)_3$ to provide compounds **20b**, **21**, and **XLVI**. Ar = 2,6-di-*iso*propylphenyl.

Whilst the calcium analogue (**20a**) is stable at room temperature, **20b**, however, rapidly undergoes hydride abstraction and $[HB(C_6F_5)_3]^-$ was detected by ^{11}B NMR after 60 minutes (Figure 5.21). Although this reactivity hampered attempts to crystallographically characterise or isolate **20b** in a pure form, standing at room temperature for a further 16 hours (or two hours at 40°C) yielded a 1:1 mixture of **XLVIa** (γ-C*H* = δ 4.82 ppm) and a second product, compound

21 (Figure 5.20). The ^{1}H NMR spectrum of **21** is unusual, with two sets of *iso*-propyl resonances and the characteristic BDI γ-C*H* signal, normally a singlet at *ca.* δ 4.5-5.0 ppm, replaced by a broad doublet centred at δ 3.90 ppm. The chemical shift of the latter peak is reminiscent to that reported by Jones *et al.* for the boron-bound γ-C*H* of compounds **XLIXa**,**b**, and **d**.[74] In addition to the two peaks of $[(C_6F_5)_3B(Ph_2P)(BH_3)]^-$ in the ^{11}B NMR spectrum at δ -11 and -36 ppm, and the doublet of **XLVIa** at δ -22 ppm, a broad resonance at δ -24 ppm was visible, suggestive of the presence of a four-coordinate boron centre in compound **21** (Figure 5.21). The corresponding ^{31}P{^{1}H} NMR spectrum presented a slightly broadened singlet at δ -42.69 ppm as well as the *pseudo*-doublet of $[(C_6F_5)_3B(Ph_2P)(BH_3)]^-$ at δ -7.31 ppm (Figure 5.22). Two {C_6F_5} species were also apparent in the ^{19}F NMR spectrum.

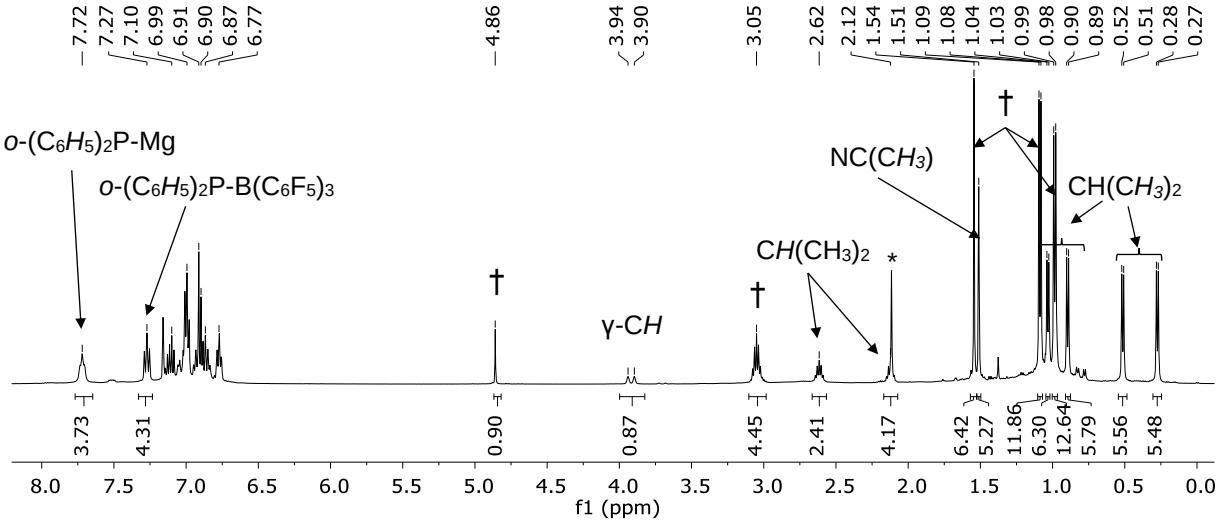

Figure 5.20: *in situ* ^{1}H NMR spectrum (500 MHz, C_6D_6, 298 K) of the reaction between compound **15** and $B(C_6F_5)_3$ after heating to 40°C for two hours to produce a 1:1 mixture of compounds **XLVIa** and **21**. Assignments refer to compound **21**, † = **XLVIa**, * = toluene impurity.

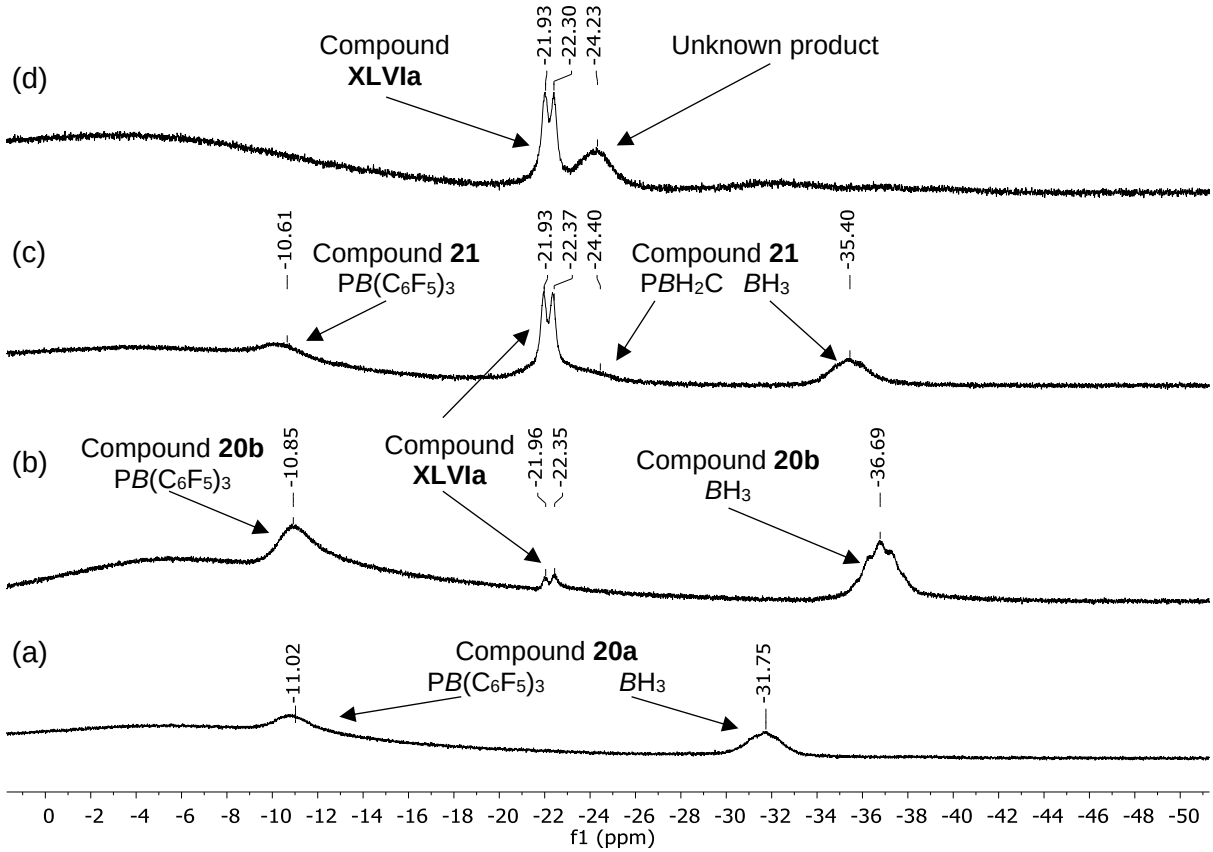

Figure 5.21: Expanded ^{11}B NMR spectra (160 MHz, C_6D_6, 298 K) of (a) compound **20a** (for comparison), (b)-(d) *in situ* reaction between compound **15** and $B(C_6F_5)_3$ (Scheme 5.10). (b) 60 minutes after addition of $B(C_6F_5)_3$ (room temperature) to give **20b**, (c) after two hours at 40°C to give **21** and **XLVIa**, (d) after approx. 16 hours at 60°C.

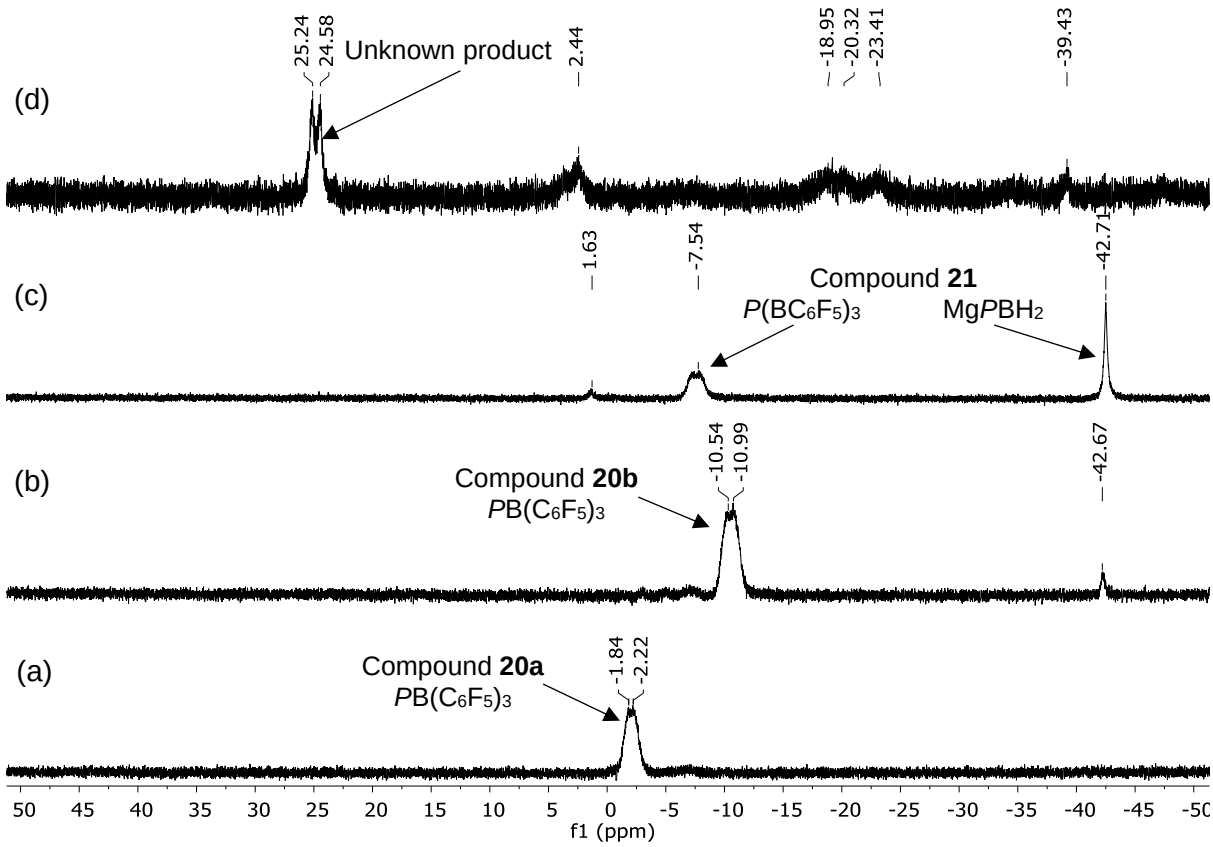

Figure 5.22: Expanded $^{31}P\{^{1}H\}$ NMR spectra (202 MHz, C_6D_6, 298 K) of (a) compound **20a** (for comparison), (b)-(d) *in situ* reaction between compound **15** and $B(C_6F_5)_3$ (Scheme 5.10). (b) 60 minutes after addition of $B(C_6F_5)_3$ (room temperature), (c) after two hours at 40°C, (d) after approx. 16 hours at 60°C.

The molecular structure of compound **21** was revealed by X-ray diffraction, following the deposition of single crystals by addition of hexane/toluene to the crude product (Figure 5.23) to consist of a $[(C_6F_5)_3B(Ph_2P)(BH_3)]^-$ anion and a cationic magnesium centre chelated by an *N,P,N*-ligand. Formation of the latter moiety can be rationalised by γ-C centred nucleophilic attack of the BDI-π-system upon an unsaturated phosphinoborane monomer, to form the C3-B1 bond (Scheme 5.10). Examples of ligand centred reactivity are fairly common amongst BDI-Ae complexes,[67, 74-79] yet examples of C-B bond formation at the γ-carbon of a BDI ligand are limited to compounds **XLIXa**-**d** (Figure 5.24). These compounds were recently reported by Jones *et al.* and formed from reaction of $[(BDI)Mg]_2$ dimers with B_2pin_2 *via* complex and poorly defined mechanisms.[74] Similar reactivity of unsaturated small molecules at cationic BDI-Ae or -Al centres have previously been observed for alkynes or CO_2, yielding compounds **XLXa**,**b**,[75] **XLXI**,[80] and **XLXII** (Scheme 5.11).[67]

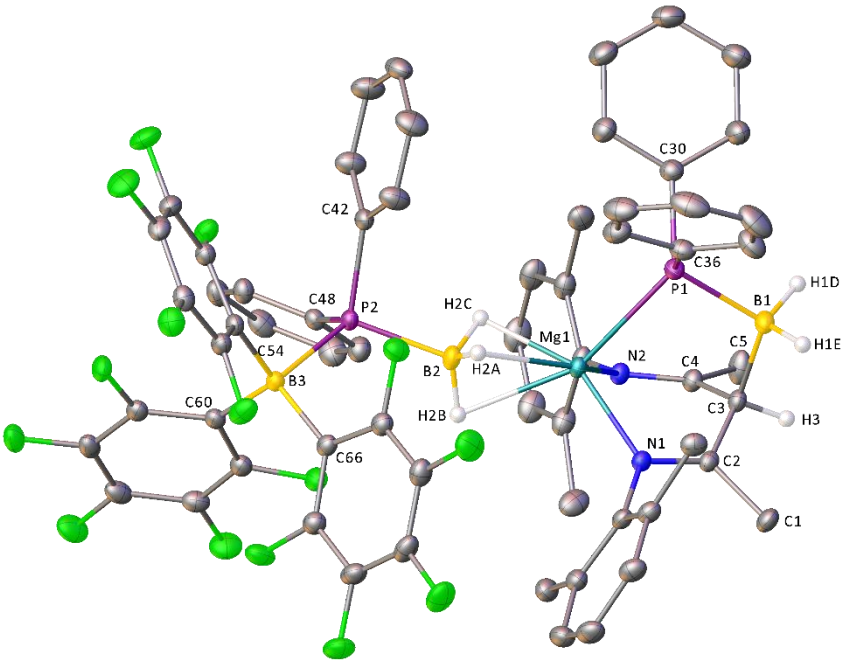

Figure 5.23: X-ray crystal structure of compound **21**. Thermal ellipsoids are shown at the 30% probability level. Hydrogen atoms except for H3 and those bound to boron are omitted for clarity, as are *iso*-propyl methyl substituents. Selected bond lengths (Å) and angles (°): P1-Mg1 2.5701(6), P1-C30 1.8389(17), P1-C36 1.8358(17), P1-B1 1.9791(18), P2-C42 1.8403(15), P2-C48 1.8339(16), P2-B2 1.9251(17), P2-B3 2.1100(16), Mg1-N1 2.0986(13), Mg1-N2 2.1057(13), N1-C2 1.2950(19), N2-C4 1.293(2), C1-C2 1.502(2), C2-C3 1.494(2), C3-C4 1.488(2), C3-B1 1.726(2), C54-B3 1.649(2), C60-B3 1.636(2), C66-B3 1.655(2), C4-C5 1.504(2), C30-P1-Mg1 121.60(6), C30-P1-B1 111.06(8), C36-P1-Mg1 119.50(6), C36-P1-C30 97.43(7), C36-P1-B1 112.27(8), B1-P1-Mg1 95.60(6), C42-P2-B2 102.12(8), C42-P2-B3 117.18(7), C48-P2-C42 104.20(7), C48-P2-B2 106.70(8), C48-P2-B3 110.48(7), B2-P2-B3 115.06(7), N1-Mg1-P1 94.86(4), N1-Mg1-N2 92.73(5), N2-Mg1-P1 96.01(4), N1-C2-C1 123.85(14), N1-C2-C3 122.85(13), C3-C2-C1 113.27(13), C2-C3-B1 110.54(12), C4-C3-C2 119.41(13), C4-C3-B1 112.13(13), N2-C4-C3 122.49(13), N2-C4-C5 123.50(14), C3-C4-C5 114.00(13), C3-B1-P1 110.30(10), C54-B3-P2 110.68(10), C54-B3-C66 109.84(12), C60-B3-P2 103.54(10), C60-B3-C54 113.11(12), C60-B3-C66 112.61(12), C66-B3-P2 106.73(9), Mg1-B2-P2 163.63(10).

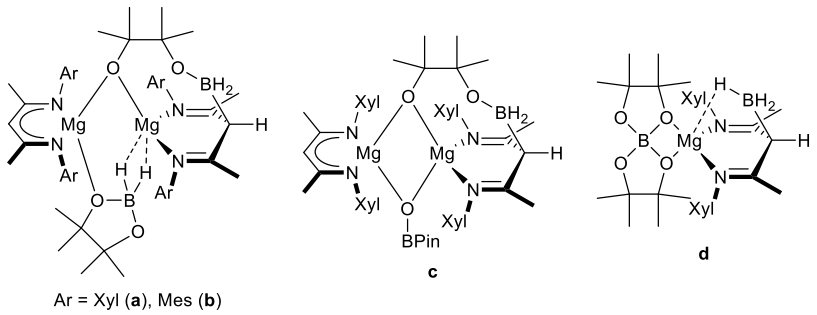

Figure 5.24: Examples of magnesium complexes (**XLIXa**-**d**) formed by γ-C centred attack of the BDI ligand on a boron centre.[74]

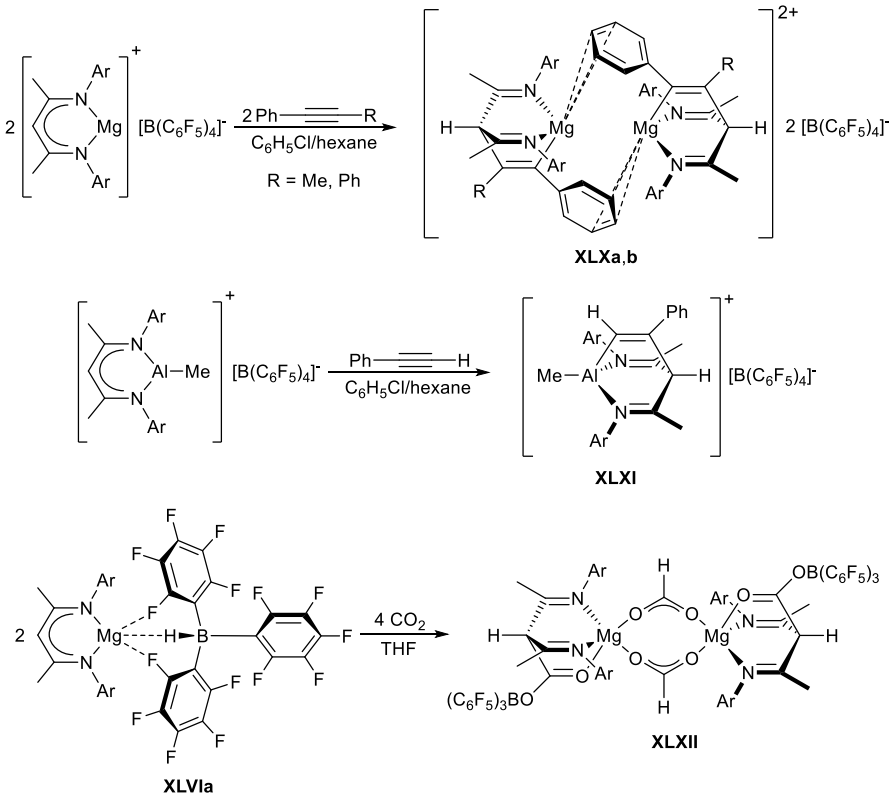

Scheme 5.11: Literature examples of ligand/metal centred activation of unsaturated small molecules at [BDI-M]$^+$ cations.[67, 75, 80] Ar = 2,6-di-*iso*propylphenyl.

Transformation of the BDI-ligand into a bis-imine-type structure with localised C=N double bonds is verified by inspection of the N1-C2 and N2-C4 bond lengths. At 1.2950(19) and 1.293(2) Å, respectively, they are significantly shorter than those typically observed in BDI ligands (for comparison, compounds **20a.toluene** and **15** display N-C bond lengths in the range 1.330(2)-1.327(4) Å). Furthermore, sp^3 hybridisation at C3 is demonstrated by a near tetrahedral geometry (C3-centred angles in the range 110.5-119.4°, compared to C2-C3-C4 = 129.7(3) for **15**), and C2-C3 and C3-C4 single-bonds of length 1.494(2) and 1.488(2) Å, respectively (*cf.* 1.410(4) and 1.416(4) Å for **15**). In conjunction with the *pseudo*-tetrahedral

magnesium centre, the bis-imine framework adopts a boat-like conformation. Interestingly, the C3-B1 bond is significantly longer (1.726(2) Å) than the analogous γ-C-B bonds in compounds **XLIXa**-**d** (1.680(2)-1.697(3) Å).[74] The B1-P1 bond (1.9791(18) Å) is significantly longer than crystallographically characterised B=P double bonds (1.763-1.913 Å), reported P-BH_3 single bonds of secondary phosphine-boranes (*ca.* 1.91 Å), and most complexes described in this chapter (except for **17** (1.9610(19) Å) and **16b** (1.9689(15) Å). The geometry at P1 is rather distorted, with P1-centred angles ranging from 95.60(6)° (B1-P1-Mg1) to 121.60(6)° (C30-P1-Mg1). The $[(C_6F_5)_3B(Ph_2P)(BH_3)]^-$ anion remains geometrically similar to that in compound **20a.toluene**.

Further heating a C_6D_6 solution of **15** and $B(C_6F_5)_3$ to 60°C overnight yielded a pale-yellow solution (Scheme 5.10). $^{31}P\{^1H\}$ and ^{11}B NMR showed that the $[(C_6F_5)_3B(Ph_2P)(BH_3)]^-$ anion of compound **21** had been consumed, with compound **XLVIa** as the only BDI-containing species visible by ^1H NMR spectroscopy. These observations suggest that two molecules of Ph_2PBH_2 monomer are produced from compound **21** on heating: one dissociating from the *N,P,N* tripodal ligand, and one originating from hydride abstraction of the $[(C_6F_5)_3B(Ph_2P)(BH_3)]^-$ anion. Neither $^{31}P\{^1H\}$, nor ^{11}B NMR spectroscopy, however, provided signals consistent with the expected oligophosphinoboranes. Rather, a yet unidentified product was characterised by an apparent doublet centred at δ 25 ppm in the $^{31}P\{^1H\}$ NMR spectrum, whilst the ^{11}B NMR spectrum displayed a broad resonance at δ -24 ppm. Work to uncover the origin of these observations is ongoing.

5.3 Conclusions

In summary, deprotonation of diphenylphosphine-borane by β-diketiminato magnesium and calcium hydride, amide, and alkyl complexes affords a series of phosphidoborate complexes, **15**-**18**. Although compound **15** is dimeric in the solid state by X-ray crystallography, NMR spectroscopy advocates a more dynamic system in solution. Whilst the calcium analogue **16a** could not be crystallographically characterised, addition of THF provides the monomeric compound **16b**. The dimeric magnesium- and trimeric-calcium complexes, **17** and **18**, display solid-state structures in which the metal centres are bridged by both hydride and phosphidoborate ligands. Addition of diphenylphosphine-borane to the magnesium phosphidoborate **15** results in P-B bond cleavage to afford diphenylphosphine, whilst insertion of BH_3 into a Mg-P bond provides the diphenylphosphinodiborate complex **19**, preventing the realisation of catalytic phosphine-borane dehydrogenation. Stoichiometric dehydrogenation was possible, however, through stepwise deprotonation and hydride abstraction utilising $[K\{N(SiMe_3)_2\}]$ and $B(C_6F_5)_3$. Addition of $B(C_6F_5)_3$ to compound **16a** results in P-$B(C_6F_5)_3$ adduct formation and an unusual calcium complex, **20a**, which was isolated as its η^6-toluene

adduct **20a.toluene**. The analogous magnesium complex **20b** was identified by NMR spectroscopy, but rapidly undergoes hydride abstraction at room temperature to provide the known borate complex **XLVIa** and compound **21**. The latter complex is thought to result from the *in situ* generation of an unsaturated phosphinoborane molecule and its reaction with the β-diketiminate ligand of compound **20b**, to result in a tripodal *N,P,N*-ligand framework. These studies highlight the diverse reactivity of alkali- and alkaline-earth complexes towards *p*-block element-containing substrates. Further investigations into this underexploited field promise to provide inorganic chemists with a range of interesting and useful tools for the rational construction of main-group element-containing molecules and polymers.

5.4 Experimental details

5.4.1 Synthesis of compound 15

In Schlenk flask: A Schlenk flask was charged with 1.0 g **Va** (2.0 mmol) and 0.4 g $Ph_2PH{\cdot}BH_3$ (2.0 mmol). The mixture was stirred and approx. 20 ml toluene was added *via* cannula, resulting in an off-white suspension. After stirring at room-temperature for 2 hours, the reaction mixture was heated to 50°C, resulting in dissolution of the precipitate and formation of a pale-yellow solution. The mixture was slowly cooled to room temperature and placed in a freezer at -30°C, resulting in the deposition of colourless crystals. Filtration and washing with fresh toluene resulted in the isolation of pure compound **15**. Yield 0.66 g, 51%.

In NMR tube: In a J. Young's NMR tube, 50 mg **Va** (0.1 mmol) was dissolved in 0.6 ml d_8-toluene. 20 mg $Ph_2PH{\cdot}BH_3$ (0.1 mmol) was dissolved in 0.1 ml d_8-toluene and added to the reaction mixture, providing a cloudy colourless suspension. After 24 hours, the NMR tube contained a large quantity of colourless solid and complete consumption of the starting materials was demonstrated by multinuclear NMR spectroscopy. The solid was re-dissolved by heating to 80°C, then allowed to slowly cool to room temperature to yield a crop of colourless crystals suitable for single crystal X-ray diffraction analysis. Yield 42.5 mg, 66%. A second crop of crystals (8 mg, 12%) could be obtained by cooling the supernatant to -30°C. Compound **15** is poorly soluble in aromatic solvents at room temperature and NMR spectra recorded at 298 K were broad and uninformative. Heating a d_8-toluene solution to 349 K within the spectrometer resulted in well-defined, sharp signals and allowed good-quality spectra to be recorded. ^{1}H NMR (400 MHz, d_8-toluene, 349 K) δ 7.12-7.03 (m, 4H, *o*-P(C_6H_5)$_3$), 7.03 – 6.93 (m, 6H, NAr), 6.93 – 6.82 (m, 6H, *m*+*p*-P(C_6H_5)$_3$), 4.95 (s, 1H, NC(CH_3)C*H*), 3.20 (hept, *J* = 6.8 Hz, 4H, (H_3C)$_2$C*H*), 1.70 (s, 6H, NC(CH_3)CH), 1.11 (m, 24H, (*H*$_3$C)$_2$CH). Boron-bound hydrogen atoms could not be detected. ^{31}P{^{1}H} NMR (162 MHz, d_8-toluene, 349 K) δ -57.09 (*br*). ^{11}B NMR (128 MHz, d_8-toluene, 349 K) δ -34.01 (qd, J_{1H} = 91.1, J_{31P} = 44.3 Hz). ^{13}C{^{1}H} NMR (101 MHz, d_8-toluene, 349 K) δ 170.89 (N*C*(CH_3)CH), 144.37 (NAr-C_{ipso}), 143.06 (NAr-

C_{ortho}), 133.83 (d, J_{31P} = 12.4 Hz, *o*-P(C_6H_5)$_3$), 127.63(*m*-P(C_6H_5)$_3$), 126.27 (*p*-P(C_6H_5)$_3$), 125.71 (NAr-C_{para}), 124.49 (NAr-C_{meta}), 95.41 (NC(CH_3)*C*H), 29.00 (NC(*C*H_3)CH), 24.69 (H_3C)$_2$CH), 24.50 (H_3C)$_2$CH), 24.32 (NC(*C*H_3)CH). Analysis calculated for $C_{82}H_{108}B_2Mg_2N_4P_2$: C 76.83, H 8.49, N 4.37 %. Found: C 76.32, H 8.38, N 4.25%.

5.4.2 Synthesis of compound 16a

In the glove box, 200 mg **IVb** (0.324 mmol) was added to a Schlenk flask and dissolved in 5 ml toluene with stirring. $Ph_2PH{\cdot}BH_3$ (65 mg, 0.324 mmol) was dissolved in 1 ml of toluene in a vial, then added to the Schlenk flask. The reaction was removed from the glove box and stirred at room temperature for 16 hours before volatiles were removed under vacuum. The resulting pale-yellow solid was washed with three portions of hexane, then vacuum dried to yield compound **16a** in near analytical purity. Yield 52 mg, 24%. Despite repeated attempts to crystallise compound **16a** from various solvent systems, we were unable to obtain satisfactory single crystals. Although the NMR spectra were broad and uninformative at 298 K (probably due to monomer/dimer equilibration), analysis by multinuclear NMR spectroscopy at 320 K was unambiguous. Furthermore, addition of two molar equivalents of THF to a C_6D_6 solution of **16a** lead to the quantitative formation of the THF adduct **16b**. ^{1}H NMR (400 MHz, d_8-toluene, 320.6 K) δ 7.28 (br, 4H, *o*-P(C_6H_5)$_3$), 7.08-7.02 (m, 6H, NAr), 6.95-6.85 (m, 6H, *m*+*p*-P(C_6H_5)$_3$), 5.03 (s, 1H, NC(CH_3)C*H*), 3.10 (br m, 4H, (H_3C)$_2$C*H*), 1.74 (s, 6H, NC(CH_3)CH), 0.99 (br m, 24H, (H_3C)$_2$CH). Boron-bound hydrogen atoms could not be detected. ^{13}C{^{1}H} NMR (101 MHz, d_8-toluene, 320.6 K) δ 166.57 (N*C*(CH_3)CH), 145.80 (NAr-C_{ipso}), 142.08 (NAr-C_{ortho}), 134.22 (d, $^2J_{13P}$ = 12.7 Hz, *o*-P(C_6H_5)$_3$), 128.51 (*m*-P(C_6H_5)$_3$), 127.46 (*p*-P(C_6H_5)$_3$), 125.02 (NAr-C_{para}), 124.08 (NAr-C_{meta}), 93.24 (NC(CH_3)*C*H), 28.76 (H_3C)$_2$*C*H), 25.45 (H_3C)$_2$CH), 24.77 (NC(*C*H_3)CH), 24.42 (H_3C)$_2$CH). ^{11}B NMR (128 MHz, d_8-toluene, 320.6 K) δ -30.16 (br m). ^{31}P{^{1}H} NMR (162 MHz, d_8-toluene, 320.6 K) δ -44.96 (br). Although the reluctance of compound **16a** to crystallise prevented us from obtaining the compound in sufficient purity for satisfactory elemental microanalysis, the results are nevertheless shown here for completeness. Analysis calculated for $C_{41}H_{54}BCaN_2P$: C 74.98, H 8.29, N 4.27%. Found: C 73.13, H 8.30, N 4.12%.

5.4.3 Synthesis of compound 16b

In a Schlenk flask from IVc: In the glove box, a Schlenk flask was charged with 200 mg **IVc** (0.29 mmol) and 58 mg $Ph_2PH{\cdot}BH_3$ (0.29 mmol). Toluene (approx. 5 ml) was added *via* cannula on the Schlenk line. The reaction was stirred at room temperature for 60 minutes, before being concentrated to two-thirds volume and placed in a freezer at -20°C, yielding colourless crystals of compound **16b**. The product was isolated by filtration, washed with hexane, dried under vacuum. Colourless block-like crystals suitable for X-ray diffraction analysis were obtained by cooling a saturated toluene solution to -30°C. Yield 66 mg, 31%.

In a J. Young's NMR tube from VIc: A d_8-toluene solution (0.3 ml) of **VIc** (20 mg, 0.019 mmol) was added to a J. Young's NMR tube containing a d_8-toluene solution (0.3 ml) of $Ph_2PH{\cdot}BH_3$ (7.5 mg, 0.038 mmol). The reaction mixture bubbled immediately and was concentrated to approx. 0.2 ml under vacuum after 24 hours at room temperature. Colourless crystals were obtained by cooling the concentrated reaction mixture to -30°C. Yield 5.2 mg, 38%. ^{1}H NMR (500 MHz, C_6D_6) δ 7.28 – 7.22 (m, 4H, *o*-P(C_6H_5)$_2$), 7.22 – 7.17 (m, 6H, 3,4,5-NAr), 7.06 – 6.93 (m, 6H, *m*+*p*-P(C_6H_5)$_2$), 4.83 (s, 1H, NC(CH_3)C*H*), 3.68 (t, *J* = 6.2 Hz, 4H, 2,5-THF), 3.23 (hept, *J* = 6.8 Hz, 4H, C*H*(CH_3)), 1.69 (s, 6H, NC(C*H*$_3$)CH), 1.4-1.0 (br, B*H*$_3$), 1.22 (t, *J* = 7.0 Hz, 28H, CH(C*H*$_3$) + 3,4-THF). ^{13}C{^{1}H} NMR (126 MHz, C_6D_6) δ 166.35 (N*C*(CH_3)CH), 145.63 (*1*-NAr), 142.03 (2,6-NAr), 133.96 (*o*-P(C_6H_5)$_2$), 133.85 (*o*-P(C_6H_5)$_2$), 128.17 (*m*-P(C_6H_5)$_2$), 127.97 (*p*-P(C_6H_5)$_2$), 126.91 (*i*-P(C_6H_5)$_2$), 125.08 (4-NAr), 124.21 (3,5-NAr), 94.04 (NC(CH_3)*C*H), 69.85 (2,5-THF), 28.59 (*C*H(CH_3)), 25.28 (CH(*C*H$_3$), 25.22 (3,4-THF), 24.66 (CH(*C*H$_3$), 24.49 (NC(*C*H$_3$)CH). Boron-bound hydrogen atoms could not be detected. ^{11}B NMR (160 MHz, C_6D_6) δ -27.10. ^{31}P NMR (202 MHz, C_6D_6) δ -38.06 (br). Analysis calculated for $C_{45}H_{62}BCaN_2OP$: C 74.16, H 8.57, N 3.84%. Found: C 73.62, H 8.47, N 3.97%.

5.4.4 Synthesis of compound 17

In a J. Young's NMR tube, 20 mg **VIa** (0.023 mmol) was dissolved in 0.5 ml d_8-toluene. A solution containing 4.6 mg $PH_2PH{\cdot}BH_3$ (0.023 mmol) in 0.1 ml d_8-toluene was added. The tube was shaken, with immediate and vigorous bubbling. The reaction was left to stand at room temperature for 24 hours, before being decanted into a vial and placed in a freezer at -30°C, yielding a crop of colourless crystals suitable for single-crystal X-ray diffraction analysis. Yield: 16 mg, 64%. Although crystals of **17** could be isolated in an analytically pure form, when redissolved in d_8-toluene, the ^{1}H NMR spectrum was complex and accompanied by the appearance of an additional minor species containing resonances corresponding to BDI and Ph_2P environments. Thus, unambiguous assignment of the spectrum was precluded. Addition of a small quantity of d_8-THF, however, produced a well-defined spectrum that presumably results from formation of the THF-adducts [LMgH·THF]$_2$ (**VIb**)[32] and [LMg(Ph_2PBH_3) THF] (**15.THF**), allowing the constituent parts of compound **17** to be unambiguously identified. ^{1}H NMR (500 MHz, d_8-toluene) δ 7.95 (t, *J* = 7.9 Hz, 1H, *o*-(C_6H_5)P)*, 7.30-6.80 (m, *N*Ar), 6.89 (m, 4H, *o*-(C_6H_5)P), 6.73 (t, *J* = 8.8 Hz, 2H, *p*-(C_6H_5)P), 6.70-6.65 (m, 1H, *m*-(C_6H_5)P)*, 6.65-6.58 (m, 4H, *m*-(C_6H_5)P), 6.56-6.44 (br, 2H), 4.83 (s, 2H, NCC*H*), 4.78 (s, 0H, NCC*H*)*, 3.46 (br, 4H (H_3C)$_2$C*H*), 3.40 (s, 1H, Mg*H*), 3.34-3.17 (m, br, 4H, (H_3C)$_2$C*H*), 3.04 (hept, *J* = 7.0 Hz, 1H, (H_3C)$_2$C*H*)*, 2.67 (br, 2H, (H_3C)$_2$C*H*), 1.60-1.50 (m, br, 18H), 1.50-1.41 (m, br, 15H (NC(C*H*$_3$)CH + (*H*$_3$C)$_2$CH), 1.38 (br, 12H, (*H*$_3$C)$_2$CH), 1.28-1.10 (m, br, 23H, (*H*$_3$C)$_2$CH), 1.09 (d, *J* = 6.9 Hz, 6H, (*H*$_3$C)$_2$CH)*, 1.01 (br, 9H, (*H*$_3$C)$_2$CH), 0.85 (d, *J* = 6.7 Hz, 3H)*, 0.49 (br, m, 5H), -0.35 (br, 1H), -0.71 (br, 2H). Boron-bound hydrides could not be unambiguously

detected. ^{1}H NMR (500 MHz, d_8-toluene + d_8-THF) δ 7.21-7.14 (m, 6H, *o*+*p*-(C_6H_5)P), 7.13-7.06 (m, 10H, *N*Ar + *m*-(C_6H_5)P), 6.96-6.92 (m, 6H, *N*Ar), 4.82 (s, 1H, NCC*H*), 4.74 (s, 1H, NCC*H*), 4.05 (s, 1H, Mg*H*), 3.43 (hept, *J* = 6.7 Hz, $(H_3C)_2CH$), 3.13 (m, br), 1.68 (s, 6H, NCCH_3), 1.58 (s, 6H, NCCH_3), 1.30 (d, *J* = 6.8 Hz, 6H, $(H_3C)_2CH$), 1.20 (d, *J* = 6.8 Hz, 6H, $(H_3C)_2CH$), 1.15 (d, *J* = 6.3 Hz, 12H, $(H_3C)_2CH$), 0.59 (q, $^{1}J_{11B}$ = 79 Hz, 3H, BH_3). ^{13}C{^{1}H} NMR (126 MHz, d_8-toluene) δ 169.14 (N*C*(CH_3)CH), 148.04 (1-*N*Ar)*, 146.92 (1-*N*Ar), 143.74 (2,6-*N*Ar), 142.07 (2,6-*N*Ar)*, 138.97 (*i*-(C_6H_5)P), 135.34 (d, *J*(^{31}P-^{13}C) = 11.1 Hz, *o*-(C_6H_5)P), 133.96 (*o*-(C_6H_5)P)*, 132.75 (d, *J*(^{31}P-^{13}C) = 9.9 Hz, *p*-(C_6H_5)P), 127.52 (3,5-*N*Ar), 127.46 (3,5-*N*Ar), 127.20 (d, *J*(^{31}P-^{13}C) = 8.1 Hz, *m*-(C_6H_5)P), 125.85 (*m*-(C_6H_5)P)*, 123.98 (4-*N*Ar), 123.51 (4-*N*Ar), 95.28 (NC(CH_3)*C*H), 28.26 ($(H_3C)_2CH$), 24.83 ($(H_3C)_2CH$), 24.67 ($(H_3C)_2CH$), 24.51 ($(H_3C)_2CH$), 24.07 (NC(CH_3)CH). ^{31}P NMR (202 MHz, d_8-toluene) δ -42.8*, -46.80. ^{11}B NMR (160 MHz, d_8-toluene) δ -31.21. * = unidentified minor product formed upon dissolution of crystals. Analysis calculated for $C_{70}H_{96}BMg_2N_4P$: C 77.56, H 8.93, N 5.17 %. Found: C 77.50, H 8.80, N 4.79 %.

5.4.5 Synthesis of compound 18

A solution of **VId** (20 mg, 0.0218 mmol) in 0.3 ml C_6D_6 was added to a J. Young's NMR tube containing 4.3 mg $Ph_2PH{\cdot}BH_3$ (0.0218 mmol) in 0.2 ml C_6D_6. On mixing, the reaction mixture bubbled. After 30 minutes at room temperature, solvent was removed under vacuum and the resulting solid dissolved in toluene. Cooling the toluene solution to -30 °C yielded colourless crystalline blocks suitable for single-crystal X-ray diffraction analysis. Yield 5.0 mg, 19%. Although crystals of **18** could be isolated in an analytically pure form, when re-dissolved in d_8-toluene, the ^{1}H NMR spectrum was complex and appeared to be composed of more than one species, accompanied by the appearance of an additional minor species. Thus, unambiguous assignment of the spectrum was precluded. ^{1}H NMR (500 MHz, d_8-toluene) δ 7.70 (t, *J* = 7.9 Hz, 4H, *o*-(C_6H_5)P), 7.50-7.11 (br, 8H, *o*-(C_6H_5)P), 7.09-7.03 (m, 13H, *p*-(C_6H_5)P + NAr), 7.01-6.98 (m, 12H, NAr + (C_6H_5)P), 6.97-6.85 (m, 10H, *m*-(C_6H_5)P), 5.04 (s, br, 1H, (NCC*H*)), 4.86 (s, 2H, (NCC*H*)), 4.50 (d, *J* = 14 Hz, 1H, (Ca*H*)), 3.50-3.30 (m, br, 9H, (C*H*(CH_3)$_2$)) 2.97 (hept, *J* = 6.4 Hz, 9H, (C*H*(CH_3)$_2$)), 1.74 (s, 11H, (NCCH_3)), 1.65 (s, 13H, (NCCH_3)), 1.22-1.16 (m, 14H, (CH(CH_3)$_2$)), 1.14 (d, *J* = 6.8 Hz, 9H, (CH(CH_3)$_2$)), 1.14 (d, *J* = 6.8 Hz, 28H, (CH(CH_3)$_2$)), 0.99 (d, *J* = 6.8 Hz, 24H, (CH(CH_3)$_2$)). Hydrogen atoms attached to boron could not be detected by ^{1}H NMR spectroscopy. ^{13}C{^{1}H} NMR (126 MHz, d_8-toluene) δ 166.41 (N*C*(CH_3)CH), 166.08 (N*C*(CH_3)CH), 161.39 (N*C*(CH_3)CH), 145.08 (*i*-NAr), 142.69 (*o*-NAr), 141.74 (*o*-NAr), 139.05 (d, *J* = 10.2 Hz, *i*-(C_6H_5)P), 137.76 (toluene), 136.29 (*o*-NAr), 134.19 (*o*-(C_6H_5)P), 134.07 (*o*-(C_6H_5)P), 133.98 (*o*-(C_6H_5)P), 128.45 (*m*-NAr), 128.22 (*p*-(C_6H_5)P), 126.97 (*m*-(C_6H_5)P), 124.07 (*p*-NAr), 124.01 (*m*-(C_6H_5)P), 123.48 (4-*N*Ar), 123.26 (4-*N*Ar), 91.99 (NC*C*H), 28.69 (*C*H(CH_3)$_2$), 28.63 (*C*H(CH_3)$_2$), 28.57 (*C*H(CH_3)$_2$), 28.36 (*C*H(CH_3)$_2$),

25.39 (CH(*C*H$_3$)$_2$), 24.80 (CH(*C*H$_3$)$_2$), 24.72 (CH(*C*H$_3$)$_2$), 24.47 (CH(*C*H$_3$)$_2$), 24.15 (NC*C*H$_3$), 23.92 (NC*C*H$_3$), 23.70 (CH(*C*H$_3$)$_2$), 23.35 (CH(*C*H$_3$)$_2$), 23.08 (CH(*C*H$_3$)$_2$).^{31}P NMR (202 MHz, d$_8$-toluene) δ -45.50. ^{11}B NMR (160 MHz, d$_8$-toluene) δ -30.54. Analysis calculated for $C_{111}H_{150}B_2Ca_3N_6P_2$: C 75.23, H 8.53, N 4.74%. Found: C 75.39, H 8.51, N 4.63%.

5.4.6 Synthesis of compound 19

A 0.3 ml C_6D_6 solution containing 8 mg $Ph_2PH{\cdot}BH_3$ (0.04 mmol) was added to a J. Young's NMR tube containing 20 mg **Va** (0.04 mmol). A colourless solid rapidly precipitated from the reaction mixture. After 3 hours, a further 8 mg $Ph_2PH{\cdot}BH_3$ (0.04 mmol) was added as a solution in 0.1 ml C_6D_6 and the reaction mixture was heated to 60°C for 16 h, resulting in a colourless solution. The solution was concentrated and a colourless solid was deposited. The mother liquor was decanted and the solid washed twice with hexane then vacuum dried to obtain **19**. Yield 20 mg, 76%. Single crystals suitable for X-ray diffraction were obtained by slowly cooling a saturated toluene solution from 80°C to room temperature. ^{1}H NMR (300 MHz, C_6D_6) δ 7.29-7.21 (m, 4H, *o*-(C$_6$*H*$_5$)$_2$P), 7.11 (s, 6H, NAr-*H*), 6.87 (m, 6H, *m*+*p*-C$_6$*H*$_5$), 4.96 (s, 1H, NC(CH$_3$)C*H*), 3.38 (hept, *J* = 6.9 Hz, 4H, C*H*(CH$_3$)$_2$), 1.74 (s, 6H, NC(C*H*$_3$)CH), 1.33 (d, *J* = 6.8 Hz, 12H, CH(C*H*$_3$)$_2$), 1.16 (d, *J* = 6.8 Hz, 12H, CH(C*H*$_3$)$_2$). The hydrogen atoms attached to boron could not be detected by ^{1}H NMR spectroscopy. ^{31}P{^{1}H} NMR (122 MHz, C_6D_6) δ -24.83 (br). ^{11}B NMR (96 MHz, C_6D_6) δ -34.28 (br). ^{13}C{^{1}H} NMR (76 MHz, C_6D_6) δ 169.79 (N*C*(CH$_3$)CH), 144.10 (NAr-*C*$_{ipso}$), 143.14 (NAr-*C*$_{ortho}$), 132.83 (d, $^2J_{31P}$ = 9.0 Hz, *o*-(*C*$_6$H$_5$)$_2$P), 130.47 (d, $^1J_{31P}$ = 54.0 Hz, *i*-(*C*$_6$H$_5$)$_2$P), 129.86 (d, $^4J_{31P}$ = 2.5 Hz, *p*-(*C*$_6$H$_5$)$_2$P), 128.60 (d, $^3J_{31P}$ = 10.1 Hz, *m*-(*C*$_6$H$_5$)$_2$P), 125.91 (NAr-*C*$_{para}$), 124.35 (NAr-*C*$_{meta}$), 95.19 (NC(CH$_3$)*C*H), 28.69 (*C*H(CH$_3$)$_2$), 25.25 (NC(*C*H$_3$)CH), 24.57 (CH(*C*H$_3$)$_2$), 24.54 (CH(*C*H$_3$)$_2$). Elemental analysis calculated for $C_{41}H_{57}B_2MgN_2P$: C 75.20, H 8.77, N 4.28%. Found: C 74.87, H 8.60, N 4.12%.

5.4.7 Sequential reaction of $Ph_2PH{\cdot}BH_3$ with [K{N(SiMe$_3$)$_2$}] and B(C$_6$F$_5$)$_3$

NMR scale: A C_6D_6 solution of $Ph_2PH{\cdot}BH_3$ (10 mg, 0.05 mmol, in 0.6 ml C_6D_6) was added to a J. Young's NMR tube containing 10 mg K{N(SiMe$_3$)$_2$} (0.05 mmol). Analysis by ^{1}H, ^{11}B, and ^{31}P NMR confirmed quantitative conversion to the potassium phosphidoborane, [K{Ph_2PBH_3}] and HN(SiMe$_3$)$_2$ in under 60 minutes.[42] B(C$_6$F$_5$)$_3$ (26 mg, 0.05 mmol) was added to the reaction mixture, which was then heated to 60°C for 16 hours. Colourless crystalline plates of **XLVa** were deposited and identified in solution by comparison of the ^{11}B and ^{19}F NMR with the literature,[55] and in the solid state by single-crystal X-ray diffraction. ^{31}P,^{11}B, and ^{1}H NMR data were consistent with the formation of cyclic oligophosphinoboranes **P-XXIVb** and/or **c**.[16]

Schlenk scale: In the glove box, three Schlenk flasks were separately charged with 50 mg [K{N(SiMe$_3$)$_2$}], 130 mg B(C$_6$F$_5$)$_3$ and 50 mg $Ph_2PH{\cdot}BH_3$ (each 0.25 mmol). Using standard Schlenk techniques, toluene (approx. 2 ml) was added to each flask *via* cannula. The $Ph_2PH{\cdot}BH_3$ solution was subsequently added to the stirred [K{N(SiMe$_3$)$_2$}] solution *via* cannula

to produce a slightly cloudy colourless solution. After 60 minutes at room temperature, the $B(C_6F_5)_3$ solution was added *via* cannula and stirred at 60°C for two days, resulting in a pale pink solution and colourless precipitate. The reaction mixture was cooled, first to room temperature, then -20°C, after which the colourless crystalline solid of **XLVa** was isolated by cannula filtration. Removing solvent from the filtrate under vacuum yielded a soft, pale orange solid, the NMR of which was in agreement with low purity cyclic oligophosphinoboranes.

5.4.8 Reaction of 16a with $B(C_6F_5)$ and isolation of compound 20a.toluene

In an NMR tube from VId: A J. Young's NMR tube was charged with 20 mg **VId** (0.0218 mmol) and 8.7 mg $Ph_2PH{\cdot}BH_3$ (0.0436 mmol). The addition of 0.5 ml d_8-toluene was accompanied by vigorous bubbling. After 10 minutes, 22 mg $B(C_6F_5)_3$ (0.0436 mmol) was added as a solution in 0.2 ml d_8-toluene. Analysis of the reaction mixture by multinuclear NMR spectroscopy showed almost instantaneous and quantitative conversion to compound **20a**. After solvent evaporation under vacuum, the resulting pale-yellow residue was re-dissolved in minimal toluene. Colourless block-like single crystals of **20a.toluene** suitable for X-ray diffraction were obtained by slow evaporation at room temperature. Yield 13.2 mg, 96%.

In a Schlenk flask from 16a: In the glove box, a Schlenk flask was charged with 50 mg **16a** (0.076 mmol) and 39 mg $B(C_6F_5)_3$ (0.076 mmol). The flask was transferred to the Schlenk line, and toluene (~5 ml) was added *via* cannula. The reaction mixture was stirred for 5 minutes, during which time a clear pale-yellow solution formed. Solvent was removed under vacuum to obtain compound **20a.toluene** as a pale-yellow powder. Yield 22 mg, 23%. ^{1}H NMR (300 MHz, C_6D_6) δ 7.58 – 7.45 (m, 4H, *o*-P(C_6H_5)), 7.13 (m, 2H, *3,5*-$H_3C(C_6H_5)$), 7.09 (m, 6H, *N*Ar), 7.00 (m, 5H, 2,4,6- $H_3C(C_6H_5)$ + *p*-P(C_6H_5)), 6.90 (td, *J* = 7.5, 2.1 Hz, 4H, *m*-P(C_6H_5)), 4.77 (s, 1H, NC(CH_3)C*H*), 2.85-2.60 (br, 4H, $(H_3C)_2CH$), 2.11 (s, 3H, $H_3C(C_6H_5)$), 1.58 (s, 1H, NC(CH_3)CH), 1.06 (d, *J* = 5.0 Hz, 12H, $(H_3C)_2CH$), 0.99 (d, *J* = 6.6 Hz, 12H, $(H_3C)_2CH$), 0.80-0.00 (br, BH_3). ^{11}B NMR (96 MHz, C_6D_6) δ -7.38 (br, $B(C_6F_5)_3$), -28.42 (br, BH_3). ^{19}F NMR (470 MHz, d_8-toluene) δ -125.46 (s, *o*-C_6F_5), -158.64 (t, *J* = 21.0 Hz, *p*-C_6F_5), -165.03 (td, *J* = 23.4, 7.1 Hz, *m*-C_6F_5). ^{31}P{^{1}H} NMR (122 MHz, C_6D_6) δ -1.43 (br). ^{13}C{^{1}H} NMR (126 MHz, C_6D_6) δ 166.72 (N*C*(CH_3)CH), 146.12 (*1*-*N*Ar), 141.30 (2,6-*N*Ar), 137.91 (*1*-$H_3C(C_6H_5)$), 133.91 (*o*-P(C_6H_5)$_2$), 133.33 (d, $^1J_{31P}$ = 42.9 Hz, *i*-P(C_6H_5)$_2$), 129.74 (*p*-P(C_6H_5)$_2$), 129.33 (*2,6*-$H_3C(C_6H_5)$), 128.57 (*3,5*-$H_3C(C_6H_5)$), 127.79 (*m*-P(C_6H_5)$_2$), 125.70 (*4*-$H_3C(C_6H_5)$), 125.38 (4-*N*Ar), 124.12 (3,5-*N*Ar), 89.92 (NC(CH_3)*C*H), 28.50 (*C*H(CH_3)), 24.99 (NC(*C*H_3)CH), 24.49 (CH(*C*H_3), 24.41 (CH(*C*H_3), 21.43 ($H_3C(C_6H_5)$). Resonances corresponding to C_6F_5 carbon atoms could not be unambiguously detected. Analysis calculated for $C_{66}H_{62}B_2F_{15}N_2P$: C 62.87, H 4.96, N 2.22%. Found: C 62.48, H 4.96, N 2.33%.

5.4.9 Reaction of compound 15 with $B(C_6F_5)_3$: *in situ* identification of compound 20b and isolation of compound 21

A J. Young's NMR tube was charged with 30 mg compound **15** (0.0468 mmol) and a C_6D_6 solution of $B(C_6F_5)_3$ (24 mg, 0.0468 mmol) was added. The tube was vigorously shaken until a clear, colourless solution was obtained after approx. two minutes. ^{1}H, $^{31}P\{^{1}H\}$, ^{11}B, and ^{19}F NMR spectra were recorded after 20 minutes at room temperature, showing quantitative conversion of the starting compounds to compound **20b**. Small quantities of **XLVIa** and compound **21** also visible. The reaction mixture was left to stand at room temperature for 16 hours, or at 40°C for two hours. Further analysis by ^{1}H, $^{31}P\{^{1}H\}$, ^{11}B, and ^{19}F NMR spectroscopy presented a 1:1 mixture of **XLVIa** and compound **21**, with complete consumption of **20b**. Solvent was removed under vacuum, then 0.5 ml hexane and ~0.05 ml toluene were added to result in isolate of a colourless crystalline solid by decantation. A single crystal of compound **21** suitable for X-ray diffraction analysis was selected under the microscope.

NMR characterisation of compound **20b** from *in situ* reaction in C_6D_6: ^{1}H NMR (300 MHz, C_6D_6) δ 7.13 (dd, *J* = 8.3, 6.9 Hz, 2H, *o*-P(C_6H_5)), 7.08 – 6.95 (m, 8H, *N*Ar + *o*-P(C_6H_5)), 6.94 – 6.85 (m, 2H, *p*-P(C_6H_5), 6.76 (td, *J* = 7.7, 2.1 Hz, 4H, *m*-P(C_6H_5)), 4.83 (s, 1H, NC(CH_3)C*H*), 2.86 (hept, *J* = 6.7 Hz, 4H, (H_3C)$_2$C*H*), 1.52 (s, 6H, NC(CH_3)CH), 1.04 (d, *J* = 6.8 Hz, 12H, (H_3C)$_2$CH), 0.92 (d, *J* = 6.9 Hz, 12H, (H_3C)$_2$CH). Boron-bound hydrogen atoms could not be detected. ^{31}P NMR (122 MHz, C_6D_6) δ 0.42 (br, m). ^{11}B NMR (96 MHz, C_6D_6) δ -10.44 (br, *B*(C_6F_5)$_3$), -36.67 (br, *B*H_3). ^{19}F NMR (282 MHz, C_6D_6) δ -126.18 (6F, d, *J* = 24.2 Hz, *o*-C_6F_5), -157.52 (3F, td, *J* = 21.0, 3.6 Hz, *p*-C_6F_5), -163.51 – -164.12 (6F, m, *m*-C_6F_5). Neither satisfactory $^{13}C\{^{1}H\}$ NMR spectra, nor elemental analysis of compound **20b** could be obtained on account of its low thermal stability with respect to onward reaction to compounds **21** and **XLVIa**.

NMR characterisation of compound **21** from *in situ* reaction in C_6D_6, * = resonance corresponding to compound **XLVIa**, in agreement with those reported in the literature.[67] ^{1}H NMR (500 MHz, C_6D_6) δ 7.72 (t, *J* = 7.6 Hz, 4H, *o*-(C_6H_5)PMg), 7.27 (t, *J* = 9.0 Hz, 4H, *o*-(C_6H_5)$_2$PB(C_6F_5)$_3$), 7.15 – 7.07 (m, 2H, *p*-(C_6H_5)PMg), 7.07 – 6.96 (m, 8H, *p*-(C_6H_5)$_2$PB(C_6F_5)$_3$ + *N*Ar*), 6.96 – 6.82 (m, 10H, *m*-(C_6H_5)PMg + *N*Ar), 6.77 (td, *J* = 7.9, 1.8 Hz, 4H, *m*-(C_6H_5)$_2$PB(C_6F_5)$_3$), 4.86 (s, 1H, NC(CH_3)C*H**), 3.92 (d, *J* = 21.8 Hz, 1H, NC(CH_3)C(*H*)BH_2), 3.05 (hept, *J* = 6.5, 5.9 Hz, 4H, (H_3C)$_2$C*H**), 2.62 (hept, *J* = 6.2 Hz, 2H, (H_3C)$_2$C*H*), 2.13 (hept, *J* = 6.6 Hz, 2H, (H_3C)$_2$C*H*), 1.54 (s, 6H, NC(CH_3)CH*), 1.51 (d, *J* = 1.3 Hz, 6H, NC(CH_3)CH), 1.09 (d, *J* = 6.8 Hz, 12H, (H_3C)$_2$CH*), 1.03 (d, *J* = 6.7 Hz, 6H, (H_3C)$_2$CH), 0.99 (d, *J* = 6.9 Hz, 12H, (H_3C)$_2$CH*), 0.90 (d, *J* = 6.7 Hz, 6H, (H_3C)$_2$CH), 0.51 (d, *J* = 6.7 Hz, 6H, (H_3C)$_2$CH), 0.27 (d, *J* = 6.5 Hz, 6H, (H_3C)$_2$CH). Boron-bound hydrogen atoms could not be detected. ^{11}B NMR (160 MHz, C_6D_6) δ -10.18 (P*B*(C_6F_5)$_3$), -21.08 (d, *J* = 63.4 Hz, H*B*(C_6F_5)$_3$*), -24.66 (P*B*H_2), -

35.26 (P*B*H$_3$). ^{31}P{^{1}H} NMR (202 MHz, C_6D_6) δ -7.31 (d, *J* = 108.9 Hz, *P*B(C_6F_5)$_3$), -42.69 (br, Mg*P*Ph$_2$). ^{19}F NMR (470 MHz, C_6D_6) δ -125.84 (d, *J* = 23.2 Hz, 6F, *o*-C_6F_5), -137.01 (br, 6F, *o*-C_6F_5*), -156.71 (t, *J* = 20.8 Hz, 3F, *p*-C_6F_5*), -157.69 (t, *J* = 20.9 Hz, 3F, *p*-C_6F_5), -161.00 (t, *J* = 18.8 Hz, 6F, *m*-C_6F_5*), -164.61 (dt, *J* = 20.6, 11.9 Hz, 6F, *m*-C_6F_5). ^{13}C{^{1}H} NMR (126 MHz, C_6D_6) δ 191.84 (N*C*(CH$_3$)C(H)BH$_2$), 172.05 (N*C*(CH$_3$)CH*), 150.14 (br, *C*$_6$F$_5$), 149.27 (br, *C*$_6$F$_5$), 148.25 (br, *C*$_6$F$_5$), 147.41 (br, *C*$_6$F$_5$), 143.29 (1-*C*-NDipp*), 141.66 (2,6-*C*-NDipp*), 141.39 (2,6-*C*-NDipp), 140.95 (1-*C*-NDipp), 140.14 (2,6-*C*-NDipp), 139.16 (br, *C*$_6$F$_5$), 138.45 (br, *C*$_6$F$_5$), 137.65 (d, *J* = 29.6 Hz, *i*-(*C*$_6$H$_5$)PMg), 136.40 (br, *C*$_6$F$_5$), 135.04 (br, *o*-(*C*$_6$H$_5$)PMg), 133.43 (d, *J* = 5.2 Hz, *o*-(*C*$_6$H$_5$)$_2$PB(C$_6$F$_5$)$_3$)), 132.49 (d, *J* = 45.0 Hz, *i*-(*C*$_6$H$_5$)$_2$PB(C$_6$F$_5$)$_3$), 129.52 (d, *J* = 2.3 Hz, *m*-(*C*$_6$H$_5$)$_2$PB(C$_6$F$_5$)$_3$), 128.95 (d, *J* = 8.2 Hz) (*m*-(*C*$_6$H$_5$)PMg), 128.76 (*p*-(*C*$_6$H$_5$)$_2$PB(C$_6$F$_5$)$_3$), 127.71 (*p*-(*C*$_6$H$_5$)$_2$PMg)$_3$, 126.32 (4-*C*-NDipp*), 125.55 (4-*C*-NDipp), 124.84 (3,5-*C*-NDipp*), 124.24 (3,5-*C*-NDipp), 96.45 (NC(CH$_3$)*C*H*), 56.58 (H*C*BH$_2$), 29.31 (*C*H(CH$_3$)), 29.29 (*C*H(CH$_3$)), 28.75 (*C*H(CH$_3$)), 28.67 (*C*H(CH$_3$)*), 25.19 (NC(*C*H$_3$)), 25.08 (CH(*C*H$_3$)), 24.68 (CH(*C*H$_3$)), 24.45 (NC(*C*H$_3$)*), 24.29(CH(*C*H$_3$)*), 24.23 (CH(*C*H$_3$)), 24.14(CH(*C*H$_3$)*), 23.89 (CH(*C*H$_3$)).

5.4.10 Reaction of compound 15 with B(C_6F_5)$_3$ at 60°C: generation of XLVIa and unknown product

The above procedure (5.4.9) was followed, but instead of solvent removal and crystallisation, the reaction mixture was heated to 60°C for 16 hours to provide a pale-yellow solution. The only BDI-containing product detected by ^{1}H NMR spectroscopy was **XLVIa** (also verified by ^{11}B and ^{19}F NMR spectroscopy). The ^{31}P{^{1}H} NMR spectrum displayed an apparent doublet centred at δ 25 ppm, corresponding to an unknown product. A broad resonance at δ -24 ppm was also present in the ^{11}B NMR spectrum.

5.4.11 X-ray crystallography

Identification code	**15**	**16b**	**17**	**18**	**19**	**20a.toluene**	**21**
Empirical formula	$C_{110}H_{165}B_2Mg_2N_4P_2$	$C_{45}H_{62}BCaN_2OP$	$C_{80.5}H_{108}BMg_2N_4P$	$C_{139}H_{181}B_2Ca_3N_6P_2$	$C_{92.5}H_{126}B_4Mg_2N_4P_2$	$C_{66}H_{62}B_2CaF_{15}N_2P$	$C_{71}H_{66}B_3F_{15}MgN_2P_2$
Formula weight	1675.63	728.82	1222.10	2139.69	1447.77	1260.84	1350.93
Temperature/K	150.00(10)	150.0(3)	150.00(10)	149.9(3)	100(2)	150.01(10)	150.00(10)
Crystal system	monoclinic	triclinic	triclinic	monoclinic	triclinic	triclinic	monoclinic
Space group	$P2_1/n$	P-1	P-1	C2/c	P-1	P-1	$P2_1/n$
a/Å	18.8895(2)	11.8835(3)	13.1986(3)	24.9783(5)	13.4773(6)	14.2828(3)	13.4493(1)
b/Å	16.2536(2)	12.2918(3)	13.8418(3)	17.9983(3)	15.8128(8)	15.1493(3)	22.3275(1)
c/Å	34.1206(5)	15.4936(4)	20.1666(3)	58.5938(8)	22.6902(11)	15.1514(3)	22.2182(1)
α/°	90	82.120(2)	95.509(2)	90	104.5820(10)	96.633(2)	90
β/°	105.7783(13)	74.020(2)	93.735(2)	100.806(2)	92.9400(10)	95.263(2)	95.912(1)
γ/°	90	83.995(2)	98.781(2)	90	109.9620(10)	109.145(2)	90
Volume/Å^3	10081.1(2)	2149.83(10)	3612.34(13)	25874.7(8)	4348.3(4)	3046.84(11)	6636.40(7)
Z	4	2	2	8	2	2	4
ρ_{calc}g/cm^3	1.104	1.126	1.124	1.099	1.106	1.374	1.352
μ/mm^{-1}	0.863	1.857	0.838	1.713	0.110	1.907	1.431
F(000)	3668.0	788.0	1326.0	9256.0	1566.0	1304.0	2792.0
Crystal size/mm^3	0.317 × 0.189 × 0.028	0.163 × 0.093 × 0.072	0.143 × 0.073 × 0.055	0.166 × 0.145 × 0.073	0.27 × 0.23 × 0.11	0.158 × 0.132 × 0.063	0.239 × 0.204 × 0.136
Radiation	CuKα (λ = 1.54184)	CuKα (λ = 1.54184)	CuKα (λ = 1.54184)	CuKα (λ = 1.54184)	MoKα (λ = 0.71073)	CuKα (λ = 1.54184)	CuKα (λ = 1.54184)
2Θ range for data collection/°	6.068 to 146.942	5.972 to 146.948	6.498 to 147.196	6.09 to 146.492	2.86 to 61.16	5.93 to 146.978	7.704 to 146.242
Index ranges	-23 ≤ h ≤ 20, -20 ≤ k ≤ 19, -41 ≤ l ≤ 42	-12 ≤ h ≤ 14, -15 ≤ k ≤ 15, -19 ≤ l ≤ 18	-16 ≤ h ≤ 16, -17 ≤ k ≤ 17, -19 ≤ l ≤ 25	-29 ≤ h ≤ 30, -15 ≤ k ≤ 22, -69 ≤ l ≤ 72	-19 ≤ h ≤ 19, -22 ≤ k ≤ 22, -31 ≤ l ≤ 32	-15 ≤ h ≤ 17, -18 ≤ k ≤ 18, -18 ≤ l ≤ 18	-15 ≤ h ≤ 16, -25 ≤ k ≤ 27, -27 ≤ l ≤ 27
Reflections collected	133709	25453	46467	77627	104431	37670	87586
Independent reflections	20547 [R_{int} = 0.0641, R_{sigma} = 0.0355]	8620 [R_{int} = 0.0243, R_{sigma} = 0.0247]	14438 [R_{int} = 0.0447, R_{sigma} = 0.0448]	24925 [R_{int} = 0.0329, R_{sigma} = 0.0409]	26663 [R_{int} = 0.0388, R_{sigma} = 0.0413]	12199 [R_{int} = 0.0369, R_{sigma} = 0.0369]	13269 [R_{int} = 0.0370, R_{sigma} = 0.0219]
Data/restraints/parameters	20547/0/878	8620/2/491	14438/264/889	24925/0/1277	26663/282/1085	12199/0/811	13269/0/881
Goodness-of-fit on F^2	1.031	1.030	1.022	1.041	1.032	1.036	1.029
Final R indexes [I>=2σ (I)]	R_1 = 0.0738, wR_2 = 0.2127	R_1 = 0.0322, wR_2 = 0.0819	R_1 = 0.0452, wR_2 = 0.1115	R_1 = 0.0536, wR_2 = 0.1204	R_1 = 0.0516, wR_2 = 0.1279	R_1 = 0.0371, wR_2 = 0.0879	R_1 = 0.0377, wR_2 = 0.0972
Final R indexes [all data]	R_1 = 0.0816, wR_2 = 0.2209	R_1 = 0.0348, wR_2 = 0.0838	R_1 = 0.0591, wR_2 = 0.1198	R_1 = 0.0659, wR_2 = 0.1275	R_1 = 0.0768, wR_2 = 0.1424	R_1 = 0.0482, wR_2 = 0.0928	R_1 = 0.0423, wR_2 = 0.1006
Largest diff. peak/hole / e Å^{-3}	0.53/-0.47	0.26/-0.26	0.42/-0.38	0.38/-0.33	1.26/-0.57	0.31/-0.29	0.47/-0.51

Notes on crystallographic refinement

For compound **15**, an orthorhombic C type was a metric possibility, but the arising solution was poor and accompanied by a despicable *R*(int). After some 150 various refinements, all roads led back to the original solution in space group $P2_1/n$. However, in treating the data as arising from a single crystal rendered afforded a refinement that was accompanied by in excess of 130 systematic absence violations – mostly related to the *n*-glide – which could not be neglected. Scrutiny of the raw data suggested the potential for pseudo-merohedral twinning of the sample to be present but efforts to resolve this at the point of integration were unsuccessful (probably because of the degree of overlap). Ultimately, the data were integrated as arising from a single component, and the twinning (approx. 9%) was addressed 'after the fact' i.e. during convergence of the model. The lattice in this structure contains a very high level of solvent, for which the electron density was smeared and disorder was prevalent. On balance, a heavily parameterized disorder-model treatment was abandoned in favour of using a solvent mask. An allowance for four molecules of toluene, per asymmetric unit, has been made in the model as presented to account for the electron density evidence prior to invoking the solvent mask algorithm.

The boron-bound hydrogen atoms in compound **16b** were located and refined without restraints. C31 was modelled to take account of 80:20 disorder. Chemically equivalent C-C distances involving the arising fractional occupancy carbons were restrained to being similar in the final least-squares cycles.

In compound **17**, the asymmetric unit was seen to contain 1.5 molecules of guest toluene in addition to one molecule of the main feature. The hydride ligand in the latter, plus the hydrogens attached to B1, were readily located and refined without restraints. Both solvent moieties were disordered. In particular, the full toluene based on C78, was refined over 2 proximate sites in a 55:45 ratio. The second toluene moiety, based on C71, is disordered with itself and is present in the asymmetric unit at half site-occupancy. Distance and ADP restraints were included in the disordered regions, to assist convergence, and rings were treated as rigid hexagons.

The asymmetric unit in compound **18** comprises one molecule of the calcium containing trimer, one ordered molecule of toluene (based on C120), ½ of one molecule of toluene (based on C8S) and 3 other regions of solvent. The boron bound hydrogens and the hydride ligand, in the main feature, were all readily located, and refined without restraints. Atoms C8S and C11S (in the ½ toluene molecule) were found to be coincident with a 2-fold rotation axis intrinsic to the space group. This necessarily means that the methyl group therein exhibits 50:50 crystallographic disorder about this symmetry element; hence, C14S is present at half site-

occupancy in the asymmetric unit. The unresolved regions of solvent were treated using the solvent mask algorithm available in Olex-2. It was evident that these regions amounted to 2.5 molecules of toluene, albeit disordered in all cases. Consequently, an allowance for these 2.5 lattice guest has been made in the formula as presented.

The asymmetric unit in compound **19** contains two crystallographically independent dimer halves and two regions of solvent. Each dimer can be completed by virtue of inversion symmetry which is present in the space group. The boron-bound hydrogen atoms were located and refined without restraints. The first of the two solvent regions was modelled as a full molecule of toluene, disordered over two proximate sites, in a 55:45 ratio. ADP restraints were applied in this region. The second solvent region straddles a crystallographic inversion centre which necessarily means that disorder is present. Ultimately the motif in the asymmetric unit was modelled as a toluene moiety, with half site occupancy, in which the methyl group was disordered over two sites in a 35:15 ratio. The fractional occupancy hydrogen atoms which were disordered with this methyl functionality were tentatively assigned and refined with restraints.

Boron bound hydrogens in the structure of compounds **20a.toluene** and **21** were located and refined without restraints.

5.5 References

1. A. Staubitz, A. P. M. Robertson, M. E. Sloan and I. Manners, *Chemical Reviews*, 2010, **110**, 4023-4078.
2. A. Rossin and M. Peruzzini, *Chemical Reviews*, 2016, **116**, 8848-8872.
3. C. W. Hamilton, R. T. Baker, A. Staubitz and I. Manners, *Chemical Society Reviews*, 2009, **38**, 279-293.
4. A. Staubitz, A. P. M. Robertson and I. Manners, *Chemical Reviews*, 2010, **110**, 4079-4124.
5. H. Dorn, J. M. Rodezno, B. Brunnhofer, E. Rivard, J. A. Massey and I. Manners, *Macromolecules*, 2003, **36**, 291-297.
6. J. R. Turner, D. A. Resendiz-Lara, T. Jurca, A. Schäfer, J. R. Vance, L. Beckett, G. R. Whittell, R. A. Musgrave, H. A. Sparkes and I. Manners, *Macromolecular Chemistry and Physics*, 2017, **218**, 1700120.
7. A. Schäfer, T. Jurca, J. Turner, J. R. Vance, K. Lee, V. A. Du, M. F. Haddow, G. R. Whittell and I. Manners, *Angewandte Chemie-International Edition*, 2015, **54**, 4836-4841.
8. T. L. Clark, J. M. Rodezno, S. B. Clendenning, S. Aouba, P. M. Brodersen, A. J. Lough, H. E. Ruda and I. Manners, *Chemistry-a European Journal*, 2005, **11**, 4526-4534.
9. C. Marquardt, T. Jurca, K. C. Schwan, A. Stauber, A. V. Virovets, G. R. Whittell, I. Manners and M. Scheer, *Angewandte Chemie - International Edition*, 2015, **54**, 13782-13786.
10. C. A. D. Pinheiro, C. Roiland, P. Jehan and G. Alcaraz, *Angewandte Chemie-International Edition*, 2018, **57**, 1519-1522.
11. J. R. Vance, A. Schafer, A. P. M. Robertson, K. Lee, J. Turner, G. R. Whittell and I. Manners, *Journal of the American Chemical Society*, 2014, **136**, 3048-3064.

12. H. Helten, B. Dutta, J. R. Vance, M. E. Sloan, M. F. Haddow, S. Sproules, D. Collison, G. R. Whittell, G. C. Lloyd-Jones and I. Manners, *Angewandte Chemie-International Edition*, 2013, **52**, 437-440.
13. A. Staubitz, A. P. Soto and I. Manners, *Angewandte Chemie-International Edition*, 2008, **47**, 6212-6215.
14. C. A. Jaska, K. Temple, A. J. Lough and I. Manners, *Journal of the American Chemical Society*, 2003, **125**, 9424-9434.
15. H. Dorn and I. Manners, *Phosphorus Sulfur and Silicon and the Related Elements*, 2001, **168**, 185-190.
16. H. Dorn, R. A. Singh, J. A. Massey, J. M. Nelson, C. A. Jaska, A. J. Lough and I. Manners, *Journal of the American Chemical Society*, 2000, **122**, 6669-6678.
17. J. M. Denis, H. Forintos, H. Szelke, L. Toupet, T. N. Pham, P. J. Madec and A. C. Gaumont, *Chemical Communications*, 2003, 54-55.
18. G. M. Adams, A. L. Colebatch, J. T. Skornia, A. I. McKay, H. C. Johnson, G. C. Lloyd-Jones, S. A. Macgregor, N. A. Beattie and A. S. Weller, *Journal of the American Chemical Society*, 2018, **140**, 1481-1495.
19. F. Anke, D. Han, M. Klahn, A. Spannenberg and T. Beweries, *Dalton Transactions*, 2017, **46**, 6843-6847.
20. A. Gluer, M. Forster, V. R. Celinski, J. S. auf der Gunne, M. C. Holthausen and S. Schneidert, *ACS Catalysis*, 2015, **5**, 7214-7217.
21. N. T. Coles, M. F. Mahon and R. L. Webster, *Organometallics*, 2017, **36**, 2262-2268.
22. A. L. Colebatch and A. S. Weller, *Chemistry-a European Journal*, 2019, **25**, 1379-1390.
23. U. S. D. Paul, H. Braunschweig and U. Radius, *Chemical Communications*, 2016, **52**, 8573-8576.
24. A. Staubitz, M. E. Sloan, A. P. M. Robertson, A. Friedrich, S. Schneider, P. J. Gates, J. Gunne and I. Manners, *Journal of the American Chemical Society*, 2010, **132**, 13332-13345.
25. D. L. Han, F. Anke, M. Trose and T. Beweries, *Coordination Chemistry Reviews*, 2019, **380**, 260-286.
26. T. N. Hooper, A. S. Weller, N. A. Beattie and S. A. Macgregor, *Chemical Science*, 2016, **7**, 2414-2426.
27. H. C. Johnson, E. M. Leitao, G. R. Whitten, I. Manners, G. C. Lloyd-Jones and A. S. Weller, *Journal of the American Chemical Society*, 2014, **136**, 9078-9093.
28. N. L. Oldroyd, S. S. Chitnis, V. T. Annibale, M. I. Arz, H. A. Sparkes and I. Manners, *Nature Communications*, 2019, **10**, 1370.
29. J. Spielmann, G. Jansen, H. Bandmann and S. Harder, *Angewandte Chemie - International Edition*, 2008, **47**, 6290-6295.
30. J. Spielmann and S. Harder, *Journal of the American Chemical Society*, 2009, **131**, 5064-5065.
31. J. Spielmann, M. Bolte and S. Harder, *Chemical Communications*, 2009, 6934.
32. J. Spielmann, D. F. J. Piesik and S. Harder, *Chemistry-a European Journal*, 2010, **16**, 8307-8318.
33. D. J. Liptrot, M. S. Hill, M. F. Mahon and D. J. MacDougall, *Chemistry-a European Journal*, 2010, **16**, 8508-8515.
34. P. Bellham, M. S. Hill, D. J. Liptrot, D. J. MacDougall and M. F. Mahon, *Chemical Communications*, 2011, **47**, 9060.
35. M. S. Hill, M. Hodgson, D. J. Liptrot and M. F. Mahon, *Dalton Transactions*, 2011, **40**, 7783-7790.
36. S. Harder, J. Spielmann and B. Tobey, *Chemistry-a European Journal*, 2012, **18**, 1984-1991.
37. P. Bellham, M. S. Hill, G. Kociok-Köhn and D. J. Liptrot, *Dalton Transactions*, 2013, 737-745.
38. P. Bellham, M. D. Anker, M. S. Hill, G. Kociok-Köhn and M. F. Mahon, *Dalton Transactions*, 2016, **45**, 13969-13978.

39. P. Bellham, M. S. Hill, G. Kociok-Köhn and D. J. Liptrot, *Chemical Communications*, 2013, **49**, 1960-1962.
40. A. Staubitz, J. Hoffmann and P. Gliese, in *Smart Inorganic Polymers: Synthesis, Properties, and Emerging Applications in Materials and Life Sciences*, eds. E. Hey-Hawkins and M. Hissler, Wiley-VCH, Weinheim, First Edition edn., 2019, ch. 2, pp. 19-39.
41. K. Izod, J. M. Watson, S. M. El-Hamruni, R. W. Harrington and P. G. Waddell, *Organometallics*, 2017, **36**, 2218-2227.
42. F. Dornhaus, M. Bolte, H. W. Lerner and M. Wagner, *European Journal of Inorganic Chemistry*, 2006, 5138-5147.
43. F. Dornhaus and M. Bolte, personal communication to the Cambridge Structural Database.
44. T. N. Hooper, M. A. Huertos, T. Jurca, S. D. Pike, A. S. Weller and I. Manners, *Inorganic Chemistry*, 2014, **53**, 3716-3729.
45. I. Abdellah, E. Bernoud, J. F. Lohier, C. Alayrac, L. Toupet, C. Lepetit and A. C. Gaumont, *Chemical Communications*, 2012, **48**, 4088-4090.
46. W. Angerer, W. S. Sheldrick and W. Malisch, *Chemische Berichte-Recueil*, 1985, **118**, 1261-1266.
47. C. A. Jaska, A. J. Lough and I. Manners, *Dalton Transactions*, 2005, 326-331.
48. C. A. Jaska, H. Dorn, A. J. Lough and I. Manners, *Chemistry-a European Journal*, 2003, **9**, 271-281.
49. A. C. Gaumont, M. B. Hursthouse, S. J. Coles and J. M. Brown, *Chemical Communications*, 1999, 63-64.
50. K. Lee, T. J. Clark, A. J. Lough and I. Manners, *Dalton Transactions*, 2008, 2732-2740.
51. J. Spielmann, D. E. J. Piesik and S. Harder, *Chemistry - A European Journal*, 2010, **16**, 8307-8318.
52. C. Jones, S. J. Bonyhady, S. Nembenna and A. Stasch, *European Journal of Inorganic Chemistry*, 2012, 2596-2601.
53. J. Langer, T. M. A. Al-Shboul, F. M. Younis, H. Gorls and M. Westerhausen, *European Journal of Inorganic Chemistry*, 2011, 3002-3007.
54. M. R. Crimmin, A. G. M. Barrett, M. S. Hill, P. B. Hitchcock and P. A. Procopiou, *Organometallics*, 2007, **26**, 2953-2956.
55. M. R. Crimmin, A. G. M. Barrett, M. S. Hill, P. B. Hitchcock and P. A. Procopiou, *Inorganic Chemistry*, 2007, **46**, 10410-10415.
56. M. Gartner, H. Gorls and M. Westerhausen, *Organometallics*, 2007, **26**, 1077-1083.
57. M. Gartner, H. Gorls and M. Westerhausen, *Zeitschrift Fur Anorganische und Allgemeine Chemie*, 2007, **633**, 2025-2031.
58. N. R. Thompson, *Journal of the Chemical Society*, 1965, 6290.
59. J. W. Gilje, K. W. Morse and R. W. Parry, *Inorganic Chemistry*, 1967, **6**, 1761.
60. E. Mayer and Laubenga.Aw, *Monatshefte Fur Chemie*, 1970, **101**, 1138.
61. L. D. Schwartz and P. C. Keller, *Inorganic Chemistry*, 1971, **10**, 645.
62. F. Dornhaus and M. Bolte, *Acta Crystallographica Section E-Structure Reports Online*, 2006, **62**, M3573-M3575.
63. M. R. Anstey, M. T. Corbett, E. H. Majzoub and J. G. Cordaro, *Inorganic Chemistry*, 2010, **49**, 8197-8199.
64. A. V. Blake, T. V. Fetrow, Z. J. Theiler, B. Vlaisavljevich and S. R. Daly, *Chemical Communications*, 2018, **54**, 5602-5605.
65. F. Dornhaus, M. Bolte, H. W. Lerner and M. Wagner, *European Journal of Inorganic Chemistry*, 2006, 1777-1785.
66. M. D. Anker, M. Arrowsmith, R. L. Arrowsmith, M. S. Hill and M. F. Mahon, *Inorganic Chemistry*, 2017, **56**, 5976-5983.
67. M. D. Anker, M. Arrowsmith, P. Bellham, M. S. Hill, G. Kociok-Köhn, D. J. Liptrot, M. F. Mahon and C. Weetman, *Chemical Science*, 2014, **5**, 2826-2830.
68. K. Yan, G. Schoendorff, B. M. Upton, A. Ellern, T. L. Windus and A. D. Sadow, *Organometallics*, 2013, **32**, 1300-1316.

69. G. R. Fulmer, A. J. M. Miller, N. H. Sherden, H. E. Gottlieb, A. Nudelman, B. M. Stoltz, J. E. Bercaw and K. I. Goldberg, *Organometallics*, 2010, **29**, 2176-2179.
70. J. Pahl, S. Brand, H. Elsen and S. Harder, *Chemical Communications*, 2018, **54**, 8685-8688.
71. L. Garcia, M. D. Anker, M. F. Mahon, L. Maron and M. S. Hill, *Dalton Transactions*, 2018, **47**, 12684-12693.
72. A. Friedrich, J. Pahl, H. Elsen and S. Harder, *Dalton Transactions*, 2019, **48**, 5560-5568.
73. A. M. Fuller, A. J. Mountford, M. L. Scott, S. J. Coles, P. N. Horton, D. L. Hughes, M. B. Hursthouse and S. J. Lancaster, *Inorganic Chemistry*, 2009, **48**, 11474-11482.
74. D. D. L. Jones, A. J. R. Matthews and C. Jones, *Dalton Transactions*, 2019, **48**, 5785-5792.
75. J. Pahl, T. E. Stennett, M. Volland, D. M. Guldi and S. Harder, *Chemistry-a European Journal*, 2019, **25**, 2025-2034.
76. W. S. Ren, S. H. Zhang, Z. Y. Xu and X. B. Ma, *Dalton Transactions*, 2019, **48**, 3109-3115.
77. J. Pahl, A. Friedrich, H. Eisen and S. Harder, *Organometallics*, 2018, **37**, 2901-2909.
78. M. T. Ma, A. Stasch and C. Jones, *Chemistry-a European Journal*, 2012, **18**, 10669-10676.
79. A. J. Boutland, I. Pernik, A. Stasch and C. Jones, *Chemistry-a European Journal*, 2015, **21**, 15749-15758.
80. T. E. Stennett, J. Pahl, H. S. Zijlstra, F. W. Seidel and S. Harder, *Organometallics*, 2016, **35**, 207-217.

6 Summary

In summary, this thesis describes the use of alkaline-earth catalysis in addressing some key issues in inorganic polymer synthesis.

Firstly, new types of metallopolymer structures were targeted. The catalytic dehydrocoupling of ferrocenylsilane monomers with diamines and diols satisfied the requirement for a highly selective and efficient element-element bond-forming reaction. Importantly, synthetically accessible homoleptic bis-amide pre-catalysts **IIb**-**d** provided the desired reactivity. The installation of ferrocene as a pendent- or main-chain substituent demanded careful tuning of the steric and electronic demands of both co-monomers to achieve high selectivity towards well-defined linear polymer.

Ferrocene-containing polycarbosilazanes were found to be promising precursors to magnetic ceramic materials, whose magnetism was found to originate from iron-nanoparticles formed during pyrolysis. Pre-crosslinking was superfluous to the requirements of pyrolysis, and good ceramic yields were thought to originate from *in situ* cross-linking reactivity of the functionalised polymer backbone. This presents an advantage with respect to solution-phase precursor processing.

The generality of alkaline-earth centred σ-bond cross-metathesis of a variety of hydridic and protic substrates was demonstrated by a detailed investigation of a previously unexplored silane-alcohol system. Stoichiometric and kinetic investigations highlighted the substantial influence that subtle changes in catalyst and substrate concentration exert on the mechanism. In particular, the inhibitory effect of coordinating substrate molecules and the involvement of alkoxide-based dimers and higher aggregates were key considerations in the absence of bulky chelating ligands.

The potential for calcium to participate in homodehydrocoupling reactions was demonstrated through investigations into the reactivity of organo- and hydrido-calcium complexes toward organostannanes. Although tin-tin coupling was possible, this reactivity was challenged by a complex manifold of interesting calcium-mediated Sn-Sn and Sn-C activation pathways in which nucleophile-directed reactivity is favoured over classical σ-bond metathesis. Furthermore, the resultant stannyl calcium complexes open new avenues for alkaline-earth chemistry involving the heavier *p*-block elements.

Finally, a series of structurally diverse magnesium- and calcium-phosphidoborane complexes were prepared by deprotonation of the parent phosphine-borane adduct. In contrast to previously explored amidoborane systems, β-hydride elimination was not promoted by the

addition of further phosphine-borane. Instead, adduct dissociation and formation of a phosphinodiboronate complex was favoured. Although sequential deprotonation and hydride-abstraction reactions was found to provide a viable stoichiometric route towards phosphine-borane oligomerisation, ligand-centred reactivity resulted in selective sequestration of phosphinoborane monomer. These studies highlight the importance of ligand design in the development of transition metal-free catalysts for phosphine-borane dehydropolymerisation.

7 Further work

Although this work demonstrates the potential for alkaline-earth mediated catalysis in the advancement of inorganic polymer synthesis, it has uncovered some important questions and avenues for future work.

Chapter 2. Further work is required to realise the full potential of dehydrocoupling-based polycondensation. Specific aspects that deserve attention include an exploration of inter-ferrocene bridge structures and their influence on polymer properties, non-iron-based metallocenes, monomers combining silane and amine functionality within the same molecule, and the synthesis of alternating bimetallic co-polymers. The use of ferrocene-containing polycarbosilazanes as ceramic precursors demands further study. Optimisation of polymer structure and processing as well as pyrolysis conditions will help to improve and build upon this work.

Chapter 3. Comments pertaining to the polymers in chapter 2 also apply here. Importantly, the moisture tolerance of polysilylethers facilitates further exploration of the properties and applications of such polymers. Ae-mediated catalytic dehydrocoupling of silanes and alcohols should be extended towards a greater range of substrates in order to fully realise its synthetic potential. Additional mechanistic investigations into this reaction will help to improve upon and optimise reaction parameter and catalyst design.

Chapter 4. The catalytic dehydrocoupling of alkyl-stannanes offers interesting comparison to literature transition metal-catalysed processes. Expanding the reaction scope, exploring catalyst design, and performing mechanistic investigations will advance this work. The general reactivity of stannyl-calcium complexes and other polar calcium-element bonds merits attention.

Chapter 5. The reluctance for phosphine-boranes and phosphidoborane species to undergo dehydrogenative coupling or β-hydride elimination at alkaline-earth centres is a key limitation. Further work should focus on alternative catalysts systems in order to favour P-B coupling over adduct dissociation. Structural and spectroscopic investigations into alkaline-earth centred phosphine-boranes reactivity will facilitate this. The fate of the $B(C_6F_5)_3$-mediated hydride abstraction reactions described also remains to be fully elucidated.

Appendix i. Experimental details

i.1. General experimental procedures

All reactions dealing with air and moisture-sensitive compounds were carried out under an argon or N_2 atmosphere using standard Schlenk line techniques, in an MBraun Labmaster glovebox under an argon atmosphere, or in an MBraun 200B glovebox under an atmosphere of N_2. NMR experiments using air-sensitive compounds were conducted in J. Young's tap NMR tubes prepared and sealed in a glovebox. NMR data were acquired at 298 K unless otherwise specified, using a Bruker 300 Ultrashield instrument for ^{1}H (300 MHz), Bruker 400 Ultrashield instrument for ^{1}H (400 MHz), ^{13}C (125.76 MHz), ^{29}Si (79.5 MHz), ^{31}P (162 MHz), ^{11}B (128 MHz) Bruker 500 Ultrashield instrument for ^{1}H (500 MHz), ^{29}Si (99 MHz) and ^{119}Sn (186 MHz), Agilent ProPulse instrument for ^{1}H (500 MHz), ^{13}C (126 MHz), ^{29}Si (99 MHz), ^{119}Sn (186 MHz), ^{19}F (490 MHz), ^{31}P (122 MHz), ^{11}B (160 MHz), and a Bruker AVIII 300 instrument for ^{1}H (300 MHz), ^{13}C (76 MHz), ^{31}P (122 MHz), ^{11}B (96 MHz), and ^{19}F (282 MHz). ^{1}H/^{13}C NMR spectra were referenced using residual solvent resonances whilst ^{29}Si, ^{119}Sn, ^{31}P, ^{11}B, and ^{19}F NMR spectra were referenced using an external standard. Elemental microanalysis was carried out by Stephen Boyer of London Metropolitan University or by Elemental Analysis Ltd. of Okehampton, Devon, UK. Transmission electron microscopy and high-resolution transmission electron microscopy (HRTEM) was carried out on a JEOL1200EX II instrument. Scanning electron microscopy was carried out on a JEOL SEM 5600LV scanning electron microscope. Powder X-ray diffraction patterns were obtained on a Bruker D8 Advance diffractometer using Cu K_α radiation. Hexane, pentane, and toluene for air- and moisture-sensitive reactions were provided by an MBraun Solvent Purification System and stored over 4Å molecular sieves. THF, Et_2O, and benzene for use in air- and moisture-sensitive reactions were dried over sodium or potassium/benzophenone and distilled before use. Heptane was dried over sodium metal (chunks) and distilled before use. Methanol was dried over activated 3Å molecular sieves. Anhydrous 1,2-dichloroethane was purchased from Sigma-Aldrich and stored over activated 4Å molecular sieves. C_6D_6 was purchased from Sigma-Aldrich and dried over a potassium mirror prior to vacuum transfer into a sealed ampoule and storage in the glovebox under argon. Dry d_8-THF was purchased from Sigma Aldrich and used as received or purchased from Fluorochem. In the latter case, it was either: dried over 4Å molecular sieves followed by a potassium mirror or dried over sodium/benzophenone before being vacuum transferred into a sealed ampoule and stored in the glovebox under argon. Terephthaldehyde was purchased from Sigma-Aldrich and further purified by sublimation. Ferrocene was purchased from Sigma-Aldrich or Avocado, and purified by sublimation before use. Diphenylsilane, *N*,*N*,*N*',*N*'-tetramethylethylenediamine, and benzyl amine were purchased

from Sigma-Aldrich and distilled from CaH_2. 2,6-di-*iso*propylphenol was purchased from Sigma-Aldrich and dried as an Et_2O solution over 4 Å molecular sieves, then distilled and stored in a sealed ampoule. Pinacol was purchased from Sigma-Aldrich and dried by azeotropic distillation of a benzene solution followed by recrystallisation from dry Et_2O. 1,4-benzenedimethanol was purchased from Sigma-Aldrich and sublimed before use. Other alcohols were purchased anhydrous from Sigma-Aldrich and stored over activated 4Å molecular sieves in a sealed ampoule. Bu_3SnH was purchased from Sigma-Aldrich and distilled before use. All tin hydrides were stored in the glove box at -30°C. Tris(pentafluorophenyl)borane was purchased from Tokyo Chemical Industry, sublimed before use, and stored at -30°C. All other commercially available compounds were purchased from Sigma-Aldrich, Fisher Scientific or Tokyo Chemical Industry and used as received. *N*,*N*'-dimethyl-*p*-xylylenediamine,[1] $[Ae(N(SiMe_3)_2)_2.(THF)_2]$ (**IIb**-**d**),[2-4] $[Ae(CH(SiMe_3)_2)_2.(THF)_2]$ (**IIIb**-**d**),[5] $[Sr(N\{SiMe_3\})_2]_2$ (**Ic**),[6] 1,1'-bis(amino)ferrocene,[7-9] ruthenocene,[10] $[(BDI)CaH]_2$ (**VId**),[11] $[(BDI)CaHex]_2$ (**Vb**),[11] Ph_2SnH_2,[12] Ph_3SnH,[13] $MesSnH_3$,[13] Ph_4Sn,[13, 14] *n*Bu_2SnH_2,[12] and *t*Bu_2SnH_2,[15] were synthesised according to literature procedures. $Ph_2PH{\cdot}BH_3$ was prepared from Ph_2PH and either $BH_3{\cdot}SMe_2$ or $BH_3{\cdot}THF$ using a method analogous to that reported in the literature and stored at -30°C.[16] 1,1'-(1,4-phenylene)diethanol was prepared by $NaBH_4$ reduction of 1,4-diacetylbenzene, and was sublimed before use.

i.2. X-ray crystallography

Data for compounds **1**, **10a**, and **10b** was collected on an Agilent Xcalibur diffractometer equipped with a Mo Kα source. The crystals were kept at 150.01(10) K during data collection. Data for compounds **2**-**9**, **10c**, **11**, **12**, **14**, **15**, **16b**, **17**, **18**, **20a.toluene**, **XLVa**, and **21** were collected on a SuperNova machine using Cu Kα radiation. The crystals were kept at 150.00(10) K during data collection. Data for compound **19** was collected on a Bruker APEX-II CCD diffractometer using a Mo Kα source and with the crystal kept at 100(2) K. Using Olex2,[17] all structures were solved with the ShelXT[18] structure solution program using Intrinsic Phasing and refined with the ShelXL[18] refinement package using Least Squares minimisation.

i.3. Diffusion ordered spectroscopy (DOSY) experiments

Diffusion Ordered NMR Spectroscopy (DOSY) experiments were carried out on a Bruker 500 Ultrashield instrument. Samples were analysed at 1-2 mg/ml concentrations in C_6D_6. To avoid distorted diffusion coefficients, the spectra were collected without sample spinning. The Bruker dstebpgp3s convection corrected pulse sequence was used, with a diffusion delay of Δ = 60 ms and gradient pulse length of δ = 5 ms. Spectra were obtained over a 16-step gradient range from 10-90%. Spectra were processed using the MestReNova Bayesian DOSY transform function at a resolution factor of 0.1, 5 repetitions, and 512 points in the diffusion

dimension over a range of ($1x10^{-7}$ – $1x10^{-4}$) cm^2s^{-1}. Molecular weights were estimated using a method described by Grubbs *et.al.*,[19] using six polystyrene standards of known molecular weight from 2000 to 30000 Da, purchased from Sigma-Aldrich. Plotting logD against logM_n produced a linear calibration curve, to which all polymers were compared (Figure i.1).

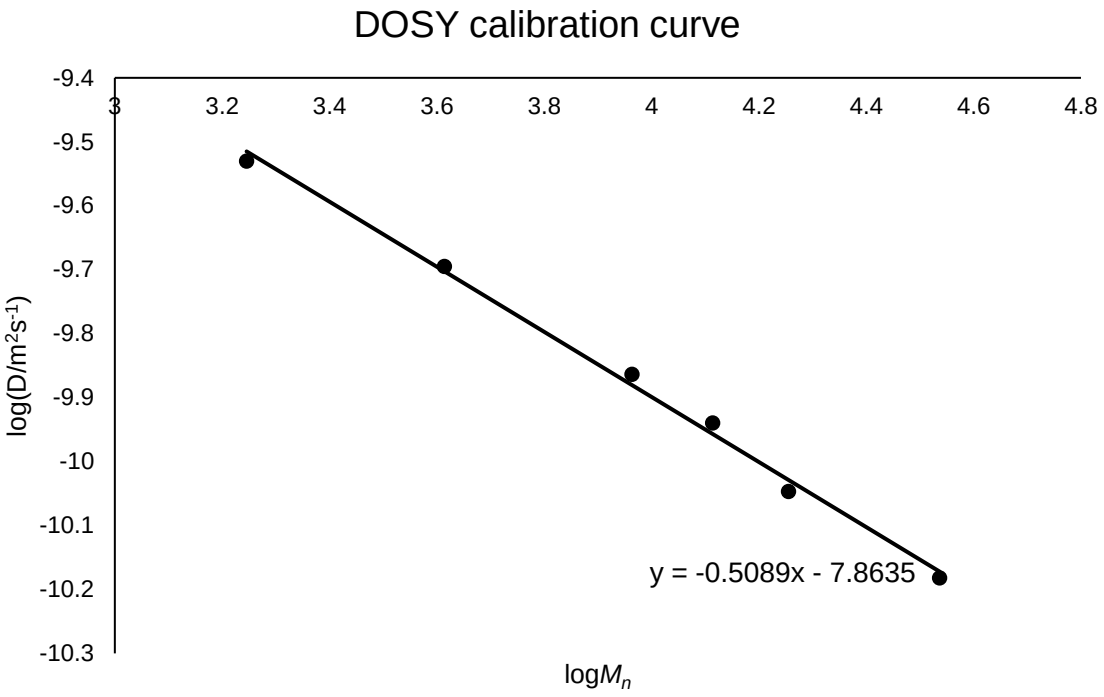

Figure i.1 Calibration curve for log(D/m^2s^{-1}) vs log(M_n/Da) obtained from DOSY NMR experiments of monodisperse polystyrene standards.

i.4. Cyclic voltammetry experiments

Cyclic voltammetry experiments were performed using an Ivium Technologies Compactstat potentiostat. Working, counter, and pseudo-reference electrodes were all platinum disks, 1 mm in diameter. Samples were prepared under a dry argon atmosphere in 1,2-dichloroethane (15 ml), at 1 mM concentration (molecular or monomer concentration), except for compounds **4** (0.4 mM), **5** (0.6 mM), and **7** (0.4 mM). After measurements cobaltocenium hexafluorophosphate was added as an internal potential standard. The Cc^+/Cc reduction wave was found to occur at -1.39 V vs Fc/Fc^+, allowing comparison to the latter, more familiar internal reference system. Tetrabutylammonium hexafluorophosphate was used as the electrolyte at 0.1 M concentration.

i.5. Gel Permeation Chromatography (GPC)

GPC was performed on a Malvern RI max Gel Permeation Chromatograph, equipped with an automatic sampler, a pump, an injector, and inline degasser. The columns (T5000) were

contained within an oven (35°C) and consisted of styrene / divinyl benzene gels. Sample elution was detected by means of a differential refractometer. THF (Fisher) containing 1 %w/w [*n*Bu$_4$N][Br] was used as the eluent at a flow rate of 1 mL min^{-1}. Samples were dissolved in the eluent (2 mg mL^{-1}), spiked with toluene to serve as a flow rate marker and filtered with a Ministart SRP15 filter (poly(tetrafluoroethylene) membrane of 0.45 μm pore size) before analysis. The calibration was conducted using monodisperse polystyrene standards obtained from Aldrich.

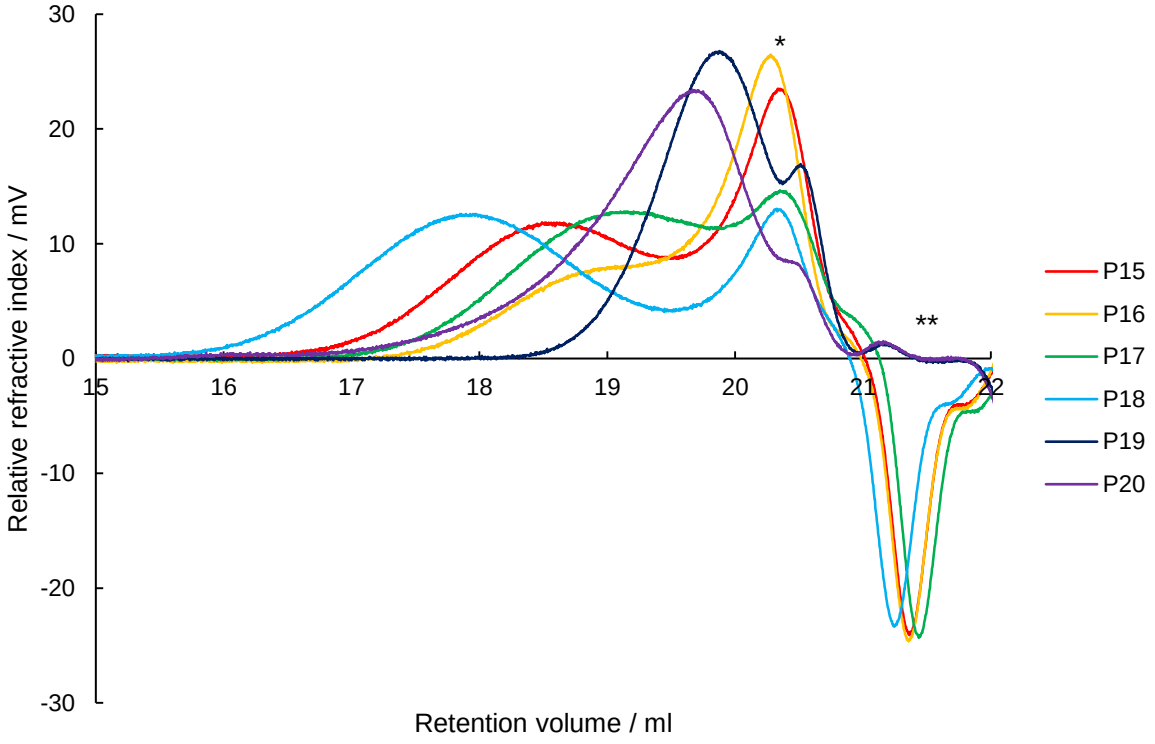

Figure i.2: GPC chromatograms of polymeric and oligomeric materials **P15**-**P20**. * oligomeric peak, ** system peak.

i.6. Thermal analysis (TGA and DSC), pyrolysis experiments, and additional ceramic characterisation data

Thermogravimetric analysis (TGA) was carried out using a Universal Instruments TGA Q500. The temperature was ramped from room temperature to 800°C at 10°C/min under a 40 ml/min flow of nitrogen. Differential scanning calorimetry (DSC) was carried out on a TA Instruments DSC Q20. Samples were ramped from 0°C to 300°C at 10°C/min under an 18 ml/min nitrogen flow. Bulk pyrolysis experiments on **P5** and **P8** were carried out under a flow of nitrogen, using the same heating protocol as for the TGA experiments, in a quartz tube furnace that was thoroughly purged with N_2 before the sample was loaded in a quartz boat. Following pyrolysis,

the sample was cooled to ambient temperature under nitrogen before removal from the furnace. The pyrolysis products were stored in the glove box.

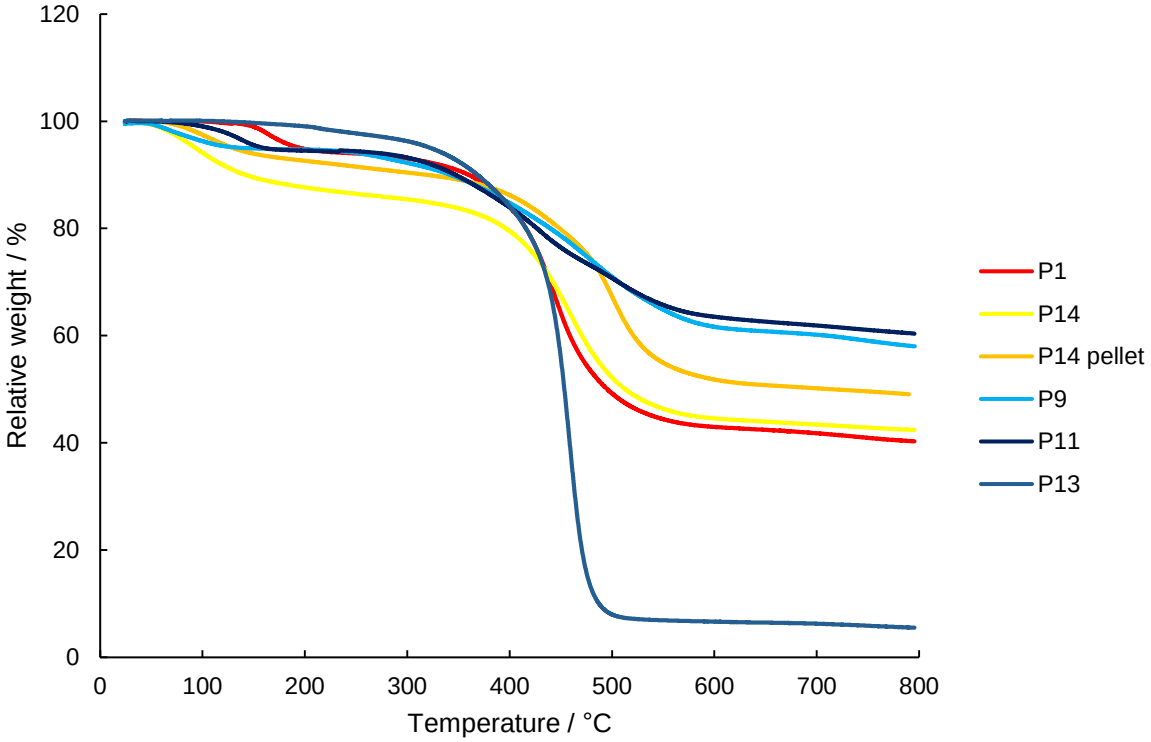

Figure i.3: TGA thermogram of polymers described in chapter 2, without correction for solvent loss.

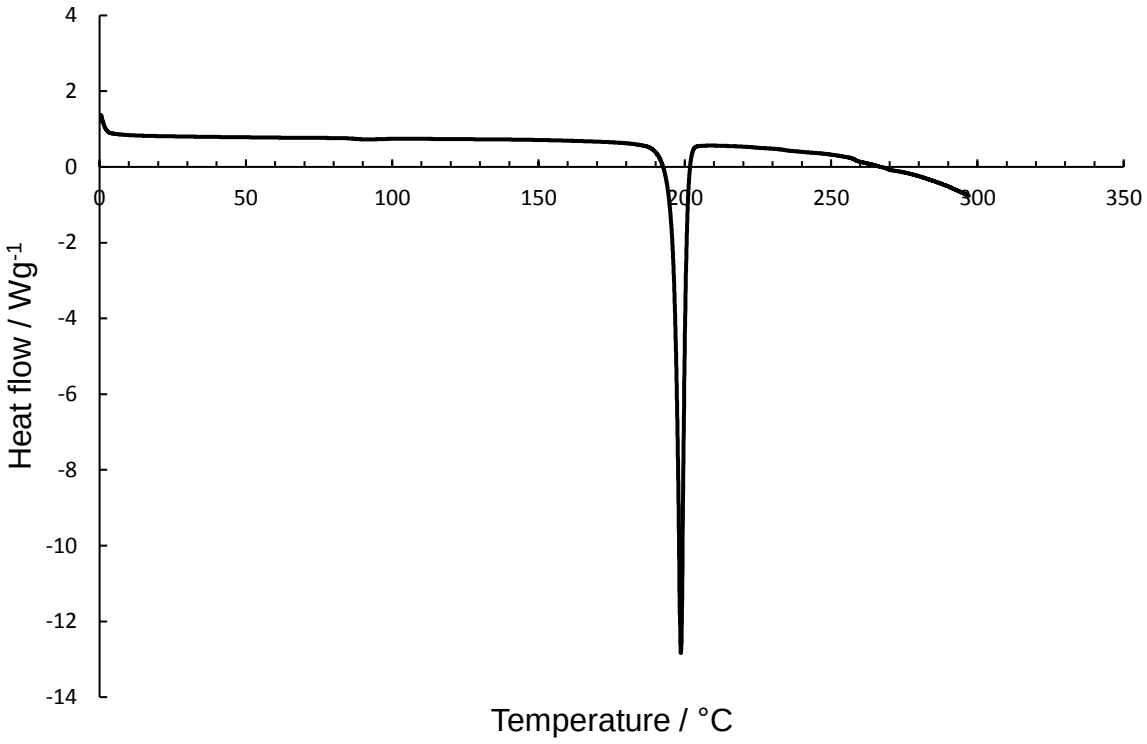

Figure i.4: DSC thermogram of compound **5**.

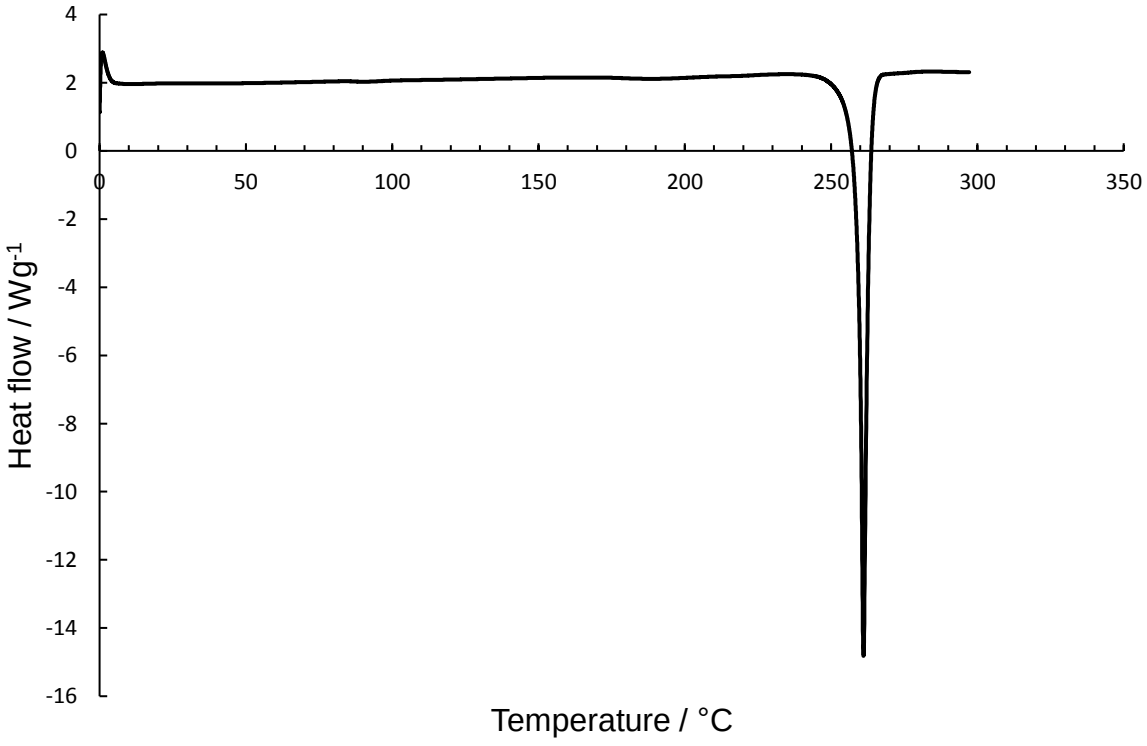

Figure i.5: DSC thermogram of compound **7**.

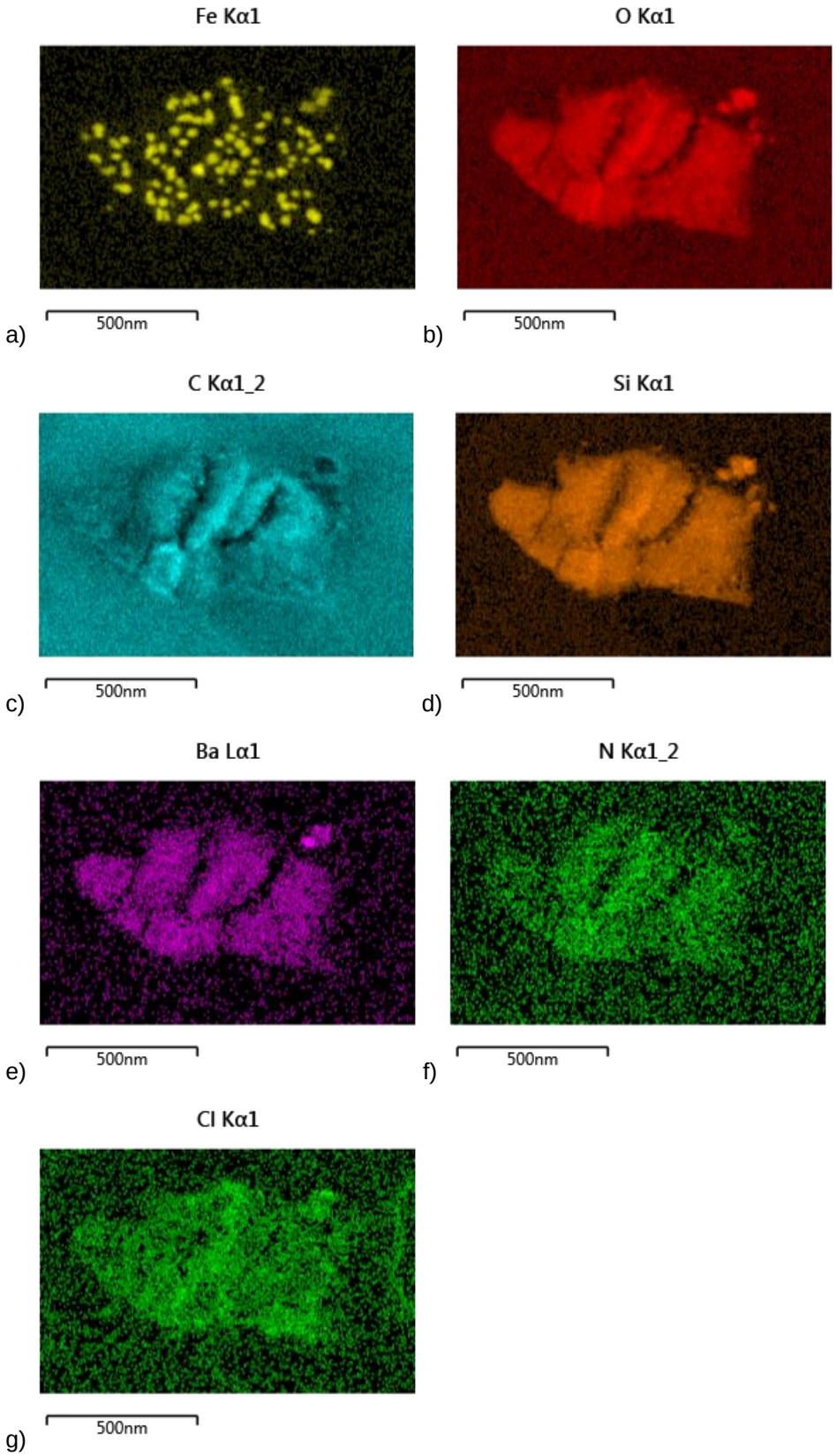

Figure i.6: TEM-EDX elemental maps of **P5py** for a) Fe Kα1, b) O Kα1, c) C Kα1_2, d) Si Kα1, e) Ba Lα1, f) N Kα1_2, g) Cl Kα1.

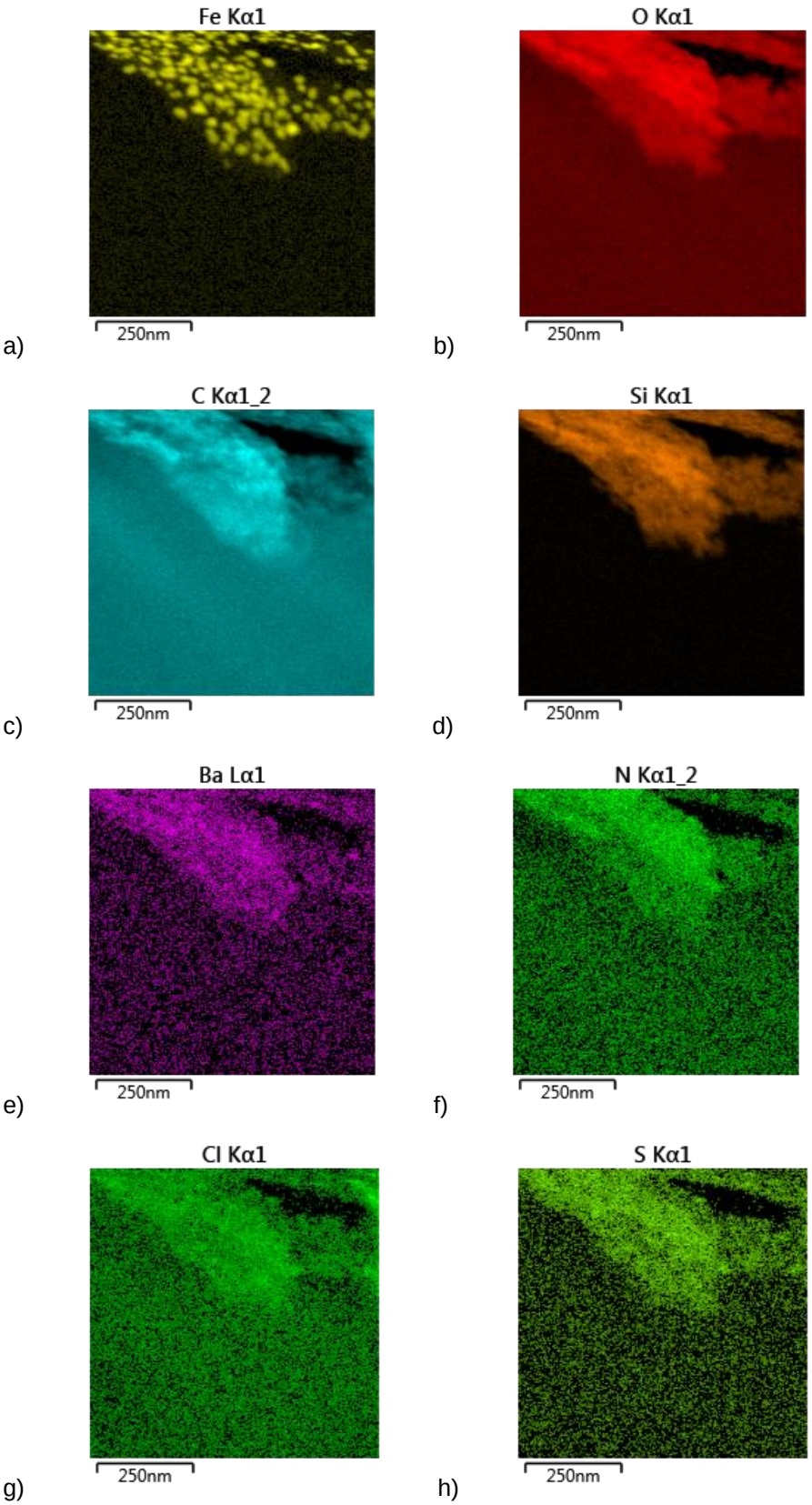

Figure i.7 TEM-EDX elemental maps of **P8py** for a) Fe Kα1, b) O Kα1, c) C Kα1_2, d) Si Kα1, e) Ba Lα1, f) N Kα1_2, g) Cl Kα1, h) S Kα1.

i.7. References

1. J. R. Stevens and P. G. Plieger, *Dalton Transactions*, 2011, **40**, 12235.
2. M. Westerhausen, *Inorganic Chemistry*, 1991, **30**, 96-101.
3. Y. Sarazin, R. H. Howard, D. L. Hughes, S. M. Humphrey and M. Bochmann, *Dalton Transactions*, 2006, 340-350.
4. J. S. Wixey and B. D. Ward, *Dalton Transactions*, 2011, **40**, 7693-7696.
5. M. R. Crimmin, A. G. M. Barrett, M. S. Hill, D. J. MacDougall, M. F. Mahon and P. A. Procopiou, *Chemistry - A European Journal*, 2008, **14**, 11292-11295.
6. M. S. Hill, M. D. Anker and A. S. S. Wilson, in *Inorganic Syntheses*, ed. P. P. Power, Wiley, 111 River Street, Hoboken, NJ 07030, USA, 2018, vol. 37, ch. 2, pp. 24-25.
7. A. N. Nesmeyanov, V. A. Sazonova and V. N. Drozd, *Doklady Akademii Nauk Sssr*, 1963, **150**, 321-&.
8. A. Shafir, M. P. Power, G. D. Whitener, J. Arnold and N. J. Long, *Inorganic Syntheses: Volume 36*, 2014, 65-72.
9. A. Shafir, M. P. Power, G. D. Whitener and J. Arnold, *Organometallics*, 2000, **19**, 3978-3982.
10. E. P. Kundig and F. R. Monnier, *Advanced Synthesis & Catalysis*, 2004, **346**, 901-904.
11. A. S. S. Wilson, M. S. Hill, M. F. Mahon, C. Dinoi and L. Maron, *Science*, 2017, **358**, 1168-1171.
12. S. Harrypersad and D. Foucher, *Chemical Communications* , 2015, **51**, 7120-7123.
13. C. Zeppek, J. Pichler, A. Torvisco, M. Flock and F. Uhlig, *Journal of Organometallic Chemistry*, 2013, **740**, 41-49.
14. C. Schneiderkoglin, B. Mathiasch and M. Dräger, *Journal of Organometallic Chemistry*, 1994, **469**, 25-32.
15. U. Englich, U. Hermann, I. Prass, T. Schollmeier, K. Ruhlandt-Senge and F. Uhlig, *Journal of Organometallic Chemistry*, 2002, **646**, 271-276.
16. K. Bourumeau, A. C. Gaumont and J. M. Denis, *Journal of Organometallic Chemistry*, 1997, **529**, 205-213.
17. O. V. Dolomanov, L. J. Bourhis, R. J. Gildea, J. A. K. Howard and H. Puschmann, *Journal of Applied Crystallography*, 2009, **42**, 339-341.
18. G. M. Sheldrick, *Acta Crystallographica a-Foundation and Advances*, 2015, **71**, 3-8.
19. W. Li, H. Chung, C. Daeffler, J. A. Johnson and R. H. Grubbs, *Macromolecules*, 2012, **45**, 9595-9603.

Appendix ii. Literature compounds, polymers, and oligomers described herein

ii.1. Molecular compounds

Ar = 2,6-di-*iso*propylphenyl unless otherwise specified.

*Compound crystallises as dimer.

I $[M(N\{SiMe_3\}_2)_2]_2$

	a	**b**	**c**	**d**
M =	Mg	Ca	Sr	Ba

II $[M(N\{SiMe_3\}_2)_2.(THF)_2]$

	a	**b**	**c**	**d**
M =	Mg	Ca	Sr	Ba

III $[M(CH\{SiMe_3\}_2)_2.(THF)_2]$

	a	**b**	**c**	**d**
M =	Mg	Ca	Sr	Ba

IV

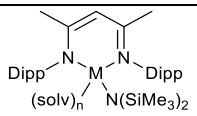

	a	**b**	**c**	**d**
M =	Mg	Ca	Ca	Ca
n =	0	0	1	1
Solv =	-	-	THF	Et_2O

V

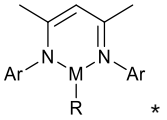

	a	**b**	**c**
M =	Mg	Ca	Sr
R =	*n*-Bu	*n*-Hex	Et
Ar =	Dipp	Dipp	Dipep

VI

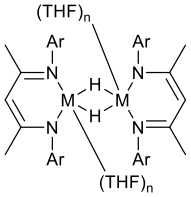

	a	**b**	**c**	**d**	**e**
M =	Mg	Mg	Ca	Ca	Sr
n =	0	1	1	0	0
Ar =	Dipp	Dipp	Dipp	Dipp	Dipep

VII		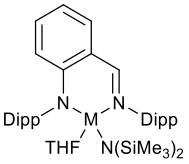		
		a	**b**	**c**
	M =	Ca	Sr	Ba
VIII		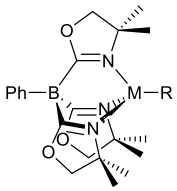		
		a		**b**
	M =	Mg		Zn
	R =	Me		H
IX		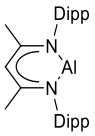		
X		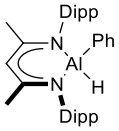		
XI		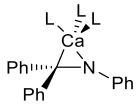		
		L = hexamethylphosphoramide		
XII		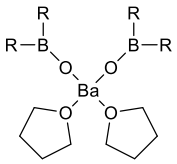	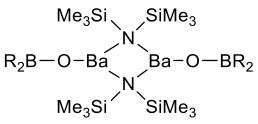	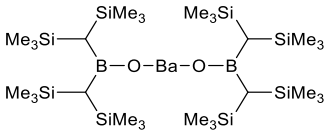
		a	**b**	**c**
		R = $CH(SiMe_3)_2$		
XIII		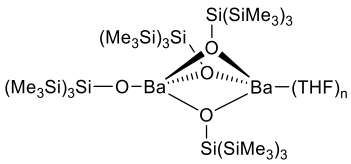		
		a		**b**
	n =	1		0
XIV		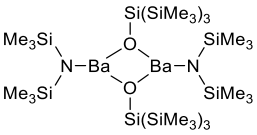		

XV

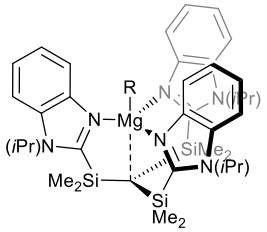

	a	**b**
R =	H	Me

XVI

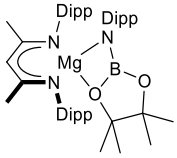

XVII

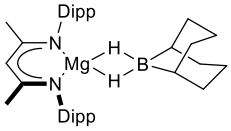

XVIII

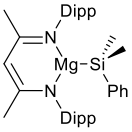

XIX

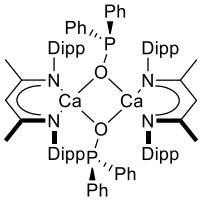

XX

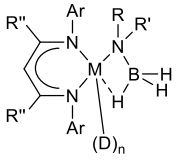

	a	**b**	**c**	**d**	**e**	**f**	**g**	**h**	**i**	**j**	**k**	**l**	**m**	**n**
M	Mg	Ca	Mg	Mg	Mg	Ca	Ca	Ca	Ca	Ca	Ca	Ca	Ca	Ca
R	Me	Me	Dipp	H	Me	H	Me	*i*Pr	Dipp	H	H	Me	*i*Pr	Dipp
R’	Me	Me	H	H	H	H	H	H	H	H	H	H	H	H
R’’	*t*Bu	Me	Me	Me	Me	Me	Me	Me	Me	Me	Me	Me	Me	Me
D	-	THF	-	THF	THF	THF	THF	THF	THF	NH_3	NH_3	NH_3	NH_3	NH_3
x	0	1	0	1	1	2	1	1	1	2	3	2	2	1

XXI

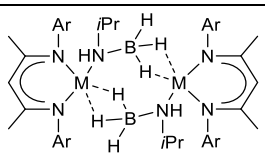

	a	**b**
M	Mg	Ca

XXII

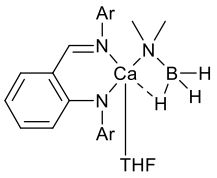

XXIII

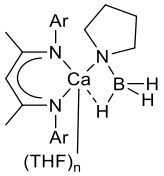

XXIV

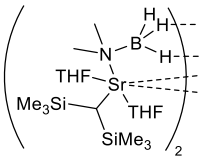

[{({Me$_3$Si}$_2$CH)Sr(*t*BuNHBH$_3$)$_2$}{(THF)$_2$Sr(*t*BuNHBH$_3$)}]

a **b**

XXV

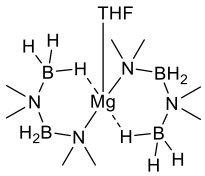

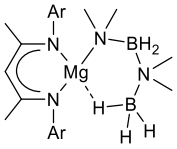

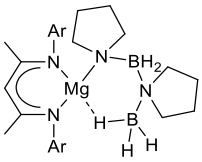

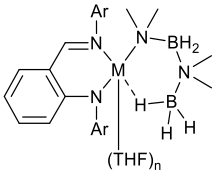

	a	**b**	**c**	**d**	**e**
M =				Mg	Ca
n =				0	1

XXVI

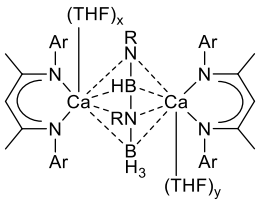

	a	**b**	**c**
R	H	Me	*i*Pr
x	1	1	1
y	1	0	0

XXVII

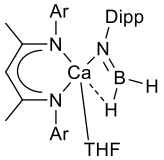

XXVIII

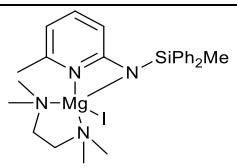

					$[(R_2O)_nM\{OC(CF_3)_3\}_2]$				
		a	**b**	**c**	**d**	**e**	**f**	**g**	**h**
XXIX	M =	Ca	Ca	Ca	Sr	Sr	Sr	Ba	Ba
	R_2O =	THF	DME	diglyme	THF	DME	diglyme	DME	diglyme
	n =	4	2	2	4	2	2	2	3

		$[(THF)_3M\text{-}\mu\text{-}(OC(CF_3)_3)_3K(THF)]$	
XXX		**a**	**b**
	M =	Sr	Ba

XXXI	$[(Odpp)Ca\text{-}\mu\text{-}(Odpp)_2]_2$

		$[(Odpp)M\text{-}\mu\text{-}(Odpp)_3M]$	
XXXII		**a**	**b**
	M =	Sr	Ba

XXXIII	$[Ca(OCPh_3)_2(THF)_4]$

XXXIV	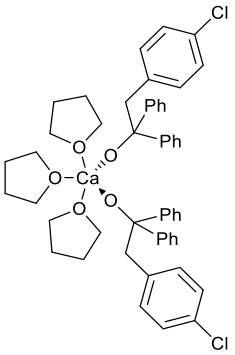

XXXV	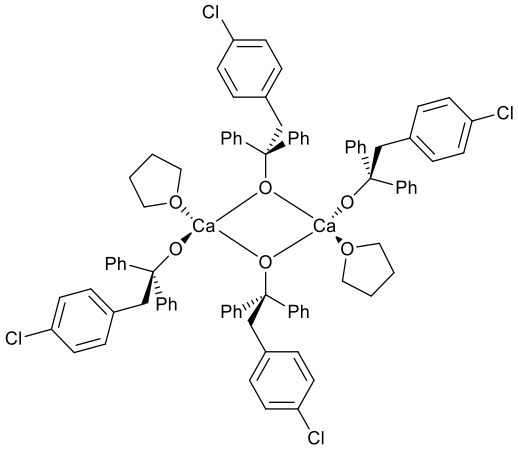

XXXVI	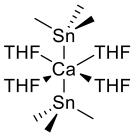

XXXVII	$[Ba(18\text{-crown-}6)(HMPA)_2][SnPh_3]_2$

		$[M(18\text{-crown-}6)(HMPA)_2][Sn(SnPh_3)_3]_2$	
XXXVIII		**a**	**b**
	M =	Ca	Sr

XXXIX

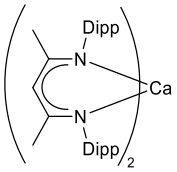

XL $[(Ph_3PO)_2Ca(CH(SiMe_3)_2)_2]$

XLI

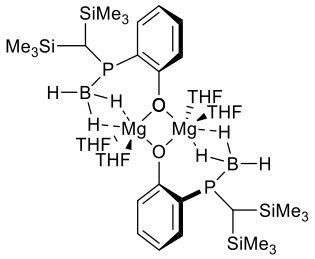

a

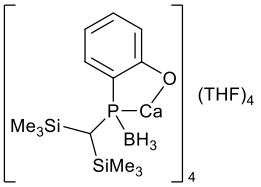

b

XLII

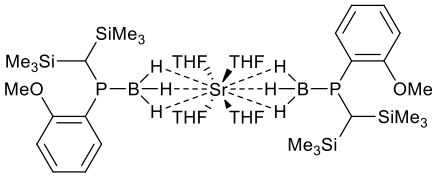

XLIII

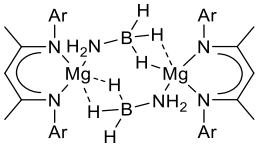

XLIV

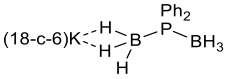

XLV $[K\{HB(C_6F_5)_3\}]$

a

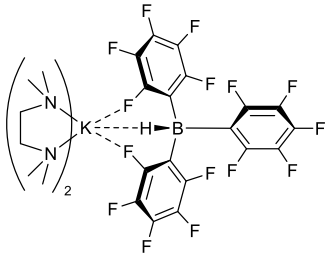

b

XLVI

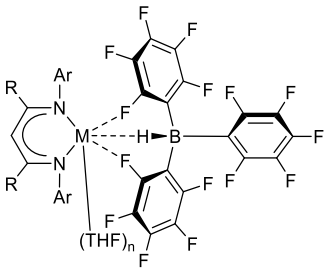

	a	**b**	**c**
M =	Mg	Mg	Ca
R =	Me	*t*Bu	Me
n =	0	0	1

XLVII

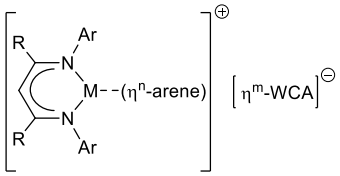

	a	b	c	d	e	f	g	h	i
M	Mg	Mg	Mg	Ca	Mg	Ca	Mg	Mg	Mg
R	Me	Me	*t*Bu	Me	Me	Me	*t*Bu	*t*Bu	*t*Bu
arene	C_6D_6	d_8-toluene	d_8-toluene	C_6D_6	C_6H_6	C_6H_6	C_6H_6	toluene	*m*-xylene
n	6	6	3	6	3	6	2	2	2
WCA		$[Al\{OC(CF_3)_3\}_4]^-$					$[B(C_6F_5)_4]^-$		
m	0	0	0	0	1	1	0	0	0

XLVIII

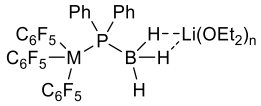

	a	b
M =	B	Al
n =	3	2

XLIX

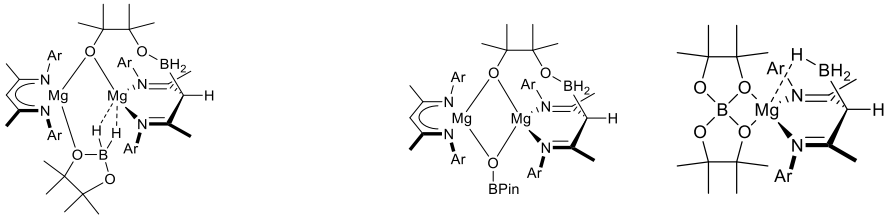

	a	b	c	d
Ar =	Xyl	Mes	Xyl	Xyl

XLX

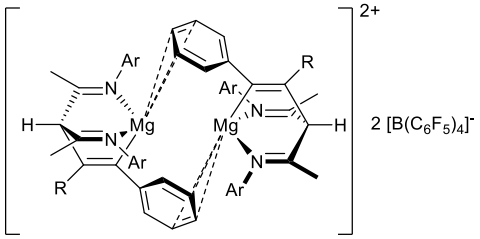

	a	b
R =	Me	Ph

XLXI

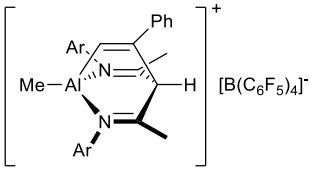

XLXII

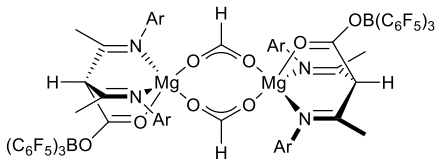

ii.2. Polymers and oligomers

P-I	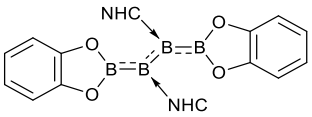	
P-II	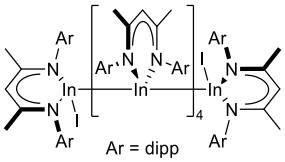	
P-III	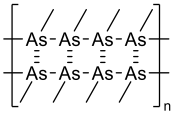	
P-IV	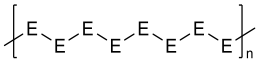	
	a	**b**
E =	S	Se
P-V	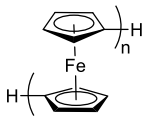	
P-VI	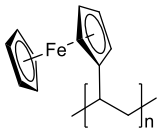	
P-VII	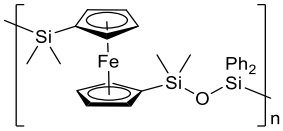	
P-VIII	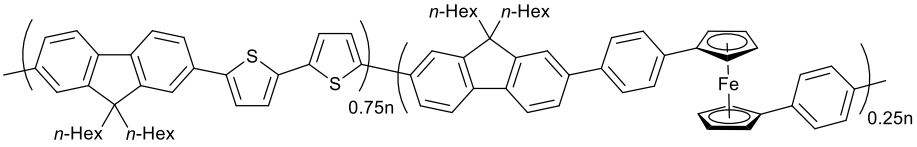	
P-IX	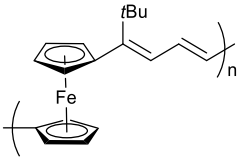	

P-X	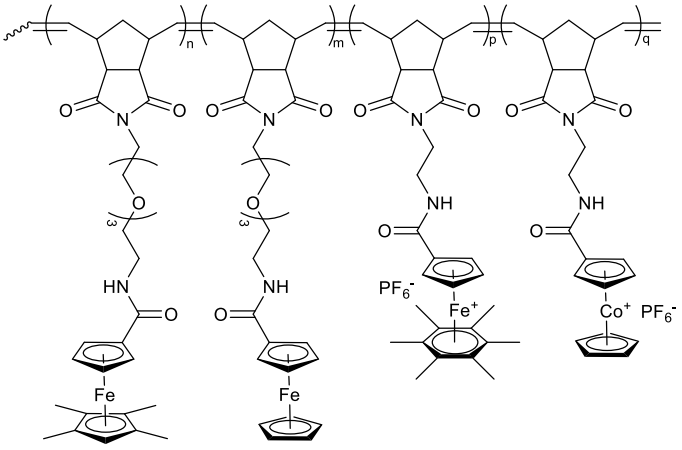
P-XI	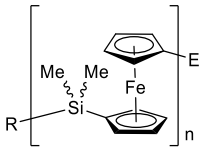 R = Fc, Ph E = H, $SiMe_3$
P-XII	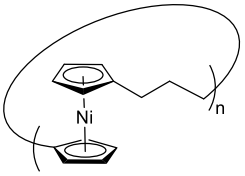
P-XII'	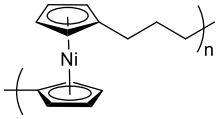
P-XIII	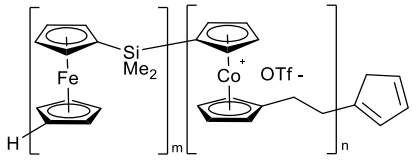
P-XIV	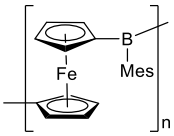
P-XV	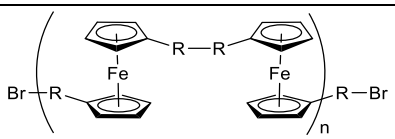 R = thiophene or thiophene-methane groups
P-XVI	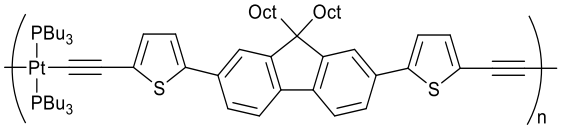

P-XVII

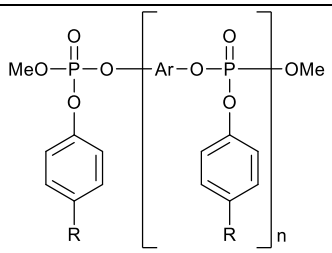

P-XVIII

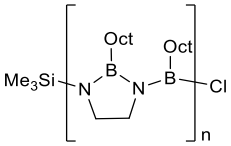

P-XIX

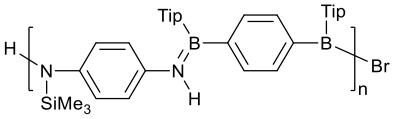

Tip - 2,4,6-tri-*iso*propylphenyl

P-XX

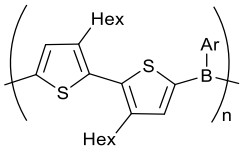

P-XXI

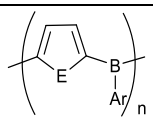

E = S, O

P-XXII

P-XXIII

	a	**b**	**c**	**d**	**e**
R =	*n*Bu	*n*Hex	*n*Oct	Me	Ph

P-XXIV

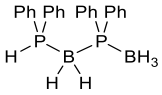

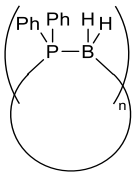

	a	**b**	**c**
n =		3	4

P-XXV

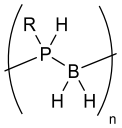

	a	**b**
R =	Ph	*i*-Bu

P-XXVI	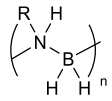 R = alkyl substituent		
P-XXVII			
		a	**b**
	Ar =	Ph	*p*-$F_3C(C_6H_4)$
P-XXVIII	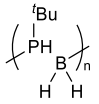		
P-XXIX	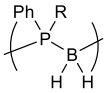		
		a	**b**
	R =	Ph	Et
P-XXX	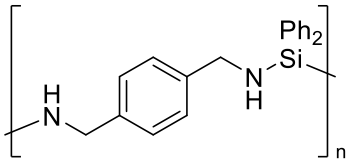		
P-XXX'	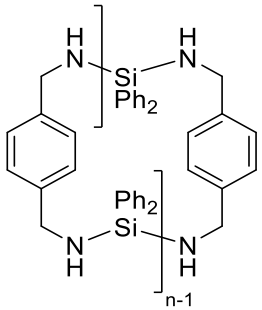		
P-XXXI	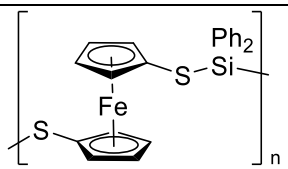		
P-XXXII	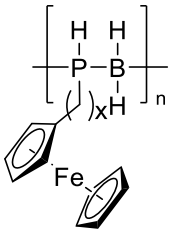		
		a	**b**
	x =	0	1

Appendix iii. Novel compounds, polymers and oligomers described herein

iii.1. Molecular compounds

Ar = 2,6-di-*iso*propylphenyl, BDI = HC{C(Me)N(Ar)}$_2$

1	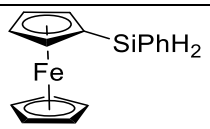
2	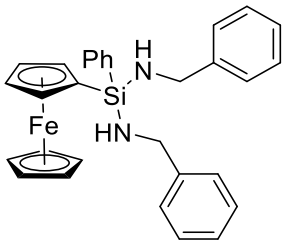
3	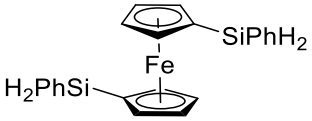
4	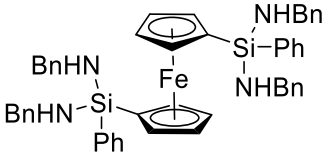
5	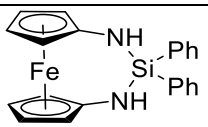
6	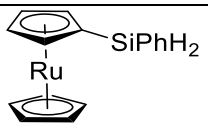
7	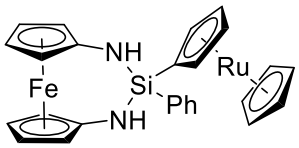
8	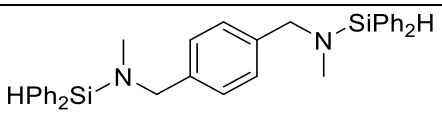

9	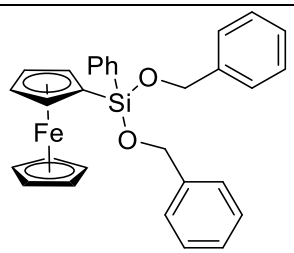			
10	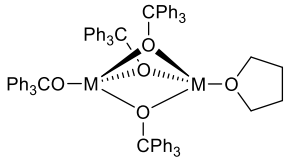			
		a	**b**	**c**
	M =	Ca	Sr	Ba
11	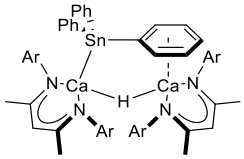			
12	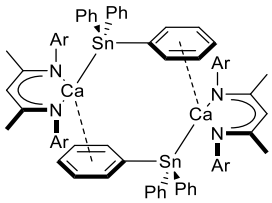			
13	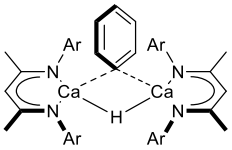			
14	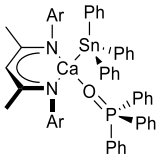			
15	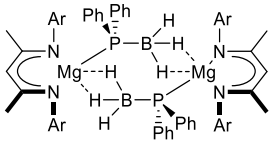			
16	[(BDI)Ca(Ph_2PBH_3)]		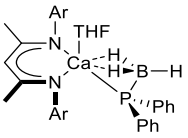	
		a		**b**
17	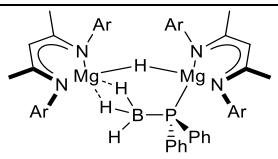			

18	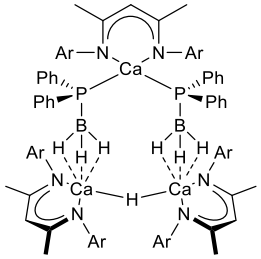			
19	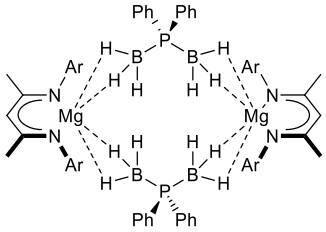			
20	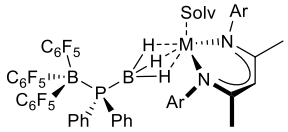			
		a	**a**.toluene	**b**
	M =	Ca	Ca	Mg
	Solv =	-	η^6-toluene	-
21	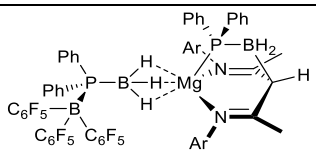			

iii.2. Polymers and oligomers

P1-**P7**	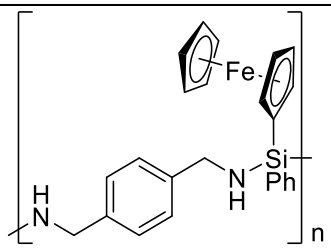
P8-**P10**	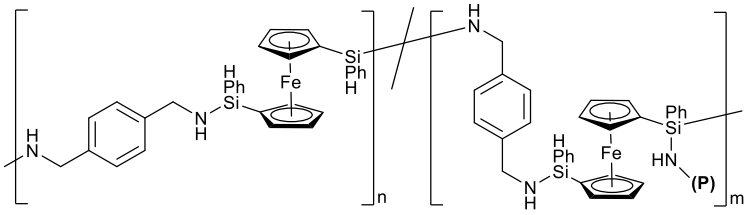

(**P**) denotes an oligomeric or polymeric side chain

P11	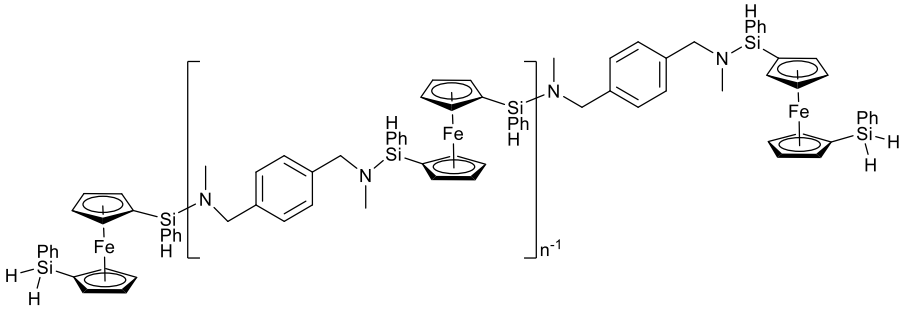
P12	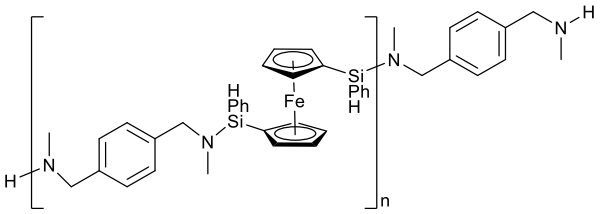
P13	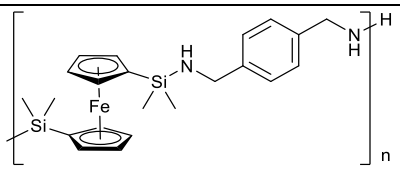
P14	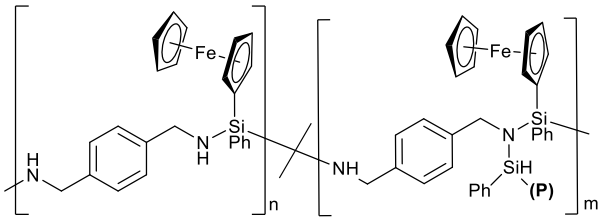 **(P)** denotes another polymer chain of similar structure
P15-P18	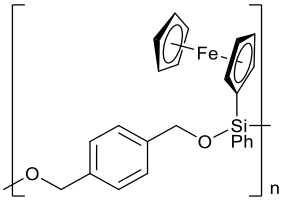
P19-P20